INVESTIGATION OF DIRECT AND INDIRECT HYDRAULIC PROPERTY LABORATORY CHARACTERIZATION METHODS FOR HETEROGENEOUS ALLUVIAL DEPOSITS: APPLICATION TO THE SANDIA-TECH VADOSE ZONE INFILTRATION TEST SITE

by

Kristine E. Baker

Submitted in Partial Fulfillment
of the Requirements for the

Masters of Science in Hydrology

New Mexico Institute of Mining and Technology
Department of Earth and Environmental Science

Socorro, NM

August 2001

I would like to dedicate this thesis to my children, for their support and understanding while their mother was “preoccupied” the majority of their childhood. I would also like to apologize for not attending all the soccer games, PTA meetings, and band concerts, all of which I had a responsibility to attend, and so dearly regret missing. I only hope that someday they will respect my accomplishments and be proud of the person I have struggled so hard to become.

On a lighter note, I would like to tell my grandfather that he was a huge inspiration to me. He knew more about groundwater than I could ever learn in a lifetime of schooling. I miss you Grandpa and I know that you are proud of me. I only wish you could be here to celebrate my achievement (and it will be one heck of a celebration).

ABSTRACT

The need to predict water flow and solute transport at contaminated waste storage facilities has shifted the focus of unsaturated flow research from near surface soils to deep vadose zone alluvium deposits. The primary objective of this research was to characterize the hydraulic properties of deep vadose zone deposits collected from a vadose zone research facility in Socorro, NM using both direct and indirect laboratory methods. Samples collected from the site were analyzed for moisture retention, electrical resistivity, hydraulic conductivity, porosity, and particle-size distributions. The measured results were then compared to properties reported for similar sandy soils and alluvial sands to determine the need to characterize heterogeneous vadose zones independently. Correlations between measured parameters were examined to minimize the number of measurements required in site characterization. The Haverkamp and Parlange (1986) parameter estimation model and a similar estimation model developed as part of this research (to predict the van Genuchten parameters) were used to estimate moisture retention parameters for samples collected at the site.

Direct laboratory measurements of moisture retention for the site deposits showed curve fitting parameters which vary from values reported for sandy soils of similar texture, however, they appeared to be similar to values reported for sandy alluvial deposits. This suggests that values reported for soils in many soil databases should not be used to predict flow and transport in deep, alluvial, vadose zone

environments. In addition, the STVZ deposits all exhibited a non-unique relationship between moisture content and matric potential (known as hysteresis), while the relationship between measurements of electrical conductivity and moisture content did not appear to be hysteretic. It is possible that a porous medium may not exhibit hysteresis in electrical resistivity measurements even if hysteresis is observed in moisture retention measurements because the potential energy state of a porous medium is determined by conditions at the air-water-solid interfaces, and the nature of surface films rather than by the quantity of water present in pores. On the other hand, electrical conductivity is a function of the pore scale fluid distribution within the medium. This research suggests that the non-unique relationship between moisture content and matric potential is less appealing than the relationship between electrical resistivity and moisture content for monitoring changes in moisture content over intermittent periods of wetting/draining conditions.

Both the parameter estimation models evaluated in this study appeared to produce estimates of moisture retention properties comparable to results obtained using direct laboratory methods, however, both models require individual calibration for narrow distributions of particle sizes and porosities. Although the separate calibrations may be cumbersome, this research suggests that property estimation models can be used to reduce the time intensity of direct laboratory measurements, thus increasing the number of samples analyzed for site characterization. Model predictions could be improved by reducing sample disturbance during collection and analysis, and increasing sample sizes for laboratory analysis. Direct measurements of air entry pressure, porosity, and residual moisture content would also improve the model predictions.

ACKNOWLEDGMENTS

I am very grateful to all the “labites” at Sandia National Laboratories for their guidance, support, encouragement and especially their tolerance of me during late nights in which “creative expressions” could be heard bellowing out of my cubicle. Special thanks goes out to Jim Brainard for teaching me skills which may come in handy if this hydrologist thing doesn’t work out. Thanks to him, I am qualified to work as a plumber, driller, and an electrician (sort of). I am also grateful for his friendship, which I will always cherish, and for introducing me to the exciting world of whitewater sports. I am particularly grateful for the support of my office-mate and good friend, Bob Holt, who not only gave me the courage to keep trying in times of adversity, but also made me believe I could actually become a scientist someday.

I am very grateful to my advisor Dr. Robert J. Glass for taking the time to teach me everything I know about vadose zone hydrology and giving me the opportunity to work with the most talented group of scientists I will most likely encounter in my career. Without his support and guidance, I would certainly not be where I am today.

And last but not least, I would like to thank my manager, Bob Smith, at the Idaho National Environmental and Engineering Laboratory (INEEL) for the support he has shown while “patiently” waiting for me to finish my thesis. I only hope that I can become the best vadose zone hydrologist in his department someday (look out Earl –

I’m after your job). I cannot forget to mention Rich Martineau for sacrificing his own dissertation to review my final draft. I appreciate his efforts and recommendations.

This project was funded by the U.S Department of Energy (DOE) under EMSP work project ER-EM-EMSP-96. Laboratory analysis was conducted at the Sandia National Laboratory Flow and Visualization Lab in Albuquerque, NM. The field research site is located in the New Mexico Institute of Mining and Technology research park. The INEEL partially funded completion of my thesis and supported presentation of the research at the DOE TIE conference in Augusta, GA in November, 2000.

TABLE OF CONTENTS

Page

ABSTRACT iii

ACKNOWLEDGMENTS v

TABLE OF CONTENTS vii

LIST OF TABLES x

LIST OF FIGURES xi

LIST OF NOTATIONS xv

CHAPTER 1.0 – INTRODUCTION 1

1.1 Research Motivation 1

1.2 Thesis Outline 2

1.3 Standard Method for Hydraulic Property Characterization 3

1.4 Application of Standard Methods for Characterization of Deep Vadose Zone Deposits 5

1.5 Research Objectives 7

1.6 Research Summary 8

CHAPTER 2.0 – Laboratory Methods for Characterizing Sandy Alluvial Deposits: Application to the STVZ Research Site 10

2.1 Abstract 10

2.2 Introduction 11

2.3 Site Description 12

2.4 Methods 20

2.5 Results 35

2.6 Discussion 57

2.7 Measurement Error and Uncertainty 75

2.8 Conclusions 81

2.9 Recommendations for Future Work 83

CHAPTER 3.0 – PREDICTIVE METHODS FOR CHARACTERIZING HYDRAULIC PROPERTIES OF SANDY ALLUVIAL DEPOSITS: APPLICATION TO THE STVZ RESEARCH SITE 86

3.1 Abstract 86

3.2 Introduction 87

3.3 Haverkamp and Parlange (1986) Model Theory 90

3.4 Haverkamp and Parlange (1986) Model Application to the STVZ Samples 95

3.5 Haverkamp and Parlange (1986) Model Application to the Fabricated Samples 101

3.6 Haverkamp and Parlange (1986) Pedotransfer Model Application Conclusions 110

3.7 Development and Application of the Parameter Estimation Model for Predicting the van Genuchten Curve Fitting Parameters.....117

3.8 Model Sensitivity Analysis.....124

3.9 Chapter Summary and Conclusions 126

CHAPTER 4.0 – CONCLUSIONS 128

4.1 Research Summary.....128

4.2 Laboratory Methods 129

4.3 Measured Results.....131

4.4 Pedotransfer Model Predictions.....133

4.5 Recommendations for Future Work 135

Appendix A—STVZ Subsurface Stratigraphy and IN SITU Moisture Profile 138

Appendix B—Preliminary Studies 148

Appendix C—Sample Preparation 170

Appendix D1—Electrical Resistivity Measurement Procedures.....174

Appendix D2—Electrical Resistivity Measured Data and Resistivity Versus Moisture Content Curves 179

Appendix E1—Moisture Retention Measurement Procedures 209

Appendix E2—Moisture Retention Measurement Data and Moisture Characteristic Curves 223

Appendix F—Sample Saturation Procedures 259

Appendix G—Saturated Hydraulic Conductivity Measurement Procedures and Measured Data 263

Appendix H—Particle Size Analysis Procedures and Measured Data 274

Appendix I—Curve Fitting Procedures 290

Appendix J—Parameter Correlation Methods and Results 297

Appendix K—Measurement Error 322

Appendix L—Haverkamp and Parlange Estimation Model Calibration to the STVZ Alluvial Sand Deposits 334

Appendix M—Haverkamp and Parlange Estimation Model Results 352

Appendix N—Fabricated Samples PSD and Brooks and Corey Fit to PDC Data 372

Appendix O—Modified Parameter Estimation Model Procedures 393

Appendix P—Modified Parameter Estimation Model Results 402

Appendix Q—Model Sensitivity and Analysis Procedures 422

Appendix R—Model Sensitivity Analysis Results 462

REFERENCES 471

LIST OF TABLES

2.1 Utten-Wentworth classification for sand sized sedimentary deposits (Prothero and Schwab, 1996) 33

2.2 Hydraulic properties of samples collected from the northwest quadrant of the STVZ infiltration test site 37

2.3 van Genuchten fitting parameters estimated using RETC 38

2.4 Table of electrical resistivity fitting parameters 50

2.5 Textural properties of NW core samples 56

2.6 Published hydraulic properties (mean values) for sandy soils and alluvial sands 60

2.7 Error analysis of porosity measurements made using the saturation chamber (3 samples analyzed 5 times each) 76

2.8 Error analysis of moisture content measurements made at 1 bar pressure using the pressure chambers (3 samples analyzed 5 times each) 77

2.9 Error analysis of electrical resistivity measurements made at saturation using the impedance analyzer (3 samples analyzed 5 times each) 77

2.10 Error analysis of moisture content measurements made using the hanging column apparatus (5 replicate samples analyzed once each – statistics represent population statistics for the set) 77

2.11 Error analysis of saturated hydraulic conductivity measurements made using the constant head permeameter (4 replicates measured three times each) 78

2.12 Error analysis of particle-size measurements made using the sieve method (2 replicate samples measured 10 times each) 78

3.1 Moisture retention curve fitting parameters for the STVZ samples and the sandy soils used in the original Haverkamp and Parlange (1986) model 88

3.2 Model input parameters used in model calibration for application to the STVZ site deposits 97

3.3 Fabricated sample descriptions 106

3.4 Model input parameters used in model calibration. 119

LIST OF FIGURES

2.1 Sandia-Tech Vadose Zone Research Site Location 13

2.2 Sandia Tech Vadose Zone Infiltration Test Site Layout 14

2.3 Instrumentation schematic and core locations 15

2.4 Three dimensional representation of the complex, heterogeneity of subsurface deposits within the vadose zone below the STVZ site (to a depth of 6m) 16

2.5 Fine-medium grained sands and gravels exposed in nearby sand pit 16

2.6 Close up of gravel layer in Figure 2.5. Lens cap shows scale of images 17

2.7 Transfer of core to PVC for storage 19

2.8 Transfer of core to PVC for storage 19

2.9 Correlated geologic stratigraphic columns of the subsurface sedimentary deposits below the STVZ infiltration pad 21

2.10 Visibly structureless sands collected from the NW quadrant 22

2.11 Iron oxide layers observed in intact section of core collected from the SE quadrant at the STVZ test site 22

2.12 Iron oxide layers in fine grained sands collected from the NW quadrant 23

2.13 Clay conglomerate collected from core in the NW quadrant 23

2.14 Example of artificial moisture content values at 0 cm tension (plotted as 2 cm tension at center of sample ring) 27

2.15 Moisture retention curves for a coarse grained sand collected from the NW core at a depth of approximately 1 meter below ground surface 39

2.16 Moisture-retention curves for a gravel collected from the NW core at a depth of approximately 2 m ground surface 40

2.17 Moisture retention curves for a silty sand collected from the NW core at approximately 5 meters below ground surface 41

2.18 Moisture retention curves for a pebbly clay collected from the NW core at approximately 6 meters below ground surface 42

2.19 Moisture-retention curves for a fine-medium-grained sand collected from the NW Core at approximately 8 meters below ground surface 43

2.20 Electrical resistivity curve for a coarse-grained sand located at approximately 1 meter below ground surface 45

2.21 Electrical resistivity curve for a gravel located at approximately 2 meters below ground surface 46

2.22 Electrical resistivity curve for a silty sand located at approximately 5 meters below ground surface 47

2.23 Electrical resistivity curve for a pebbly clay located at approximately 6 meters below ground surface 48

2.24 Electrical resistivity curve for a fine grained sand located at approximately 8 meters below ground surface 49

2.25 Particle-size distribution for a coarse-grained sand collected from the STVZ research site at approximately 1 meter below ground surface 52

2.26 Particle-size distribution for a gravel collected from the STVZ research site at approximately 2 meters below ground surface 53

2.27 Particle-size distribution for a silty sand collected from the STVZ research site at approximately 5 meters below ground surface 54

2.28 Particle-size distribution for a fine grained sand collected from the STVZ research site at approximately 8 meters below ground surface 55

2.29 Plot of van Genuchten parameter ($1/\alpha$) during a drainage sequence (MDC) versus wetting sequence (MWC) 63

2.30 Plot of van Genuchten parameter ($1/\alpha$) during a drainage sequence from satiation (MDC) versus a drainage sequence from saturation (PDC) 64

2.31 Plot of van Genuchten parameter ($1/\alpha$) during a wetting sequence (MWC) versus a drainage sequence from saturation (PDC) 65

2.32 Slope of the primary drainage curve versus the slope of the main drainage curve 66

2.33 Slope of the PSD versus slope of the PDC 67

2.34 PDC $1/\alpha$ versus average grain diameter d_g 68

2.35 Correlation between electrical resistivity curve fitting parameter “k” versus grain diameter 74

2.36 Correlation between saturated hydraulic conductivity and grain size 70

2.37 Correlation between saturated hydraulic conductivity and grain sorting.....71

2.38 Relationship between the pore-size distribution fitting parameter α and saturated hydraulic conductivity for the PDC 72

2.39 Correlation between porosity and saturated hydraulic conductivity 73

2.40 Typical moisture retention curves for sandy soils (Carsel and Parish, 1988) and sandy alluvial deposits of similar texture (mean fitting parameter values for sandy alluvial deposits collected from the STVZ site).....62

3.1 Moisture characteristic curves showing hysteresis in air entry pressure values 93

3.2 Regression analysis of curve fitting parameters (λ / (n_d-1)) versus bulk density for the STVZ site deposits. Data for the samples used in the original model calibration are included in the plot for comparison.....97

3.3 Regression analysis of packing parameter (γ) versus estimated particle index (λ) values for the STVZ samples 98

3.4 Example of the moisture retention curve estimates for sample number NW4.....102

3.5 Example of the moisture retention curve estimates for sample number NW10.....103

3.6 Example of the moisture retention curve estimates for sample number NW2.....104

3.7 Example of the moisture retention curve estimates for sample number NW21.....105

3.8 Estimate of the model parameter λ for the fabricated samples 107

3.9 Estimate of the model parameter γ for the fabricated samples.....108

3.10 Estimated curves using model estimation equations calibrated to the STVZ samples.....111

3.11 Estimated curves using model estimation equations re-calibrated to the fabricated samples.....112

3.12 Estimated curves using model estimation equations calibrated to the STVZ samples.....113

3.13 Estimated curves using model estimation equations re-calibrated to the fabricated samples.....114

3.14 Estimated curves using model estimation equations calibrated to the STVZ samples.....115

3.15 Estimated curves using model estimation equations re-calibrated to the fabricated samples.....116

3.16 Regression analysis used to determine estimation equation for the van Genuchten curve fitting parameter *n* for the PDC.....118

3.17 Example of the model predictions for sample NW11 121

3.18 Example of the model predictions for sample NW2 122

LIST OF NOTATIONS

θ	=	Volumetric moisture content (ml/ml)
θ_r	=	Residual moisture content (ml/ml)
θ_s	=	Saturated moisture content (ml/ml)
ϕ	=	porosity (volume of sample void space/total sample volume)
α	=	van Genuchten (1980) model curve fitting parameter
n	=	van Genuchten (1980) model curve fitting parameter
h	=	matric potential (cm)
h_{ae}	=	Brooks and Corey (1964) model curve fitting parameter representing air entry pressure (cm)
h_{we}	=	Brooks and Corey (1964) model curve fitting parameter representing water entry pressure (cm)
λ	=	Brooks and Corey (1964) model curve fitting parameter representing the slope of the pore size distribution curve
$F(d)$	=	Particle size distribution function
d_g	=	Curve fitting parameter in *F(d)* representing the average grain diameter (cm) of a sample.
n_d	=	Curve fitting parameter in *F(d)* representing the slope of the distribution curve
ρ	=	Electrical resistivity (ohm meters)
k	=	Curve fitting parameter in Archie's law describing the relationship between electrical resistivity and moisture content.
m	=	Curve fitting parameter in Archie's law describing the relationship between electrical resistivity and moisture content.
K_{sat}	=	Saturated hydraulic conductivity [L/T]

K(h)	=	Unsaturated hydraulic conductivity as a function of pressure head [L/T]
Bd, ρ_d	=	Sample dry bulk density (g/cc)
Pd, ρ_p	=	Particle density (g/cc)
γ	=	Packing parameter in the Haverkamp and Parlange (1986) pedotransfer model (unitless)
MWC	=	moisture retention main wetting curve
MDC	=	moisture retention main draining curve
PDC	=	moisture retention primary draining curve

CHAPTER 1.0 – INTRODUCTION

1.1 Research Motivation

Understanding unsaturated fluid flow and transport within deep vadose zones is currently at the forefront of environmental research. It is estimated that approximately 800 million cubic meters of subsurface media in the United States and Puerto Rico (location of many U.S. Department of Energy facilities) have been or are being contaminated at present. Although only 7% of the media are estimated to be within the vadose zone, it is of particular interest because the vadose zone is considered to act as a continuing source of groundwater contamination. Remediation has been hampered by the lack of a comprehensive understanding of the interdependence of physical, geochemical, and microbial processes as they are manifested in spatially and temporally heterogeneous subsurface environments.

The vadose zone consists of near surface soils above the plant root zone and sedimentary geologic deposits and rock formations within the deep vadose zone. Previous vadose zone research has been driven by the need to improve water use efficiency and reduce soil salinity for agricultural purposes, and to reduce the impact of leachate on groundwater quality (Istok et al., 1994; Healy and Mills, 1991). The need to predict water flow and solute transport at contaminated waste storage facilities has shifted the focus of unsaturated flow research from soils to deep vadose zone alluvium deposits because trenches excavated in alluvium are currently being used to store toxic

materials and low-level radioactive waste at many U.S. Department of Energy (DOE) facilities (Istok et al., 1994). These sedimentary deposits consist of heterogeneous layered materials with distinctly differing biogeochemical and hydrologic properties which are spatially and temporally variant.

One of the major technical focus areas of the U.S. DOE Subsurface Science Initiative is to improve the understanding of physical flow and transport of fluids in complex heterogeneous subsurface matrices. Physical properties of vadose zone materials which determine the behavior of water flow systems are the hydraulic conductivity and water-retention characteristics. The hydraulic conductivity of a porous material is the measure of its ability to transmit water, while the water retention characteristics reflect its ability to store water.

1.2 Thesis Outline

- **Chapter 1 – Introduction**

  This chapter includes motivation for the research, a brief description of methods used to characterize hydraulic properties of vadose zone materials, research objectives and a research summary.

- **Chapter 2 – Laboratory Methods for Characterizing Hydraulic Properties of Sandy Alluvial Deposits: Application to the STVZ Research Site.**

  This chapter describes methods used for laboratory analysis, examples of measured results for moisture retention curves, electrical resistivity curves, saturated hydraulic conductivity, and particle-size distributions. Correlations between hydraulic and geophysical parameters are examined and discussed in the chapter in order to minimize the number of measurements required for site characterization. A discussion

of the results, chapter conclusions, and recommendations for future work are included at the end of the chapter.

- **Chapter 3 – Predictive Methods for Characterizing Hydraulic Properties for Sandy Alluvial Deposits: Application to the STVZ Research Site.**

This chapter includes an evaluation of a pedotransfer model developed by Haverkamp and Parlange (1986) for application to sandy alluvial deposits. The chapter also includes development and application of a similar pedotransfer model designed to estimate the van Genuchten (1980) parametric model parameters often used in flow and transport models for unsaturated porous media. The chapter concludes with an examination of the conditions for pedotransfer model application using Monte Carlo simulations.

- **Chapter 4 – Conclusions and Recommendations for Future Research**

The final chapter of the thesis summarizes the research, discusses key research topics and results, and includes recommendations for future work related to the research.

1.3 Standard Method for Hydraulic Property Characterization

Fluid flow and transport within the vadose zone are highly dependent on the unsaturated hydraulic conductivity K(h) of subsurface porous media. Current methods for determining K(h) include direct field and laboratory measurements, and indirect estimation methods. Direct field measurements are associated with a high degree of uncertainty due to difficulties in calibrating monitoring equipment to heterogeneous geologic materials and due to uncertainty in the volume of the wetted region (van Genuchten et al., 1999). Although laboratory measurements typically have a higher degree of measurement precision compared to *in situ* analysis, direct laboratory

measurements are extremely time consuming, often limiting the number of measurements which can be reasonably obtained. Standard laboratory methods are also restricted to K(h) measurements during the drainage cycle, prohibiting knowledge of the hysteretic behavior of the porous medium (Stephens, 1995 pg 171-172).

As an alternative, indirect methods have been developed for estimating K(h) from direct measurements of hydraulic and textural properties of soils and geologic materials. Indirect methods consist of pore-size distribution models (also referred to as parametric models), inverse methods, and pedotransfer functions (van Genuchten et al., 1999).

Pore-size distribution models estimate K(h) based on the distribution, connectivity, and tortuosity of pores within a porous medium. The pore-size distribution is represented by the moisture retention curve (also referred to as the moisture characteristic curve). The moisture retention curve is determined from a power law fit to moisture content data as a function of equilibrium matric potential (negative pressure head). The data can be measured during wetting and draining sequences to describe the hysteretic moisture retention behavior of porous materials.

Inverse models combine a numerical solution of Richard's equation with an optimization algorithm to estimate pore-size distribution model parameters from observed time series of infiltration, water content and/or pressure head. Although results are based on data collected from real flow conditions, the results are non-unique (van Genuchten et al., 1999).

Pedotransfer functions (PTFs) estimate hydraulic properties of soils based on textural and physical properties of a porous medium (e.g., particle-size distributions and bulk density or porosity). Physical PTFs such as the models developed by Arya and

Paris (1981), Arya et al. (1999), and Haverkamp & Parlange (1986) are based on the concept of shape similarity between pore-size distribution and particle-size distribution curves (van Genuchten et al., 1999). The vast majority of PTFs are completely empirical and require some form of surrogate input data for model calibration (van Genuchten et al., 1999). Although PTFs are appealing for hydraulic property characterization, cumbersome model calibration may not improve efficiency over direct laboratory determinations. In addition, the evaluation of calibration sample size (i.e., number of samples), number of data points required, and impact of measurement error may show that PTF models are not feasible for estimating properties of vadose zone materials with a great deal of certainty. PTF model results can be improved, however, when one or more moisture content data points at pressure equilibrium are included as model input parameters. Recently, neural network analyses have been introduced to further improve the predictions. An advantage of neural networks is that they require no *a priori* model concept. Instead the model is calibrated through an iterative process (van Genuchten et al., 1999).

1.4 Application of Standard Methods for Characterization of Deep Vadose Zone Deposits

Most published studies and testing standards for hydraulic property characterization have focused on near surface soils within the root zone, primarily because of the ease of sample and data collection and because agricultural processes have motivated research in near surface soils (Healy and Mills, 1991; Istok et al., 1994). Therefore, the ASTM laboratory methods for measuring moisture retention properties, developed for characterizing homogeneous soils, may not be applicable for characterization of poorly consolidated alluvial deposits.

For deep vadose zone materials, the sampling procedures often require driving or auguring techniques which are costly and often lead to severe sample disturbance in poorly consolidated materials For this reason, many researchers refer to hydraulic property databases such as the Unsaturated Soil Database (UNSODA) compiled by the U.S. Environmental Protection Agency (EPA) to determine hydraulic properties of vadose zone materials based on textural classifications. Although these databases serve as useful repositories for hydraulic property analyses of soils, it remains unclear that hydraulic properties within heterogeneous deep vadose zones are similar to those reported in the literature for soils (Healy and Mills, 1991). In addition, many hydraulic property databases do not include moisture retention properties and unsaturated flow behavior during wetting (infiltration) events. Even though the relationship between matric potential and moisture content has been shown to be dependent on the wetting/draining history of a porous medium, referred to as hysteresis (Haverkamp and Parlange, 1986; Stephens, 1995), it is often neglected by researchers because it generally takes much longer to obtain the data due to the very low initial conductivity and low starting flow rates. The wetting history may also impact the relationship between electrical conductivity and moisture content due to changes in pore-size distribution and pore connectivity.

Particle sorting, grain size distributions, packing geometry, and geologic structure all impact unsaturated flow behavior of materials in the vadose zone (Fetter, 1991 pg. 82; Klute, 1986 pg. 635; Jury et al., 1991 pg. 228). Therefore, correlations between hydraulic property parameters such as saturated hydraulic conductivity, moisture retention parameters, particle-size distribution parameters, and sample porosity or bulk density should be observed during analysis. These correlations can then be used

to minimize the number of parameters requiring direct observation, improving cost and time efficiency in characterizing vadose zone materials.

Research is required to develop standard procedures for characterizing deep vadose zone materials below the root zone. These studies should include sample collection techniques which preserve the integrity of *in situ* geologic and hydrologic conditions, procedures for determining hysteretic moisture retention and hydraulic conductivity behavior, scaling procedures for application of laboratory results to field study sites, and procedures for estimating hydraulic properties from correlated physical properties which are more cost efficient and timely to measure directly.

1.5 Research Objectives

The DOE is interested in methodologies for determining the spatial variability of K(h) due to the possibility of contaminant transport within regions of the western United States where buried waste has been introduced to deep vadose zones (Alumbaugh et al., 1996). Researchers at the Sandia National Laboratories and the University of Arizona have collaborated as part of a DOE Environmental Management Science Program (EMSP) to investigate field, laboratory, and predictive methods for describing the spatial variability of vadose zone materials. The Sandia-Tech Vadose Zone (STVZ) research facility was constructed in Socorro, NM to examine hydraulic properties within vadose zone materials during various infiltration events. The geologic materials located at the field site represent common alluvial and fluvial deposits underlying a majority of DOE facilities in the western United States. The overall research objective is to develop and test an integrated Hybrid Hydrologic-Geophysical Inverse Technique (HHGIT) for vadose zone characterization at contaminated DOE sites. The HHGIT is a geostatistical based estimation technique. The results of the

HHGIT technique represent conditional mean hydraulic property fields and contaminant distributions. The study incorporates field and laboratory measurements of geophysical and hydrologic data as input parameters for the inverse model. The HHGIT model simulates changes in hydraulic properties during an unsaturated infiltration event (Alumbaugh et al., 1996).

The focus of the research included in this thesis includes characterization of hydraulic properties of the vadose zone deposits located at the infiltration field site using direct laboratory and indirect predictive methods to obtain moisture retention curve fitting parameters often used in unsaturated zone flow and transport numerical models. The hydraulic properties will be used as input parameters in the HHGIT inverse model. Predictive methods for determining hydraulic properties are appealing because they allow analysis of large sample sets, required in geostatistical based modeling. Most laboratory methods for determining moisture retention curves limit the number of samples which can be analyzed due to long periods required to reach steady state conditions.

1.6 Research Summary

Alluvial deposit samples were collected from continuous core to a depth of 12 m below ground surface at the STVZ site and transported to Sandia National Laboratories for analysis. Properties measured include wetting and draining moisture retention curves, porosity, saturated hydraulic conductivity, electrical resistivity, and particle-size distributions. Functional forms (equations fit to measured data through regression analysis – described in Chapter 2) describing the shape of the moisture retention curves, electrical resistivity curves, and particle-size distribution curves were fit to measured data to obtain curve fitting parameters. Correlations were examined between

parameters to minimize the number of measurements required in hydraulic property characterization of vadose zone materials. The correlations were then used to estimate hydraulic properties using prediction models. Model predictions were compared to results obtained using direct methods to determine application for site characterization. A sensitivity analysis was conducted to determine model requirements for achieving optimum results and to examine the impact of measurement error on the predictions.

CHAPTER 2.0 – LABORATORY METHODS FOR CHARACTERIZING SANDY ALLUVIAL DEPOSITS APPLICATION TO THE STVZ RESEARCH SITE

2.1 Abstract

The primary objective of this research is to characterize the hydraulic properties of deep vadose zone deposits collected from the Sandia-Tech Vadose Zone (STVZ) research facility in Socorro, NM. Measured results were compared to properties reported for similar sandy soils and alluvial sands to determine the need to characterize heterogeneous vadose zones individually. Correlations between parameters were examined to minimize the number of measurements required in hydraulic property characterization of deep vadose zone materials.

The results of this study indicate that moisture retention properties for sandy alluvial deposits vary from properties reported for sandy soils. In addition, moisture retention relationships show dependence on the wetting history and grain texture of the deposits. Although the relationship between electrical resistivity and moisture content was also a function of grain textures, hysteresis was not observed in the electrical resistivity measurements. Correlations observed between measured properties indicate that physical properties of alluvial deposits can be used to predict hydraulic properties. For example, the porosity of a sample can be coupled with grain-size distribution data to estimate moisture retention properties of the deposits. In addition, the relationship

between curve fitting parameters for wetting and draining moisture retention curves can be used to estimate wetting parameters from data measured during a draining sequence.

2.2 Introduction

2.2.1 Problem Statement

Buried waste within deep vadose zones has shifted the focus of unsaturated flow research from near surface soils to heterogeneous geologic units often consisting of thick layers of alluvial sands and gravels. Although hydraulic property databases have been compiled for near surface soils, limited data is available for hydraulic properties of alluvial geologic deposits. It has not yet been established that soil properties are valid for modeling flow and transport within deep vadose zones, therefore, the use of soil properties for modeling contaminant transport within deep vadose zones could lead to erroneous predictions. In addition, characterization methods were developed for soils and have not been fully examined for application to poorly compacted, heterogeneous alluvial deposits.

2.2.2 Motivation

This research supports hydraulic and geophysical site characterization of the STVZ field experiment which incorporates both hydraulic and geophysical data collected during infiltration events within alluvial subsurface deposits. Coupling laboratory and field data to characterize hydraulic and geophysical properties of subsurface materials will reduce the uncertainty inherent in data collected independently.

2.2.3 Research Objectives

The objectives of this research are to: 1) examine, modify, and apply laboratory methods for hydraulic and geophysical site characterization, 2) quantify property and

parameter correlations to minimize cumbersome direct laboratory measurement of properties, and 3) examine measurement error and uncertainty in laboratory measurements.

2.2.4 Chapter Outline

This chapter includes a geologic description of the STVZ research site, instrument borehole layout, and continuous core locations; a description of preliminary studies conducted to examine possible shortcomings of the laboratory methods; presentation of laboratory results and parameter correlations; a sequential description of methods used for site characterization; and a discussion of laboratory measurement error and uncertainty. Data presented in the results section of the chapter represent measurements made for distinct geologic units located at the STVZ site (e.g., sands, silts, clays, gravels). A discussion of major topics, chapter conclusions, and recommendations for future work are presented at the end of this chapter. This chapter includes a condensed discussion of the research conducted for this thesis. Refer to the appendices for a detailed description of the research site, instrumentation, preliminary studies, measurement techniques, and research results.

2.3 Site Description

2.3.1 Introduction

The STVZ field site is located at the New Mexico Institute of Mining and Technology (NMT) research park located in Socorro, NM (Figure 2.1). The site was developed to monitor hydraulic properties such as moisture content, pressure, and electrical resistivity during an infiltration event (Figures 2.2 and 2.3). The top meter of soil within the root zone was removed from the research infiltration and monitoring pad in order to examine infiltration and redistribution into geologic alluvial deposits.

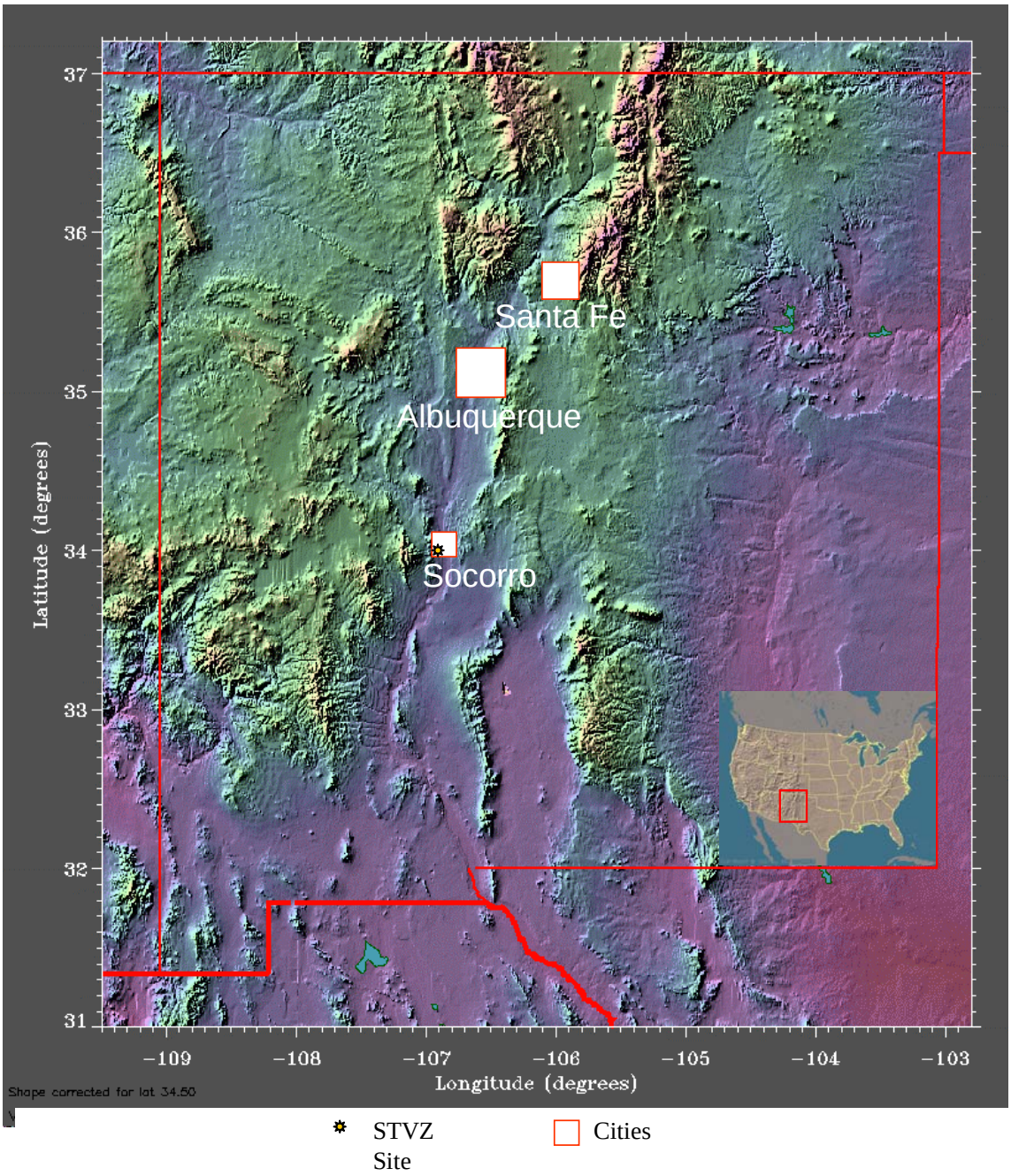

Figure 2.1 – Sandia-Tech Vadose Zone Research Site Location.

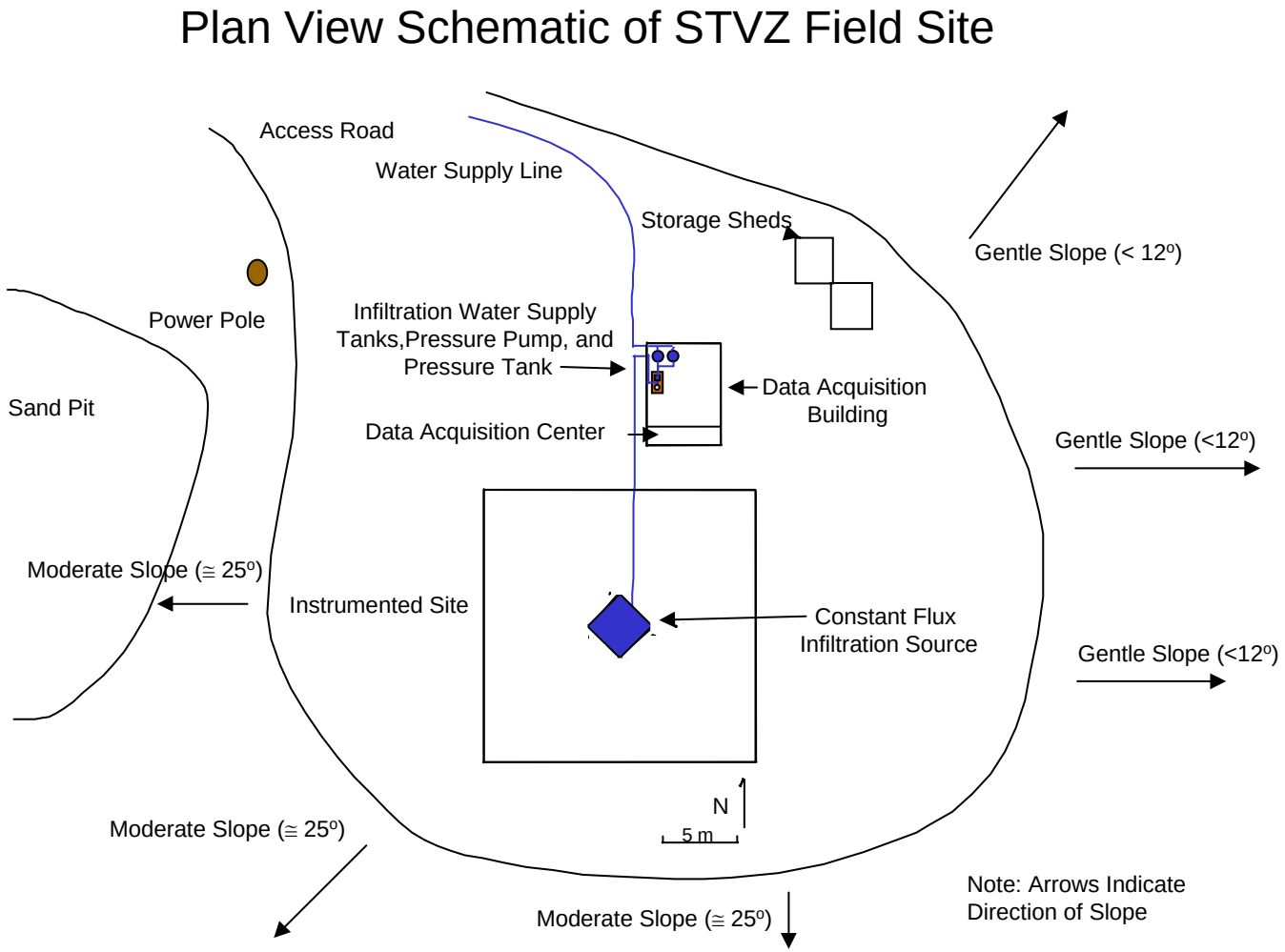

Figure 2.2 – Sandia Tech Vadose Zone Infiltration Test Site Layout.

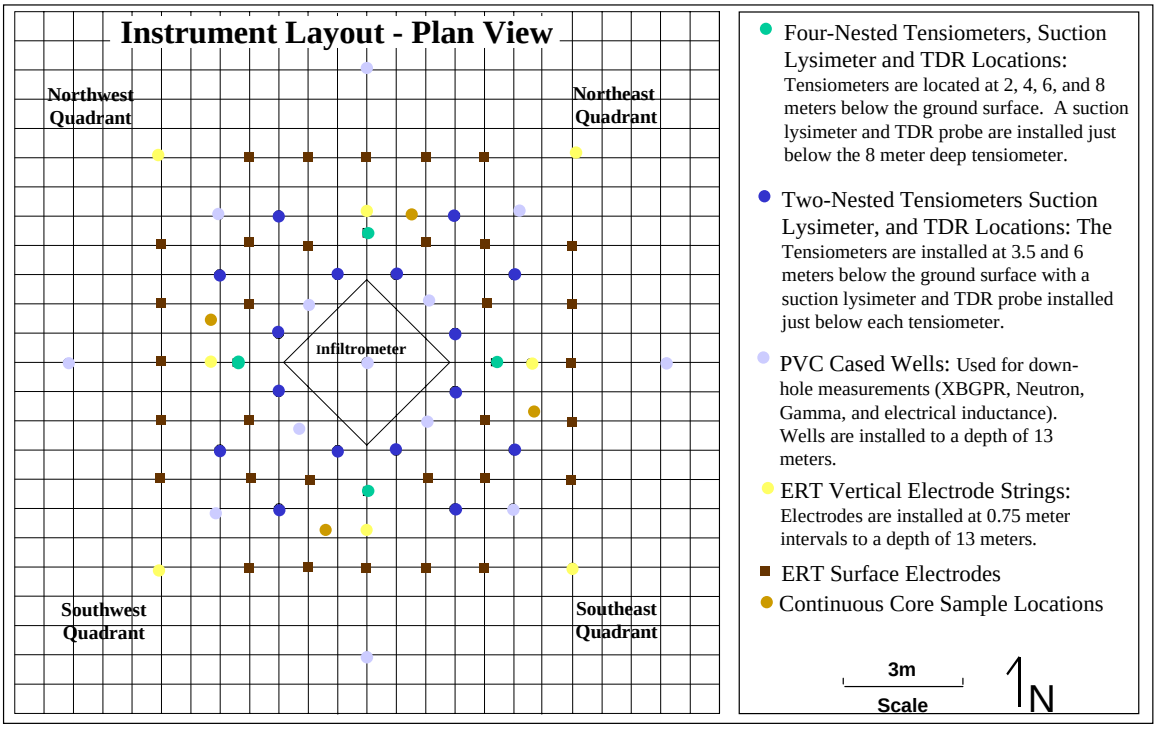

Figure 2.3 – Instrumentation schematic and core locations.

The complex, heterogeneous geology (Figure 2.4) provides a challenging testing ground for investigating the application of geophysical techniques to vadose zone flow and transport problems and is an analog to many DOE sites in the western United States.

The field site is located on the top of a knoll providing access to correlated deposits exposed in a nearby excavated sand pit (Figure 2.2). The geologic units exposed in the pit are displayed in Figures 2.5 and 2.6. In addition, proximity of the NMT campus provides the opportunity for student participation in this research and continued use of the site by NMT when the project has been completed.

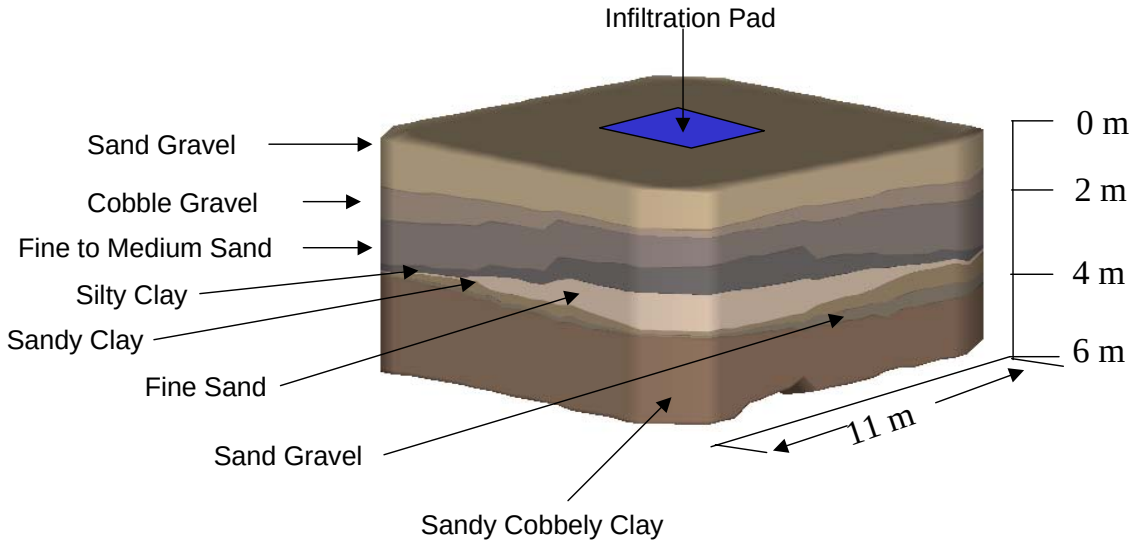

Figure 2.4 – Three dimensional representation of the complex, heterogeneity of subsurface deposits within the vadose zone below the STVZ site (to a depth of 6m). Below 6m, the deposits consist of inter-bedded layers of fine-medium grained sands.

Figure 2.5 – Fine-medium grained sands and gravels exposed in nearby sand pit.

Figure 2.6 – Close up of gravel layer in Figure 2.5. Lens cap shows scale of images.

2.3.2 Geology

The field site deposits are mapped as part of the Sierra Ladrones Formation, Upper Santa Fe Group consisting of fine-coarse grained, poorly consolidated, ancestral Rio Grande axial-river deposits with intermittent layers of debris flow sediments and sedimentary layers of eolian sands. The axial-river deposits range from approximately 300-800 meters in thickness between the Socorro Basin and the Socorro Mountain block (Hawley, 1983). Hydraulic mapping of the basin indicates that the water table within the vicinity of the infiltration site is located from 20 m to 30 m below the ground surface (Anderholm, 1983).

2.3.3 Monitoring Equipment Instrumentation

The site is instrumented to a depth of approximately 12 m consisting of 13 PVC cased access tubes for down-borehole geophysical monitoring of moisture content,

9 vertical arrays of electrical resistivity electrodes and 32 surface electrodes for ERT data collection, 32 thermocouples for monitoring subsurface temperatures, and 80 tensiometers for monitoring matric potential (negative pressure). Additional instruments include time domain reflectometer probes and suction lysimeters for measuring tracer concentrations. All instruments were installed within a 10.6 m by 10.6 m area in an axisymmetric pattern outside a 3 m by 3 m infiltration pad located at the center of the site (Figure 2.3). The axisymmetric instrument layout minimizes uncertainties that might otherwise occur due to an unbalanced distribution of instruments. Further details on installation and instrumentation may be found in Paprocki (2000) and Brainard et al. (2000).

2.3.4 Core Collection Procedures

Rodgers and Company (Albuquerque, NM) was contracted to auger boreholes while collecting continuous core samples from the subsurface. A CME 75 high torque drill rig was used to auger the holes. Eight sections of 6 ¼ inch ID x 5 ft long split spoon samplers were inserted into a hollow stem wire line auger with a 10 ½ inch bit to collect core samples from four boreholes located within the site instrumentation pad (Figure 2.3).

Sediment removed from the shoe of the samplers was immediately weighed and recorded before and after oven drying at the NMT soil's lab to determine the gravimetric moisture content of the deposits at depth. Intact core was preserved and transferred to Sandia National Laboratory in Albuquerque, NM in 5 ft long sections of PVC pipe marked with location, core orientation, and geologic boundaries (Figures 2.7 and 2.8).

Figure 2.7 – Transfer of core to PVC for storage.

Figure 2.8 – Transfer of core to PVC for storage.

2.3.5 Geologic Characterization

Field site geology was characterized from inspection of the continuous core sections and drilling logs recorded during installation of monitoring equipment boreholes. A general representation of subsurface stratigraphy and location of geologic units is shown in Figure 2.9. Extensive geologic description of the individual cores and initial *in situ* moisture profiles at depth are included in Appendix A.

Although the majority of the core contains visibly structureless, moderately dry, poorly consolidated sands (Figure 2.10), geologic structure was visible in sections of core containing iron oxide deposits (Figures 2.11 and 2.12). Visible structure consists primarily of thin laminations (Figures 2.5 and 2.6), however occasional sections of core contain convoluted layers of iron oxide deposits and/or rip-up clasts of clay and angular rhyolite (Figure 2.13). These convoluted layers represent occasional high velocity channel flow deposition intermittent with fluvial and eolian depositional environments.

2.4 Methods

2.4.1 Introduction

Preliminary studies were conducted prior to measuring hydraulic properties to examine optimum experimental techniques for hydraulic and geophysical property characterization. The studies include 1) examination of sample compaction during desorption measurements, 2) impact of natural structure on moisture retention properties, 3) cause of artificially high moisture contents at saturation, 4) determination of moisture equilibrium times, 5) sample contact required for electrical resistivity measurements, and 6) sample disturbance due to sub-sampling methods. An overview of the studies is included in this chapter, while a detailed description of the studies is presented in Appendix B.

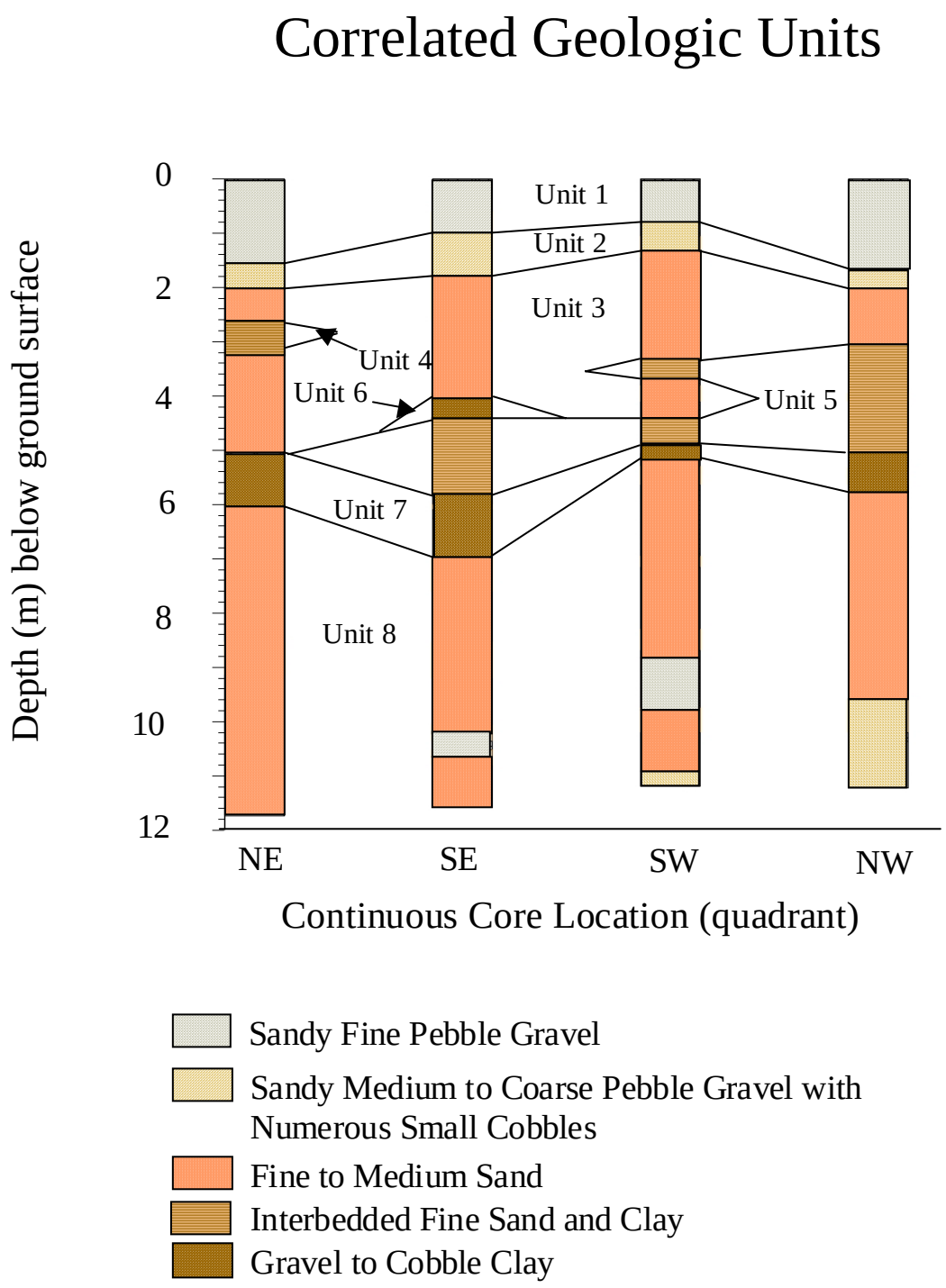

Figure 2.9 – Correlated geologic stratigraphic columns of the subsurface sedimentary deposits below the STVZ infiltration pad.

Figure 2.10 – Visibly structureless sands collected from the NW quadrant.

Figure 2.11 – Iron oxide layers observed in intact section of core collected from the SE quadrant at the STVZ test site.

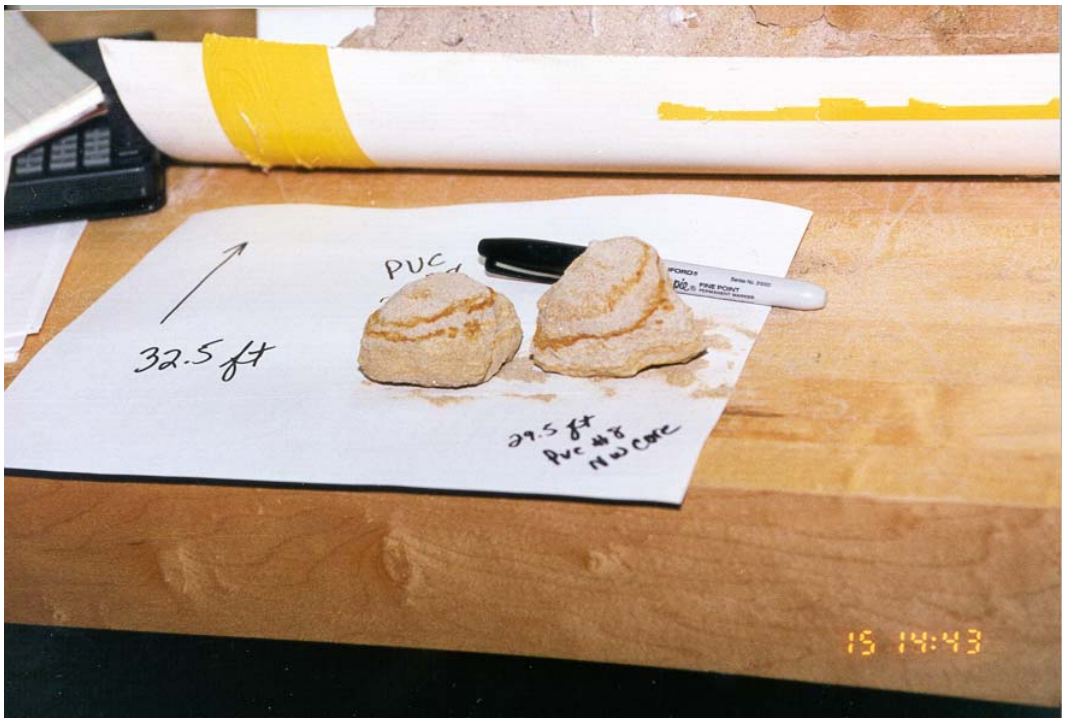

Figure 2.12 – Iron oxide layers in fine grained sands collected from the NW quadrant.

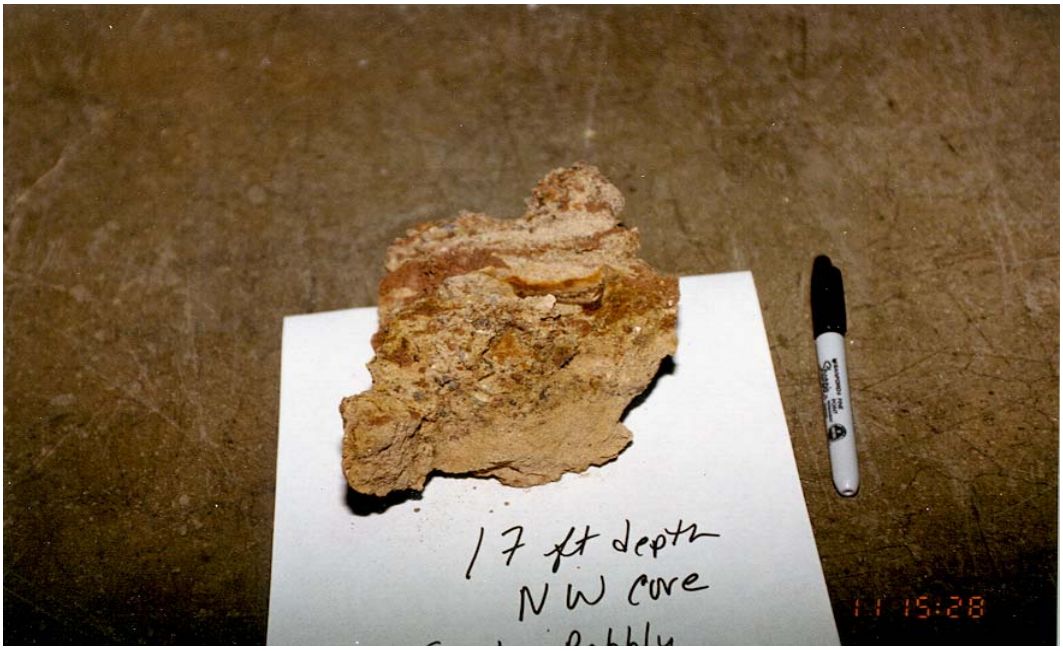

Figure 2.13 – Clay conglomerate collected from core in the NW quadrant.

Initial laboratory techniques were based on ASTM standards for analysis of soil properties. ASTM standard laboratory procedures for determination of soil hydraulic properties include: sample collection procedures (ASTM, 1999 and ASTM, 1994a), techniques for preserving and transporting soil samples (ASTM, 1995), wetting and draining procedures relating moisture content to the energy state of soils (ASTM, 1994b and ASTM, 1994c), procedures for determining soil hydraulic conductivity (ASTM, 1994d), and procedures for measuring soil particle-size distribution (ASTM, 1963). Additional references for hydraulic property characterization methods are found in Klute (1986), Stephens (1995), and Jury et al. (1991). ASTM standards have not been established for electrical resistivity measurements, therefore Knight (1991) was used as a reference for the procedure.

These techniques were evaluated to determine applicability for measurement of poorly consolidated alluvial deposits located at the STVZ research site. Deviation from ASTM standards and published recommendations were based on results of preliminary experiments designed to examine possible procedural shortcomings (Appendix B). Laboratory measurement techniques were evaluated for measurement precision and accuracy when possible.

2.4.2 Preliminary Studies

2.4.2.2 Compaction

Because volume changes during analysis greatly impact the moisture retention characteristics of a porous medium, a preliminary study was conducted as part of this research to examine compaction during desorption of various sample textures, identify the cause of the compaction, and determine if compaction during analysis could be prevented. Intact near-surface, coarse-grained sands, and fine-grained sands located at

approximately 3.5 m below ground surface were collected from the STVZ site for analysis during desorption. The fine-grained sands did not compact during desorption using two separate wetting solutions (Socorro tap water at approximately 1000 μS/cm conductivity and a 0.005M calcium sulfate solution), while the coarse-grained sands compacted using both solutions. Compaction observed in near surface sands may have been due to destruction of fine-particle "bridges" deposited between sand grains during natural recharge. Destruction of these "bridges" has been observed in previous studies conducted by the New Mexico Bureau of Mines (Love et al., 1987) during infiltration and subsequent drainage events. Compaction was greater for the coarse-grained sands saturated with the calcium sulfate solution compared to the samples saturated with tap water, by as much as 5% by volume (Appendix B). The reason for the increased compaction using the calcium sulfate solution was not evident, however, based on the results of this study, a calcium sulfate solution was not used to saturate the samples during moisture retention and hydraulic conductivity analysis. Instead, tap water collected from the STVZ site was used as the wetting solution for all the laboratory experiments. Although a calcium sulfate solution is recommended for characterizing hydraulic properties of soils to prevent flocculation of clays during analysis (Klute, 1986, pg. 692), this was not a major concern in this research due to the low percentage of clays present in most of the samples.

2.4.2.3 Impact of Natural Structure on Moisture Retention Properties

A study to examine the impact of geologic structure on moisture retention properties was conducted to examine the impact of sample disturbance on the measured results. The study was necessary to address difficulties in preserving intact samples of poorly consolidated sands collected from the STVZ site. To conduct this experiment,

intact samples were collected from a shallow trench located on the south slope of the infiltration site. Drainage curves were measured for undisturbed samples starting at complete saturation (porosity) to a maximum tension of 100 cm. The measurements were repeated after homogenizing and repacking individual samples. The results of the study indicate that moisture retention properties for repacked and undisturbed samples of sandy alluvial deposits are similar (i.e., within the margin of measurement error).

2.4.2.4 Oversaturation Study

Preliminary moisture retention primary drainage curve measurements (desorption from complete saturation) consistently showed rapid moisture loss from 0-12 cm tension by as much as 0.07 volumetric moisture content followed by a small change in moisture content with increasing tension until air entry pressure was reached (Figure 2.14). Stephens and Rehfeldt (1985) observed similar artificial water contents at 0 cm tension, which they hypothesized was due to large void spaces between the sediment and the sample ring. The results of this study indicate that an excess of approximately 0.04 volumetric moisture content was retained by the cotton cloth attached at the ends of the sample rings and approximately 0.02 volumetric moisture content was retained along the edges of the ring at saturation, accounting for 0.06 volumetric moisture content overestimate in saturation (Appendix B).

2.4.2.5 Equilibrium Time Determinations

Moisture equilibrium times and methods for determining equilibrium during wetting and draining moisture retention measurements were examined in order to minimize measurement uncertainty. Two methods of establishing moisture equilibrium using the hanging column apparatus (shown in Appendix E1) were compared. The first method established moisture equilibrium after daily measurements of sample mass

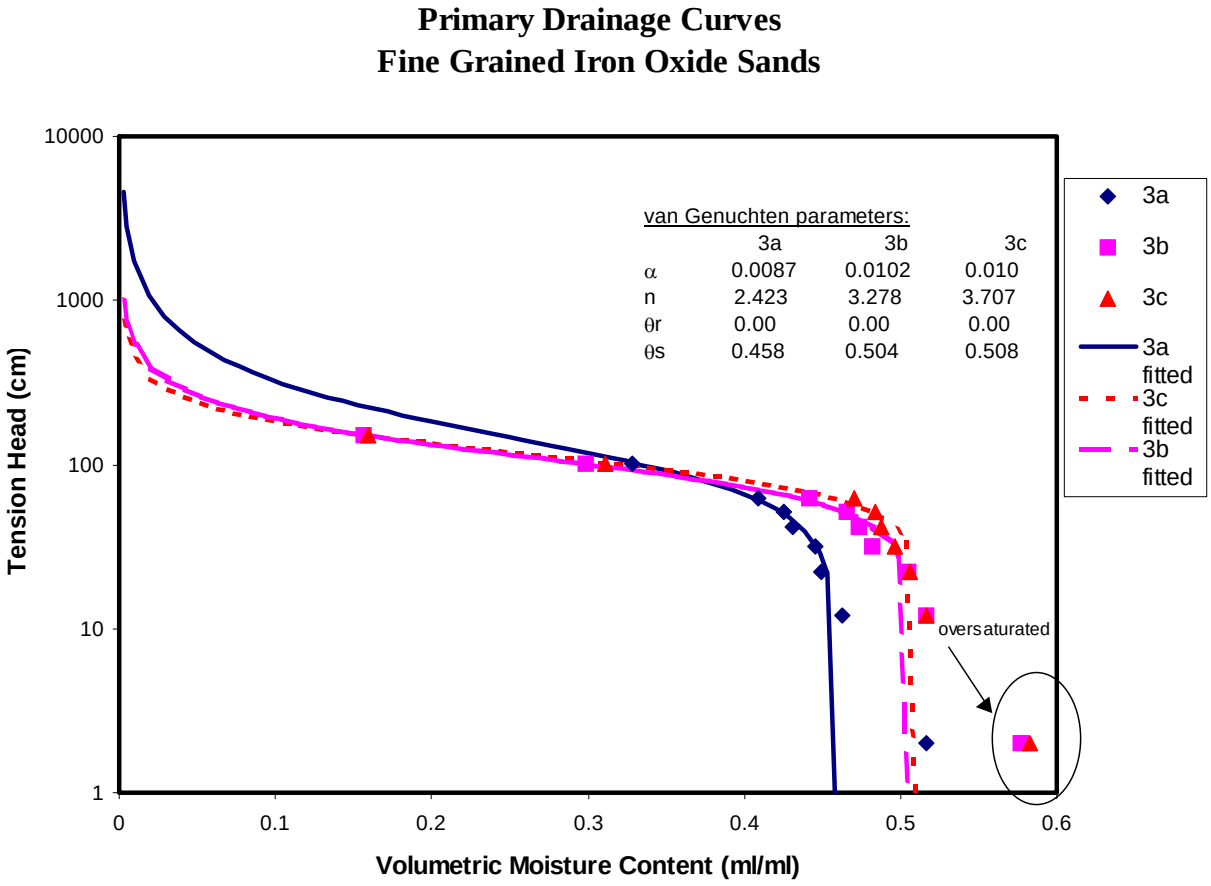

Figure 2.14 – Example of artificial moisture content values at 0 cm tension (plotted as 2 cm tension at center of sample ring).

reached a steady value (within +/- 0.05 g), while the second method established equilibrium after the water level in the burette ceased to increase. Although evaporation occurred in the burettes, monitoring the burette daily was sufficient for determining when the sample stopped draining (as opposed to monitoring the volume of water that drained from the sample). The results indicate that equilibrium moisture contents using both methods were very similar (+/-0.01 volumetric moisture content). Because monitoring the water level in the burette is less time consuming and minimizes sample disturbance (compared to removing and weighing the sample daily), this method is more practical for determining moisture equilibrium during desorption. The second method examined

moisture equilibrium during drainage of sands in a hanging column apparatus using a "mini-tensiometer" constructed of PVC tubing and a 1 bar ceramic cup. The results of the study indicate that moisture equilibrium at 40 cm tension was reached after approximately 7 hours. At 95 cm tension, moisture equilibrium was reached in approximately 10 hours for the same sands (Appendix B).

2.4.2.6 Sample Contact During Electrical Resistivity Measurements

To determine the optimum degree of sample contact (without sample disturbance) with the electrodes for electrical resistivity measurements, samples of a highly conductive porous material (clay) and a highly resistive material (coarse-grained sand) were saturated and drained at 30 cm tension, then the electrical resistivity was measured at different degrees of sample contact. Impedance (related to resistivity by Equation 2-4) was measured without tightening the nuts on the holder (Figure D1.1 in Appendix D1), hand tightening the nuts, tightening the nuts three turns with a wrench, and tightening the nuts six turns with a wrench. The impedance varied by more than 10% between the hand tightened measurements and the measurements when the nuts were tightened three turns with a wrench (for both samples). Alternatively, the impedance varied by less than 5% between measurements taken when the nuts were tightened three turns and measurements taken when the nuts were tightened six turns with a wrench. Tightening the nuts six turns resulted in flow out of the bottom of the ring suggesting compaction within the samples. The results show that tightening the nuts three turns during sample analysis provides sufficient contact between the porous material and the silver plates, yet minimizes sample compaction. Refer to Appendix D1 for a detailed description of the study.

2.4.2.7 Disturbance of Intact Sub-Samples Collected From Core

Intact samples for laboratory analysis were initially obtained by gently pushing 100 cubic centimeter (cc) rings into intact core, however the attempt to collect "undisturbed" samples was unsuccessful, primarily due to poor sediment consolidation and dry conditions of the core. Higher population variability between hydraulic properties was observed among samples collected adjacent to each other in the core (same geologic units) compared to parameters measured between repacked samples of similar textures (Section 2.4.2.3). The high variability was most likely due to sub-sampling disturbance along the edge of the sample ring rather than due to spatial variability or measurement uncertainty (refer to Appendix K for measurement error determinations). Therefore, laboratory derived hydraulic properties were measured from repacked samples rather than intact sub-cores.

2.4.3 Laboratory Measurements

2.4.3.1 Main Wetting Curve and Resistivity Measurements

Samples were prepared by dividing 11 m of core collected from the northwest (NW) quadrant into 6 inch sections. The samples were homogenized, air dried, then repacked in 100 cm^3 polycarbonate rings. The mass of the sample was estimated from approximate *in situ* bulk density values determined for individual grain types (i.e., fine sands, coarse sands, clays, and gravels) from intact core collected during borehole drilling. Appendix C contains a detailed description of sample preparation.

For correspondence with the test conducted at the field site, moisture retention characteristics of the STVZ deposits starting from *in situ* (or near *in situ*) conditions during a wetting event were measured initially. To achieve a uniform moisture content near *in situ* conditions, the samples were dried in a relative humidity oven at 65%

humidity and 65^{o}C (Flint, 1996) after compacting the sediment in the rings using wetting/draining packing methods (Appendix C). After reaching the desired initial moisture contents, a cotton cloth was placed on top of the samples to prevent sediment from sticking to the silver plates in the impedance analyzer sample holder during resistivity measurements (Appendix D1). The samples were then placed in the hanging column apparatus directly on top of approximately 1 teaspoon of a diatomaceaous earth slurry to maintain hydraulic contact. The samples were allowed to reach moisture equilibrium starting at 100 cm, incrementally decreasing the tension to 80, 60, 50, 40, 30, 20, 10 and 0 cm to obtain the main wetting curve (MWC) data (Appendix E2). Moisture equilibrium during sample wetting was assumed once the samples reached a steady weight during daily monitoring. This method was used instead of monitoring the water level in the burette (section 2.4.2.5) to determine moisture equilibrium because evaporation resulted a continual decrease in the burette water level, making it difficult to determine when imbibition had ceased. Due to the presence of entrapped air during imbibition, the samples did not reach complete porosity at 0 cm tension. Instead they reached a satiated moisture content (also referred to as field saturation), equal to approximately 80-90% porosity.

Electrical resistivity was measured at each moisture equilibrium point by placing the sample in the impedance analyzer sample holder, then tightening down the nuts on the sample holder to obtain adequate contact, and applying a logarithmic sweep of frequencies across the sample (a detailed description of the methods is included in Appendix D1). The impedance associated with the frequency not affected by polarization at the sample/electrode interface was used to calculate electrical resistivity

by multiplying the impedance by the ratio of the sample cross-sectional area to the sample length (Knight, 1991).

2.4.3.2 Main Drainage Curve and Resistivity Measurements

In order to examine hysteresis, the MWC process was reversed and moisture retention for the main drainage curve (MDC) was measured starting at the satiated moisture content. Pressure chambers were used to drain the samples at pressures greater than 100 cm due to loss of hydraulic contact at tensions greater than 100 cm in the hanging columns (Appendix E1). Silica flour was used as the hydraulic contact material in the pressure cells since the air entry pressure of diatomaceaous earth was exceeded in the pressure cells (refer to Appendix E1 for air entry pressures of diatomaceous earth and silica flour). The samples were drained to a maximum of 5 bars pressure in the pressure chambers. Most of the sandy deposits ceased to drain at 1 to 3 bars pressure, therefore data at higher pressures may not be included in the data set for these samples. Residual moisture content was determined from functional form model fits to data (described in section 2.4.4). Equilibrium was determined during drainage in the pressure cells by monitoring daily changes in sample weight, since the effluent water volume was too low to monitor changes in burette water levels in the presence of evaporation. Electrical resistivity was measured at each moisture equilibrium point using the methods described previously for the MWC.

2.4.3.3 Saturation and Primary Drainage Curve Measurements

Since many researchers measure moisture retention characteristics by draining a fully saturated sample (van Genuchten et al., 1991; Healy and Mills, 1991; Yeh and Harvey, 1990), data obtained from desorption starting at porosity (primary drainage curve) was compared to data collected along the MWC and MDC.

After draining the samples to residual moisture content in the pressure chamber during the MDC measurements, the samples were air dried 2 to 3 days (still intact) and then saturated from the bottom under a vacuum with deaerated tap water collected from the infiltration site. The samples were flushed twice in a vacuum chamber with CO_2 (vacuuming between flushes) to minimize entrapped air during saturation, then were imbibed under a vacuum (Appendix F). The samples were placed back in the hanging column apparatus directly on top of the diatomaceous earth slurry and drained starting at 0 cm tension incrementally increasing tension head to 10, 20, 30, 40, 50, 80, 100 cm tension to obtain the primary drainage curve (PDC) data. Higher pressures (1 bar, 3 bars, and 5 bars) were measured in pressure cells with silica flour as the hydraulic contact material.

2.4.3.4 Saturated Hydraulic Conductivity Measurements

After completing all moisture retention measurements, the samples were oven dried (105^{o}C) to determine dry sample weight for calculation of volumetric moisture contents. This was necessary before measuring hydraulic conductivity because sediment is often lost by sticking to the top and bottom of the permeameter ends. After oven drying, the samples were saturated under a vacuum flushing with CO_2 to ensure complete saturation (Appendix F). Saturated hydraulic conductivity was determined from measurements of outflow flux rates and differences in hydraulic head between a constant head water reservoir and the outflow port of sample permeameters for high permeable materials. A falling head permeameter was used to determine saturated hydraulic conductivity of low permeable samples (clay samples). A complete description of the two methods is included in Appendix G, along with diagrams of the permeameters.

2.4.3.5 Particle-Size Analysis

After completion of the hydraulic property measurements, the samples were oven dried and particle-size distributions were measured using dry sieving techniques for particles greater than 0.053 mm. Since the majority of the deposits contained less than 5 weight percent of silt and clay sized particles (Appendix H), dispersion methods were used only for samples containing higher percentages of clays. Due to problems with laboratory equipment, four clay samples were not analyzed as a part of this research. The data will be available in future publications.

Since the ASTM recommended stack of sieves does not include a wide range of sand-sized sieves (Klute, 1986), the Utten-Wentworth classification of sand-sized particles (Prothero and Schwab, 1996) was used to determine sieve sizes for grain-size distributions for the STVZ deposits. Table 2.1 includes the sieve numbers, range of particle sizes (mm) per sieve, grain classifications, and phi units (grain size expressed as the negative logarithm of grain diameter in mm to the base 2) for the Utten-Wentworth scale of sand-sized particles.

Table 2.1 – Utten-Wentworth classification for sand sized sedimentary deposits (Prothero and Schwab, 1996).

Particle Classification (sieve number in parentheses)	Range of Particle Sizes (mm) per Sieve	ϕ Units
very coarse sand (#20)	1 to 2	-1 to 0
coarse sand (#40)	0.5 to 1	0 to 1
medium sand (#60)	0.25 to 0.5	1 to 2
fine sand (#150)	0.16 to 0.25	2 to 3
very fine sand (#270)	0.053 to 0.16	3 to 4

2.4.4 Curve Fitting Procedures

Moisture retention curve fitting parameters were obtained by fitting the van Genuchten equation (van Genuchten et al., 1991) to the moisture retention data for the MWC, MDC, and PDC using the Retention Curve (RETC) fitting program developed by the U.S. Salinity Laboratory. The van Genuchten equation is

$$\theta = (\theta_s - \theta_r)\left[1+(\alpha h)^n\right]^{-m} + \theta_r \qquad (2\text{-}1)$$

where θ is the volumetric moisture content, θ_r is the residual moisture content, θ_s is the saturated/satiated moisture content, α is a curve fitting parameter [cm^{-1}] representing the pressure ($1/\alpha$ cm) required to drain the average pore size of the sample, n is a curve fitting parameter that describes the slope of the pore-size distribution, *m* is assumed to equal *1-1/n*, and h is the tension head [cm]. Residual moisture content and saturation were determined from fitting (2-1) to measured data (i.e., they were established as unknown parameters in the RETC curve fitting program).

The Brooks and Corey equation (van Genuchten et al., 1991) was fit to the PDC for evaluation of the Haverkamp and Parlange (1986) estimation model (Chapter 3) using the MATHCAD mathematics program. The Brooks and Corey equation is

$$\theta = (\theta_s - \theta_r) * \left[\frac{h_{ae}}{h}\right]^{\lambda} + \theta_r \quad \text{for } h > h_{ae} \qquad (2\text{-}2)$$

$$\theta = \theta_s \quad \text{otherwise}$$

where h_{ae} is the tension head [cm] required to drain the largest pore size (also referred to as the air entry pressure) and λ is a curve fitting parameter which describes the slope of the pore-size distribution. Residual moisture content was assumed to equal zero (for application to the Haverkamp and Parlange, 1986 prediction model). Saturation was

assumed to be equal to porosity (for the PDC) and was calculated from bulk density measurements.

A modified version of the van Genuchten equation (Haverkamp and Parlange, 1986) was used to describe the shape of the particle-size distribution curve by

$$F(d) = \left[1 + \left(\frac{d_g}{d} \right)^{n_d} \right]^{-\left(1 - 1/n_d\right)} \tag{2-3}$$

where $F(d)$ is the fraction finer than grain diameter (d [mm]), d_g represents the average grain diameter of the medium [mm], and n_d is the slope of the particle-size distribution. Both d_g and n_d are curve fitting parameters.

Microsoft ® Excel was used to obtain curve fitting parameters for Archie's Law (Knight, 1991) by fitting a power law function to resistivity data as a function of moisture content. Archie's Law is described by

$$\rho = k\theta^{-m} \tag{2-4}$$

where ρ is the electricity resistivity of the partially saturated porous material (in units of ohm meters), θ is the volumetric moisture content, and k and m are curve fitting parameters.

2.5 Results

2.5.1 Hydraulic Properties

The majority of the STVZ deposits consist of poorly consolidated, well sorted fine-medium grained sands with sample porosities ranging from 0.33 to 0.43, saturated hydraulic conductivity values for the sandy deposits equal to approximately 10^{-3} cm s^{-1}, low residual moisture contents less than 10 percent by volume, air entry pressures ranging from 20 to 60 cm, and moderately uniform pore-size distributions.

Tables 2.2 and 2.3 list hydraulic properties measured for samples collected from the NW quadrant at the STVZ site. Missing sections in depth below ground surface (bgs) are due to the fact that the split spoon samplers did not always contain a full 5 ft of core during collection. This occurred as a result of dry sediment spilling out of the sampler as it was being extracted from the borehole and/or because large clasts plugged the shoe (opening at bottom of sampler) preventing core from entering the sampler during drilling. Raw laboratory measurements used for property determinations are included in Appendices D through H.

2.5.2 Moisture retention curves

Figures 2.15 through 2.19 show main wetting, main drainage, and primary drainage curves for representative medium-coarse grained sands, gravels, silty sands, clays, and fine-grained sands collected from the NW quadrant of the STVZ research site. For the complete set of moisture retention curves, refer to Appendix E2.

Data points were initially measured in the pressure chambers for the MDC sequence at 1 bar, 3 bars, and 5 bars pressure, however there was not a major change in moisture content between 1 bar and 3 bar measurements, therefore the measurements were made at 1 bar and 5 bar pressures for a majority of the samples.

Due to time constraints, measurements were not made in the pressure chambers (pressures greater than 100 cm) for a majority of the samples during the PDC sequence. The oversaturated values at pressures below 20 cm tension were not used in the RETC fit to obtain van Genuchten fitting parameters, therefore, the coefficient of variation (R^2) does not reflect a fit to those data points for the PDC (Appendix E2 and Appendix J). The PDC was not measured for samples containing large percentages of

Table 2.2 – Hydraulic properties of samples collected from the northwest quadrant of the STVZ infiltration test site.

sample ID	depth bgs (m)	texture	repacked bulk density (g/cc)	repacked porosity **	Ksat (cm/s)	estimated residual moisture content *	estimated porosity *	satiation *
NW1	0.30	coarse sand	1.58	0.404	1.80E-03	0.098	0.336	0.238
NW2	0.61	coarse sand	1.61	0.392	1.80E-03	0.067	0.376	0.315
NW4	1.52	coarse sand	1.66	0.374	1.10E-02	0.031	0.378	0.325
NW5	1.81	gravel	1.75	0.340	1.25E-03	0.018	0.390	0.276
NW6	2.72	silty sand	1.37	0.483	1.79E-03	0.09	0.422	0.396
NW7	3.05	fine sand	1.48	0.442	7.13E-03	0.068	0.413	0.375
NW8	3.35	fine sand	1.67	0.370	4.06E-03	0.099	0.386	0.371
NW9	3.66	fine sand	1.73	0.347	9.05E-04	0.049	0.368	0.320
NW10	4.27	Fine sand	1.53	0.423	1.75E-03	0.051	0.372	0.319
NW11	4.57	silty sand	1.5	0.434	1.75E-03	0.098	0.404	0.372
NW12	4.88	silty sand	1.47	0.445	4.90E-03	0.077	0.399	0.378
NW13	5.18	sandy clay	1.44	0.374	1.03E-04	0.12	N/A	0.365
NW14	5.79	pebbly clay	1.65	0.283	7.23E-04	0.07	N/A	0.312
NW15	6.10	clay	1.31	0.430	5.42E-05	0.12	N/A	0.434
NW16	6.40	fine sand	1.5	0.434	3.69E-03	0.067	0.399	0.385
NW17	6.71	fine sand	1.53	0.423	5.66E-03	0.05	0.399	0.386
NW19	7.32	fine sand	1.55	0.415	9.03E-04	0	0.400	0.373
NW20	7.92	fine sand	1.58	0.404	6.59E-03	0.03	0.387	0.373
NW21	8.23	fine sand	1.55	0.415	8.14E-03	0.077	0.424	0.363
NW22	8.84	silty sand	1.51	0.430	4.10E-03	0.095	0.383	0.366
NW23	9.14	fine-coarse sand	1.64	0.381	5.28E-03	0.11	0.400	0.341
NW24	9.75	fine-coarse sand	1.65	0.377	4.59E-03	0.097	0.389	0.325
NW25	10.36	fine-coarse sand	1.63	0.385	4.59E-03	0.07	0.364	0.286
NW27	10.97	fine-coarse sand	1.68	0.366	4.59E-03	0.041	0.381	0.303

NOTES:
* Based on RETC fit to PDC data.
** Calculated from bulk density
density = 2.65 g/cc for sands and 2.30 g/cc for clays.

Table 2.3 – van Genuchten fitting parameters estimated using RETC.

sample ID	depth bgs (m)	texture	MWC α (cm^{-1})	MDC α (cm^{-1})	PDC α (cm^{-1})	MWC n	MDC n	PDC n	1/α MWC (cm)	1/α MDC (cm)	1/α PDC (cm)
NW1	0.30	coarse sand	0.068	0.029	0.044	9.983	4.278	5.669	14.691	34.412	22.676
NW2	0.61	coarse sand	0.061	0.054	0.038	8.488	2.973	3.949	16.313	18.587	26.247
NW4	1.52	coarse sand	0.105	0.040	0.031	2.761	3.567	5.011	9.552	24.783	32.051
NW5	1.81	gravel	0.255	0.109	0.020	1.826	1.797	1.582	3.922	9.141	51.282
NW6	2.72	silty sand	0.018	0.010	0.008	3.998	4.775	2.560	56.561	100.200	123.457
NW7	3.05	fine sand	0.046	0.023	0.020	4.513	4.029	4.217	21.877	43.535	49.751
NW8	3.35	fine sand	0.034	0.018	0.014	4.755	4.327	5.734	29.481	54.795	69.930
NW9	3.66	fine sand	0.045	0.023	0.019	2.924	3.090	3.766	22.442	43.215	53.476
NW10	4.27	fine sand	0.048	0.028	0.020	3.322	3.267	3.597	21.053	36.036	49.751
NW11	4.57	silty sand	0.028	0.016	0.016	4.866	4.442	7.690	35.689	64.309	62.893
NW12	4.88	silty sand	0.041	0.018	0.015	3.782	4.687	6.161	24.231	54.675	64.935
NW13	5.18	sandy clay	0.02	7.90E-04	N/A	14.83	1.23	N/A	52.63	1265.82	N/A
NW14	5.79	pebbly clay	0.08	0.04	N/A	3.36	2.09	N/A	12.05	24.65	N/A
NW15	6.10	clay	see plot	0.02	N/A	see plot	1.10	N/A	higher than measured	49.60	N/A
NW16	6.40	fine sand	0.030	0.013	0.013	3.955	4.904	6.549	33.546	76.104	75.758
NW17	6.71	fine sand	0.033	0.015	0.014	4.834	5.628	6.947	29.913	64.893	70.423
NW19	7.32	fine sand	0.026	0.012	0.010	2.573	3.312	3.872	39.063	85.985	96.154
NW18	7.62	fine sand	0.036	0.016	0.018	3.035	3.684	5.367	28.035	60.500	54.645
NW20	7.92	fine sand	0.043	0.017	0.017	7.633	5.175	4.951	23.041	58.720	60.241
NW21	8.23	fine sand	0.024	0.019	0.017	2.757	5.329	6.120	41.806	53.079	60.606
NW22	8.84	silty sand	0.037	0.015	0.015	16.093	4.896	5.724	26.717	65.920	66.225
NW23	9.14	fine-coarse sand	0.046	0.018	0.015	5.832	3.287	5.724	21.566	55.096	66.225
NW24	9.75	fine-coarse sand	0.050	0.023	0.041	7.805	3.424	1.677	19.932	44.287	24.631
NW25	10.36	fine-coarse sand	0.057	0.025	0.021	4.016	3.350	4.506	17.637	39.541	48.780
NW27	10.97	fine-coarse sand	0.058	0.024	0.055	6.367	8.390	5.421	17.182	42.230	35.804

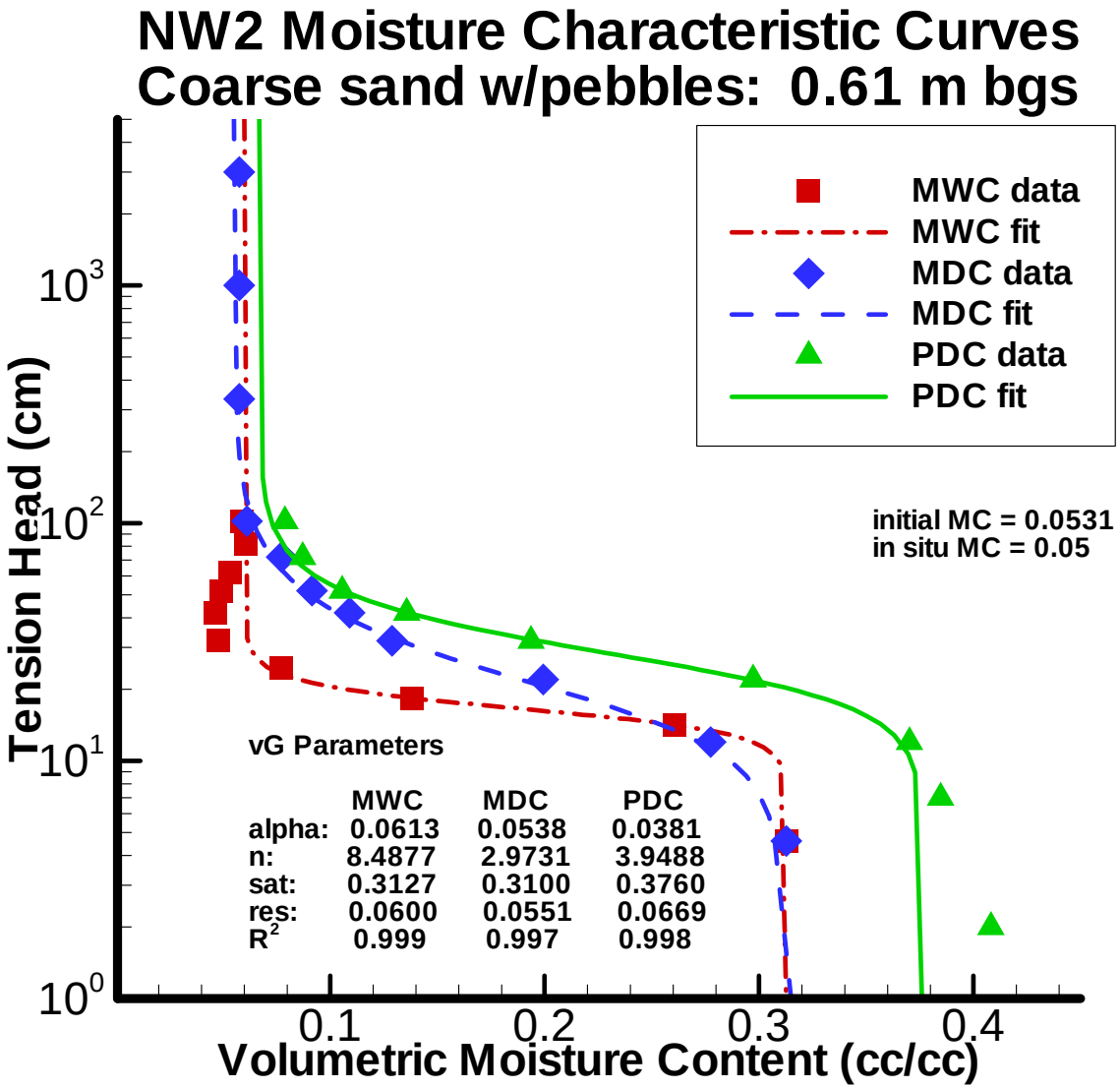

Figure 2.15 – Moisture retention curves for a coarse grained sand collected from the NW core at a depth of approximately 1 meter below ground surface.

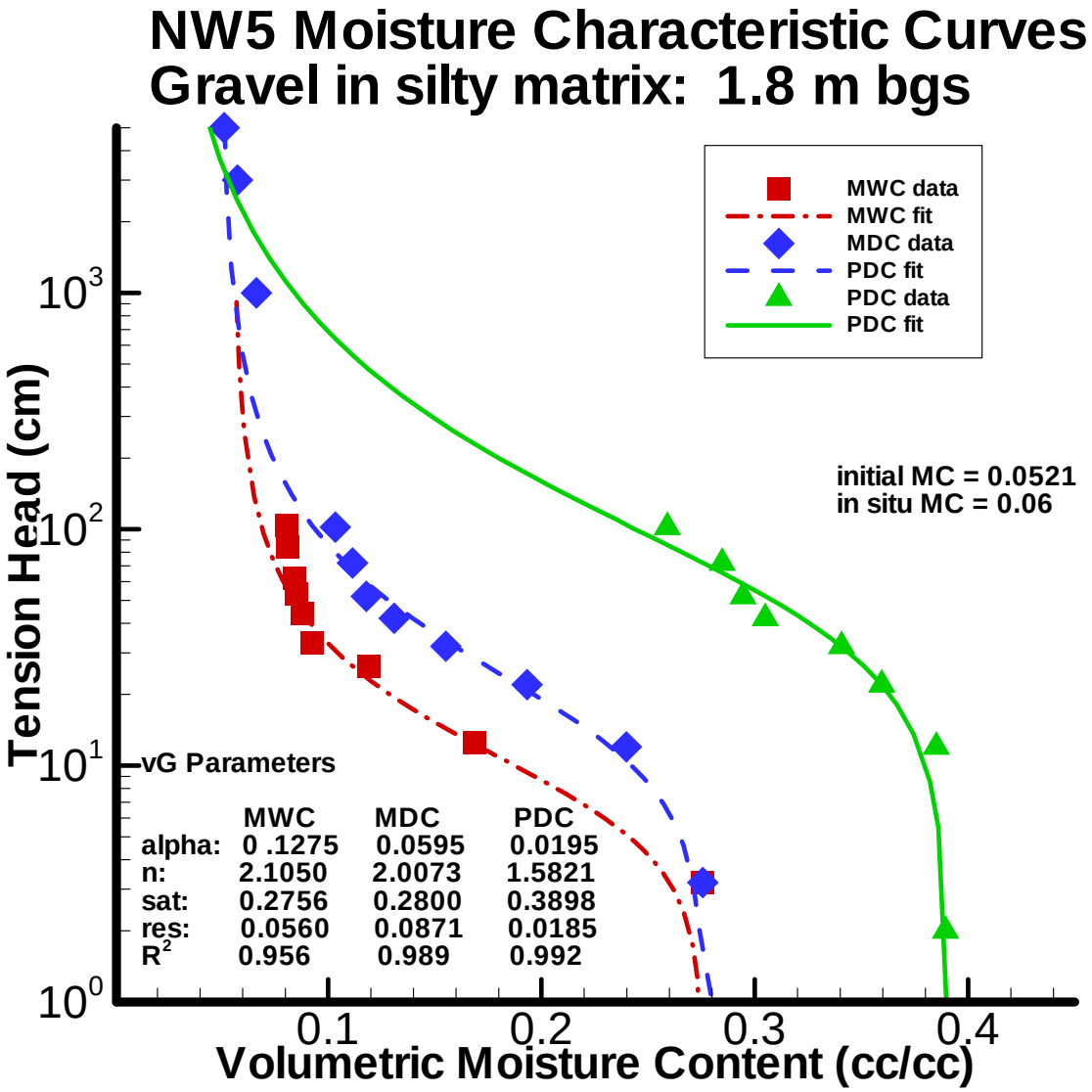

Figure 2.16 – Moisture-retention curves for a gravel collected from the NW core at a depth of approximately 2 m ground surface.

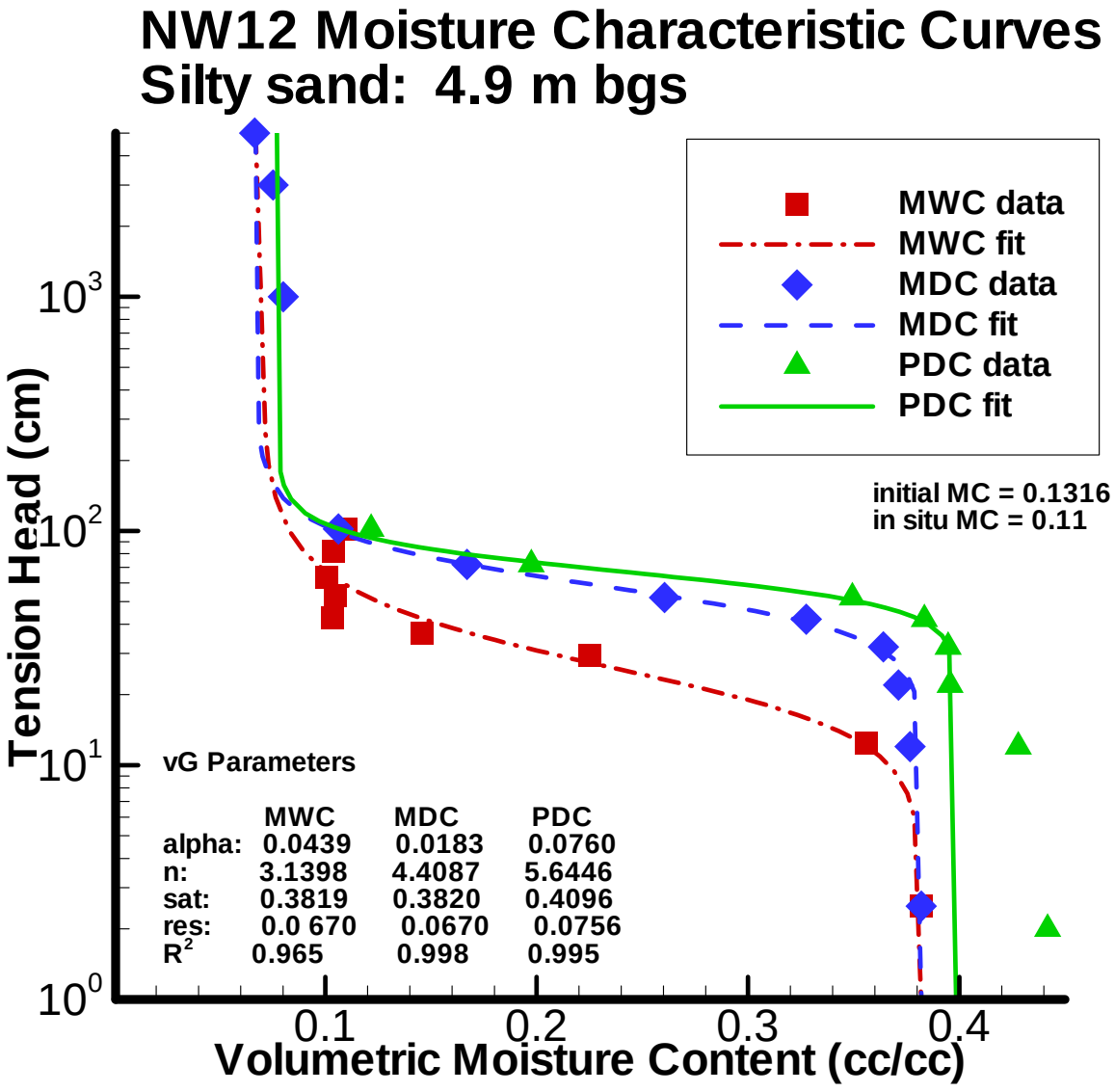

Figure 2.17 – Moisture retention curves for a silty sand collected from the NW core at approximately 5 meters below ground surface.

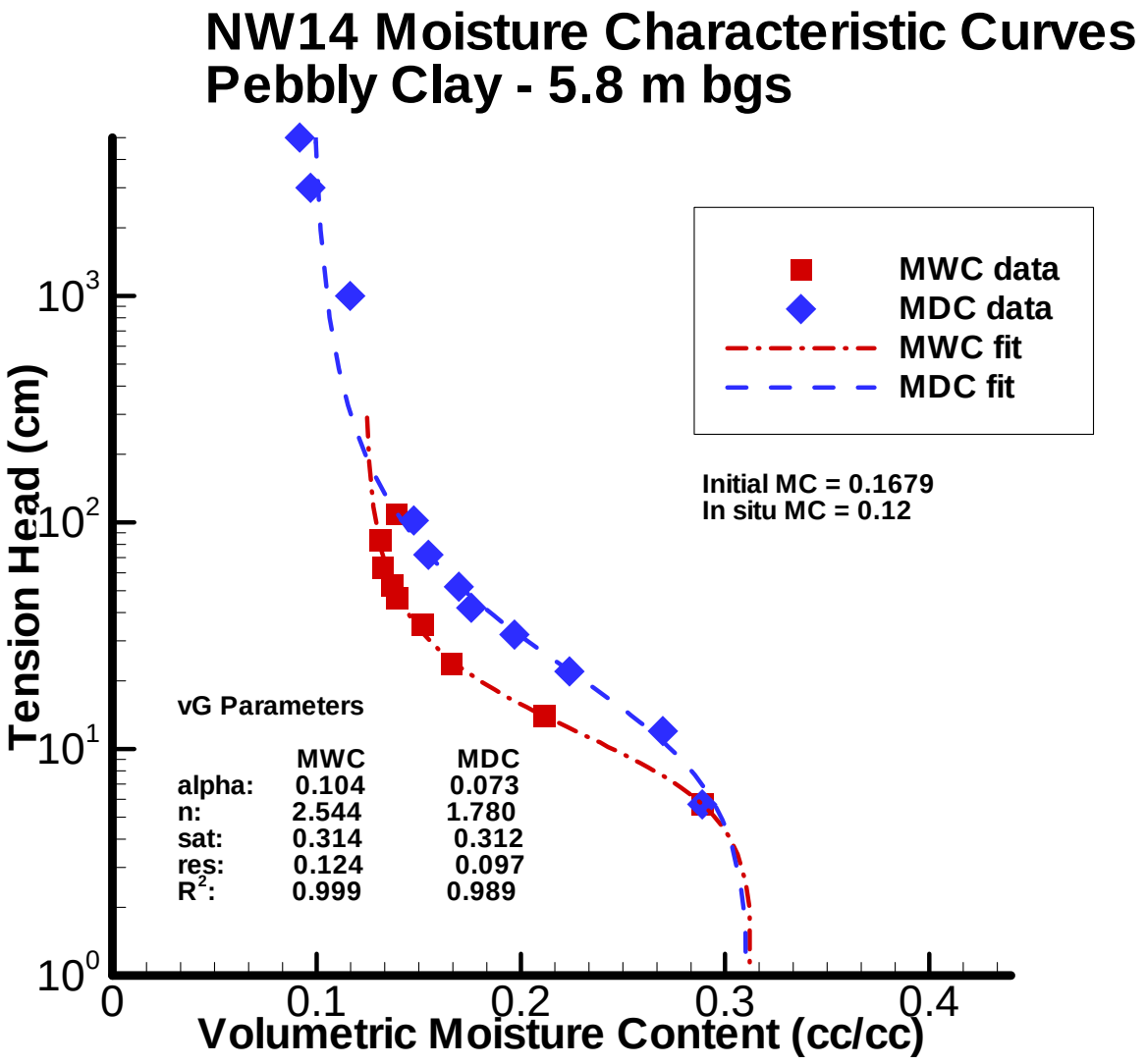

Figure 2.18 – Moisture retention curves for a pebbly clay collected from the NW core at approximately 6 meters below ground surface.

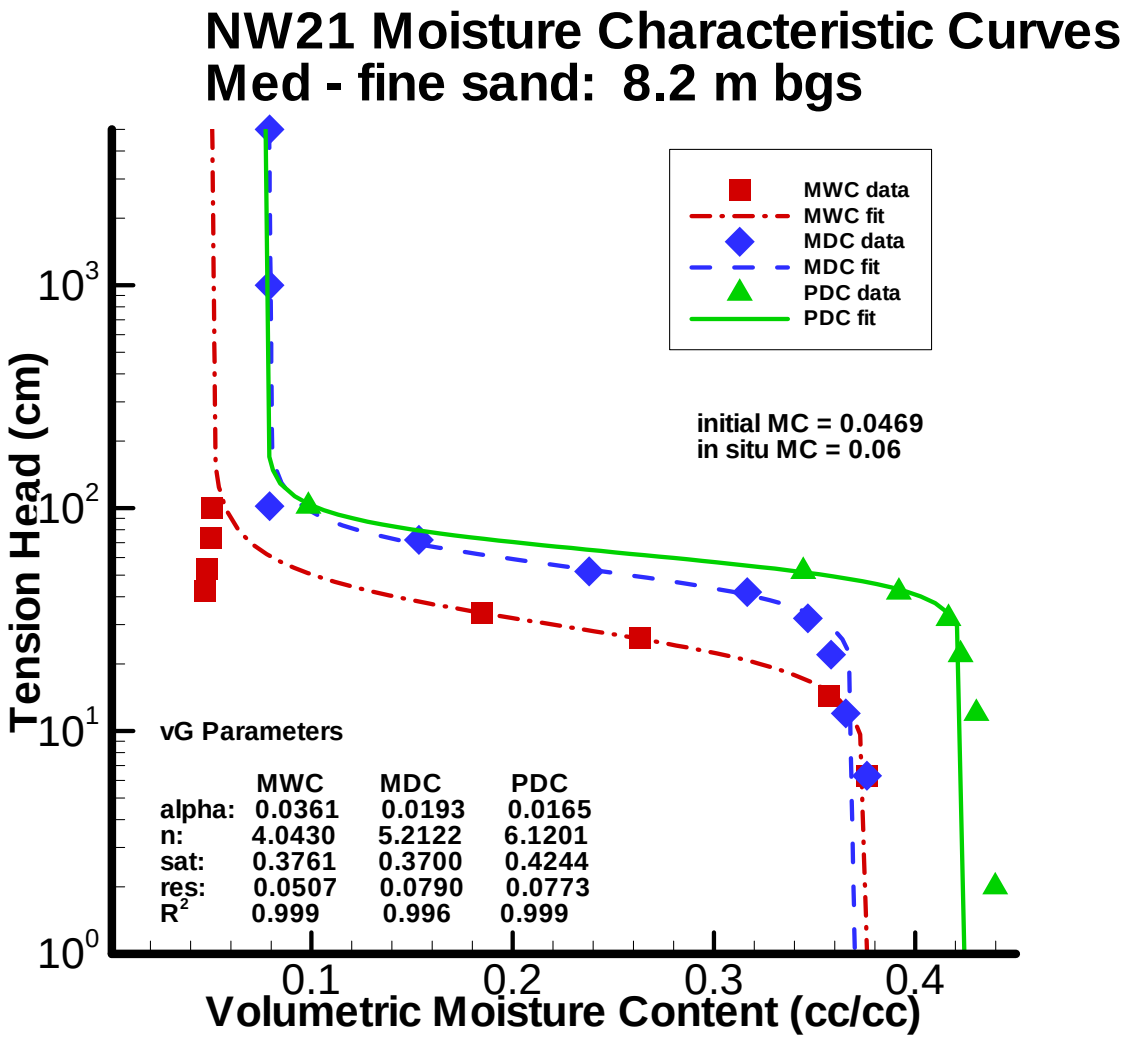

Figure 2.19 – Moisture-retention curves for a fine-medium-grained sand collected from the NW Core at approximately 8 meters below ground surface.

swelling clays (NW6, NW13, NW14, and NW15) primarily because the PDC data was used to evaluate the Haverkamp and Parlange (1986) estimation model for sandy deposits (Chapter 3). The Haverkamp and Parlange model is not valid for soils/deposits which contain swelling clays.

The MWC data at high tensions show an anomalous decrease in moisture content with decrease in tension due to sample evaporation prior to reaching water entry negative pressures. This behavior was observed in samples with very low initial moisture contents (i.e., sandy deposits) most likely due to a higher degree of isolated pores (disconnected) at low moisture contents. These data points were not used in the RETC fits, therefore the coefficient of variation (R^2) reported for the fits does not reflect a fit to those points.

2.5.3 Electrical Resistivity

Electrical resistivity data was recorded during both MWC and MDC sequences. Figures 2.20 through 2.24 represent resistivity relationships for representative coarse-grained sands, gravels, silty sands, clays, and fine-medium grained sands as a function of volumetric moisture content. The squares represent data collected during a wetting sequence (MWC) while the circles represent data collected during a draining sequence (MDC). The complete set of data (wetting and draining) was used for the power law curve fit to data (Archie's law) because the relationship between resistivity and moisture content does not appear to be hysteretic and limited data was available for individual sequences.

The electrical resistivity curves vary with sample texture, indicating steeper slopes for finer grained deposits and shallower slopes for coarser grained deposits. The

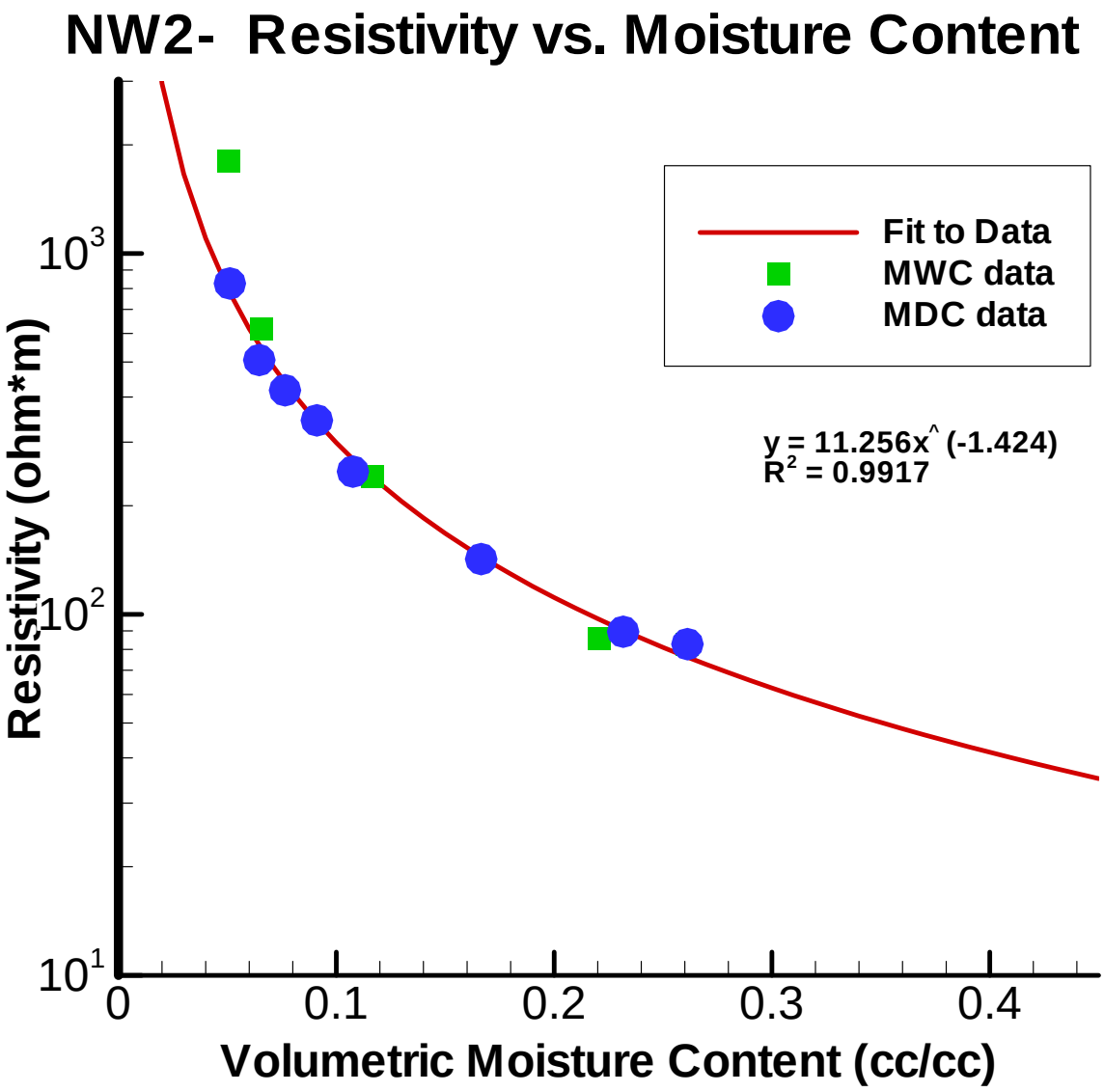

Figure 2.20 – Electrical resistivity curve for a coarse-grained sand located at approximately 1 meter below ground surface.

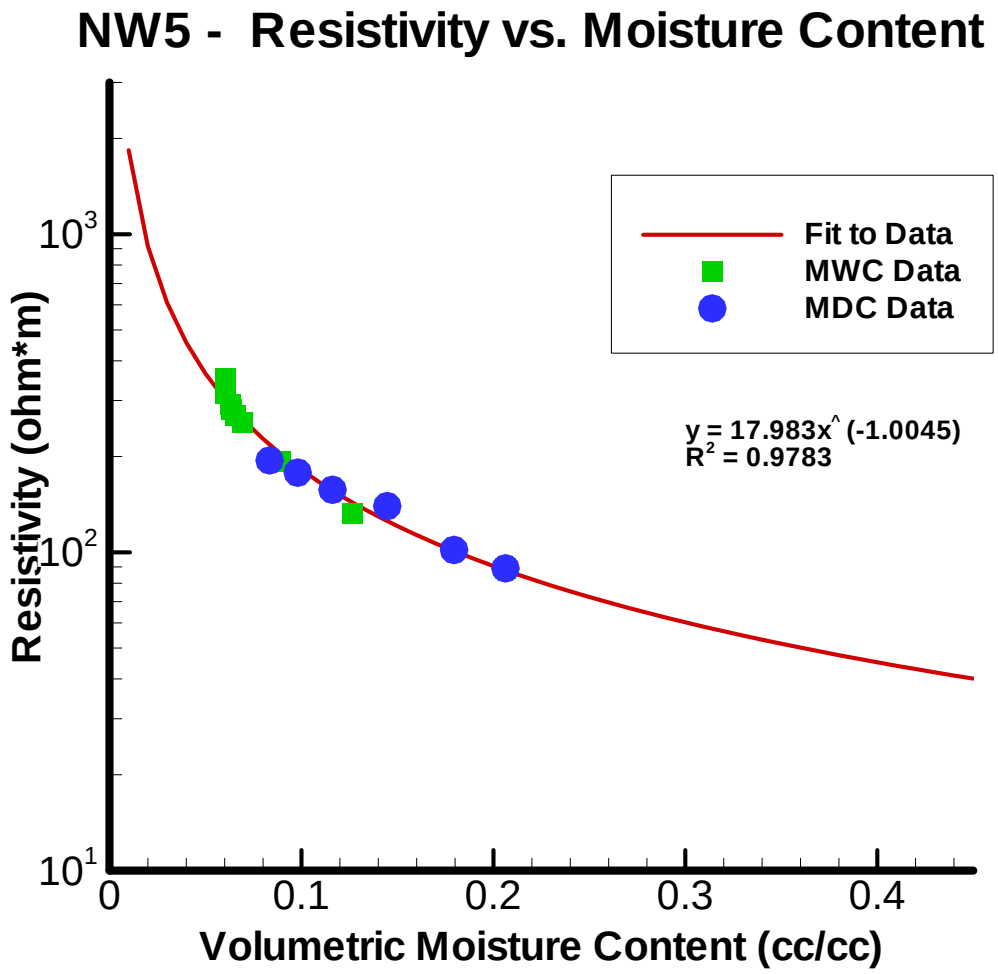

Figure 2.21 – Electrical resistivity curve for a gravel located at approximately 2 meters below ground surface.

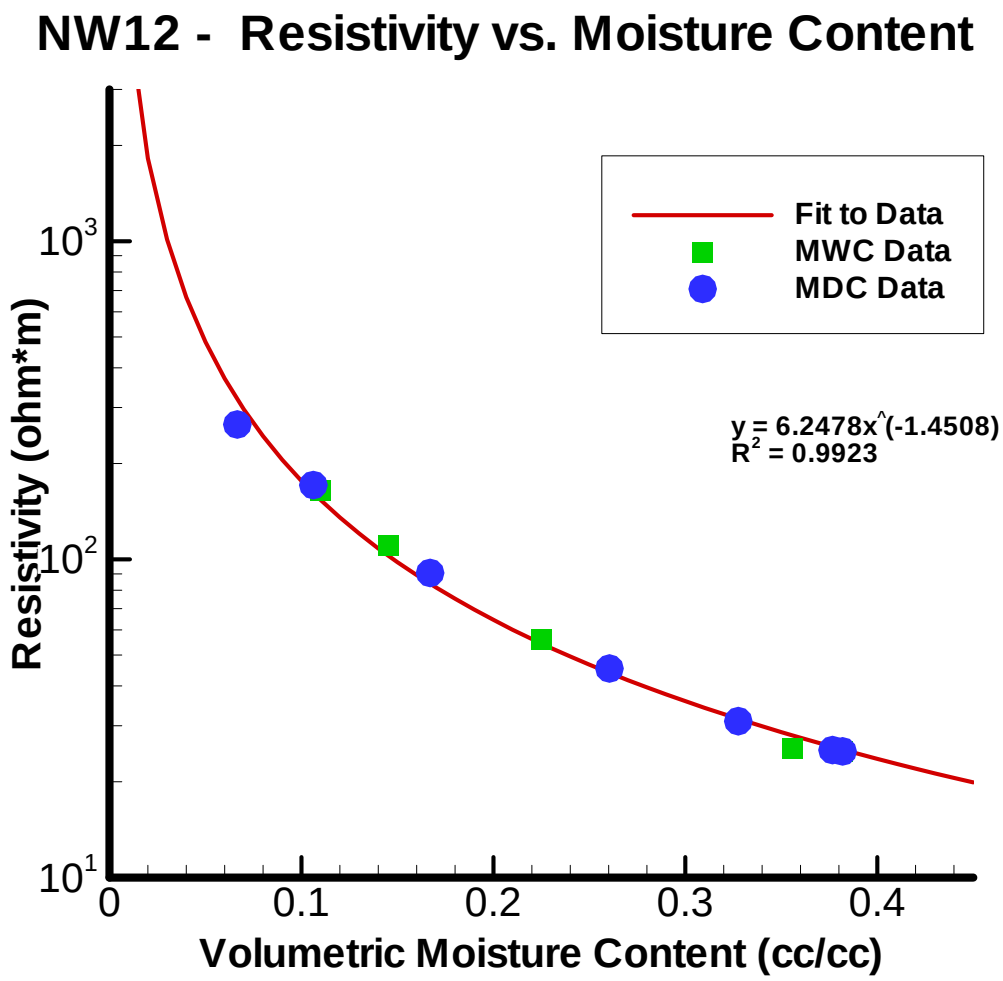

Figure 2.22 – Electrical resistivity curve for a silty sand located at approximately 5 meters below ground surface.

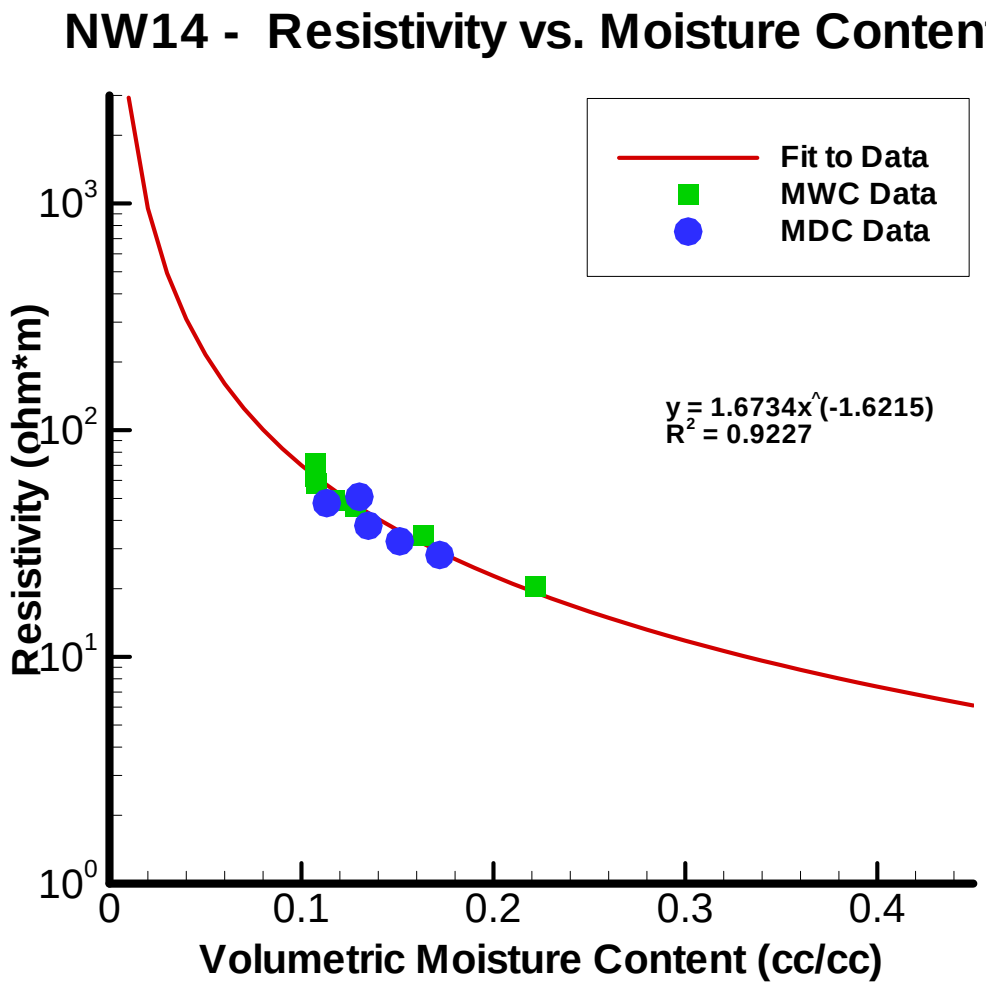

Figure 2.23 – Electrical resistivity curve for a pebbly clay located at approximately 6 meters below ground surface.

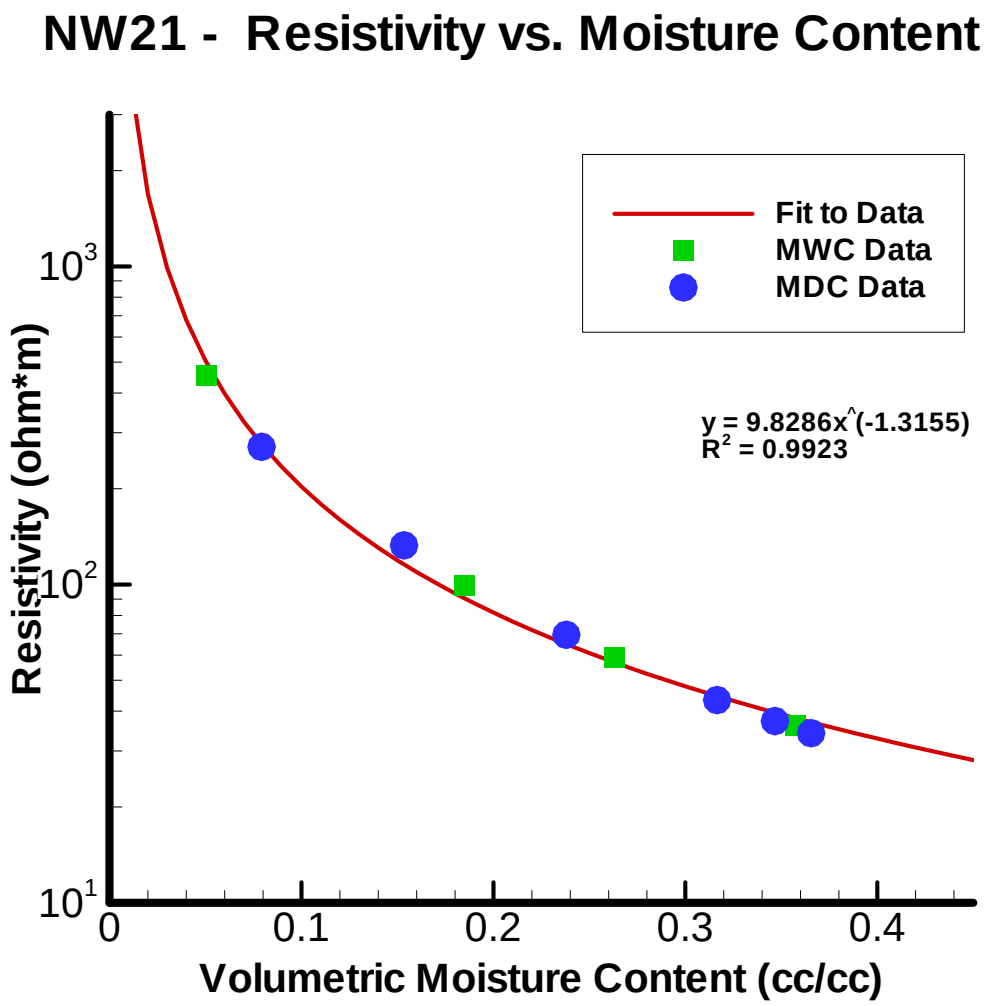

Figure 2.24 – Electrical resistivity curve for a fine grained sand located at approximately 8 meters below ground surface.

majority of the sandy deposits had a very high resistivity value at moisture contents less than 10 volume percent, with exceptions for deposits containing higher percentages of clay minerals. Table 2.4 lists the curve fitting parameters for the NW core samples. For the complete set of resistivity curves, refer to Appendix D2.

2.5.4 Particle-Size Distributions

Figures 2.25 through 2.28 represent the particle-size distributions for representative coarse-grained sands, gravels, silty sands, and fine-medium grained sands collected from the STVZ research site. The fitting parameter "nfit" represents the slope of the curve while the parameter "dgfit" represents the average grain diameter (mm). Table 2.5 lists the particle-size distribution fitting parameters (d_g and n_d), the coefficient of uniformity (C_u) describing grain sorting, and the median grain diameter (d_{50}). The coefficient of uniformity is determined by dividing the grain size in which 60% of the deposits are finer than by the grain size in which 10% of the deposits are finer than (i.e., d_{60}/d_{10}). The complete set of PSD curves are included in Appendix H. The distributions do not include particles greater than 2 mm since rock clasts are not considered to retain moisture and are not included (mass or volume) in the moisture retention calculations for volumetric moisture content.

2.5.5 Parameter Correlations

Correlations were identified between pore-size distribution fitting parameters, particle-size distribution fitting parameters, resistivity curve fitting parameters, grain texture, and saturated hydraulic conductivity. Correlations with R^2 greater than 0.50 were not observed in the analysis for a large combination of parameters. This may be a result of measurement error and uncertainty and/or model uncertainty in determining

Table 2.4 – Table of electrical resistivity fitting parameters.

sample ID	sample depth (m bgs)	k	m	description
NW1	0.30	21.296	1.059	coarse sand
NW2	0.61	11.256	1.424	coarse sand
NW4	1.52	9.708	1.678	coarse sand
NW5	1.81	17.983	1.005	silty gravel
NW6	2.72	6.190	1.350	silty sand
NW7	3.05	7.341	1.534	fine sand
NW8	3.35	5.762	1.598	fine sand
NW9	3.66	9.231	1.214	fine sand
NW10	4.27	5.177	1.312	fine sand
NW11	4.57	4.068	1.508	silty sand
NW12	4.88	6.248	1.451	silty sand
NW13	5.18	0.510	2.240	sandy clay
NW14	5.79	1.513	3.092	pebbly clay
NW15	6.10	1.451	1.434	clay
NW16	6.40	6.369	1.319	fine sand
NW17	6.71	7.306	1.300	fine sand
NW19	7.32	8.501	1.087	oxidized fine sand
NW18	7.62	8.391	1.268	fine sand
NW20	7.92	7.577	1.415	fine sand
NW21	8.23	9.829	1.316	fine sand
NW22	8.84	10.279	1.223	silty sand
NW23	9.14	12.883	1.119	fine-coarse sand
NW24	9.75	10.254	1.300	fine-coarse sand
NW25	10.36	11.767	1.212	fine-coarse sand
NW27	10.97	11.496	1.318	fine-coarse sand

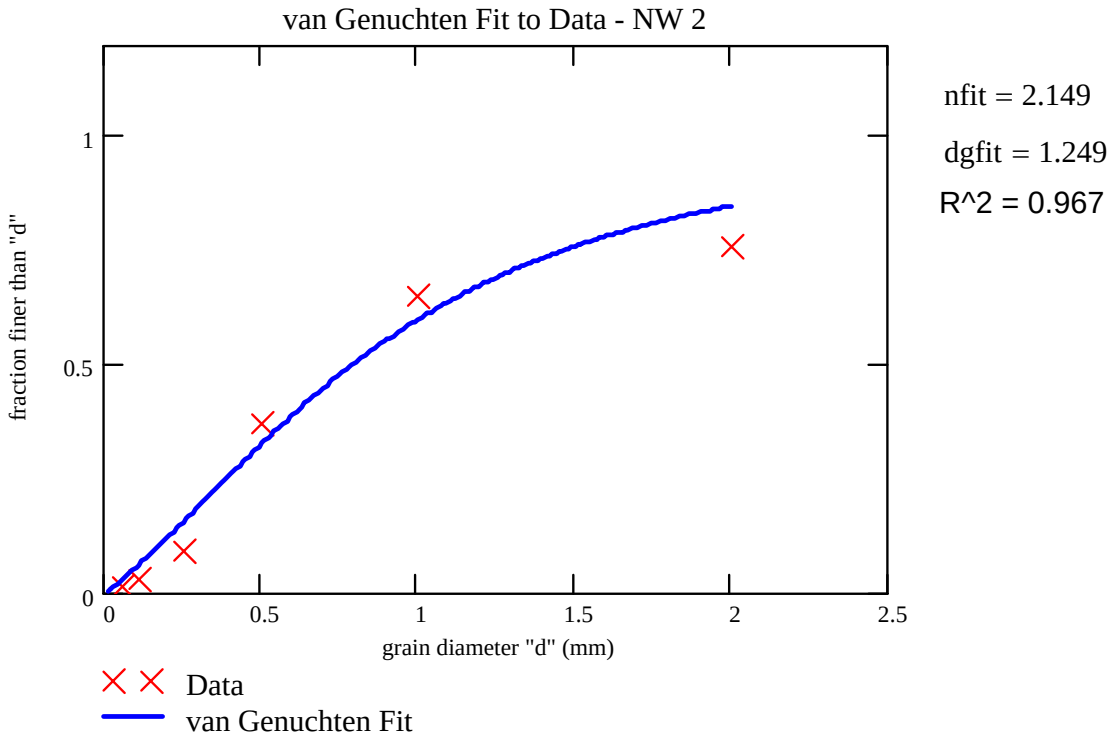

Figure 2.25 – Particle-size distribution for a coarse-grained sand collected from the STVZ research site at approximately 1 meter below ground surface.

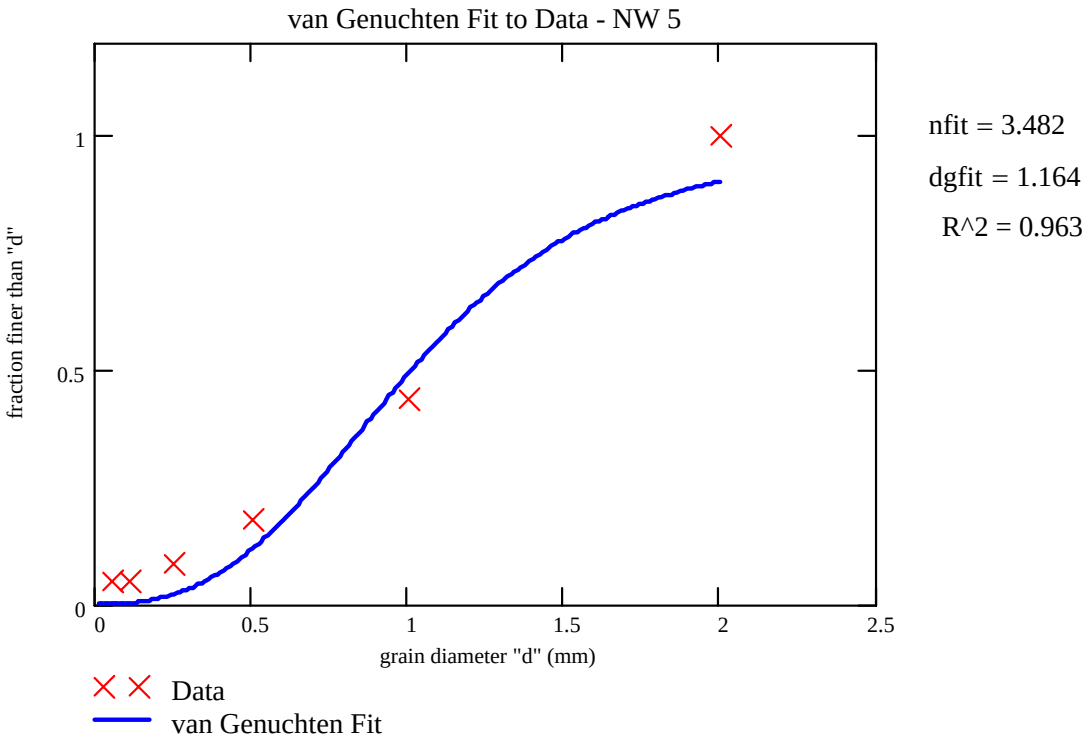

Figure 2.26 – Particle-size distribution for a gravel collected from the STVZ research site at approximately 2 meters below ground surface.

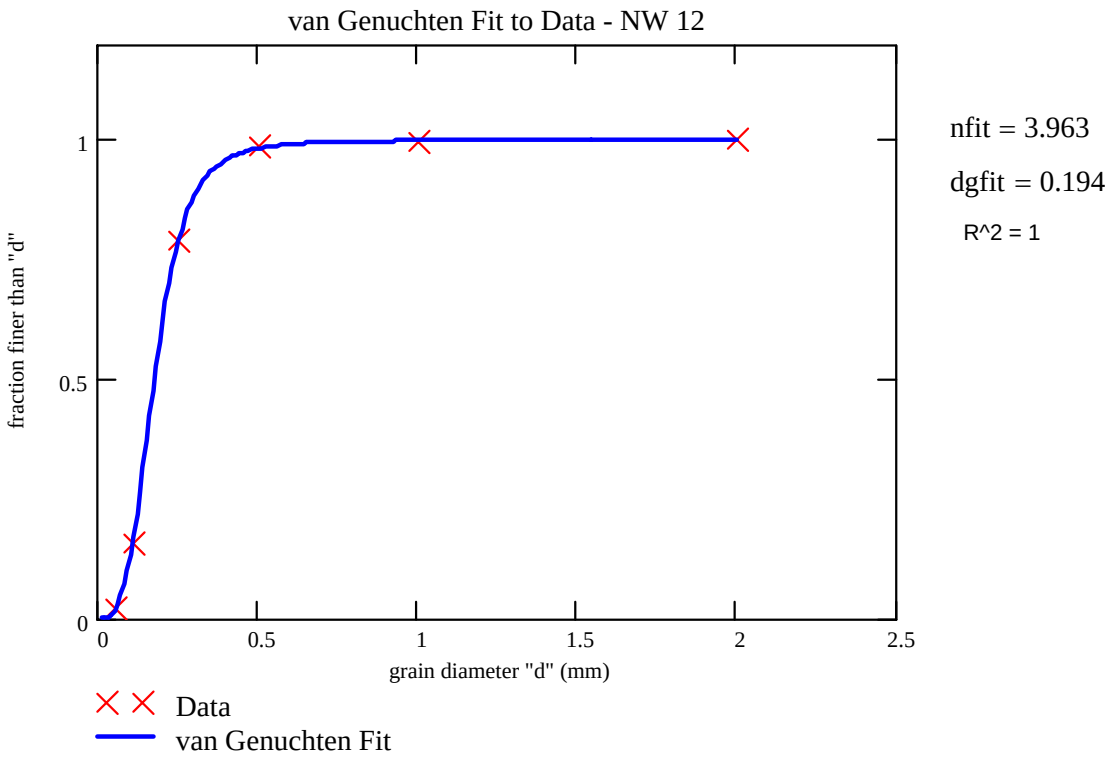

Figure 2.27 – Particle-size distribution for a silty sand collected from the STVZ research site at approximately 5 meters below ground surface.

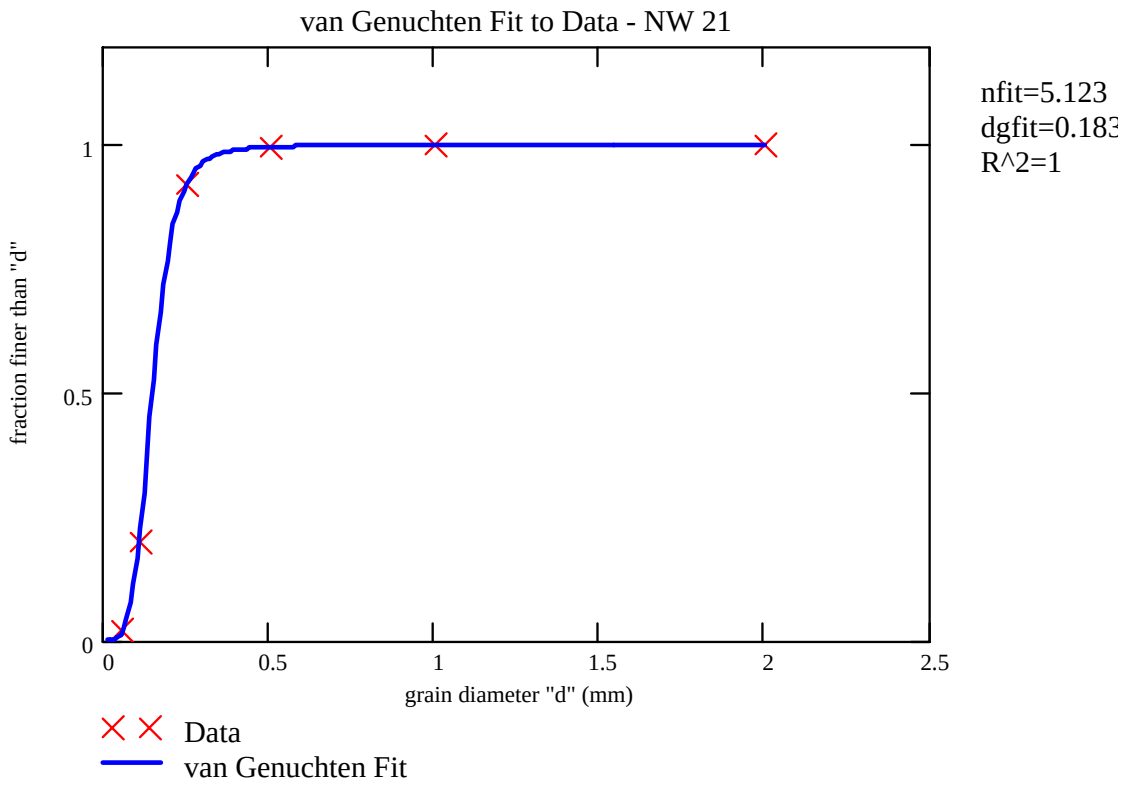

Figure 2.28 – Particle-size distribution for a fine grained sand collected from the STVZ research site at approximately 8 meters below ground surface.

Table 2.5 – Textural properties of NW core samples.

sample ID	depth (m bgs)	texture	d_{50} (mm)	$C_u = d_{60}/d_{10}$	d_g (mm)	n_d
				*	**	**
NW1	0.30	coarse sand	0.80	3.24	0.711	3.332
NW2	0.61	coarse sand	0.68	3.27	0.621	3.118
NW4	1.52	coarse sand	0.40	1.88	0.452	4.334
NW5	1.81	gravel	1.10	7.68	0.807	2.384
NW6	2.72	silty sand	N/A	N/A	N/A	N/A
NW7	3.05	fine sand	0.22	2.94	0.248	3.492
NW8	3.35	fine sand	0.21	2.89	0.232	3.160
NW9	3.66	fine sand	0.30	3.08	0.427	2.499
NW10	4.27	fine sand	0.24	2.55	0.284	3.207
NW11	4.57	silty sand	0.16	2.39	0.180	3.732
NW12	4.88	silty sand	0.17	2.38	0.197	3.909
NW13	5.18	sandy clay	N/A	N/A	N/A	N/A
NW14	5.79	pebbly clay	N/A	N/A	N/A	N/A
NW15	6.10	clay	N/A	N/A	N/A	N/A
NW16	6.40	fine sand	0.15	2.46	0.133	5.998
NW17	6.71	fine sand	0.16	2.27	0.149	5.805
NW18	7.62	fine sand	0.17	2.25	N/A	N/A
NW19	7.32	fine sand	0.14	3.08	0.133	4.079
NW20	7.92	fine sand	0.17	1.64	0.175	5.543
NW21	8.23	fine sand	0.15	1.64	0.183	5.123
NW22	8.84	silty sand	0.16	2.13	0.157	4.783
NW23	9.14	fine-coarse sand	0.18	1.33	0.227	3.450
NW24	9.75	fine-coarse sand	0.22	1.60	0.267	3.264
NW25	10.36	fine-coarse sand	0.33	3.00	0.393	3.020
NW27	10.97	fine-coarse sand	0.32	2.57	0.375	3.455
NOTES	*	C_u >6 - poor sorting; C_u <4 - well sorting				
	**	van Genuchten fitting parameters for PSD				

parameters (calculated from direct measurements of related properties). Figures included in this section represent best correlations between parameters. Appendix J includes figures for all parameter correlations examined in this study.

2.6 Discussion

2.6.1 Sample Disturbance

Although undisturbed samples are preferred for analysis of soil hydraulic properties, sample disturbance to some degree is virtually unavoidable (Stephens, 1996). Therefore, using laboratory analysis of intact core samples to infer true hydraulic properties of a geologic formation may not always yield correct results. Laboratory sample data usually provides satisfactory information on mineralogy and chemistry, but moisture retention characteristics are frequently altered by the sampling process, especially in deep vadose zone materials cored at depth using auguring techniques (Hearst et al., 1994). In friable materials, the bulk density and porosity can also be significantly altered during sampling. Although the results presented in this study may not reflect the true hydraulic properties for the STVZ vadose zone materials, they appear to reflect similar results as those that would have been obtained using intact sampling techniques for the sandy deposits (Appendix B).

2.6.2 Hysteresis in Moisture Retention Measurements

Hydrogeologic studies of the unsaturated zone have established that the relationship between hydraulic conductivity, fluid pressure, and water content are hysteretic (Knight, 1991). Hysteresis can significantly influence water flow and solute transport in partially saturated porous materials (Simunek et al., 1999). Although the importance of hystersis has been demonstrated in several numerical studies (e.g., Gillham et al., 1979; Kaluarachchi and Parker, 1987; Russo et al., 1989) and has been

recognized by researchers for many years, it is typically neglected in water flow studies because it takes a considerably longer amount of time to collect moisture retention data during a wetting sequence than a drainage sequence (Simunek et al., 1999; Yeh and Harvey, 1990). For this reason, many researchers measure moisture retention data along a drainage curve starting from either field saturation or porosity. The fitting parameters obtained from these curves are often reported in databases for flow and transport predictions within soils and deep vadose zone deposits using parametric or estimation models. In order to adequately model unsaturated flow and transport within the vadose zone, unsaturated flow models require integration of parameters obtained separately for individual flow conditions. This research clearly shows hysteresis in moisture retention curves for the STVZ site deposits (shown in Figures 2.15 through 2.19 and Table 2.3). Therefore, hydraulic parameters for separate flow scenarios should be uniquely quantified to accurately predict flow and transport in unsaturated environments.

2.6.3 Hysteresis in Electrical Resistivity Measurements

Although Knight (1991) observed a hysteretic relationship between electrical resistivity and moisture content in consolidated sandstone during main wetting and main draining sequences, the observations of this study indicate that the electrical resistivity relationship is not hysteretic for the STVZ alluvial deposits (shown in Figures 2.20 through 2.24). Water content and potential energy of soil water are not uniquely related because the potential energy state is determined by conditions at the air-water-solid interfaces and the nature of surface films rather than by the quantity of water present in pores (Jury et al., 1991). Electrical conductivity is a function of pore scale fluid distribution (Knight, 1991), similar to soil water potential, however, pore

connectivity and transport tortuosity within a lithified geologic unit is very different than pore connectivity within an unconsolidated porous medium. Cementation within a consolidated porous medium blocks pathways between pores creating isolated pore spaces within the medium during imbibition and draining (e.g., pores may be hydraulically connected in one direction only). During imbibition and draining of an unconsolidated porous medium, small pores may be filled while large pores are virtually empty, however the pores may be hydraulically connected through films along the edges of the empty pores, allowing an electrical current to pass through the medium measuring the entire moisture content of the medium. Therefore, it is possible that unconsolidated deposits and soils may not exhibit hysteresis in electrical resistivity measurements even if hysteresis is observed in moisture retention measurements.

2.6.4 Significance of the Curve Fitting Parameters Determined for the STVZ Alluvial Deposits

This research indicates that the van Genuchten moisture retention curve fitting parameters α and n (obtained from PDC data) for the STVZ sandy alluvial deposits differ from values reported in published literature for soil cores of similar texture (i.e., percent sands, silts, and clays –Table 2.6). Specifically, the parameter n for samples analyzed in this study has a higher population mean compared to values reported for sandy soils of similar texture, while the parameter α has a lower population mean than tabulated values reported for sandy soils. The van Genuchten fitting parameters from this study are, however, in agreement with values reported for sandy alluvial deposits of similar textures (Table 2.6). Although standard deviations between measurements were not reported in all the studies, the results of this research suggest that sandy alluvial

Table 2.6 – Published hydraulic properties (mean values) for sandy soils and alluvial sands. Population standard deviation is expressed in parentheses (if reported). The sandy soils and alluvial deposits were reported as undisturbed samples in the literature. B&C refers to Brooks and Corey (1964) parameteric model where λ is approximately equal to (n-1) and h_{ae} is approximately equal to $1/\alpha$ (van Genuchten et al., 1991).

Type of Sediment	van Genuchten n	van Genuchten α (1/cm)	$1/\alpha$ (cm)	Ksat (cm/s)	Porosity	θ_r
Alluvial Sands						
STVZ Sand (coarse-fine)	4.50 (1.75)	0.021 (0.01)	47.62	0.004 (0.0025)	0.389 (0.02)	0.066 (0.03)
Healy and Mills (1991) Sand (coarse-fine)	4.79 (0.881)	0.067 (0.013)	14.92	0.0385	0.384	0.055
Yeh and Harvey (1990) Sand (coarse - med)	4.72 (0.924)	0.074 (0.0006)	13.51	0.1126 (0.003)	0.436 (0.016)	0.05 to 0.10
Stephens et al. (1986) Sand (coarse – fine)	4.05 (2.01)	0.0279 (0.0067)	35.84	0.024 (0.011)	0.415 (0.043)	0.05 to 0.10
Sandy Soils						
Carsel and Parrish (1988) Sand	2.68	0.145	6.90	0.00825	0.43	0.045
Rawls et al. (1982) Sand	1.592	0.138	7.25	0.0058	0.417	0.020
Anderson and Carsel (1986) Loamy sand	1.629	0.100	10.0	0.0017	0.358	0.044
Mallants et al. (1996) Sandy loam	1.386	0.013	76.92	5.3e-5	0.360	0.012
Haverkamp and Parlange (1986) Sand	B&C λ 1.872 (0.485)	N/a	B&C h_{ae} 27.787 (7.421)	N/a	0.39 (0.03)	0.00

deposits have a more uniform pore-size distribution and higher air entry pressures than sandy soils of similar textures (Figure 2.29).

The difference in pore volume distributions and average pore sizes (reflected by the parameter α) between soils and alluvial deposits may be due to weathering of soils at the surface, forming cracks, root channels, and deposition of fine particles in larger void spaces in the soil (Mitchell, 1975 pg. 54; Buol et al., 1973 pg. 28; Stephens, 1996 pg. 89), thus forming a larger distribution and larger average pore sizes for soils than for deeper alluvial deposits. These results suggests that the use of tabulated soil properties (based on particle textures alone) for flow and transport predictions may not be appropriate for predicting flow and transport within deep vadose zones.

2.6.5 Parameter Correlations

The strongest observed correlations exist between the van Genuchten fitting parameters for α values observed for the separate moisture retention curves (MWC, MDC, PDC). The correlations for α between the MWC, MDC, and the PDC all appear to be linear (Figures 2.30, 2.31, and 2.32). The slope of the moisture retention curves do not appear to be strongly correlated, although there does appear to be a slight linear relationship between the slope of the MDC and the slope of the PDC (Figure 2.33). Although a linear relationship exists between the slopes of the PDC and the PSD, the parameters are not strongly correlated (Figure 2.34). The van Genuchten parameter α, however, shows a fairly strong correlation to the average particle size of the deposits (Figure 2.35).

Saturated hydraulic conductivity typically decreases with decrease in grain size (Jury et al., 1991), however the correlations observed between saturated hydraulic

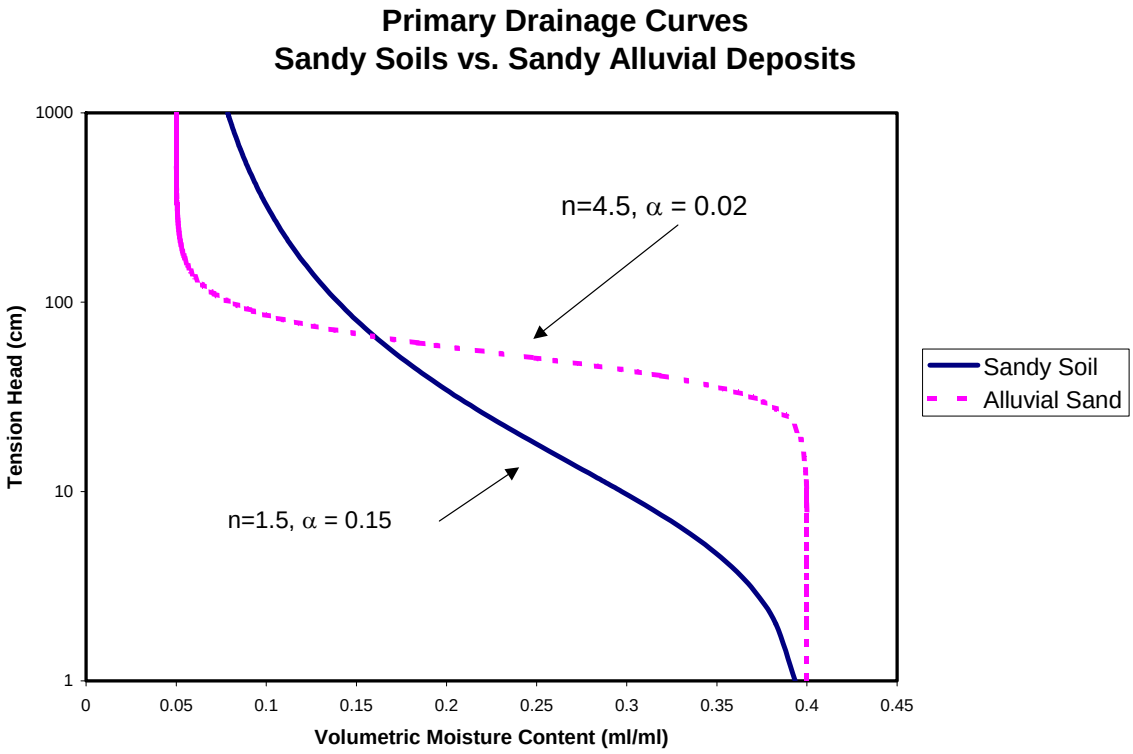

Figure 2.29 – Typical moisture retention curves for sandy soils (Carsel and Parish, 1988) and sandy alluvial deposits of similar texture (mean fitting parameter values for sandy alluvial deposits collected from the STVZ site).

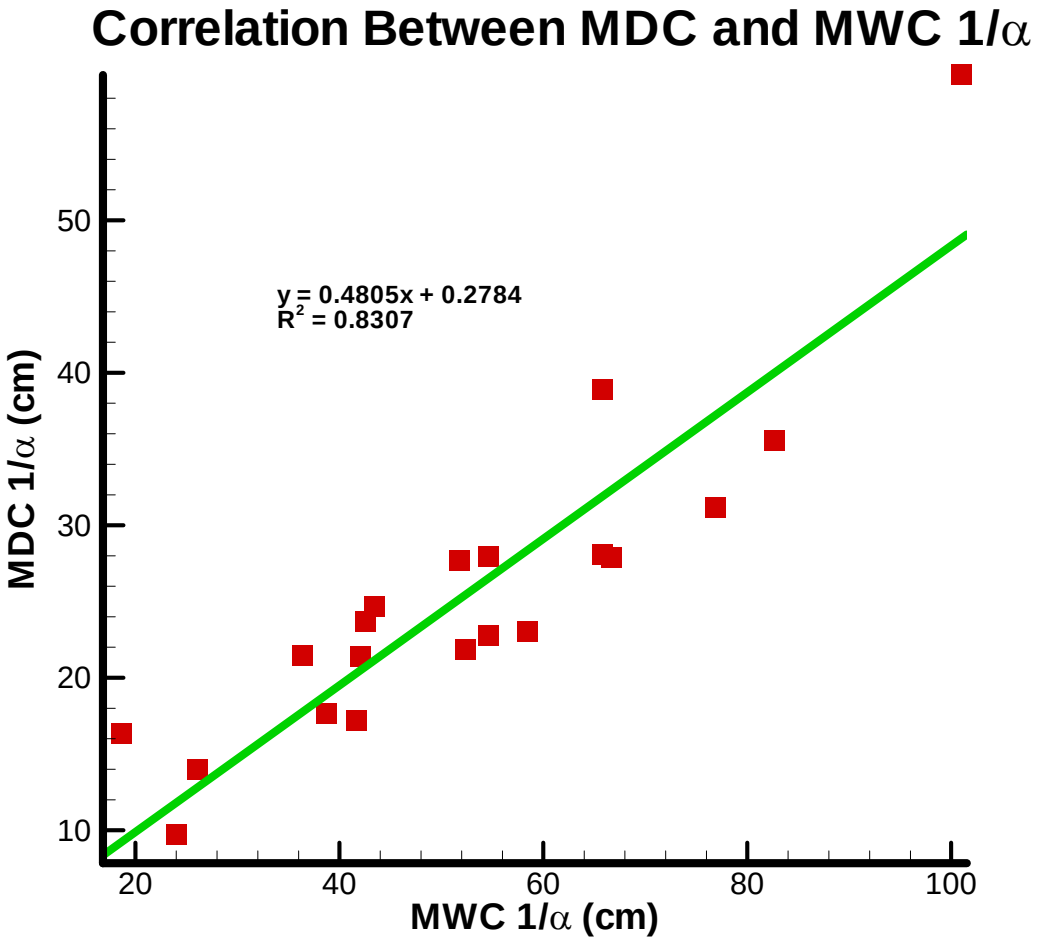

Figure 2.30 – Plot of van Genuchten parameter (1/α) during a drainage sequence (MDC) versus wetting sequence (MWC).

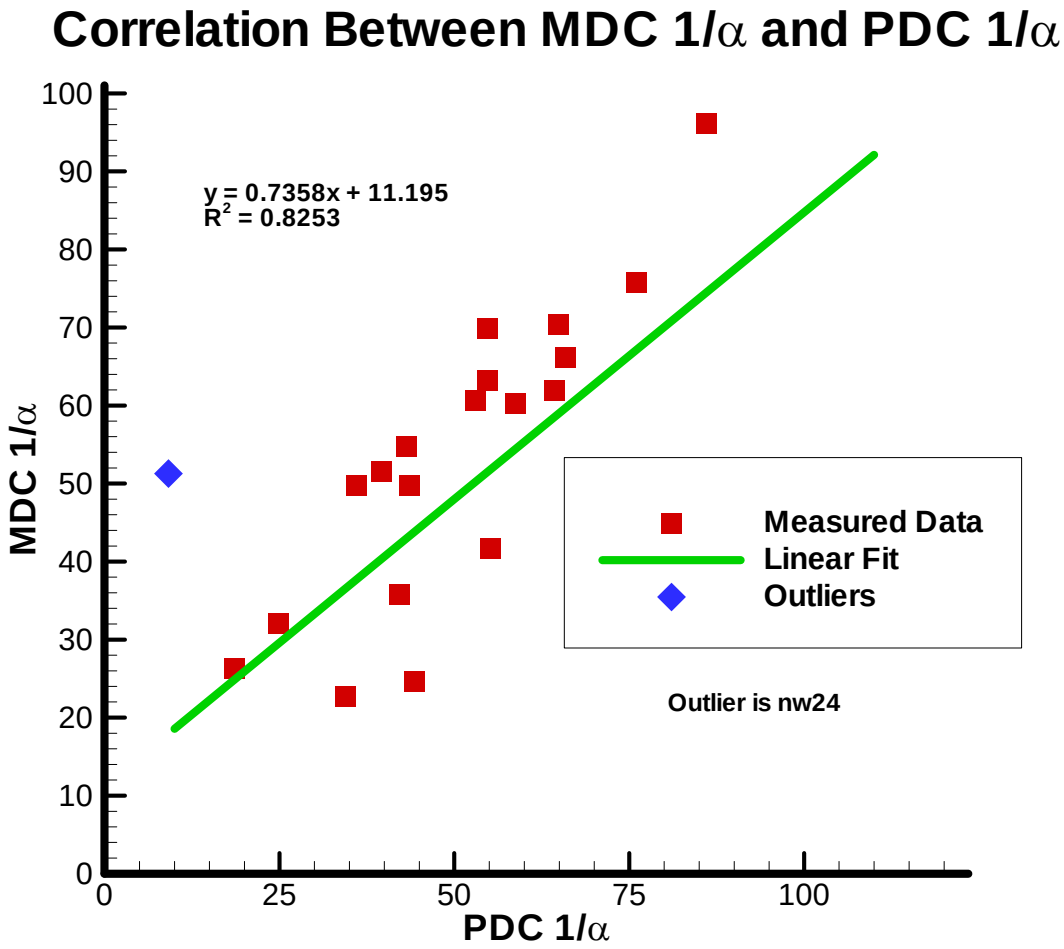

Figure 2.31 – Plot of van Genuchten parameter (1/α) during a drainage sequence from satiation (MDC) versus a drainage sequence from saturation (PDC).

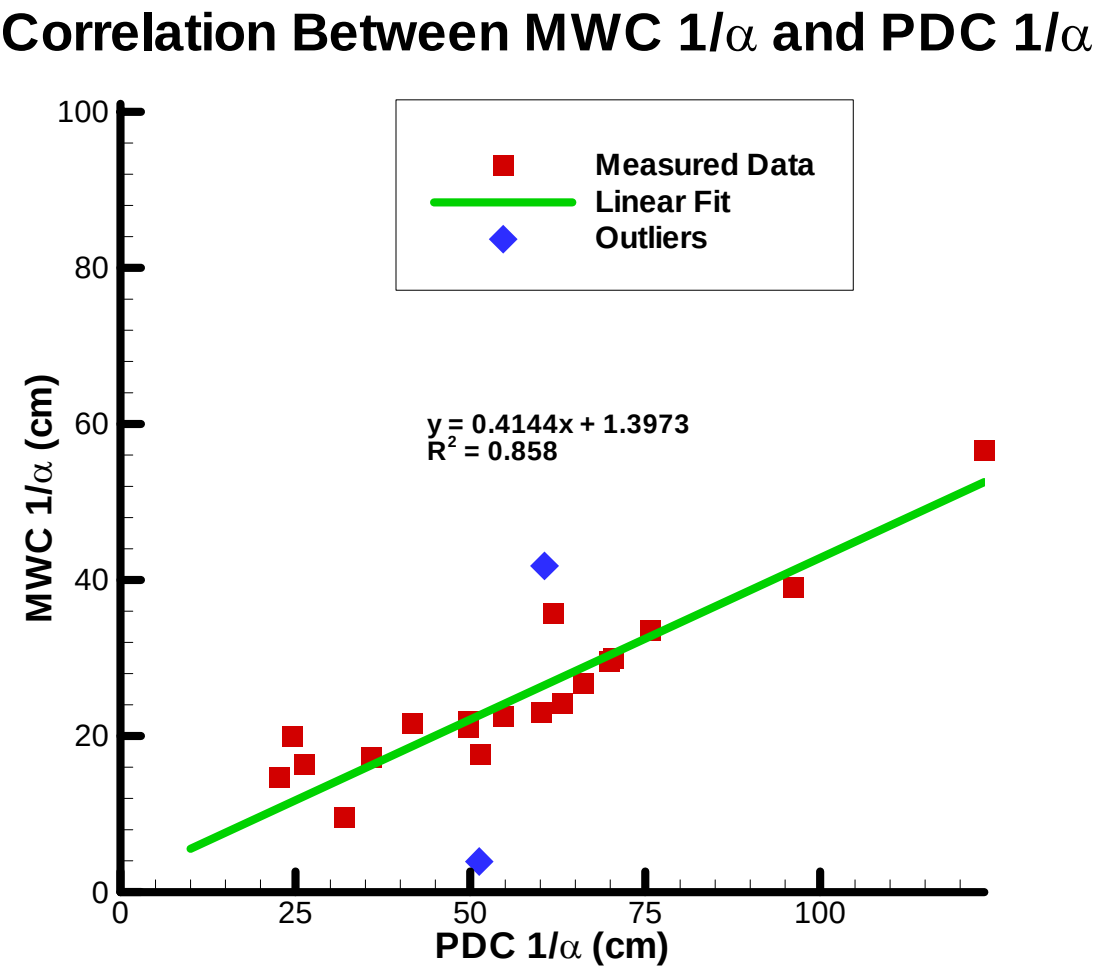

Figure 2.32 – Plot of van Genuchten parameter (1/α) during a wetting sequence (MWC) versus a drainage sequence from saturation (PDC).

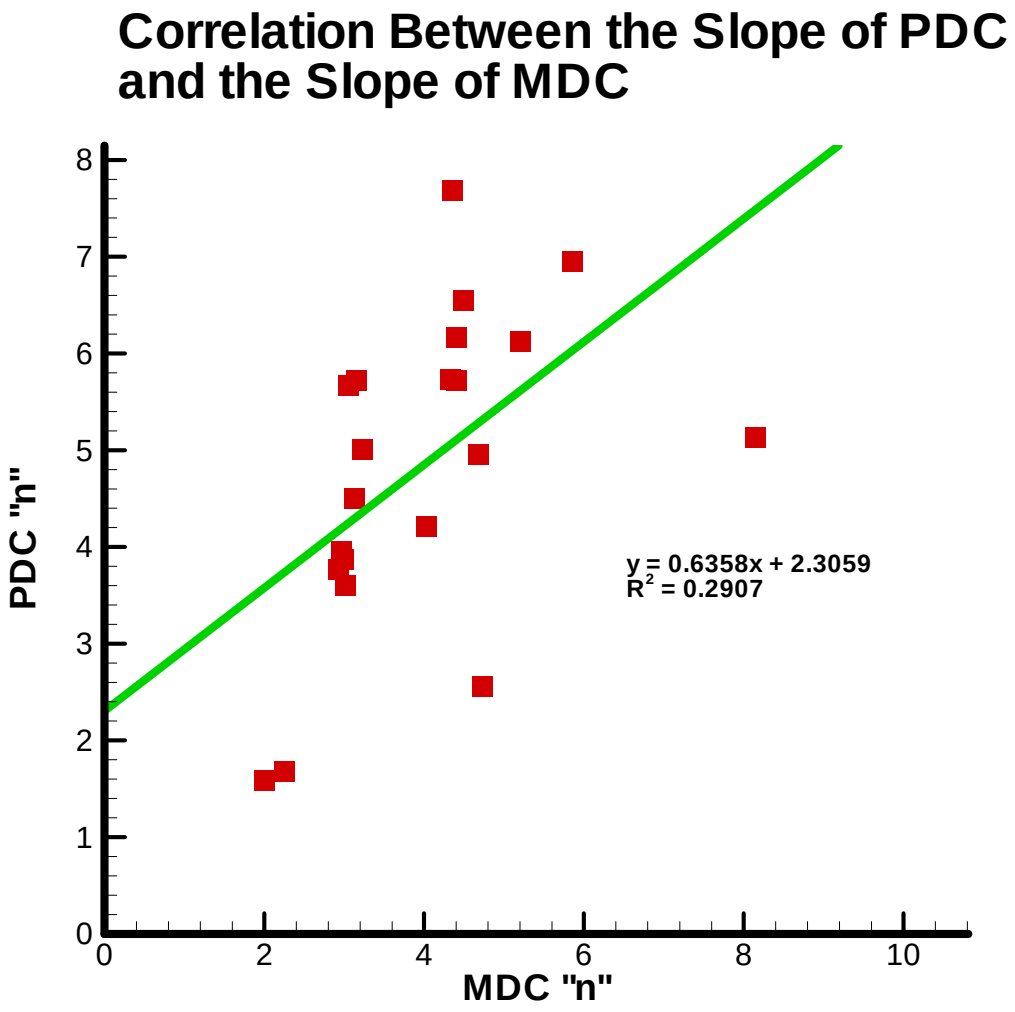

Figure 2.33 – Slope of the primary drainage curve versus the slope of the main drainage curve.

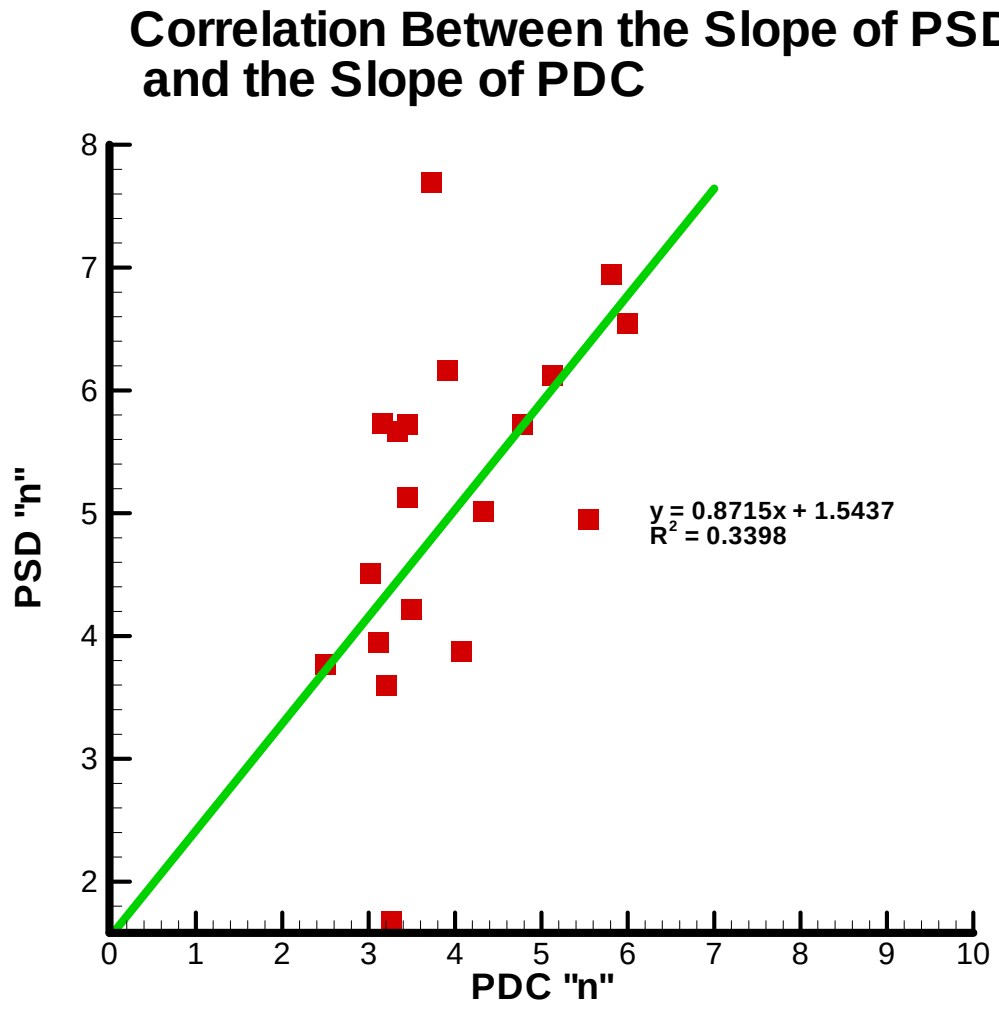

Figure 2.34 – Slope of the PSD versus slope of the PDC.

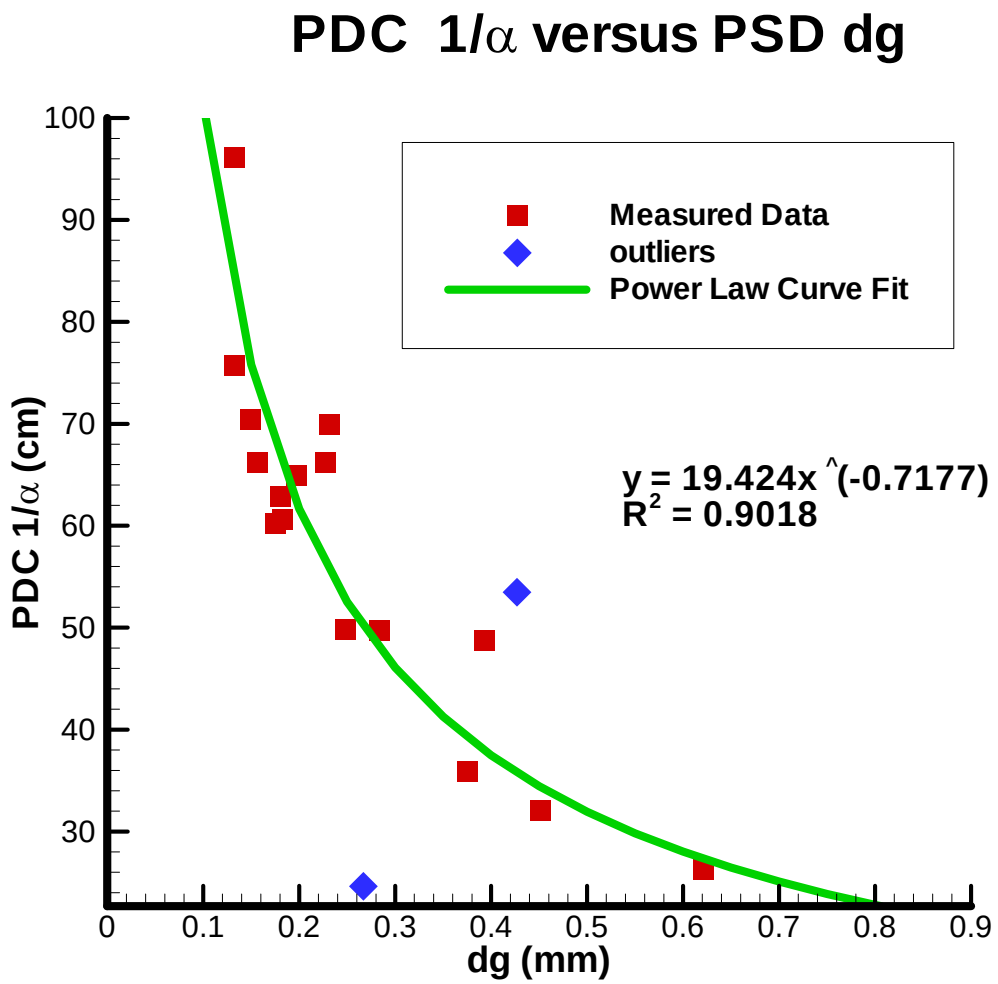

Figure 2.35 – PDC *1/α* versus average grain diameter d_g.

conductivity and average grain size (Figure 2.36), show an anomalous increase in conductivity with decrease in grain size. This may be due to the fact that particles greater than 2 mm were removed from the particle-size distribution measurements, but were included in samples used to measure saturated hydraulic conductivity. Although the larger clasts may not contribute to moisture retention, the clasts do impact the hydraulic conductivity measurements, in particular if the sample is poorly sorted. In fact, grain sorting plays a major role in saturated hydraulic conductivity (Jury et al., 1991) as shown in Figure 2.37. Therefore, the samples with larger average grain sizes may also represent samples which are more poorly sorted, resulting in lower conductivity values. The same holds true for the relationship between $1/\alpha$ and hydraulic conductivity shown in Figure 2.38. The figure shows that hydraulic conductivity appears to increase with decrease in average pore diameter. Intuitively, samples with larger mean pore sizes should also have higher hydraulic conductivity values at saturation, but again sorting of pore sizes plays a major role in the conductivity of the sample. For instance, the presence of large clasts in sample NW5 may have resulted in a poor distribution of pore sizes by filling large voids with finer particles. Although trends were observed between saturated hydraulic conductivity and other parameters (Figure 2.39), it does not appear to be strongly related to any one parameter, suggesting that multiple factors control the hydraulic conductivity of a porous medium at saturation.

Figure 2.40 shows that the slope of the linear resistivity curves (log of Equation 2-4) increases with increase in grain size, however, the slope does not appear to be directly related to moisture retention curve fitting parameters.

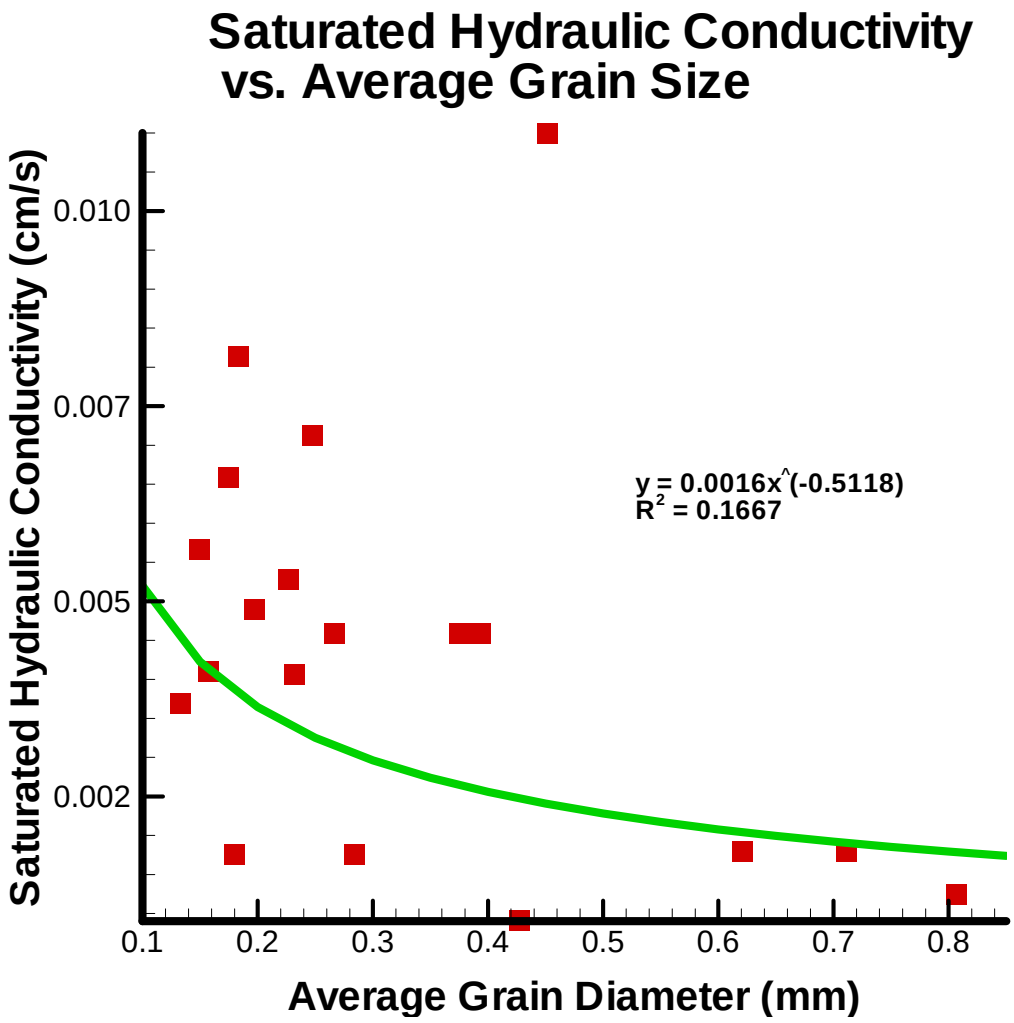

Figure 2.36 – Correlation between saturated hydraulic conductivity and grain size.

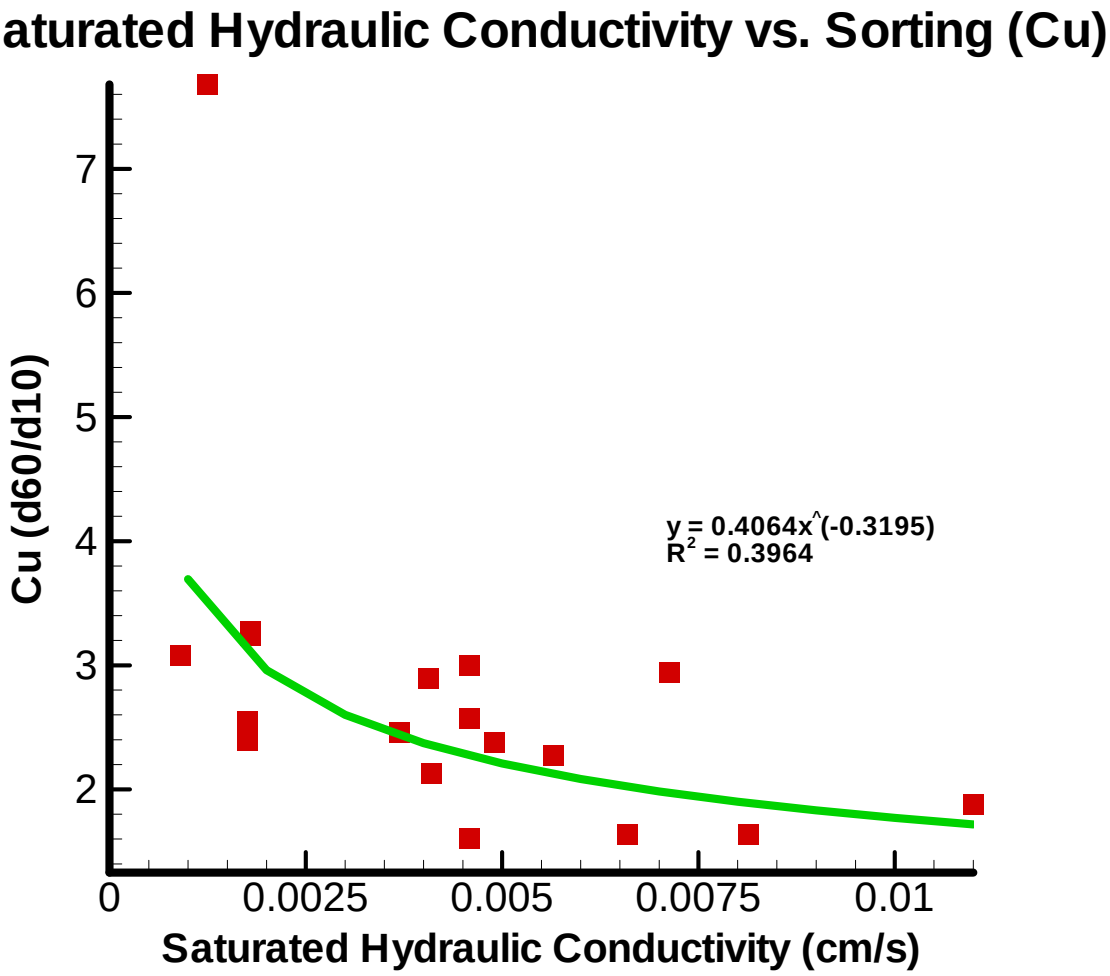

Figure 2.37 – Correlation between saturated hydraulic conductivity and grain sorting. Conductivity appears to decrease exponentially with better sorted samples (well sorted samples have C_u value <4).

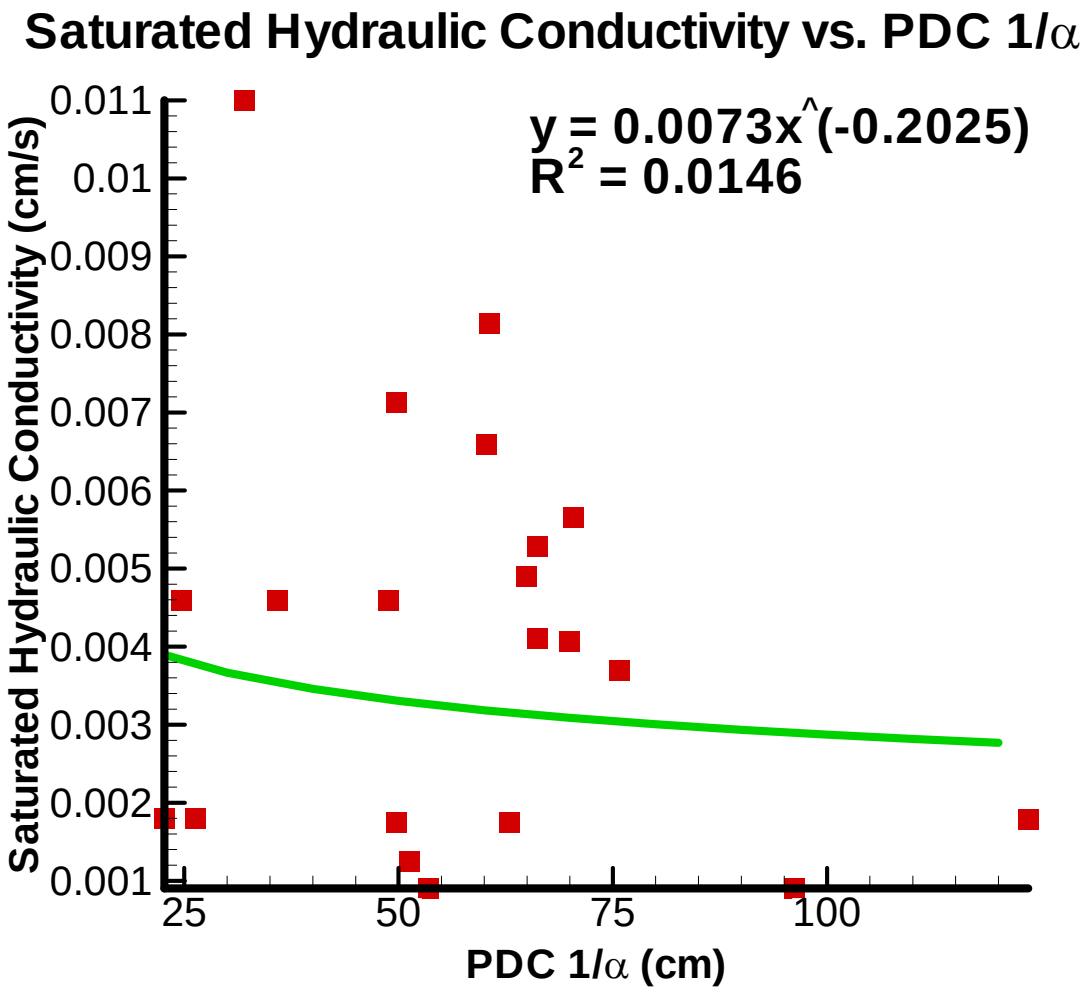

Figure 2.38 – Relationship between the pore-size distribution fitting parameter α and saturated hydraulic conductivity for the PDC. Conductivity appears to decrease with a decrease in α.

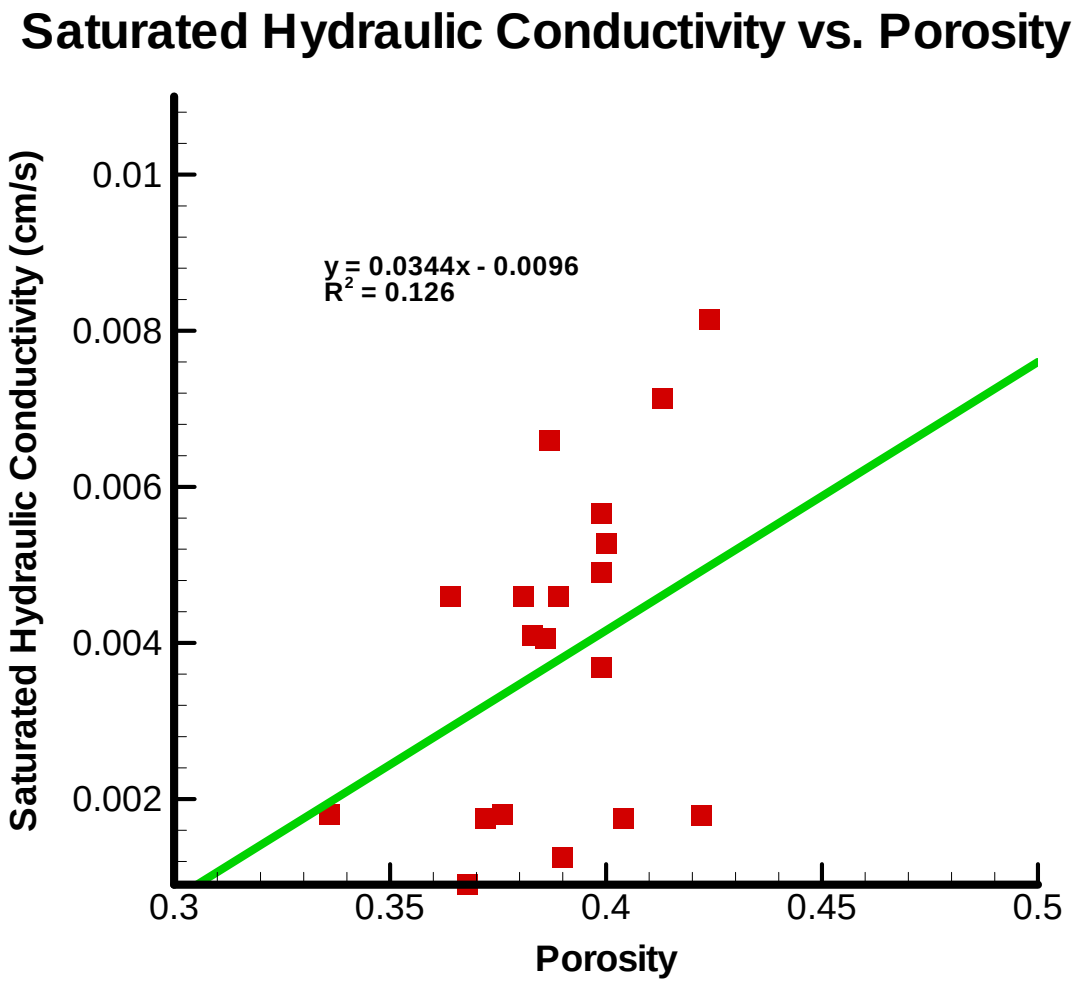

Figure 2.39 – Correlation between porosity and saturated hydraulic conductivity. Although the correlation is not strong, conductivity appears to increase with increase in porosity.

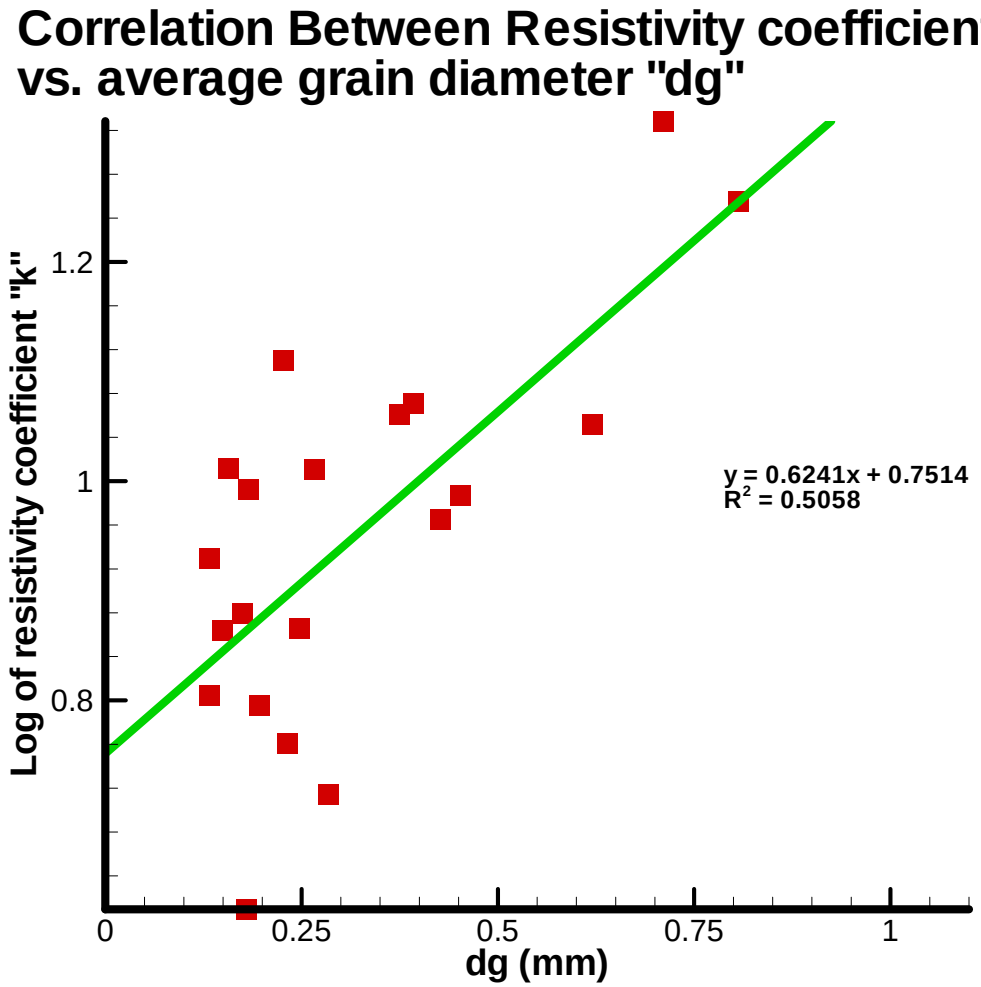

Figure 2.40 – Correlation between electrical resistivity curve fitting parameter "k" versus grain diameter.

2.7 Measurement Error and Uncertainty

2.7.1 Measurement Error

2.7.1.1 Introduction

Direct measurements of hydraulic properties consist of both the "true" value and measurement error contributed by factors which cannot be completely avoided. Imprecision and bias in the measuring device and/or researcher errors, such as misread values and transcription errors, may occur. In order to determine the relevance of laboratory data, the degree of measurement error should be identified and included in the data, typically in the form of the standard deviation from the mean value (Mandel, 1964).

The two major components of measurement error are precision and accuracy (Scheaffer and McClave, 1995). Precision refers to the reproducibility of measurements and accuracy refers to the ability to produce unbiased measurements. Measurement bias is the result of a constant deviation in the results. For example, measurements which are continually skewed in a particular direction from the "true" value due to improper instrument calibration are considered to be biased. Model estimates are considered biased if the estimated value does not equal the mean value (Isaaks and Srivastava, 1989).

Measurement accuracy is typically determined by comparing results to a known value. Unfortunately, this is difficult to do when measuring hydraulic properties since actual hydraulic properties are rarely known. Measurement precision can be determined by repeating a measurement several times using the same procedure and noting the deviation in the results. The data would be considered precise within +/- the standard deviation in the repeatability measurements.

2.7.1.2 Measured results

Repeatability tests were conducted for moisture retention measurements in the hanging column apparatus and the pressure cells, hydraulic conductivity measurements in the constant head permeameters, electrical resistivity measurements in the impedance analyzer, porosity measurements in the saturation chamber, and particle-size analysis using dry sieve methods. Measurements were repeated for duplicate samples for all measurement methods except the hanging column apparatus. Because the hanging column drainage procedure alters the grain orientation of the samples, identical measurements were made for replicate samples as an alternative to repeating the measurements for each sample. The standard deviation between replicate samples (in the hanging column measurements) was actually lower than the standard deviations between repeated measurements made for individual samples (all other measurement devices). Tables of results are included in this section with details listed in Appendix K. Sample statistics represent measurements repeated for an individual sample while population statistics represent statistics for measurements made for replicates. The coefficient of variation is equal to the standard deviation divided by the mean. Refer to Appendix K for a detailed description of the methods used to determine measurement error.

Table 2.7 - Error analysis of porosity measurements made using the saturation chamber (3 samples analyzed 5 times each).

Sample ID	Sample Mean	Sample Stdev	Coefficient of Variation
36	0.332	0.009	0.027
37	0.321	0.019	0.060
46	0.336	0.014	0.043
average	**0.330**	**0.014**	**0.043**

Table 2.8 – Error analysis of moisture content measurements made at 1 bar pressure using the pressure chambers (3 samples analyzed 5 times each).

Sample ID	Sample Mean	Sample Stdev	Coefficient of Variation
36	0.032	0.008	0.250
37	0.035	0.006	0.171
46	0.037	0.006	0.162
average	**0.035**	**0.007**	**0.200**

Table 2.9 – Error analysis of electrical resistivity measurements made at saturation using the impedance analyzer (3 samples analyzed 5 times each).

Sample ID	Sample Mean	Sample Stdev	Coefficient of Variation
36	47.776	8.561	0.179
37	48.926	8.246	0.169
46	48.828	8.097	0.166
average	**48.510**	**8.301**	**0.171**

Table 2.10 – Error analysis of moisture content measurements made using the hanging column apparatus (5 replicate samples analyzed once each – statistics represent population statistics for the set).

Tension Head (cm)	Sample Mean	Sample Stdev	Coefficient of Variation
200	0.048	0.003	0.059
100	0.077	0.003	0.036
50	0.319	0.006	0.020
40	0.381	0.013	0.033
30	0.399	0.004	0.009
20	0.402	0.005	0.011
10	0.407	0.005	0.011
0	0.434	0.003	0.007
	average	**0.0052**	**0.023**

Table 2.11 – Error analysis of saturated hydraulic conductivity measurements made using the constant head permeameter (4 replicates measured three times each).

Sample Statistics:				
Sample ID:	A	B	C	D
mean	1.10E-03	1.05E-03	1.14E-03	8.77E-04
stdev	8.62E-05	1.37E-11	8.70E-05	1.37E-11

Population Statistics:	mean	stdev	Coefficient of variation
	1.04e-03	5.00e-05	4.80E-02

Table 2.12 – Error analysis of particle-size measurements made using the sieve method (2 replicate samples measured 10 times each).

	Sieve No.	Grain Size	Mean fraction by Weight	Std Dev	Coefficient of Variation
sample 1	5	pebbles	0.037	0.0007	0.0194
	10	granules	0.031	0.0003	0.0123
	18	VC sand	0.075	0.0016	0.0215
	35	C sand	0.275	0.0037	0.0135
	60	M sand	0.338	0.0023	0.0068
	140	F sand	0.195	0.0049	0.0253
	270	VF sand	0.032	0.0022	0.0686
	Bottom	Silt & clay	0.0135	0.0011	0.0881
			Average all sieves	**0.0021**	**0.0319**
sample 2	5	pebbles	0.028	0.0028	0.0984
	10	granules	0.032	0.0002	0.0065
	18	VC sand	0.076	0.0009	0.0125
	35	C sand	0.275	0.0006	0.0024
	60	M sand	0.340	0.0014	0.0042
	140	F sand	0.198	0.0030	0.0154
	270	VF sand	0.034	0.0012	0.0364
	Bottom	Silt & clay	0.014	0.0008	0.0561
			Average all sieves	**0.0014**	**0.0290**

2.7.2 Measurement Uncertainty

2.7.2.1 Introduction

Qualitatively speaking, measurement uncertainty refers to the fact that measured values are in some sense only a reasonable or useful guess at what the unknown value might be (Isaaks and Srivastava, 1989 pg 489). In other words, no matter the measurement approach, there will always be a degree of error which may not be easily quantified. Although not quantified, the existence of measurement uncertainty in this research is recognized and possible sources are discussed in this section.

2.7.2.2 Moisture Retention Uncertainty

The hydraulic contact material used in the moisture retention experiments (silica flour and diatomaceous earth) most likely contributed to measurement uncertainty in the moisture content measurements. The material stuck to the bottom of the cotton cloth attached to the sample rings and possibly permeated the samples to some degree creating lower permeability at the base of the samples. Removing the samples at equilibrium to obtain a sample weight may have resulted in a minor degree of evaporation, also contributing to measurement uncertainty. It is possible that complete moisture equilibrium may not have been achieved during moisture retention analysis, even though standard methods and direct determinations (Appendix B) suggest that moisture equilibrium is reached within a matter of hours in the wet range of tensions between 0 and 100 cm to days in the dry range of tensions greater than 100 cm. If the evaporation rate in the hanging column apparatus was higher than the drainage rate (or rate of imbibition), actual moisture equilibrium could not have been detected. This would lead to an overestimate in moisture content at each tension head measured during drainage and an underestimate in moisture content during imbibition.

2.7.2.3 Lack of Microbial Growth

The use of thymol during moisture retention analysis to prevent bacterial growth in the porous plates (Appendix F) may have had an impact on the moisture retention properties of the deposits, however, the percent organic matter was very minimal since the deposits were all collected below the root zone. Of more concern than destruction of bacteria in sediments, was the potential of bacterial growth in the porous plates which would have resulted in a greater degree of measurement uncertainty by impeding flow through the plates. Therefore, thymol as added to the wetting solution for all analyses.

2.7.2.4 Uncertainty in Electrical Resistivity Measurements

Electrical impedance measurements are dependent on the degree of contact between the porous material and the silver plates (Appendix K). In the preliminary study, measurements based on degree of contact at varying moisture contents were not compared. It is possible that the optimum degree of contact may have been higher at lower moisture contents (as the resistivity increased). Sample compaction during analysis was of greater concern, which would have resulted in a higher degree of measurement uncertainty for all measured properties (in addition to electrical resistivity) because of a decrease in sample porosity. Therefore, the same method was used to ensure sample contact regardless of moisture content.

2.7.2.5 Uncertainty in Saturated Hydraulic Conductivity Measurements

The high flux rate applied to the samples during measurement of saturated hydraulic conductivity in the constant head permeameters (Appendix G) may have contributed to sample disturbance during analysis, leading to overestimated conductivity values because of possible formation of preferential flow paths. Another

possible contributor to measurement uncertainty may have been the small time period used to measure outflow and the small volumes measured to determine volumetric flux. It is also possible that not enough time was allowed to reach steady state flow within the samples before measurements were made.

2.7.2.6 Uncertainty in Particle-Size Distribution Measurements

Although care was taken during analysis, uncertainty in particle-size distribution measurements using sieve methods may have resulted from sediment sticking to the sides of individual sieves (not passing through openings) and from particles sticking in the sieve openings instead of passing through. Soil hydrometer methods include measurement uncertainty primarily from sample loss while taking measurements (sediment sticking to the hydrometers) and from evaporation of the soil slurry during analysis (takes 24 hours to complete the measurements).

2.7.2.7 Uncertainty in Moisture Retention Curve Fitting Parameters

The van Genuchten equation was fit to moisture retention data requiring the RETC curve fitting program to estimate four unknown parameters (θ_s, θ_r, α, and n). The RETC program is limited to non-unique results which contribute to model uncertainty (van Genuchten et al., 1991). The model uncertainty increases with the number of unknown parameters and fewer number of measured data points. Weighting individual data points improves the fit to data, however, measurement uncertainty and error is included in the data, making the weighted fits somewhat subjective.

2.8 Conclusions

Samples collected from the NW quadrant of the STVZ infiltration test site were used to analyze moisture retention during wetting and draining sequences, porosity, electrical resistivity, saturated hydraulic conductivity, and particle-size distributions for

site characterization of deep vadose zone materials. Methods for characterizing hydraulic properties of alluvial vadose zone deposits were based on standard methods developed for soil characterization and results of preliminary studies conducted as part of this research. Functional forms (equations 2-1 through 2-4) were fit to the moisture retention, electrical resistivity, and particle-size distribution data, and correlations between hydraulic and geophysical parameters were examined.

Major differences in moisture retention curves between intact and repacked sandy deposits were not observed (Appendix B), therefore it was assumed that properties measured for repacked sands were similar to properties that would have been made for intact samples. Although sample compaction was observed in undisturbed near surface sandy deposits, significant compaction in the repacked samples during imbibition or subsequent desorption was not evident. The electrical resistivity measurements did not appear to disturb the samples during analysis. On the other hand, saturated hydraulic conductivity measurements resulted in some sample loss by sticking to the permeameter sample holders. Although high flux rates used in hydraulic conductivity analysis were higher than *in situ* conditions, sample disturbance and turbulent flow did not occur as a result.

Hysteresis was observed in moisture retention wetting and draining, but not in the electrical resistivity data. The moisture retention fitting parameters for the sandy alluvial deposits appear to differ from parameters reported for sandy soils while the porosity, saturated hydraulic conductivity, and bulk density are similar to values reported for both sandy alluvial deposits and sandy soils.

Correlations between parameters were the strongest for the van Genuchten parameter α between wetting and draining moisture retention curves. Although

correlations between the other parameters were not strong, relationships were observed between saturated hydraulic conductivity and pore-size distribution parameters, saturated hydraulic conductivity and particle-size distribution parameters, and electrical resistivity and particle-size distribution parameters.

Measurement error for the majority of measurement techniques was identified by conducting measurement repeatability tests. Measurement uncertainty, which could not be quantified, most likely exists due to sample disturbance inherent in sample preparation and analysis, possible insufficient equilibrium times, influence of evaporation, and low permeability boundary conditions caused by hydraulic contact material.

2.9 Recommendations for Future Work

2.9.1 Sample collection

Although environmental conditions can be better controlled in a laboratory setting and laboratory measurements typically have a higher degree of measurement precision compared to *in situ* analysis, laboratory measured properties using standard techniques do not represent field scale hydraulic properties. Even though similar hydraulic properties between intact and repacked alluvial sand samples were observed, it is unlikely that natural structure was captured and/or preserved during sample collection. Collecting undisturbed samples of poorly consolidated deposits, often found in vadose zone environments, is nearly impossible and certainly improbable. Most standard laboratory methods are limited to analysis of inadequate sample sizes for capturing natural structures such as aggregates, concretions, and lenses of low permeability sediments, which strongly influence unsaturated flow behavior.

Development of methods for collecting and analyzing undisturbed meso-scale samples are required to preserve the integrity of *in situ* conditions.

2.9.2 Cost and Time Efficient Methods

It took approximately six months to complete the laboratory sample analyses for twenty five samples after collection and transport to the laboratory for analysis. Based on this time frame, this research confirms the perception that laboratory analysis of a large number of samples using standard methods is unrealistic. Time efficient methods for measuring moisture retention properties of soils and alluvial deposits are needed for characterizing large sample sets. Methods which reduce laboratory experimentation time include desorption by centrifugation (Nimmo et al., 1987) and hydraulic property predictive methods based on surrogate data which is less time consuming to measure directly (Arya et al., 1999; Arya, et al., 1981, Haverkamp, and. Parlange, 1986; van Genuchten, et al., 1999). At present, these methods require further examination to develop standard techniques, application conditions, and impact of measurement and model uncertainty on moisture retention parameters.

Direct measurements of air entry pressure, porosity, and residual moisture content prior to data collection would allow researchers to focus on the active region of moisture retention curves resulting in better estimates of curve fitting parameters using a limited number of data points. Methods for measuring these properties could be easily developed in a laboratory setting in a reasonably time frame. For example, centrifugation could be used to measure residual moisture content, a method for measuring air entry pressure could be developed using air injection methods, and porosity measurements using the vacuum saturation techniques could be improved by

reducing measurement uncertainty (e.g., using hydrophobic materials to hold sediment in sample rings).

2.9.3 Examination of Alluvial Geologic Hydraulic Properties

This research suggests that curve fitting parameters for moisture retention characteristics of deep vadose zone alluvial deposits differ from reported values for soils of similar texture. This implication could have a significant impact on flow and transport modeling in deep vadose zone environments. Further investigations involving larger sample sets and sample sizes of both soils and deep vadose zone deposits are required to support the findings. The investigations should examine the impact of natural structure on moisture retention and hydraulic conductivity measurements. Because an investigation of large sample sets is unrealistic using standard laboratory techniques, the examination should be conducted using innovative time efficient methods for attaining curve fitting parameters. The initial part of the study should include an in-depth examination of procedures using desorption centrifugation and predictive modeling. Methods for direct time-efficient measurements of air entry pressure, porosity, and residual moisture content should be included in the study. Impact of measurement error and model uncertainty should be examined to determine conditions for application.

CHAPTER 3.0 – PREDICTIVE METHODS FOR CHARACTERIZING HYDRAULIC PROPERTIES OF SANDY ALLUVIAL DEPOSITS: APPLICATION TO THE STVZ RESEARCH SITE

3.1 Abstract

Pedotransfer functions developed for estimating hydraulic properties of vadose zone porous media are appealing to many researchers because hydraulic properties for a large number of samples can be estimated from a relatively small sample set. This chapter includes an evaluation of a pedotransfer model developed by Haverkamp and Parlange (1986) for application to sandy alluvial deposits often found in deep vadose zones. Because the model was developed for application to sandy soils, the model was calibrated to the STVZ alluvial deposits and the results were compared to model predictions made using the original model estimation equations. Since the Haverkamp and Parlange (1986) model predicts the Brooks and Corey (1964) moisture retention fitting parameters, the model was modified to predict the van Genuchten (1980) fitting parameters which tend to better describe the moisture retention curve for finer grained deposits with wider pore-size distributions.

Results show that both models predict moisture retention curves similar to direct functional form fits to measured data for a majority of the samples analyzed. Exceptions include application to deposits exhibiting dissimilar physical properties from samples used in the model calibrations. A model sensitivity analysis was

conducted to examine optimum conditions for model calibration and application. The analysis showed that the number of samples and data points used in the model calibrations was adequate, however, model estimates improved when the model was calibrated to deposits with narrower distributions of particle sizes.

3.2 Introduction

3.2.1 Problem Statement

Characterizing heterogeneous unsaturated materials requires a large number of hydraulic property measurements. It is impractical, however, to directly measure unsaturated hydraulic properties on a large number of samples. Pedotransfer functions for estimating hydraulic properties are appealing because properties are empirically predicted from a limited number of direct measurements, and a larger number of indirect or surrogate measurements which are less time consuming to obtain.

Pedotransfer functions (PTFs) were developed to estimate hydraulic properties of soils based on textural and physical properties of a porous medium (e.g., particle-size distributions and bulk density or porosity). Early PTFs used statistical models relating volumetric moisture content to particle-size analysis (e.g., Salter et al., 1996; Gupta and Larson, 1976). Because the standard deviations between predicted and experimental water content values for the statistical models were much greater than laboratory errors (Haverkamp and Parlange, 1986), alternative pedotransfer functions that assume shape similarity between the particle-size distribution and the pore-size distribution of soils were developed (e.g., Arya and Paris, 1981; Haverkamp and Parlange, 1986). The Arya and Paris (1981) model relates pore radius to the pore volume for fractions of particle-sizes along the particle-size distribution curve. Although this model is the most commonly used pedotransfer model, it has been criticized for it's non-unique pore-

size/particle-size relationship in the basic equation of the model (Haverkamp and Parlange, 1986).

3.2.2 Motivation

The Haverkamp and Parlange (H&P) model was selected to examine application to the STVZ deposits because it was developed for sandy soils similar in texture to the deposits located at the STVZ site and because the model includes predictions of hysteretic curves. The model was modified as part of this study in order to predict the van Genuchten fitting parameters rather than the Brooks and Corey parameters. The van Genuchten parameter estimation model was also based on shape similarities between the particle-size distributions and the pore-size distributions, along with additional parameter correlations (Chapter 2).

3.2.3 Hypotheses

The Haverkamp and Parlange (1986) pedotransfer model was originally calibrated using 10 sandy soils exhibiting lower air entry pressures and steeper moisture retention slopes (higher values for λ) than the curve fitting parameters measured for the STVZ samples (Table 3.1).

Table 3.1 – Moisture retention curve fitting parameters for the STVZ samples and the sandy soils used in the original Haverkamp and Parlange (1986) model. The model parameters represent population mean values +/- population standard deviation.

Samples	Range of Bulk Densities (g/cc)	Range of Particle Sizes (mm)	h_{ae} (cm)	λ
H&P model sandy soils	1.50 to 1.75	0.2 to 0.5	28.78 +/- 7.42	1.87 +/- 0.48
STVZ sandy alluvial deposits	1.47 to 1.68	0.13 to 0.45	37.36 +/- 13.93	1.42 +/- 0.53

The differences in parameters are similar to the differences described in Chapter 2 between soils and deep vadose zone alluvial deposits of similar texture. Differences in moisture retention properties will lead to differences in parameter correlation between pore-size distributions and particle-size distributions. For this reason, we hypothesize that the H&P model will require calibration to individual geologic environments. To test this hypothesis, model results were compared between the H&P model and an empirical model calibrated to the STVZ infiltration test site deposits. To examine the optimum range of sample texture and porosity for model application, both the H&P model and the empirical model were used to estimate curves for well sorted, moderately sorted, and poorly sorted sandy alluvial deposits repacked at various bulk densities (referred to as fabricated samples).

In addition, we hypothesize that the size of the sample set used for model calibration, the number of measured moisture retention data points, and laboratory measurement error associated with pore-size and particle-size distribution data will impact model predictions. To test this hypothesis, a model sensitivity analysis was conducted to examine optimum conditions for model application.

3.2.4 Chapter Outline

This chapter includes a discussion of the basic theory behind the Haverkamp and Parlange (1986) pedotransfer model, application of the model to the STVZ site deposits, and model application results. Development and application of an empirical predictive model for estimating van Genuchten fitting parameters from the correlations presented in Chapter 2 are then presented. In conclusion, optimum conditions for model application based on results of a model sensitivity analysis are discussed, followed by recommendations for future work

3.3 Haverkamp and Parlange (1986) Model Theory

The objective of the Haverkamp and Parlange (1986) pedotransfer model is to predict soil moisture retention curves during either a wetting or draining process from direct measurements of the particle-size distribution, bulk density, and saturation of a soil (referred to in this chapter as "static material properties"). The model is calibrated using input parameters obtained from direct measurements of these static material properties using a representative sample set.

The Haverkamp and Parlange (1986) model is based on the shape similarity between the moisture characteristic curve and the particle-size distribution function. The particle-size distribution is described by a form of the van Genuchten (1980) equation for uniform sandy soils without organic matter by

$$F(d) = \left[1 + \left(\frac{d_g}{d} \right)^{n_d} \right]^{-\left(1 - 1/n_d\right)} \tag{3-1}$$

where $F(d)$ is the fraction finer than grain diameter (d), d_g represents the average grain diameter of the medium, and n_d is the slope of the particle-size distribution. The relationship between pore-size distributions (represented by the MCC) and $F(d)$ is based on the fundamental relationship between capillary pressure head (h) assumed to equal negative pressure head (cm), and the pore radius (R, also in cm) described by

$$h = \frac{2\sigma}{R\rho_w g} \tag{3-2}$$

where σ is the interfacial surface tension between water and air, g is the gravitational constant, and ρ_w is the density of water. For soils of similar texture (e.g., grain geometry

and grain size) without swelling particles, the grain diameter is related to the pore radius through the packing arrangement of the grains by

$$d = \gamma R \tag{3-3}$$

where the packing parameter *(γ)* varies as a function of grain texture and is assumed to be constant for soils of similar textures. The relationship between capillary pressure head and the grain diameter is determined by substituting (3-3) into (3-2) for pore radius *(R)* by

$$h = 0.149 \frac{\gamma}{d} \tag{3-4}$$

where 0.149 (cm^2) is the product of $2\sigma/\rho_w g$ in (3-2) at a constant temperature of 20 ^oC.

Haverkamp and Parlange (1986) suggest that the relationship between the particle diameter (*d*) and the pore radius (*R*) expressed in (3-3) relates pore fraction to the relative solid fraction of particles by

$$S(R) = F(d) \tag{3-5}$$

where S is the degree of saturation (θ / θ_s), θ is the volumetric moisture content, and θ_s is saturation. Haverkamp and Parlange (1986) define the moisture content as a function of the particle size distribution by

$$\theta = \theta_s F(d) \tag{3-6}$$

and derive equations for predicting moisture characteristic curves from particle-size distribution data by combining (3-6) with the Brooks and Corey (1964) model for calculating θ as a function of *h* by

$$\theta = (\theta_s - \theta_r) * \left[\frac{h_{ae}}{h} \right]^{\lambda} + \theta_r \tag{3-7}$$

where θ_r is residual moisture content assumed to equal zero in the model, h_{ae} is air entry pressure (cm), and λ is a fitting parameter describing the slope of the moisture characteristic curve. Because (3-7) does not account for hysteresis, Haverkamp and Parlange (1986) modify (3-7) to calculate $\theta(h)$ during draining and wetting sequences. For the MWC (Figure 3.1), the model equation for calculating the moisture content for *h* greater than h_{ae} is

$$\theta = \frac{\phi}{1+\lambda}\left[\frac{h_{ae}}{h}\right]^{\lambda} \tag{3-8}$$

where ϕ is porosity defined by

$$\phi = 1-\left(\frac{\rho_d}{\rho_p}\right) \tag{3-9}$$

ρ_d is the soil dry bulk density and ρ_p is the particle density assumed to equal 2.65 g/cc. The moisture content for *h* greater than h_{we} (water entry pressure) and less than h_{ae} for the MWC (Figure 3.1) is

$$\theta = \phi\left[1-\left(\frac{\lambda}{1+\lambda}\right)\frac{h}{h_{ae}}\right]. \tag{3-10}$$

For the MDC (Figure 3.1), the moisture content for *h* greater than h_{ae} is

$$\theta = \phi\left[\frac{h_{ae}}{h}\right]^{\lambda}\left[1-\frac{h_{ae}}{h}\left(1-\frac{\theta_s}{\phi}\right)\right] \tag{3-11}$$

For the MDC and the MWC, θ_s is assumed to equal natural field saturation, (approximately equal to 80-90% porosity due to entrapped air). The moisture content for *h* less than or equal to h_{ae} for the MDC and h_{we} for the MWC is

$$\theta = \theta_s \tag{3-12}$$

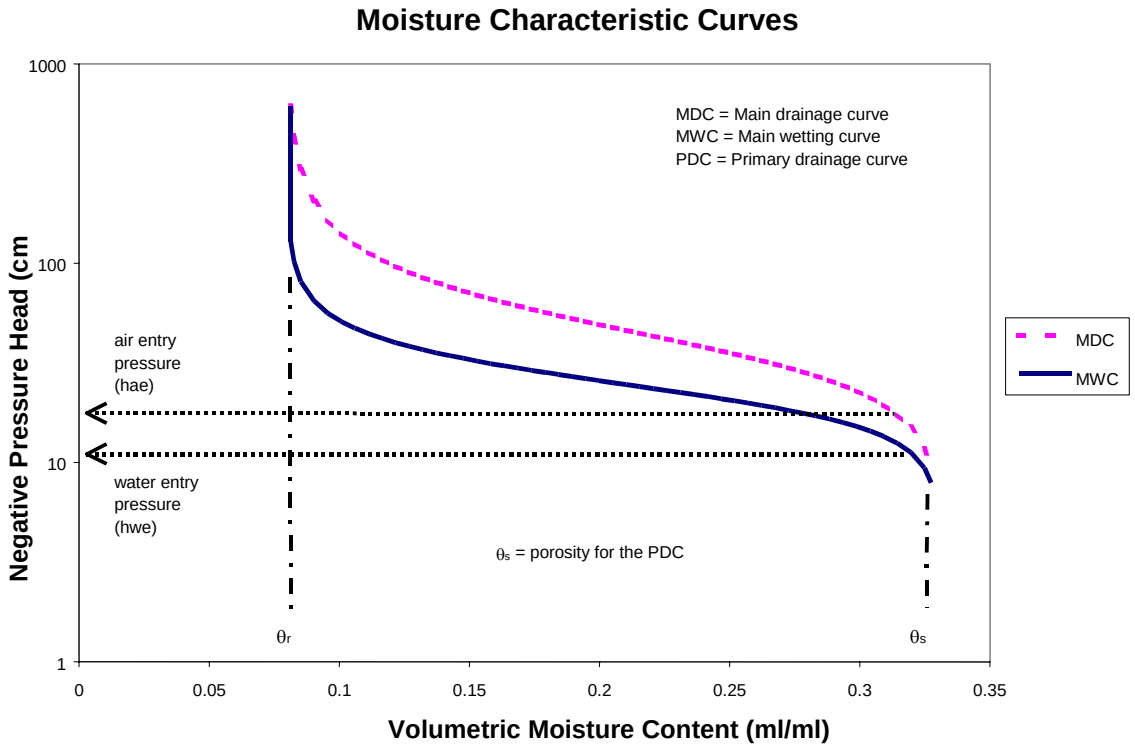

Figure 3.1 – Moisture characteristic curves showing hysteresis in air entry pressure values. Air entry pressure is determined from fitting the Brooks and Corey equation (3-10 for the MWC and 3-11 for the MDC) to measured data.

For the PDC, (3-11) and (3-12) are used to calculate $\theta(h)$, assuming θ_s is equal to ϕ (void of entrapped air).

The Haverkamp and Parlange (1986) model was originally calibrated through regression analysis of moisture retention measurements during desorption from field saturation, dry bulk density measurements, and particle-size distribution measurements of 10 sandy soils ranging in particle sizes from 0.2 to 0.5 mm in diameter. The estimated fitting parameter ($\hat{\lambda}$) is defined by

$$\hat{\lambda} = a1(\rho_d{}^{a2})(n_d - 1) \qquad (3\text{-}13)$$

where "^" represents the parameter estimate and the coefficients a1 and a2 are fitting parameters. The estimated air entry pressure ($\hat{h}_{ae}$) is defined by

$$\hat{h}_{ae} = \frac{\hat{\gamma}^* 0.149}{d_g}\left(\left[\frac{\theta_{ae}}{\phi}\right]^{-1/m_d} - 1\right)^{-1/n_d} \frac{h_{ae}}{h(\theta_{ae})} \tag{3-14}$$

where $\hat{\gamma}$ is the estimated packing parameter defined by

$$\hat{\gamma} = b1 + b2\,\hat{\lambda} + b3\,\hat{\lambda}^2 \tag{3-15}$$

and b1, b2, and b3 are fitting parameters determined from regression analysis of the plot of γ, (calculated from (3-4) using h_{ae} and d_g) versus the estimated slope of the moisture retention curve ($\hat{\lambda}$) for the sample set. The estimated packing parameter can be calculated from either the wetting or drying boundary curve, leading to two different values: γ_{wet} or γ_{dry}. Since the two parameters are strictly related to one another, the two boundary curves can be used interchangeably.

θ_{ae} is the moisture content along the wetting curve at air entry pressure defined by

$$\theta_{ae} = \frac{\phi}{1+\hat{\lambda}} \tag{3-16}$$

$\frac{h_{ae}}{h(\theta_{ae})}$ represents the ratio of the packing parameter during the wetting cycle to the packing parameter during the draining cycle $\left(\gamma_{wet}/\gamma_{dry}\right)$ defined by

$$\frac{h_{ae}}{h(\theta_{ae})} = \left[\left(1+\hat{\lambda}\right)\left(1 - \frac{h_{ae}}{h(\theta_{ae})}\left[1 - \frac{\theta_s}{\phi}\right]\right)\right]^{-1/\hat{\lambda}} \tag{3-17}$$

Equation (3-17) is solved iteratively for the MWC, the MDC, and all scanning curves, but reduces to

$$\frac{h_{ae}}{h(\theta_{ae})} = \left(1+\hat{\lambda}\right)^{-1/\hat{\lambda}} \tag{3-18}$$

for the PDC where saturation equals porosity. Haverkamp and Parlange (1986) define the model parameter estimation coefficients a1, a2, b1, b2, and b3 in equations (3-13) and (3-15) to be 0.0723, 3.8408, 17.1736, -4.7043, and 0.1589, respectively. The coefficient of determination for regression analysis was 0.981 and 0.993 for equations (3-13) and (3-15), respectively, suggesting good correlation between parameters used in model calibration.

3.4 Haverkamp and Parlange (1986) Model Application to the STVZ Samples

3.4.1 Methods

The H&P model was initially applied to estimate hydraulic properties of samples collected from the STVZ infiltration test site assuming the original model coefficients a1, a2, b1, b2, and b3 were valid for the STVZ site deposits. The model was then calibrated using input parameters determined from a representative sample set of the site deposits to obtain empirical coefficients for (3-13) and (3-15). The estimated parameters $\hat{\lambda}$ and $\hat{h}_{ae}$ were then used from each model scenario (H&P model and empirical model) to estimate $\theta(h)$ curves during desorption (PDC) using (3-11) and (3-12) for all the measured STVZ and fabricated samples. The estimated curves were then compared to the original Brooks and Corey fit to measured data. The coefficient of determination (R^2) for the estimated curves and the direct Brooks and Corey fit to data does not include fits to data in the very dry or very wet range of measurements due to

measurement uncertainty in these regions of the curves (Chapter 2). The model also assumes a residual moisture content of zero, which does not agree with measured data in the dry range for a majority of the STVZ samples, possibly due to lack of hydraulic contact during drainage.

3.4.2 Model calibration to the STVZ Deposits

A set of 15 sandy alluvial STVZ site samples was selected for model calibration. The model input parameters required for calibration are the Brooks and Corey fitting parameters (h_{ae} and λ), porosity (ϕ) calculated from dry bulk density, dry bulk density (ρ_d), slope of the particle-size distribution function (n_d), and mean grain diameter (d_g). The empirical coefficients a1 and a2 for estimation of the particle index ($\hat{\lambda}$) were determined from regression analysis of the plot of $\lambda/(n_d - 1)$ versus the measured dry bulk density (ρ_d) (Figure 3.2). The Brooks and Corey fitting parameters λ and h_{ae} were determined from linear regression analysis of the logarithmic plot of measured moisture content and pressure data (fitting the log of (3-11) to the log of the measured data). The van Genuchten fitting parameters n_d and d_g were determined by fitting (3-1) to the measured particle-size distribution data for each sample (Appendix I includes detailed procedures for the Brooks and Corey fit to moisture retention data and the van Genuchten fit to the particle size data). The empirical coefficients b1, b2, and b3 for estimation of the packing parameter ($\hat{\gamma}$) were determined from regression analysis of the plot of γ versus $\hat{\lambda}$ (Figure 3.3). The parameter γ was calculated from (3-4) using h_{ae} and d_g obtained from the Brooks and Corey equation fit to data. Model input parameters used in calibration are listed in Table 3.2. Appendix L describes detailed

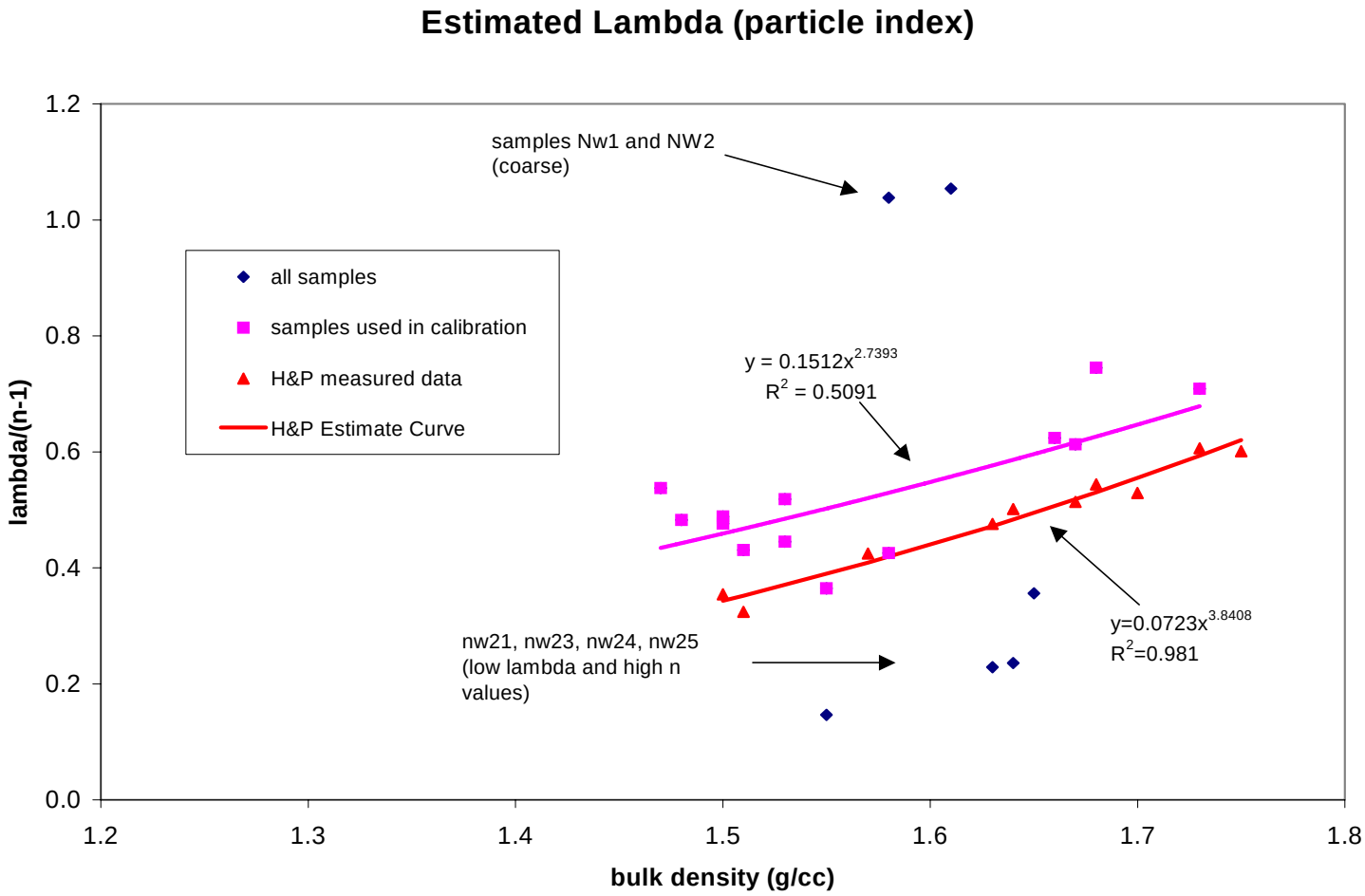

Figure 3.2 – Regression analysis of curve fitting parameters (λ / (n_d-1)) versus bulk density for the STVZ site deposits. Data for the samples used in the original model calibration are included in the plot for comparison.

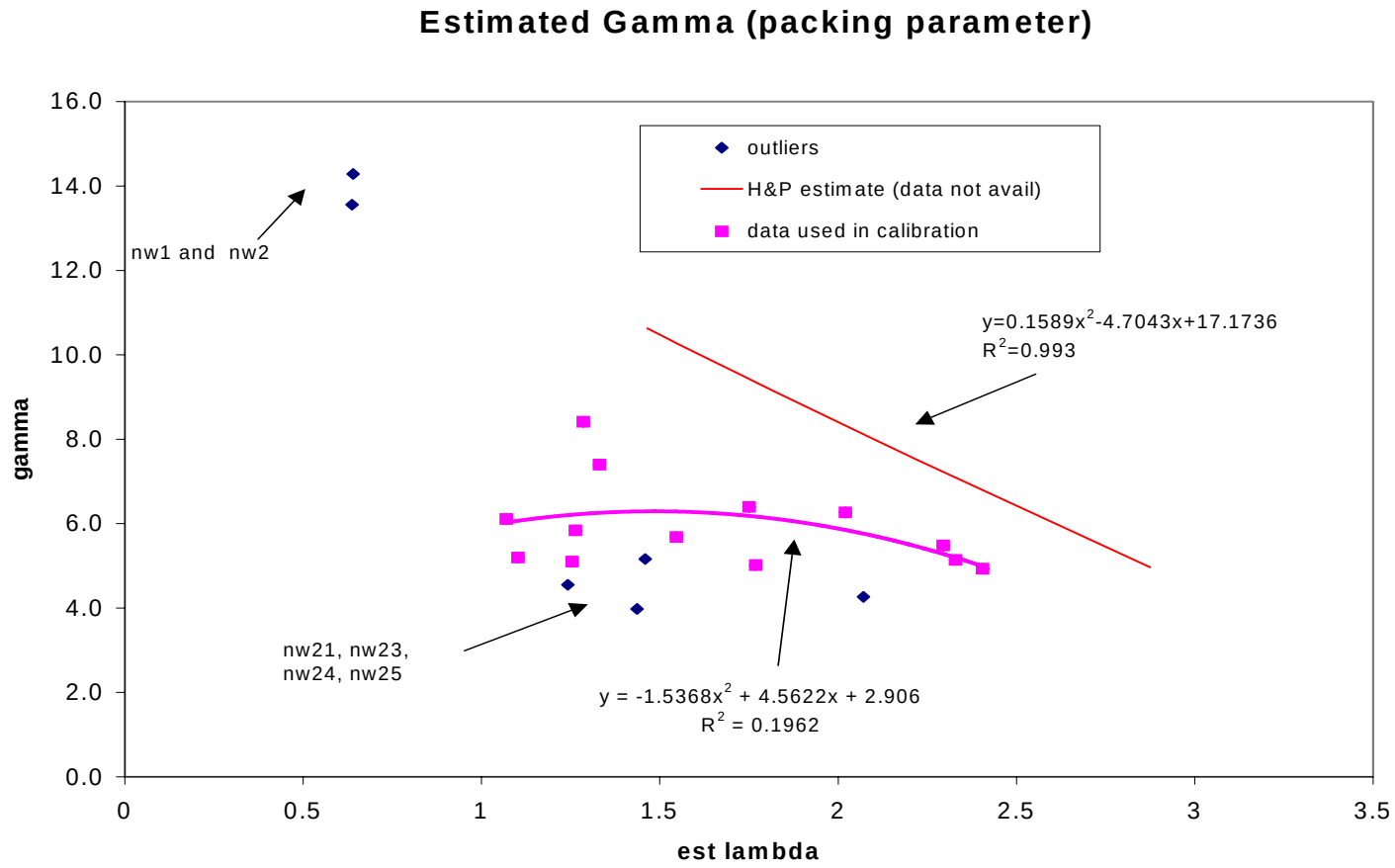

Figure 3.3 – Regression analysis of packing parameter (γ) versus estimated particle index (λ) values for the STVZ samples. The curve obtained in the original model calibration is included for comparison. The data used to obtain the curve was not available, however R^2 is shown for the fit to data

Table 3.2 – Model input parameters used in model calibration for application to the STVZ site deposits.

sample	h_{ae} cm	λ	n_d(PSD)	d_g(PSD) mm	γ	B_d g/cc	Porosity
NW1	16.386	1.249	2.203	1.458	16.034	1.77	0.336
NW2	18.473	1.211	2.149	1.249	13.241	1.69	0.376
NW4	21.165	2.080	4.334	0.452	6.421	1.65	0.378
NW7	31.560	1.042	3.492	0.248	5.253	1.51	0.413
NW9	34.408	1.343	2.499	0.427	9.861	1.66	0.363
NW10	31.768	1.034	3.207	0.284	5.584	1.50	0.372
NW12	43.626	1.364	3.909	0.197	5.768	1.47	0.399
NW16	52.427	1.675	5.998	0.133	4.680	1.45	0.399
NW17	52.202	2.138	5.805	0.149	5.220	1.53	0.399
NW19	66.950	1.123	4.079	0.133	5.976	1.47	0.400
NW20	46.745	2.254	5.543	0.175	5.490	1.50	0.387
NW21	46.581	1.858	5.123	0.183	5.721	1.55	0.424
NW22	49.292	1.630	4.783	0.157	5.194	1.51	0.383
NW24	30.148	0.872	3.264	0.267	6.106	1.63	0.389
NW27	27.464	2.083	3.455	0.375	7.184	1.68	0.381

procedures used in model calibration and includes plots showing the Brooks and Corey fit to the PDC data. Appendix H includes plots showing the van Genuchten fit to the PSD data. Porosity was calculated from bulk density values assuming a particle density of 2.65 g/cc. Unlike the H&P model regression analysis which shows good correlation between model parameters, the coefficient of determination (R^2) for empirical estimation of the particle index (λ) and the packing parameter (γ) was less than 0.80 suggesting a weak relationship between model parameters. Measurement error, the small sample set used for calibration (15 samples) and/or the limited number of data points measured along

the moisture characteristic curve (resulting in uncertainty in λ) may have contributed to these poor parameter correlations.

3.4.3 Air Entry Pressure Estimation Equations

Haverkamp and Parlange (1986) based the derivation of (3-14) on properties associated with a wetting sequence, assuming a hysteretic relationship between the MWC and the MDC, which may not be valid. For this reason, an alternative equation was used to estimate air entry pressure ($\hat{h}_{ae}$) from the estimated packing parameter ($\hat{\gamma}$) and the average particle diameter (d_g) for each sample by

$$\hat{h}_{ae} = \frac{\hat{\gamma} * 0.149}{d_g}. \qquad (3\text{-}19)$$

For comparison, moisture characteristic curves were estimated using both (3-14) and (3-19) to predict air entry pressure, then the estimated pressures were compared to pressures determined from direct methods (i.e., fitting the Brooks and Corey equation to measured PDC data).

3.4.4 Haverkamp and Parlange (1986) Model Results

The best model results were obtained using the empirical model equations for estimating λ and γ and equation (3-19) for estimating h_{ae}. Predictions for samples used in model calibration were much better than predictions for samples not used in calibration. Predictions made using the H&P model equations show similar slopes to curves obtained using the empirical equations, however, the estimate of air entry pressure was lower in most cases. This suggests that equation (3-19) provides better estimates of air entry pressure for the STVZ samples than (3-14).

Figures 3.4 and 3.5 represent examples of the best model results for the STVZ samples, while Figures 3.6 and 3.7 represent examples of the worst model results for the STVZ samples. Refer to Appendix M for model results for all the STVZ samples collected in the NW quadrant of the infiltration test site. The model results include the original Brooks and Corey (1964) model fit to data (B&C fit to data), estimated curves using the empirical model equations (calibrated fit) and estimated curves using the H&P model equations (H&P estimate). The coefficient of determination (R^2) does not represent curve fits to data in the extreme dry or wet range of measured data due to measurement uncertainty in these regions.

3.5 Haverkamp and Parlange (1986) Model Application to the Fabricated Samples

3.5.1 Purpose

To examine the optimum range of textures and bulk densities valid for model application using the STVZ empirical model equations, 10 samples (with 1 replicate each) were fabricated with varying grain sizes, sorting, and bulk densities. Sands collected from the STVZ site were sieved and sorted into narrow ranges of grain diameters, then were repacked to represent samples of well sorted, moderately sorted, and poorly sorted samples for median grain diameters of 0.16 mm (fine grained sands) and 0.50 mm (medium grained sands). Each set of samples was repacked to a high bulk density (~1.80 gcm^{-1}) and a low bulk density (~1.40 gcm^{-1}), however, after the samples were saturated and allowed to drain, the grains settled to a more uniform bulk density of approximately 1.75 g cm^{-1} (Table 3.3).

3.5.2 Model Application

The STVZ sample empirical model was initially used to estimate moisture retention parameters for the fabricated samples to determine how well the model works

Sample Number NW4

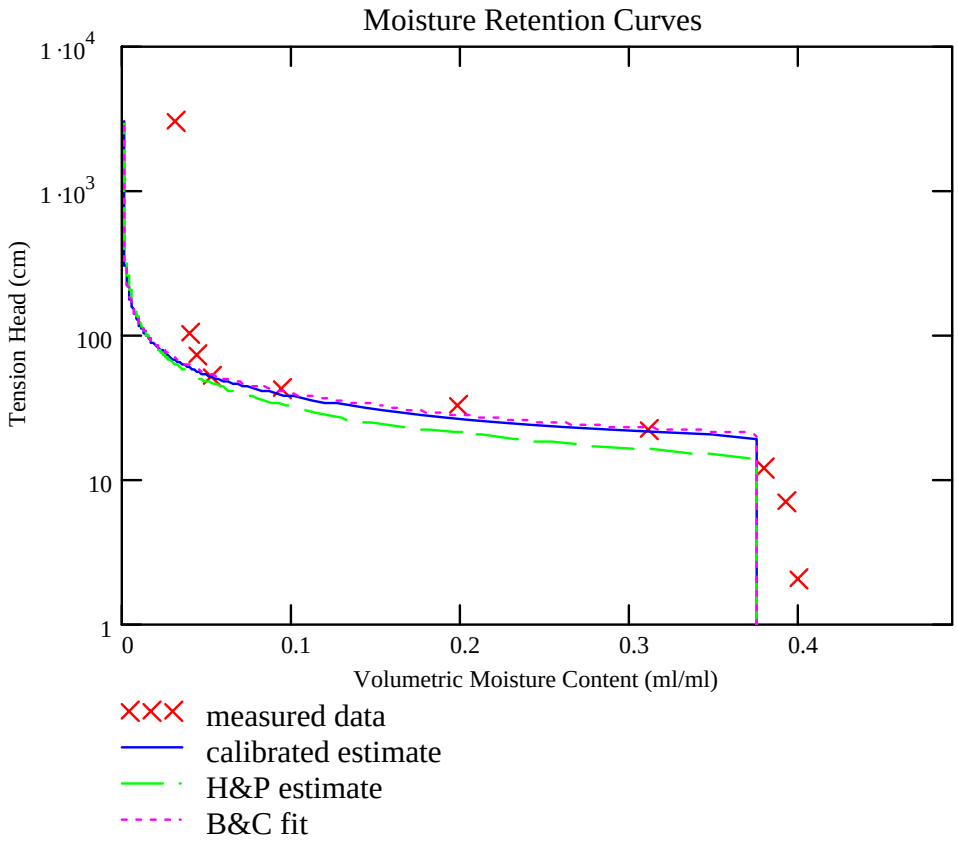

RSQ1 = 0.883
RSQ2 = 0.284
RSQ3 = 0.936

RSQ1= R^2 for calibrated estimate
RSQ2=R^2 for H&P estimate
RSQ3 = R^2 for B&C fit to data

Figure 3.4 – Example of the moisture retention curve estimates for sample number NW4.

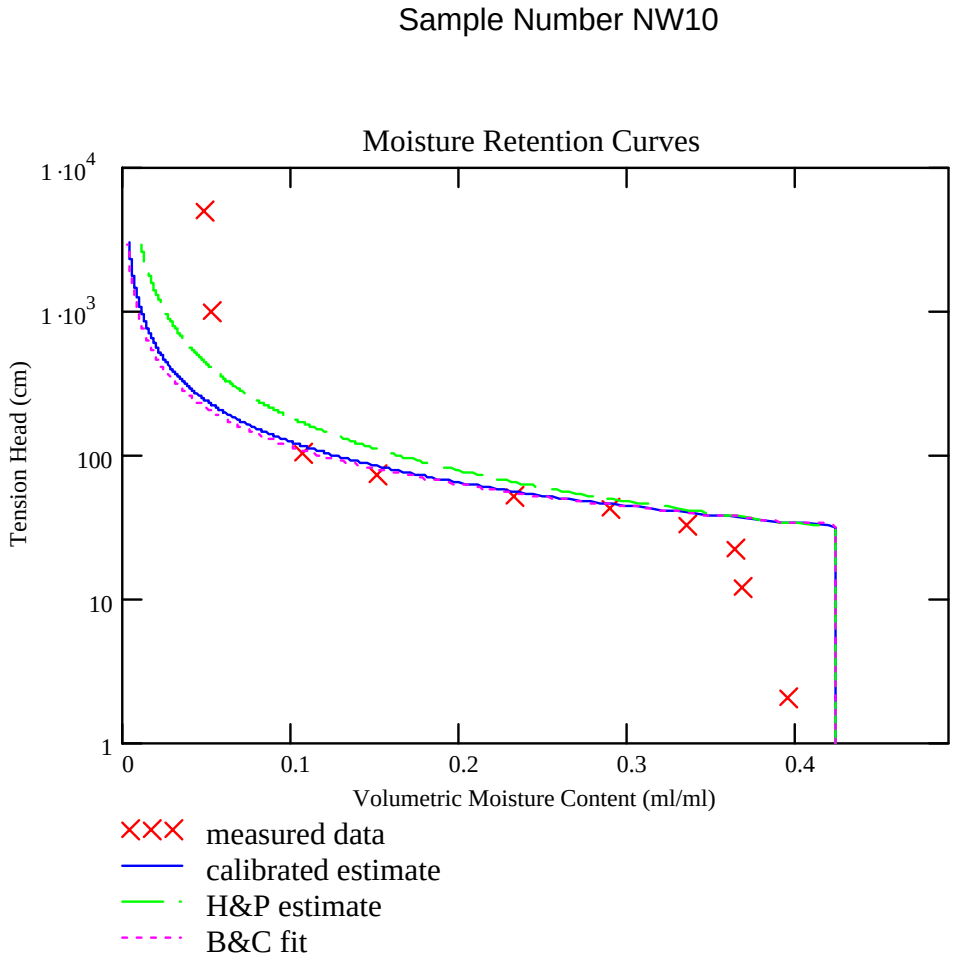

Figure 3.5 – Example of the moisture retention curve estimates for sample number NW10.

Sample Number NW2

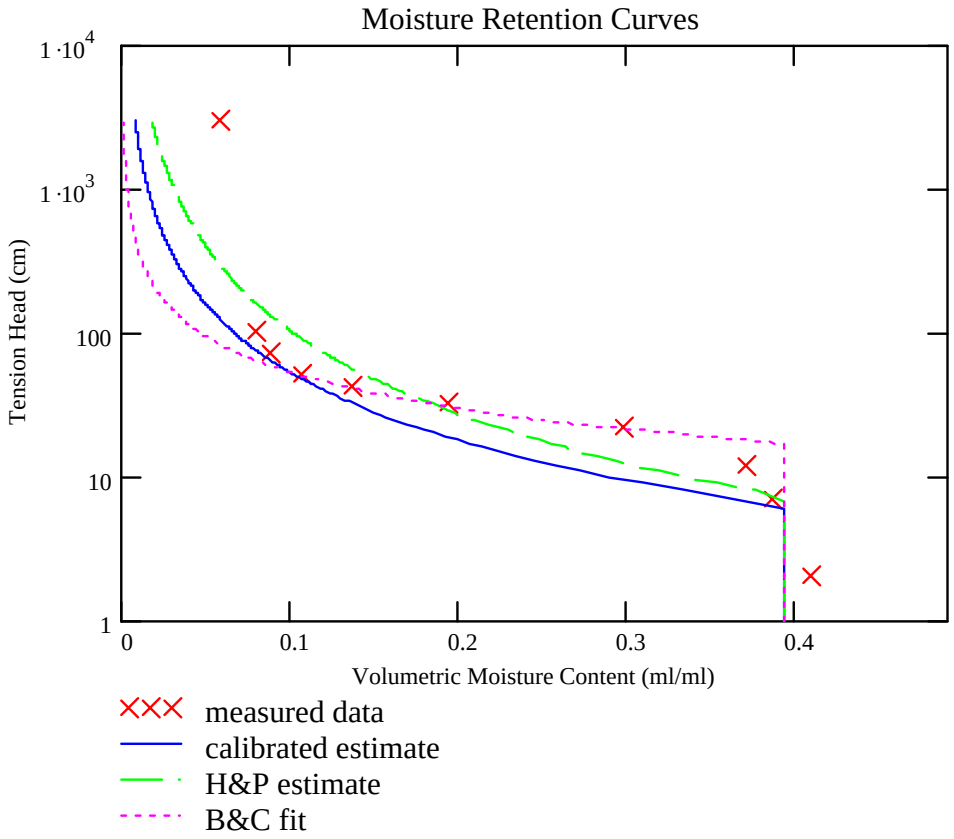

RSQ1 = 0.345
RSQ2 = 0.694
RSQ3 = 0.979

RSQ1= R^2 for calibrated estimate
RSQ2=R^2 for H&P estimate
RSQ3 = R^2 for B&C fit to data

Figure 3.6 – Example of the moisture retention curve estimates for sample number NW2. This sample was not used in model calibration to the STVZ samples due to poor correlation between parameters.

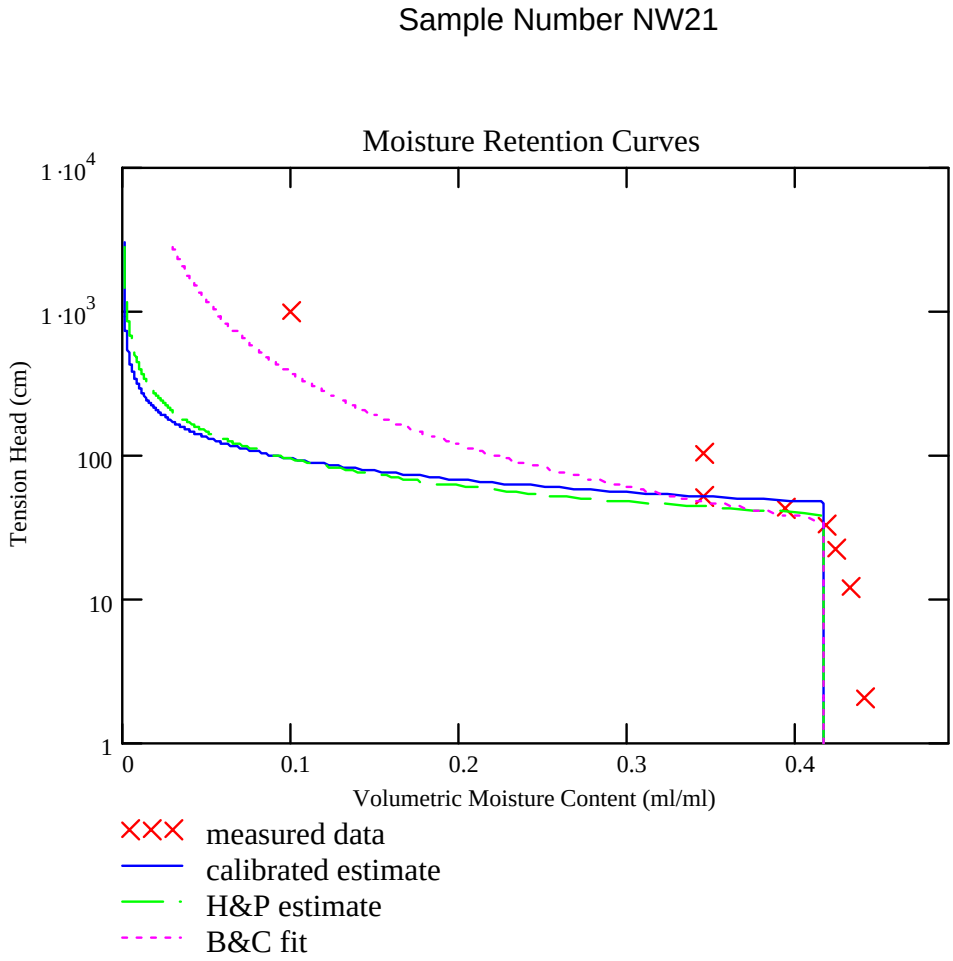

Figure 3.7 – Example of the moisture retention curve estimates for sample number NW21. This sample was not used in model calibration to the STVZ samples due to poor correlation between parameters.

Table 3.3 – Fabricated sample descriptions.

Sample Replicates	Median Grain Diameter	Sorting	Final Bulk Density (g/cc)
A1	0.16mm	poor	1.72
A2	0.16mm	poor	1.76
B1	0.5mm	poor	1.84
B2	0.5mm	poor	1.79
C1	0.16mm	poor	1.67
C2	0.16mm	poor	1.66
D1	0.5mm	poor	1.74
D2	0.5mm	poor	1.70
E1	0.16mm	moderate	1.67
E2	0.16mm	moderate	1.58
F1	0.5mm	moderate	1.80
F2	0.5mm	moderate	1.80
G1	0.16mm	moderate	1.67
G2	0.16mm	moderate	1.54
H1	0.5mm	moderate	1.74
H2	0.5mm	moderate	1.74
I1	0.16mm	well	1.55
K1	0.16mm	well	1.58
J1	0.5mm	well	1.63
L1	0.5mm	well	1.64

for samples with a large range of physical properties. The model was then calibrated to the fabricated samples in an attempt to improve model estimates. The fabricated sample empirical equations obtained from regression analysis are shown in Figures 3.8 and 3.9. The data used in the STVZ empirical model calibration and the data used in the H&P model calibration are plotted in Figures 3.8 and 3.9 for comparison. Note the narrower

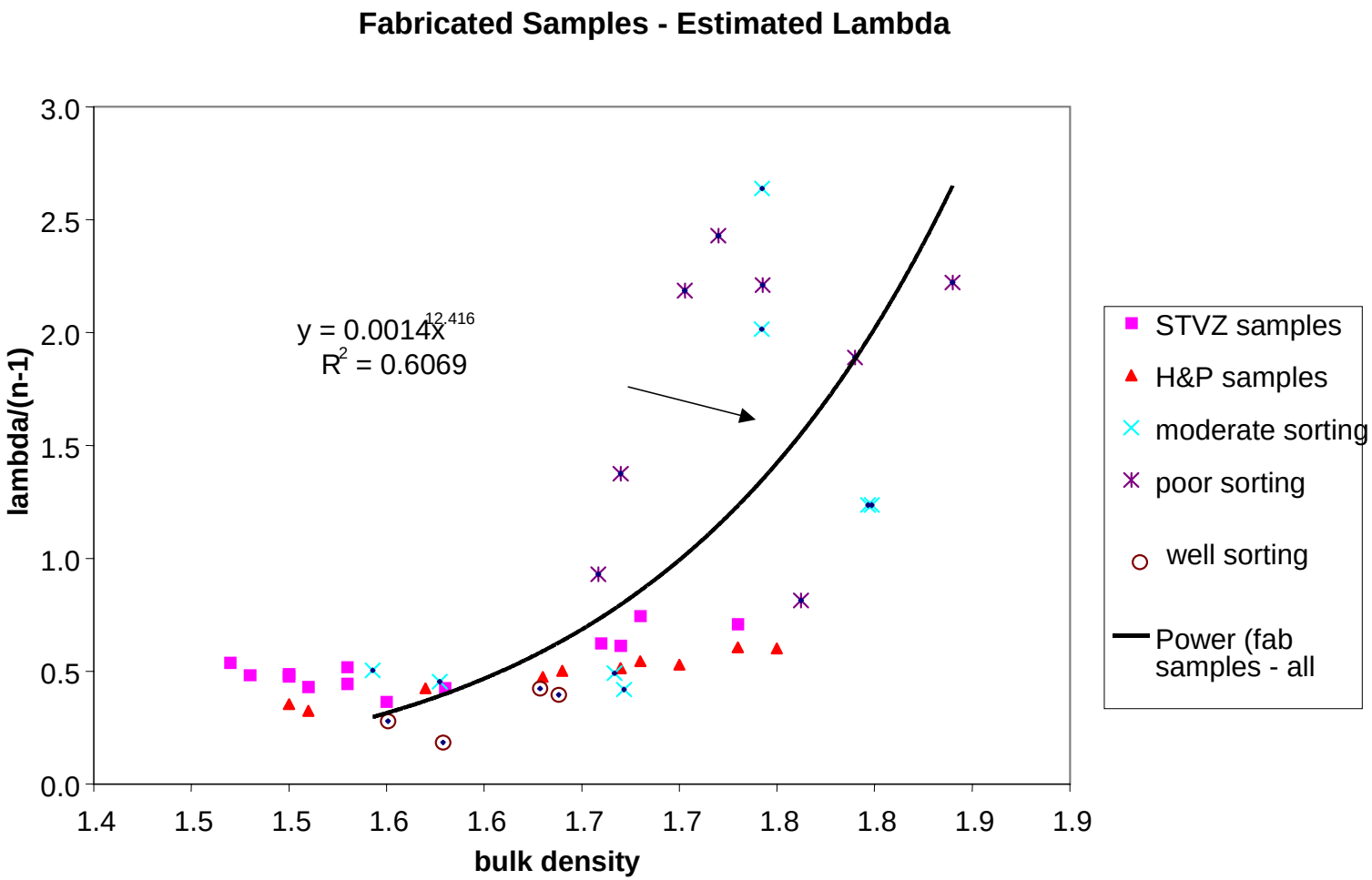

Figure 3.8 – Estimate of the model parameter λ for the fabricated samples.

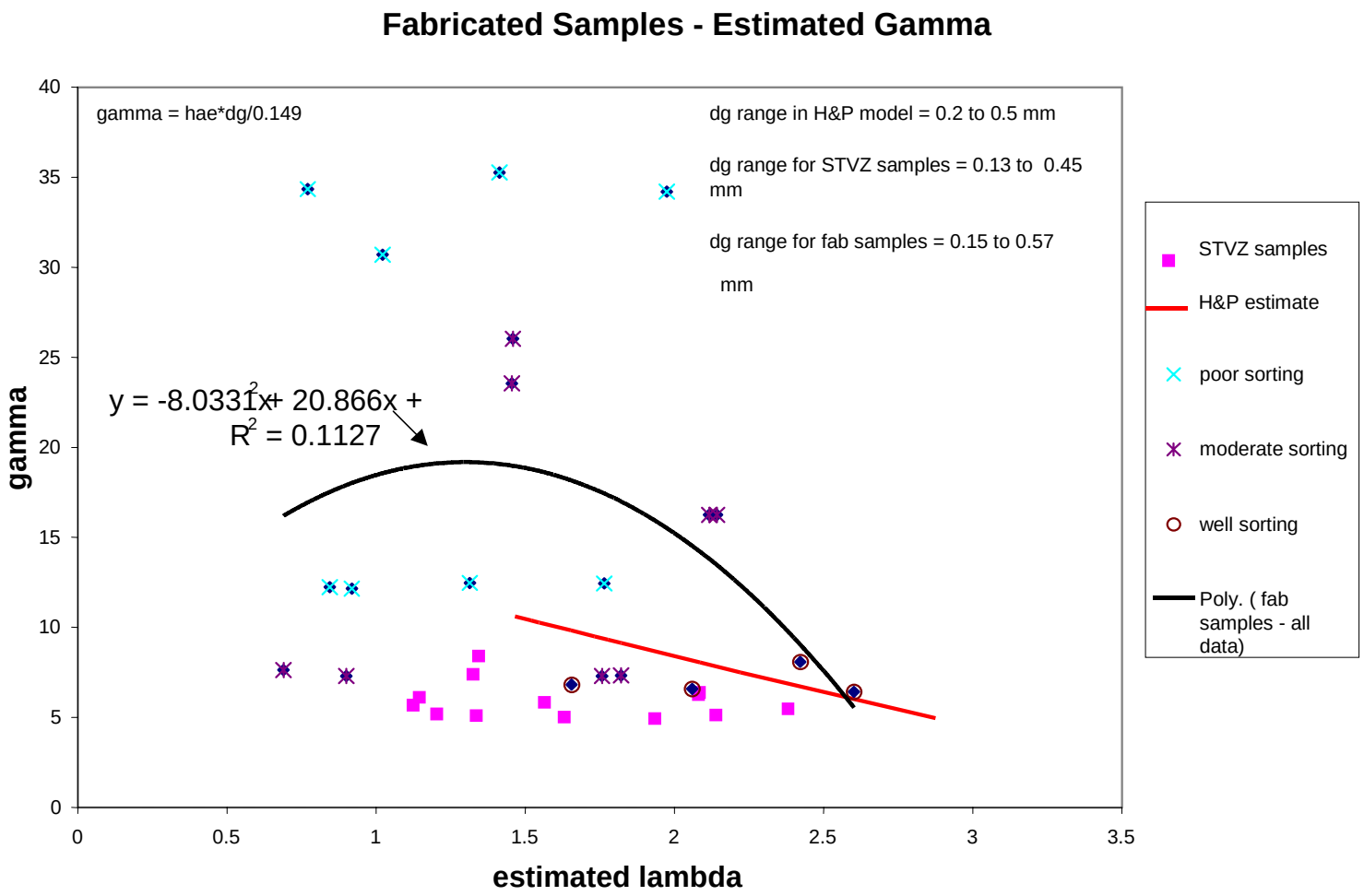

Figure 3.9 – Estimate of the model parameter γ for the fabricated samples.

range of $\lambda/(n-1)$ for both the STVZ and H&P model data than for the fabricated samples.

In particular, the poorly sorted and moderately sorted fabricated samples packed at high bulk densities (greater than 1.75 g/cc) have a much higher ratio of $\lambda/(n-1)$ than the values observed for both the STVZ samples and the H&P samples. The regression analysis curve for the estimated packing parameter (γ) for the fabricated samples (Figure 3.9) also shows much higher values for γ for the poorly sorted and moderately sorted samples packed to high bulk densities than for the STVZ samples or the H&P samples. Because of the distinct differences in these values, the model was calibrated separately for poorly sorted and moderate to well sorted samples.

Appendix N describes the calibration procedures and results for the fabricated samples, including all attempts to improve parameter estimates by calibrating to different sample types (e.g., well sorted, moderately sorted, etc.)

3.5.3 Results

Direct model calibration to the fabricated samples did not improve the estimates for the majority of the fabricated samples compared to estimates obtained using the STVZ sample empirical model. In fact the estimates were worse for most of the samples, with exception for the well sorted samples. This may have been due to a wide scatter in the parameter values observed in regression analysis (Figures 3.8 and 3.9). For this reason, only the initial estimates for the fabricated samples (using the STVZ empirical model) and the H&P estimates are included in the results (both this chapter and Appendix N).

Figures 3.10 and 3.11 show estimates for a poorly sorted sample with a high bulk density. Figures 3.12 and 3.13 show estimated curves for a moderately sorted sample with a bulk density similar to the STVZ samples (1.58 g/cc). Figures 3.14 and 3.15 show estimated curves for a sample that was well sorted with a bulk density also similar to the STVZ samples.

The estimated curves shown in the figures include an estimate using the H&P model equations for comparison. In most cases, the H&P model estimates do not estimate the air entry pressure very well, however the slope of the curves are similar to the calibrated estimates. The coefficient of determination (R^2) does not represent a fit to data in the very dry range (greater than 100 cm tension) due to possible lack of hydraulic contact in this region (in addition, the model assumes a residual moisture content of zero).

3.6 Haverkamp and Parlange (1986) Pedotransfer Model Application Conclusions

Both the H&P model and the STVZ empirical model applications to the STVZ sands resulted in predictions very similar to the direct Brooks and Corey (1964) model fit to data for a majority of the samples. Although application of the H&P model resulted in under-estimated air entry pressures, the predictions were much better than anticipated. The STVZ empirical model application to the fabricated samples indicated that sample texture, sorting, and packing significantly impact model results. The results support our hypothesis that pedotransfer models are appropriate for predicting hydraulic properties for deposits of similar textural and physical properties, yet require separate calibration for narrow ranges of particle size distributions and porosities.

Sample Number B1

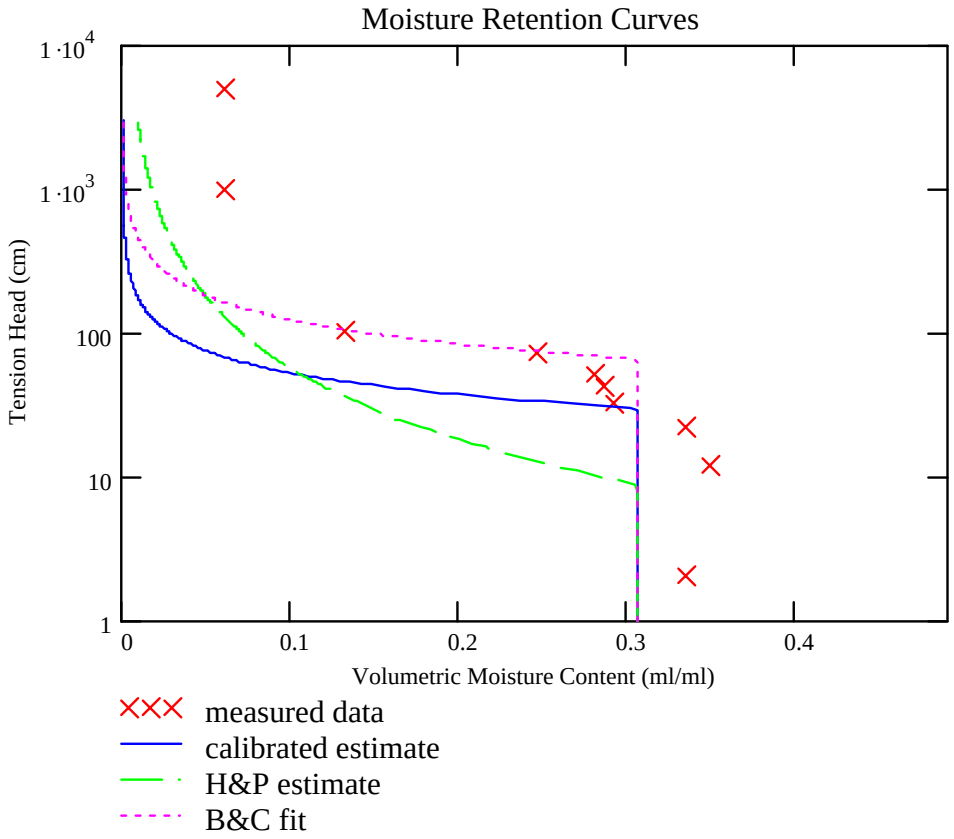

RSQ1 = –1.987
RSQ2 = –3.295
RSQ3 = 0.855

RSQ1= R^2 for calibrated estimate
RSQ2=R^2 for H&P estimate
RSQ3 = R^2 for B&C fit to data

Figure 3.10 – Estimated curves using model estimation equations calibrated to the STVZ samples. Sample B1 has a wide range of particle sizes with a median grain size of 0.50mm. The sample was packed to a high bulk density of 1.84 g/cc.

Sample Number B1

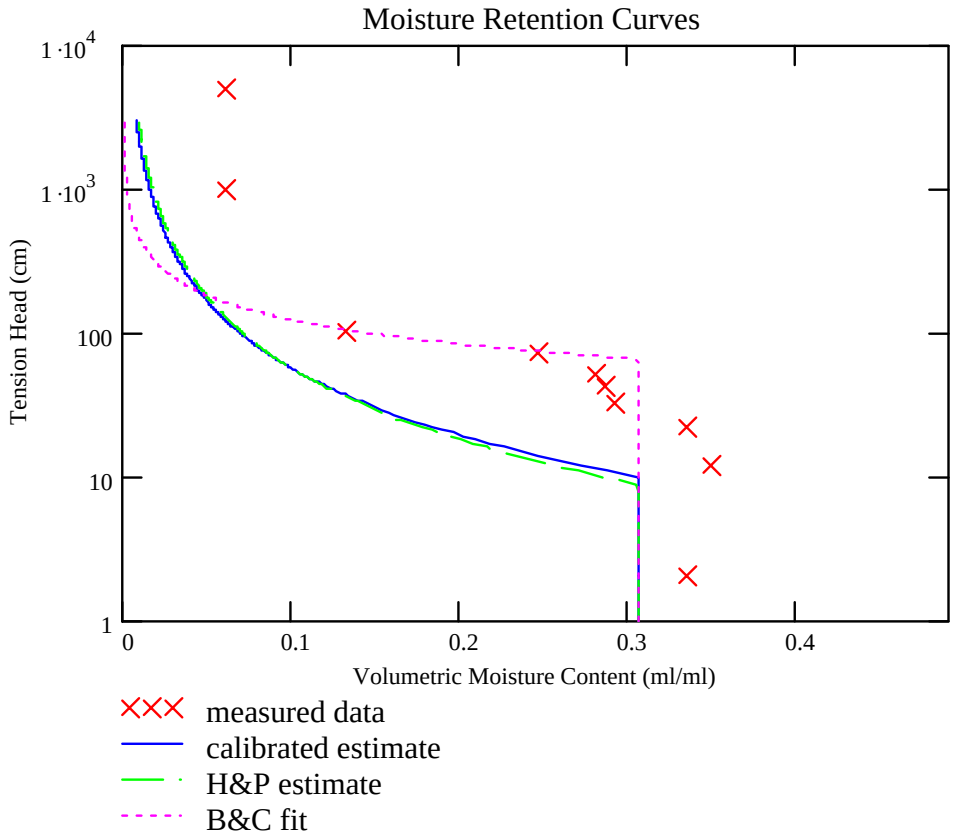

RSQ1 = –3.103
RSQ2 = –3.295
RSQ3 = 0.855

RSQ1= R^2 for calibrated estimate
RSQ2=R^2 for H&P estimate
RSQ3 = R^2 for B&C fit to data

Figure 3.11 – Estimated curves using model estimation equations re-calibrated to the fabricated samples. Sample B1 has a wide range of particle sizes with a median grain size of 0.50mm. The sample was packed to a high bulk density of 1.84 g/cc.

Sample Number E2

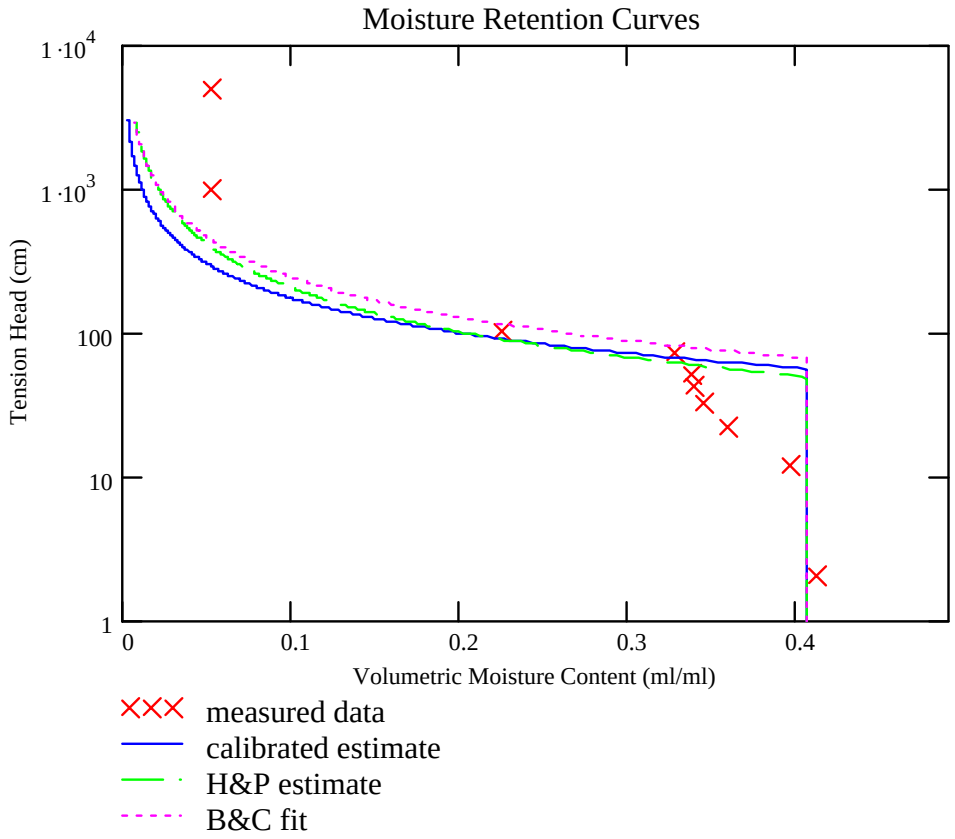

RSQ1 = 0.228
RSQ2 = 0.278
RSQ3 = 0.19

RSQ1= R^2 for calibrated estimate
RSQ2=R^2 for H&P estimate
RSQ3 = R^2 for B&C fit to data

Figure 3.12 – Estimated curves using model estimation equations calibrated to the STVZ samples. Sample E2 has a moderate range of particle sizes with a median grain size of 0.16mm. The sample was repacked to a bulk density of 1.58 g/cc.

Sample Number E2

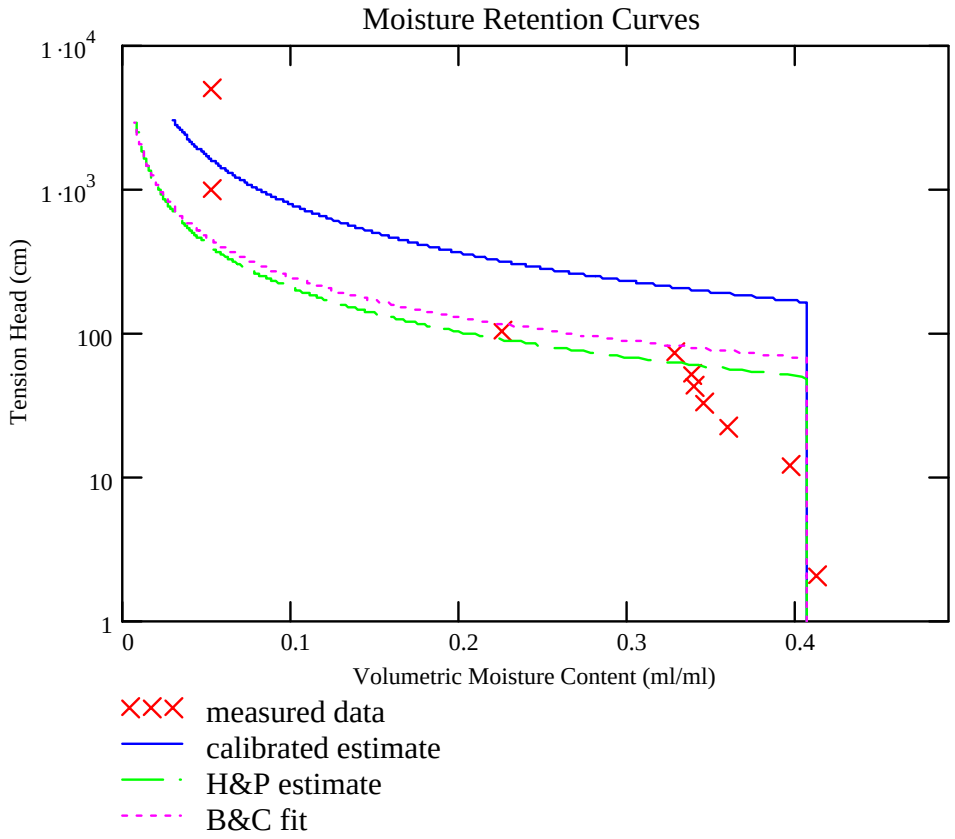

RSQ1 = −1.451
RSQ2 = 0.278
RSQ3 = 0.19

RSQ1= R^2 for calibrated estimate
RSQ2=R^2 for H&P estimate
RSQ3 = R^2 for B&C fit to data

Figure 3.13 – Estimated curves using model estimation equations re-calibrated to the fabricated samples. Sample E2 has a moderate range of particle sizes with a median grain size of 0.16mm. The sample was repacked to a bulk density of 1.58 g/cc.

Sample Number L1

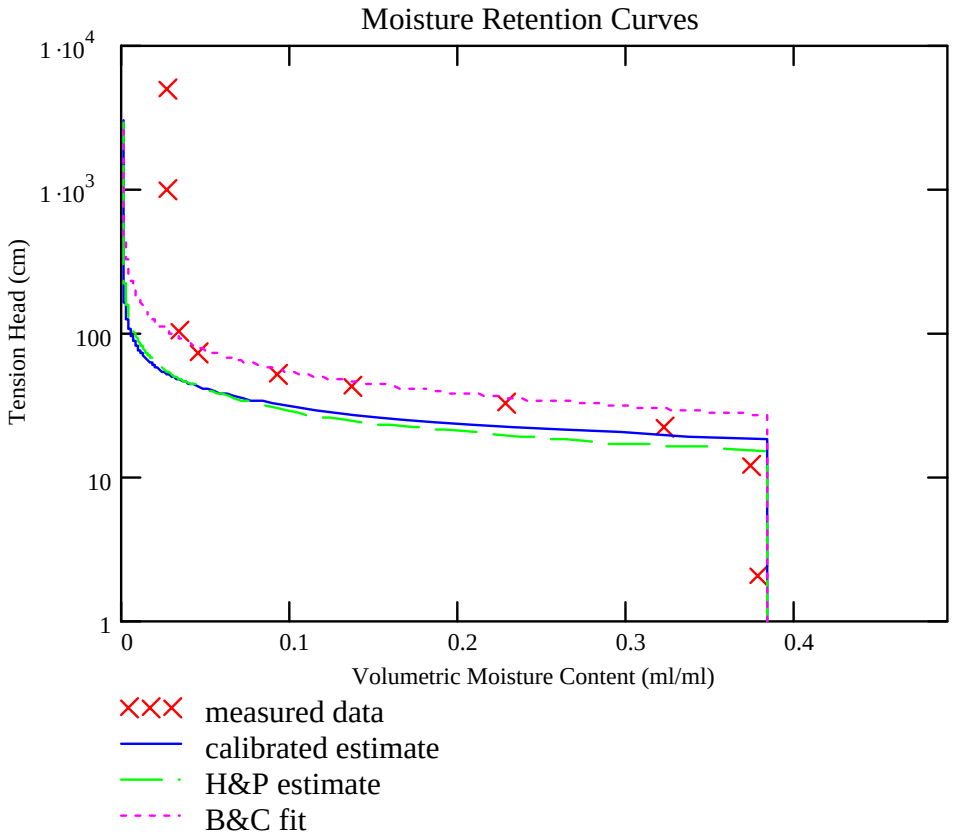

RSQ1 = 0.711
RSQ2 = 0.594
RSQ3 = 0.952

RSQ1= R^2 for calibrated estimate
RSQ2=R^2 for H&P estimate
RSQ3 = R^2 for B&C fit to data

Figure 3.14 – Estimated curves using model estimation equations calibrated to the STVZ samples. Sample L1 has a narrow range of particle sizes with a median grain size of 0.50 mm. The sample was packed to a bulk density of 1.64 g/cc.

Sample Number L1

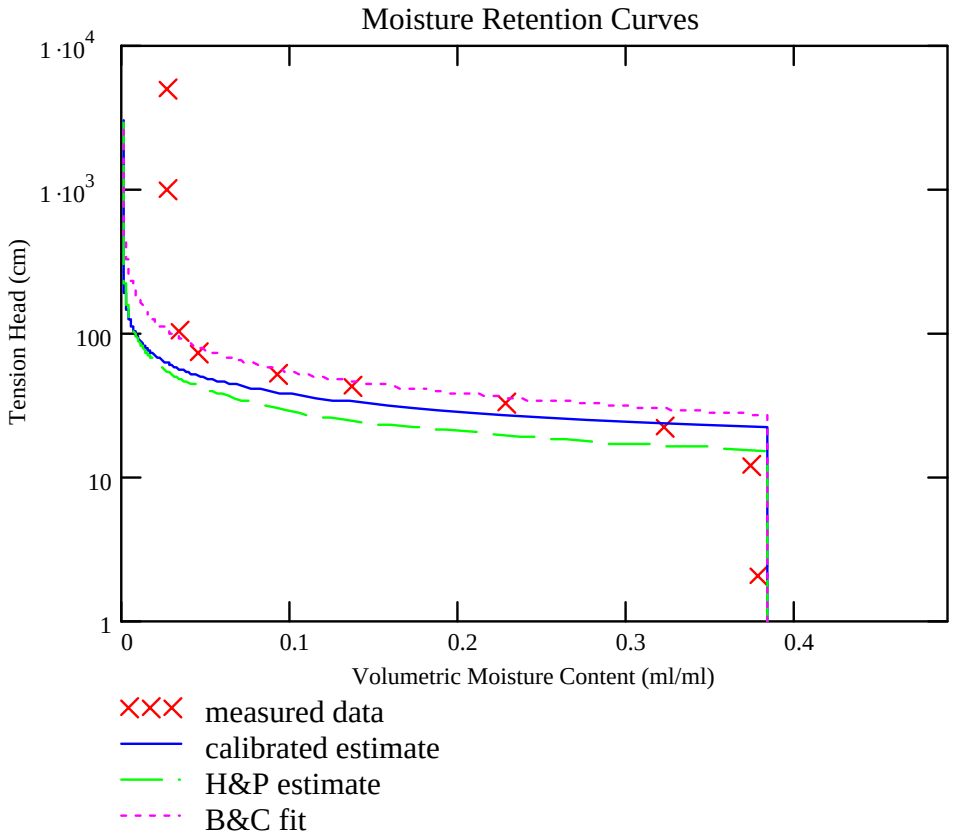

RSQ1 = 0.897
RSQ2 = 0.689
RSQ3 = 0.957

RSQ1= R^2 for calibrated estimate
RSQ2=R^2 for H&P estimate
RSQ3 = R^2 for B&C fit to data

Figure 3.15 – Estimated curves using model estimation equations re-calibrated to the fabricated samples. Sample L1 has a narrow range of particle sizes with a median grain size of 0.50 mm. The sample was packed to a bulk density of 1.64 g/cc.

3.7 Development and Application of the Parameter Estimation Model for Predicting the van Genuchten Curve Fitting Parameters.

3.7.1 Model Development

We used the static material properties described in Section 3.3 along with correlations between parameters described in Chapter 2 (Appendix O) to develop van Genuchten parameter estimation equations. The van Genuchten fitting parameter *n* representing the slope of the PDC was first estimated by plotting the ratio of the PDC *n* to the slope of the PSD (n_d) versus the sample dry bulk density (Figure 3.16). Correlations between the slope of the MWC, MDC, and PDC were poor (Chapter 2), therefore the slope of the curves was assumed to be constant and equal to the PDC *n*.

Satiation was assumed to equal values obtained from RETC fits to MDC data (Chapter 2), and porosity was calculated from bulk density values. Satiation was estimated from the correlation between satiation and saturation for the PDC (Figure 3.17). The fitting parameter α was estimated for the PDC from the correlation between $1/\alpha$ (cm) and the PSD fitting parameter d_g (Figure 2.35 in Chapter 2), then α was estimated for the MDC and the MWC from correlations between these curves and the PDC (Figures 2.31 and 2.32 in Chapter 2). Estimation model input parameters are listed in Table 3.4.

3.7.2 van Genuchten Parameter Estimation Model Results

The estimated van Genuchten parameters were generally statistically the same as the parameters derived from fitting the van Genuchten equation directly to the moisture retention data. Estimates for samples not used in model calibration (due to anomalous relationships between parameters) exhibit the greatest deviations from measured values.

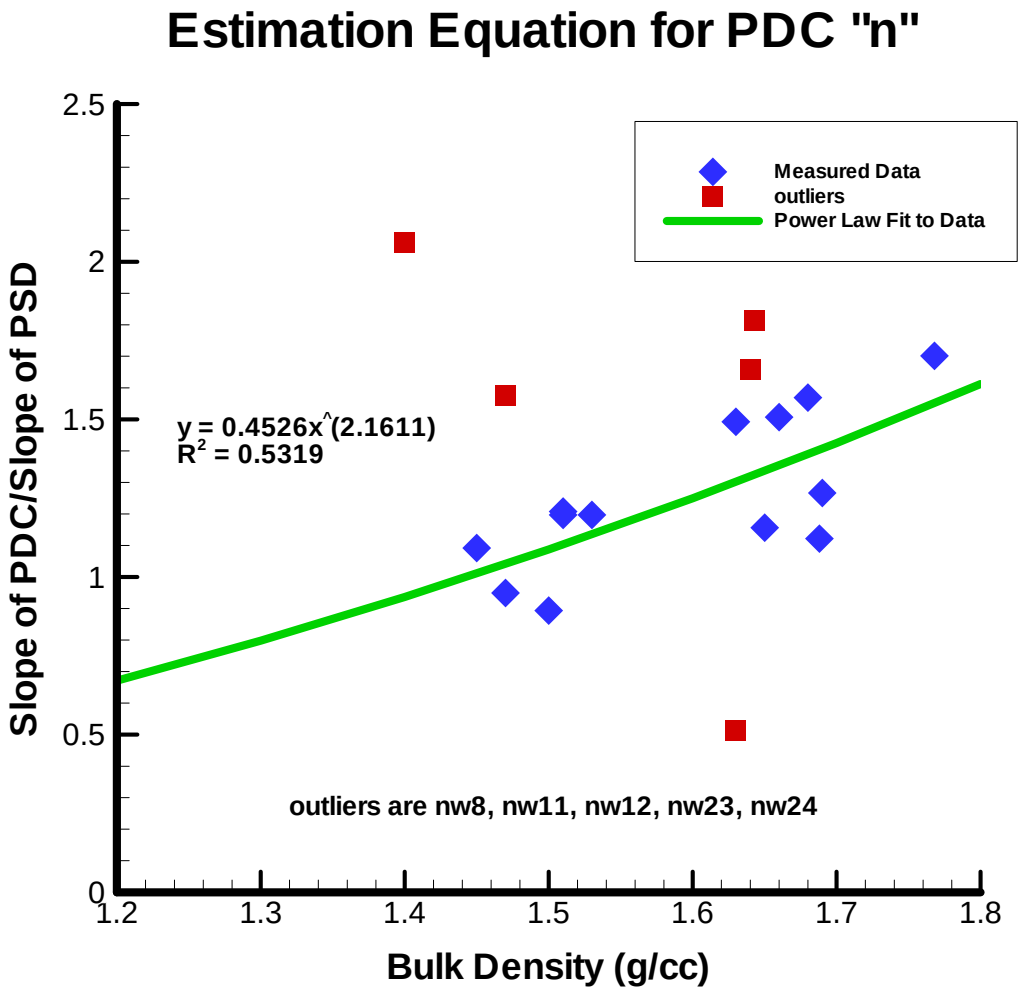

Figure 3.16 – Regression analysis used to determine estimation equation for the van Genuchten curve fitting parameter *n* for the PDC.

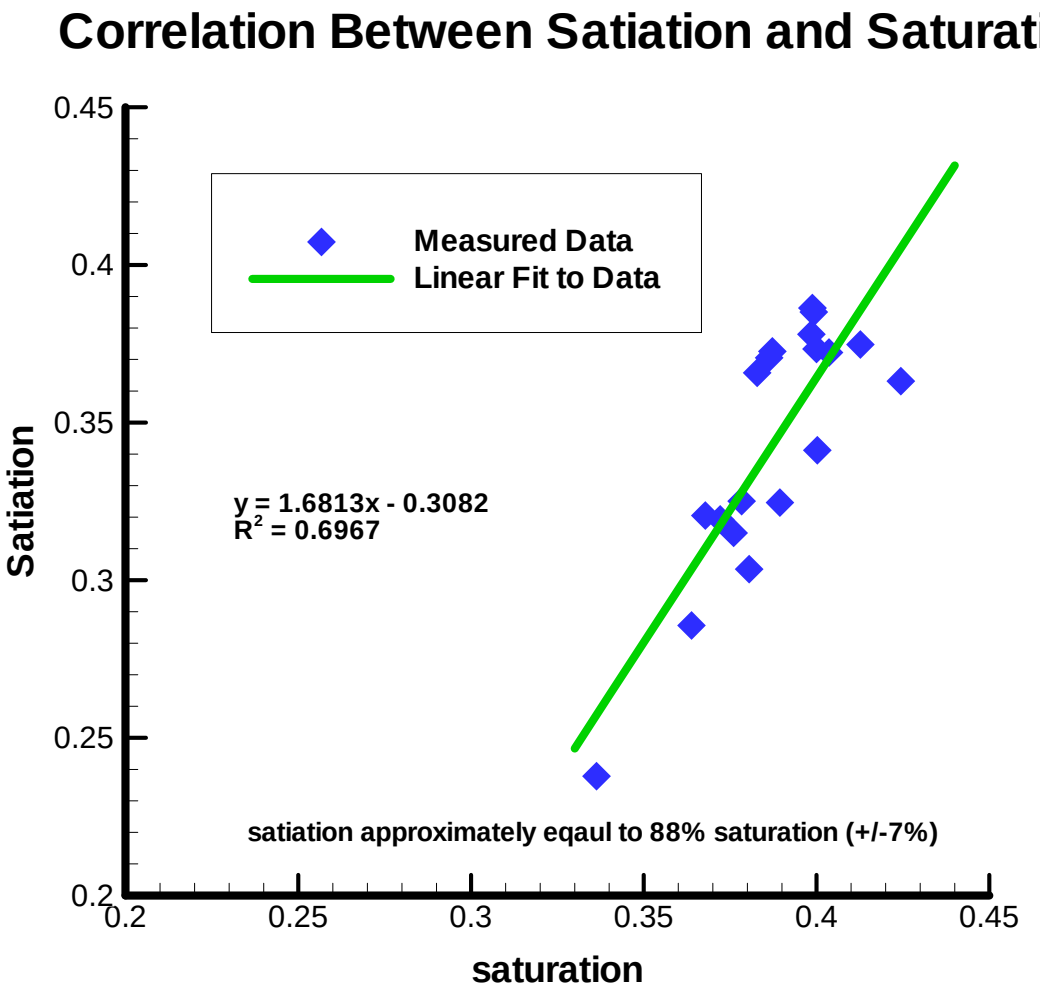

Figure 3.17 – Relationship between saturation and satiation.

Table 3.4 – Model input parameters used in van Genuchten parameter model calibration.

	MWC n	MDC n	PDC n	MWC 1/α	MDC 1/α	PDC 1/α	ϕ	θs	PSD n (n_d)	dg
NW1	9.983	4.278	5.669	14.691	34.412	22.676	0.336	0.238	3.332	0.711
NW2	8.488	2.973	3.949	16.313	18.587	26.247	0.376	0.315	3.118	0.621
NW4	2.761	3.567	5.011	9.552	24.783	32.051	0.378	0.325	4.334	0.452
NW7	4.513	4.029	4.217	21.877	43.535	49.751	0.413	0.375	3.492	0.248
NW8	4.755	4.327	5.734	29.481	54.795	69.930	0.386	0.371	3.160	0.232
NW9	2.924	3.090	3.766	22.442	43.215	53.476	0.368	0.320	2.499	0.427
NW10	3.322	3.267	3.597	21.053	36.036	49.751	0.372	0.319	3.207	0.284
NW11	4.866	4.442	7.690	35.689	64.309	62.893	0.404	0.372	3.732	0.180
NW12	3.782	4.687	6.161	24.231	54.675	64.935	0.399	0.378	3.909	0.197
NW16	3.955	4.904	6.549	33.546	76.104	75.758	0.399	0.385	5.998	0.133
NW17	4.834	5.628	6.947	29.913	64.893	70.423	0.399	0.386	5.805	0.149
NW19	2.573	3.312	3.872	39.063	85.985	96.154	0.400	0.373	4.079	0.133
NW20	7.633	5.175	4.951	23.041	58.720	60.241	0.387	0.373	5.543	0.175
NW21	2.757	5.329	6.120	41.806	53.079	60.606	0.424	0.363	5.123	0.183
NW22	16.093	4.896	5.724	26.717	65.920	66.225	0.383	0.366	4.783	0.157
NW23	5.832	3.287	5.724	21.566	55.096	66.225	0.400	0.341	3.450	0.227
NW24	7.805	3.424	1.677	19.932	44.287	24.631	0.389	0.325	3.264	0.267
NW25	4.016	3.350	4.506	17.637	39.541	48.780	0.364	0.286	3.020	0.393
NW27	6.367	8.390	5.421	17.182	42.230	35.804	0.381	0.303	3.455	0.375

Examples of the best model predictions are shown in Figure 3.18 while Figure 3.19 is an example of the worst model predictions. The figures include estimates of the MWC, MDC, and PDC along with measured data. Measured data includes overestimates in moisture content at complete saturation along the PDC, and anomalous decreases in moisture content along the MWC at pressures higher than water entry pressure. R^2 does not represent a fit to data points in those regions for a majority of the samples.

Sample NW 11

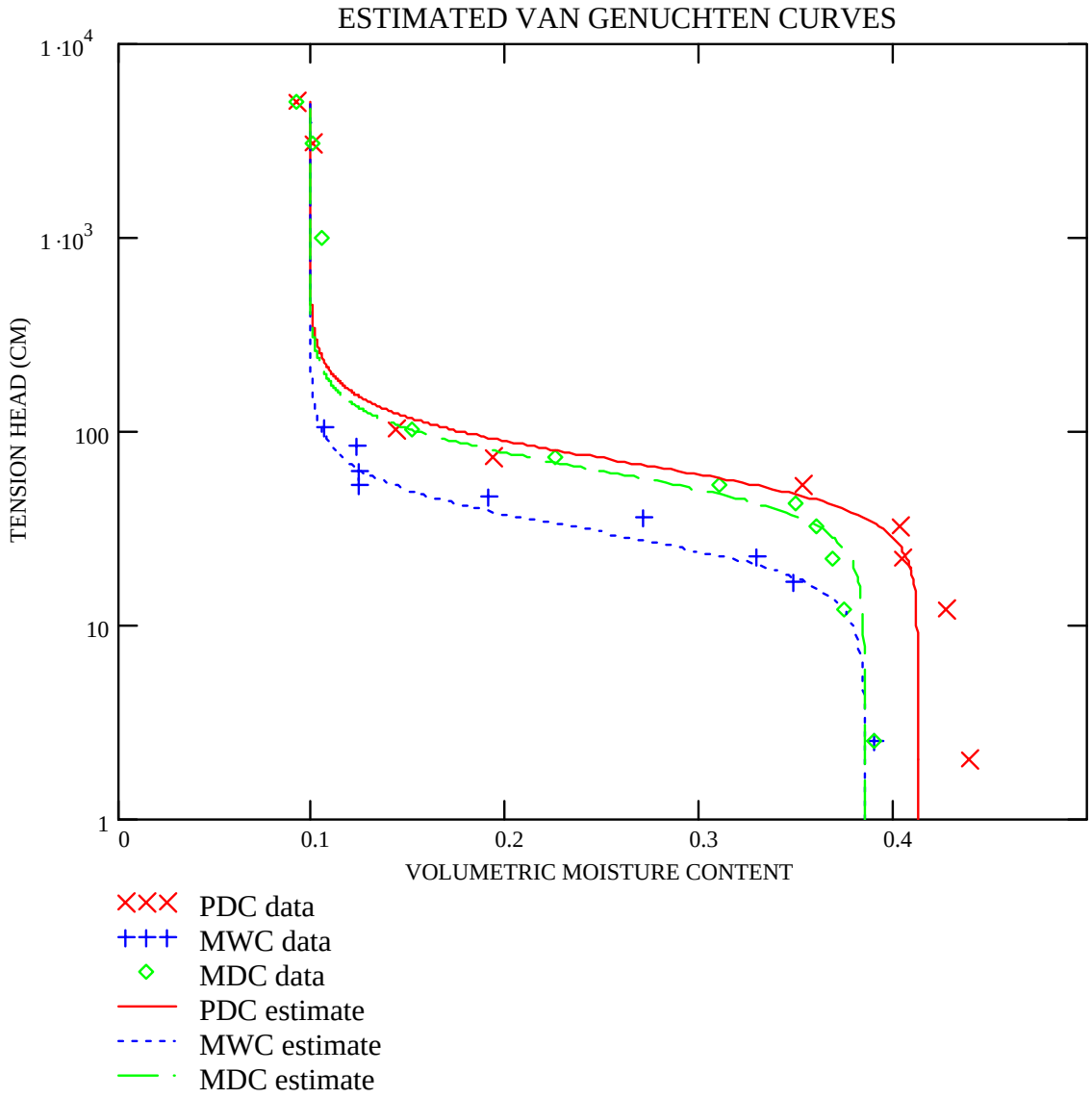

RSQ1 = 0.949

RSQ2 = 0.932

RSQ3 = 0.992

RSQ1 = R^2 for PDC
RSQ2 = R^2 for MWC
RSQ3 = R^2 for MDC

Figure 3.18 – Example of the model predictions for sample NW11. Residual moisture content was assumed to equal moisture content at highest pressure measured to be consistent with direct fit of the van Genuchten equation.

Sample NW 2

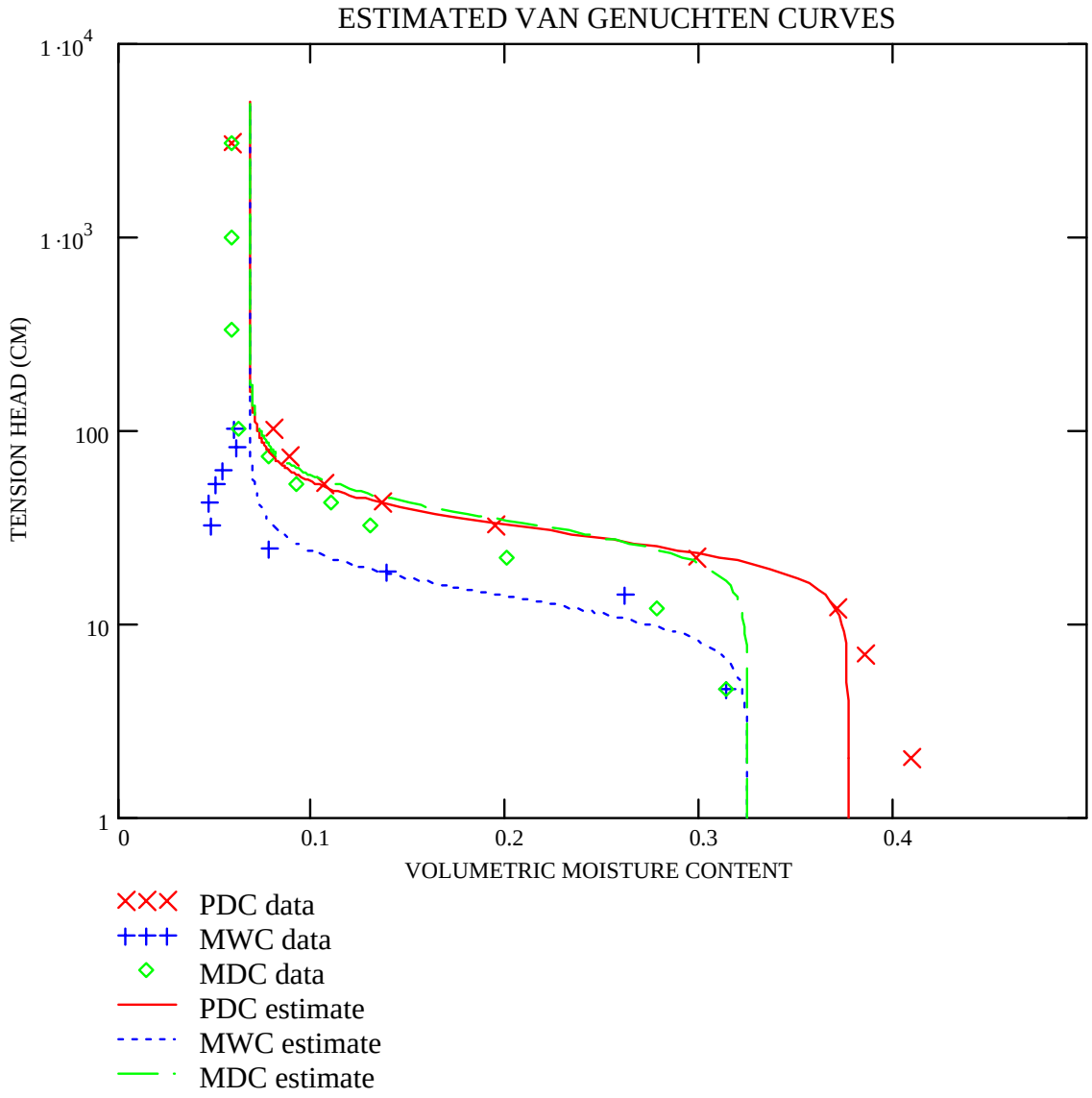

RSQ1 = 0.997

RSQ2 = 0.912

RSQ3 = 0.765

RSQ1 = R^2 for PDC
RSQ2 = R^2 for MWC
RSQ3 = R^2 for MDC

Figure 3.19 – Example of the model predictions for sample NW2. Residual moisture content was assumed to equal moisture content at highest pressure measured to be consistent with direct fit of the van Genuchten equation.

3.7.3 Discussion

Both the van Genuchten parameter estimation model and the Haverkamp and Parlange (1986) model applications resulted in statistically similar estimates of the moisture retention curves for the STVZ samples compared to the direct fit of functional forms to measured data. The ease of calibration and application of the van Genuchten parameter model was more appealing than the H&P model, however. Another advantage of the van Genuchten parameter estimation model is that it allows prediction of the MWC and MDC from PDC measurements, which is appealing because the PDC is often the only curve researchers examine due to the simplicity in sample preparation and experimental conditions. The H&P model also allows prediction of various wetting/draining sequences from measured values obtained during a single sequence of measurements (typically draining), however, the H&P model hysteresis equations are difficult to decipher and include time intensive iterative solutions. Although the van Genuchten parameter estimation model does not include estimation of scanning curves (while the H&P model does), the estimated parameters obtained from model application can be used in hysteretic models (e.g., Scott et al., 1983; Mualem, 1976) to predict scanning curves if desired. Additional parameters required by hysteretic models include the residual moisture content and the saturated moisture content (i.e., the starting and stopping points) associated with individual scanning curves (Scott, et al., 1983).

3.7.4 Conclusions

The van Genuchten parameter predictive model, developed as part of this study, provides estimates very similar to the direct fit of the van Genuchten equation to measured data using the RETC curve fitting model (Chapter 2) for the majority of the samples. Similar to application of the H&P model, estimates for samples used in model

calibration were much better than estimates for samples excluded from calibration. Although estimates for fabricated samples were not examined for the van Genuchten parameter model, the results would most likely be similar, based on model sensitivity to properties used in model calibration. Even though the model also requires calibration to deposits with narrow particle-size distributions, this model can be easily calibrated and applied to a relatively small number of representative samples to predict properties for a large data set. Reduction of measurement error and careful determination of fitting parameters (i.e., careful weighting of data points and reduction of free parameters in parametric model applications) would result in improved predictions.

3.8 Model Sensitivity Analysis

3.8.1 Model Development and Application

Based on the model application results discussed in the previous sections, it appears that pedotransfer models provide the best results for geologic deposits composed of very similar textures and that the impact of measurement error, sample size, and the number of measured data points along the moisture characteristic curves may seriously impact the model results (based on poor correlations observed between parameters). To test this hypothesis, Monte Carlo simulations were used to examine the optimum conditions for model application.

The Haverkamp and Parlange (1986) model with original model coefficient values for a1, a2, b1, b2, and b3 were used to represent reality (i.e., true data). Since both estimation models are based on similar concepts, it is assumed that the optimum conditions determined for one model will apply to pedotransfer models of similar governing equations and basic parameter derivations. Measurements of moisture characteristic and particle-size distribution data in the presence of error was simulated

by introducing error to the true data. To identify the optimum number of data points for the moisture characteristic curves, the Brooks and Corey equation was fit to the measurements (in the presence or error) with an increasing number of data points. The optimum number of samples required for model calibration was defined by randomly selecting samples from a total population of artificially generated samples (1000 total) of increasing sample set sizes. The statistics of the results were examined for each model scenario and estimated curves were compared to the true moisture characteristic curves. To examine the impact of particle diameters on the model results, the process was repeated using a narrower range of mean particle diameters. Appendix Q includes a detailed description of the procedures including FORTRAN codes and algorithms.

3.8.2 Model Sensitivity Analysis Results

Results of the analysis indicate that increasing the number of moisture retention data points and/or the number of samples used in model calibration did not significantly improve model results, however calibration to a narrower range of particle sizes improved the results substantially (see Appendix R).

Although the analysis showed that introduction of measurement error strongly influences pedotransfer model predictions, measurement error most likely impacts parametric model estimates (i.e., direct curve fits to data) to the same degree. Because the impact of measurement error on parametric model results was not examined in this study, comparison between the two methods cannot be made at present. Nevertheless, the impact of measurement error on both parametric and pedotransfer model results could be quite substantial when coupled with spatial variability model predictions and should be examined further.

3.9 Chapter Summary and Conclusions

Haverkamp and Parlange (1986) calibrated their pedotransfer model to 10 sandy soils ranging in particle diameters from 0.20 to 0.50 mm (fine to medium grained sands). The regression analysis for the 10 sandy soils resulted in a coefficient of determination (R^2) for estimates of both λ and γ of greater than 0.90. In contrast, R^2 for the regression analysis of the STVZ field site data was less than 0.80 for these parameters. The higher degree of uncertainty may have been due to increased measurement error for the infiltration site samples compared to the samples used in the Haverkamp and Parlange (1986) model or possibly due to the larger range of particle sizes for the STVZ samples, which ranged from 0.053 to 2.0 mm in diameter (very fine to coarse grained sands). Regardless of these differences in model calibration, both the empirical model and the H&P model equations predicted curves similar to curves obtained from the direct fit of the Brooks and Corey equation to measured data for the majority of samples used in model calibrations. In contrast, model results were much poorer for samples with significantly different physical properties from the samples used in the model calibrations.

Because the van Genuchten parametric model is often used to estimate moisture retention curves of vadose zone materials, a predictive model similar to the H&P model for estimating moisture retention curves was developed and examined. The research indicates that the model was much easier to calibrate and implement than the H&P model. Although equations for estimating scanning curves were not included in the model, the model does include methods for estimating the MWC and the MDC from PDC data. The ease of model calibration and application makes the van Genuchten

parameter estimation model much more appealing for estimating properties of large data sets.

The model sensitivity analysis indicated that the number of samples and data points measured in the STVZ sample moisture retention measurements was adequate for model calibration, however the analysis showed improved results for samples of narrower particle-size distributions. For heterogeneous vadose zone environments, spatial variability in sediment physical properties can be quite significant. For this reason, pedotransfer models would require separate calibrations for a large number of textural classes of sediments. Although the process would still be somewhat cumbersome, predictive models are more feasible for obtaining parameters for large data sets than standard laboratory techniques.

The model sensitivity analysis also indicates that model predictions appear to be quite sensitive to measurement error (see Appendix R). The erroneous predictions would be expected to significantly propagate through non-linear geostatistical models used in predicting spatial variability of properties within the vadose zone. For this reason, further examination of measurement error and the impact on unsaturated flow and transport predictions, which rely heavily on spatial variability of vadose zone hydraulic properties, is highly recommended.

CHAPTER 4.0 – CONCLUSIONS

4.1 Research Summary

This research is part of a collaborative project designed to investigate field, laboratory, and predictive methods for describing the spatial variability of vadose zone materials. The Sandia-Tech Vadose Zone (STVZ) research facility in Socorro, NM is used to examine hydraulic properties of deep vadose zone materials during various infiltration events as part of this investigation. The study incorporates field and laboratory measurements of geophysical and hydrologic data as input parameters for a numerical inverse model which simulates the response during an unsaturated infiltration event (Alumbaugh et al., 1996).

The focus of the research described in this document is to characterize the hydraulic properties of the vadose zone deposits located at the infiltration field site using laboratory and indirect estimation techniques. Laboratory methods for determining moisture retention curves are often limited to analysis of a small number of samples due to the time intensive process associated with the analysis. Estimation methods for determining hydraulic properties are appealing because they allow analysis of large sample sets required in geostatistical based modeling.

Samples collected from the STVZ site were analyzed at the Sandia National Laboratory (Albuquerque, NM) flow and visualization lab for hydraulic properties by measuring wetting and draining moisture retention curves, porosity, saturated hydraulic

conductivity, electrical resistivity, and particle size distributions. Functional forms describing the shape of the moisture retention curves, electrical resistivity curves, and particle-size distribution curves were then fit to the measured data. The results were compared to properties reported in the literature for similar sandy soils and alluvial deposits. Correlations between parameters were examined to minimize the number of measurements required in hydraulic property characterization of vadose zone materials. Pedotransfer models were used to predict hydraulic properties based on the parameter correlations. Model predictions were compared to results obtained using direct methods and finally a sensitivity analysis was conducted to determine model requirements for achieving optimum results and to examine the impact of measurement error on the predictions.

4.2 Laboratory Methods

4.2.1 Establishment of Laboratory Methods

Methods for characterizing hydraulic properties of alluvial vadose zone deposits were based on standard methods developed for soil characterization and preliminary studies designed to address methodologies specific to poorly consolidated alluvial sands. Modifications to standard soil characterization methods were based on preliminary test results. Deviations from standard methods include analysis of repacked samples instead of intact undisturbed samples, moisture retention measurements in the hanging columns from 0 to 100 cm due to loss of hydraulic contact at negative pressures greater than 100 cm, use of a wetting solution made from tap water as opposed to a calcium sulfate solution, and dry sieving sand particles using a stack of sieves for particle size analysis better suited for sand sized particle distribution analysis.

4.2.2 How Well Do the Methods Work?

- **Sampling techniques**

Although similar hydraulic properties were observed between undisturbed and repacked alluvial sand samples, it is unlikely that natural structure was captured and/or preserved during sample collection. Collecting undisturbed samples of poorly consolidated deposits, often found in vadose zone environments, is nearly impossible and certainly improbable. In addition, most standard laboratory methods are limited to analysis of inadequate sample sizes for capturing natural structures such as aggregates, concretions, and lenses of low permeability sediments, which strongly influence unsaturated flow behavior. For these reasons, laboratory analysis of representative samples should be recognized as an estimate of hydraulic properties based on differences in textures only and that further examination of the impact of geologic structure should be considered when making critical remediation and/or long term waste management decisions.

- **Curve Fitting Procedures**

The van Genuchten equation was fit to moisture retention data requiring four unknown parameters in the RETC curve fitting program. The RETC program is limited to non-unique results which contribute to model uncertainty. Model uncertainty increases with the number of unknown parameters and fewer number of measured data points. Weighting individual data points improves the fit to data, however measurement uncertainty and error is included in the data, making the weighted fits somewhat subjective. For this reason, careful interpretation should be used in curve fitting results, examining highly weighted data points and possible anomalous data used in the fits.

- **Time Consuming Methods**

It took approximately 6 months to complete the laboratory sample analysis for 25 repacked samples, after the samples had been collected and transported to the laboratory for analysis. Based on this time frame, this research confirms the perception that laboratory analysis of a large sample set is unrealistic.

- **Influence of Measurement Error**

Non-linear functional forms (e.g., van Genuchten and Brooks and Corey models) are highly sensitive to measurement and model uncertainty resulting in uncertain curve fitting parameters. Parametric models incorporate the curve fitting parameters in most flow and transport predictions which could lead to a high degree of uncertainty in the predictions.

4.3 Measured Results

4.3.1 Summary of Hydraulic Properties

The majority of the STVZ deposits consist of poorly consolidated, well sorted fine-medium grained sands with sample porosities ranging from 33 to 43%, saturated hydraulic conductivities approximately equal to 10^{-3} cm/s, residual moisture contents less than 10%, air entry pressures ranging from 20 to 60 cm, and moderately well sorted pore size distributions. Hysteresis was observed in the wetting and draining moisture retention curves for all of the samples analyzed. Curve fitting parameters for the van Genuchten model fit to data appear to vary from parameters often reported for sandy soils of similar texture, while the hydraulic conductivity and porosity are similar to values reported for sandy soils and alluvial sands.

This research shows that shape of the electrical resistivity curves as a function of moisture content vary with sample texture, exhibiting steeper slopes for finer grained

deposits and shallower slopes for coarser grained deposits. Hysteresis was not observed in resistivity measurements, however, suggesting that the relationship between moisture content and resistivity is unique, as opposed to the relationship between matric potential and moisture content which is dependent on the wetting/draining history. The majority of the sandy deposits had a very high resistivity value at moisture contents less than 10 volume percent, with exceptions for deposits containing higher percentages of clay minerals.

4.3.2 Parameter Correlations

Moderate to weak correlations were identified between moisture-retention parameters, electrical resistivity parameters, and particle-size distribution parameters, even though these parameters are in theory strongly inter-related. The weak parameter correlations may be due in part to measurement error and uncertainty. Saturated hydraulic conductivity did not appear to be correlated to any one parameter, which suggests that it is a function of multiple sample conditions, such as sorting, porosity, texture, and structure. The slopes of the moisture retention curves are all poorly correlated to the slopes of the particle-size distributions. This suggests that pore volume distributions are not solely related to particle-size distributions, but also depend on the packing arrangement and geometry of the grains.

4.3.3 Soils Versus Alluvial Sands

Although the majority of the measured hydraulic properties resemble properties reported for soils of similar texture, the measured van Genuchten curve fitting parameters n and α are statistically different from values reported for intact soils of similar textures characterized by percentages of sand, silt, and clay sized particles. This suggests that tabulated soil moisture characteristic properties often used to predict

unsaturated flow and contaminant transport could result in erroneous predictions within deep vadose zone environments.

4.3.4 Impact of Hysteresis on Flow and Transport Model Predictions

This research clearly shows hysteretic moisture retention behavior for sandy alluvial deposits. In order to adequately model unsaturated flow and transport within the vadose zone, unsaturated flow models require integration of unique parameters for various flow conditions. Reported values for soils and geologic deposits are typically measured during a drying sequence starting from complete saturation (porosity. For this reason, the use of tabulated values should be used with caution in numerical models which incorporate curve fitting parameters to predict flow and transport in the vadose zone.

4.4 Pedotransfer Model Predictions

Although the STVZ empirical model predictions for the Haverkamp and Parlange (1986) model were similar to measured data, regression analysis of parameters for model estimation equations during calibration to the STVZ samples resulted in poor correlations between parameters compared to the original model development. The regression analysis for the original model resulted in a coefficient of determination (R^2) for both model parameters (λ and γ) of greater than 0.90. In contrast, R^2 for the regression analysis of the STVZ field site samples was less than 0.80 for both parameters. This may be due to the fact that the original model was calibrated to 10 sandy soils of narrow particle diameters from 0.20 to 0.50 mm (fine to medium grained sands) while the STVZ samples ranged in particle diameters from 0.053 to 2.0 mm in diameter (very fine to coarse grained sands), or possibly due to increased measurement error for the STVZ samples. Regardless of these differences in model calibration, both

the empirical model and the original model equations appear to predict curves similar to the original functional form fits to measured data for the majority of samples used in model calibration. In contrast, model results were much poorer for samples exhibiting dissimilar physical properties from the calibration samples.

The van Genuchten parametric model is often used in numerical models to estimate flow and transport in unsaturated porous media and is therefore more appealing to many researchers for characterizing hydraulic properties of vadose zone materials. For this reason, a van Genuchten parameter predictive model similar to the Haverkamp and Parlange model was developed and evaluated for estimating moisture retention curves. This research indicates that the model is much easier to calibrate and implement than the Haverkamp and Parlange pedotransfer model. Although the model does not include equations for estimating scanning curves, the model does include methods for estimating the MWC and the MDC from PDC data alone. The ease of model calibration and application makes the van Genuchten parameter estimation model much more appealing for estimating properties of large data sets.

Model sensitivity analysis indicates that a moderate sample size (20-40 samples) and the number of data points measured in the STVZ sample moisture retention measurements (10-12) would provide adequate results, however the model requires separate calibration for deposits of significantly varying textural differences. For heterogeneous vadose zone environments, spatial variability in sediment physical properties is quite significant. For this reason, pedotransfer models require separate calibrations for a large number of textural classes. Although the process is still be quite cumbersome, efficiency in obtaining a large data set required for spatial variability studies would be improved compared to standard laboratory methods.

This research indicates that model predictions appear to be quite sensitive to measurement error. The model uncertainties would be expected to propagate quite drastically through non-linear geostatistical models used in predicting spatial variability of properties within the vadose zone. For this reason, further examination of measurement error and the impact on unsaturated flow and transport predictions is recommended.

4.5 Recommendations for Future Work

4.5.1 Meso-Scale Experiments

Although environmental conditions can be better controlled in a laboratory setting and laboratory measurements typically have a higher degree of measurement precision compared to *in situ* analysis, laboratory measured properties using standard techniques do not represent field scale hydraulic properties. Innovative methods are needed for collecting and analyzing undisturbed meso-scale samples in which the integrity of *in situ* conditions is preserved. Meso-scale samples large enough to capture large scale heterogeneity's could feasibly be analyzed in the laboratory controlled environment with minimal measurement uncertainty. Measurement methods could incorporate standard field monitoring equipment such as geophysical EM equipment for monitoring moisture content, tensiometers for measuring matric potential, and suction lysimeters for analyzing geochemical reactions and/or tracking flow paths by the use of tracers. Methods are needed, however, to reduce the amount of time typically required for a meso-scale sample to reach steady-state conditions. Geo-centrifuges have been proposed for dealing with these larger scale samples. The impact of high pressures on monitoring equipment would have to be fully explored before this technique is fully developed. The possibility of large pressure gradients along a large column is also of

concern. Centrifugation on a smaller assumes the pressure throughout the column is equal to the average pressure in the samples. For small columns (less than 5 cm) this assumption is acceptable, however, it may not be valid for meso-scale samples or samples with a high degree of heterogeneity.

4.5.2 Time Efficient Measurement Techniques

Time efficient methods for measuring moisture retention properties of soils and alluvial deposits are required for characterizing meso-scale and/or a large number samples for site characterization. Innovative methods include desorption by centrifugation and predictive methods based on surrogate data which is much less time consuming to measure directly. At present, these methods require further examination to develop standard techniques, application conditions, and impact of measurement and model uncertainty on moisture retention parameters.

Direct measurements of air entry pressure, porosity, and residual moisture content prior to data collection would allow researchers to focus on the active region of moisture retention curves resulting in better estimates of curve fitting parameters using a limited number of data points. Innovative methods for measuring these properties could be easily developed in a laboratory setting and could be obtained in a reasonably short time frame.

4.5.3 Unique Vadose Zone Properties

Many vadose zone studies are concerned with relatively large areas of land in which direct hydraulic property measurements are extremely cumbersome and costly (van Genuchten et al., 1999). As an alternative, researchers have recently begun to utilize tabulated hydraulic property databases, such as the Unsaturated Soil Database (UNSODA) available through the U.S. EPA and U.S. Dept. of Agriculture, to obtain

properties necessary for flow and transport predictions within deep vadose zones. These data bases are categorized by soil textures (Leij et al., 1996), similar to textures for deep vadose zone deposits. However, this research suggests that moisture retention properties of sedimentary alluvial deposits, commonly found in deep vadose zones, differ statistically from parameters reported for soils of similar texture. These differences could result in erroneous flow and transport predictions within deep vadose zone environments.

Due to the time intensive nature of this research, further investigation involving a larger sample set of both soils and deep vadose zone deposits is required to support these findings. The investigations should examine the impact of natural structures on moisture retention properties in addition to hydraulic conductivity measurements (saturated and unsaturated) and measurements of electrical conductivity at moisture equilibrium. Since an investigation of large sample sets is unrealistic using standard laboratory techniques, the examination should be conducted using innovative time efficient methods for attaining curve fitting parameters. The initial part of the study should include an in-depth examination of procedures using desorption centrifugation and predictive modeling. Methods for direct and time efficient measurements of air entry pressure, porosity, and residual moisture content should be included in the study. Impact of measurement error and model uncertainty should be examined to determine conditions for application.

Appendix A

STVZ Subsurface Stratigraphy and *In Situ* Moisture Profile

DESCRIPTION OF GEOLOGIC UNITS

The upper 2 m consist of a laterally continuous fine grained sandy pebble gravel (Unit 1) which abruptly coarsens to a medium-coarse grained sandy pebble gravel with numerous small cobbles (Unit 2). A layer of fine-medium grained sand underlies Unit 2 ranging in depth below ground surface from approximately 2 to 4.5 m (Unit 3). An apparently isolated lens of inter-bedded sand and clay (Unit 4) is present within Unit 3 in the northeast (NE) core. Another inter-bedded sand and clay deposit in the southwest (SW) core can be correlated with a similar deposit in the northwest (NW) core (Unit 5). Unit 5 is present again in the southwest core below an intervening layer of sand characterized as Unit 3, and in the southeast (SE) core where it intervenes between two sandy gravel clay layers, reaching a maximum depth of almost 6 m. The upper clay layer in the SE core may be an isolated lens (Unit 6) while the lower clay layer (Unit 7) appears to be continuous across the site. Unit 7 contains numerous small cobbles, coarse gravels, and sandy deposits reaching a maximum depth of almost 7 m. Underlying Unit 7 is a thick layer of fine-medium grained sand with occasional intervening sandy gravel lenses, and a gravel cobble layer at the base of the SW and NW boreholes (Unit 8).

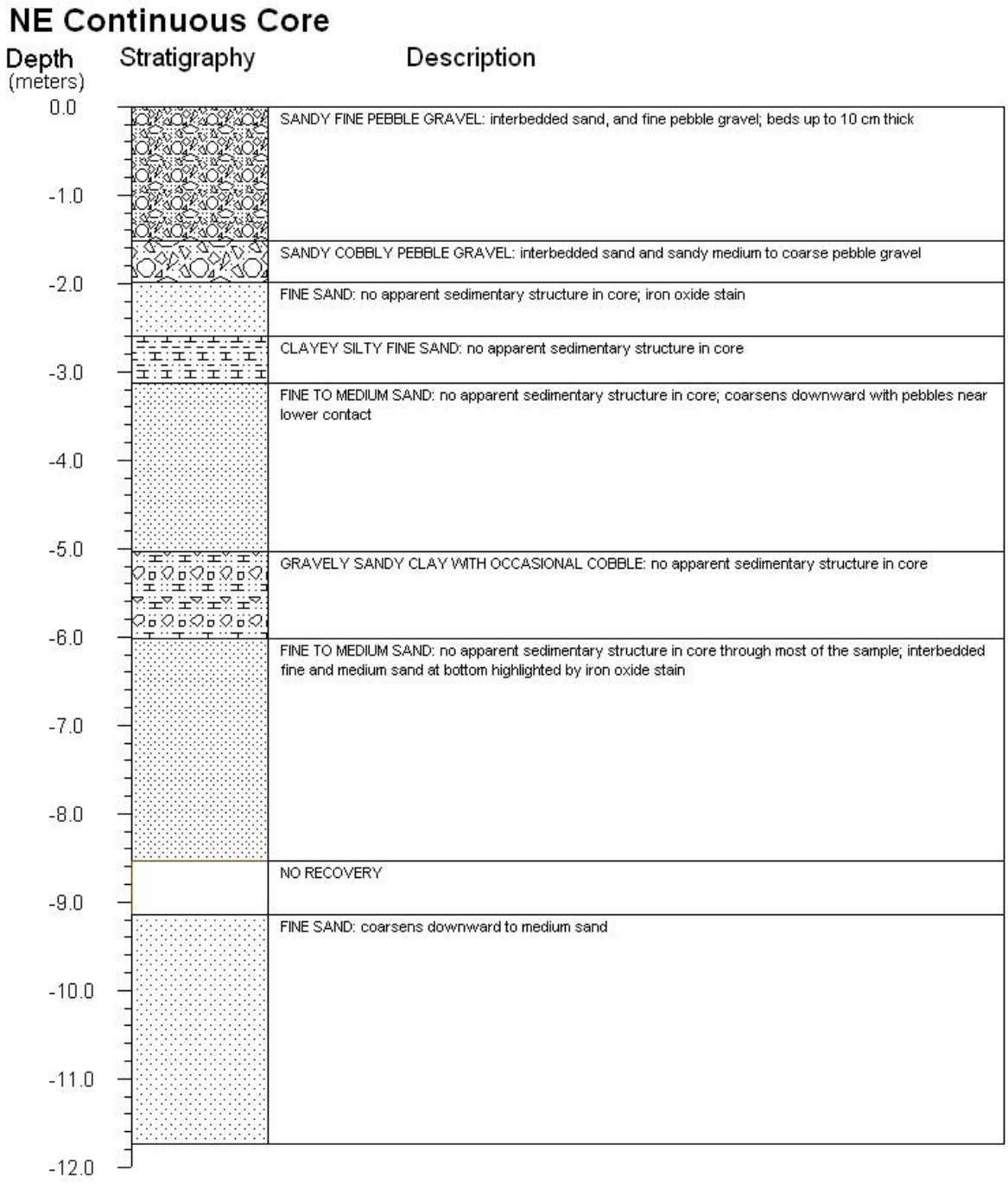

Figure A.1 – Stratigraphic Column of NE Core. Depth is in meters below ground surface.

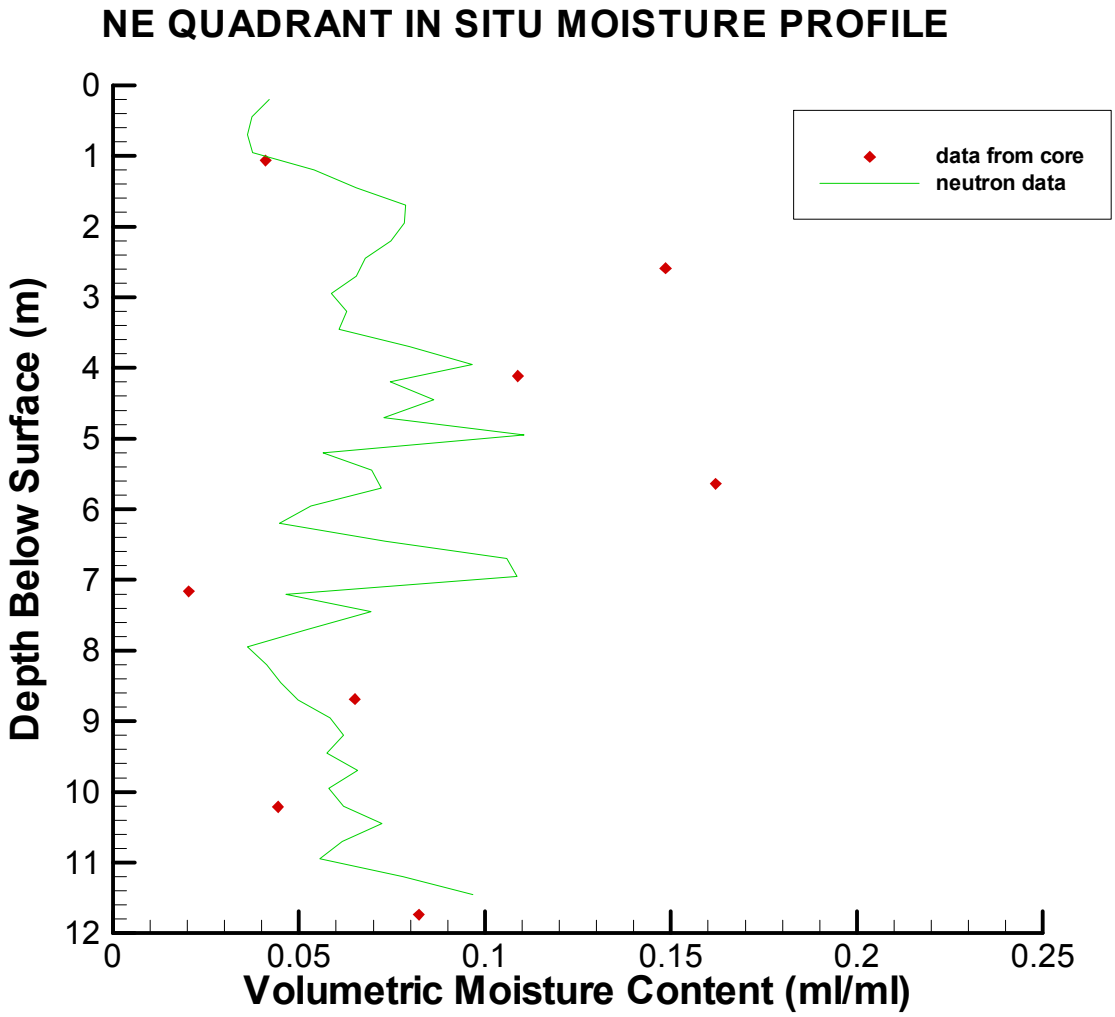

Figure A.2 – In situ moisture profile NE Quadrant. Diamonds represent estimated volumetric moisture content from gravimetric data collected from drilling. Solid line represents moisture profile estimated from neutron data. The neutron probe was not calibrated to the clay deposits, therefore the profile from 4-6 m bgs is questionable.

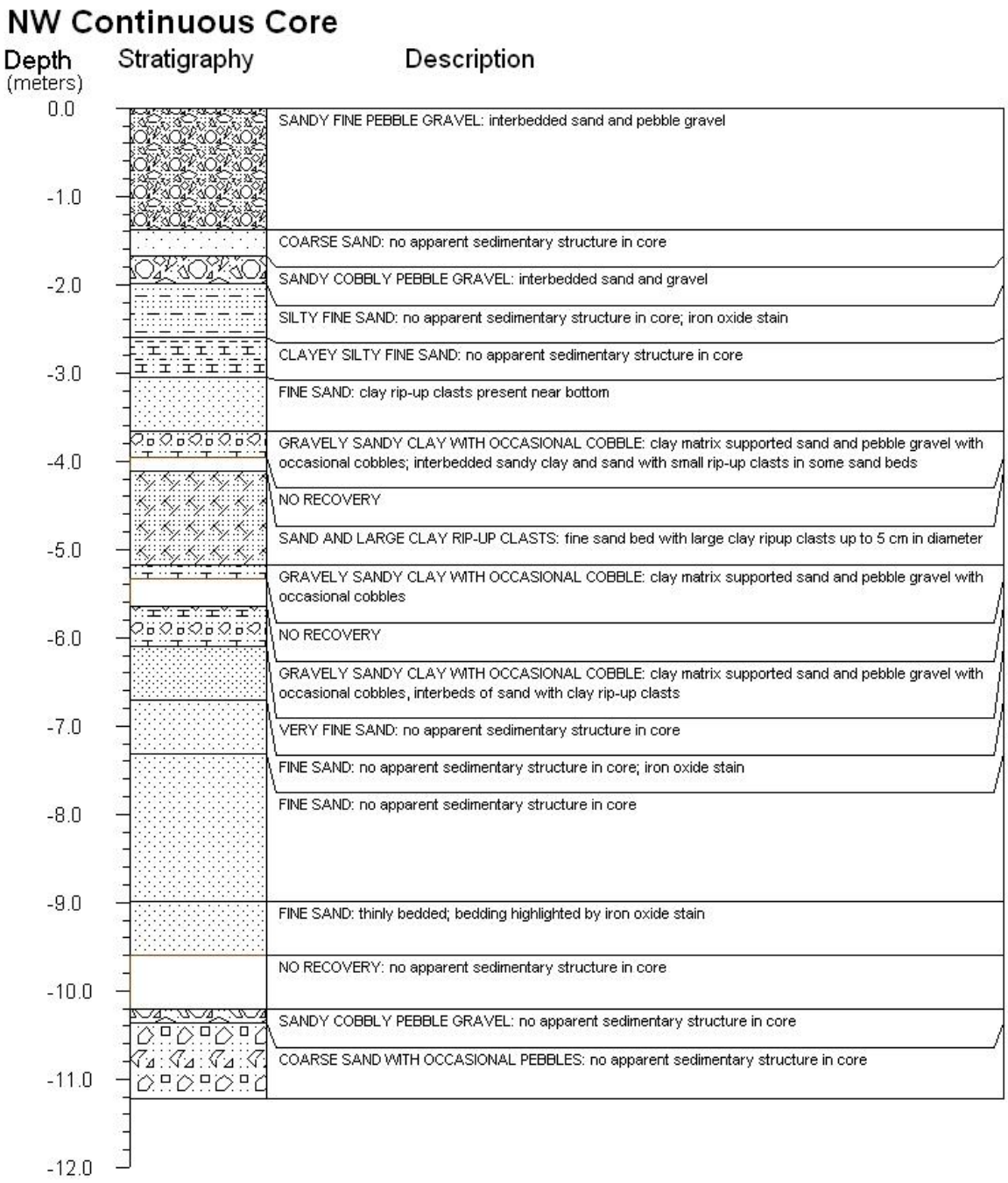

Figure A.3 – Stratigraphic column of NW Core. Depth is in meters below ground surface.

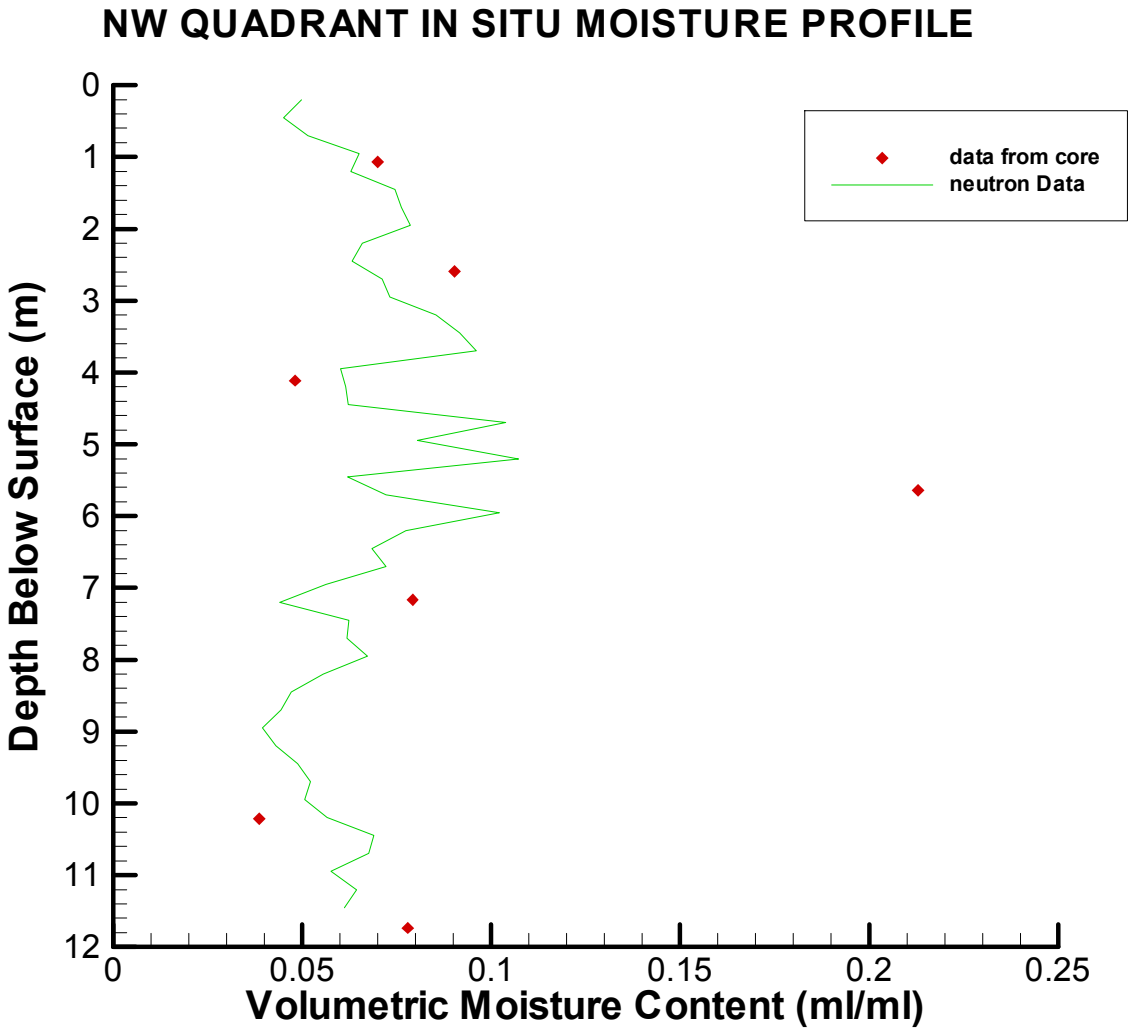

Figure A.4 – In situ moisture profile NE Quadrant. Diamonds represent estimated volumetric moisture content from gravimetric data collected from drilling. Solid line represents moisture profile estimated from neutron data. The neutron probe was not calibrated to the clay deposits, therefore the moisture profile between 4-6 m bgs is questionable.

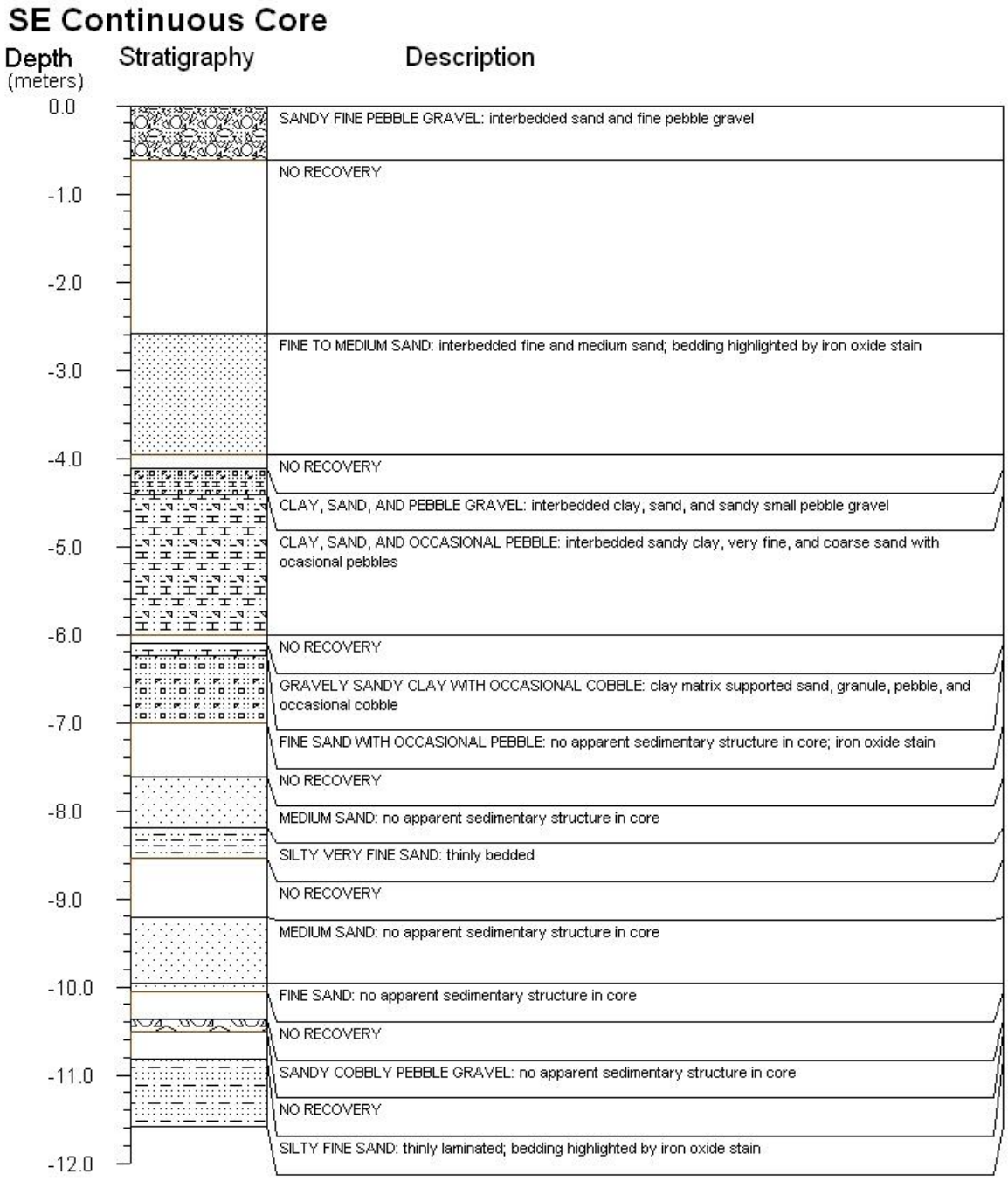

Figure A.5 – Stratigraphic column of SE Core. Depth is in meters below ground surface.

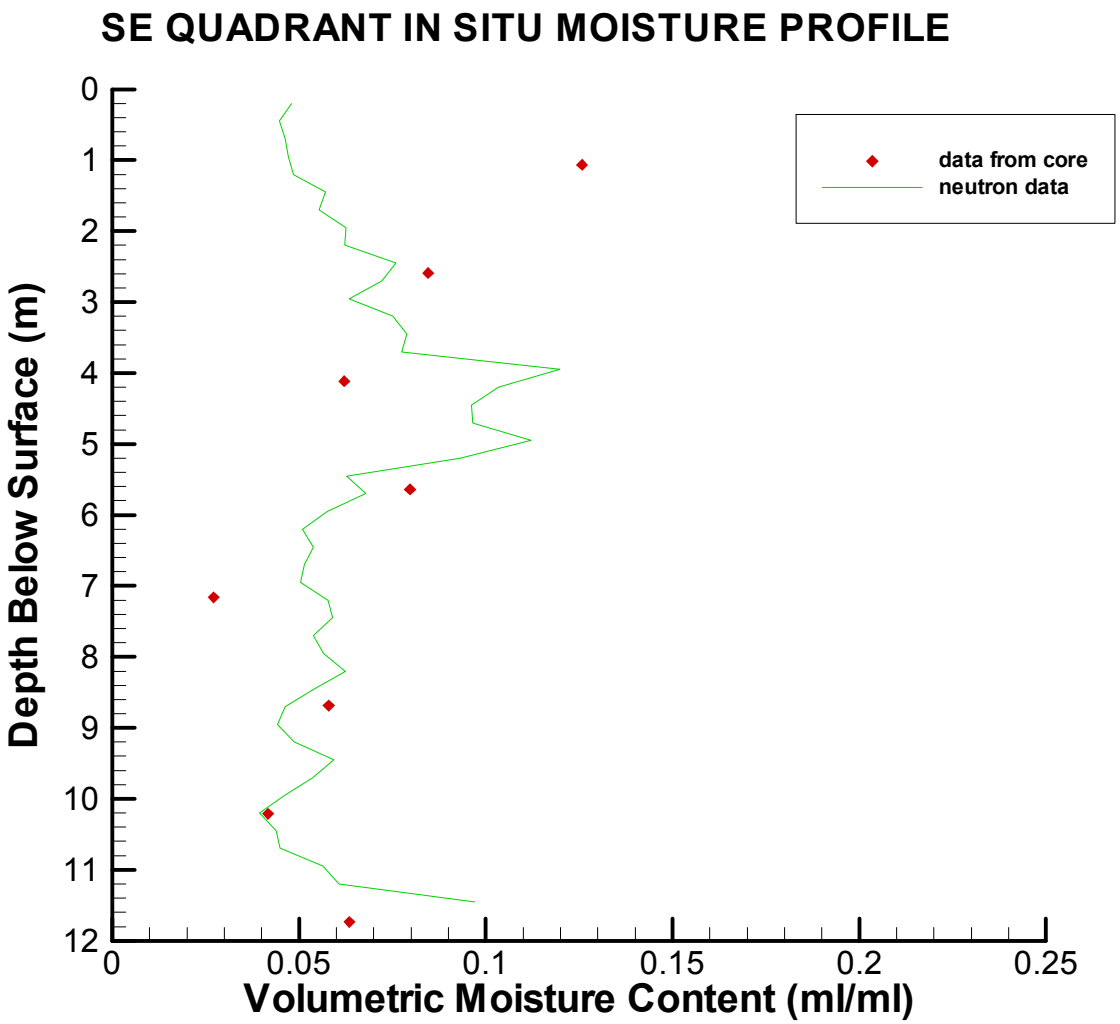

Figure A.6 – In situ moisture profile SE Quadrant. Diamonds represent estimated volumetric moisture content from gravimetric data collected from drilling. Solid line represents moisture profile estimated from neutron data. The neutron probe was not calibrated to the clay deposits, therefore the moisture profile between 4-6 m bgs is questionable.

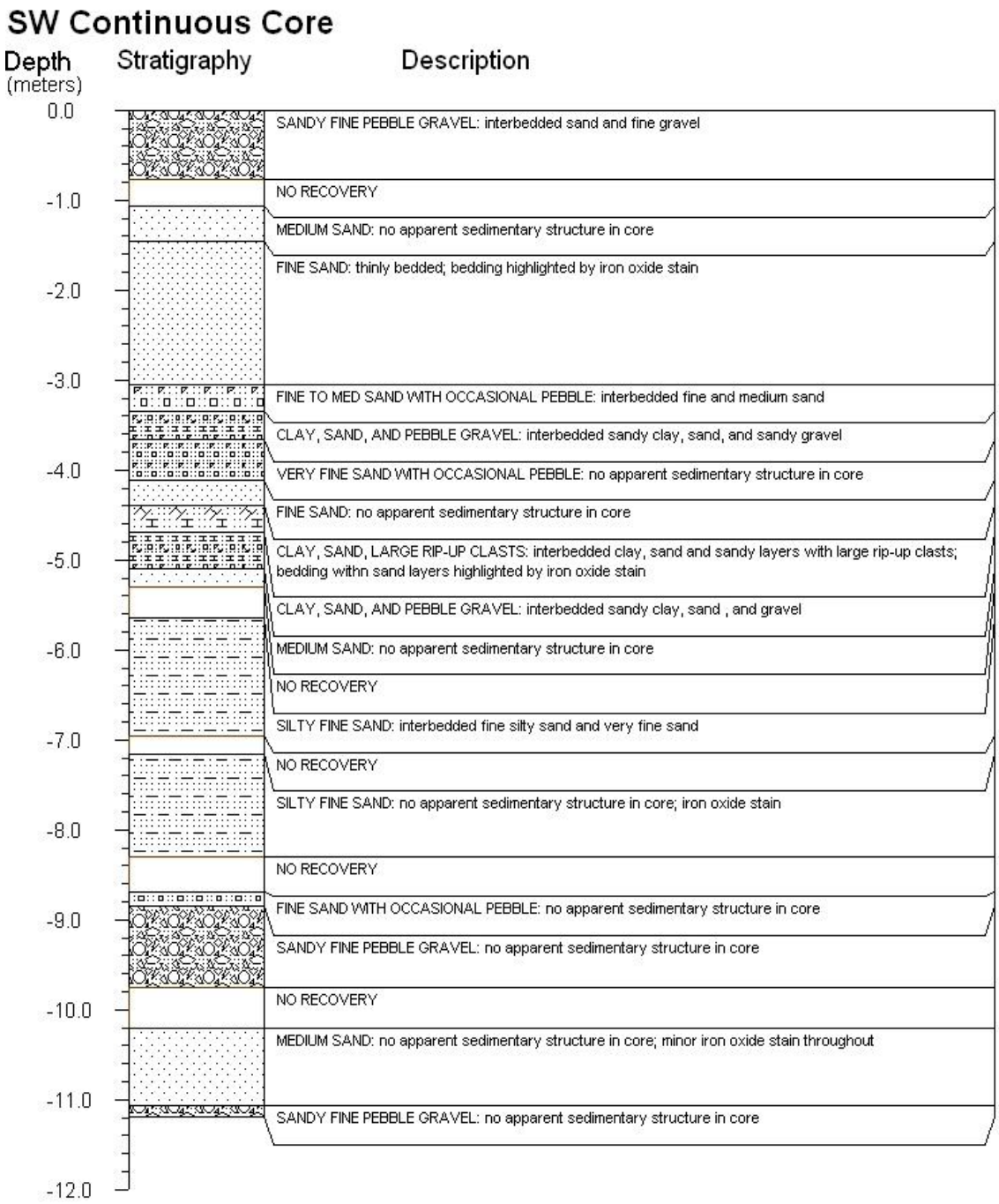

Figure A.7 – Stratigraphic column of SW Core. Depth is in meters below ground surface.

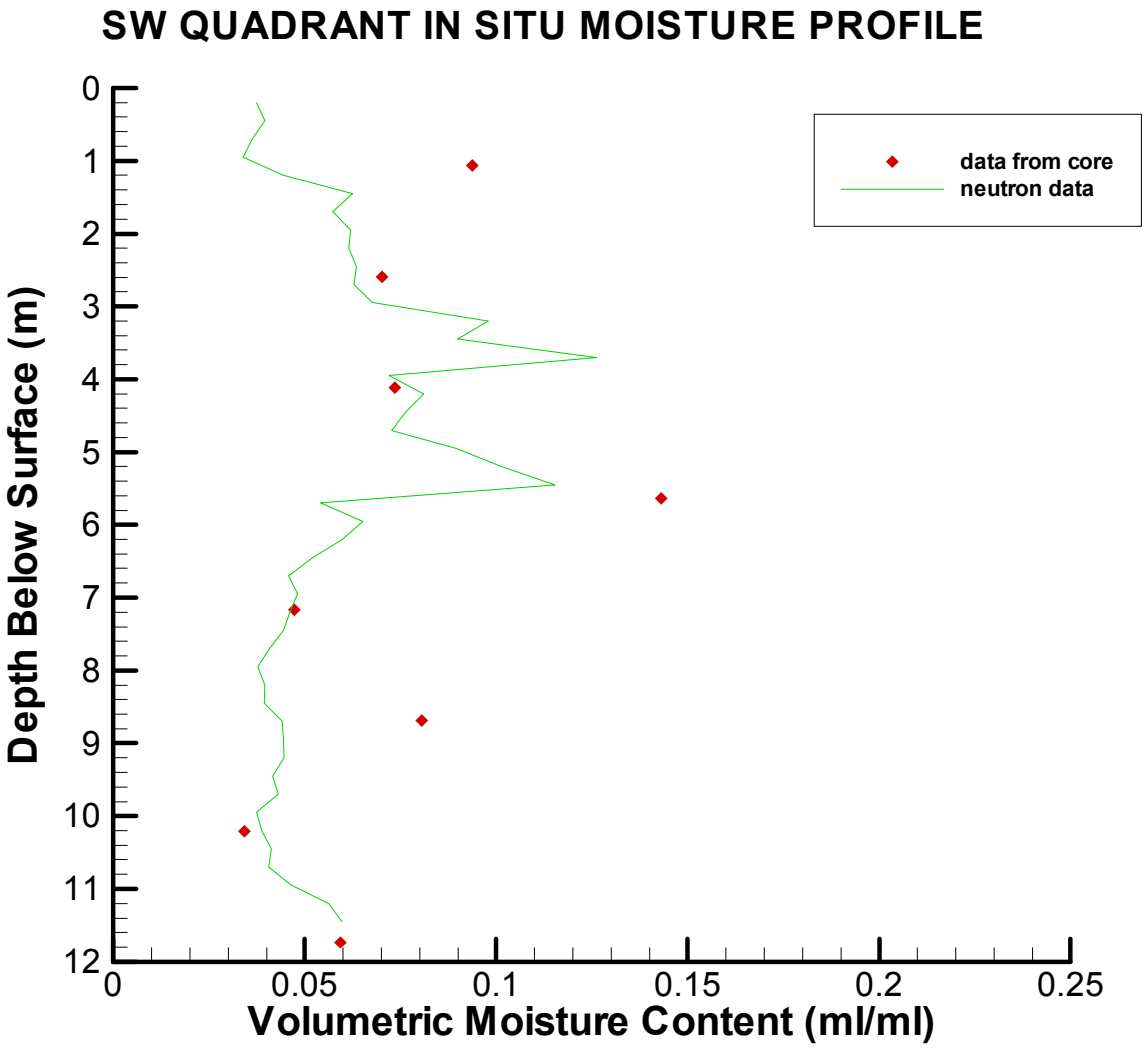

Figure A.8 – In situ moisture profile SW Quadrant. Diamonds represent estimated volumetric moisture content from gravimetric data collected from drilling. Solid line represents moisture profile estimated from neutron data. The neutron probe was not calibrated to the clay deposits, therefore the moisture profile between 4-6 m bgs is questionable.

Appendix B

Preliminary Studies

B.1 Highly Disturbed Intact Core Moisture Retention Measurements

Soil hydraulic properties are strongly influenced by natural structure, particularly in the wet range of matric potentials (Klute, 1986). Exposed geologic units adjacent to the infiltration test site reveal geologic structures such as laminations and cross-bedding (see Chapter 2). Geologic structure was also observed in the intact core collected from the field site (see Chapter 2). Because of these observations, we initially intended to collect undisturbed samples for laboratory analysis by gently pushing 100 cc rings into intact core, however our attempt to collect "undisturbed" samples was unsuccessful, primarily due to poor consolidation of the deposits and dry conditions of the core. Measured moisture retention parameters exhibited a higher degree of variability among samples collected from visibly similar geologic units at adjacent locations compared to parameters measured between repacked samples of similar textures. We believe the high degree of variation in the parameters was primarily due to sub-sampling disturbance along the edge of the sample ring rather than due to spatial variability or measurement uncertainty (based on examination of parameter variability between samples – see Appendix K). Therefore, laboratory derived hydraulic properties were measured from repacked soil samples rather than "undisturbed" sub-cores.

B.1.1 Methods and Results

Four five ft sections of core collected from the NE quadrant were split open and 100 cc polycarbonate rings were gently pushed into moderately moist (*in situ* moisture

content ranging from 2 to 10% by volume) sections of core. Three samples each were collected from four geologic units (units 1 through 4 – see Appendix A) at approximately the same location (depth below surface). The rings were pushed into the core to preserve the *in situ* vertical orientation. Despite careful laboratory techniques, cracks and void spaces formed within the samples while pushing the rings into the core. These structures were not evident within the sections of core prior to insertion of the rings. We hypothesize that friction along the edges of the rings caused this disturbance while pushing the rings into the core.

The samples were saturated under a vacuum (flushing with CO_2 – see Appendix D) and placed in the hanging column apparatus. The samples were drained incrementally in the hanging columns from 0 to 150 cm tension. Although three samples were collected from each geologic unit, one sample fell apart during drainage, therefore the following results do not contain data for all samples originally collected. The observed data, along with fitted curves obtained from the RETC fitting FORTRAN program, (M.Th. van Genuchten, et al., 1991) are displayed in Figures B.1-B.5. Tables B.1-B.4 list the moisture retention data for all the samples analyzed.

Table B.1 – Primary drainage data for medium to coarse grained sands (Unit 1).

sample ID:	1b		1c
θ	**Ψ (cm)**	**θ**	**Ψ (cm)**
0.3751	2	0.4147	2
0.3400	12	0.4096	12
0.2757	22	0.3526	22
0.1612	32	0.2010	32
0.0684	42	0.0822	42
0.0404	52	0.0506	52
0.0325	62	0.0405	62
0.0237	102	0.0302	102
0.0170	152	0.0236	152

Table B.2 – Primary drainage data for gravels (Unit 2).

sample ID:	2a		2b		2c
θ	Ψ (cm)	θ	Ψ (cm)	θ	Ψ (cm)
0.3395	2	0.2955	2	0.4396	2
0.2663	12	0.2584	12	0.3777	12
0.2522	22	0.2503	22	0.2407	22
0.1082	32	0.1605	32	0.1268	32
0.0634	42	0.1007	42	0.0868	42
0.0445	52	0.0788	52	0.0707	52
0.0445	62	0.0668	62	0.0626	62
0.0357	102	0.0547	102	0.0411	102
0.0263	152	0.0449	152	0.0302	152

Table B.3 – Primary drainage data for fine grained sands (Unit 3).

sample ID:	3a		3b		3c
θ	Ψ (cm)	θ	Ψ (cm)	θ	Ψ (cm)
0.5164	2	0.5766	2	0.5824	2
0.4625	12	0.5161	12	0.5166	12
0.4493	22	0.5051	22	0.5060	22
0.4452	32	0.4823	32	0.4958	32
0.4310	42	0.4735	42	0.4881	42
0.4256	52	0.4659	52	0.4841	52
0.4091	62	0.4415	62	0.4706	62
0.3284	102	0.2990	102	0.3109	102
		0.1564	152	0.1597	152

Table B.4 – Primary drainage data for sandy clay (Unit 4).

sample ID:	4a		4b		4c
θ	Ψ (cm)	θ	Ψ (cm)	θ	Ψ (cm)
0.3264	2	0.3778	2	0.3108	2
0.3109	12	0.3583	12	0.3011	12
0.3051	22	0.3506	22	0.2969	22
0.2932	32	0.3435	32	0.2911	32
0.2786	42	0.3378	42	0.2846	42
0.2606	52	0.3354	52	0.2813	52
0.2536	62	0.2617	102	0.2035	102
0.2251	102	0.0776	152	0.0400	152
0.1819	152				

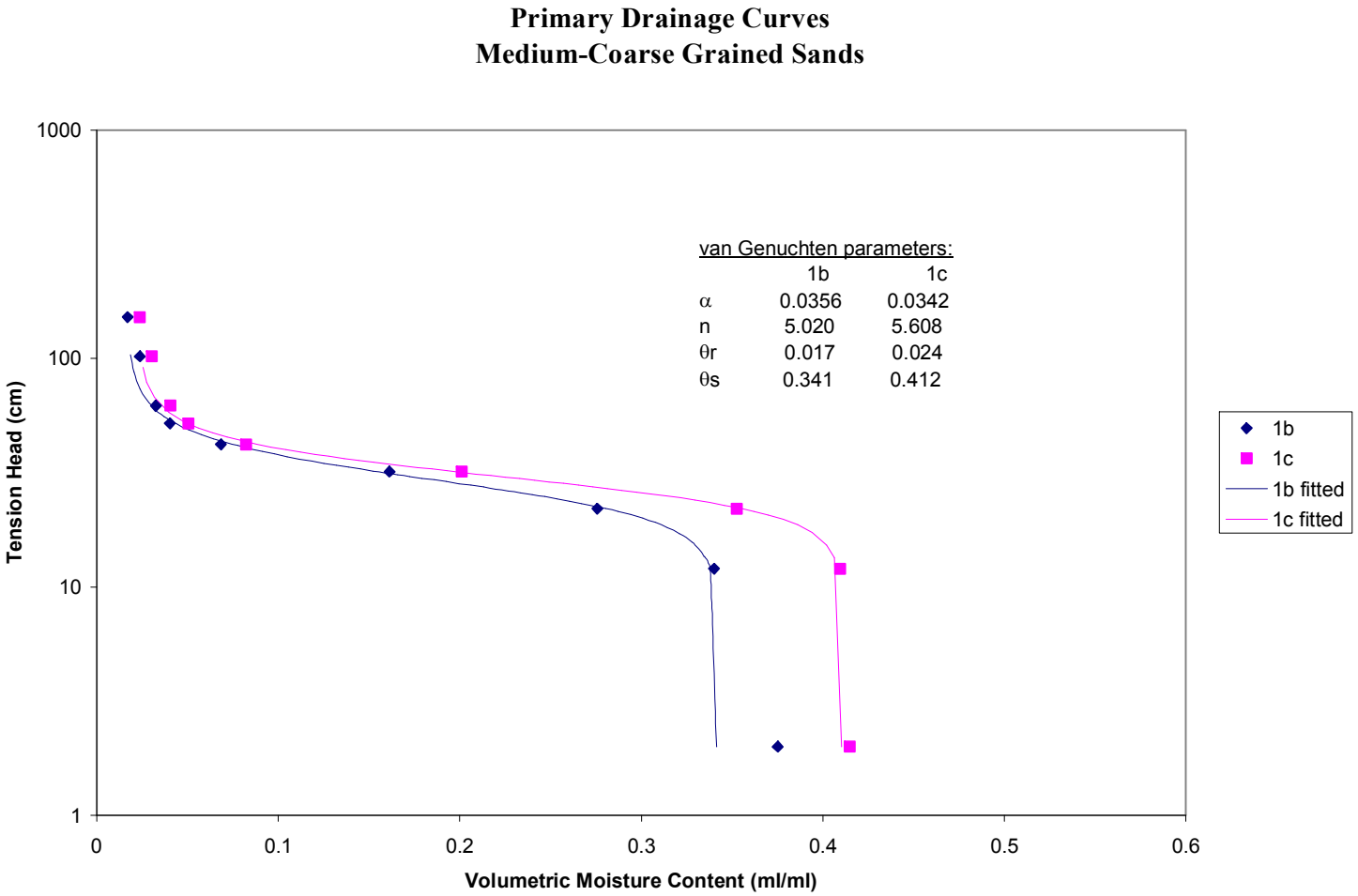

Figure B.1 – Primary drainage curves for medium - coarse grained sands.

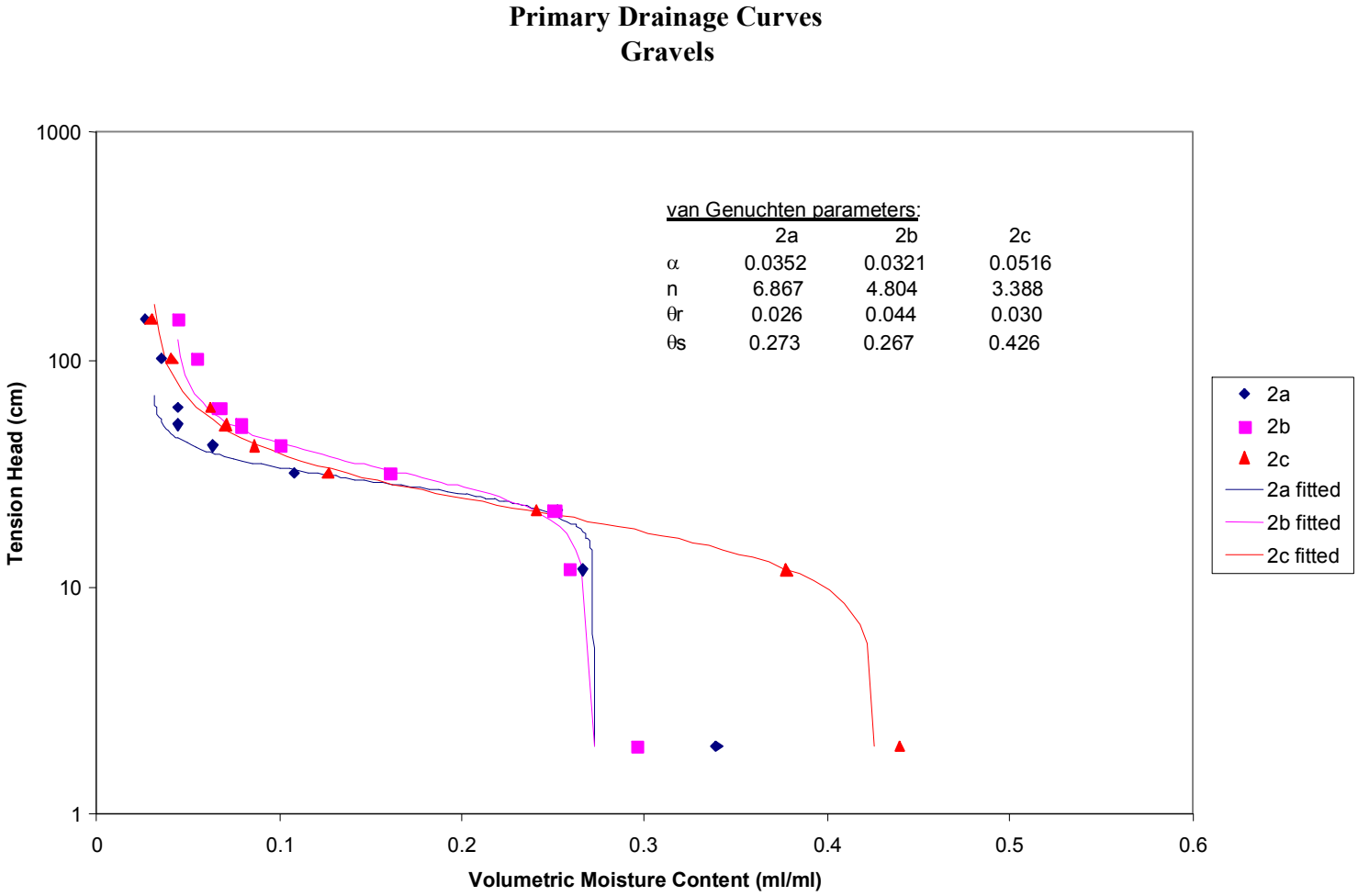

Figure B.2 – Primary drainage curves for gravels.

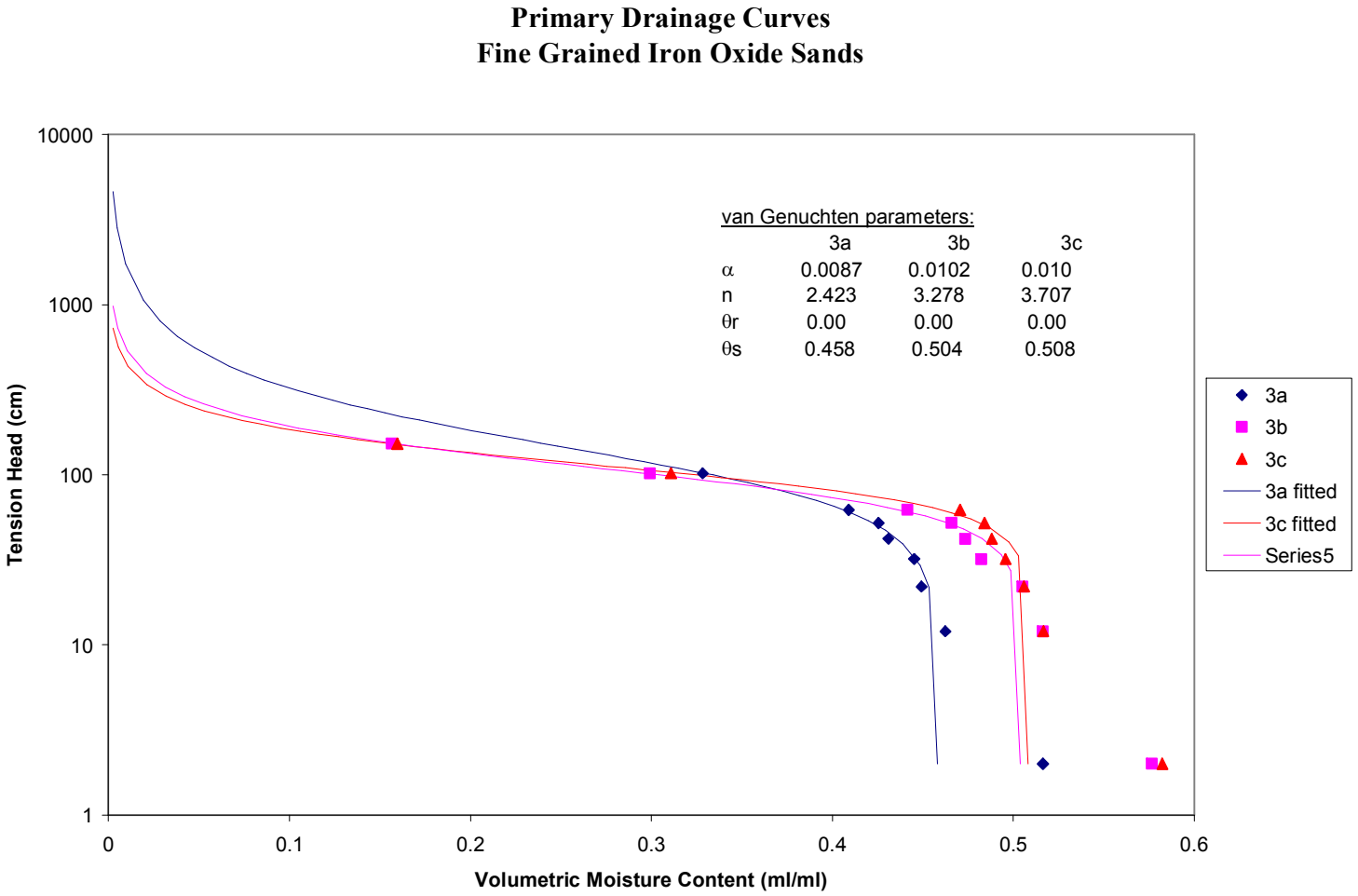

Figure B.3 – Primary drainage curves for fine grained, iron stained sands.

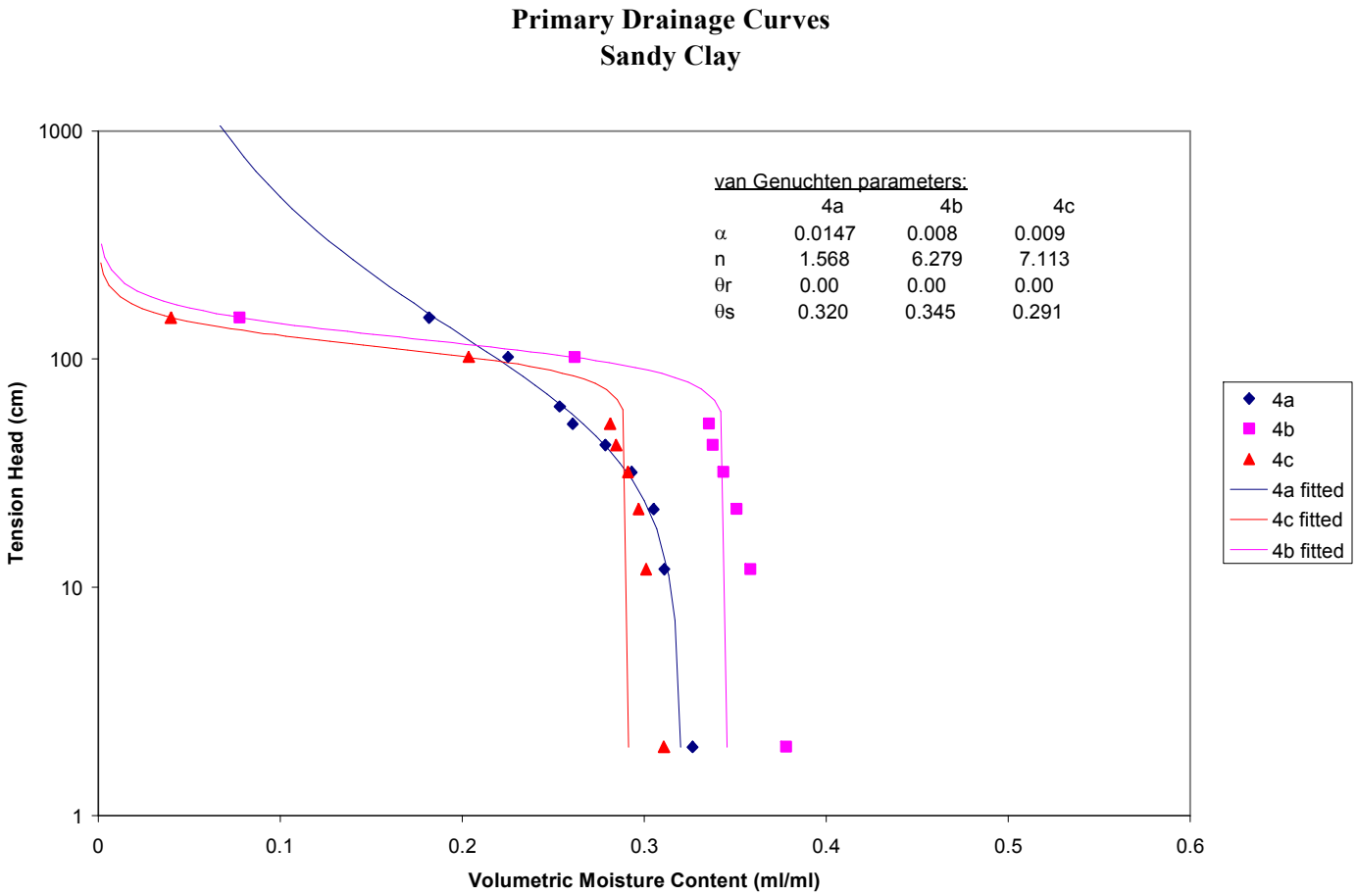

Figure B.4 – Primary drainage curves for sandy clays.

B.1.2 Conclusions

The curves reflect significant variations between properties, in particular porosity, which was impacted the most due to formation of void spaces during sub-coring. Due to the high degree of disturbance observed during our attempt to collect intact samples, we conclude that although repacked samples may not represent *in situ* conditions, the data collected from the repacked samples will better estimate hydraulic properties for alluvial deposits of similar textures than data collected from highly disturbed samples which contain large void spaces, cracks, and disturbance along the edges of the rings.

B.2 Impact of Natural Structure on Moisture Retention Properties

Since undisturbed samples of poorly consolidated deposits are difficult to obtain, we conducted a study to examine the impact of natural structure on moisture-retention characteristics of the STVZ deposits. In this study we examine the moisture retention curves obtained from undisturbed and repacked samples of sandy deposits collected from the STVZ site. Six undisturbed samples were collected from an exposed trench adjacent to the infiltration test pad (see Brainard, 2000). Geologic structures were not observed in the exposed trench or the intact transparent sample rings, possibly due to disturbance during excavation. Three of the samples were collected from a medium-coarse grained sand layer, and three were collected from a fine-medium grained sand layer. Both layers are located approximately 5-6 meters below the top of the infiltration pad. The sample textures are representative of the majority of the deposits located at the site.

Three of the samples were collected from a medium-coarse grained sand unit, denoted Unit 3 (one sample from this unit was disturbed during analysis) and three were collected from a fine-medium grained sand unit, denoted Unit 4. Both units are located approximately 5-6 meters below the top of the infiltration pad. The sample textures are

largely representative of the primary deposits located at the site. After the primary drainage curve for the undisturbed samples was measured, the samples were oven dried, homogenized (separately) and repacked to the *in situ* bulk density and the drainage sequence was repeated.

The results do not indicate a significant difference between the undisturbed and repacked sample moisture retention fitting parameters (see Figures B.5 and B.6). Statistical analysis was not performed due to the small sample set, therefore definitive conclusions cannot be drawn from these results, however we conclude that for the purpose of our research, repacked sandy deposits collected from the STVZ site exhibit similar moisture retention properties as intact samples.

The difference in shape, air entry values, and porosity between the two units (fine-grained versus coarse-grained sands) can be attributed to the difference in grain textures. The particle size distributions show a difference in d_{10} values between the two units, and indicate that Unit 4 is well sorted while Unit 3 is poorly sorted (see Figure B.7). Sorting plays a major role in the shape and fitting parameters of moisture retention curves. The well sorted deposits have a higher air entry pressure and a higher porosity than the poorly sorted deposits.

Table B.5 – Hydraulic properties of undisturbed Socorro samples (fitting parameters λ, Ψae obtained from Brooks & Corey equation fit to data using MATHCAD)

Sample ID	Initial Moisture Content	Bulk Density	Intact sample Porosity	Repacked sample Porosity	Intact λ (B&C)	Repacked λ	Intact Ψae (cm)	Repacked Ψae (cm)
S3-4	0.05	1.61	0.368	0.371	1.295	1.264	16.542	16.408
S3-5	0.05	1.62	0.367	0.378	1.138	1.032	14.260	13.745
S4-2	0.05	1.52	0.383	.0390	1.402	1.339	24.374	24.215
S4-3	0.06	1.53	0.386	0.388	1.382	1.358	24.573	24.514
S4-6	0.06	1.55	0.380	0.403	1.555	1.421	25.449	24.581

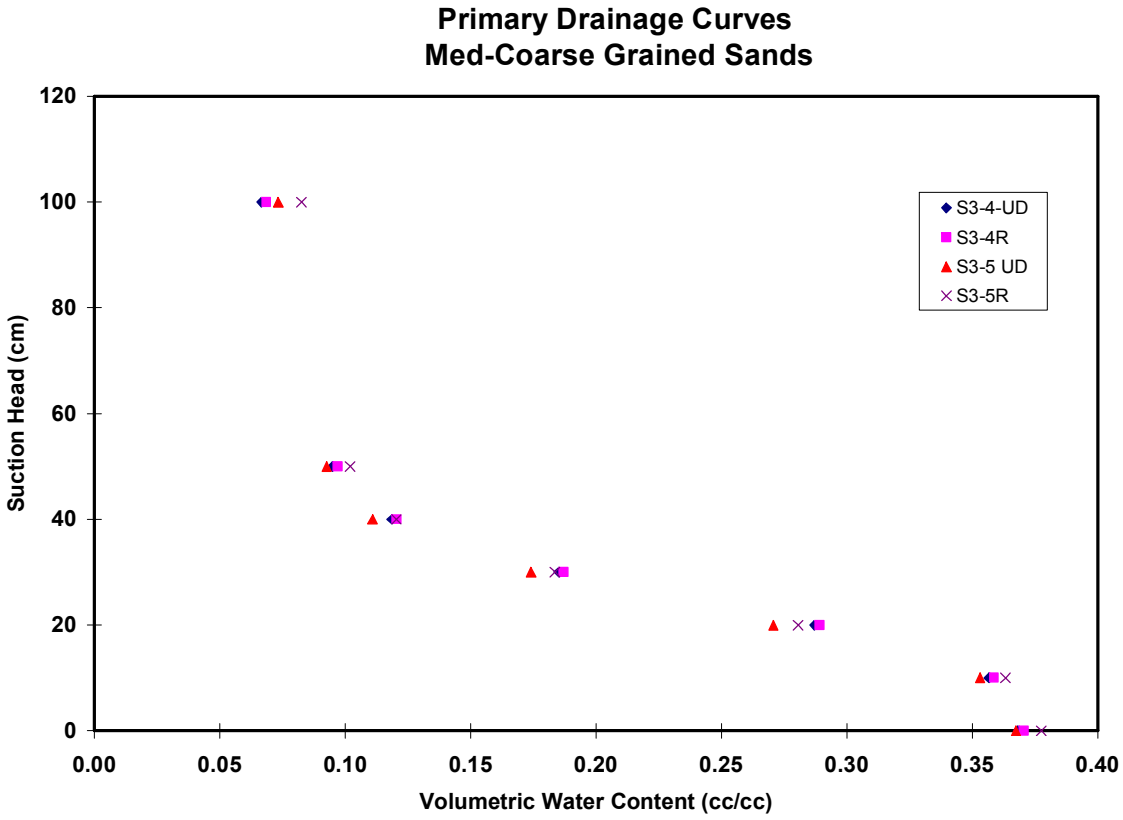

Figure B.5 – Undisturbed vs. repacked sample moisture retention curves for medium- fine grained sands.

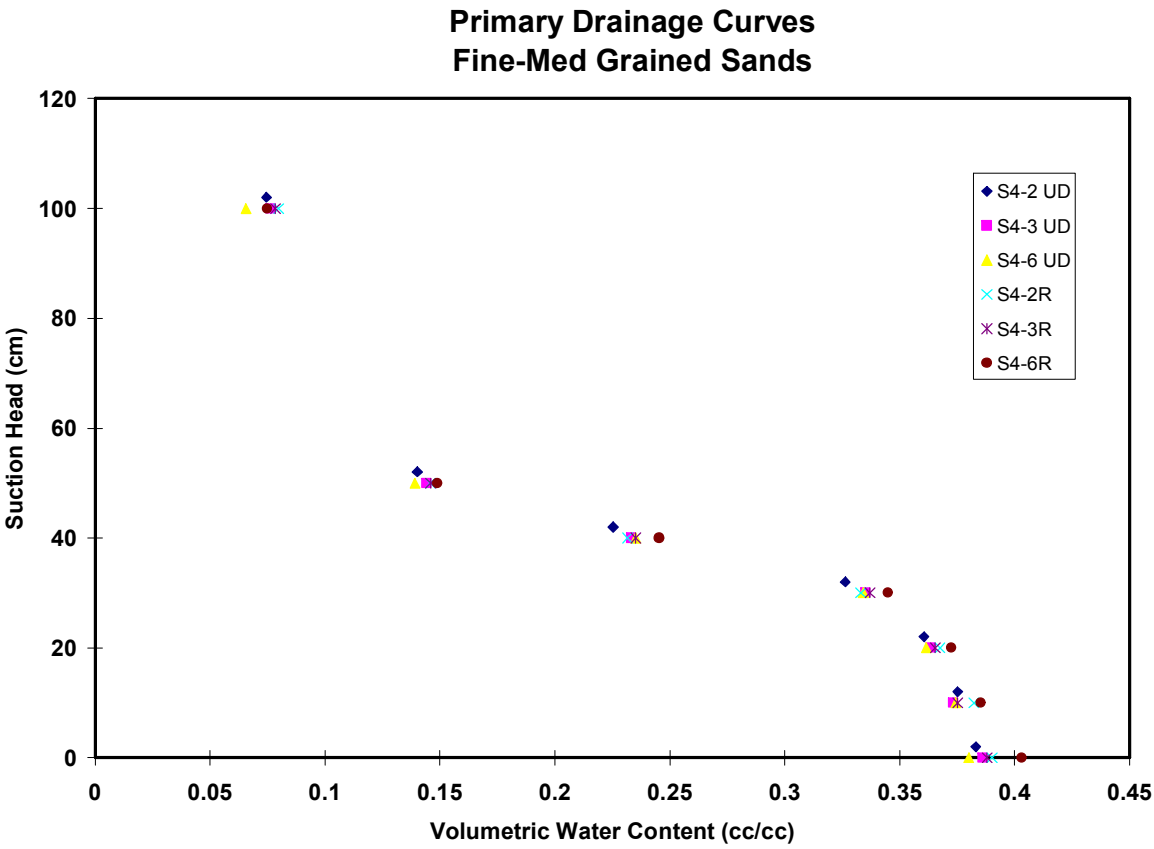

Figure B.6 – Undisturbed vs. repacked moisture retention curves for fine-medium grained sands.

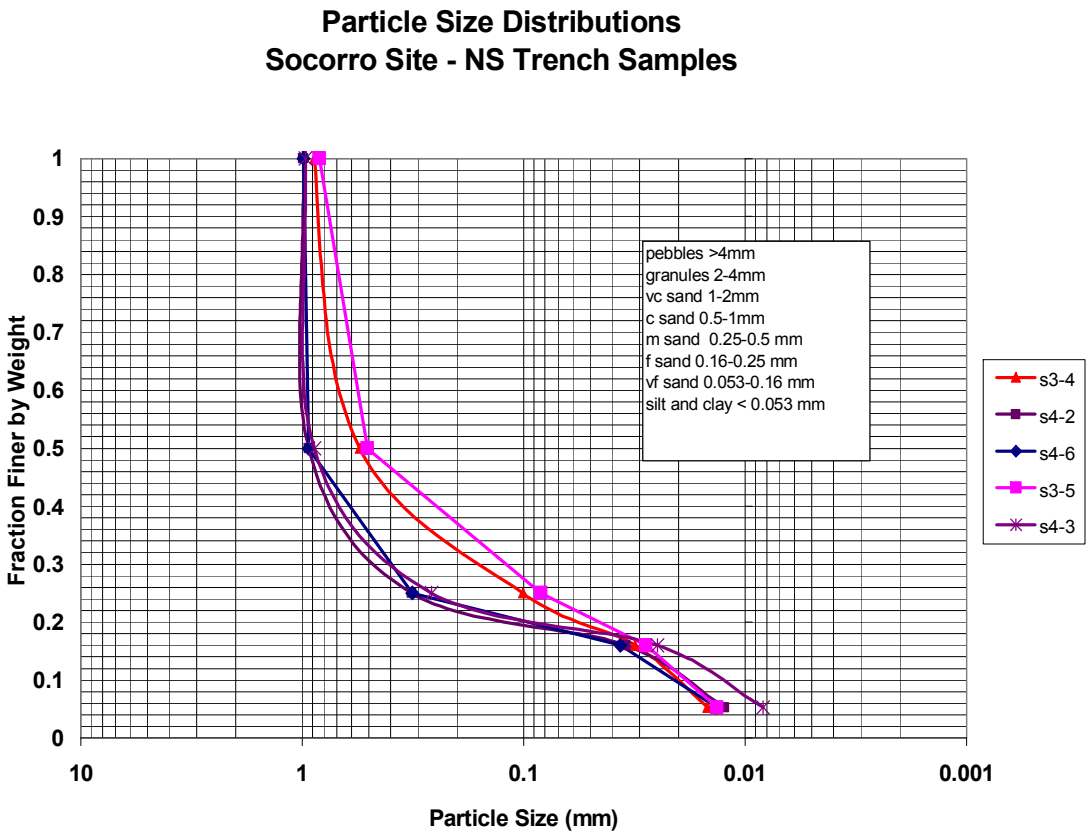

Figure B.7 – Particle size distributions for samples collected in NS trench.

B.3 Over-Saturation Estimates

Preliminary saturation tests show overestimated values of porosity compared to calculations from the bulk density measurement of the samples (see Figures 1-4). The measured primary drainage curves consistently show rapid moisture loss from 0-12 cm tension (by as much as 4-7% moisture content by volume) followed by a relatively constant moisture content with large changes in tension until air entry pressure is reached. During analysis of moisture retention properties, the samples are secured in a 100 cc ring with a section of cotton cloth at the top and bottom of each ring to prevent disturbance during resistivity measurements. We hypothesize that additional absorption of water by the cloth is contributing to the overestimates in porosity. To test this

hypothesis, we saturated empty sample rings with a cotton cloth attached to the bottom of the rings. We then drained the cloth in the hanging column apparatus to determine the degree of moisture loss from the cloth during de-saturation. The test results show that the cloth absorbs approximately 0.02 volumetric moisture content per section of cotton cloth (0.04 per sample). Although the cloth did not completely drain at 20 cm tension, the volume of water retained by the cloth was well within the margin of measurement precision for the scale used to measure the samples (+/- 0.01 g). Any additional moisture loss during de-saturation (> 0.04 volumetric moisture content) may have been due to drainage of pores along the edge of the sample ring. Stephens and Rehfeldt (1985) observed artificially large water contents at 0 cm tension, which they also hypothesized was due to large void spaces between the sample and the ring. To examine the volume absorbed along the edge of the ring, we calculated the pore radius (R) for water drained at 12 cm tension , we used the Laplace-Young equation (Jury et al., 1991)

$$R = \frac{2\sigma}{\rho g h} \qquad \text{(B-1)}$$

where σ is the surface tension of water (0.072 N/kg), ρ is the density of water (1000 kg/m^3), g is the gravitational constant (10 N/kg), and h is the tension head (0.12m). From this equation, the pore radius drained is estimated to be 0.12 mm. This would account for 0.017 volumetric water content, calculated by multiplying the circumference of ring (17.91 cm) times height of ring (4 cm) times diameter of pore (0.024 cm). This reasonably accounts for any excess water being drained from the sample.

Tables B.6 through B.8 – Cloth saturation test results.

Ring ID	Ring dry wt (g)	Ring sat wt (g)	Cloth dry wt (g)	Cloth area (cm^2)	Cloth wt @ 5 cm tension(g)	Cloth wt @ 10 cm tension(g)	Cloth wt @ 20 cm tension(g)
6a	31.64	33.41	0.7	56.75	32.88	32.75	32.6
6b	31.43	33.31	0.69	56.75	32.59	32.59	32.38
7c	29.06	31.14	0.72	56.75	30.52	30.46	30.31

Ring ID	Vol of Water @ sat (ml)	Vol drained @ 5 cm tension (ml)	Vol drained @ 10 cm tension (ml)	Vol drained @ 20 cm tension (ml)
6a	1.77	0.53	0.13	0.15
6b	1.88	0.72	0.00	0.21
7c	2.08	0.62	0.06	0.21

Ring ID	Vol moisture content @ sat (per ring)	Ring vol moisture content @ 5 cm tension	Ring vol moisture content @ 10 cm tension	Ring vol moisture content @ 20 cm tension
6a	0.0177	0.0050	0.0010	0.0015
6b	0.0188	0.0070	0.0000	0.0021
7c	0.0208	0.0060	0.0006	0.0021

In summary, the moisture content at saturation is more than likely overestimated due to excess water retained in the cotton cloth (~4%) and water retained along the edges of the ring (~2%) resulting in approximately 6% overestimation of porosity. Based on these results, sample saturation was assumed to equal volumetric moisture content at 20 cm tension for the majority of the samples (see Appendix J for curve fitting estimates of saturation).

B.4 Cause and Degree of Sediment Compaction During Desorption

Preliminary moisture retention tests involving undisturbed samples of near surface deposits collected from the STVZ infiltration test site resulted in approximately 10% volume loss during desorption experiments starting from saturation (PDC). Before we attempted to measure moisture retention characteristics from core samples, we conducted

a study to examine the cause and degree of compaction during desorption. We collected 20 undisturbed samples of coarse-grained, near surface deposits (Unit 1) and 20 undisturbed samples from a fine-grained sand located approximately 20 ft below ground surface (from a nearby sand quarry). We hypothesized that the chemical solution of the wetting fluid may have led to dissolution of minerals possibly leading to collapse during saturation/desaturation processes. To examine dissolution, we used 2 wetting solutions to saturate the samples: tap water from Socorro, NM (used for laboratory analysis), and a 0.005M $CaSO_4$ solution (to increase the ionic strength of the solution).

The average bulk density of the near surface deposits was 1.49 g/cc (0.44 porosity) while the average density of the sand quarry sands was 1.37 g/cc (0.48 porosity). We saturated the samples and allowed them to reach equilibrium at 0 cm tension. Simply saturating the samples without desorption caused collapse resulting in approximately 2% volume loss in the near surface deposits using tap water and 7 to almost 10% volume loss using the calcium sulfate solution. Only one sample from the sand quarry compacted using tap water only (see Table B.9). We then drained the samples at 30 cm tension for near surface deposits and 50 cm for fine sands (resulting in approximately 20 volume percent moisture content). The samples did not compact further after draining at these tensions for either the coarse sands or the fine sands. This suggests that simply wetting the near surface deposits disturbed the samples. The collapse does not appear to be caused by mineral dissolution, since the calcium sulfate solution caused a greater degree of compaction than the tap water. Although it is not clear why the higher ionic strength solution caused greater compaction, we concluded that tap water would result in a lesser degree of sample disturbance, therefore we used tap

Table B.9 – Compaction Test Results

sample ID	initial height in ring (cm)	tension head (cm)	final height (cm)	height lost (cm)	percent volume loss	tension head (cm)	final height (cm)	height lost (cm)	final percent volume loss
A18	4	0	3.9	0.1	2.5	30	3.9	0.1	2.5
A20	4	0	3.8	0.2	5	30	3.8	0.2	5
A37	4	0	4	0	0	50	4	0	0
A38	4.5	0	4.5	0	0	50	4.5	0	0
A34	4.2	0	4.1	0.1	2.38	50	4.1	0.1	2.38
B35	4.2	0	4.2	0	0	50	4.2	0	0
B28	4.1	0	4.1	0	0	50	4.1	0	0
B39	4.1	0	3.8	0.3	7.32	50	3.8	0	7.32
B15	4.3	0	4	0.3	6.98	30	3.9	0.4	9.3
B11	4.2	0	3.8	0.4	9.52	30	3.8	0.4	9.52
B16	4.2	0	3.8	0.4	9.52	30	3.8	0.4	9.52

NOTE: samples with a prefix of "A" were imbibed with Socorro tap water
samples with a prefix of "B" were imbibed with a 0.005M CaSO4 solution
samples in Bold are from Unit 1 (coarse grained near surface deposits)

water as the wetting solution for moisture-retention and hydraulic conductivity measurements. Since the samples analyzed were repacked, we did not observe significant collapse during wetting/draining sequences even in the near surface deposits.

B.5 Equilibrium Time Determination

We determined equilibrium was reached during drainage in the hanging columns after the water level in the burette ceased to increase over a 24 hour period. Although this is an accepted practice (Jury et al., 1991; Stephens, 1995), we validated the method by conducting two preliminary tests. In the first test, we compared the calculated moisture content determined by weighing the sample daily until the weight ceased to decrease (within +/- 0.03 g) and the moisture content determined by weighing the sample after the water level in the burette ceased to increase. Comparison between the two methods

indicates that the equilibrium moisture contents achieved at a series of tension heads were very similar (+/-0.01 volumetric moisture content – see Figure B.8). Since it took significantly less time to reach equilibrium by monitoring the water level than monitoring changes in sample weights, we determined that monitoring the water level in the burette was a more time efficient method for determining moisture equilibrium.

Our second test involved monitoring moisture equilibrium with a pressure transducer attached to a "mini-tensiometer" constructed of PVC tubing and a 1 bar ceramic cup. Figures 9 and 10 show results of the study indicating that moisture equilibrium was reached for a fine grained sand at approximately -40 cm pressure after approximately 7 hours and at -83 cm pressure after approximately 10 hours.

B.6 Impact of Sample Contact on Electrical Resistivity Measurements

To determine the optimum degree of sample contact with the impedance analyzer electrodes for electrical resistivity measurements, we saturated a highly conductance porous material (clay) and a highly resistive material (coarse-grained sand), drained the samples at 30 cm tension, allowing the samples to reach moisture equilibrium, and measured the electrical resistivity at different degrees of sample contact. We placed the samples in the impedance analyzer sample holder (see Appendix F.1) and measured impedance without tightening the bolts on the holder, hand tightening the bolts, tightening the bolts 3 turns with a wrench, and tightening the bolts 6 turns with a wrench. The impedance varied by more than 10% between the hand tightened measurements and the measurements when the bolts were tightened 3 turns with a wrench (for both samples), but the impedance varied by less than 5% between measurements taken when the bolts were tightened 3 turns and 6 turns with a wrench.

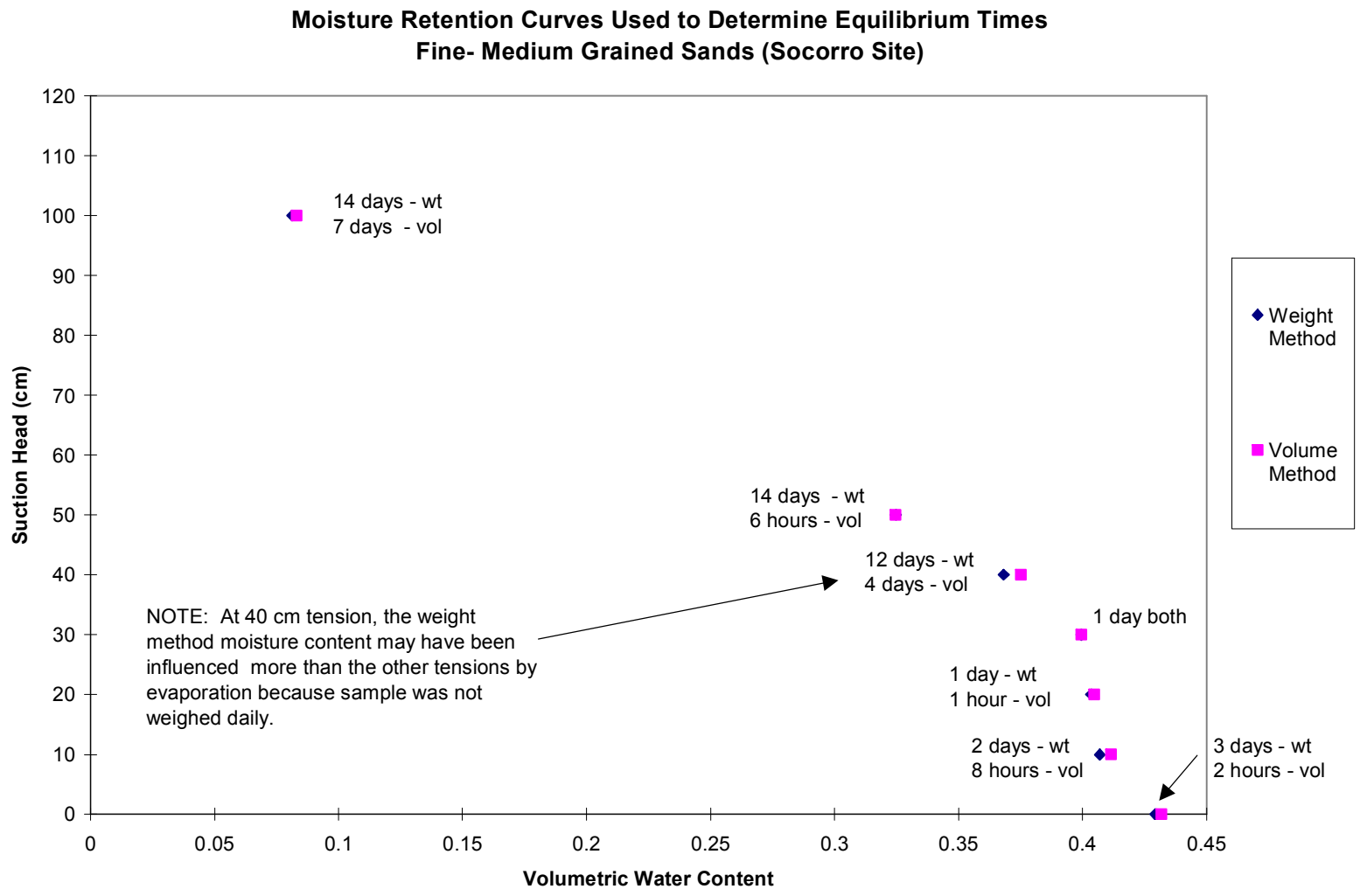

Figure B.8 – Determination of moisture equilibrium by monitoring sample weight and water level in burette.

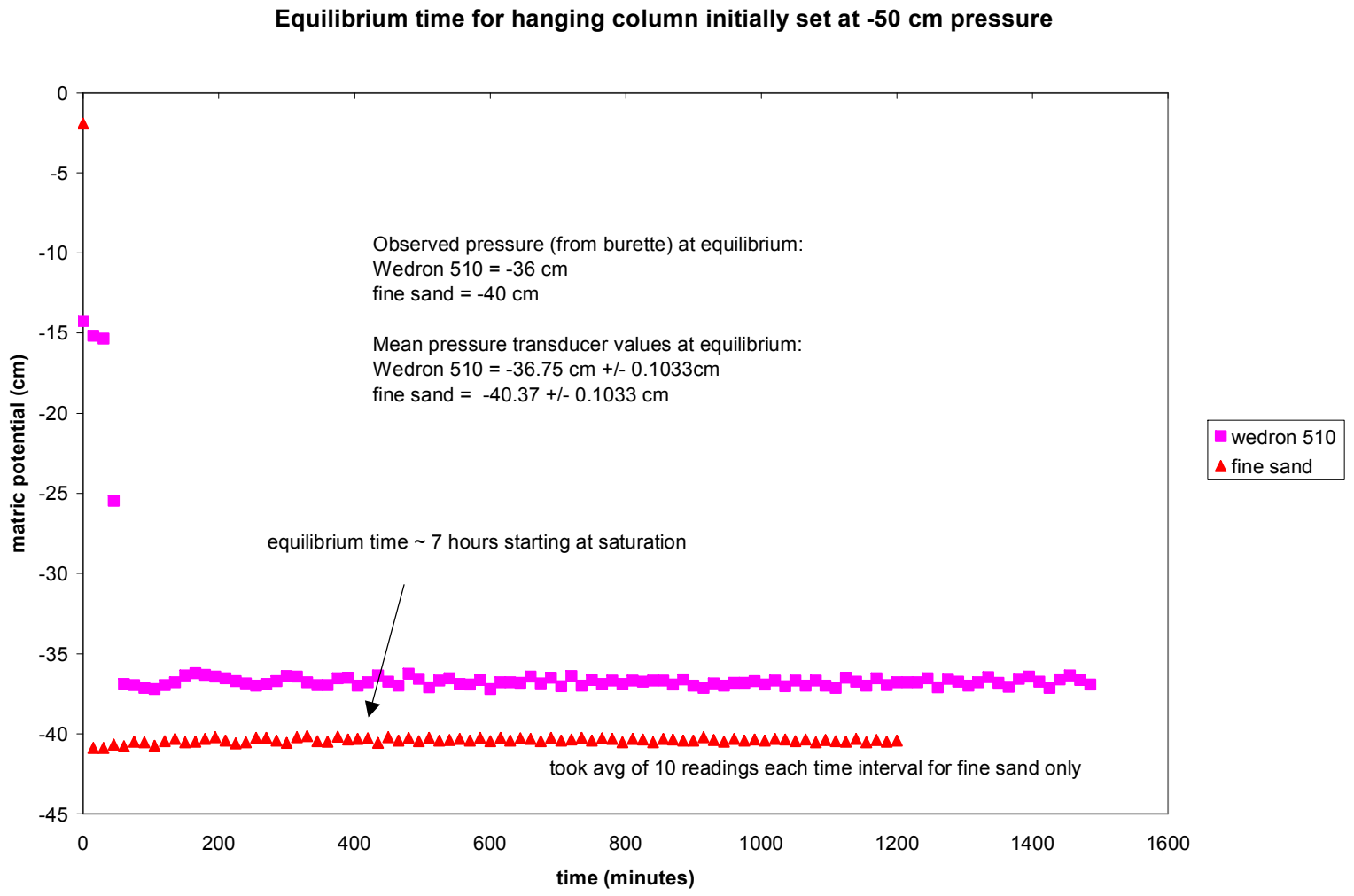

Figure B.9 – Determination of equilibrium time using a mini-tensiometer and a 5 psi automated pressure transducer starting at -50 cm pressure.

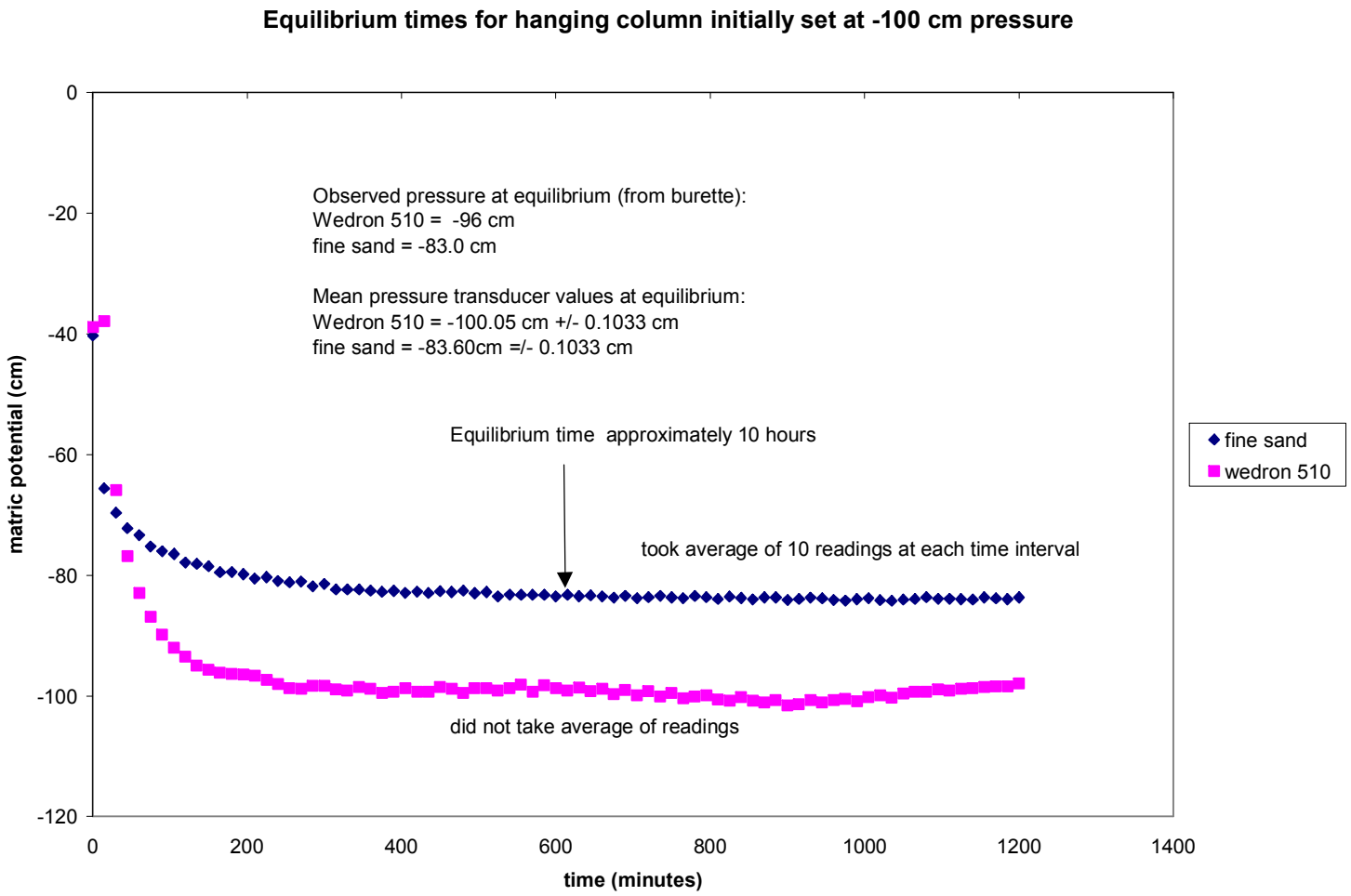

Figure B.10 – Determination of equilibrium time using a mini-tensiometer and a 5 psi automated pressure transducer starting at –100 cm pressure.

Tightening the bolts 6 turns resulted in flow out of the bottom of the ring suggesting compaction to the samples. Based on these results, we determined that tightening the bolts 2-3 turns during sample analysis would provide enough contact between the porous material and the silver plates to obtain adequate impedance measurements, yet would minimize sample compaction. When the samples were saturated, we hand tightened the bolts since we observed flow when the bolts were tightened slightly with a wrench.

Table B.10 – Degree of Contact vs. Measured Impedance

Impedance (ohms)	Resistance (ohm*m)
1) silver plate resting on sample (bolts not tightened at all)	
2b: 441.40	27.81
7b: 1333.00	83.98
2) hand tightened bolts	
2b: 323.80	20.40
7b: 1292.00	81.40
3) tightened bolts 3 turns with wrench	
2b: 268.50	16.92
7b: 1165.10	73.40
4) tightened bolts about 6 turns with wrench (water leaked out bottom)	
2b: 256.50	16.16
7b: 1154.60	72.74
Samples 2b (clay) and 7b (coarse-grained sand) drained in hanging column at 30 cm tension	

Appendix C

Sample Preparation

METHODS

We initially measured moisture retention curves from intact samples collected from the NE core, however the curves reflected a high degree of variance between fitting parameters for samples of similar texture (see Appendix B). We hypothesize this was due to disturbance from drilling and from pushing rings into core which caused formation of void spaces, cracks and disturbance along edges of the rings. Therefore, we divided approximately 36 ft of core collected from the NW quadrant into 6 inch sections, air dried and homogenized the deposits and repacked 100 cubic centimeter (cc) sample rings to a dry bulk density representative of *in situ* conditions determined from measurements made from intact samples collected during drilling and from a nearby trench (ranging from 1.4 to 1.7 g/cc). A piece of cotton cloth was attached to the bottom of the rings with a plastic zip tie to contain the sediment during analysis. Only non-conductive materials were used for the sample ring to reduce interference with electrical resistance measurements at moisture equilibrium (see Appendix F).

We weighed the desired mass of sediment (ring volume times dry bulk density), mixed the sediment in a tray and spooned it into the ring (thoroughly mixing between spoonfuls) until the ring was filled. We placed the sample ring in the hanging column directly on the porous plate (without diatomaceous earth) and quickly wet the sample by raising the burette approximately 1meter above the porous plate. We then quickly drained the sample by lowering the burette to compact the deposits. This process was

repeated until the desired bulk density was reached. Since we were not able to reach the desired bulk density for every sample, the actual bulk density was recorded and used to calculate porosity of the sample.

Once the sample was consolidated, the sample was placed in a relative humidity oven set at 60^{o}C and 65% relative humidity (Flint, 1996) until the *in situ* moisture content was obtained (takes approximately 2-6 hours depending on grain texture). The *in situ* moisture content was estimated from a moisture profile measured in a neutron access borehole located close to the NW core sampling location using a CPN 501 neutron probe (see Figure C.1). See Brainard et al. (2000) for a detailed description of the neutron probe procedures and results.

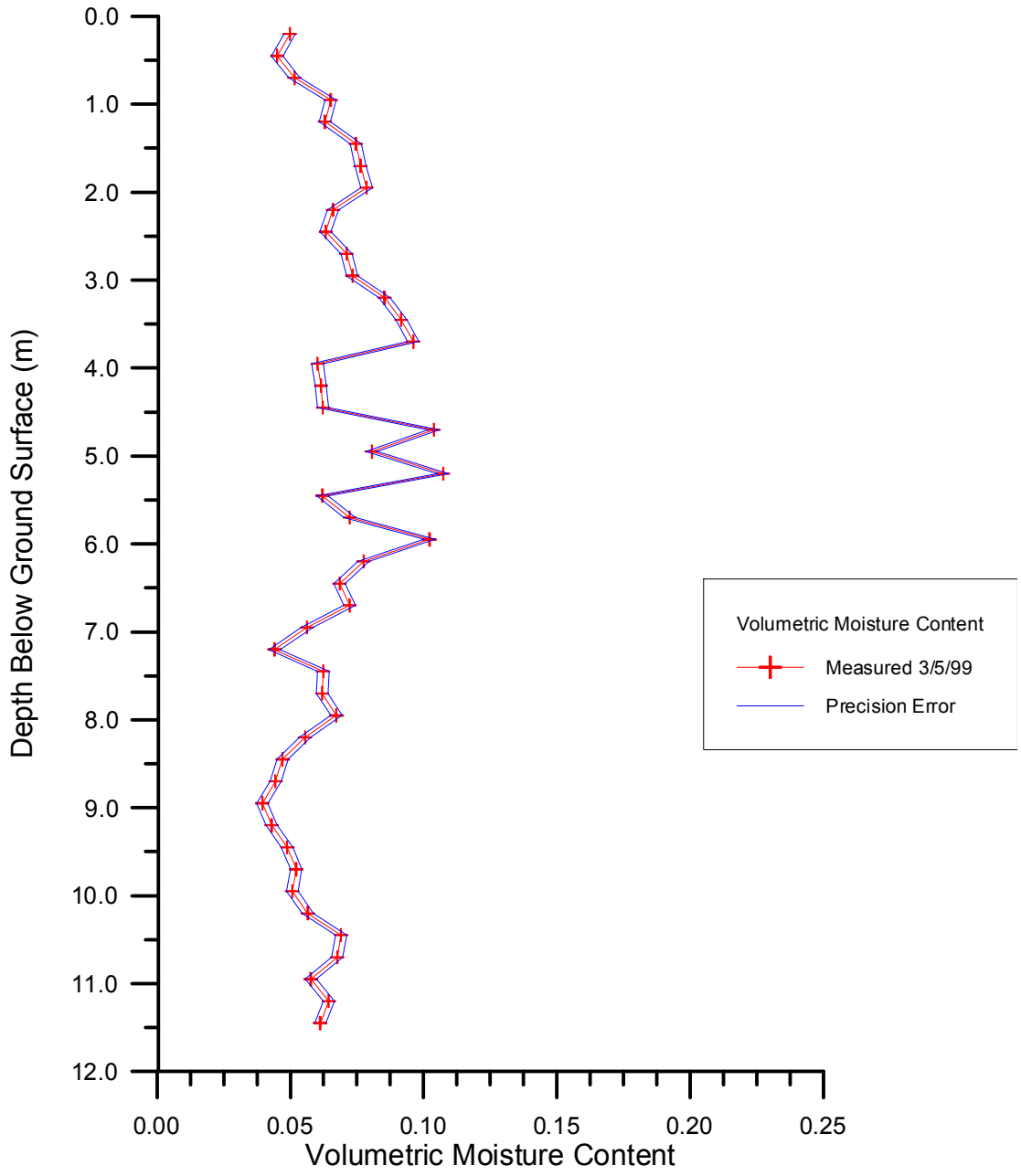

Figure C.1 – In situ moisture profile measured using a CPN 501 neutron probe.

Appendix D1

Electrical Resistivity Measurement Procedures

D1.1 Required Equipment

Sample holder (see Figure 1)

Impedance analyzer (Hewlett Packard model 4192A LF)

PC computer

D1.2 Introduction

We used a Hewlett Packard model 4129A LF impedance analyzer (Knight, 1991) to measure the electrical resistivity of a sample at each sample moisture equilibrium along the MWC and the MDC to establish a relationship between moisture content and resistivity for samples collected at the infiltration test site. This relationship was used to convert the electrical resistivity data measured at the infiltration site to volumetric moisture contents. The impedance analyzer was connected to a personal computer for automated data acquisition of impedance measurements during application of a logarithmic sweep of frequencies of current to the sample. The logarithmic sweep was used to obtain the frequency not affected by polarization at the sample/electrode interface (Knight, 1991). The two-electrode technique (Knight, 1991) was used with electrodes attached to a sample holder (see Figure F1.1). The electrodes are placed in direct contact with variably saturated samples at the top and bottom of the sample rings. Electrical resistivity is calculated from the impedance value corresponding to the lowest phase angle during a logarithmic sweep of frequencies by

$$\rho = I\frac{A}{t} \tag{D1-1}$$

where ρ is the electrical resistivity (ohm*m), I is the sample impedance (ohm), A is the sample cross sectional area (m^2), and t is the thickness (length) of the sample (m).

D1.3 Procedures

1) Connect the sample holder (Figure 1) to the impedance analyzer by inserting the lead wires into the high frequency test fixture (current plates that read "low" and "high") on the front of the analyzer (see user's manual).
2) Tighten the fixtures to obtain adequate contact.
3) Insert the sample into the sample holder and tighten the nuts 2-3 turns (see appendix B) with a wrench after hand tightening, unless the sample is saturated and subject to compaction. In the case of saturation, placing the top plate on the sample should be sufficient (or hand tightening depending on degree of saturation).
4) Turn on the analyzer (push in the button on the upper left corner).
5) If the impedance value reads an error message (such as "UCL") this means there is not sufficient contact or a reading cannot be made. Try wiggling the wires or the fixture or try tightening the nuts down tighter.
6) Turn on the computer and *cd* (DOS command for "change directory") to the NB directory.
7) At the NB prompt, type "go".
8) A message will display asking if you want to overwrite the "sweep.dat" file (output file). Type "y" for yes.

9) If a message displays stating that there is a problem, this means there is insufficient contact or that the sample is too dry for current to flow through.

10) Normally, a screen will be displayed which shows the impedance value, phase angle, and the frequency at each logarithmic frequency (executable runs through a logarithmic sweep of frequencies).

11) The sweep stops at 1000 kHz, but may be writing to the computer for a minute or two after the sweep has discontinued.

12) Once it has stopped writing to computer, hit the ESC button.

13) Edit the "sweep.dat" file to examine output.

14) Scroll through the phase angles to find the lowest angle (closest to zero) – record the corresponding impedance value (in the first column).

15) To calculate the resistivity, multiply the impedance (ohms) by the cross-sectional area of the sample (m^2) divided by the thickness of the sample (m). This will give you the resistivity (ohm*m) (Knight, 1991).

16) An option is to use the "sweep.exe" executable to search the output file for the value corresponding to the lowest phase angle and calculate the resistivity (the FORTRAN code will have to be modified somewhat to skip the first 3 lines of the output file and will either have to be compiled to run in DOS or we will have to install Windows on the computer).

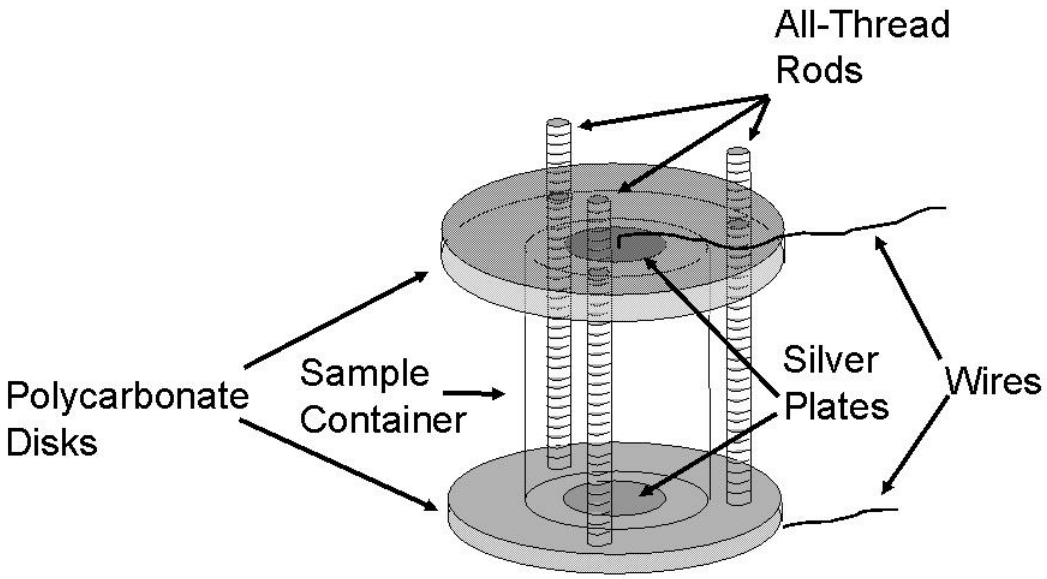

Figure D1.1 – Impedance Analyzer Sample holder.

Appendix D2

Electrical Resistivity Measured Data and Resistivity Versus Moisture Content Curves

Table D2.1 – Table of Resistivity Curve Fitting Parameters (see Equation 2-4)

sample ID	sample depth (m bgs)	k	m	slope of log-log plot	description
NW1	0.30	21.296	1.059	-1.471	coarse sand
NW2	0.61	11.256	1.424	-1.497	coarse sand
NW4	1.52	9.708	1.678	-1.653	coarse sand
NW5	1.81	17.983	1.005	-1.261	silty gravel
NW6	2.72	6.190	1.350	-1.069	sitly sand
NW7	3.05	7.341	1.534	-1.328	fine sand
NW8	3.35	5.762	1.598	-1.215	fine sand
NW9	3.66	9.231	1.214	-1.172	fine sand
NW10	4.27	5.177	1.312	-0.937	med-fine sand
NW11	4.57	4.068	1.508	-0.919	silty sand
NW12	4.88	6.248	1.451	-1.155	silty sand
NW13	5.18	0.510	2.240	0.656	sandy clay
NW14	5.79	1.513	3.092	-0.363	pebbly clay
NW15	6.10	1.451	1.434	-0.192	clay
NW16	6.40	6.369	1.319	-1.061	fine sand
NW17	6.71	7.306	1.300	-1.123	fine sand
NW19	7.32	8.501	1.087	-1.171	oxidized fine sand
NW18	7.62	8.391	1.268	-1.010	fine sand
NW20	7.92	7.577	1.415	-1.244	fine sand
NW21	8.23	9.829	1.316	-1.306	med-fine sand
NW22	8.84	10.279	1.223	-1.238	silty sand
NW23	9.14	12.883	1.119	-1.242	fine-coarse sand
NW24	9.75	10.254	1.300	-1.314	fine-coarse sand
NW25	10.36	11.767	1.212	-1.298	fine-coarse sand
NW27	10.97	11.496	1.318	-1.398	fine-coarse sand

Table D2.2 – Measured resistivity data.

	resistivity		resistivity		resistvity		resistvity		resistivity		
moist cont	NW1wet	moist cont	NW1dry	moist cont	NW2wet	moist cont	NW2dry	moist cont	NW4wet	moist cont	NW4dry
0.035	2165.805	0.216	103.538	0.051	1804.458	0.261	82.735	0.069	1407.011	0.332	58.286
0.075	370.771	0.199	120.890	0.066	619.275	0.232	89.523	0.150	283.954	0.310	61.186
0.159	141.814	0.170	144.302	0.117	240.521	0.167	142.315	0.263	93.068	0.235	102.141
0.216	103.538	0.127	193.934	0.221	85.550	0.108	248.760	0.332	58.286	0.159	217.537
		0.110	220.153	0.261	82.735	0.091	344.852			0.096	519.212
		0.039	677.556			0.076	417.686			0.067	
		0.029	856.115			0.065	506.561			0.045	1428.276
		0.022	1173.809			0.051	825.749			0.035	2133.554
	resistivity		resistivity		resistivity		resistivity		resistivity		resistivity
moist cont	NW5wet	moist cont	NW5dry	moist cont	NW6wet	moist cont	NW6dry	moist cont	NW7wet	moist cont	NW7dry
0.060	352.568	0.206	89.069	0.155	79.730	0.423	21.403	0.081	355.567	0.384	32.528
0.061	315.081	0.179	101.767	0.177	64.993	0.407	20.918	0.097	254.303	0.362	32.333
0.063	290.657	0.145	139.800	0.225	46.563	0.398	20.880	0.294	47.523	0.319	39.398
0.064	281.787	0.116	157.298	0.270	35.846	0.390	22.424	0.357	37.041	0.263	60.598
0.066	268.481	0.098	178.137	0.321	27.731	0.379	20.956	0.384	32.528	0.207	86.223
0.069	255.601	0.083	194.480	0.357	23.387	0.361	27.999			0.138	150.084
0.089	193.691			0.369	22.270	0.265	35.074				
0.126	132.327			0.387	21.971						
0.206	89.069			0.423	21.403						

Table D2.2 – (continued).

	resistivity		resistivity		resistivity		resistivity		resistivity		resistivity
moist cont	NW8wet	moist cont	NW8dry	moist cont	NW9wet	moist cont	NW9dry	moist cont	NW10wet	moist cont	NW10dry
0.115	210.137	0.382	26.309	0.097	207.937	0.326	34.517	0.109	94.798	0.320	21.205
0.135	137.667	0.373	27.903	0.134	127.215	0.318	34.019	0.229	37.989	0.293	26.034
0.178	84.080	0.364	36.522	0.176	83.026	0.298	36.372	0.288	27.903	0.251	36.987
0.229	54.506	0.318	37.262	0.228	53.077	0.266	41.034	0.320	21.205	0.198	41.619
0.359	26.602	0.270	44.426	0.326	34.517	0.225	53.512			0.171	50.812
0.382	26.309	0.186	85.165			0.188	101.884			0.135	70.837
		0.125	163.121			0.121	105.805			0.103	100.986
		0.090	262.002			0.099	136.861				
						0.043	332.227				
	resistivity		resistivity		resistivity		resistivity		resistivity		
moist cont	NW11wet	moist cont	NW11dry	moist cont	NW12wet	moist cont	NW12dry	moist cont	NW13wet	moist cont	NW13dry
0.105	142.388	0.390	21.180	0.110	165.062	0.382	24.912	0.233	13.348	0.233	13.348
0.123	134.806	0.374	18.825	0.146	110.673	0.377	25.153	0.233	14.642	0.233	14.642
0.191	39.530	0.368	20.735	0.225	55.803	0.328	31.008	0.233	12.862	0.233	12.862
0.270	23.243	0.310	20.589	0.356	25.518	0.260	45.385	0.290	7.989	0.290	7.989
0.329	19.969	0.225	33.501	0.382	24.912	0.167	90.675	0.343	6.103	0.343	6.103
0.348	17.629	0.151	64.997			0.106	171.259	0.356	5.265	0.356	5.265
0.390	21.180	0.091	135.462			0.067	265.383	0.361	5.075	0.361	5.075
								0.365	5.039		
								0.361	5.160		
								0.319	5.189		

Table D2.2 – (continued).

	resistivity		resistivity		resistivity				resistivity		
moist cont	NW14wet	moist cont	NW14dry	moist cont	NW15wet	moist cont	NW15dry	moist cont	NW16wet	moist cont	NW16dry
0.108	71.364	0.172	28.13477	0.401	5.380	0.434	4.814	0.080	179.449	0.404	19.979
0.108	71.462	0.151	32.32228	0.409	5.220	0.070	77.354	0.157	84.463	0.347	23.784
0.108	67.936	0.135	37.91652	0.413	5.090			0.206	58.315	0.255	39.425
0.108	62.538	0.130	50.84543	0.421	5.047			0.375	21.960	0.125	103.271
0.108	58.259	0.113	47.68517	0.424	4.987					0.068	188.905
0.117	48.994			0.434	4.814						
0.128	45.892			0.070	77.354						
0.163	34.396										
0.222	20.368										
			resistivity		resistivity		resistivity		resistivity		resistivity
moist cont	NW17wet	moist cont	NW17 dry	moist cont	NW18 wet	moist cont	NW18 dry	moist cont	NW19wet	moist cont	NW19dry
0.059	245.607	0.407	21.409	0.099	155.844	0.393	26.1213	0.129	73.702	0.374	25.248
0.151	97.477	0.325	32.637	0.214	60.719	0.298	34.84084	0.146	54.746	0.353	25.576
0.233	55.341	0.201	65.433	0.295	41.226	0.202	65.92873	0.207	44.342	0.341	25.751
0.318	30.991	0.098	155.019	0.397	26.358			0.214	44.576	0.297	29.841
0.381	23.878	0.063	254.602	0.423	26.165			0.248	38.327	0.218	49.504
		0.389	22.353					0.296	32.451	0.080	160.250
								0.338	27.340		
								0.357	29.280		
								0.398	25.467		

Table D2.2 – (continued).

	resistivity		resistivity		resistivity		resistivity		resistivity		resistivity
moist cont	NW20 wet	moist cont	NW20 dry	moist cont	NW21wet	moist cont	NW21 dry	moist cont	NW22 wet	moist cont	NW22 dry
0.061	368.365	0.373	29.649	0.051	452.470	0.365	34.113	0.067	250.072	0.367	35.442
0.088	261.373	0.360	30.445	0.185	99.021	0.347	37.237	0.297	46.449	0.345	36.166
0.267	53.502	0.339	33.337	0.263	59.207	0.317	43.361	0.363	33.180	0.305	45.539
0.363	32.462	0.274	42.517	0.357	36.185	0.238	69.526	0.366	33.269	0.212	75.325
0.392	30.080	0.179	95.266			0.153	132.816			0.119	155.243
		0.066	341.814			0.079	270.984				
	resistivity		resistivity		resistivity		resistivity		resistivity		resistivity
moist cont	NW23 wet	moist cont	NW23dry	moist cont	NW24 wet	moist cont	NW24 dry	moist cont	NW25 wet	moist cont	NW25 dry
0.037	410.557	0.335	38.876	0.053	397.373	0.334	36.477	0.056	339.197	0.260	56.182
0.167	102.346	0.314	42.145	0.178	110.108	0.308	43.069	0.137	126.966	0.232	70.397
0.323	39.332	0.276	56.704	0.289	53.663	0.284	48.764	0.241	64.821	0.189	98.461
		0.238	67.504			0.253	65.269	0.294	46.081	0.152	132.940
		0.159	118.346			0.206	87.908			0.105	198.975
		0.111	198.830			0.185	91.162			0.083	244.844
						0.120	164.907				
						0.113	204.651				
	resistivity		resistivity								
moist cont	NW27 wet	moist cont	NW27 dry								
0.014	2951.747	0.307	45.964								
0.080	355.013	0.293	60.764								
0.240	86.058	0.188	114.893								
0.323	44.088	0.109	223.215								
		0.062	438.775								
		0.060	471.118								
		0.057	493.064								

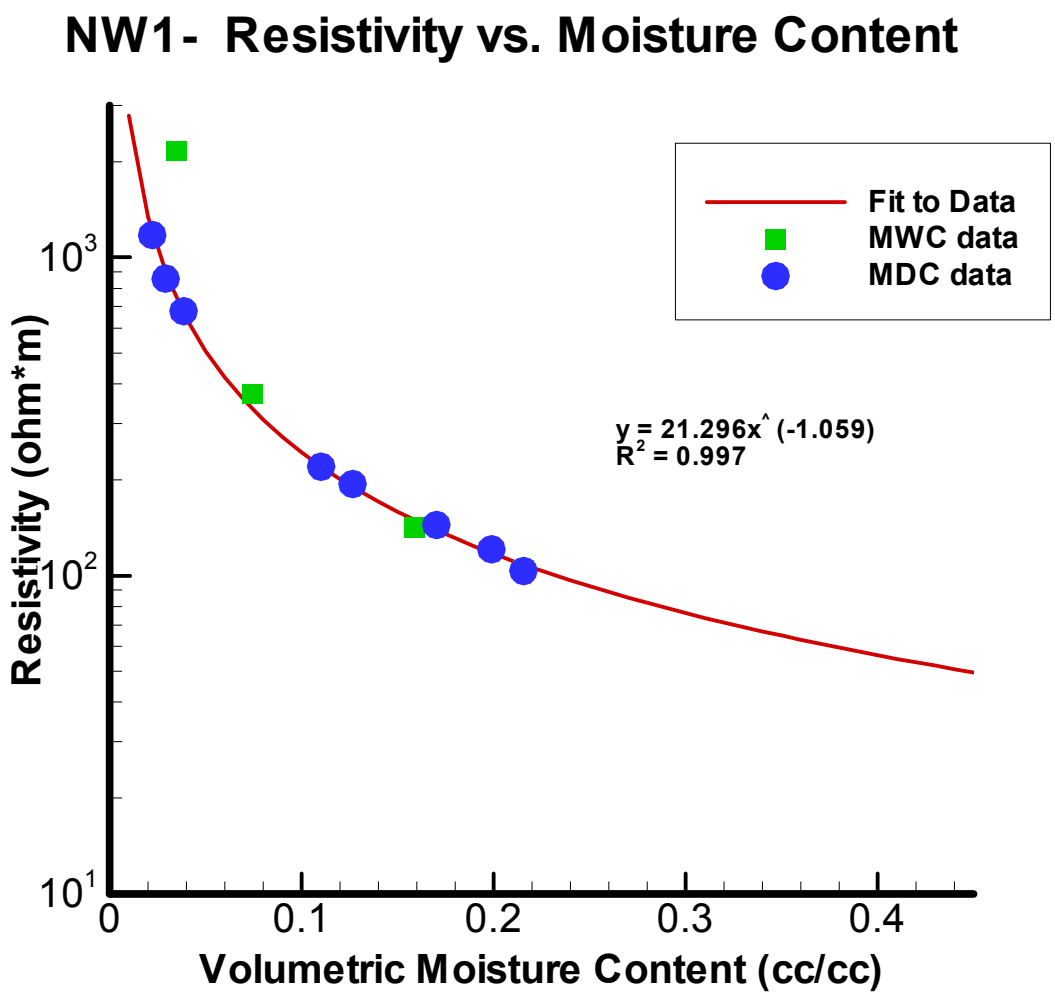

Figure D2.1– Electrical resistivity curve for a coarse sand collected at approximately 0.30 meters below ground surface. Curves were fit to data collected during wetting and draining sequences.

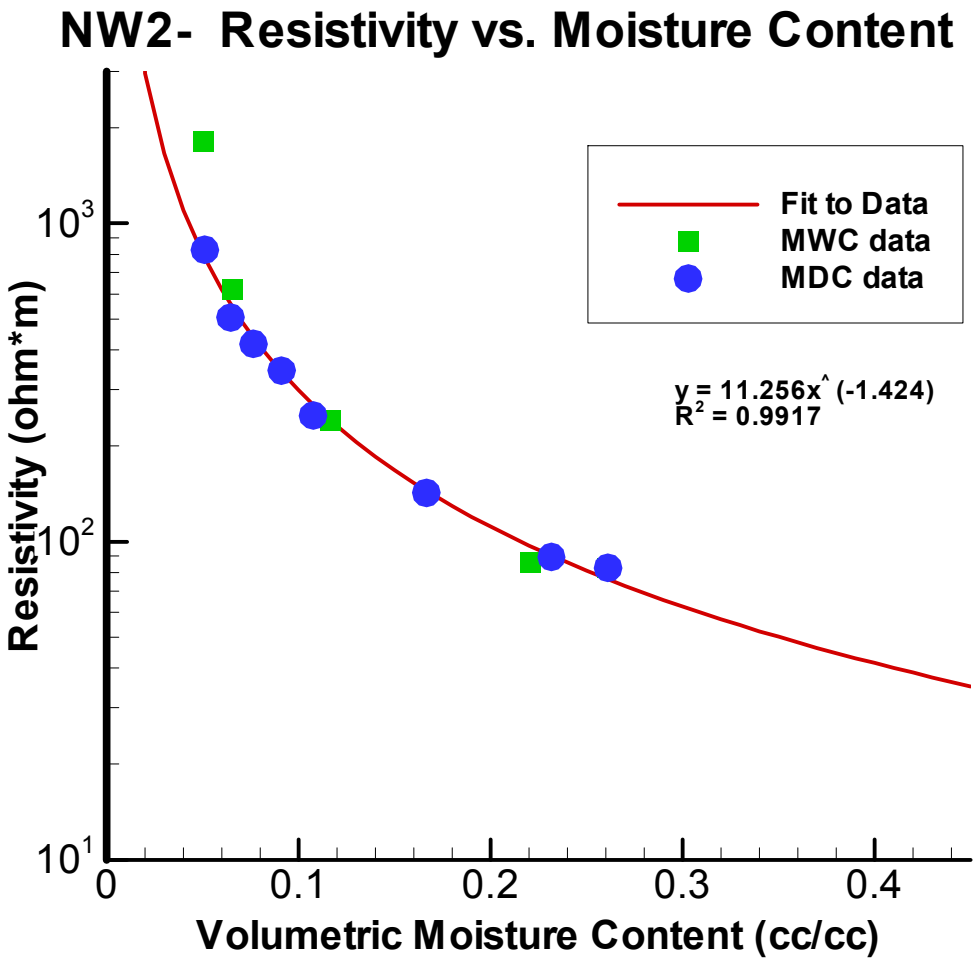

Figure D2.2 – Electrical resistivity curve for a coarse sand collected at approximately 0.61 meters below ground surface. Curves were fit to data collected during wetting and draining sequences.

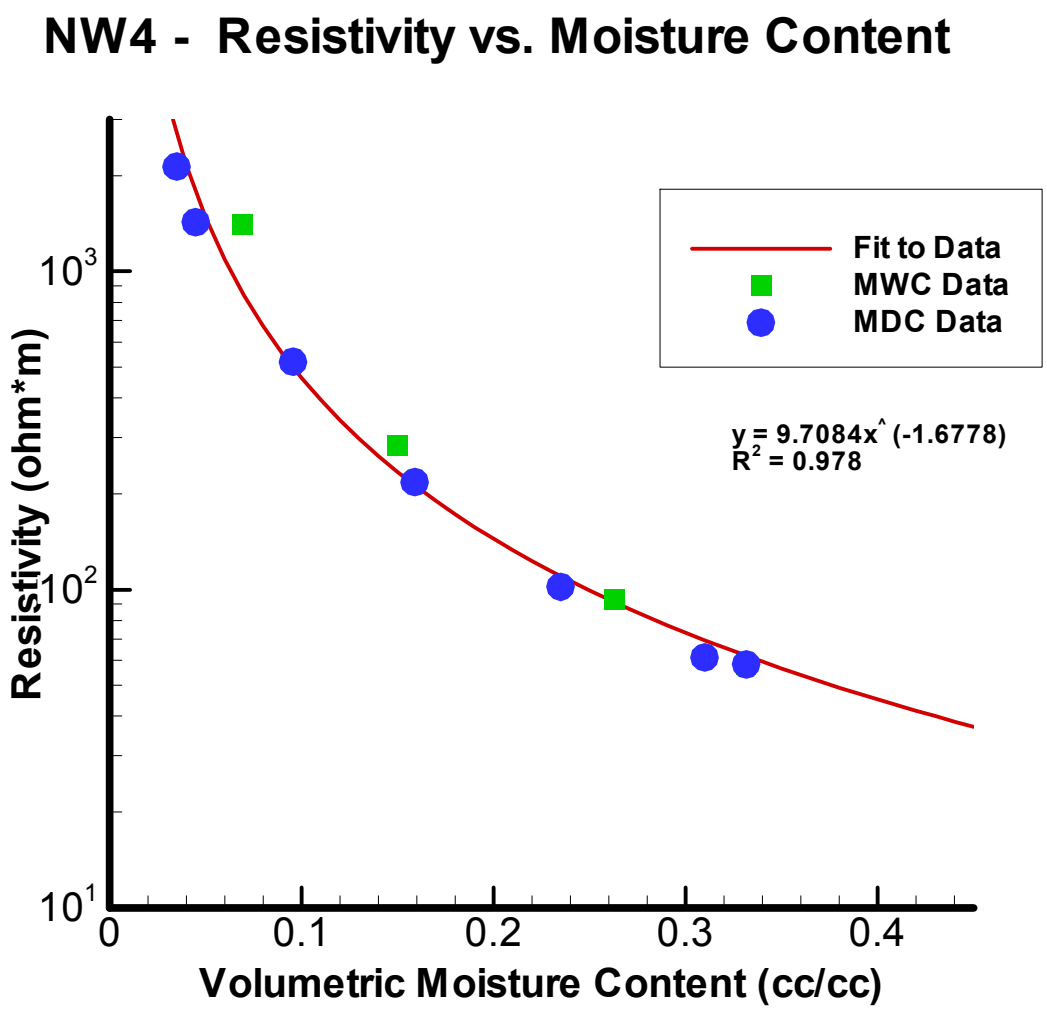

Figure D2.3 – Electrical resistivity curve for a coarse sand collected at approximately 1.52 meters below ground surface. Curves were fit to data collected during wetting and draining sequences.

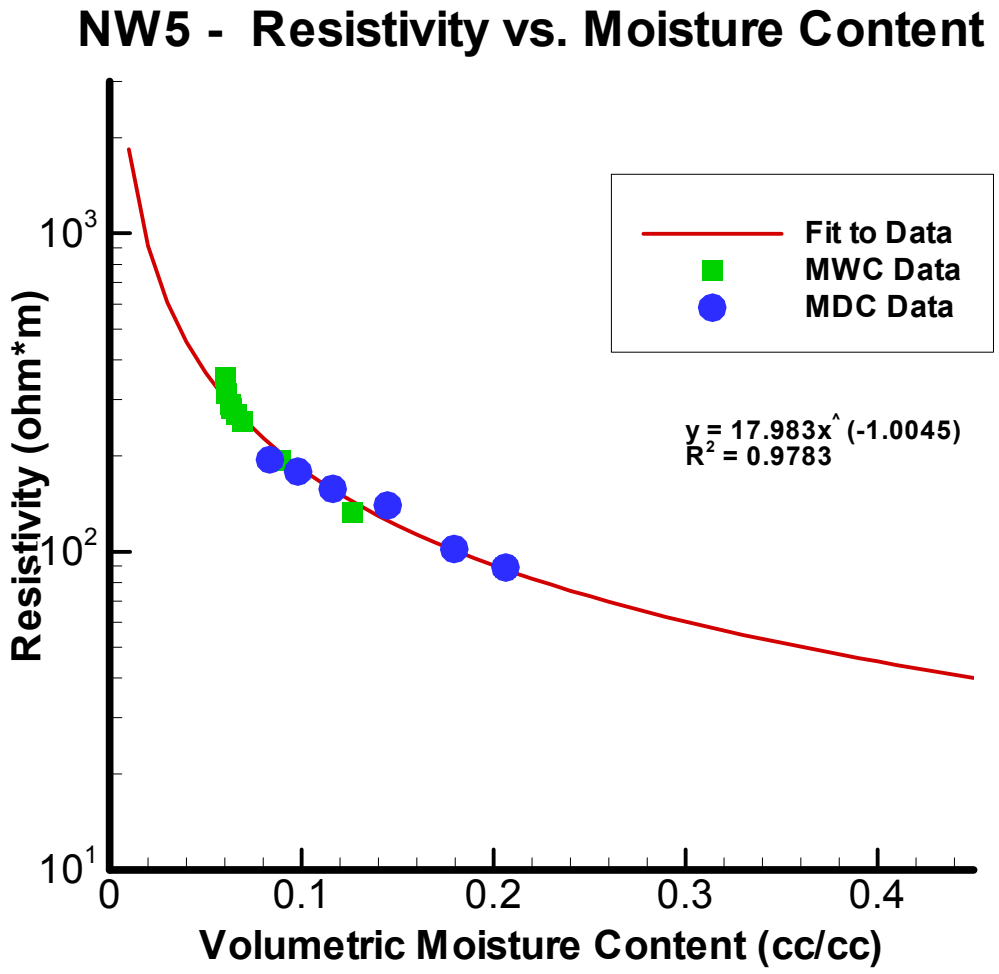

Figure D2.4 – Electrical resistivity curve for a silty gravel collected at approximately 1.81 meters below ground surface. Curves were fit to data collected during wetting and draining sequences.

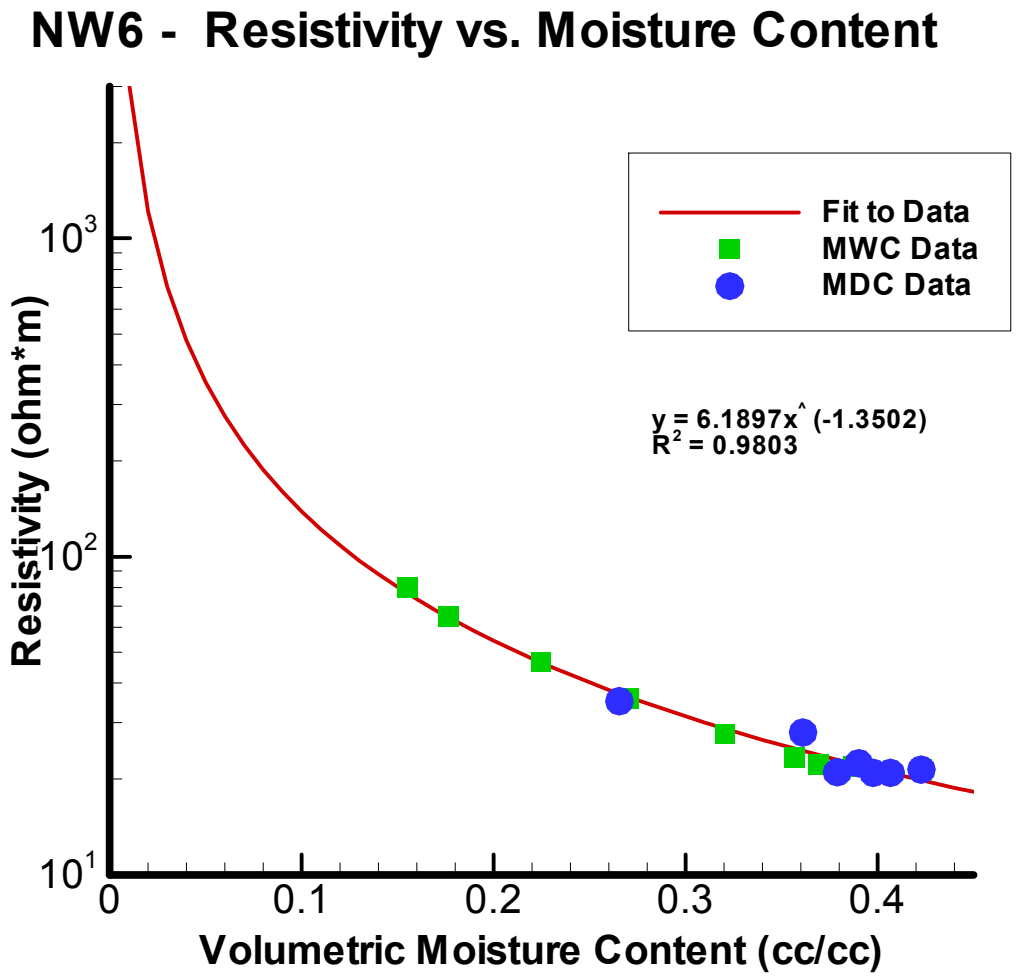

Figure D2.5 – Electrical resistivity curve for a silty sand collected at approximately 2.72 meters below ground surface. Curves were fit to data collected during wetting and draining sequences.

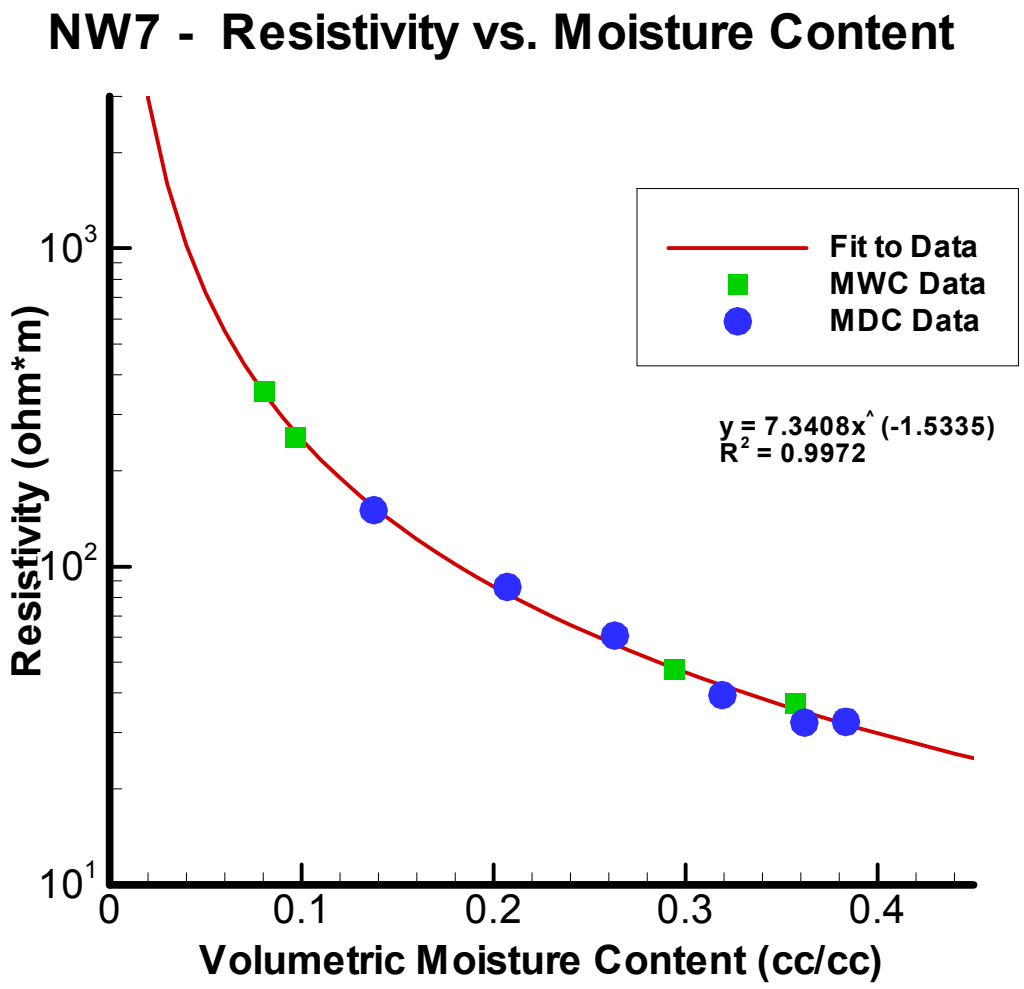

Figure D2.6 – Electrical resistivity curve for a fine sand collected at approximately 3.05 meters below ground surface. Curves were fit to data collected during wetting and draining sequences.

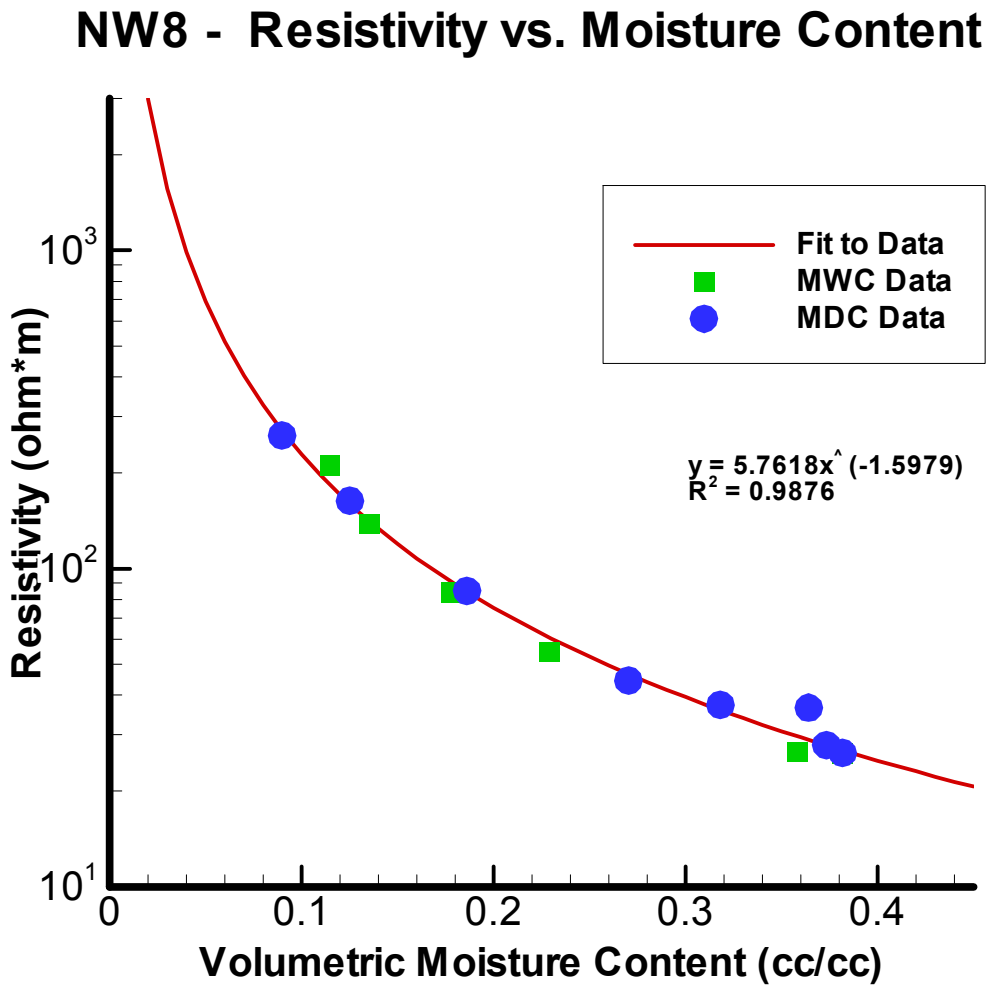

Figure D2.7 – Electrical resistivity curve for a fine sand collected at approximately 3.35 meters below ground surface. Curves were fit to data collected during wetting and draining sequences.

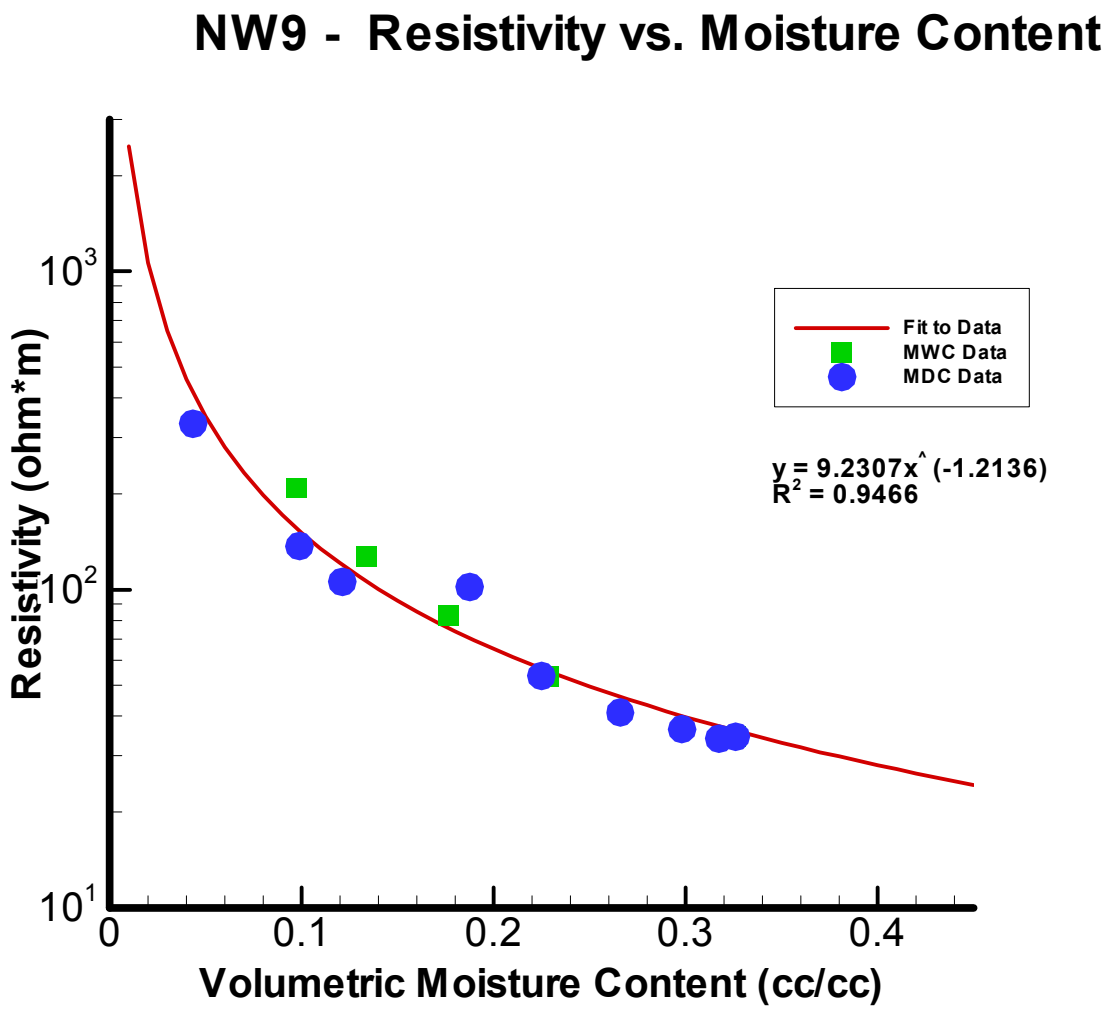

Figure D2.8 – Electrical resistivity curve for a fine sand collected at approximately 3.66 meters below ground surface. Curves were fit to data collected during wetting and draining sequences.

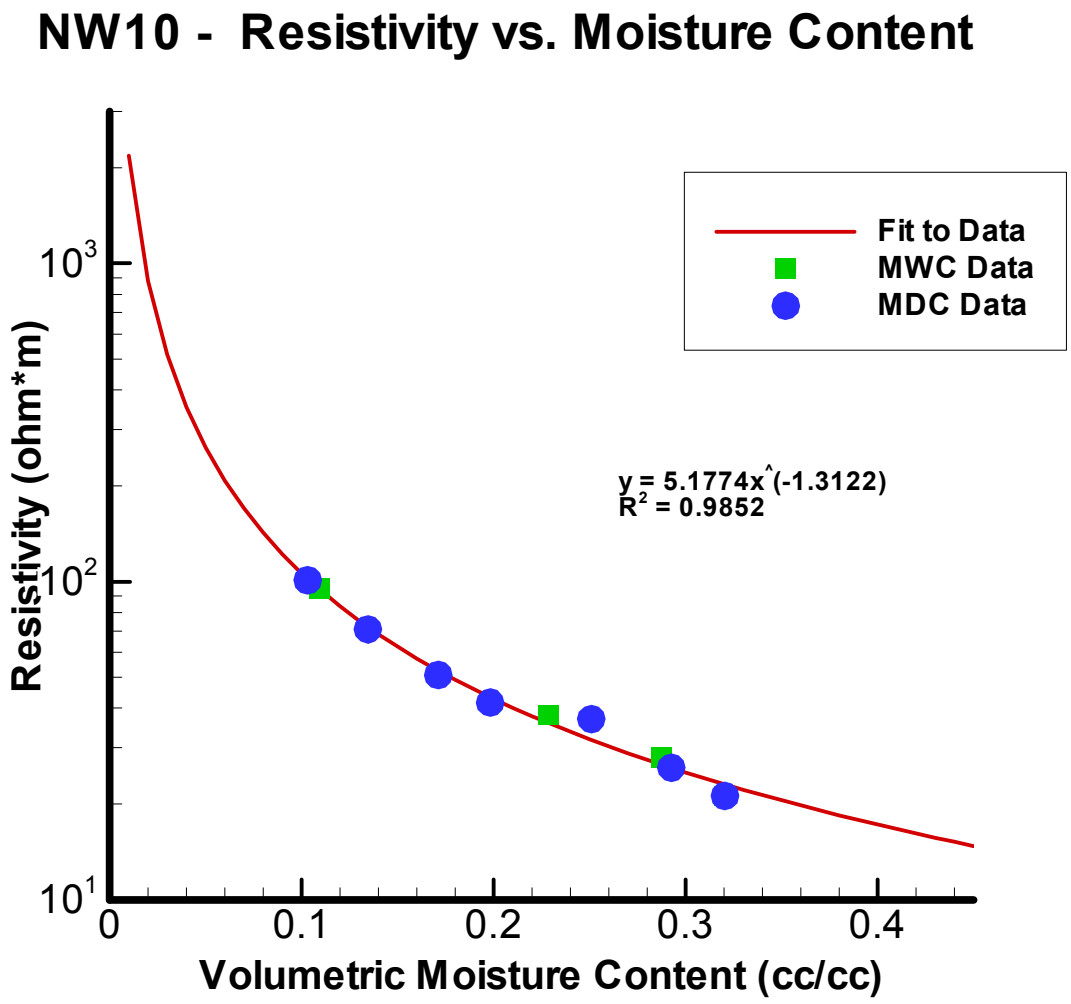

Figure D2.9 – Electrical resistivity curve for a fine-med sand collected at approximately 4.27 meters below ground surface. Curves were fit to data collected during wetting and draining sequences.

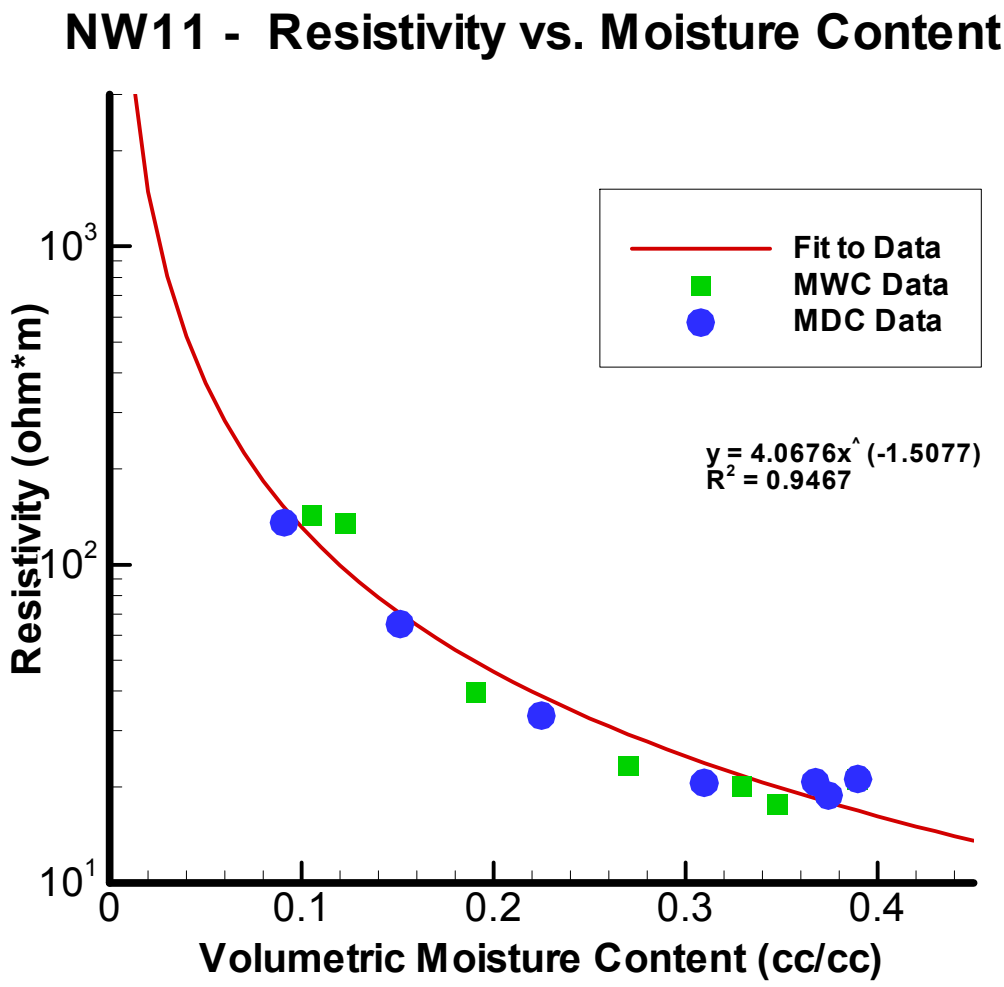

Figure D2.10 – Electrical resistivity curve for a silty sand collected at approximately 4.57 meters below ground surface. Curves were fit to data collected during wetting and draining sequences.

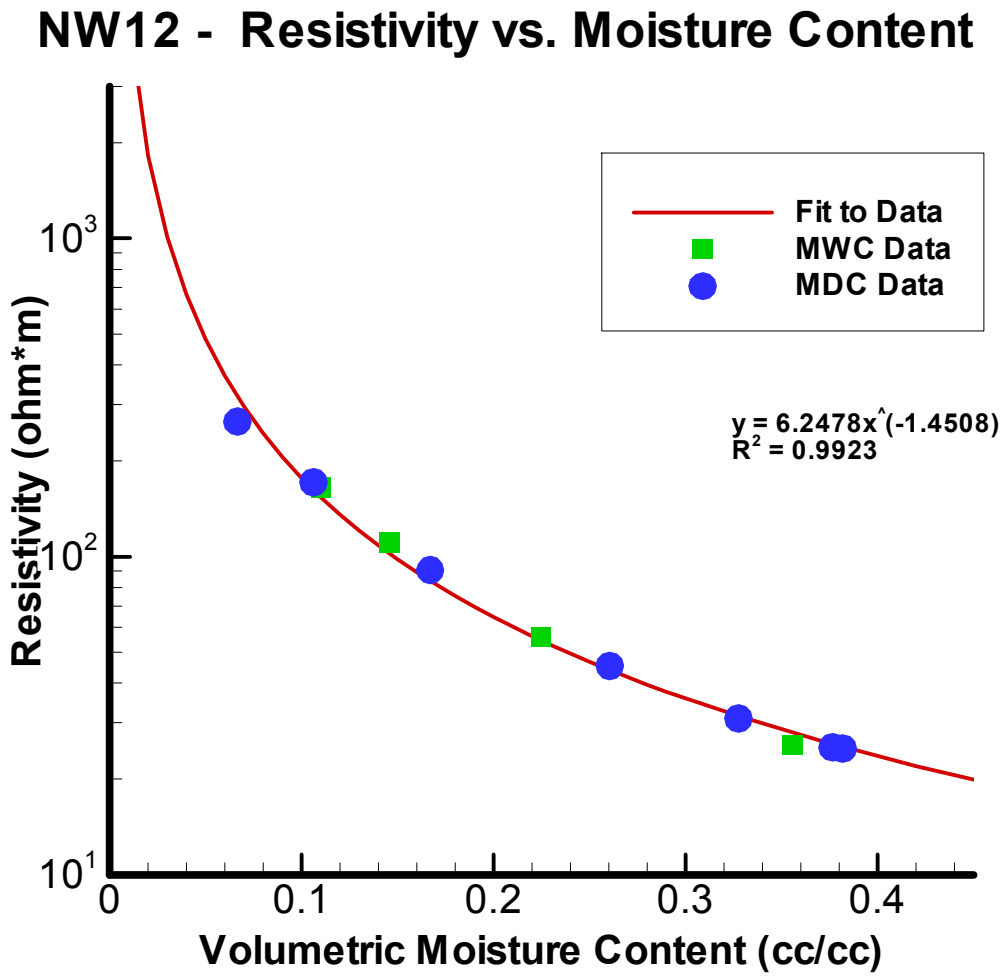

Figure D2.11 – Electrical resistivity curve for a silty sand collected at approximately 4.88 meters below ground surface. Curves were fit to data collected during wetting and draining sequences.

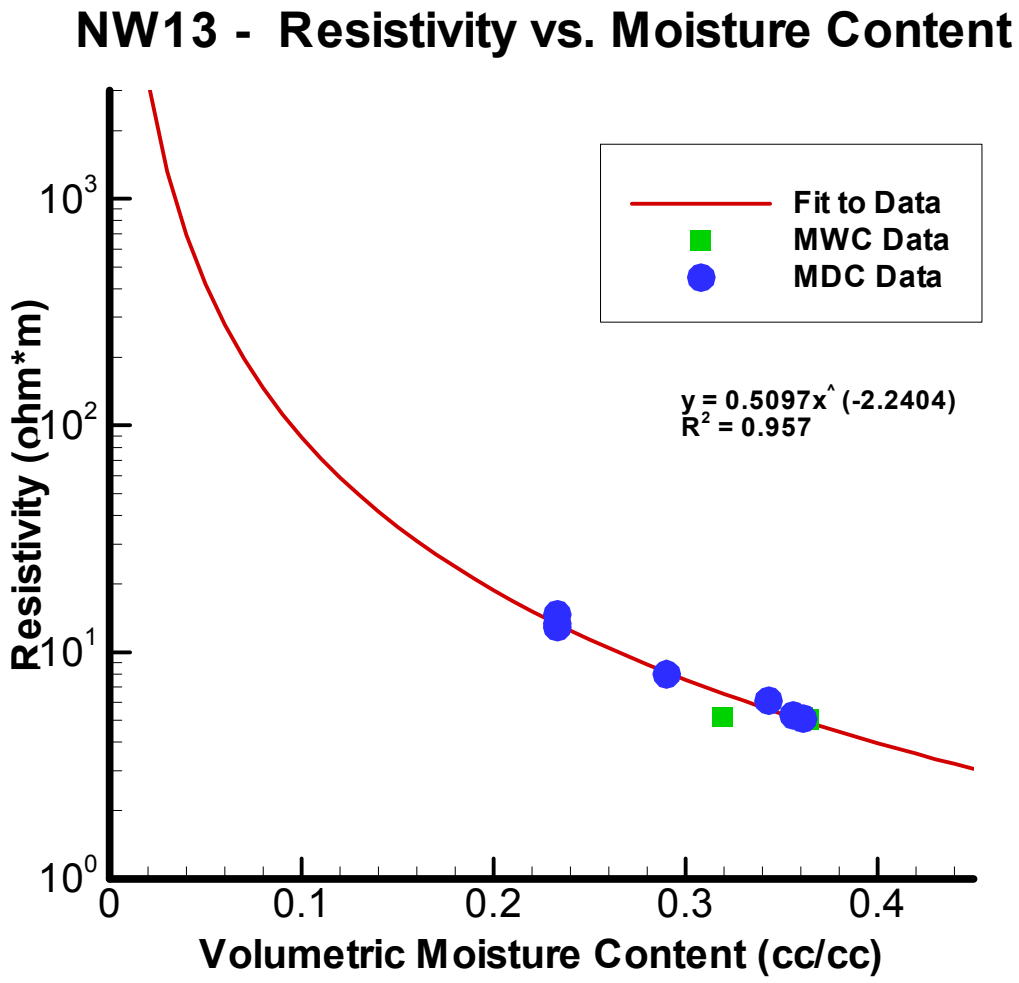

Figure D2.12 – Electrical resistivity curve for a sandy clay collected at approximately 5.18 meters below ground surface. Curves were fit to data collected during wetting and draining sequences.

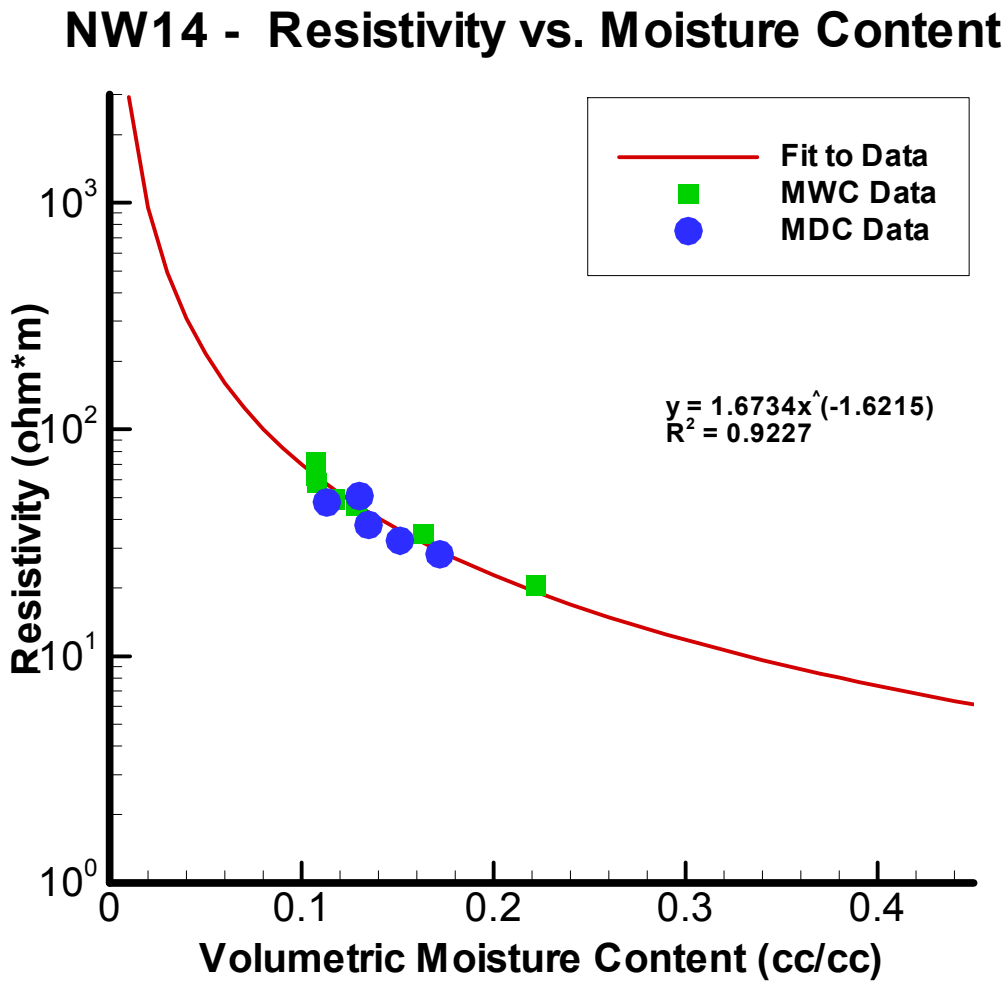

Figure D2.13 – Electrical resistivity curve for a pebbly clay collected at approximately 5.79 meters below ground surface. Curves were fit to data collected during wetting and draining sequences.

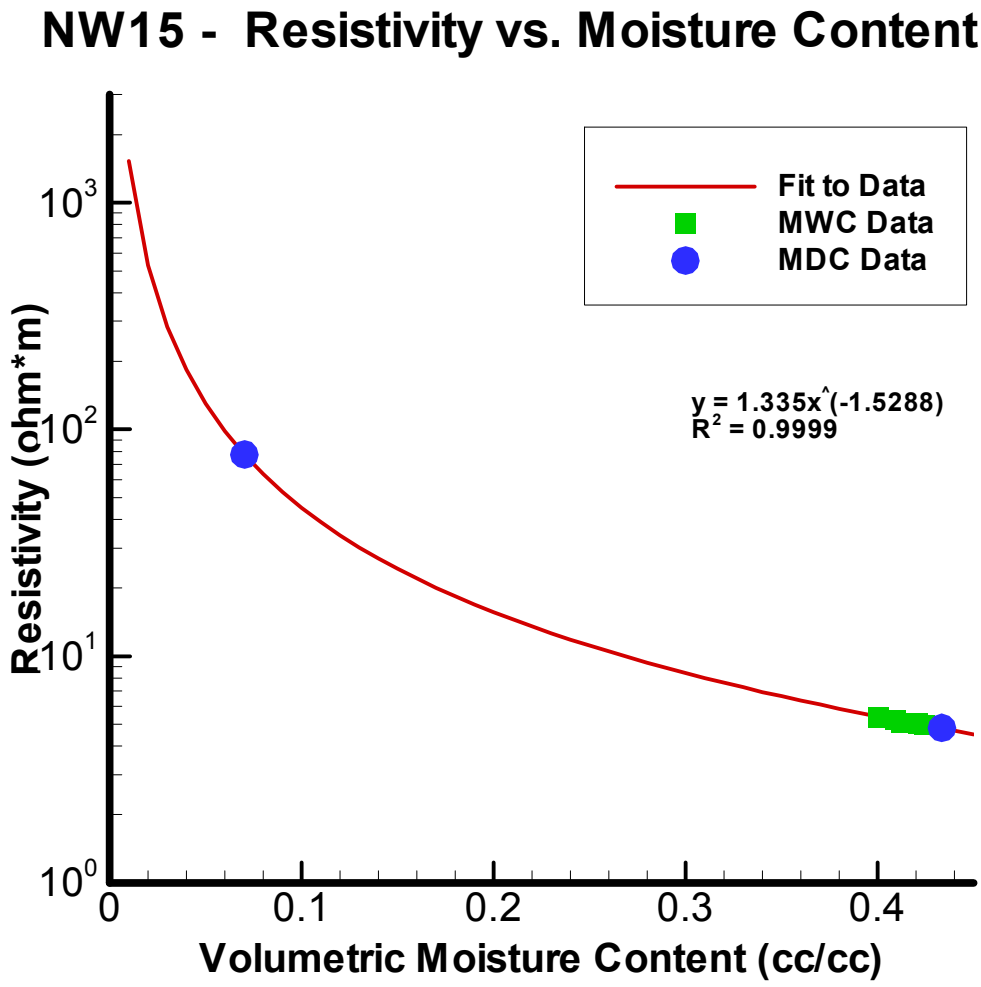

Figure D2.14 – Electrical resistivity curve for a clay collected at approximately 6.10 meters below ground surface. Curves were fit to data collected during wetting and draining sequences.

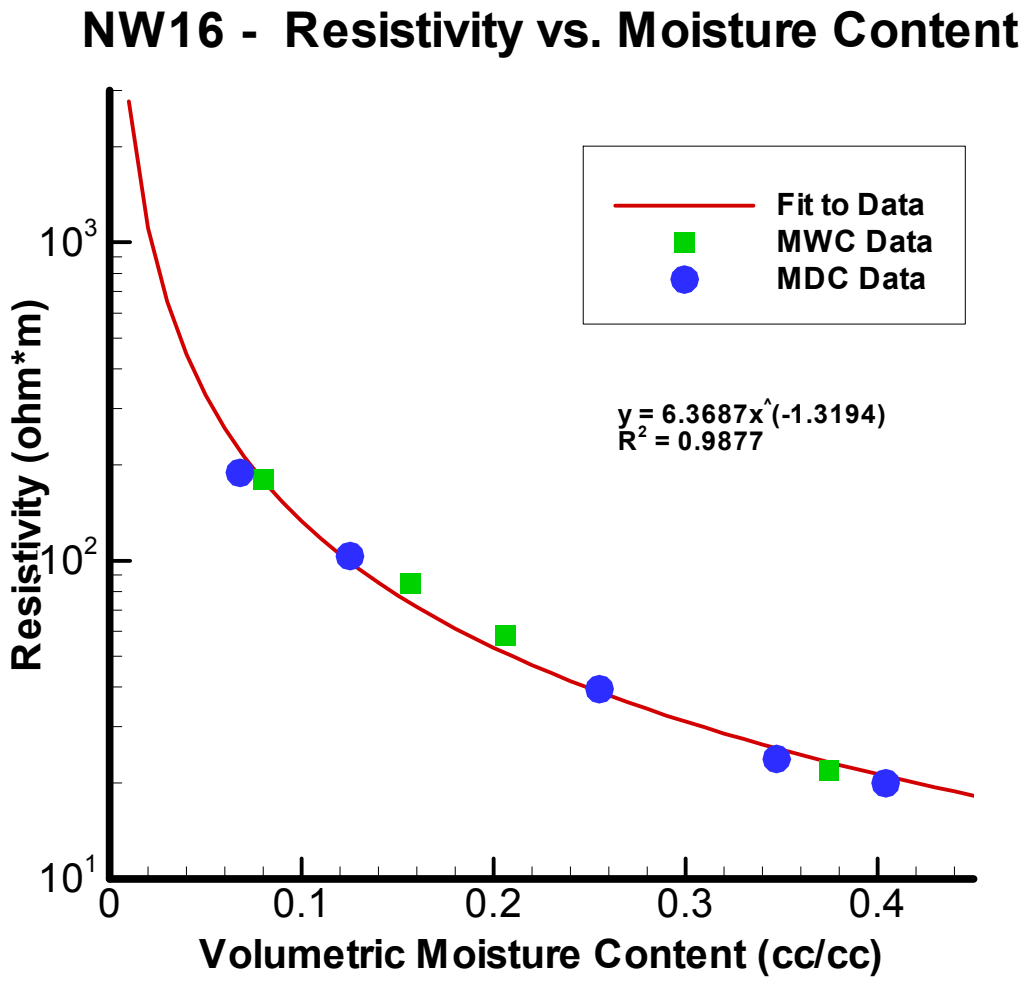

Figure D2.15 – Electrical resistivity curve for a fine sand collected at approximately 6.40 meters below ground surface. Curves were fit to data collected during wetting and draining sequences.

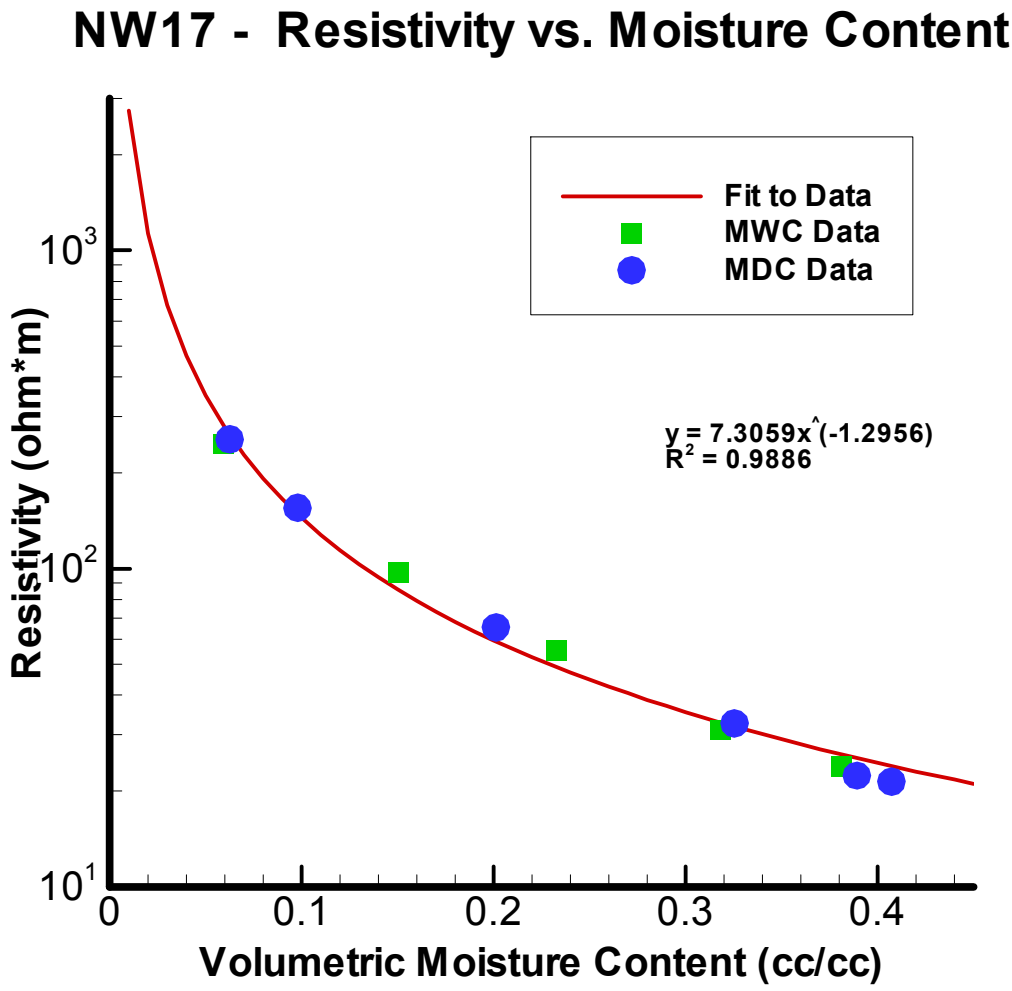

Figure D2.16 – Electrical resistivity curve for a fine sand collected at approximately 6.71 meters below ground surface. Curves were fit to data collected during wetting and draining sequences.

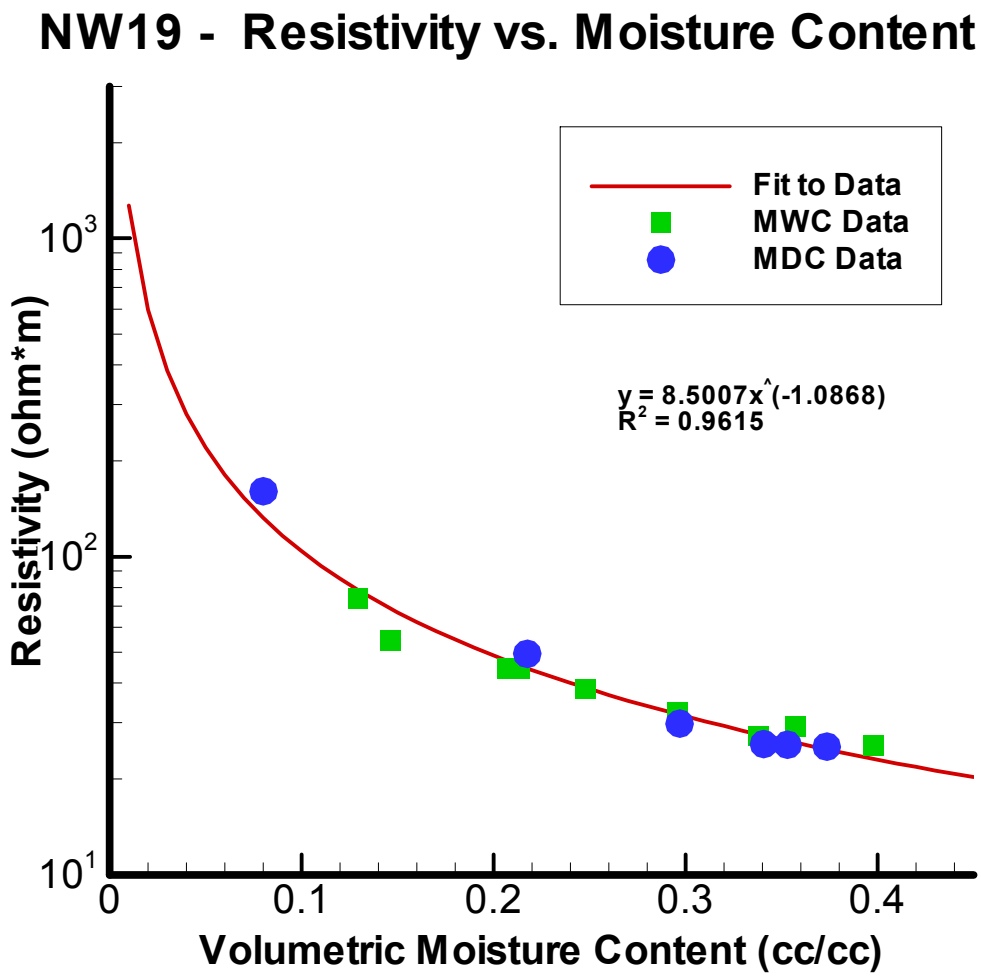

Figure D2.17 – Electrical resistivity curve for an iron oxidized fine sand collected at approximately 7.32 meters below ground surface. Curves were fit to data collected during wetting and draining sequences.

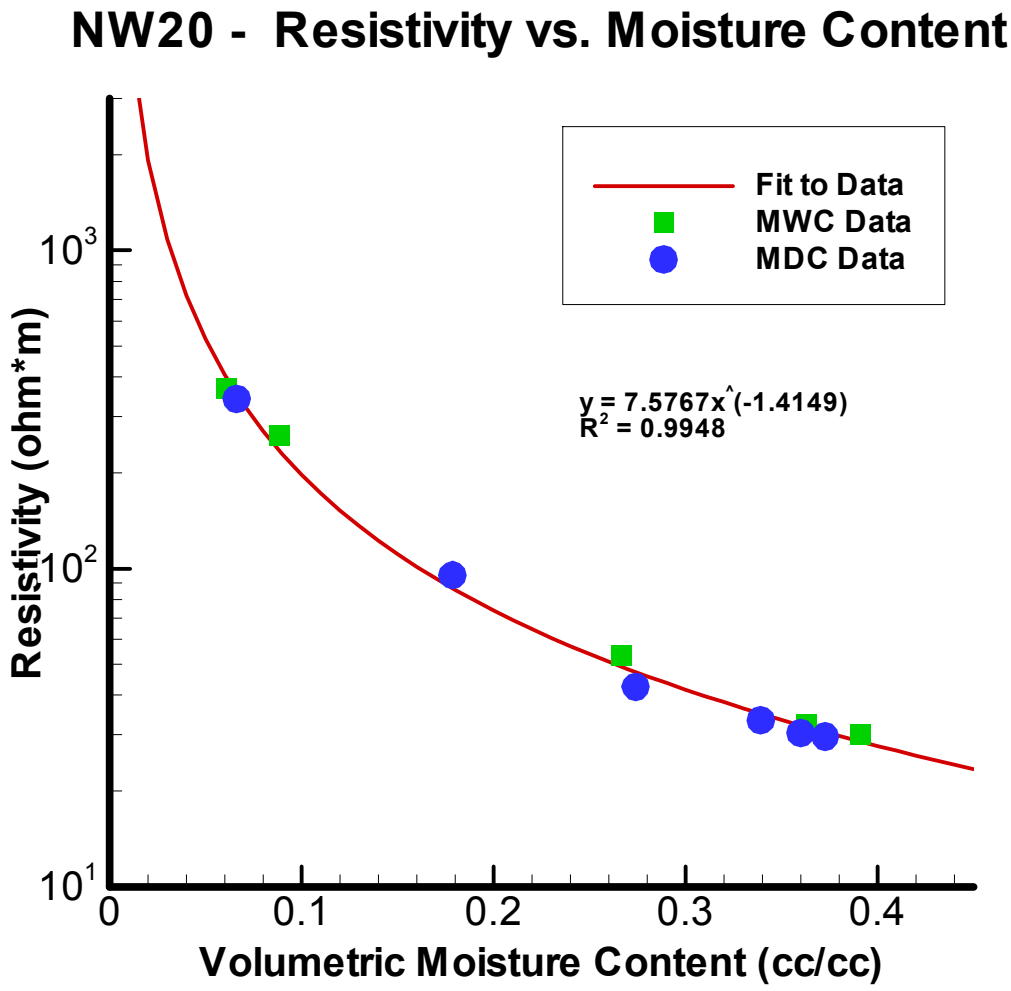

Figure D2.18 – Electrical resistivity curve for an fine sand collected at approximately 7.92 meters below ground surface. Curves were fit to data collected during wetting and draining sequences.

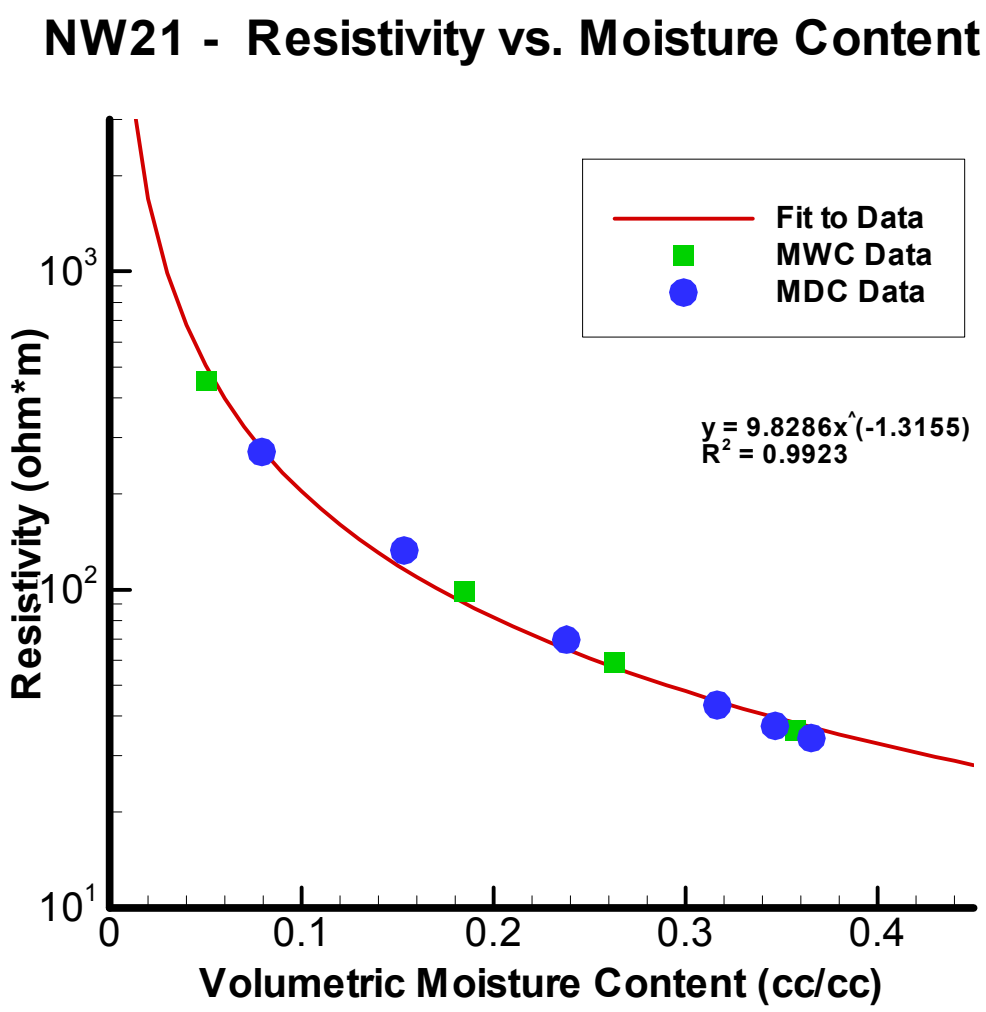

Figure D2.19 – Electrical resistivity curve for an med-fine sand collected at approximately 8.23 meters below ground surface. Curves were fit to data collected during wetting and draining sequences.

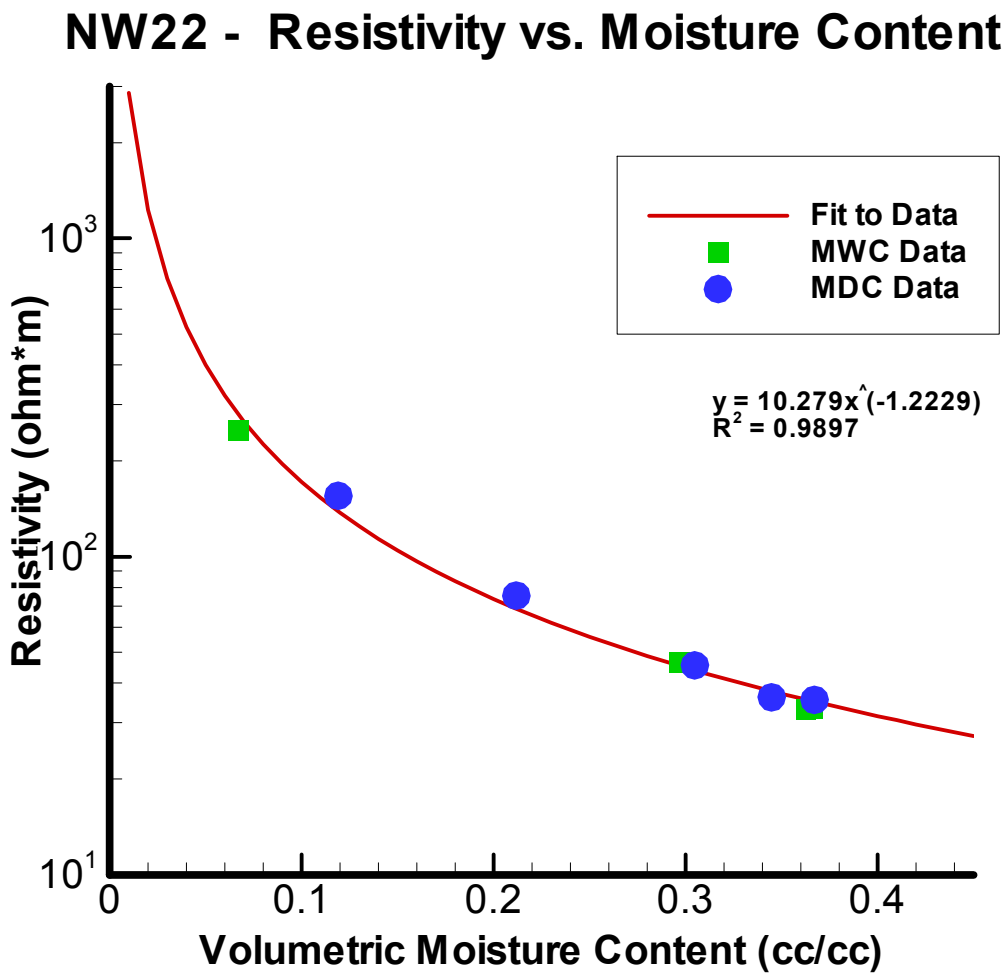

Figure D2.20 – Electrical resistivity curve for a silty sand collected at approximately 8.84 meters below ground surface. Curves were fit to data collected during wetting and draining sequences.

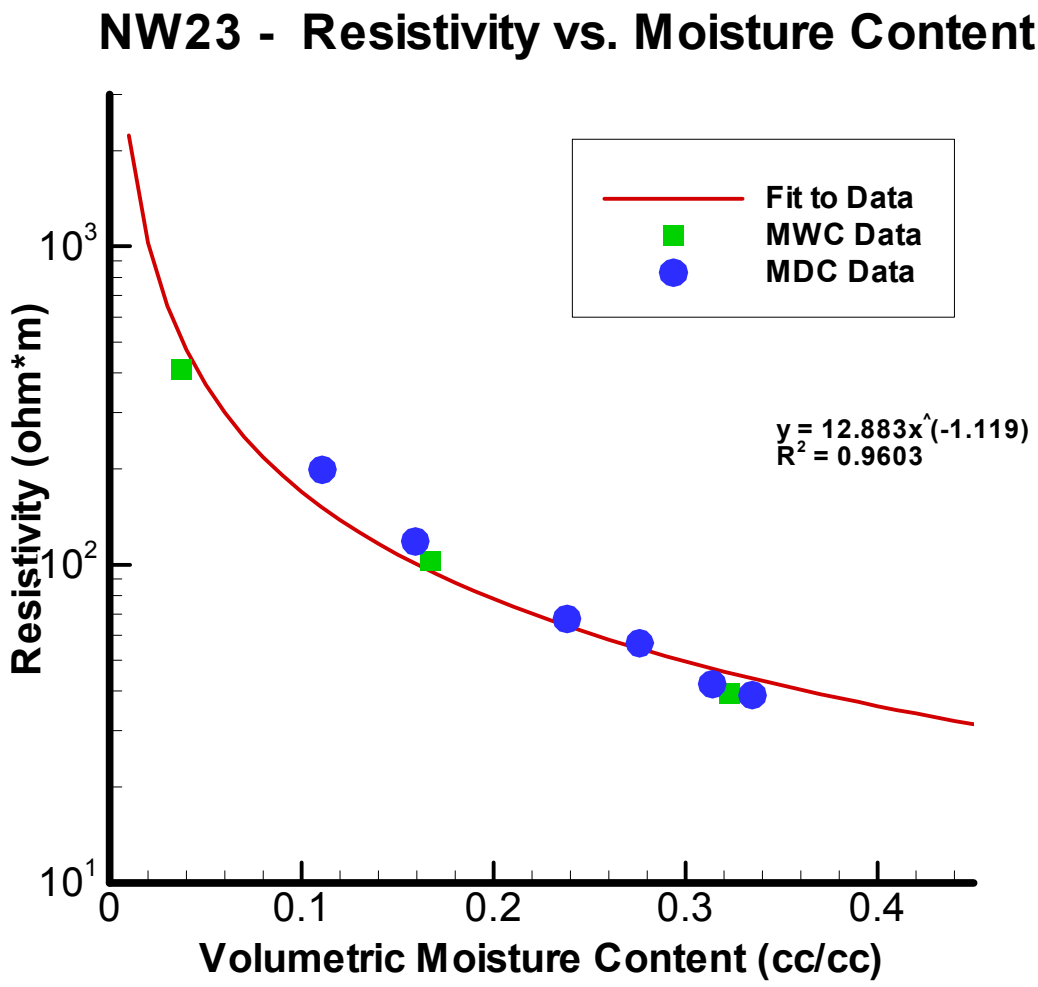

Figure D2.21 – Electrical resistivity curve for a fine-coars sand collected at approximately 9.14 meters below ground surface. Curves were fit to data collected during wetting and draining sequences.

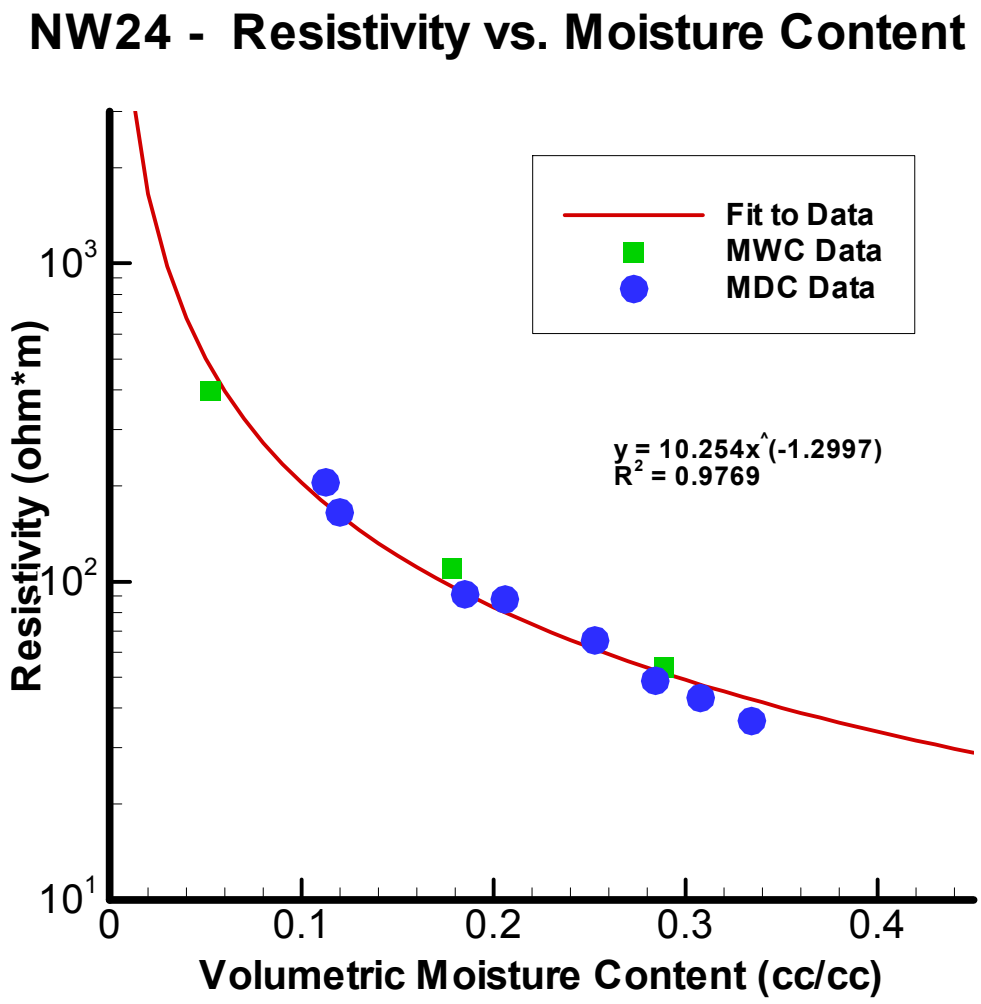

Figure D2.22 – Electrical resistivity curve for a fine-coars sand collected at approximately 9.75 meters below ground surface. Curves were fit to data collected during wetting and draining sequences.

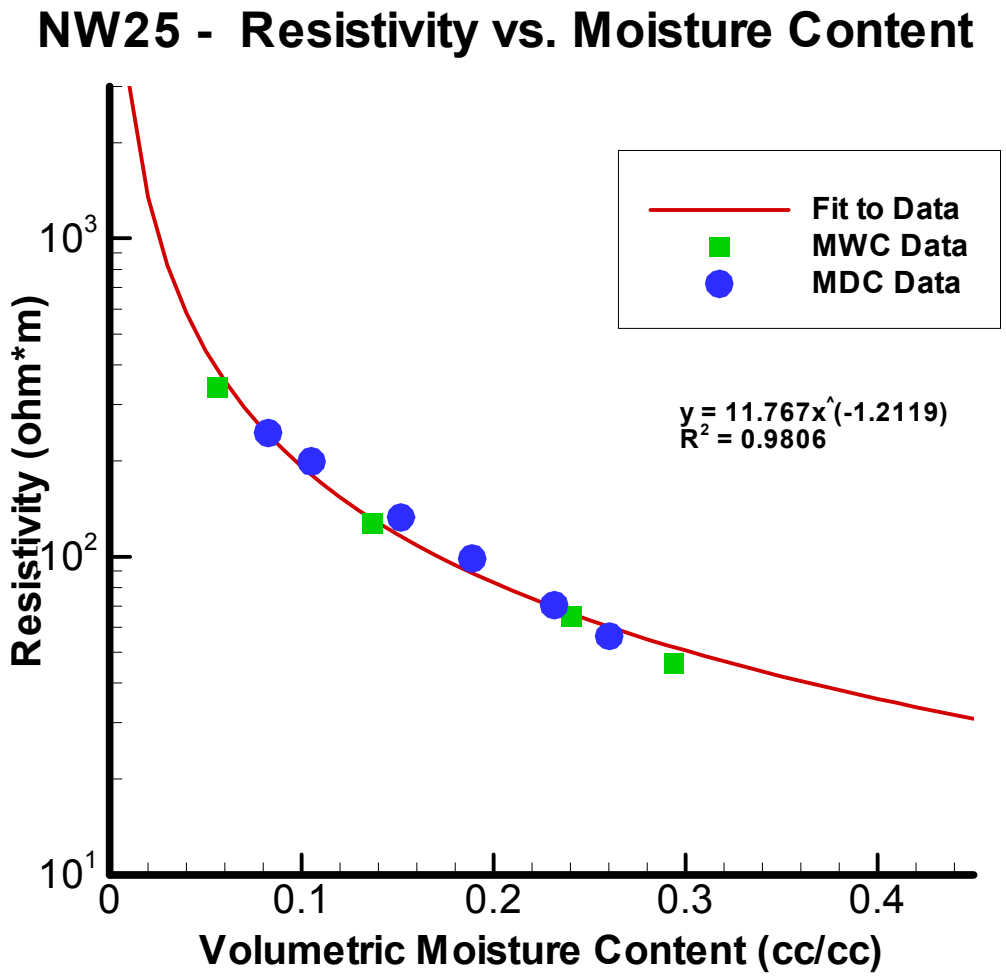

Figure D2.23 – Electrical resistivity curve for a fine-coars sand collected at approximately 10.36 meters below ground surface. Curves were fit to data collected during wetting and draining sequences.

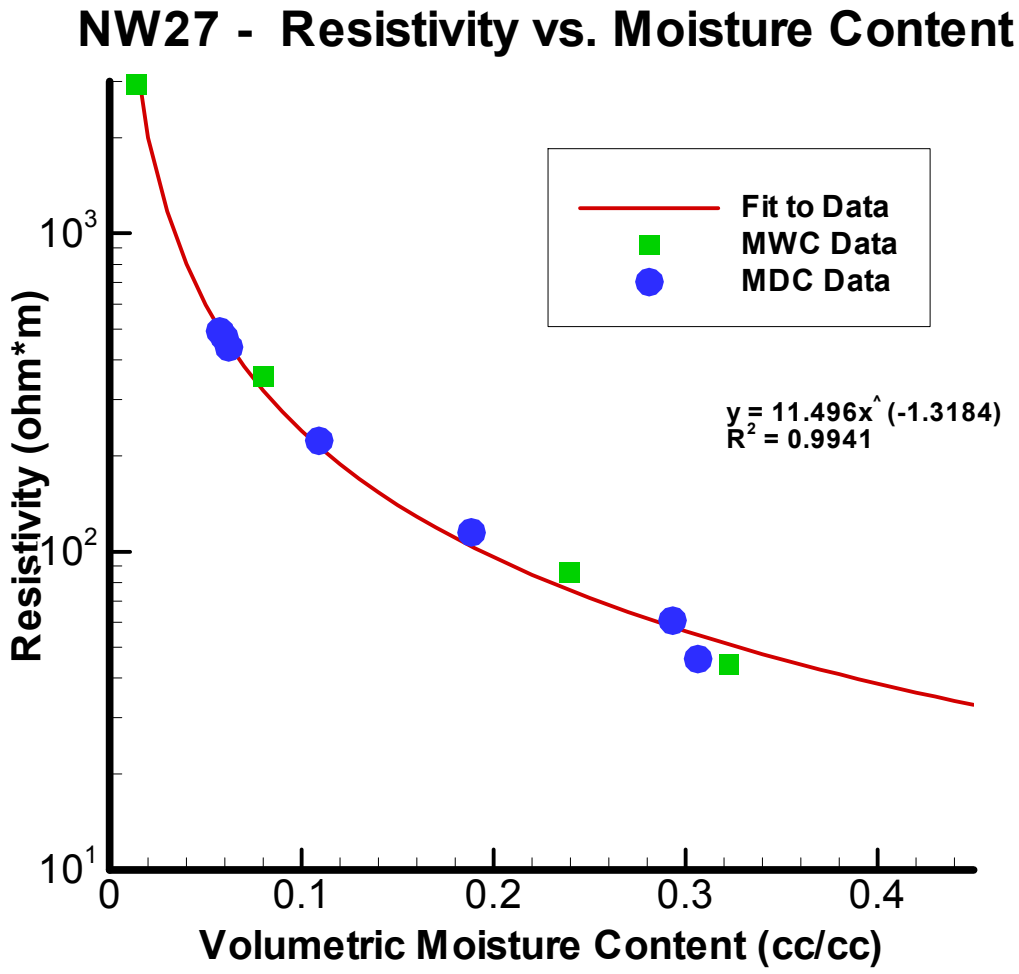

Figure D2.24 – Electrical resistivity curve for a fine-coars sand collected at approximately 10.97 meters below ground surface. Curves were fit to data collected during wetting and draining sequences.

Appendix E1

Moisture Retention Measurement Procedures

E1.1 Introduction

E1.1.1 Standard Methods for Measuring Moisture Retention Curves

The relationship between water content and matric potential of a porous medium (known as the moisture retention relationship) is a fundamental part of hydraulic property characterization of vadose zone materials (Klute, 1986 pg 635). Fitting parameters obtained from the moisture retention function [$\Psi(\theta)$] are often used in functional forms, such as the Mualem model (1976) and the van Genuchten model (1980), to estimate fluid transport within the vadose zone (Jury et al., 1991 pg 108). Two direct methods by which these functions are obtained are the suction method and the pressure cell method (de Backer and Klute, 1967).

The suction method makes use of a hanging column apparatus (Figure E1.1), also referred to as the Haines apparatus (Stephens, 1995 pg 187) and the tension plate assembly (Hillel, 1980 pg 161) to measure equilibrated moisture content at various matric potentials (i.e., negative pressures or tensions). Soil samples are placed in individual Büchner funnels (see Figure E1.2), usually on top of a slurry of fine grained material with a high bubbling pressure to insure hydraulic contact (Klute, 1986 pg 652; Stephens, 1995 pg 191).

The burette is sequentially adjusted to desired potentials, allowing moisture equilibrium at each potential during either wetting or draining cycles. The hanging

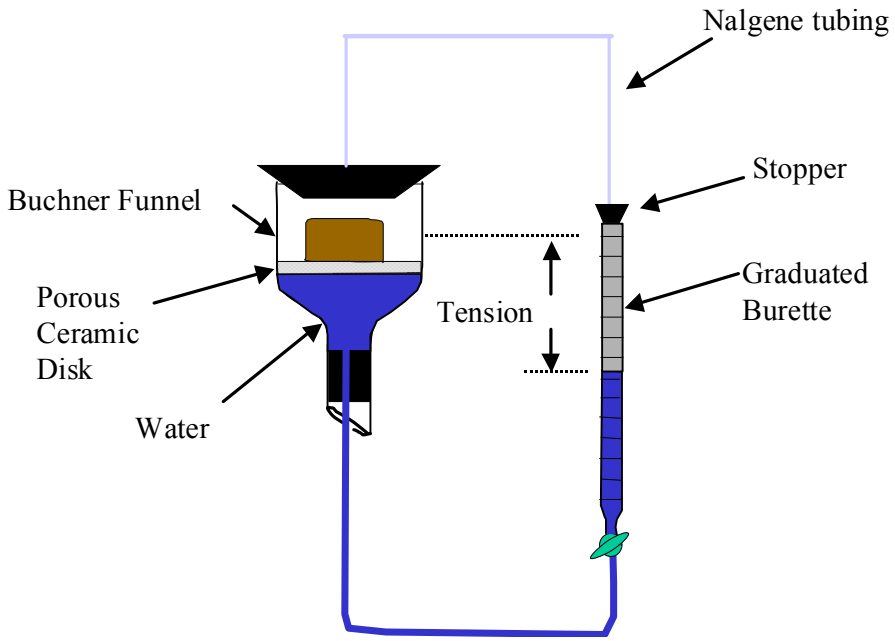

Figure E1.1 – Hanging Column Apparatus

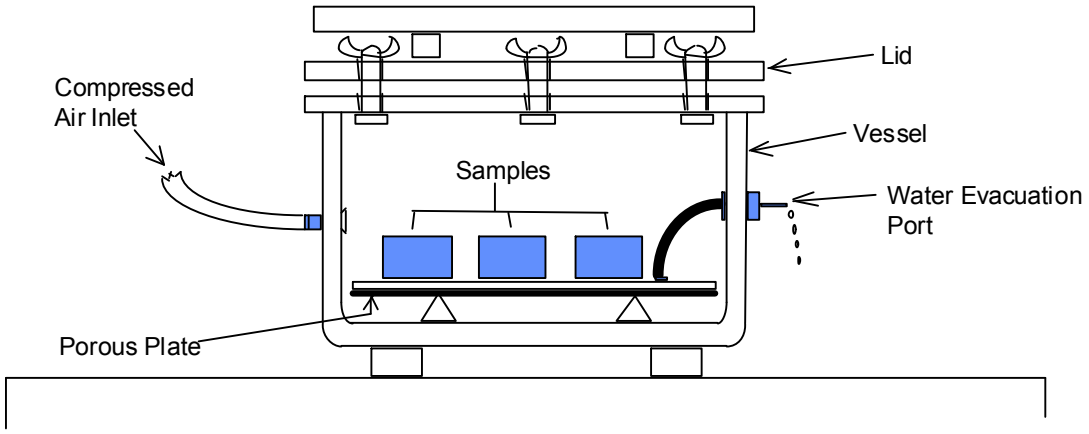

Figure E1.2 – Pressure Cell Assembly

column apparatus is more beneficial than the pressure cells for measuring moisture retention in the wet range of tensions because of the poor resolution and accuracy of most pressure gauges at low pressures (less than 1 bar) and because standard pressure cells can only be used to measure moisture retention during a drainage cycle (de Backer and Klute, 1967; Stephens, 1995 pg 190). The hanging column measurements are limited, however, by the low bubbling pressure of the porous plates, which typically range from -100 to -

300 cm (Stephens, 1995 pg 187). For tensions greater than the bubbling pressure of the porous disk, the pressure cell method is required.

The pressure cell method is designed to prevent cavitation of the water in the system (de Backer and Klute, 1967). The pressure cell assembly consists of an air-tight chamber enclosing a porous ceramic plate with a rubber membrane attached at the bottom (see Figure E1.2). The plate and membrane are connected to a tube that extends through the chamber and is open to atmospheric pressures outside the chamber. Instead of reducing the pressure in the water beneath the plate, the cell gas pressure on the sample water is increased while the water under the plate is maintained at atmospheric pressure. Under these conditions, the water is not subjected to low absolute pressures and cavitation does not occur (de Backer and Klute, 1967).

Pressure and moisture content measurements for the main wetting curve (MWC) (see Figure E1.3) in the hanging column apparatus are recorded during a wetting process starting at 100 to 300 cm tension (depending on bubbling pressure of porous disk) relative to the center of the sample. For convenience, the top of the porous plate is often used as a reference point for measuring tension. In this case, the tensions should be corrected to reflect the distance to the center of the sample. The sample is allowed to reach equilibrium moisture content at each tension, then the burette is raised by set increments (depending on sample texture), repeating the process until field saturation (~80-90% porosity) is reached. Porosity is typically not reached during imbibition due to air entrapment within the sample (Haverkamp and Parlange, 1986). The sample is often assumed to be at equilibrium after the water level in the burette remains constant (Stephens, 1995 pg 188), which usually occurs within several hours for moist soils (Jury et al., 1991 pg 62) and within 2-3 days for dry soils (Klute, 1986 pg 653). The

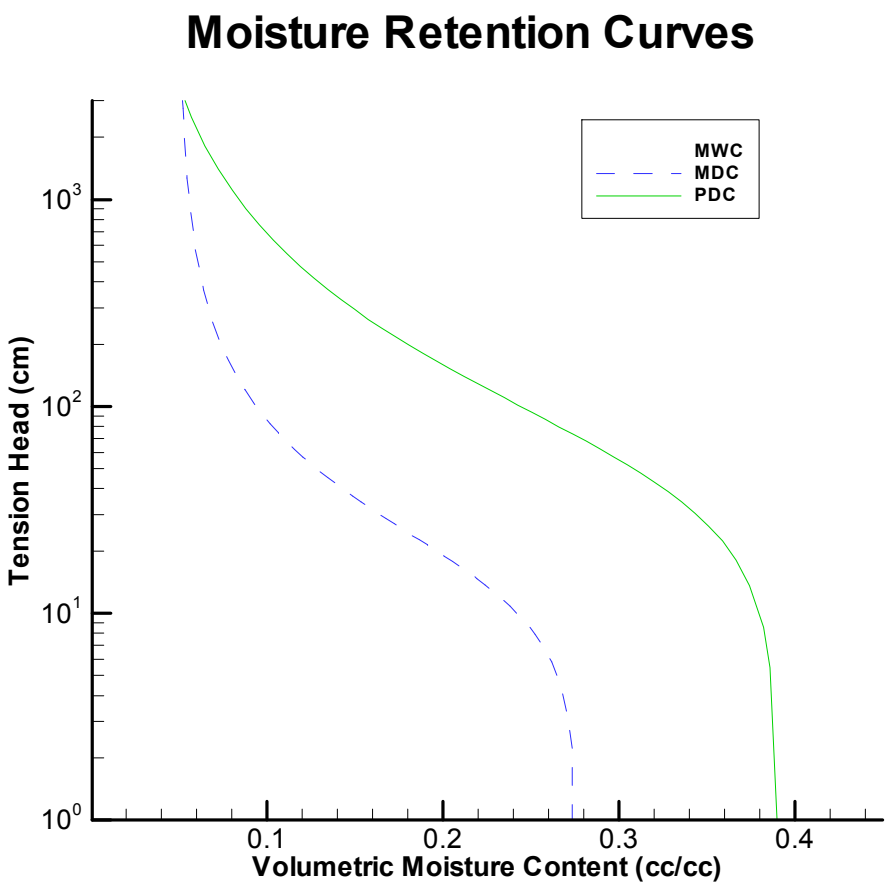

Figure E1.3 – Moisture retention curves fit to measured data (data not included to emphasize shape of the curves).

moisture content can be determined by monitoring the change in water volume in the burette (Stephens, 1995 pg 188) or by removing and weighing the sample at equilibrium (Jury et al., 1991 pg 62). Pressure and moisture content measurements for the main drainage curve (MDC) are measured starting at field saturation by reversing the order of tension head measured along the wetting curve. The primary drainage curve (PDC), sometimes referred to as the initial drainage curve, is measured by draining the sample to residual moisture content starting from complete saturation or porosity (Klute, 1986 pg 636).

Volumetric moisture content (θ_v) is calculated by measuring the mass of the sample at moisture equilibrium (M_w), subtracting the oven dry sample weight (M_d), and dividing the difference by the density of water (ρ_w) at the laboratory temperature (which needs to remain constant during analysis) and the total sample volume (V_t) by

$$\theta_v = \frac{M_w - M_d}{V_t * \rho_w} \quad [\mathrm{LL}^{-1}] \qquad \text{(E1-1)}$$

E1.2 Methods Used In Analysis

E1.2.1 Measurement Sequence

1. Repack samples to approximate *in situ* bulk density (samples are wet after packing)
2. Dry samples to approximate *in situ* moisture content in relative humidity oven
3. Wet samples in hanging column to measure MWC
   - Measure resistivity at each moisture equilibrium
4. Drain samples from satiated moisture content to measure MDC
   - Measure resistivity at each moisture equilibrium
5. Saturate samples and measure PDC in hanging column from 0-100 cm tension and pressure chambers at 1 bar, 3 bars, and 5 bars pressure.
6. Oven dry samples to determine volumetric moisture content

E1.2.2 Procedures for Hanging Column Measurements at Low Tension Heads

ASTM standards have not been published for the hanging column apparatus and the methods are not described in Klute (1986), therefore hanging column procedures were based on published methods described by Stephens (1995); de Backer and Klute (1967); and Jury et al., (1986). Deviations from these methods were based on results from preliminary tests conducted prior to analysis.

Required equipment

Pyrex #36060 (medium flow) Büchner funnels, 10 -15 μm pores

50 mL - 100 ml burettes

250 cm length ¼" ID nalgene tubing

2 – single hole rubber stoppers (to fit into bottom of funnel and top of burette)

1 - #15 rubber stopper (cut to 2 inch thickness to fit inside funnels).

4 cm polycarbonate sample rings (5.57cm ID)

Cotton cloth, cut in squares large enough to fit on the bottom of the rings

Clamps (zip ties) to hold cloth onto bottom of rings

Mettler scale for weighing samples (minimum resolution of 0.01 grams)

Water proof marker to mark water levels in burette

Metric ruler

Main Wetting Curve Measurements

Before placing the samples on the porous plate in the hanging column apparatus, we placed approximately 1 teaspoon of diatomaceous slurry in the center of the porous plate to maintain hydraulic contact between the porous plate and the sample. Air entry pressure for the diatomaceous earth is much greater than pressures exerted on the samples in the hanging columns (see Figure E1.4) suggesting that the slurry should remain moist during analysis.

The samples were placed directly on the slurry and the meniscus in the burette was raised to 100 cm below the top of the porous plate. Volumetric moisture content was determined by

$$\theta_v = \frac{\left(SW_w - SW_d\right)}{\rho_w V_t} \qquad \text{(E1-2)}$$

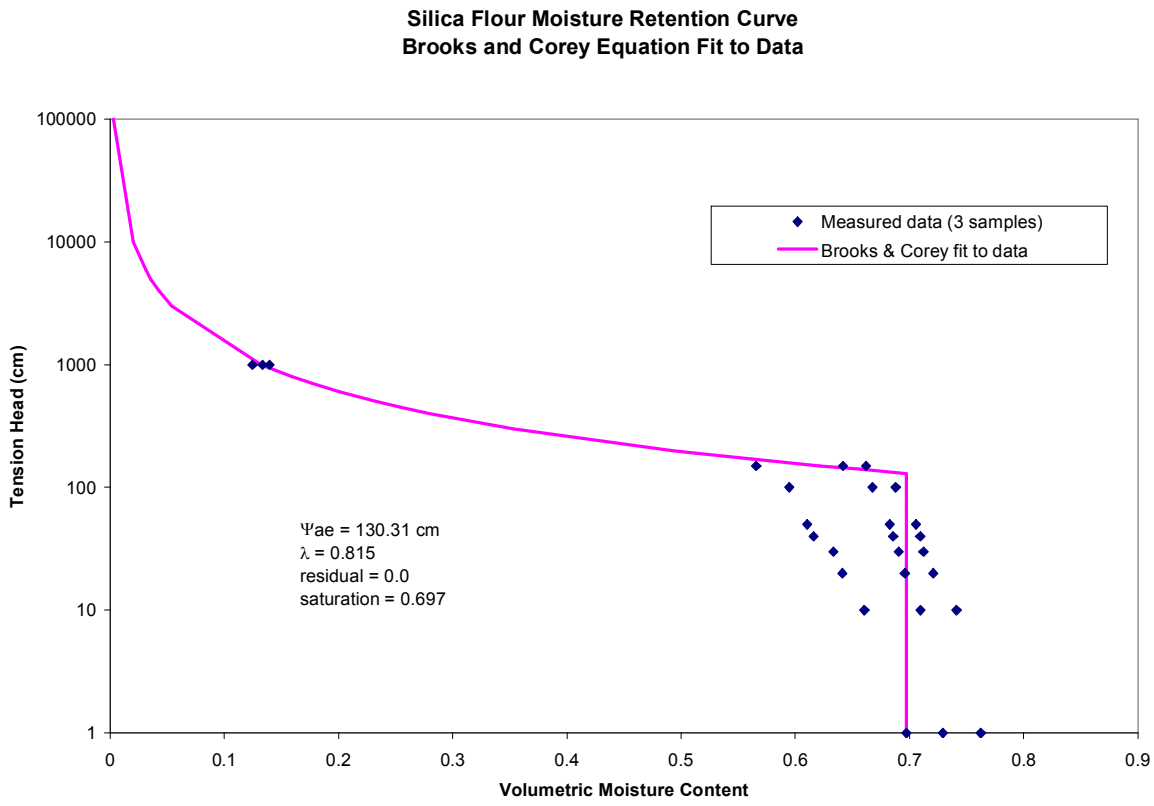

Figure E1.4 – Air entry pressure of diatomaceous earth.

where SW_w is the measured wet sample weight (g), SW_d is the measured dry sample weight (g), ρ_w is the density of water (g cm^{-3}), and V_t is the sample total volume (cm^3). The burette was then raised to 70 cm, 50 cm, and then 10 cm increments between 50 and 0 cm allowing the sample to reach equilibrium at each tension. Since the water level in the burette changes as the sample imbibes (and water evaporates), the tension measurements were adjusted accordingly to reflect the actual tension at equilibrium.

Main Drainage Curve Measurements

The main drainage curve was measured from the satiated moisture content (~ 80 - 90% porosity, also referred to as field saturation) by reversing the wetting process (lowering the burette in same sequence of tension heads) from 0 to 100 cm tension. We observed loss of hydraulic contact at tensions greater than 100 cm and air bubbles

forming in the funnels, therefore the samples were drained at higher tensions in the pressure cells.

Primary Drainage Curve

The primary drainage curve was measured following the same procedures as the main drainage curve, however the samples were initially fully saturated using saturation methods described in Appendix D.

Determination of Moisture Equilibrium

Moisture equilibrium during drainage in the hanging column assembly was assumed after the water level in the burette ceased to increase after 24 hours, based on literature (Jury et al., 1991; Stephens, 1995) and preliminary studies (see Appendix B). Moisture equilibrium was assumed for the wetting curve once the samples ceased to increase in weight during daily monitoring. This method was employed as opposed to monitoring the water level in the burette because evaporation caused a continual decrease in the burette water level making it difficult to determine moisture equilibrium.

E1.2.3 Procedures for Pressure Cell Measurements at High Tensions

Required Equipment

5 Bar System:	15 Bar System:
Air compressor and connections	Nitrogen tank and connections
700-3 pressure supply manifold	750-2 pressure supply manifold
5 bar ceramic plate extractor apparatus	15 bar ceramic plate extractor apparatus

Introduction

The pressure cell method is often used to drain samples at pressures in the dry range of matric potentials primarily because the bubbling pressures for the hanging column porous plates are lower than 1 bar. Using the pressure cell apparatus, one or more

soil samples are placed on the porous ceramic surface. The soil samples together with the porous ceramic plate are then saturated with a wetting fluid. After saturation, the cell can be mounted in the pressure chamber and air pressure is used to extract moisture from the soil samples at set pressure intervals (Klute, 1986).

We developed procedures based on published ASTM standards (D 3152, 1994), Klute (1986), and the user's manual supplied by the manufacturer (Soil Moisture Corporation of Santa Barbara, CA). The samples were imbibed and drained to 100 cm tension in the hanging column apparatus, then transferred to the pressure cells to determine moisture equilibrium at 1 bar, 3 bars, and 5 bars pressure. Measurements were not made at higher pressures due to time constraints. Silica flour was used as the hydraulic contact between the samples and the porous plate due to the low air entry pressure of diatomaceous earth. Air entry pressure of silica flour is approximately 460 cm, which we determined by measuring a primary drainage curve of silica flour (see Figure E1.5).

Pressure Cell Assembly (referenced from Soil Moisture Corporation user's manual)

1. The pressure cell apparatus which includes the pressure regulator manifolds, pressure cells, and associated equipment are manufactured by Soil Moisture Corporation (SMEC) of Santa Barbara, CA and are specifically designed for extracting water from soil samples.
2. Assemble the pressure cell apparatus according to the manufacturer's instructions.
3. Place the triangular support in the extractor chamber on the bottom before any pressure plate cells are installed. This is necessary because a seal can be created between the pressure plate cell and the bottom of the chamber.

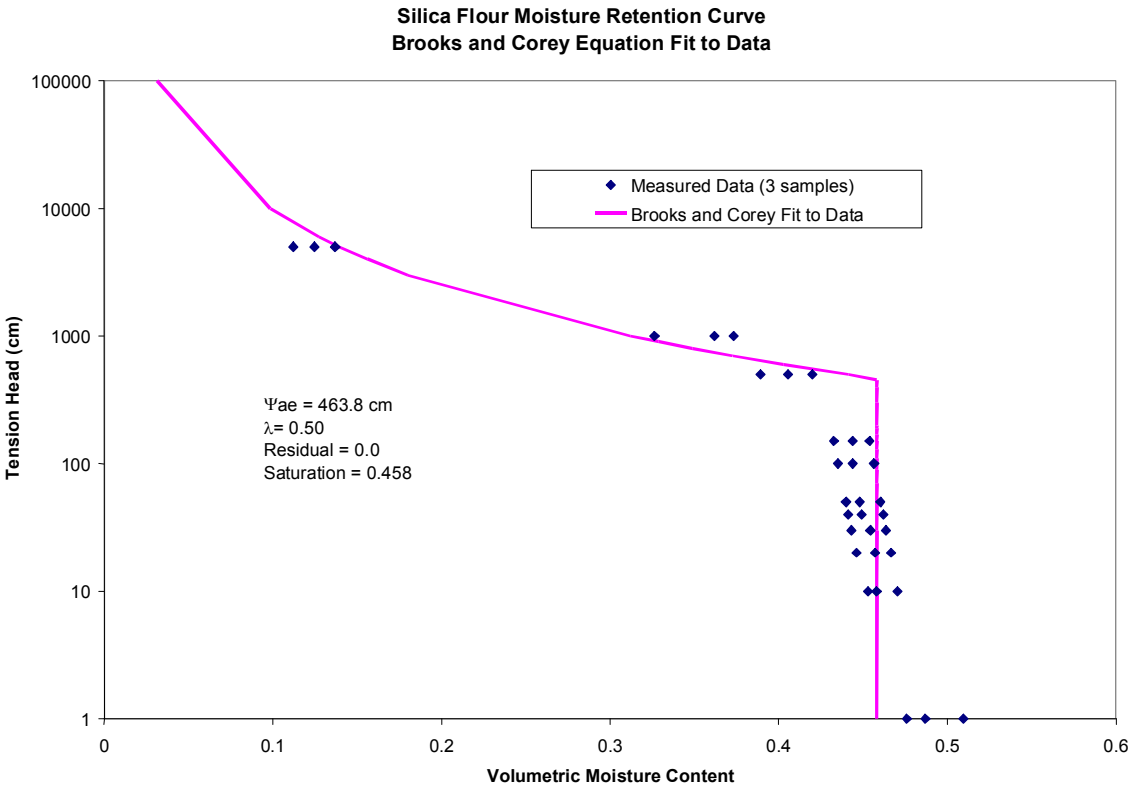

Figure E1.5 – Air entry pressure of silica flour used as the hydraulic contact in the pressure cell apparatus.

4. Saturate the pressure plates with deaerated water and mount the pressure plate cells in the tank. The 5 bar extractor is designed to accept a maximum of four ceramic pressure plate cells, one stacked on top of another. The first pressure plate cell is placed directly on the triangular support at the bottom of the extractor and connection is made through the lowest outlet port. The second pressure plate cell is set on three plastic spacers which are placed on the first ceramic plate cell near the outer edge and located about 120^{o} from each other. Connection to this cell is made through the middle outlet port. The remaining cells are mounted similar to the second cell. When mounting more than one cell, the spacing between cells should be three (3) notches apart, from top of clip to top of clip.

5. Attach the 6 in. length of rubber tube to the outflow stem of the first ceramic pressure plate cell. It is advisable to support the cell with the fingers directly behind the outlet stem when pushing the rubber tube over the outlet stem.
6. Push the free end of the rubber tube over the end of the outflow tube that projects into the tank.
7. Center the lid on the tank and clamp into place with the six clamping bolt assemblies, making sure that the rectangular heads of the bolts are properly seated in the constraining groove on the bottom side of the lower clamping ring.

Equilibration

1. Before making a run, a test run using only water should be conducted to determine if there are any leaks or damages in the system:
    - Let an excess of water stand on the surface of the porous plate cells for several hours to thoroughly wet the plate. Approximately 150 ml of water will be required to fill the pores of each plate.
    - Mount one or more of the wetted plates in the extractor and make the outflow connections.
    - Carefully add water on to the surface of each cell so that the surface is completely covered to the maximum depth permitted by the outer edge of the neoprene diaphragm.
    - Close the extractor and build up the pressure to maximum pressure of cell (5 or 15 bars), following the instructions below:
    - As the pressure builds up inside the extractor, there will be a rush of air from the outflow tubes. This is caused by the reduction of the internal

volume of the cell as the diaphragm and screen collapse under the pressure in the extractor. If the internal outflow tubing connections are tight and the cell has not been cracked or damaged, this air flow will stop after several minutes and there will be a steady flow of water.

- Small bubbles of air will come out in the flow of water at reasonably regular intervals. This is air which is slowly diffusing through the ceramic plate, and is to be expected.
- The outflow rate in ml/min should be measured soon after the flow starts, while the entire surface of the ceramic plate is covered with water. After a period of time, all of the water on the plate will have been conducted through and flow of water will stop. The slowly diffusing air will gradually conduct small amounts of water surrounding the internal screen to the outside.
- To measure the rate of diffusion, a short length of rubber tubing can be connected to the outflow tube and the end inserted under an inverted graduate which has been previously filled with water.
- The flow rate or the air should be less than 1/10 ml of air at atmospheric pressure per min with the extractor pressure at 220 psi. If the flow rate of air is appreciably higher than this, it indicates that there is a leak in the tubing connection or that the cell is cracked or not sealed properly.

2. Additionally, before making a run, it is desirable to provide a means for determining the required equilibrium time for each sample. This can be done by connecting each outflow tube to the tip of a burette with a piece of small diameter

tubing. Gas diffusing through the ceramic plate passes continuously in small bubbles through this small outflow tube, and keeps the extracted liquid transported to the burette. Read the burette periodically until equilibrium is reached. When equilibrium is reached, no measurable amount of change in the burette reading will be observed over a period of several hours or days.

E1.2.4 Moisture Content Adjustments

For deposits which contained a significant number of particles greater than 2 mm, we adjusted the sample bulk density and moisture contents by subtracting the mass and volume of the stones from the total volume and mass of the sample (Klute, 1986) after completion of all characterization procedures. Klute (1986) recommends removing larger particles before repacking samples when determining soil moisture retention, however we chose to remove the particles after completion of all characterization procedures since we were measuring multiple properties for each sample, some of which would be impacted by inclusion of larger particles (i.e., hydraulic conductivity).

Appendix E2

Moisture Retention Measurement Data and Moisture Characteristic Curves

E2. 1 Moisture Retention Data

The following tables list the measured moisture retention data. Tension head in cm reflects the tension exerted on the sample at the center of the ring. Moisture content values reflect the moisture retained by particles in the sample which are less than 2mm in diameter. The time allowed to reach equilibrium does not necessarily reflect exact equilibrium times since measurements were not always taken daily. Times represent period allowed to equilibrate, however they may exceed the actual equilibrium time.

Pressures at 333, 1000, 3000, 5000 cm correspond to 1/3 bar, 1 bar, 3 bars and 5 bars respectively. Since precision of the pressure gauges is approximately +/- 1 psi (72 cm) conversion from bars to cm was rounded to nearest 1000 cm (except for 1/3 bar which was considered to be 1/3 of 1000 cm).

Highest pressure measurement reflects pressure at which sample stopped draining. At higher pressures, sample either increased in weight (due to sorption of silica flour during analysis) or the weight did not change. Due to time constraints, measurements at high tensions were not made for the PDC sequence for all samples. Because the change in moisture content did not change much between 1 bar and 3 bars pressure, measurements were made at 1 bar and 5 bars pressure for many of the samples.

Pressure head values during wetting were adjusted to reflect effects of evaporation (i.e., drastic drop in burette meniscus due to evaporation). Pressure head values during draining remained relatively equal to the initial pressure exerted on the

samples. Changes in pressure head during drainage were usually minimal due to the effects of evaporation (typically within 1 cm), therefore the water levels were assumed to equal the initial pressures exerted on the samples.

Table E2.1 – Moisture retention measurements for samples NW1 – NW4.

nw1			**nw2**			**nw4**		
Pressure (cm)	moisture content	time (days)	Pressure (cm)	moisture content	time (days)	Pressure (cm)	moisture content	time (days)
mwc			**mwc**			**mwc**		
102	0.042	2	102	0.059	2	102.6	0.054	2
82	0.028	3	82	0.061	2	82	0.049	2
62	0.025	2	62	0.053	2	62	0.048	1
52	0.025	1	52	0.049	4	52.5	0.037	3
42	0.024	3	42	0.047	3	42.3	0.033	4
32	0.025	6	32	0.048	3	32	0.031	2
22	0.021	4	24.5	0.077	4	23.8	0.069	4
13.9	0.091	8	18.3	0.138	7	15.3	0.150	8
11.1	0.194	6	14.2	0.261	7	7.2	0.263	7
2	0.263	10	4.6	0.313	12	0.4	0.332	12
mdc			**mdc**			**mdc**		
12	0.243	1	12	0.277	3	12	0.310	5
22	0.208	6	22	0.199	7	22	0.235	10
32	0.155	13	32	0.129	12	32	0.159	5
42	0.135	3	42	0.109	2	42	0.096	2
52	0.047	4	52	0.092	3	52	0.067	5
72	0.036	2	72	0.077	3	72	0.045	5
102	0.027	5	102	0.061	5	102	0.035	3
333	0.024	2	333	0.058	2	333	0.030	2
1000	0.022	1	1000	0.058	1	1000	0.030	1
3000	0.018	1	3000	0.058	1	3000	0.030	1
pdc			**pdc**			**pdc**		
2	0.411	1	2	0.408	1	2	0.398	1
7	0.366	2	7	0.385	2	7	0.391	1
12	0.333	2	12	0.370	2	12	0.379	1
22	0.240	2	22	0.297	2	22	0.310	2
32	0.132	4	32	0.194	2	32	0.197	2
42	0.108	2	42	0.136	2	42	0.093	2
52	0.099	3	52	0.106	2	52	0.053	2
72	0.091	2	72	0.087	2	72	0.044	2
102	0.087	2	102	0.079	2	102	0.039	2

Table E2.2 – Moisture retention measurements for samples NW5 – NW7.

nw5			nw6			nw7		
Pressure (cm)	moisture content	time (days)	Pressure (cm)	moisture content	time (days)	Pressure (cm)	moisture content	time (days)
mwc			**mwc**			**mwc**		
103.4	0.081	8	100	0.155	3	102	0.081	4
84	0.081	7	84.6	0.177	4	82	0.080	1
62.1	0.084	3	66.9	0.225	4	62.3	0.076	3
53.4	0.085	4	55.1	0.270	8	52	0.072	3
44	0.088	7	46.8	0.321	4	42.5	0.075	3
33.2	0.093	4	37.6	0.357	8	34.7	0.097	4
26.3	0.119	13	23.4	0.369	6	22.4	0.294	5
12.5	0.169	9	10.5	0.387	10	12.3	0.357	12
3.2	0.276	14	0.8	0.423	8	0.8	0.384	3
mdc			**mdc**			**mdc**		
12	0.240	3	12	0.407	1	12	0.375	1
22	0.193	2	22	0.398	1	22	0.362	1
32	0.155	3	32	0.390	2	32	0.319	7
42	0.131	4	42	0.386	1	42	0.263	2
52	0.118	3	52	0.379	2	52	0.207	5
72	0.111	3	72	0.361	5	72	0.138	11
102	0.103	2	102	0.265	3	102	0.090	9
1000	0.066	7	1000	0.111	14	1000	0.083	1
3000	0.058	2	3000	0.099	3	3000	0.076	1
5000	0.051	2	5000	0.090	2	5000	0.068	6
pdc			**pdc**			**pdc**		
2	0.389	1	2	0.445	1	2	0.433	1
12	0.385	1	12	0.426	2	12	0.410	2
22	0.360	2	22	0.421	2	22	0.407	2
32	0.341	2	32	0.412	2	32	0.377	2
42	0.305	2	42	0.405	2	42	0.321	3
52	0.294	1	52	0.403	2	52	0.256	2
72	0.285	2	72	0.388	2	72	0.163	2
102	0.259	3	102	0.337	2	102	0.097	2
						1000	0.073	5
						5000	0.065	4

Table E2.3 – Moisture retention measurements for samples NW8 – NW10.

nw8			**nw9**			**nw10**		
Pressure (cm)	moisture content	time (days)	Pressure (cm)	moisture content	time (days)	Pressure (cm)	moisture content	time (days)
mwc			**mwc**			**mwc**		
102	0.115	4	99.3	0.085	2	102	0.108	4
82	0.106	3	83.2	0.080	2	83.4	0.109	6
62.9	0.106	3	65	0.080	3	62.8	0.119	5
52.9	0.105	2	56.6	0.070	3	53	0.108	2
46.2	0.135	4	47	0.093	3	44.7	0.106	3
39.4	0.178	7	38.8	0.134	3	34.3	0.104	4
31.9	0.229	4	30	0.176	4	23.8	0.229	10
16.3	0.359	12	21.3	0.228	4	12	0.288	7
3.3	0.382	6	3.9	0.326	10	7.8	0.320	3
mdc			**mdc**			**mdc**		
12	0.373	1	12	0.318	1	12	0.314	1
22	0.364	2	22	0.298	2	22	0.293	2
32	0.350	2	32	0.266	2	32	0.251	5
42	0.318	4	42	0.225	4	42	0.198	3
52	0.270	4	52	0.188	3	52	0.171	3
72	0.186	3	72	0.121	3	72	0.135	4
102	0.125	3	102	0.099	3	102	0.103	7
1000	0.100	12	1000	0.052	10	1000	0.090	4
5000	0.090	1	3000	0.047	2	3000	0.080	3
			5000	0.043	1	5000	0.073	5
pdc			**pdc**			**pdc**		
2	0.410	2	2	0.378	1	2	0.394	1
12	0.395	3	7	0.375	1	12	0.367	2
22	0.380	2	12	0.354	1	22	0.363	2
32	0.381	2	22	0.350	1	32	0.335	2
42	0.368	2	32	0.335	1	42	0.289	3
52	0.358	2	42	0.296	3	52	0.232	2
72	0.245	2	52	0.270	2	72	0.151	2
102	0.147	4	72	0.130	13	102	0.107	2
1000	0.105	5	102	0.052	4	1000	0.052	6
5000	0.091	4				5000	0.047	3

Table E2.4 – Moisture retention measurements for samples NW11 – NW13.

nw11			nw12			nw13		
Pressure (cm)	moisture content	time (days)	Pressure (cm)	moisture content	time (days)	Pressure (cm)	moisture content	time (days)
mwc			**mwc**			**mwc**		
103	0.105	5	102	0.110	2	119.9	0.233	6
83.3	0.123	7	82	0.104	2	101	0.233	8
62.4	0.123	4	63.1	0.101	4	64.3	0.233	5
52.5	0.123	2	53.2	0.105	1	53.4	0.290	34
46.4	0.191	10	42.6	0.103	2	45.7	0.343	14
36.1	0.270	4	36.6	0.146	7	35.3	0.356	4
22.3	0.329	11	29.4	0.225	11	25.3	0.361	12
16.7	0.348	7	12.4	0.356	10	12.0	0.361	2
2.5	0.390	7	2.5	0.382	2	4.4	0.365	7
mdc			**mdc**			**mdc**		
12	0.374	1	12	0.377	1	4.4	0.365	7
22	0.368	3	22	0.371	3	30	0.365	1
32	0.360	2	32	0.364	1	40	0.363	2
42	0.349	4	42	0.328	4	50	0.363	2
52	0.310	4	52	0.260	2	70	0.361	4
72	0.225	3	72	0.167	3	100	0.361	5
102	0.151	3	102	0.106	5	1000	0.336	3
1000	0.104	10	1000	0.080	10	3000	0.319	6
3000	0.099	2	3000	0.075	2	5000	0.288	3
5000	0.091	1	5000	0.067	1			
pdc			**pdc**					
2	0.439	2	2	0.442	2			
12	0.426	2	12	0.428	2			
22	0.403	1	22	0.396	2			
32	0.402	2	32	0.395	2			
52	0.352	1	42	0.383	2			
72	0.192	4	52	0.349	2			
102	0.143	2	72	0.197	2			
			102	0.122	2			

Table E2.5 – Moisture retention measurements for samples NW14 – NW16.

nw14			nw15			nw16		
Pressure (cm)	moisture content	time (days)	Pressure (cm)	moisture content	time (days)	Pressure (cm)	moisture content	time (days)
mwc			**mwc**			**mwc**		
109.2	0.139	2	104.95	0.401	16	96.95	0.080	2
83.3	0.131	3	83.6	0.409	14	83.45	0.085	8
62.8	0.133	7	65.5	0.413	2	62.45	0.074	2
52.6	0.137	4	53.1	0.413	3	52.3	0.073	1
46.5	0.140	10	46.5	0.410	1	46.1	0.157	7
35.3	0.152	6	35.3	0.413	10	37.3	0.206	6
23.8	0.166	2	23.8	0.421	7	30	0.277	4
14.0	0.212	5	17.5	0.424	7	17	0.375	9
5.7	0.289	6	8.5	0.434	7	6.1	0.404	10
mdc			**mdc**			**mdc**		
5.7	0.289	6	8.5	0.434	7	12	0.390	1
12	0.270	3	32	0.414	1	22	183.500	3
22	0.224	6	42	0.412	1	32	0.375	2
32	0.197	2	52	0.411	1	42	0.373	1
42	0.176	3	72	0.410	2	52	0.347	3
52	0.170	4	102	0.408	3	72	0.255	2
72	0.155	2	1000	0.355	7	102	0.125	7
102	0.148	4	3000	0.331	6	1000	0.068	1
1000	0.116	5	5000	0.312	3	3000	0.010	1
3000	0.097	7						
5000	0.092	3				**pdc**		
						2	0.404	1
						12	0.405	2
						22	0.402	1
						32	0.393	2
						42	0.390	2
						52	0.374	3
						72	0.279	7
						102	0.122	7

Table E2.6 – Moisture retention measurements for samples NW17 – NW18.

nw17			nw18			nw19		
Pressure (cm)	moisture content	time (days)	Pressure (cm)	moisture content	time (days)	Pressure (cm)	moisture content	time (days)
mwc			mwc			mwc		
102.8	0.059	7	102.7	0.099	5	105.7	0.129	9
82.6	0.061	3	83	0.096	2	84.3	0.146	7
62.8	0.058	4	62	0.094	1	63.2	0.207	12
52.5	0.056	2	54.7	0.088	7	53.1	0.214	5
43.8	0.151	7	43.2	0.087	5	44.8	0.248	6
32.5	0.233	3	33.8	0.214	10	32.2	0.296	1
22.7	0.318	10	23.3	0.295	7	22.2	0.338	5
12.9	0.381	8	12.5	0.397	12	13.6	0.357	3
2.4	0.407	8	4.3	0.423	2	2.3	0.398	8
mdc			mdc			mdc		
22	0.389	3	22	0.405	2	12	0.379	3
32	0.377	1	32	0.393	3	22	0.374	2
42	0.365	3	42	0.349	3	32	0.356	2
52	0.325	4	52	0.298	4	42	0.353	2
72	0.201	2	72	0.202	5	52	0.341	3
102	0.098	4	102	0.091	2	72	0.297	2
1000	0.063	2				102	0.218	4
3000	0.061	2				1000	0.080	1
5000	0.059	1				3000	0.069	2
						5000	0.067	1
pdc			pdc			pdc		
2	0.407	1	2	0.430	1	2	0.408	2
12	0.409	2	12	0.404	3	12	0.406	2
22	0.394	2	22	0.408	1	22	0.385	2
32	0.391	2	32	0.396	1	32	0.376	2
42	0.391	2	42	0.365	3	42	0.374	2
52	0.368	2	52	0.262	2	52	0.371	2
72	0.229	3	72	0.145	4	72	0.355	2
102	0.088	2	102	0.068	2	102	0.240	5
1000	0.049	4	1000	0.045	4	1000	0.063	4
			5000	0.041	3			

Table E2.7 – Moisture retention measurements for samples NW20 – NW22.

nw20			nw21			nw22		
Pressure (cm)	moisture content	time (days)	Pressure (cm)	moisture content	time (days)	Pressure (cm)	moisture content	time (days)
mwc			**mwc**			**mwc**		
105.7	0.061	5	100	0.051	2	102.7	0.067	5
84.3	0.054	2	73.6	0.050	3	74.1	0.068	4
63.2	0.047	3	53.3	0.048	4	53.7	0.068	3
53.1	0.047	5	42.4	0.047	1	42.5	0.081	10
44.8	0.047	1	33.7	0.185	8	32.2	0.080	1
32.2	0.088	6	26.1	0.263	7	25	0.297	7
22.2	0.267	9	14.3	0.357	7	16.9	0.363	6
13.6	0.363	9	6.3	0.376	4	6	0.378	4
2.3	0.392	9						
mdc			**mdc**			**mdc**		
22	0.373	3	12	0.365	5	12	0.366	3
32	0.360	3	22	0.358	2	22	0.368	2
42	0.339	2	32	0.347	2	32	0.367	2
52	0.274	4	42	0.317	6	42	0.345	2
72	0.179	5	52	0.238	4	52	0.305	2
102	0.081	2	72	0.153	3	72	0.212	2
1000	0.066	1	102	0.079	3	102	0.119	2
3000	0.071	3	1000	0.079	2	1000	0.121	1
5000	0.069	1	5000	0.079	1	5000	0.107	3
pdc			**pdc**			**pdc**		
2	0.401	1	2	0.440	5	2	0.406	5
12	0.389	2	12	0.430	2	12	0.397	1
22	0.392	2	22	0.423	5	22	0.383	1
32	0.364	3	32	0.417	5	32	0.376	2
42	0.351	2	42	0.392	2	42	0.357	5
52	0.286	5	52	0.344	7	52	0.324	4
72	0.171	4	72	0.344	1	72	0.241	1
102	0.063	10	102	0.099	2	102	0.109	3

Table E2.8 – Moisture retention measurements for samples NW23 – NW25.

nw23			nw24			nw25		
Pressure (cm)	moisture content	time (days)	Pressure (cm)	moisture content	time (days)	Pressure (cm)	moisture content	time (days)
mwc			**mwc**			**mwc**		
102.42	0.037	5	102.5	0.053	5	100.8	0.056	5
72.2	0.039	4	73.6	0.049	2	73.8	0.057	4
52.6	0.038	2	52	0.046	2	53	0.057	2
42.4	0.037	1	42	0.044	2	42.7	0.059	1
32.7	0.038	2	32	0.044	1	32.7	0.059	2
25.6	0.167	12	29.2	0.178	11	30.4	0.137	9
13.9	0.323	10	16.1	0.289	6	12.5	0.241	6
6.9	0.351	7	10	0.334	7	9.1	0.294	7
			mdc			**mdc**		
mdc			12	0.326	2	12	0.286	2
12	0.348	2	22	0.308	3	22	0.260	5
22	0.335	2	32	0.284	2	32	0.232	2
32	0.314	2	42	0.253	2	42	0.189	2
42	0.276	3	52	0.206	2	52	0.152	2
52	0.238	3	72	0.185	2	72	0.105	6
72	0.159	3	102	0.120	4	102	0.083	5
102	0.111	2	1000	0.113	2	1000	0.114	2
			5000	0.110	1	5000	0.098	1
pdc			**pdc**			**pdc**		
2	0.393	2	2	0.375	3	2	0.374	2
12	0.386	4	12	0.356	4	12	0.364	3
22	0.372	3	22	0.337	3	22	0.340	2
32	0.346	5	42	0.280	9	32	0.282	5
42	0.304	6	52	0.233	11	42	0.247	3
52	0.262	4	72	0.229	1	52	0.246	2
72	0.218	5	102	0.222	1	72	0.225	1
102	.201	11				102	0.072	13

Table E2.9 – Moisture retention measurements for samples NW27.

nw27		
Pressure (cm)	moisture content	time (days)
mwc		
105.2	0.014	7
74.5	0.013	2
52.8	0.013	2
43	0.013	2
33.8	0.015	4
32.1	0.080	5
15.5	0.240	5
6.8	0.323	7
mdc		
12	0.307	2
22	0.293	5
32	0.293	1
42	0.188	4
52	0.109	3
72	0.062	3
102	0.060	2
1000	0.057	1
5000	0.056	1
pdc		
2	0.386	3
12	0.384	3
22	0.357	2
32	0.278	7
42	0.174	6
52	0.091	1
72	0.054	2
102	0.048	1

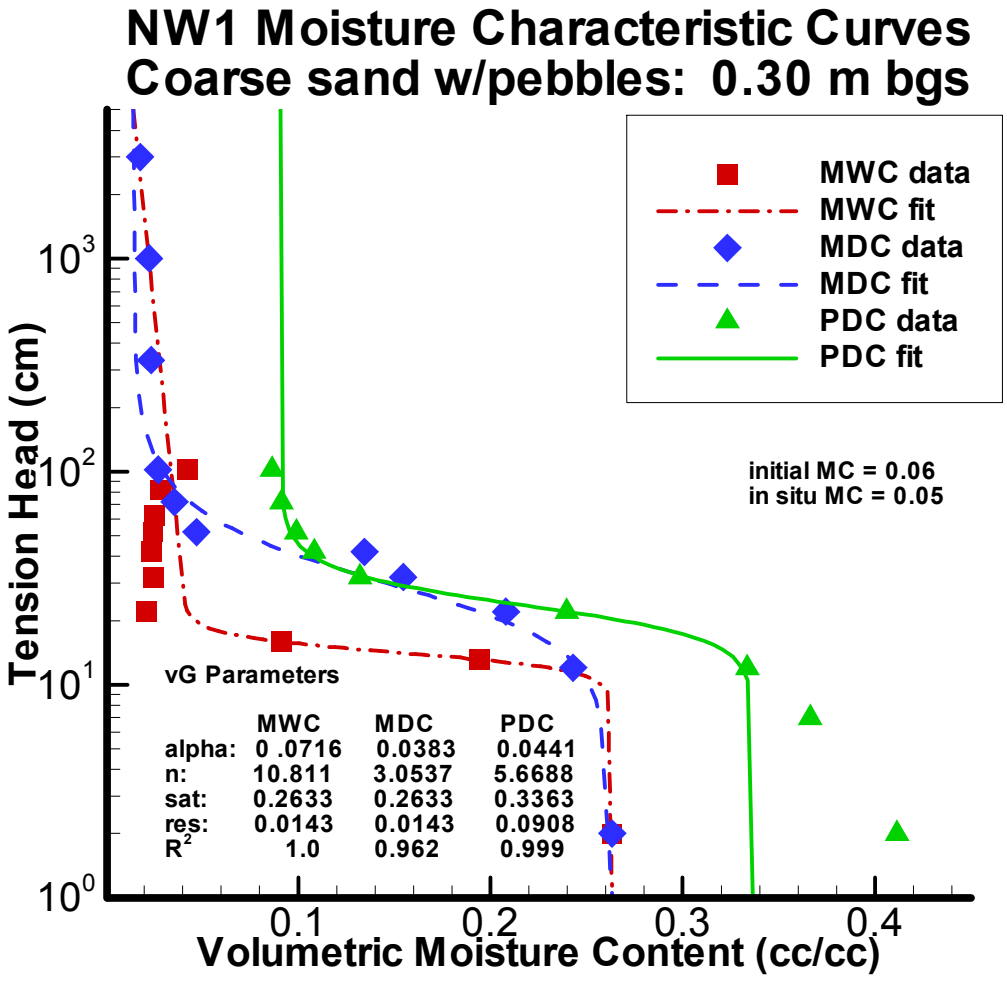

Figure E2.1 – Moisture Characteristic Curves for sample NW1 – coarse grained sand. Sample location approximately 030 meters bgs.

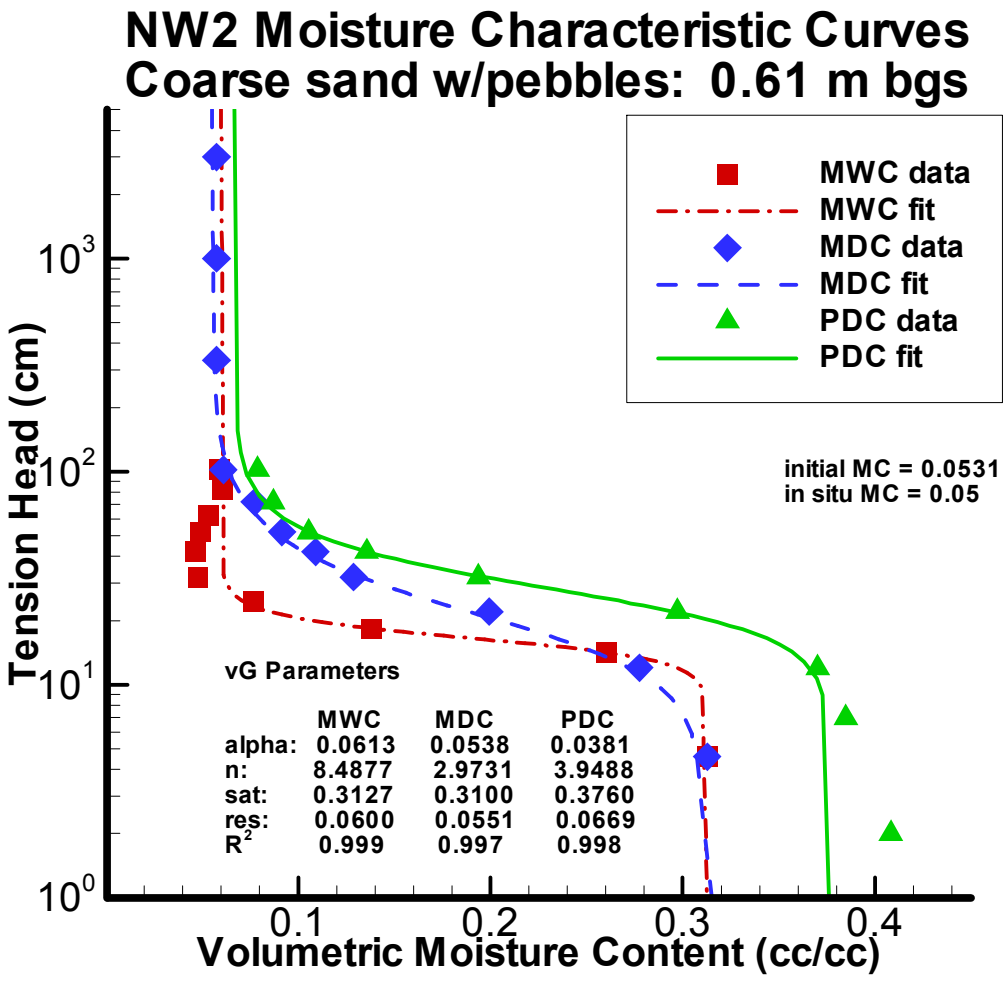

Figure E2.2 – Moisture Characteristic Curves for sample NW2 – coarse grained sand. Sample location approximately 0.61 meters bgs.

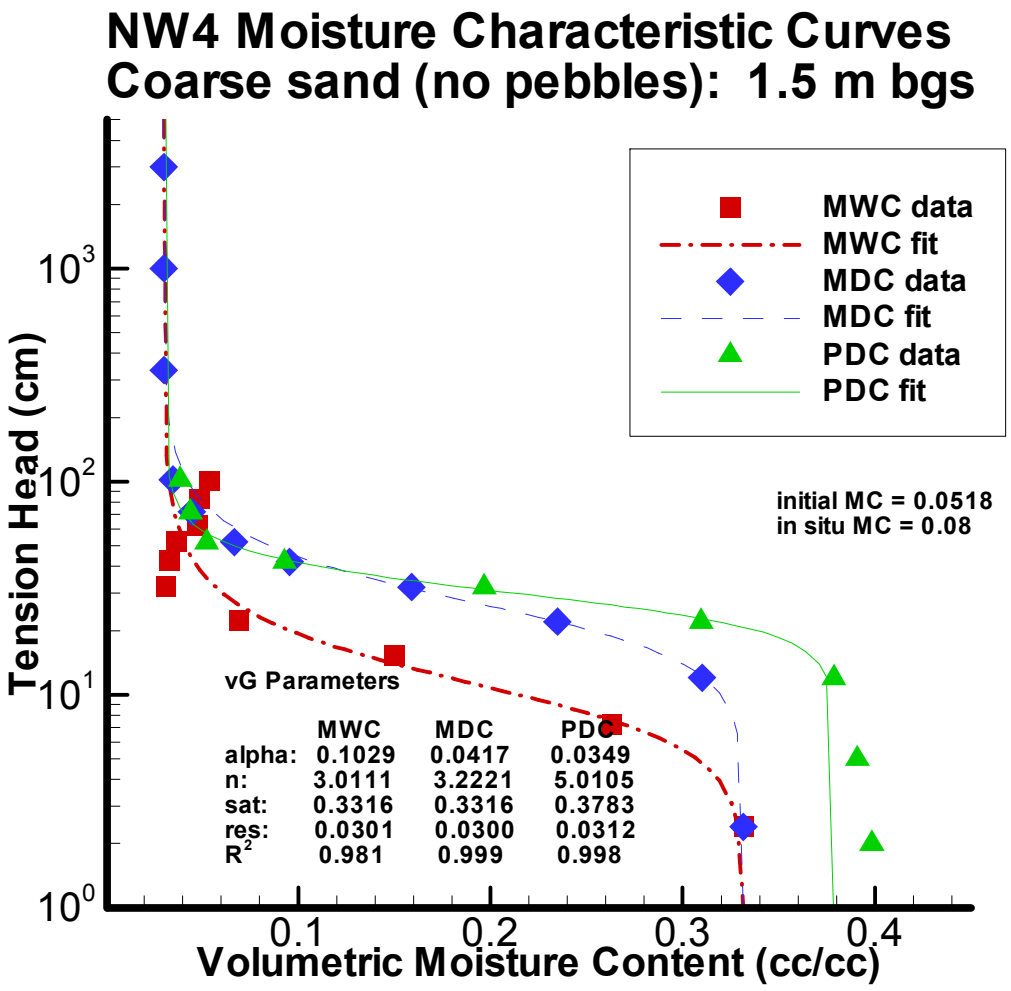

Figure E2.3 – Moisture Characteristic Curves for sample NW4 – coarse grained sand. Sample location approximately 1.5 meters bgs.

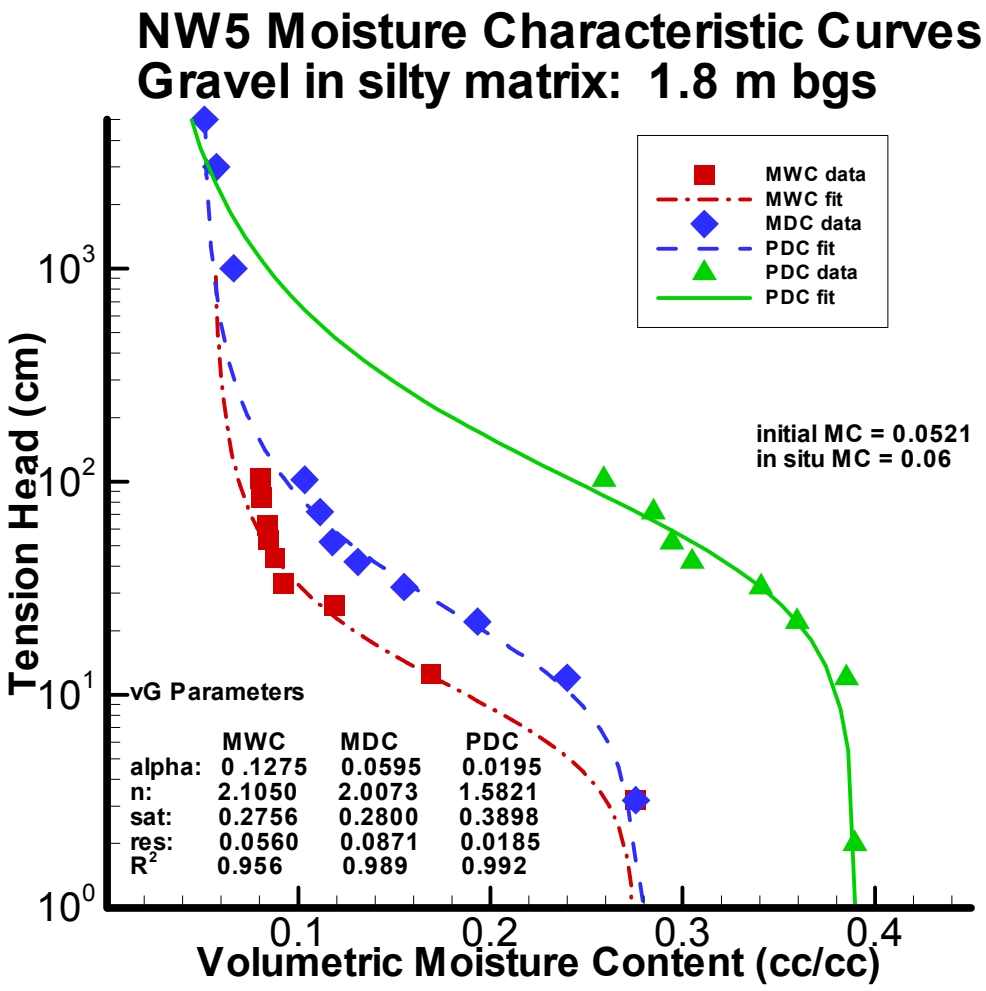

Figure E2.4 – Moisture Characteristic Curves for sample NW5 – gravel. Sample location approximately 1.8 meters bgs.

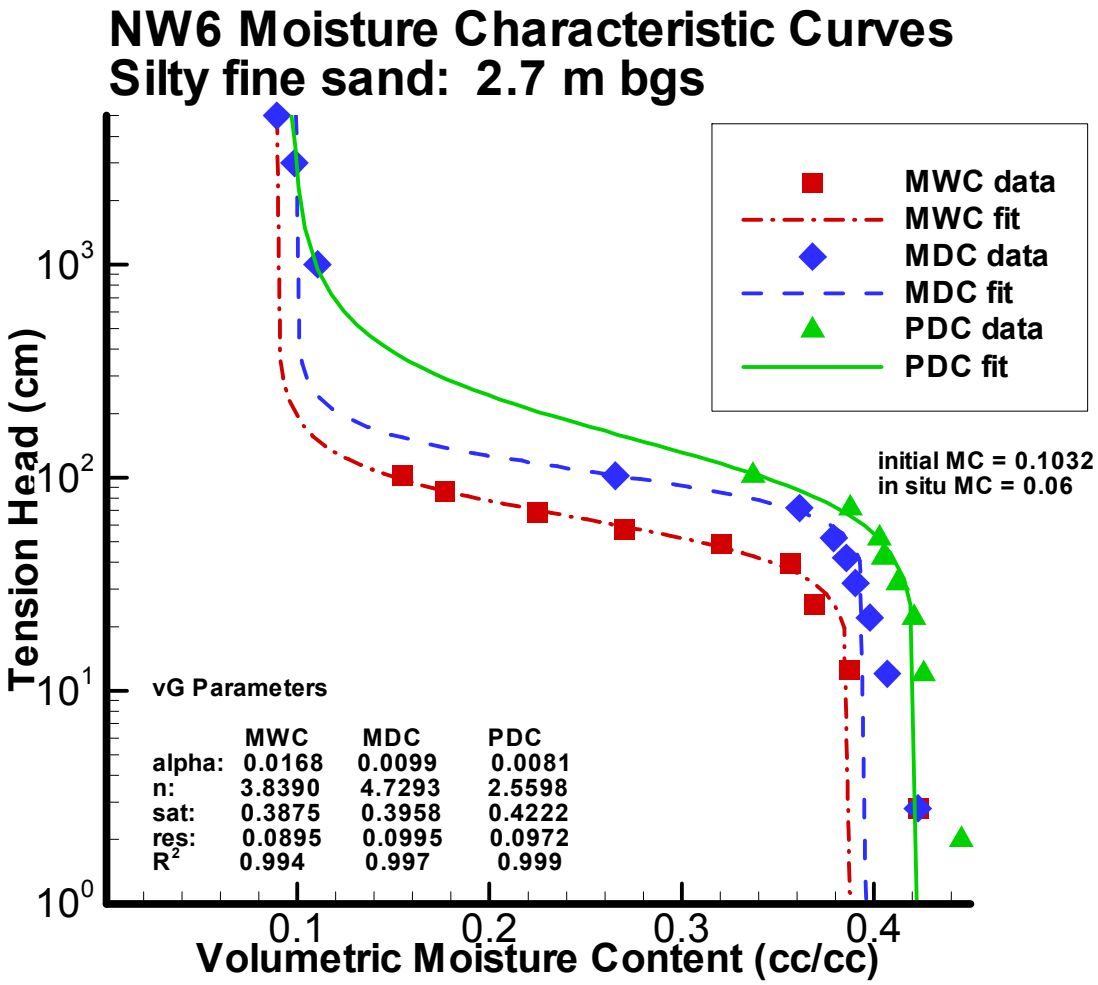

Figure E2.5 – Moisture Characteristic Curves for sample NW6 – silty fine sand. Sample location approximately 2.7 meters bgs.

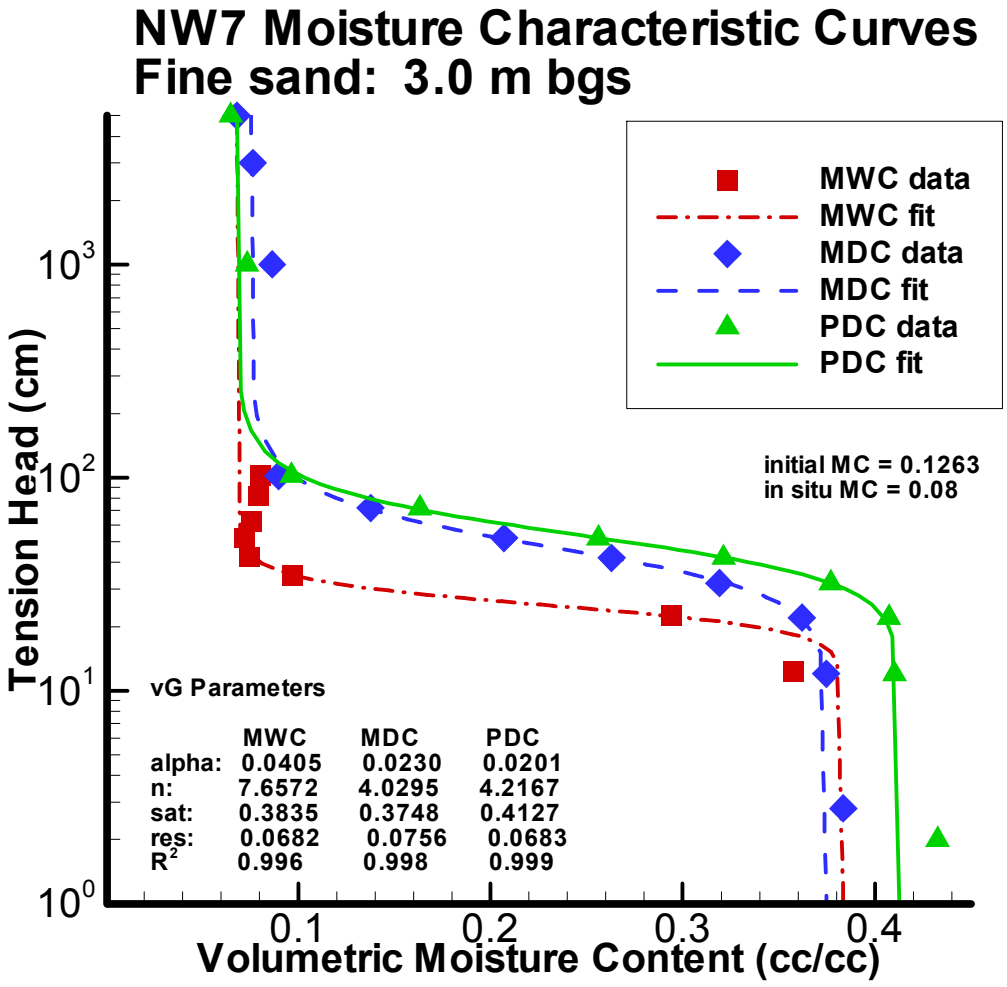

Figure E2.6 – Moisture Characteristic Curves for sample NW7 – fine sand. Sample location approximately 3.0 meters bgs.

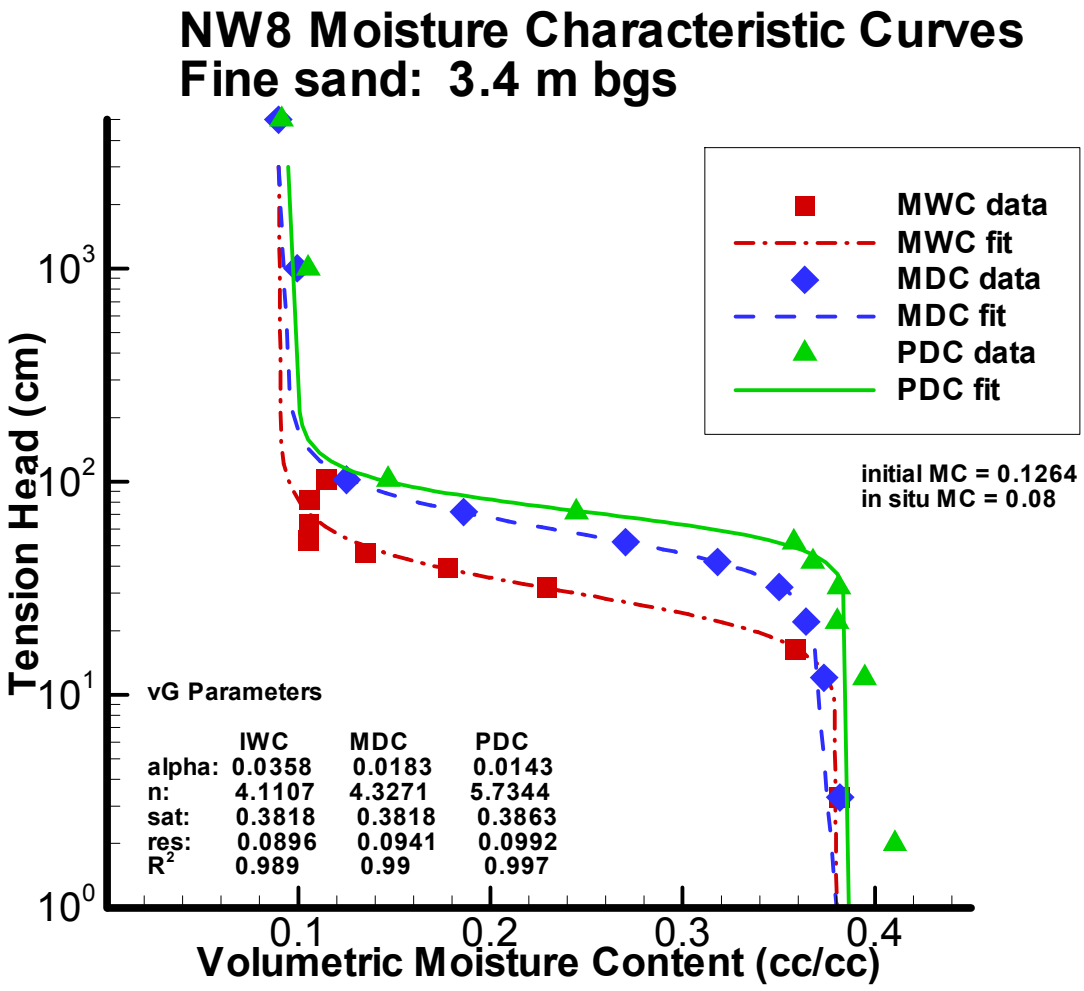

Figure E2.7 – Moisture Characteristic Curves for sample NW8 – fine sand. Sample location approximately 3.4 meters bgs.

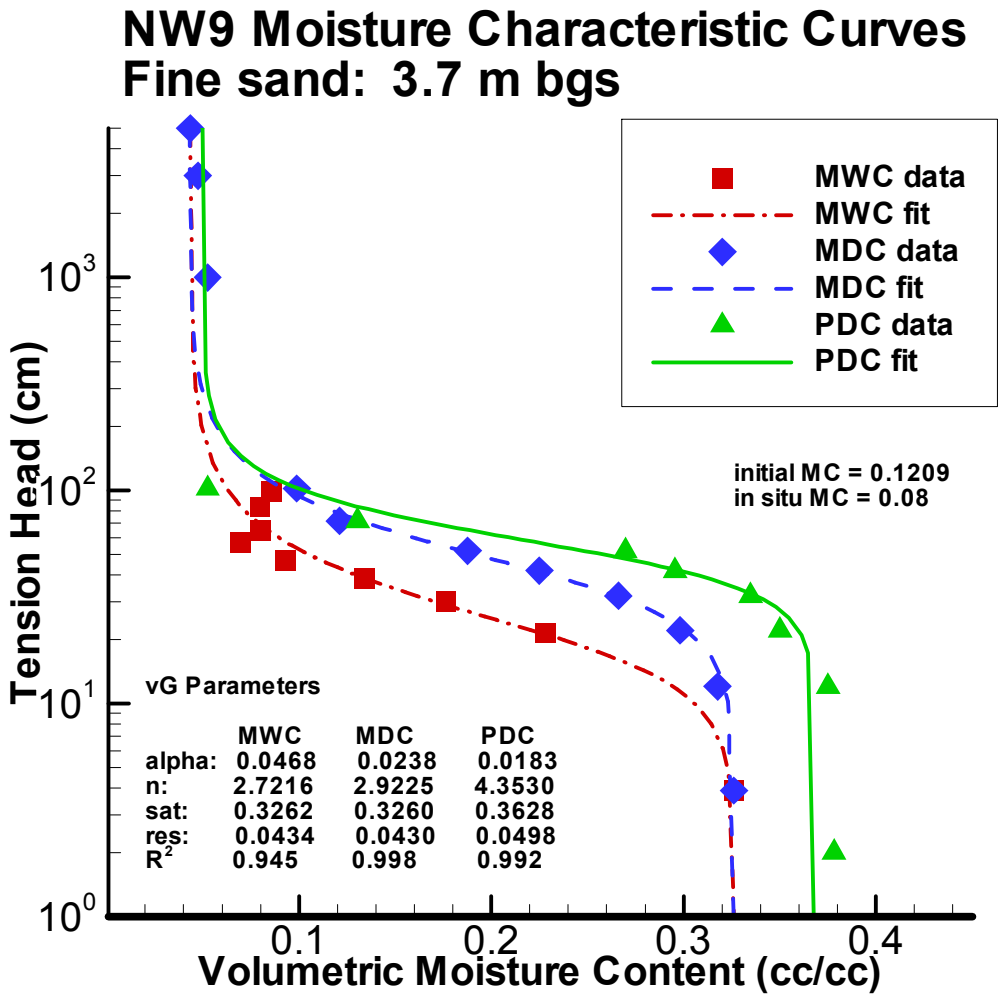

Figure E2.8 – Moisture Characteristic Curves for sample NW9 – fine sand. Sample location approximately 3.7 meters bgs.

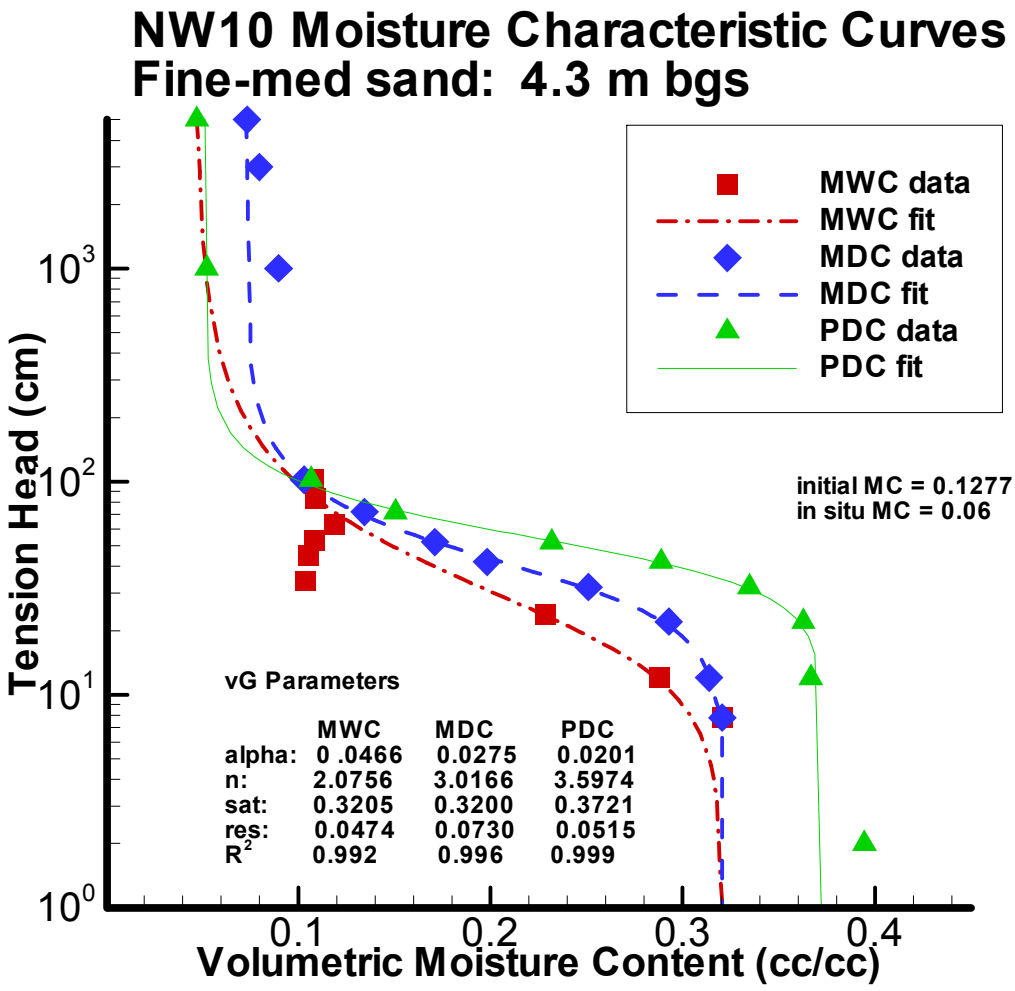

Figure E2.9 – Moisture Characteristic Curves for sample NW10. Sample location approximately 4.3 meters bgs.

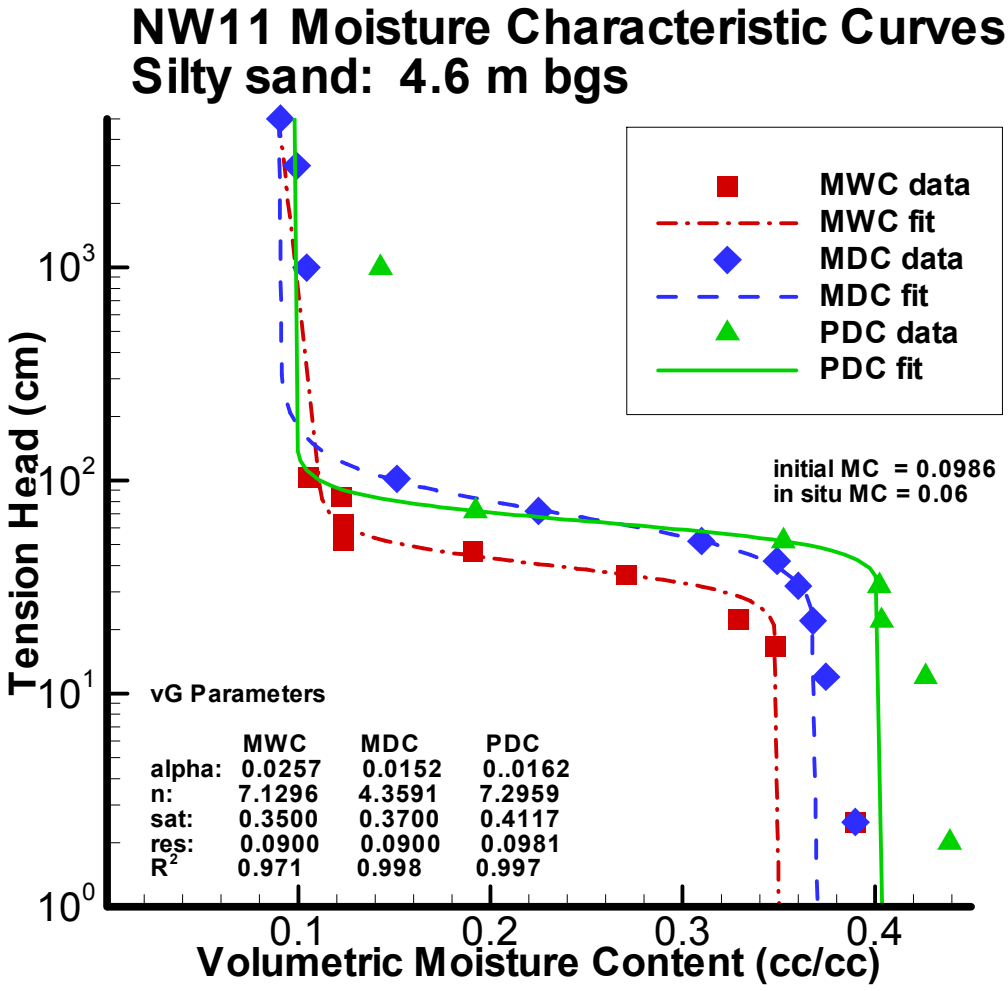

Figure E2.10 – Moisture Characteristic Curves for sample NW11 – fine sand. Sample location approximately 4.6 meters bgs.

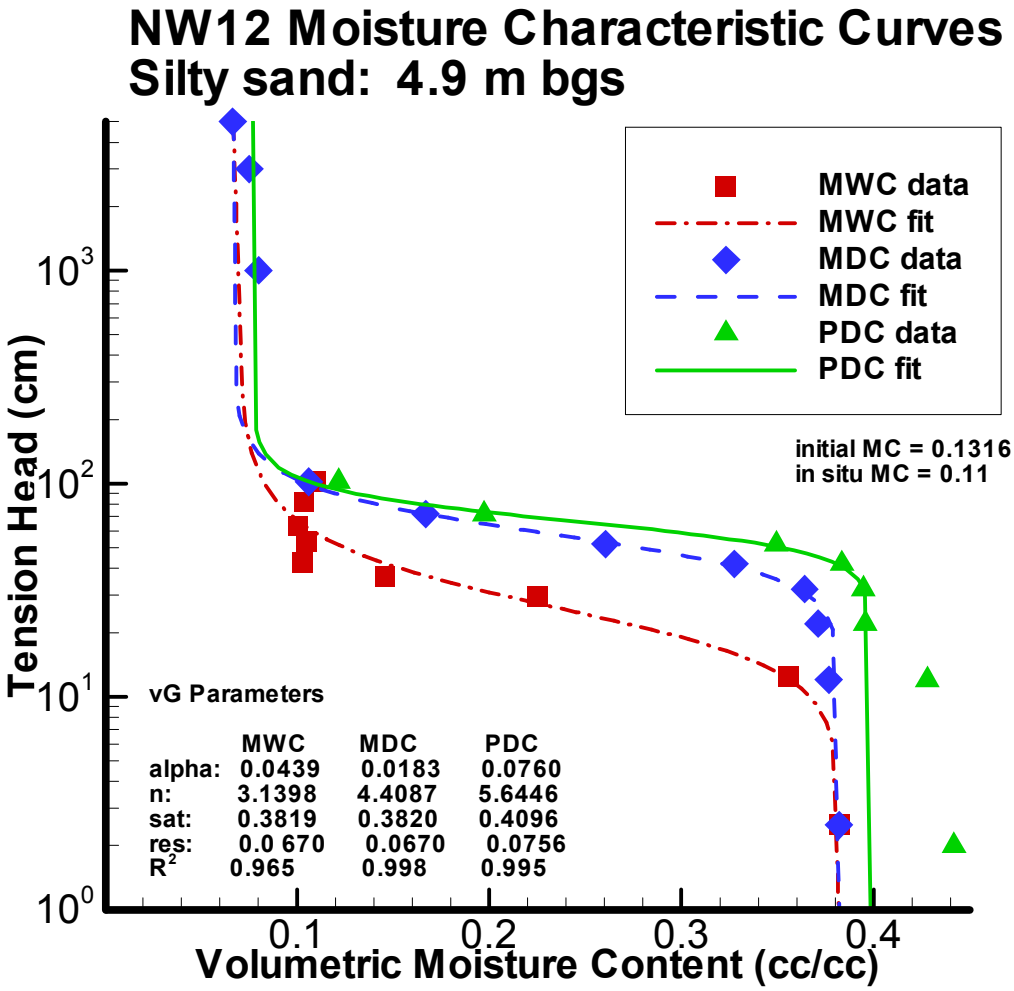

Figure E2.11 – Moisture Characteristic Curves for sample NW12 – silty sand. Sample location approximately 4.9 meters bgs.

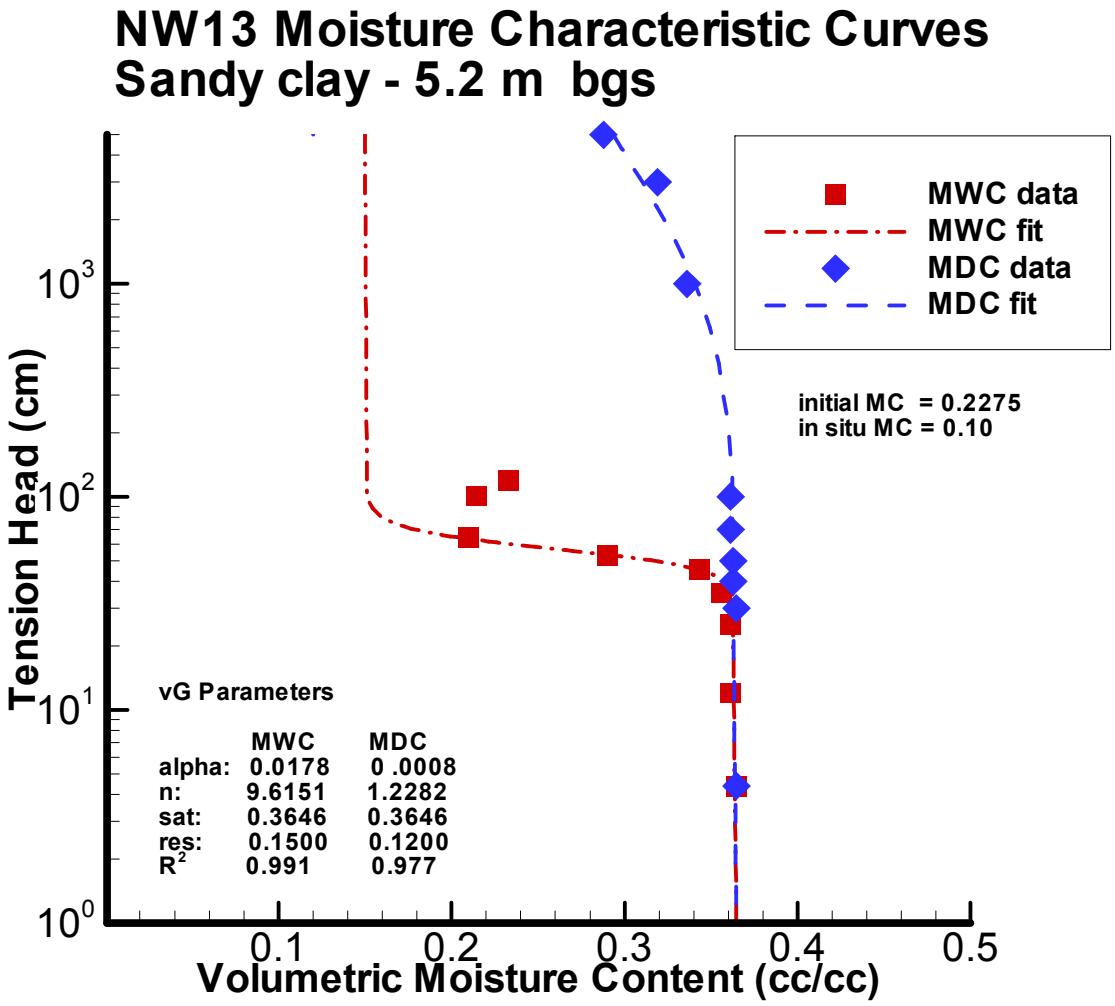

Figure E2.12 – Moisture Characteristic Curves for sample NW13 – sandy clay. Sample location approximately 5.2 meters bgs.

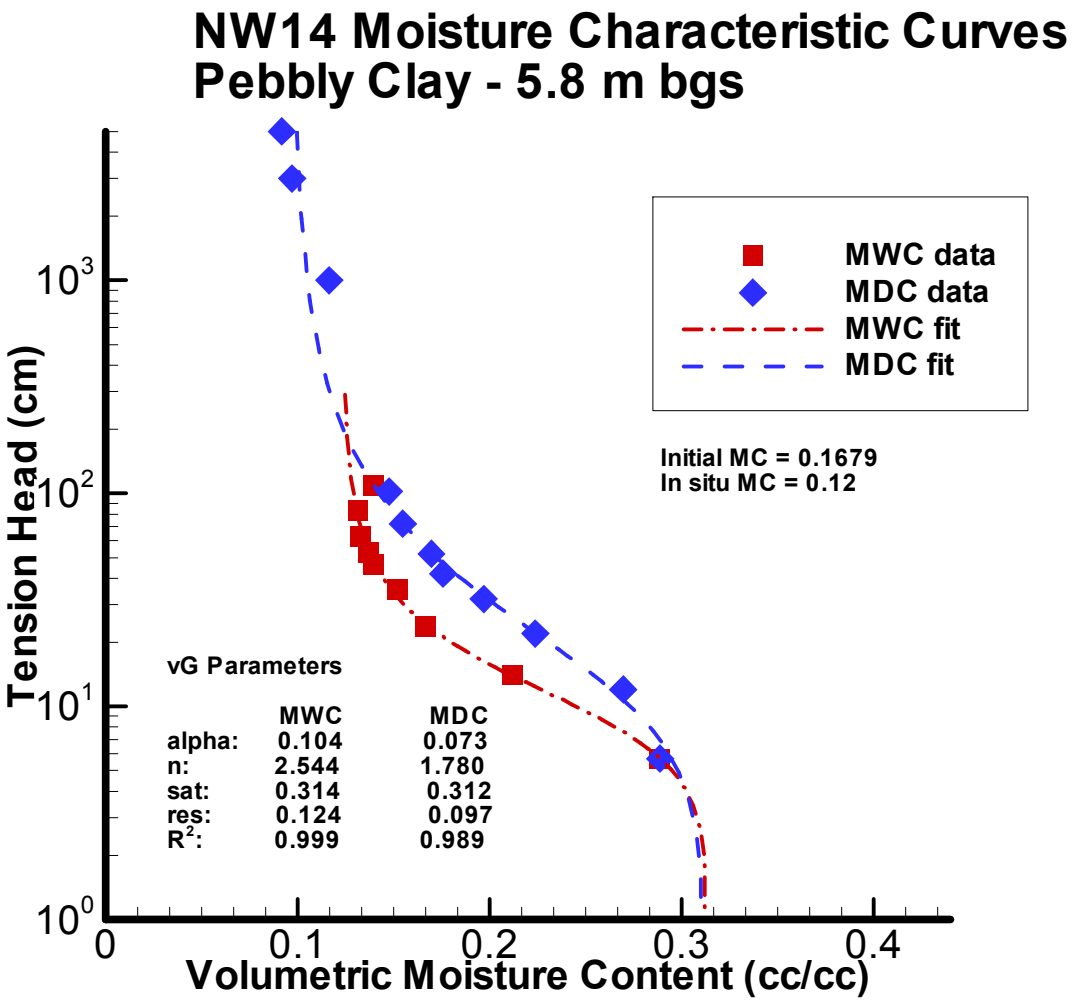

Figure E2.13 – Moisture Characteristic Curves for sample NW14 – pebbly clay. Sample location approximately 5.8 meters bgs.

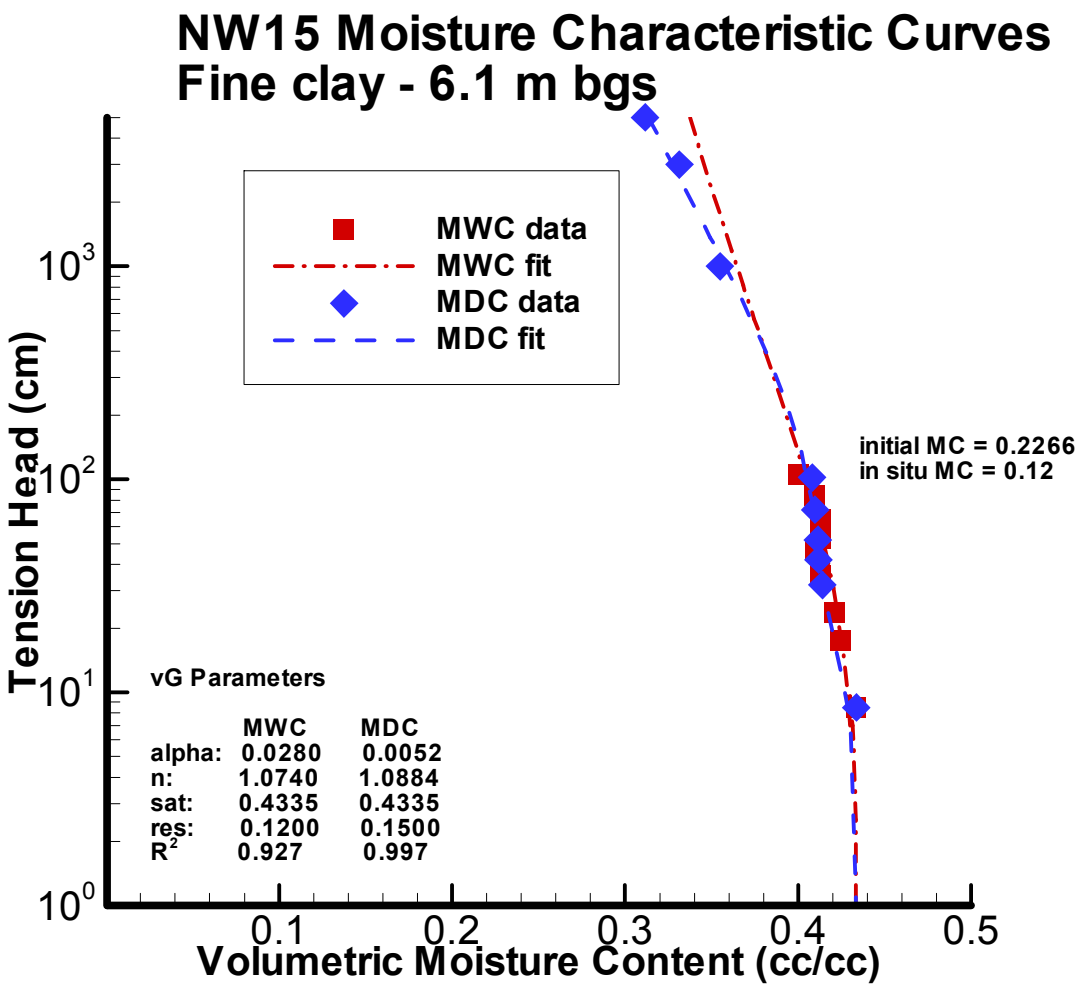

Figure E2.14 – Moisture Characteristic Curves for sample NW15 – clay. Sample location approximately 6.1 meters bgs.

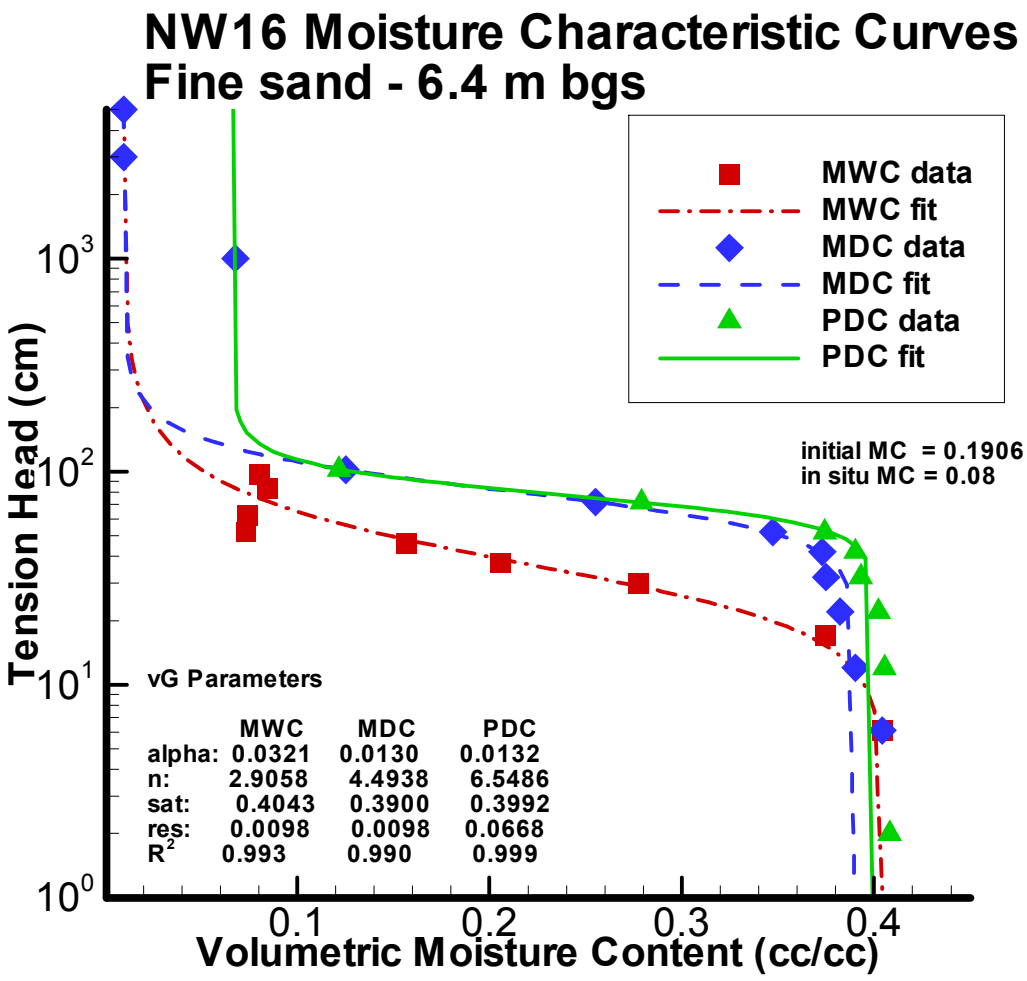

Figure E2.15 – Moisture Characteristic Curves for sample NW16 – fine sand. Sample location approximately 6.4 meters bgs.

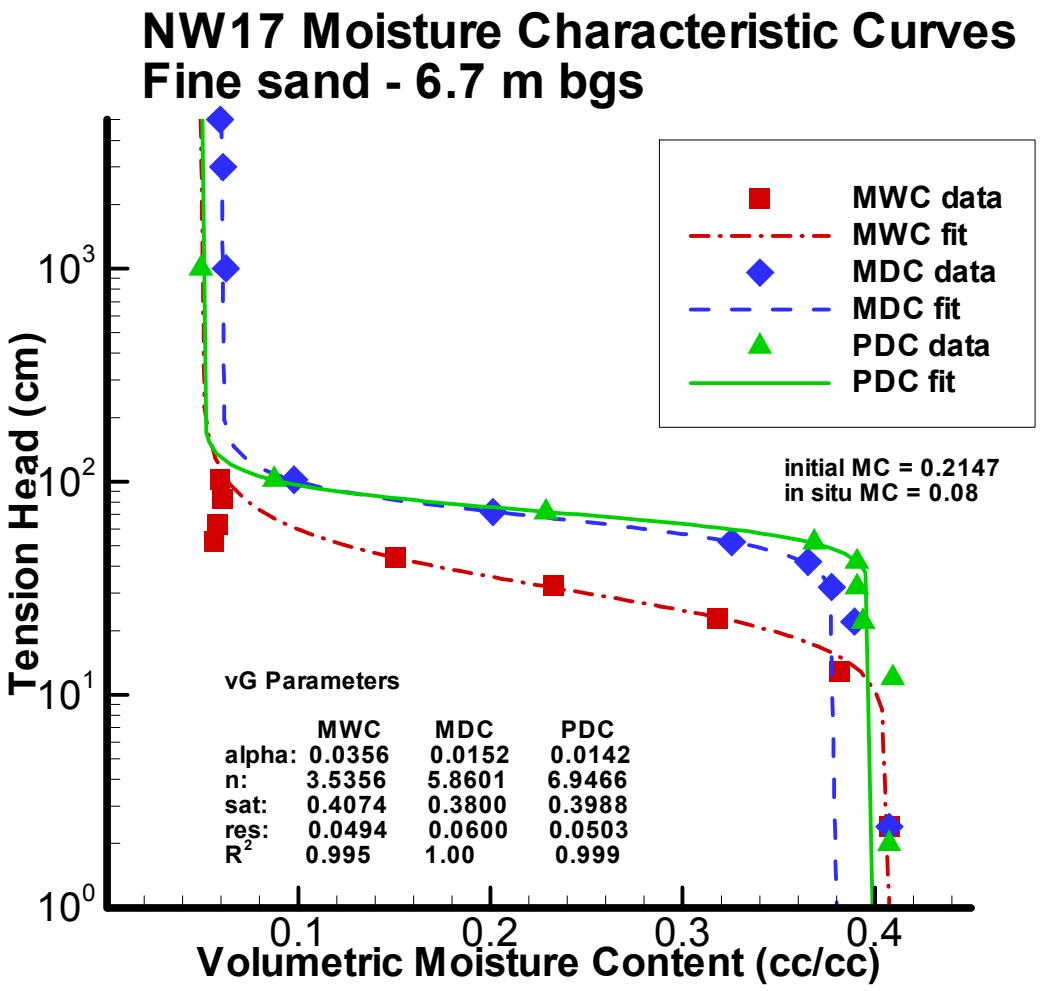

Figure E2.16 – Moisture Characteristic Curves for sample NW17 – fine sand. Sample location approximately 6.7 meters bgs.

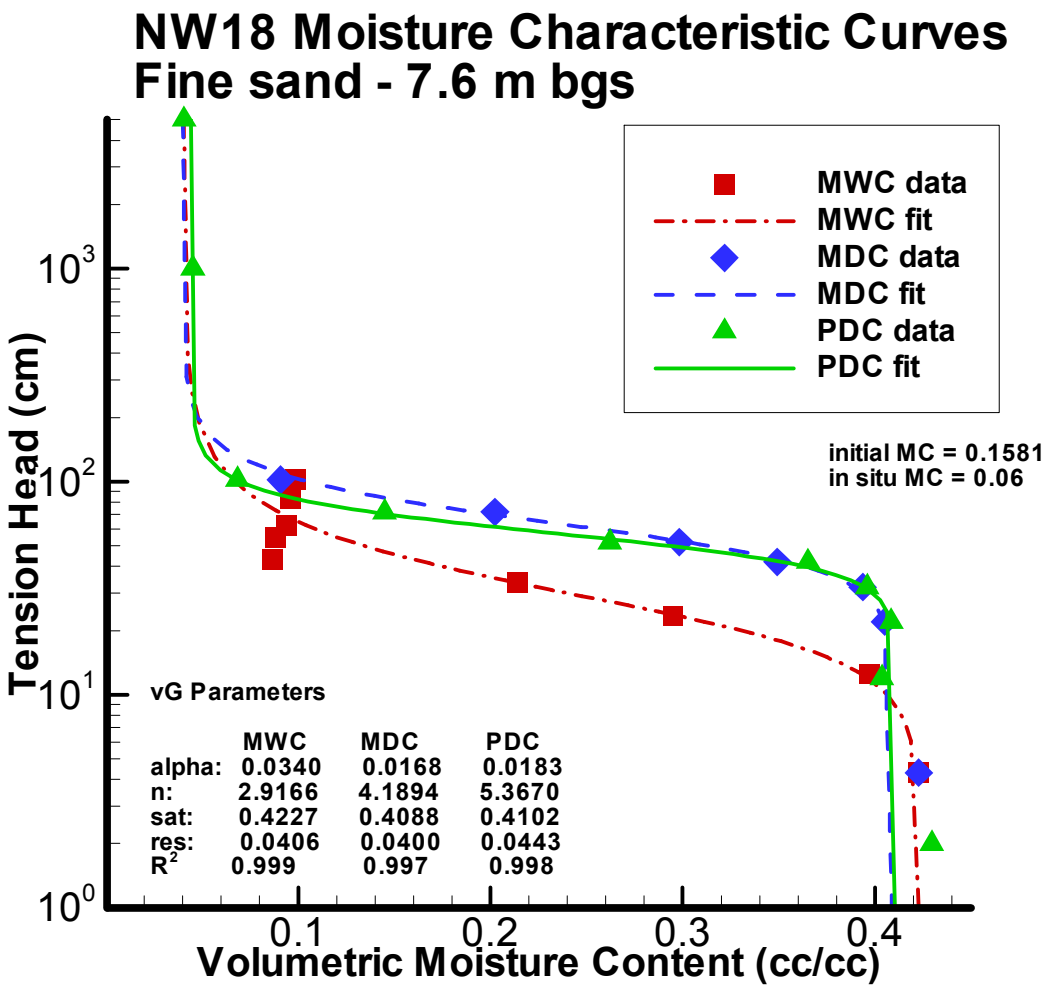

Figure E2.17 – Moisture Characteristic Curves for sample NW18 – fine sand. Sample location approximately 7.6 meters bgs.

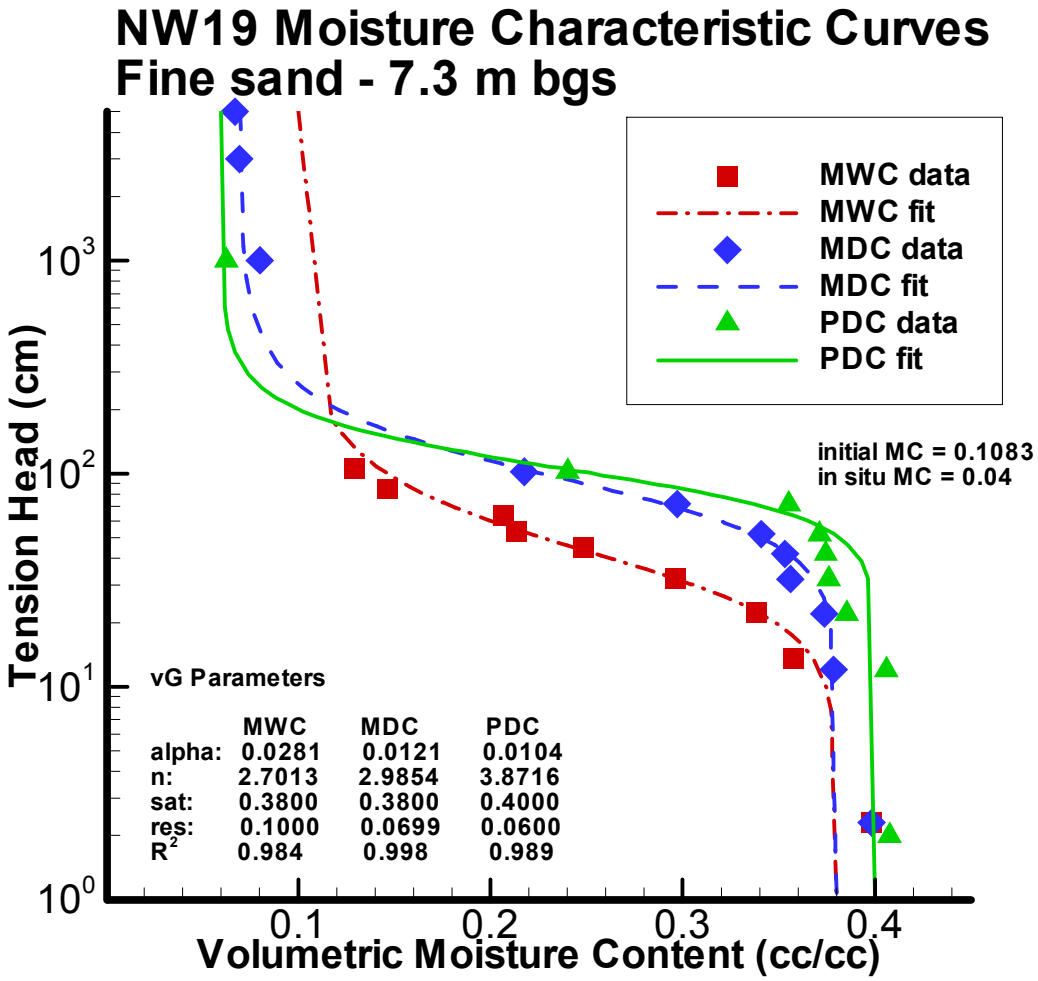

Figure E2.18 – Moisture Characteristic Curves for sample NW19 – fine sand. Sample location approximately 7.3 meters bgs.

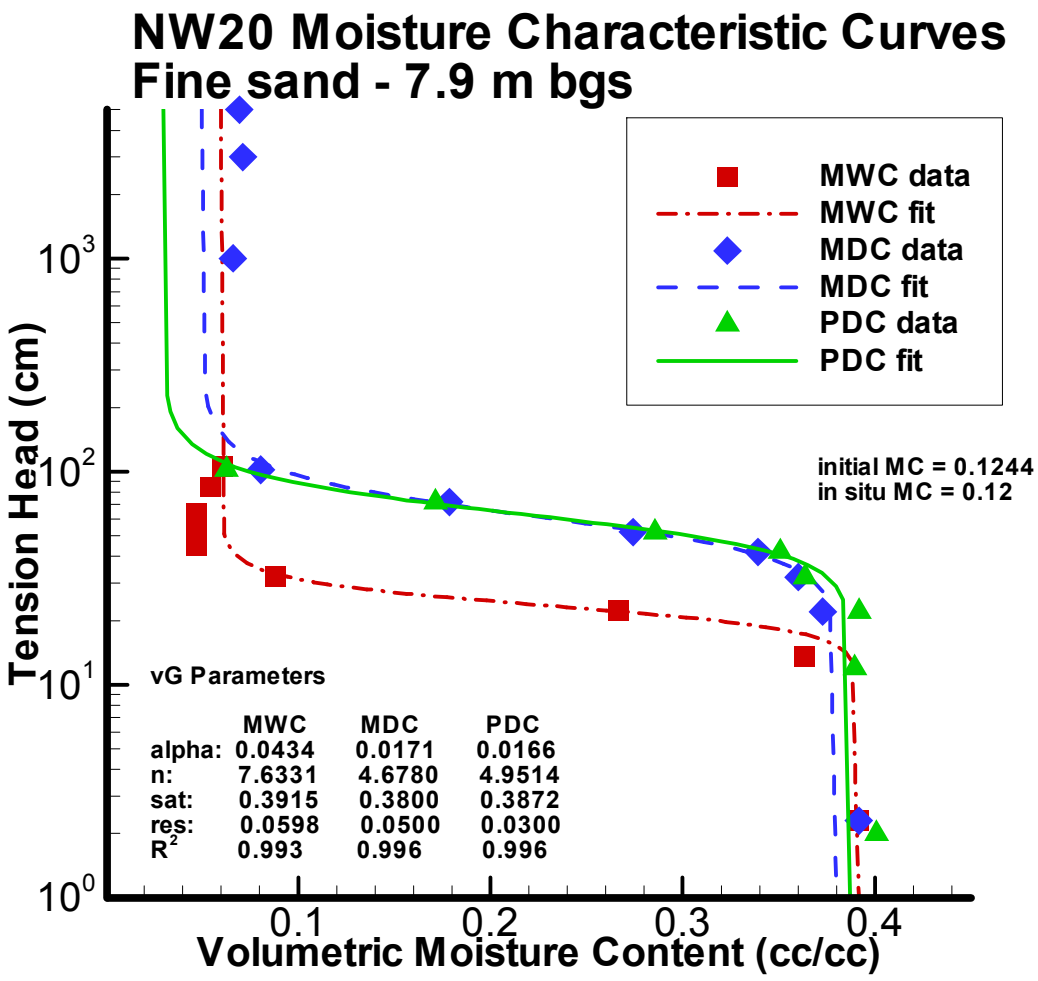

Figure E2.19 – Moisture Characteristic Curves for sample NW20 – fine sand. Sample location approximately 7.9 meters bgs.

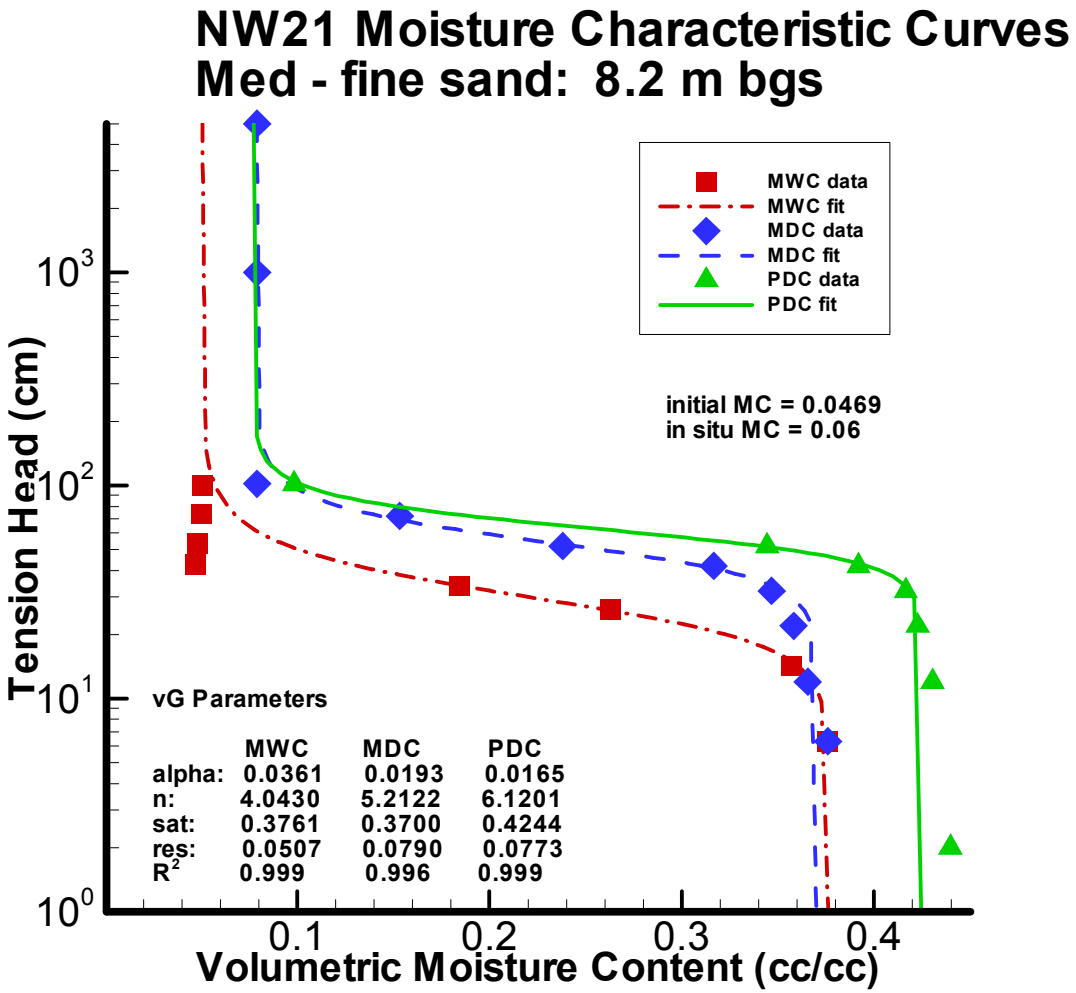

Figure E2.20 – Moisture Characteristic Curves for sample NW21 – fine to medium sand. Sample location approximately 8.2 meters bgs.

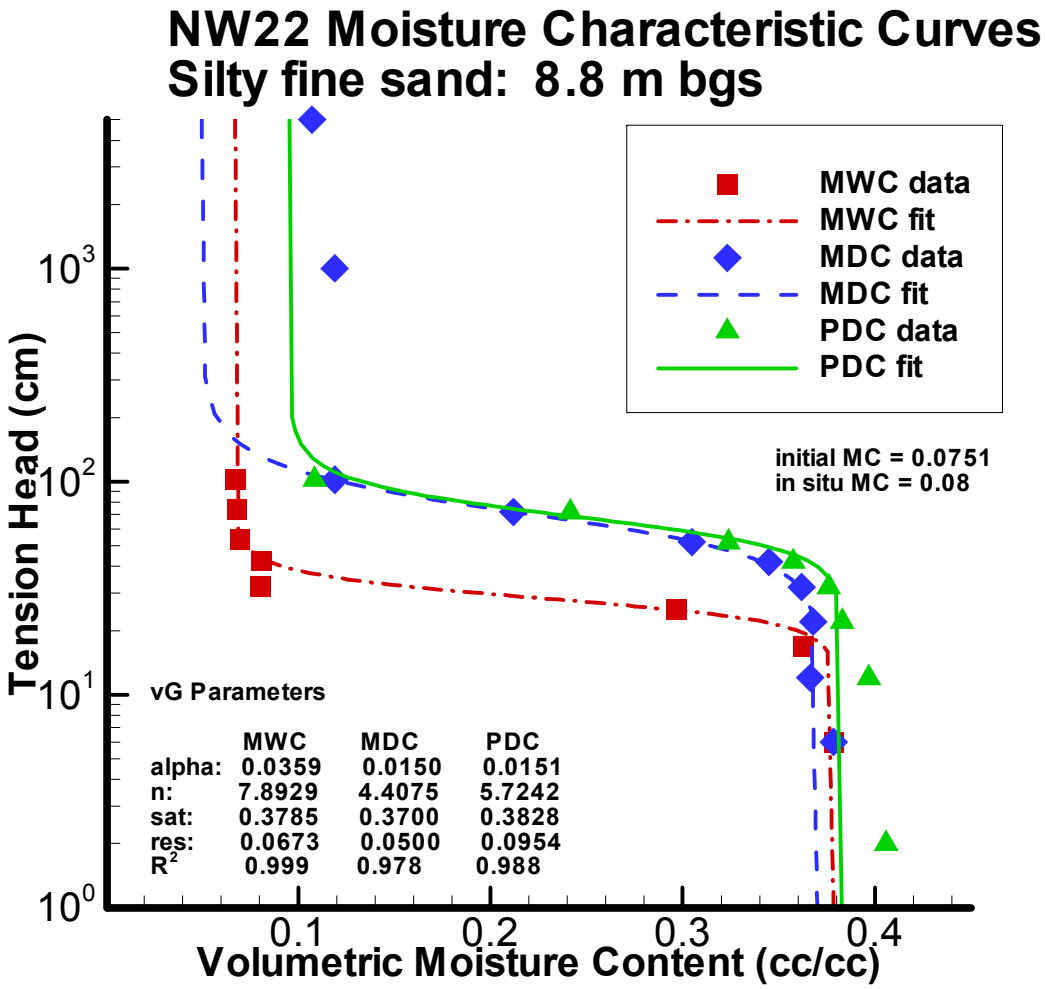

Figure E2.21 – Moisture Characteristic Curves for sample NW22 – silty fine sand. Sample location approximately 8.8 meters bgs.

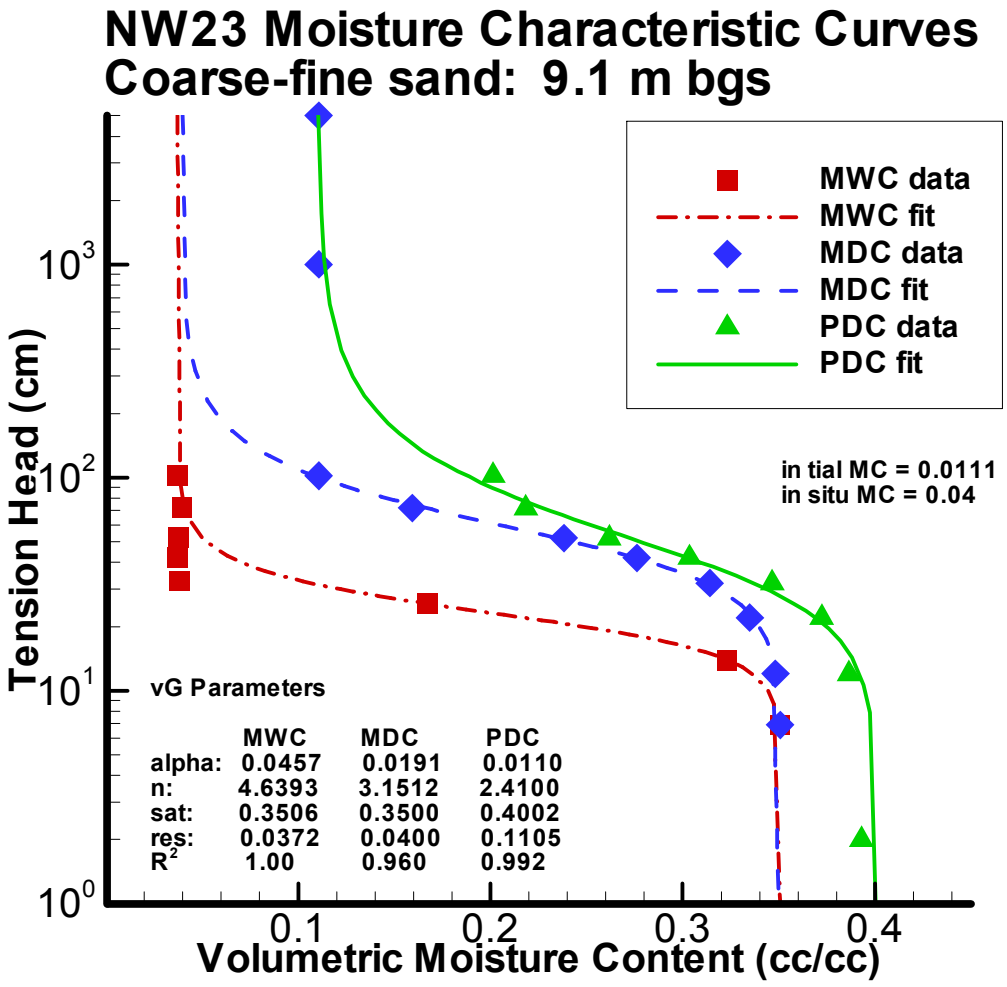

Figure E2.22 – Moisture Characteristic Curves for sample NW23 – fine to coarse sand. Sample location approximately 9.1 meters bgs.

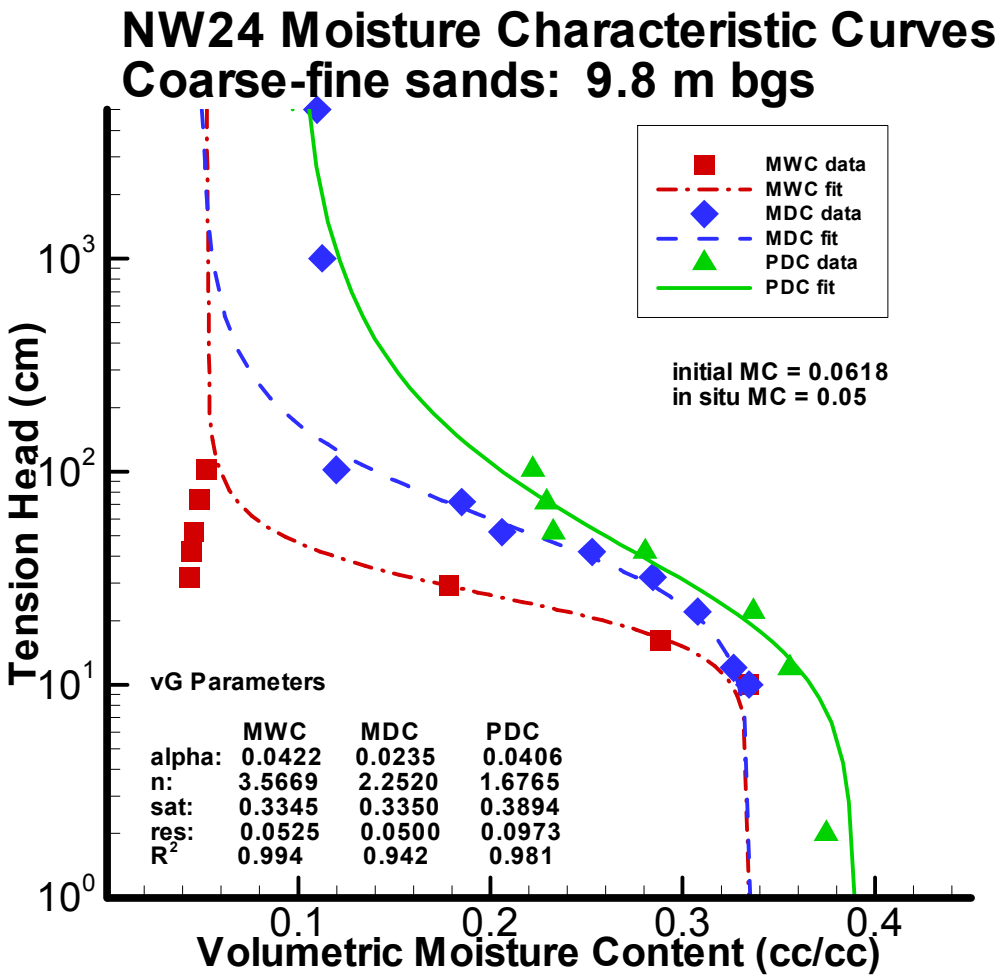

Figure E2.23 – Moisture Characteristic Curves for sample NW24 – fine sand. Sample location approximately 9.8 meters bgs.

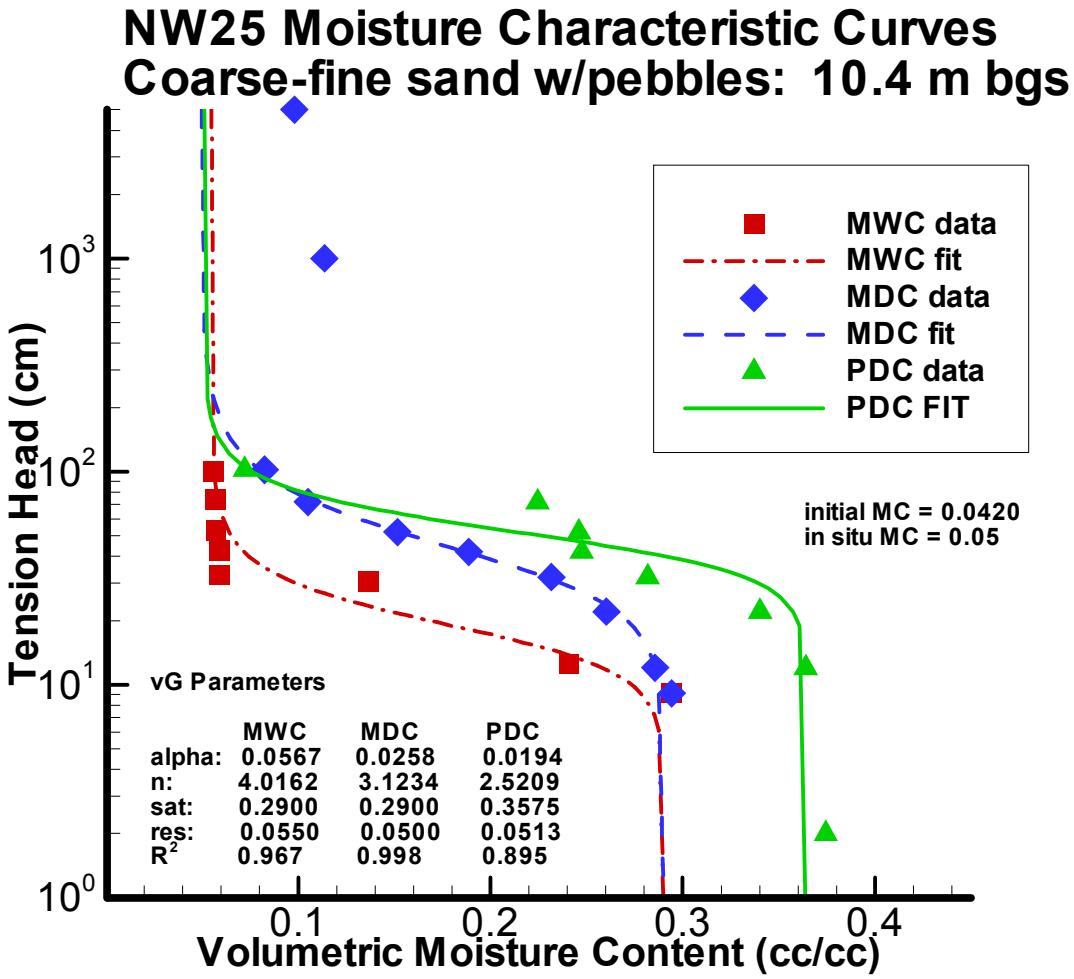

Figure E2.24 – Moisture Characteristic Curves for sample NW25 – coarse to fine sand. Sample location approximately 10.4 meters bgs.

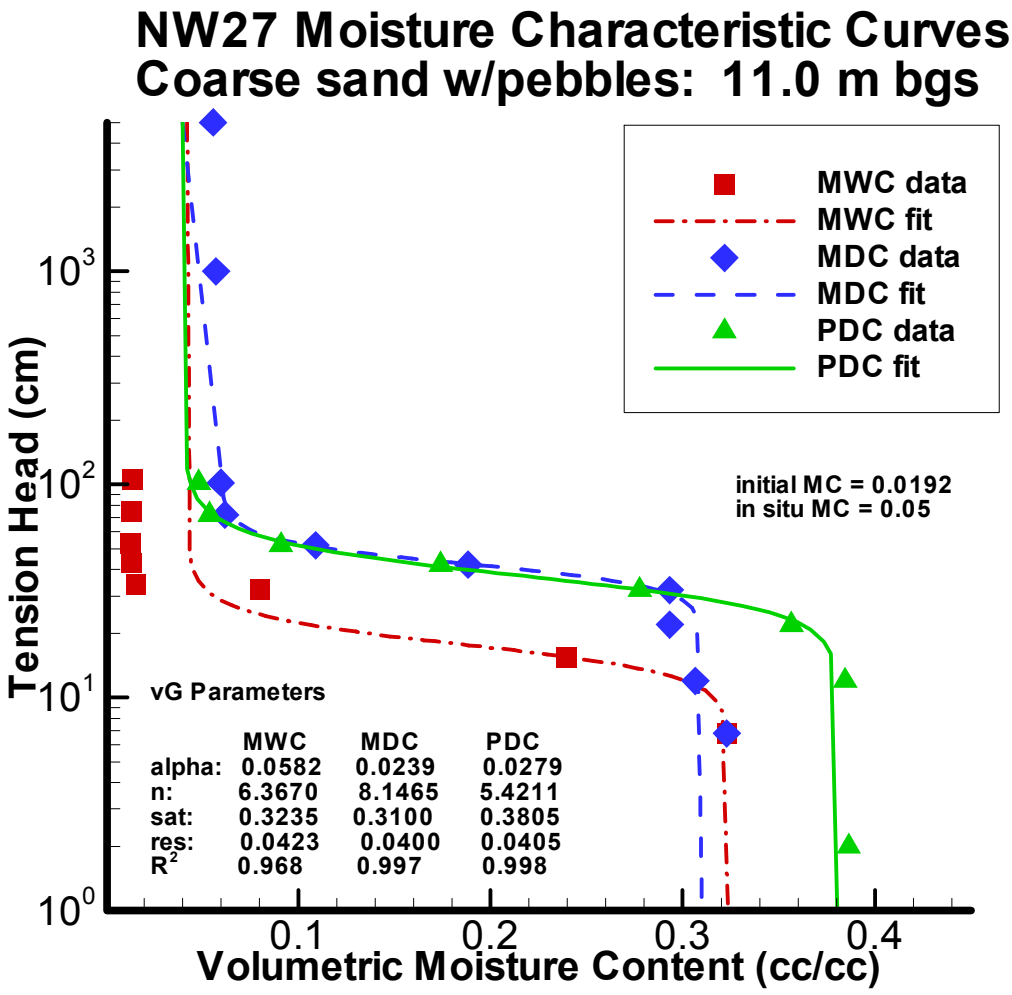

Figure E2.25 – Moisture Characteristic Curves for sample NW27 – coarse sand. Sample location approximately 11 meters bgs.

Appendix F

Sample Saturation Procedures

F.1 Required Equipment

Vacuum chamber

Vacuum pump (600 mm Hg)

CO_2 canister

Water deaerator

F.2 Introduction

The porosity of a sample is the ratio of the volume of the void spaces, within the porous medium, to the total volume of the sample. To determine the volume of the void spaces, the voids must be completely filled with a fluid that can be measured (weighed). By flushing the samples with CO_2 gas, then saturating the samples under a vacuum, the pores (in theory) will be completely filled with water, allowing calculation of sample porosity (Klute, 1986). ASTM standards for saturating samples to determine hydraulic conductivity (ASTM D 2434) and methods described in Klute (1986 pg 650-652) were referenced for direct measurements of porosity. Porosity was also estimated using bulk density values for each sample by

$$\phi = 1 - \frac{\rho_d}{\rho_p} \tag{F-1}$$

where ϕ is porosity, ρ_d is sample dry bulk density, ρ_p is the particle density, assumed to equal 2.65 g cm^{-3} since the majority of the samples are composed of silica sand (Jury et al., 1991).

F.3 Procedures

1. Place oven dried, pre-weighed samples in the saturation chamber (see Figure F.1).
2. Place the lid on the chamber and evacuate the chamber to 600 mm Hg vacuum, using a vacuum pump.
3. Fill the chamber with CO_2 gas to ensure saturation of small internal pores (CO_2 is more soluble in water than oxygen, and should prevent entrapment of air within the pores).
4. Evacuate the chamber again using the vacuum pump (to the same vacuum pressure as before).
5. Under a vacuum, fill the chamber with a deaerated thymol solution. Approximately 1 gram of thymol (1-($CH(CH_3)CH_3$)-2-(OH)-4-(CH_3)-C_6H_3) per gallon of water is used to inhibit bacterial growth (it does not significantly change the density of the water or the resistivity of the sample). ASTM standards recommend a 0.005M $CaSO_4$ solution be used to inhibit flocculation of clays (Klute, 1986) for samples containing greater than 10% clay particles, however preliminary tests showed that this solution increased the degree of compaction in the coarse grained sandy deposits of undisturbed samples (see Appendix C). Since the majority of the deposits contain less than 10% clay particles, we used tap water from the infiltration site (at ~860 μS/cm electrical conductivity) and 1 gram per gallon thymol as the wetting solution.
6. Allow samples to saturate for approximately one hour, place on a towel to remove excess moisture retained along edges of the ring (see Porosity Over-estimation Study), and weigh to obtain saturation weight.

7. Porosity is calculated by dividing the mass of the water (wet sample weight – dry sample weight) by the total volume of the sample.

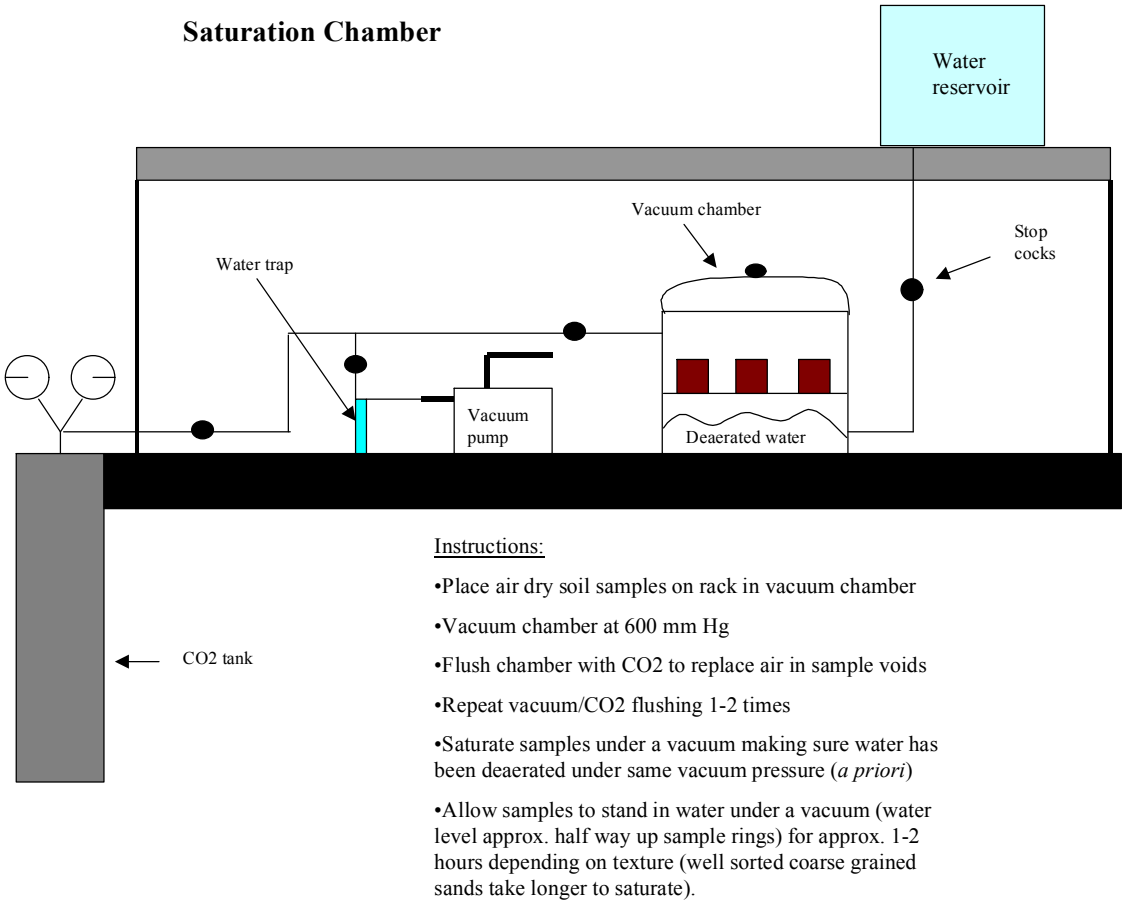

Figure F.1 – Saturation chamber, vacuum pump, and CO_2 tank.

Appendix G

Saturated Hydraulic Conductivity Measurement Procedures and Measured Data

G.1 Introduction

The hydraulic conductivity of a porous material is qualitatively defined as the ability of a saturated porous medium to transmit fluids. The physical relationship often used to describe fluid flow through porous materials is Darcy's law, (Klute, 1986 pg 735) defined by

$$q = -K(\theta)\frac{\partial H}{\partial z} \tag{G-1}$$

where q is the flux density [LT^{-1}], also referred to as the Darcy velocity, or apparent velocity (i.e., the volumetric flux per unit cross-sectional area of the flow region per unit time), $K(\theta)$ is the hydraulic conductivity [LT^{-1}], referred to as the saturated hydraulic conductivity (K) when the interstitial pores are completely filled with fluids, and $\partial H / \partial z$ [LL^{-1}] is the driving force, expressed as the negative gradient of the hydraulic head, composed of both the gravitational head (z) and the pressure head (h) by

$$H = h + z \tag{G-2}$$

The saturated hydraulic conductivity of a porous medium can be calculated from direct measurements of flux, hydraulic head, and column dimensions by

$$K = \frac{Q * L}{A * \Delta H} \tag{G-3}$$

where Q is the volumetric flux [L^3T^{-1}], A is the cross sectional area of the column [L^2], ΔH is the difference between the hydraulic head [L] at the flux inlet and outlet through the column (see Figure 1), and L is the column length [L].

There are two general laboratory methods for determination of the saturated hydraulic conductivity of porous materials: the constant head method and the falling head method (Stephens, 1995 pg 139). Column permeameters are used in both procedures with a constant head flux for deposits with a relatively high permeability, typically ranging from 1 to 10^{-5} cm s^{-1} and a falling head flux for materials with a low permeability ranging from 10^{-3} to 10^{-7} cm s^{-1} (Stephens, 1995 pg 140). In the constant head permeameter (Figure G-1), water is introduced into a saturated sample column by maintaining inflow and outflow reservoirs at constant positions relative to the sample column (Stephens, 1995 pg 139). In a falling-head permeameter, water is introduced to a saturated sample column by gravity drainage from a standpipe (or burette) while the head on the downstream end remains constant (Figure G.2).

Applicability of Darcy's law for calculating hydraulic conductivity depends on maintaining laminar flow conditions during analysis. According to ASTM standards for permeability measurements of coarse materials (using the constant head method), the following conditions are necessary for ensuring laminar flow throughout the test: 1) continuity of flow with no soil volume change during the test; 2) flow with the soil voids saturated with water and no air bubbles in the soil voids; 3) flow in the steady state with no changes in hydraulic gradient; and 4) direct proportionality of velocity of flow with hydraulic gradient below values at which turbulent flow begins (velocities

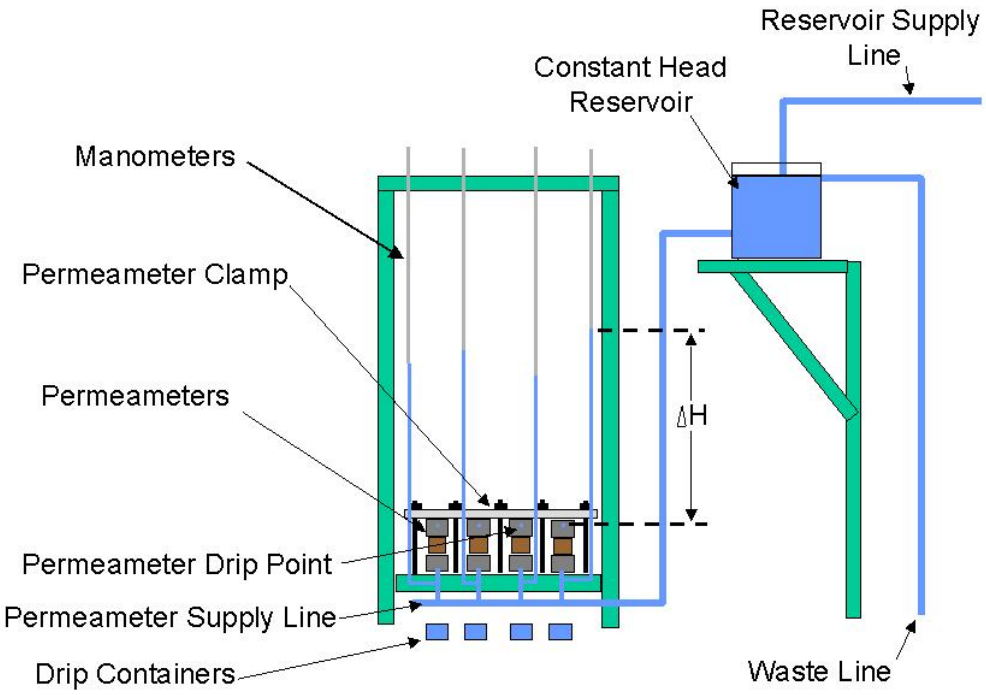

Figure G.1 – Constant head permeameter device.

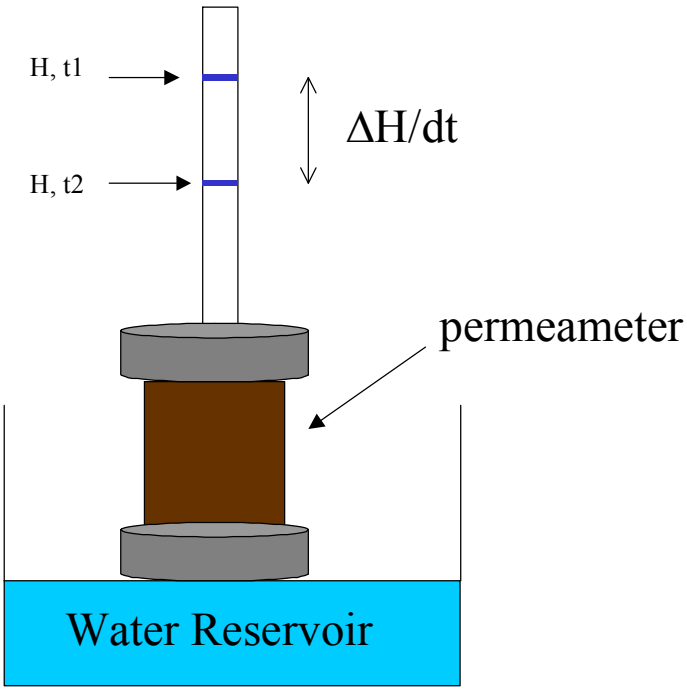

Figure G.2 – Falling head permeameter.

associated with Reynolds numbers (G-9) between 1 and 10 for porous medium; Fetter, (1988 pg 143). Modification of Darcy's law is often used to calculate hydraulic conductivity using the falling-head method (Stephens, 1995 pg 139) by

$$K = \frac{aL}{At} \ln\left(\frac{H_1}{H_2}\right) \qquad \text{(G-8)}$$

where A and L are the sample column's cross-sectional area [L^2] and length [L], respectively, a and is the burette's (or standpipe's) cross-sectional area [L^2], t is the time between measurements, and H_1 and H_2 are the water levels in the burette at t_1 and t_2, respectively.

G.2 Constant Head Permeameter Method

G.2.1 Required Equipment

Nalgene flexible tubing

Permeameter frame

Water reservoir

Sample holders

Stop watch

4 - 50 ml graduated cylinders

G.2.2 Methods

1. Saturate samples in vacuum chamber (as described in Appendix C).
2. Place samples in the sample holders (see Figure G.1).
2. Tighten nuts on sample holder to prevent leaking.
3. Make sure tubing clamps are closed, then fill the constant head tank with tap water allowing overflow to drain into sink until a constant head is established.
4. Open clamps allowing flow through samples.

5. Once a steady flow rate is established, measure volume of outflow per time using a graduated cylinder (steady state assumed when dH remains constant in all manometers).
6. Measure the head difference for each permeameter from the water level in the manometer to the outlet location of the sample (drip location).

G.3 Falling Head Permeameter Method

G.3.1 Required Equipment

Burette w/stop cock

Permeameter (Figure G-2)

Timer

G.3.2 Methods

1. Saturate sample in vacuum chamber (as described in Appendix C).
2. Place sample in permeameter (see Figure G.2).
3. Tighten nuts on permeameter to prevent leaking.
4. Make sure stop-cock on burette is closed then fill burette with water marking initial water level.
5. Set timer and open stock-cock allowing water to flow through the sample.
6. At each time interval, measure water level drop in burette.
7. Repeat process for 2-3 time intervals.

G.4 Measured Data

Preliminary tests conducted with the constant head permeameter device indicated that flow would not occur through fully saturated samples until the difference in head between the water reservoir and the permeameter outlet port was greater than 60-70 cm (greater than air entry pressure), therefore we constructed the water reservoir

approximately 70 cm higher than the top of the permeameters. In hind-sight, we recognize that the large head was required to induce flow due to entrapped air in the bottom section of the permeameter (below the saturated sample). In any event, the Reynolds number (equation G-9) for each sample was calculated to be less than 1.0 which is the lower critical Reynolds number for laminar flow (1<Re<10, Fetter, 1994 pg 143). The lower critical Reynolds number sets a limit below which laminar flow will always occur (Vennard & Street, 1982 pg 283). Since the screen in contact with the sample at each end of the permeameter has a much higher permeability than the samples measured, we assume that the entrapped air passed through the ring along the edges (largest pore space) and exited the top of the permeameter upon immediate contact (i.e., excessive sample disturbance did not occur as the entrapped air passed through the ring).

$$\mathrm{Re} = \frac{\rho v d}{\mu} \qquad \text{(G-9)}$$

where ρ is the density of water (g/cm^3), v is the fluid velocity (cm/s), d is the diameter of the pore (cm), and μ is the viscosity of the fluid (g/s*cm).

Table G.1 – Measured hydraulic conductivity data for STVZ samples collected from the NW core.

Run	sample ID	depth (m)	description	height (cm)	ΔH (cm)	area (cm^2)	Q (cm^3/sec)	K (cm/sec)	K (cm/day)	Re
1	NW1	0.4572	coarse	4.3	81	25.52	0.825	1.72E-03	148.29	0.114
2	NW1	0.4572	sand	4.3	80.9	25.52	0.883	1.84E-03	158.97	0.122
3	NW1	0.4572	w/pebbles	4.3	81.2	25.52	0.883	1.83E-03	158.38	0.122
							average	1.80E-03	155.22	0.119
							stdev	6.95E-05	6.00	0.005
1	NW2	0.6096	coarse	3.6	81.5	25.52	1.000	1.73E-03	149.56	0.109
2	NW2	0.6096	sand	3.6	81.5	25.52	1.033	1.79E-03	154.55	0.113
3	NW2	0.6096	w/pebbles	3.6	81.5	25.52	1.083	1.88E-03	162.02	0.118
							average	1.80E-03	155.38	0.114
							stdev	7.26E-05	6.27	0.005
1	NW4	1.524	coarse	3.8	68.4	25.52	4.600	1.00E-02	865.29	0.398
2	NW4	1.524	sand	3.8	66.2	25.52	5.000	1.12E-02	971.78	0.433
3	NW4	1.524	no pebbles	3.8	66.3	25.52	5.200	1.17E-02	1009.13	0.450
							average	1.10E-02	948.73	0.427
							stdev	8.64E-04	74.64	0.026
1	NW5	1.829	silty gravel	4.2	81.5	25.52	0.650	1.31E-03	113.42	0.040
2	NW5	1.829		4.2	81.5	25.52	0.608	1.23E-03	106.15	0.037
3	NW5	1.829		4.2	81	25.52	0.592	1.20E-03	103.88	0.036
							average	1.25E-03	107.81	0.038
							stdev	5.77E-05	4.98	0.002
1	NW6	2.743	silty sand	4	82.2	25.52	0.933	1.78E-03	153.78	0.021
2	NW6	2.743		4	82.2	25.52	0.933	1.78E-03	153.78	0.021
3	NW6	2.743		4	81.9	25.52	0.950	1.82E-03	157.10	0.021
							average	1.79E-03	154.89	0.021
							stdev	2.22E-05	1.92	0.000
1	NW7	3.048	fine sands	4	73.5	25.52	3.267	6.97E-03	601.94	0.158
2	NW7	3.048		4	73.8	25.52	3.400	7.22E-03	623.96	0.165
3	NW7	3.048		4	74	25.52	3.400	7.20E-03	622.27	0.165
							average	7.13E-03	616.06	0.163
							stdev	1.42E-04	12.26	0.004
1	NW8	3.353	fine sand	4.1	72.5	25.52	1.775	3.93E-03	339.87	0.087
2	NW8	3.353	w/pebbles	4.1	73	25.52	1.975	4.35E-03	375.58	0.097
3	NW8	3.353		4.1	73	25.52	1.775	3.91E-03	337.55	0.087
							average	4.06E-03	351.00	0.091
							stdev	2.47E-04	21.32	0.006

Table G.1 – (continued).

Run	sample ID	depth (m)	description	height (cm)	ΔH (cm)	area (cm^2)	Q (cm^3/sec)	K (cm/sec)	K (cm/day)	Re
1	NW9	3.658	fine sand	4.1	81.5	25.52	0.467	9.20E-04	79.49	0.025
2	NW9	3.658	w/clay and	4.1	81	25.52	0.458	9.09E-04	78.55	0.024
3	NW9	3.658	pebbles	4.1	81.5	25.52	0.450	8.87E-04	76.65	0.024
							average	9.05E-04	78.23	0.024
							stdev	1.67E-05	1.45	0.000
1	NW10	4.267	fine-med	4.1	81.4	25.52	0.933	1.84E-03	159.17	0.045
2	NW10	4.267	sands w/	4.1	81.6	25.52	0.867	1.71E-03	147.44	0.042
3	NW10	4.267	pebbles	4.1	81.6	25.52	0.867	1.71E-03	147.44	0.042
							average	1.75E-03	151.35	0.043
							stdev	7.84E-05	6.77	0.002
1	NW11	4.572	silty sand	3.5	81	25.52	1.433	2.43E-03	209.70	0.051
2	NW11	4.572		3.5	81	25.52	0.136	2.31E-04	19.95	0.005
3	NW11	4.572		3.5	80.5	25.52	1.517	2.58E-03	223.27	0.054
							average	1.75E-03	150.98	0.036
							stdev	1.32E-03	113.67	0.027
1	NW12	4.877	silty sand	4.1	73.5	25.52	2.150	4.70E-03	406.08	0.091
2	NW12	4.877		4.1	73.5	25.52	2.425	5.30E-03	458.02	0.102
3	NW12	4.877		4.1	73.5	25.52	2.150	4.70E-03	406.08	0.091
							average	4.90E-03	423.39	0.094
							stdev	3.47E-04	29.99	0.007
1	NW14	5.7912	pebbly,	4	83.3	25.52	0.383	7.21E-04	62.33	0.001
2	NW14	5.7912	sandy,	4	83	25.52	0.383	7.24E-04	62.55	0.001
3	NW14	5.7912	clay	4	83	25.52	0.383	7.24E-04	62.55	0.001
							average	7.23E-04	62.48	0.001
							stdev	1.51E-06	0.13	0.000
1	NW16	6.4008	fine sand	3.4	77.5	25.52	2.233	3.84E-03	331.75	0.067
2	NW16	6.4008		3.4	78.9	25.52	2.200	3.72E-03	321.00	0.066
3	NW16	6.4008		3.4	79.4	25.52	2.100	3.52E-03	304.48	0.063
							average	3.69E-03	319.07	0.065
							stdev	1.59E-04	13.74	0.002
1	NW17	6.7056	fine sand	4	74.3	25.52	2.600	5.49E-03	473.93	0.090
2	NW17	6.7056		4	74.4	25.52	2.733	5.76E-03	497.57	0.094
3	NW17	6.7056		4	75	25.52	2.750	5.75E-03	496.60	0.095
							average	5.66E-03	489.37	0.093
							stdev	1.55E-04	13.37	0.003

Table G.1 – (continued).

Run	sample ID	depth (m)	description	height (cm)	ΔH (cm)	area (cm^2)	Q (cm^3/sec)	K (cm/sec)	K (cm/day)	Re
1	NW19	7.3152	oxidized	3.7	83	25.52	0.517	9.03E-04	77.98	0.012
2	NW19	7.3152	silty sand	3.7	82.9	25.52	0.517	9.04E-04	78.08	0.012
3	NW19	7.3152		3.7	83	25.52	0.517	9.03E-04	77.98	0.012
							average	9.03E-04	78.02	0.012
							stdev	6.29E-07	0.05	0.000
1	NW20	7.9248	fine sand	4.3	76	25.52	3.000	6.65E-03	574.71	0.123
2	NW20	7.9248		4.3	76	25.52	3.000	6.65E-03	574.71	0.123
3	NW20	7.9248		4.3	76	25.52	2.917	6.47E-03	558.75	0.119
							average	6.59E-03	569.39	0.121
							stdev	1.07E-04	9.22	0.002
1	NW21	8.2296	med-fine	4.2	72.8	25.52	3.675	8.31E-03	717.88	0.157
2	NW21	8.2296	sand	4.2	73	25.52	3.500	7.89E-03	681.82	0.149
3	NW21	8.2296		4.2	73.8	25.52	3.690	8.23E-03	711.04	0.158
							average	8.14E-03	703.58	0.155
							stdev	2.22E-04	19.15	0.005
1	NW22	8.8392	silty fine sand	3.7	73.8	25.52	2.133	4.19E-03	362.14	0.078
2	NW22	8.8392		3.7	73.9	25.52	2.100	4.12E-03	356.00	0.076
3	NW22	8.8392		3.7	74	25.52	2.033	3.98E-03	344.23	0.074
							average	4.10E-03	354.13	0.076
							stdev	1.05E-04	9.10	0.002
1	NW23	10.0584	coarse-fine	4	77.2	25.52	2.533	5.14E-03	444.44	0.104
2	NW23	10.0584	sand - some silt	4	77.2	25.52	2.633	5.35E-03	461.98	0.108
3	NW23	10.0584		4	77.2	25.52	2.633	5.35E-03	461.98	0.108
							average	5.28E-03	456.13	0.107
							stdev	3.91E-05	3.38	0.001
1	NW24	9.7536	coarse-fine	4.1	76.9	25.52	2.300	4.81E-03	415.20	0.255
2	NW24	9.7536	sand w/pebbles	4.1	76.8	25.52	2.350	4.92E-03	424.78	0.261
3	NW24	9.7536		4.1	76.9	25.52	2.450	5.12E-03	442.28	0.272
							average	4.95E-03	427.42	0.263
							stdev	1.59E-04	13.73	0.008
1	NW25	10.3632	coarse-fine	4.2	78.5	25.52	2.200	4.61E-03	398.54	0.125
2	NW25	10.3632	sand w/pebbles	4.2	78.9	25.52	2.275	4.75E-03	410.04	0.129
3	NW25	10.3632		4.2	78.5	25.52	2.100	4.40E-03	380.43	0.119
							average	4.59E-03	396.34	0.125
							stdev	1.73E-04	14.93	0.005

Table G.1 – (continued).

Run	sample ID	depth (m)	description	height (cm)	ΔH (cm)	area (cm^2)	Q (cm^3/sec)	K (cm/sec)	K (cm/day)	Re
1	NW27	10.3632	coarse-fine	4.2	78.5	25.52	2.200	4.61E-03	398.54	0.345
2	NW27	10.3632	sand w/pebbles	4.2	78.9	25.52	2.275	4.75E-03	410.04	0.356
3	NW27	10.3632		4.2	78.5	25.52	2.100	4.40E-03	380.43	0.329
							average	4.59E-03	396.34	0.343
							stdev	1.73E-04	14.93	0.014

Appendix H

Particle Size Analysis Procedures and Measured Data

H.1 Introduction

Particle size analysis (PSA) is a measurement of the size distribution of individual particles in a soil sample. Any procedures followed should clearly specify the pretreatment, the separation method, and the purpose for which the size analysis is intended for a particular soil (Klute, 1986). The standard PSA procedures are as follows:

H.2 Pretreatment of samples

For the deposits which contain large quantities of iron oxide minerals, the samples need to be pre-treated with a bi-carbonate-buffered sodium dithionite-citrate system. Optimum pH for maximum iron oxide removal is ~7.3 (the bi-carbonate buffer holds the pH at this level). If the iron-oxides are part of the dominant mineralogy, it is not recommended that they be removed.

H.3 Separation of >2mm grains

1. Oven dry samples and record total mass
2. Sieve sample to remove the >2mm particles (10 mesh sieve)
3. Weigh and record the >2mm portion and the <2mm portion

H.4 Particle size analysis of sands

1. Use sieve method for analysis of sand sized particles. The sieve sizes for the individual particle ranges are listed in Table H.1. The sieves are stacked from highest to lowest mesh opening.

2. Pre-weigh and record the sieves and place the sand particles in the top sieve (largest mesh opening).
3. Cover the sieve stack and tape the outside of the stack to prevent the stack from tipping over during the process.
4. Shake sieves on shaker stand of equivalent device for approximately 10 minutes
5. Weigh the individual sieves and the sands.
6. Remove particles from sieve openings and wipe out sieves between sample measurements.
7. Determine the sand weight by subtracting the sieve weight from the combined weight.
8. After all measurements are made, determine the percent by weight of each particle size by dividing the individual weights by the total mass of the sample and multiplying by 100.
9. Calculate percent finer than by weight by subtracting the percent by weight of the cumulative particle sizes from 100:

Example:	4mm particles	10% (of total mass)	90% finer than 4mm
	2mm particles	20%	70% finer than 2mm
	1mm particles	50%	20% finer than 1 mm
	.05 mm particles	20%	0% finer than .05 mm

Table H.1 – Udden Wentworth particle size scale for sand size particles (Prothero and Schwab, 1996).

Particle Description (sieve)	Particle Size	ϕ Values
very coarse sand (#20)	1-2 mm	-1-0
coarse sand (#40)	0.5-1 mm	0-1
medium sand (#60)	0.25-0.5 mm	1-2
fine sand (#150)	0.16-0.25 mm	2-3
very fine sand (#270)	0.053-0.16 mm	3-4

Table H.2 – Particle size distribution data for the NW core deposits.

smallest

grain size		NW1	NW2	NW4	NW5	NW7	NW8	NW9	NW10
(mm)	sieve #	wt fraction	wt fraction	wt fraction	wt fraction	wt fraction	wt fraction	wt fraction	wt fraction
<.053	bottom	0.007	0.010	0.004	0.032	0.015	0.019	0.027	0.031
0.053	270	0.008	0.017	0.018	0.023	0.121	0.128	0.071	0.073
0.106	140	0.032	0.065	0.104	0.057	0.467	0.428	0.302	0.430
0.25	60	0.228	0.276	0.557	0.162	0.372	0.211	0.359	0.366
0.5	35	0.315	0.278	0.284	0.200	0.019	0.031	0.129	0.078
1	18	0.139	0.108	0.026	0.156	0.003	0.030	0.029	0.022
2	10	0.270	0.244	0.006	0.369	0.004	0.153	0.084	0.000

grain size		NW11	NW12	NW16	NW17	NW18	NW19	NW20	NW21
(mm)	sieve #	wt fraction	wt fraction	wt fraction	wt fraction	wt fraction	wt fraction	wt fraction	wt fraction
<.053	bottom	0.034	0.021	0.020	0.017	0.011	0.091	0.008	0.010
0.053	270	0.181	0.133	0.245	0.157	0.141	0.281	0.089	0.090
0.106	140	0.616	0.629	0.720	0.788	0.818	0.596	0.802	0.764
0.25	60	0.145	0.192	0.010	0.038	0.029	0.025	0.097	0.122
0.5	35	0.016	0.011	0.001	0.000	0.000	0.004	0.003	0.012
1	18	0.004	0.004	0.000	0.000	0.000	0.001	0.000	0.001
2	10	0.005	0.010	0.004	0.000	0.000	0.002	0.000	0.000

grain size		NW22	NW23	NW24	NW25	NW27
(mm)	sieve #	wt fraction	wt fraction	wt fraction	wt fraction	wt fraction
<.053	bottom	0.022	0.023	0.028	0.020	0.004
0.053	270	0.179	0.122	0.090	0.055	0.014
0.106	140	0.722	0.543	0.451	0.261	0.303
0.25	60	0.072	0.256	0.357	0.443	0.489
0.5	35	0.004	0.043	0.045	0.163	0.116
1	18	0.001	0.008	0.000	0.033	0.030
2	10	0.000	0.006	0.029	0.024	0.044

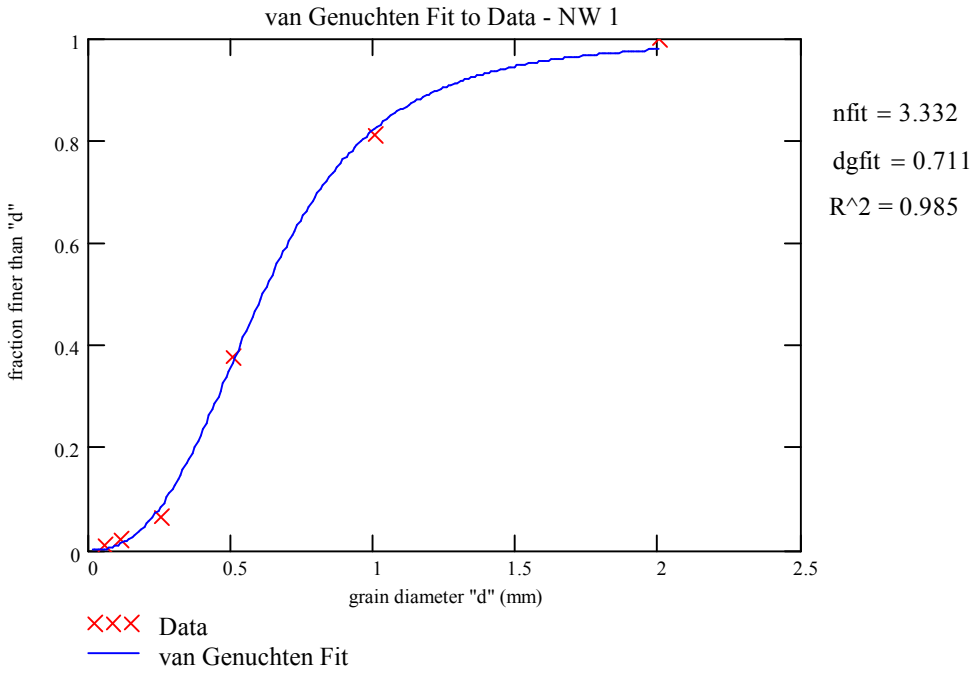

Figure H.1 – Particle size distribution curve for sample NW1.

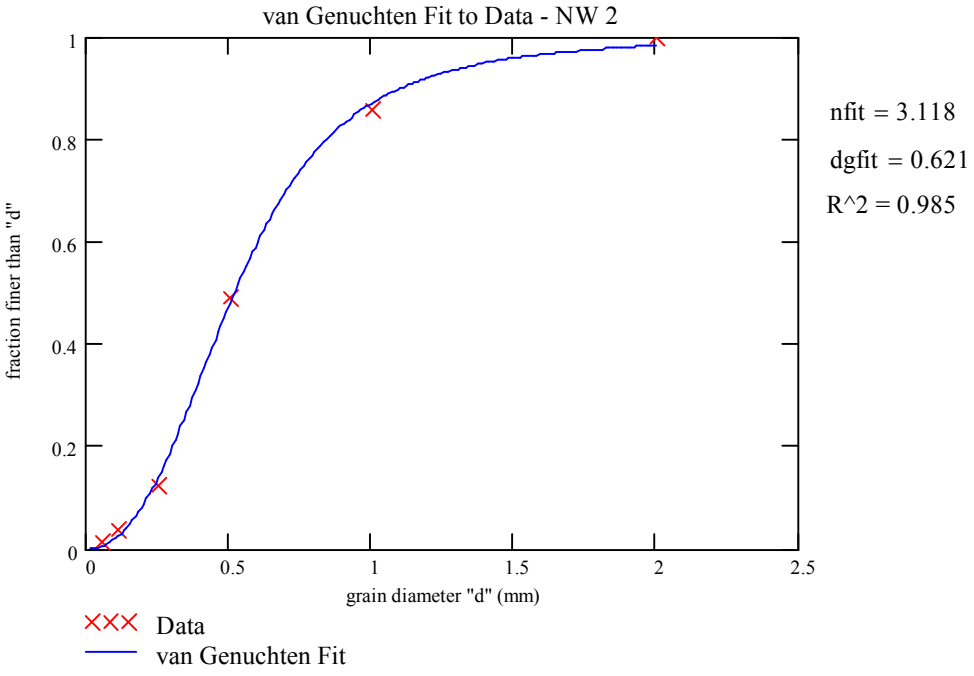

Figure H.2 – Particle size distribution curve for sample NW2.

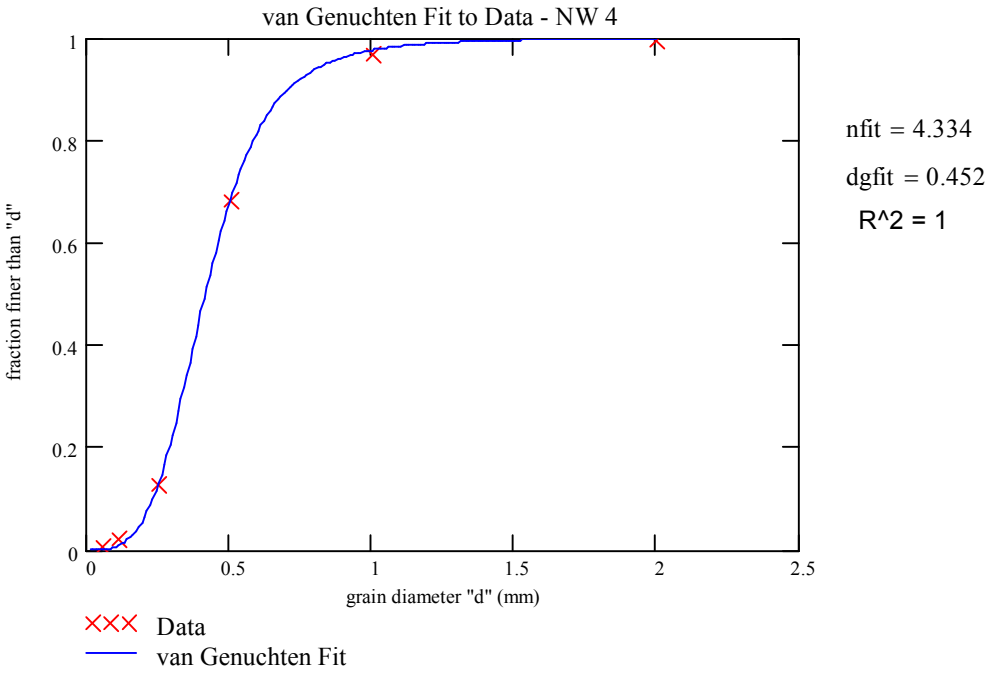

Figure H.3 – Particle size distribution curve for sample NW4.

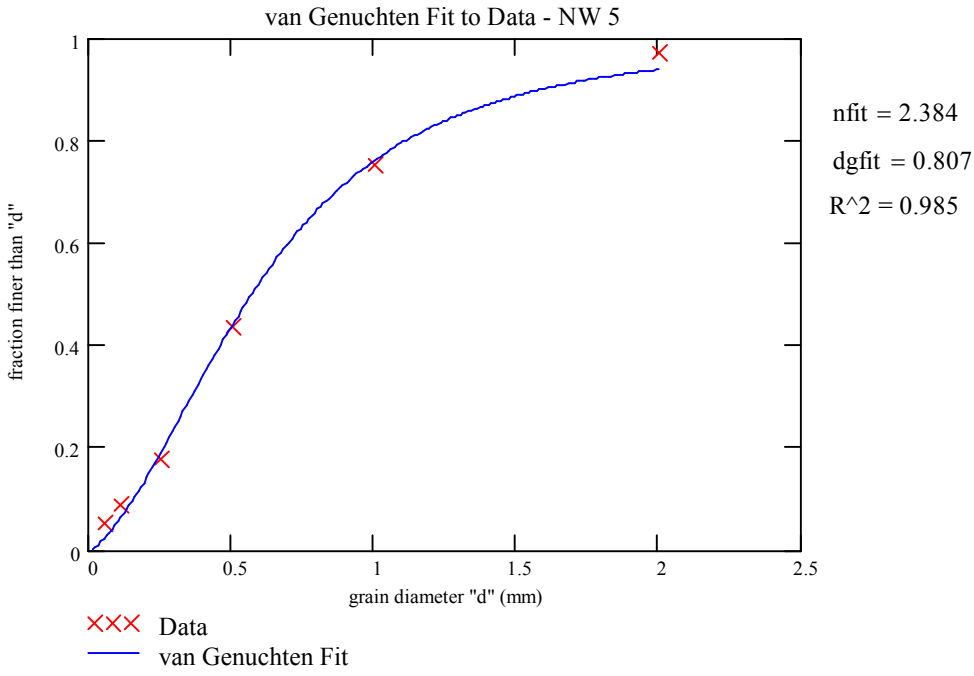

Figure H.4 – Particle size distribution curve for sample NW5.

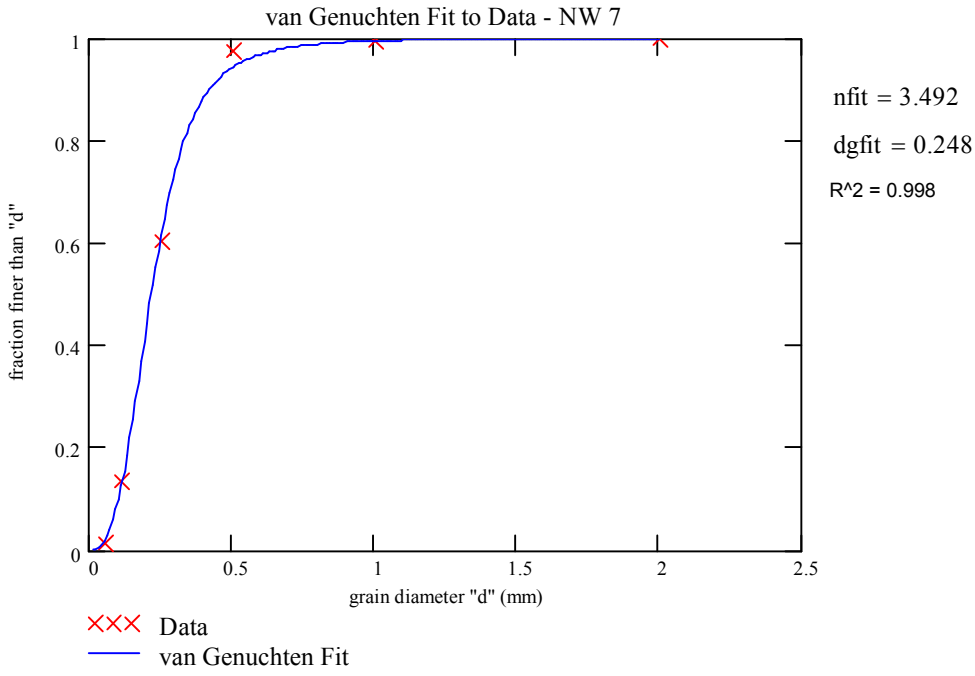

Figure H.5 – Particle size distribution curve for sample NW7.

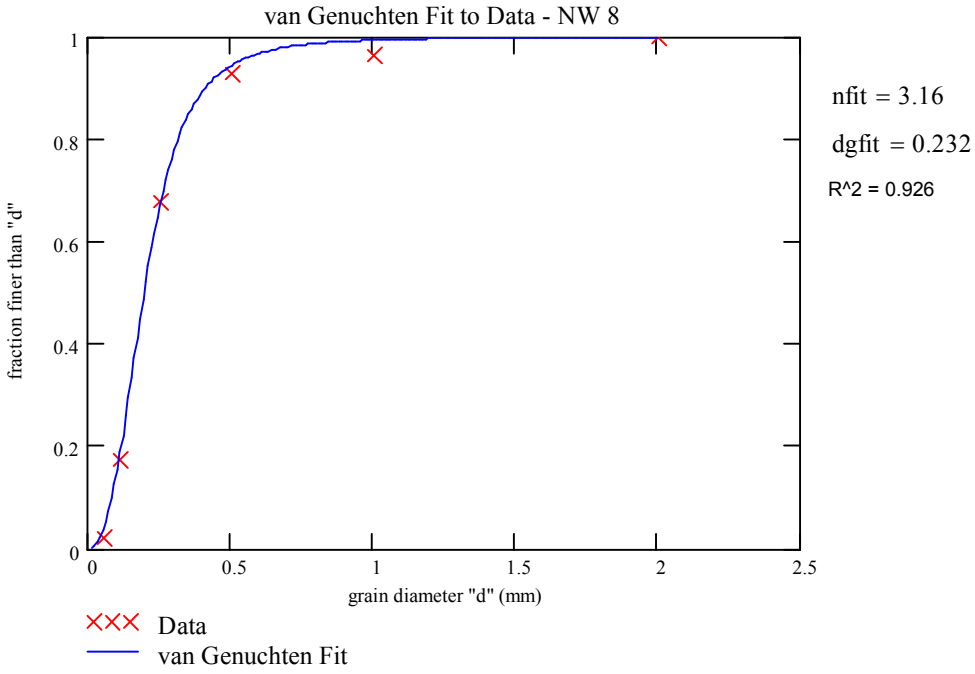

Figure H.6 – Particle size distribution curve for sample NW8.

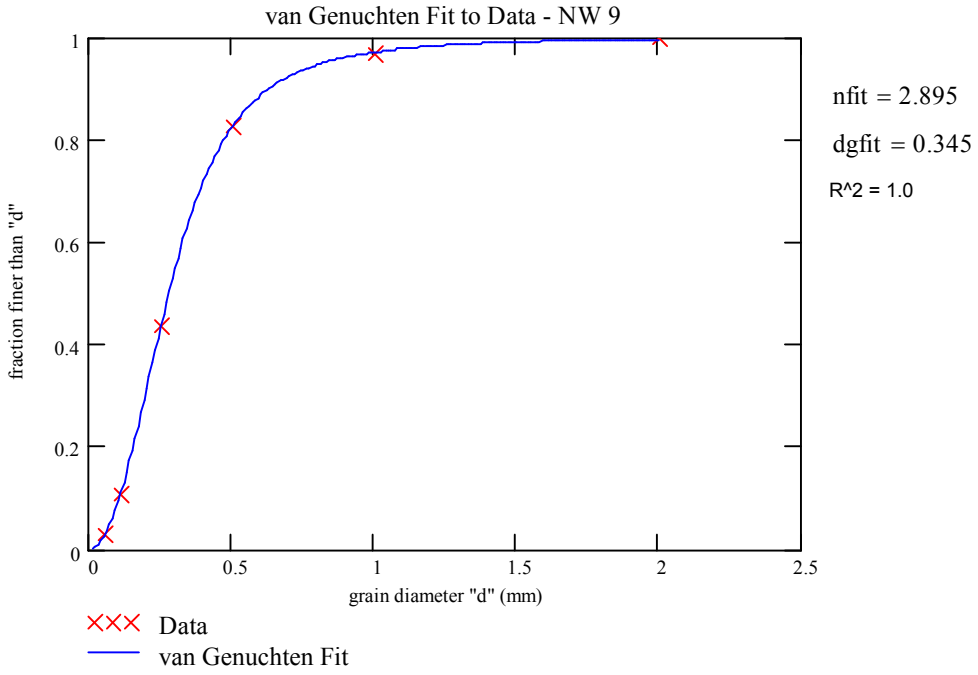

Figure H.7 – Particle size distribution curve for sample NW9.

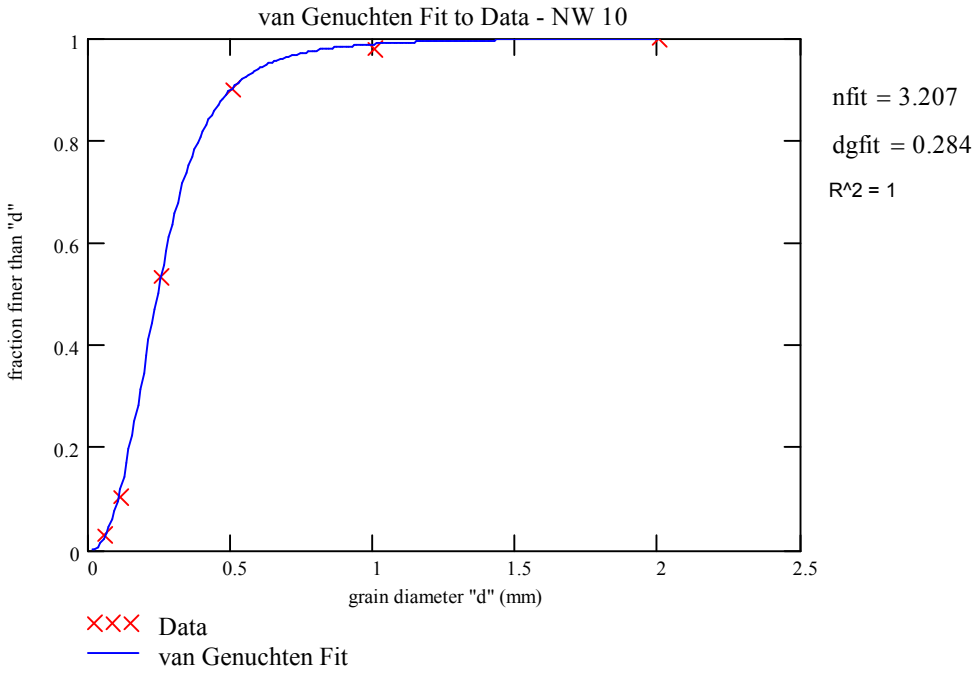

Figure H.8 – Particle size distribution curve for sample NW10.

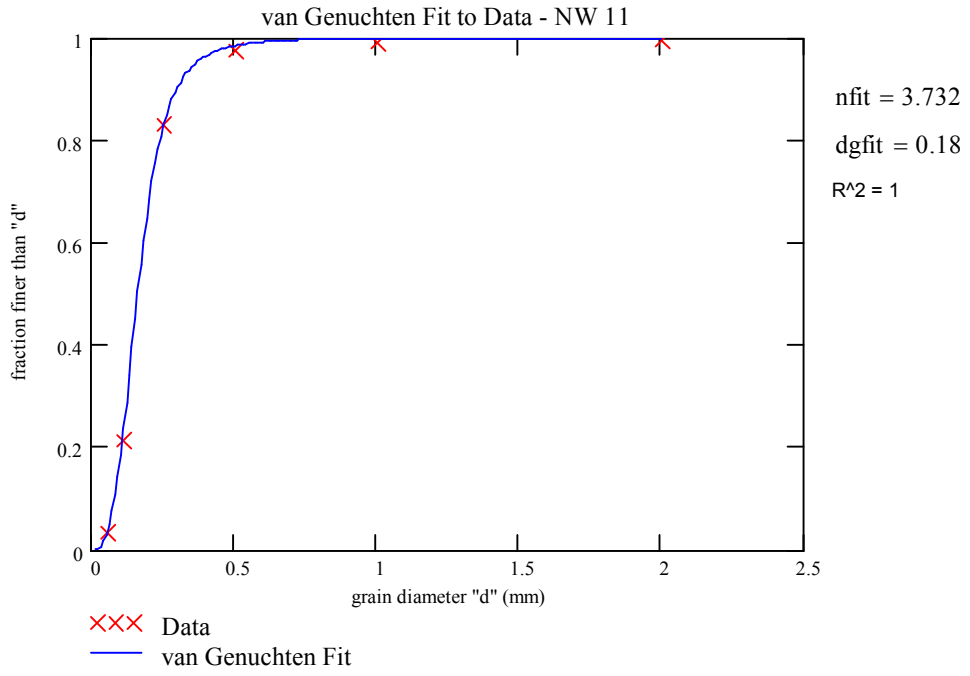

Figure H.9 – Particle size distribution curve for sample NW11.

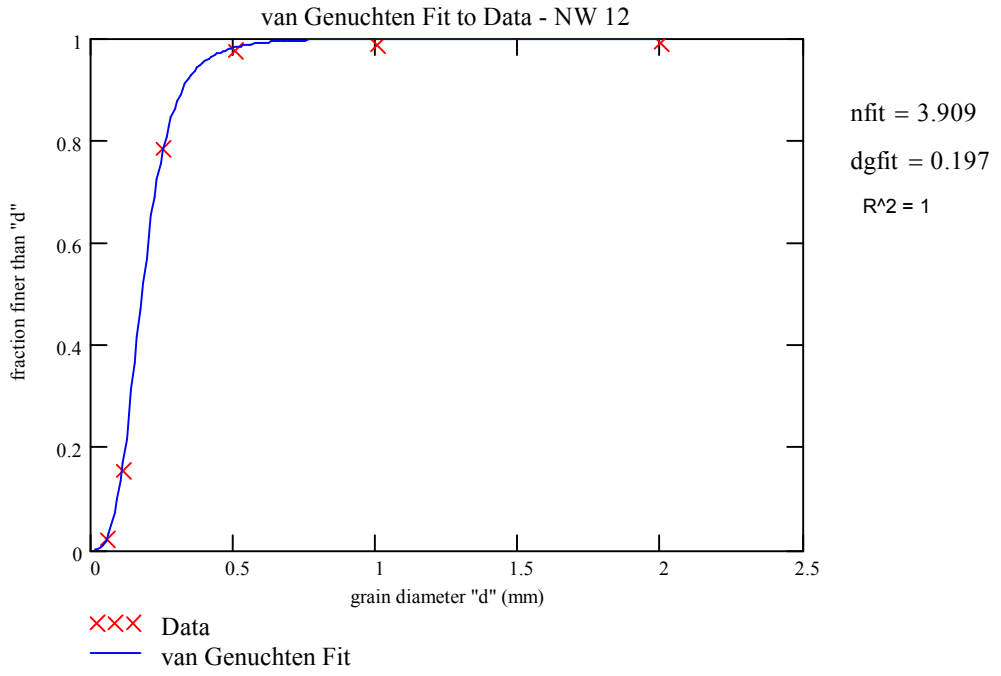

Figure H.10 – Particle size distribution curve for sample NW12.

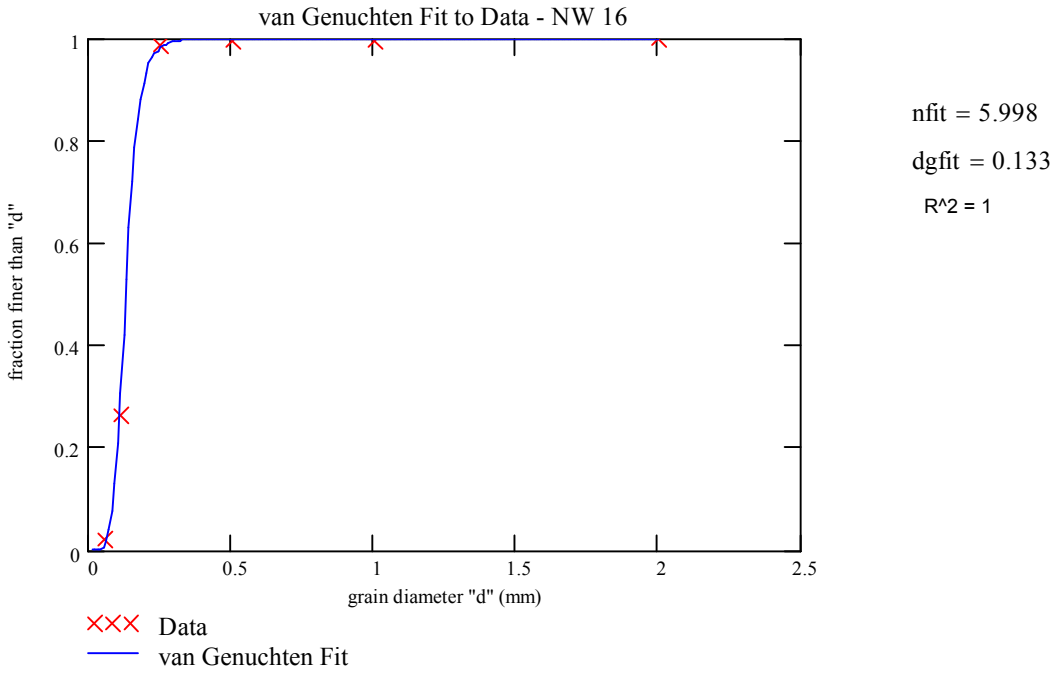

Figure H.11 – Particle size distribution curve for sample NW16.

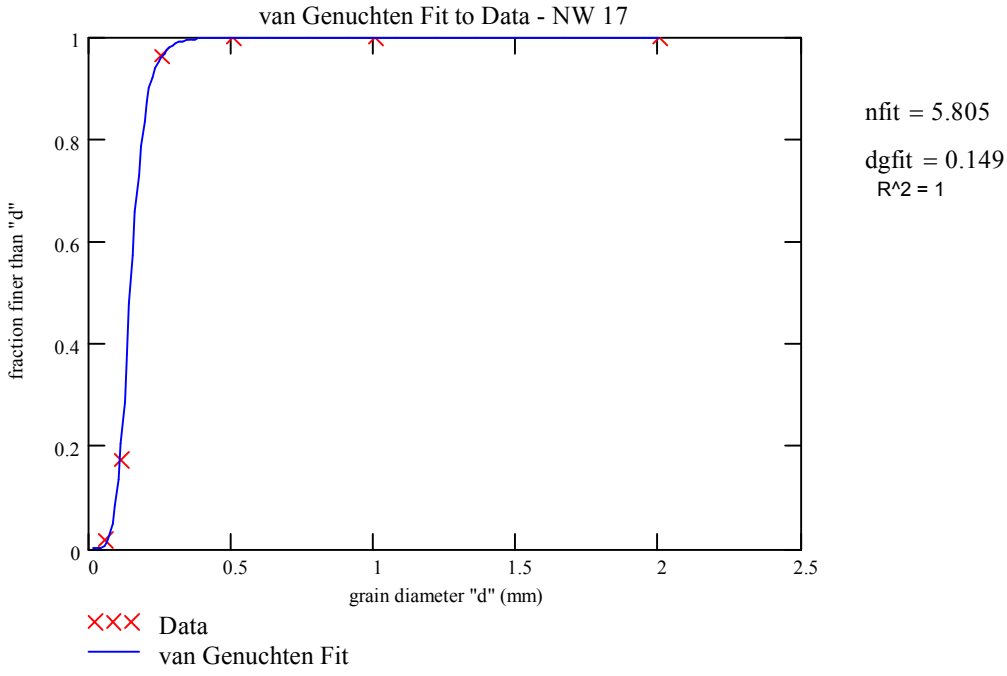

Figure H.12 – Particle size distribution curve for sample NW17.

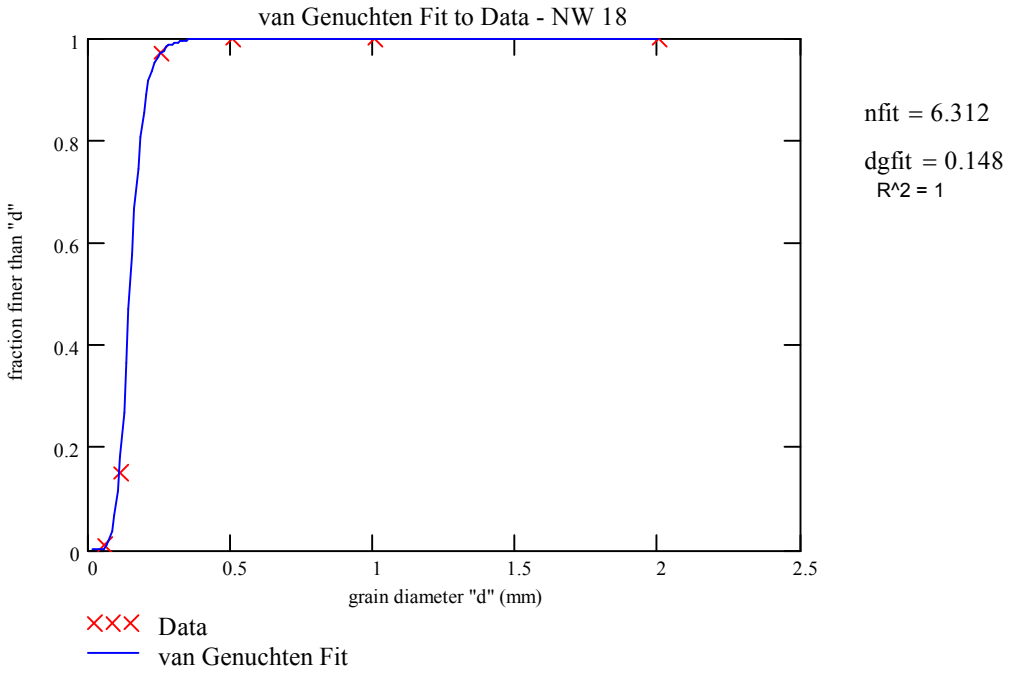

Figure H.13 – Particle size distribution curve for sample NW18.

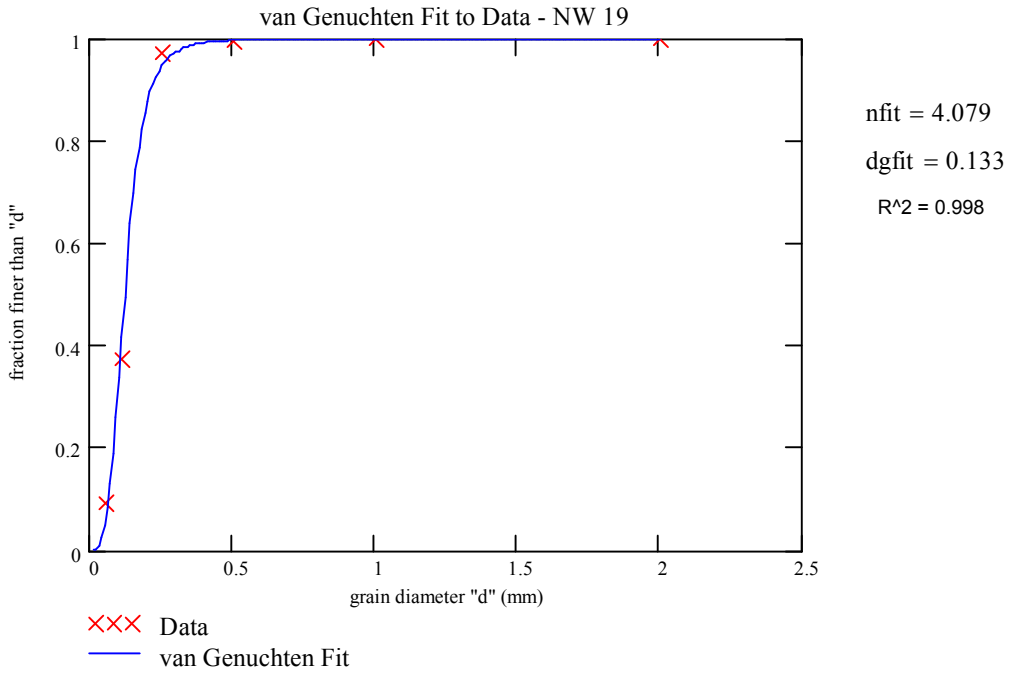

Figure H.14 – Particle size distribution curve for sample NW19.

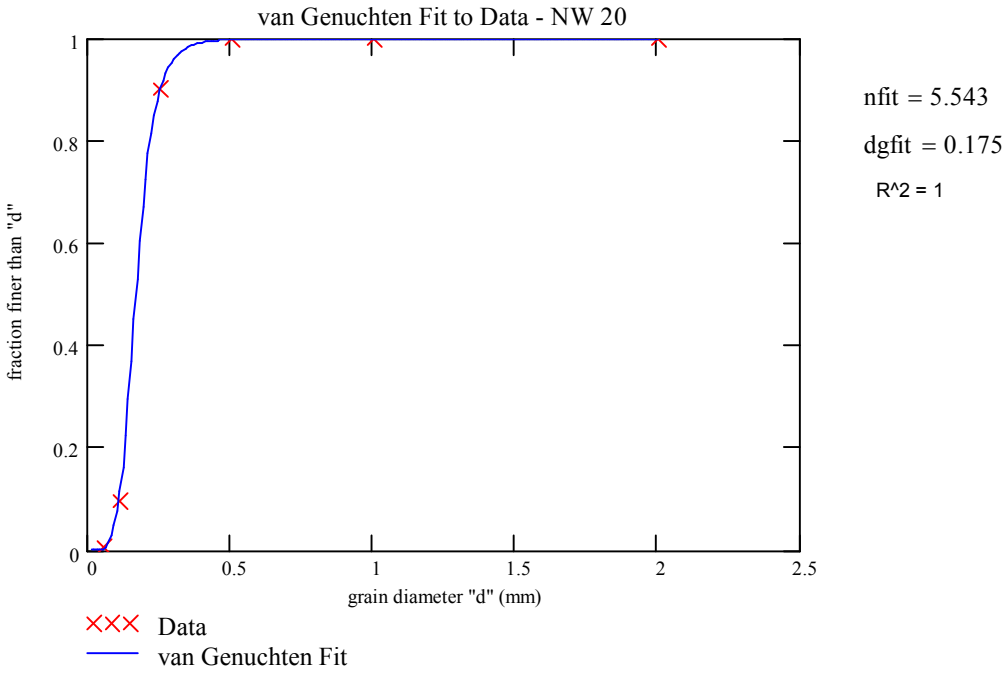

Figure H.15 – Particle size distribution curve for sample NW20.

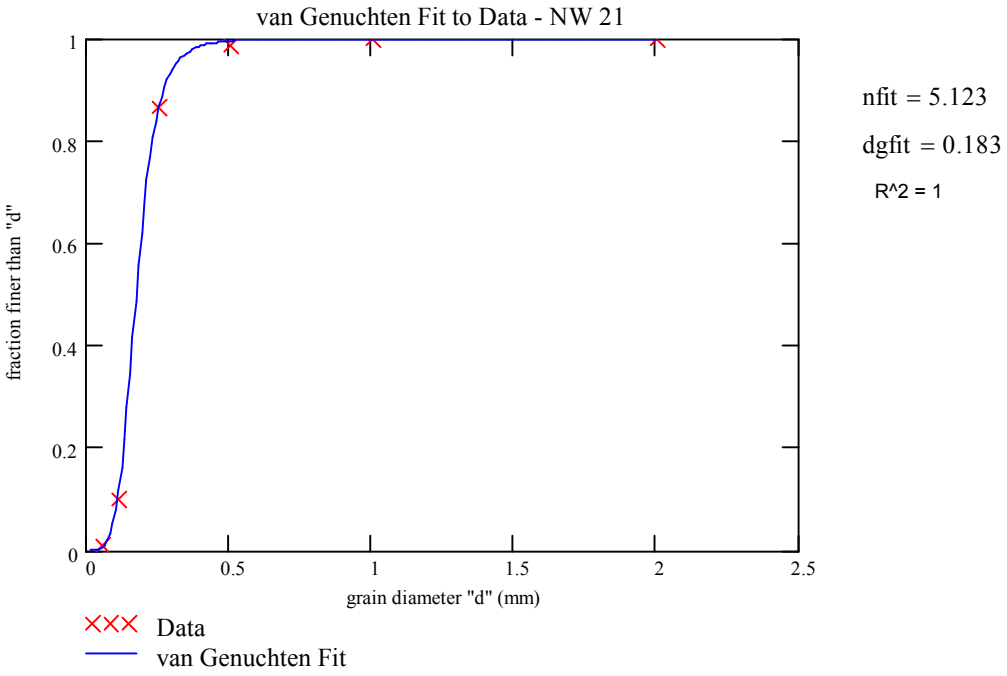

Figure H.16 – Particle size distribution curve for sample NW21.

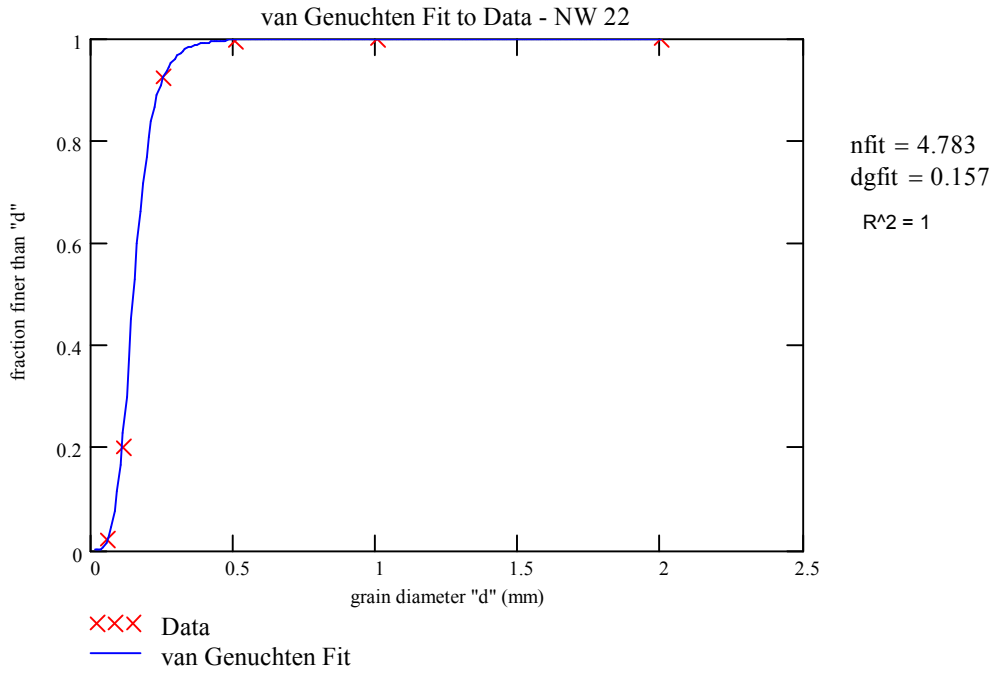

Figure H.17 – Particle size distribution curve for sample NW22.

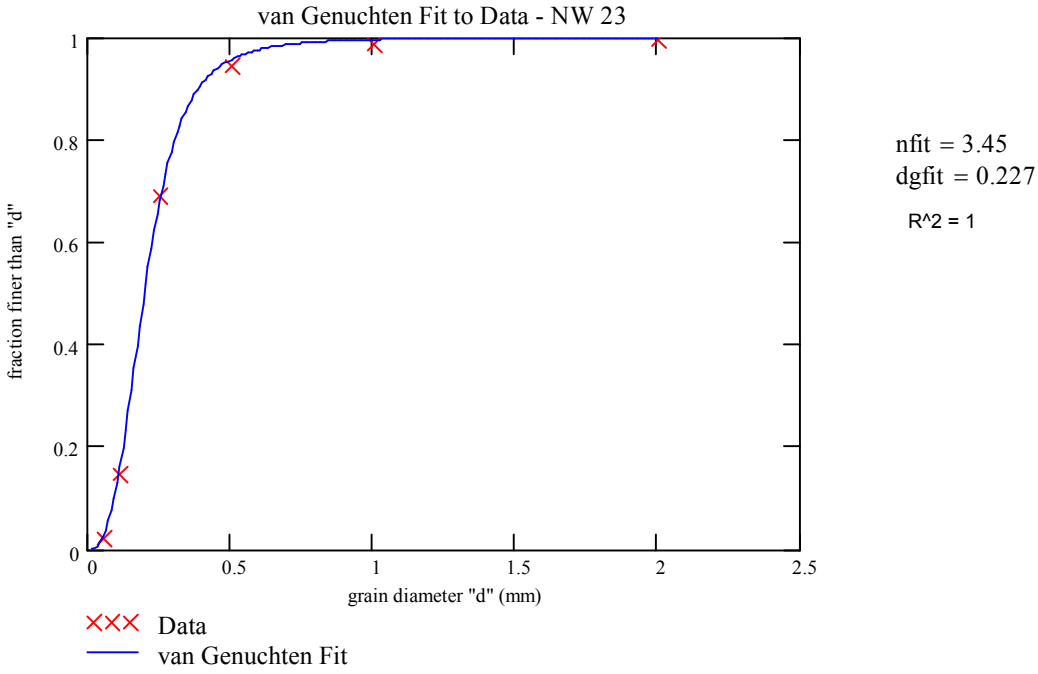

Figure H.18 – Particle size distribution curve for sample NW23.

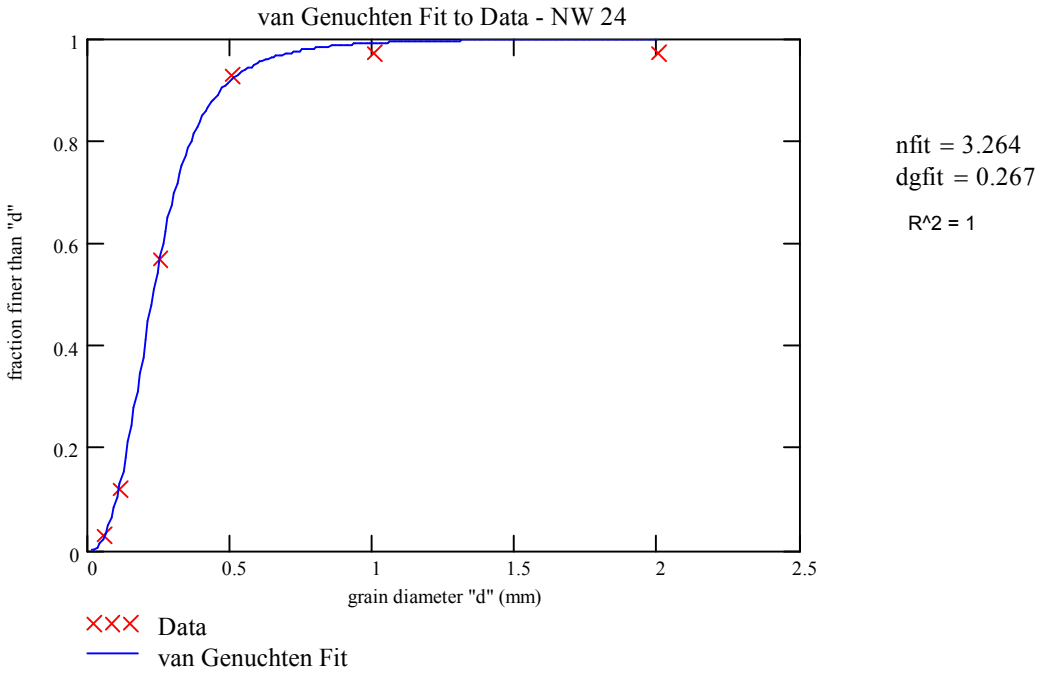

Figure H.19 – Particle size distribution for sample NW24.

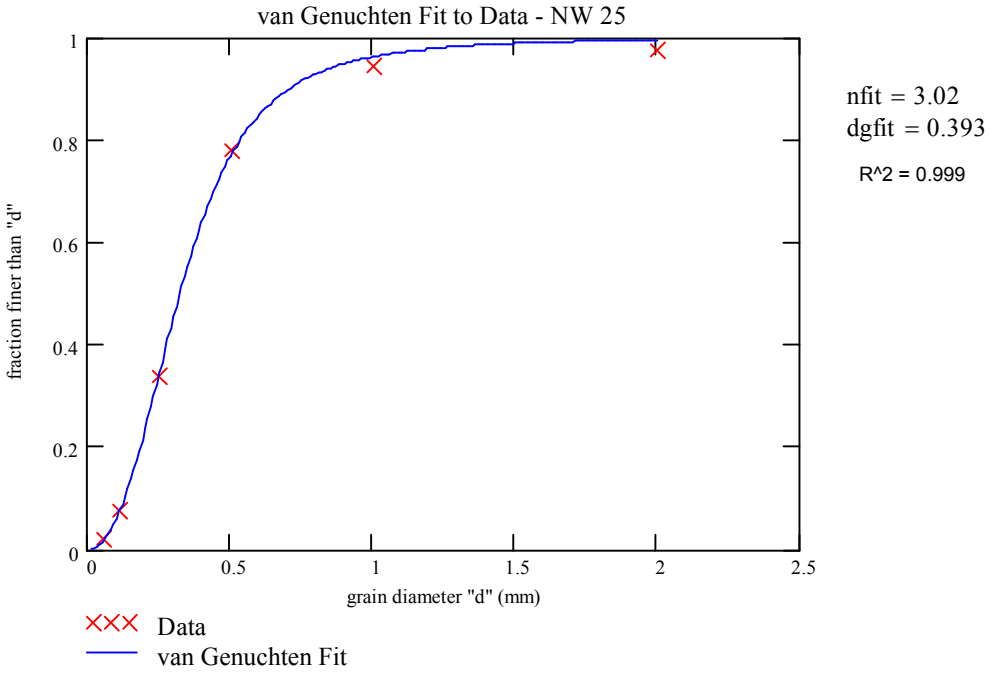

Figure H.20 – Particle size distribution for sample NW25.

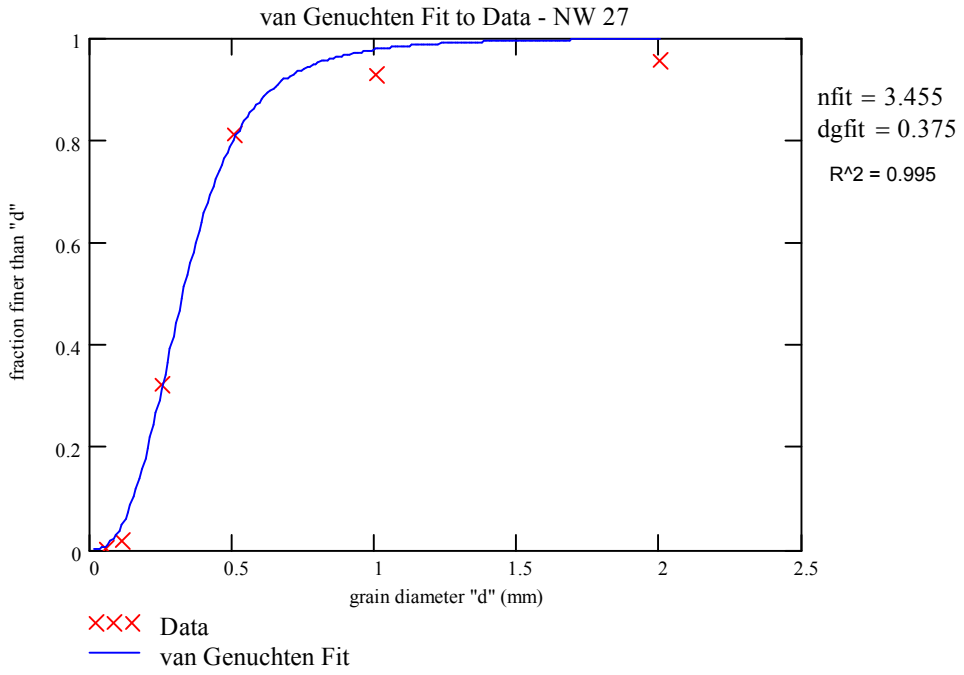

Figure H.21 – Particle size distribution for samples NW27.

H.5 Particle size analysis of silt and clay sized particles

H.5.1 Hydrometer measurements:

1. Weigh 20g (fine grained soil) or 100g (sandy soil) of sample into a 600 mL beaker, add 250 mL of distilled water and 100 mL of HMP solution and allow to soak overnight (make a "blank" sample which does not contain soil). Transfer the suspension to a sedimentation flask, stopper and shake overnight (24 hrs) on a horizontal shaker.
2. Transfer suspension to a sedimentation cylinder and add distilled water to bring the volume to 1L.
3. Allow suspension to equilibrate thermally and record temperature.
4. Insert rubber stopper and mix contents thoroughly by shaking end over end for approximately 1 min.

5. If surface is covered with foam, add a drop of amyl alcohol.

6. Lower hydrometer into suspension and take readings after 30 seconds and 1 min (R).

7. Remove hydrometer and rinse and wipe dry. Take additional readings at 3, 10, 30, 60, 90, 120, 1440 minutes, inserting hydrometer 10 s before each reading and removing, rinsing and drying after each reading. Make sure to take readings on blank solution at each time interval also (R_L).

H.5.2 Calculation of mean particle diameter (silts and clays):

$X = \theta t^{-1/2}$ (μm)

X = mean particle diameter

θ = sedimentation parameter $\theta = 1000\left(Bh'\right)^{1/2}$ [μm $min^{1/2}$]

where $B = (30\ \eta\ /[g\ (\rho_s - \rho_l)])$

η = fluid viscosity in poise [$gcm^{-1}s^{-1}$]

ρ_s = soil particle density [2.65 g/cm^3]

ρ_l = solution density [g/cm^3]

g = gravitational constant [981 cm/s^2]

t = time of measurement in seconds

h' = hydrometer settling depth (cm)

where $h' = -0.164R + 16.3$ (for ASTM 152H soil hydrometer @ 30° C)

R = uncorrected hydrometer reading (g/L)

To determine sand, silt, and clay percentages, plot P vs. log X where $P = C/C_0 \times 100$

Where $C = R - R_L$

RL = reading on blank solution

C_o = oven dry weight of sample

Appendix I

Curve Fitting Procedures

I.1 RETC Curve Fitting Procedures

The RETC curve fitting program (van Genuchten et al., 1991) was used to fit the van Genuchten equation to the MWC, MDC, and PDC data. RETC uses the Marquardt nonlinear least-squares optimization algorithm to determine moisture retention model parameters (i.e., $\theta_r, \theta_s, \alpha, n$, and m). An obvious artifact observed in the MWC data occurred because water entry pressure was not reached for most of the sandy samples for 10-15 days after beginning the wetting process. Sample evaporation during this time period resulted in a decrease in moisture content at tensions between 100 cm and water entry pressure. For this reason, the anomalous data was not used in the curve fitting process to obtain parameters for the MWC.

Residual moisture content and saturation were initially declared as free parameters when fitting curves to the MWC data using RETC, however the limited number of data points (4-5) resulted in residual moisture content values set equal to 0 and saturation equal to unrealistic values greater than 1.0. Therefore, RETC was run for the MWC setting residual moisture content equal to values obtained during RETC fits to MDC data, and saturation equal to moisture content values measured at 0 cm tension. Data points were weighed equally unless the coefficient of determination (R^2) was less than 0.95, in which case select data points were given higher weights in order to achieve a better fit to data.

The RETC program was fit to the MDC and PDC data declaring residual moisture content, saturation, α, and n as free parameters (resulting in four unknown parameters). An obvious artifact in the PDC data was observed overestimation at data points measured between 0 and 10 cm tension. This anomaly was most likely due to excess water absorbed along the edges of the ring and water absorbed by the cotton cloth (see Appendix B). For this reason, data points from 0 to 10 or 20 cm tension (depending on extent of oversaturation) were not used in the RETC fit to data for the PDC.

I.2 Mathcad Procedures

The mathematics software package MATHCAD was used to fit the linear form of the Brooks and Corey equation (Equation 2 in Chapter 2) to the log of the measured moisture retention data. MATHCAD was also used to fit the van Genuchten equation (Equation 3 in chapter 2) to the PSD data primarily because RETC resulted in poor fits to data and unrealistic fitting parameter values for the PSD data.

I.2.1 Particle Size Distributions

In order to solve for the fitting parameters in Equation 3 from Chapter 2 (d_g and n_d), the first and second derivatives were calculated (since there are two unknown parameters) and three equations were fit to the raw data by using a fitting command in MATHCAD:

I.2.2 Brooks and Corey Moisture Retention Curve

The Brooks and Corey equation was solved in MATHCAD by taking the log of the equation (making it linear) and solving for the slope and the intercept of the log of saturation (Se):

$$Se = \frac{\theta - \theta_r}{\theta - \theta_s} \tag{I-1}$$

$$Ff(d, dg, n) := \left[1 + \left(\frac{dg}{d}\right)^{n}\right]^{-\left(1-\frac{1}{n}\right)} \qquad dd := 0.01, 0.02 .. 2 \qquad dg := 0.35 \quad n := 4.5$$

$$F(d, u) := \begin{bmatrix} \left[1 + \left(\frac{u_1}{d}\right)^{u_2}\right]^{-\left(1-\frac{1}{u_2}\right)} \\ \left[1 + \left(\frac{u_1}{d}\right)^{u_2}\right]^{\left(-1+\frac{1}{u_2}\right)} \cdot \left(-1 + \frac{1}{u_2}\right) \cdot \left(\frac{u_1}{d}\right)^{u_2} \cdot \frac{u_2}{\left[u_1 \cdot \left[1 + \left(\frac{u_1}{d}\right)^{u_2}\right]\right]} \\ \left[1 + \left(\frac{u_1}{d}\right)^{u_2}\right]^{\left(-1+\frac{1}{u_2}\right)} \cdot \left(-1 + \frac{1}{u_2}\right) \cdot \left(\frac{u_1}{d}\right)^{u_2} \cdot \frac{\ln\left(\frac{u_1}{d}\right)}{\left[1 + \left(\frac{u_1}{d}\right)^{u_2}\right]} \end{bmatrix}$$

Figure I.1 – MATHCAD function used to determine values of d_g and n_d, where u_1 represents d_g and u_2 represents n_d.

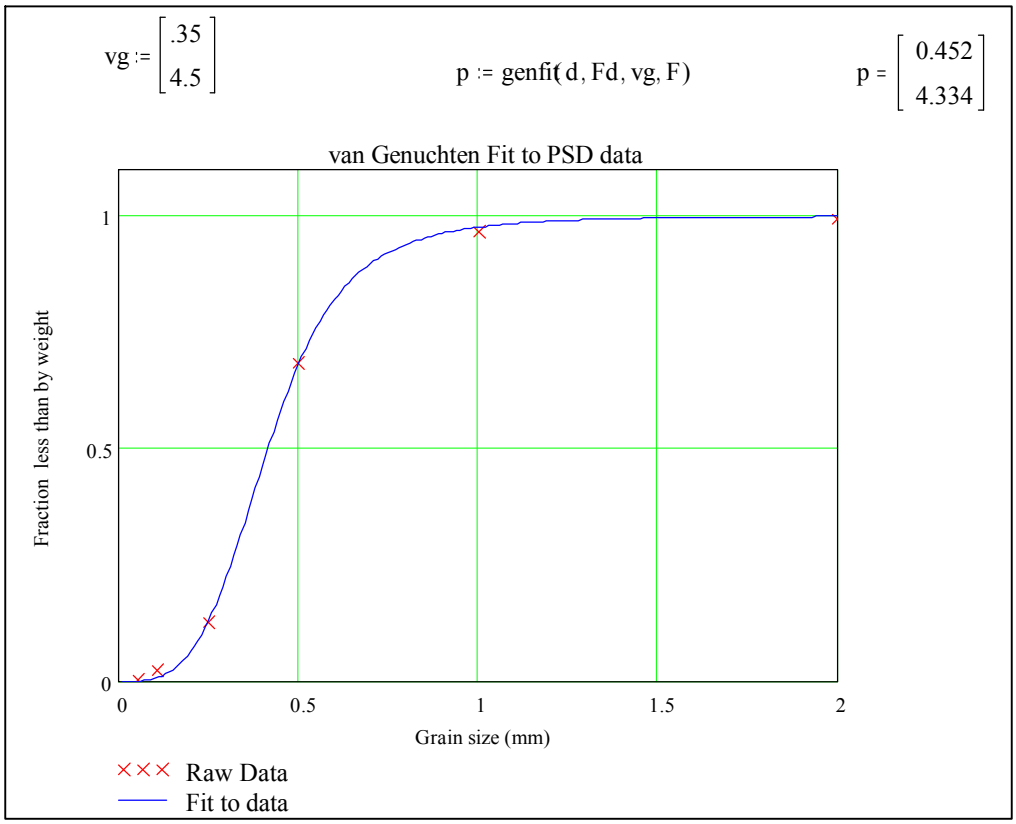

Figure I.2 – van Genuchten equation fit to PSD data. The first element in the vector "vg" is the initial guess for *dg* and the second is the initial guess for n_d. The values in the vector "p" are the fitted values for *dg* and n_d respectively.

Residual moisture content (θ_r) was set equal to zero for simplification, since only the region of drainage (or wetting) along this curve is used to determine the fitting parameters.

$$Log(Se) = Log\left[\frac{h}{h_{ae}}\right]^{-\lambda} \tag{I-2}$$

$$Log(Se) = -\lambda \log(h) + \lambda \log(h_{ae}) \tag{I-3}$$

Equation 3 shows that λ is the slope of the linear equation and h_{ae} is 10 to the power of the slope divided by the linear intercept. The following is an example of the MATHCAD file written to solve for the slope and intercept of Equation I-3. The fitted

$K := I - 2$

$Icut := 4$ Icut = #data pts at saturation

$j := 1..K - Icut$

$LS1_j := LS_{j+Icut}$

$L\Psi 1_j := L\Psi_{j+Icut}$ Used to eliminate nonlinear data near saturation

$\lambda := -slope(L\Psi 1, LS1)$

$\lambda = 1.144$

$\Psi ae := (10)^{\frac{intercept(L\Psi 1, LS1)}{\lambda}}$

$\Psi ae = 32.06$

$F_j := -\lambda \cdot L\Psi 1_j + \lambda \cdot \log(\Psi ae)$

F = linear fit
= log (Ψ/Ψae)^-λ
= -λ*log(Ψ)-(-λ*log(Ψae)
= -λlog(Ψ)+λlog(Ψae)

Figure I.3 – MATHCAD procedures for fitting the Brooks and Corey equation to the PDC data.

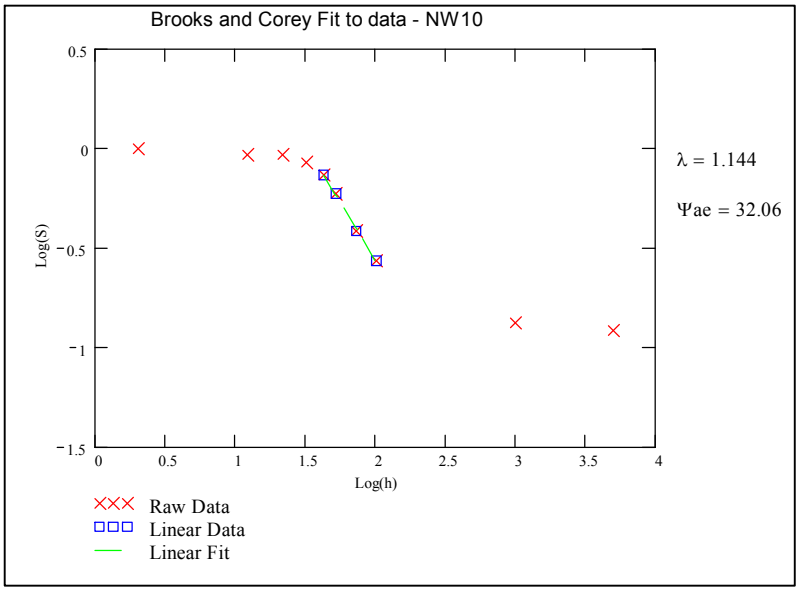

Figure I.4 –Linear Brooks and Corey fit to the PDC data.

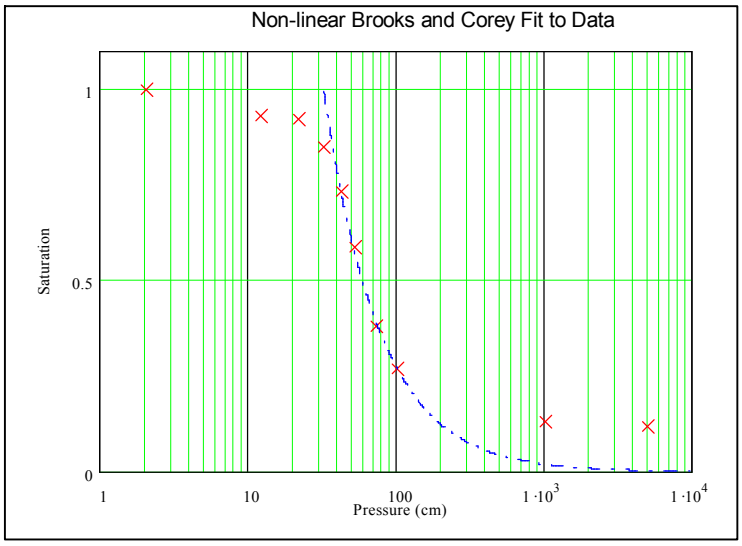

Figure I.5 – Nonlinear Brooks and Corey fit to the PDC data.

parameters were then used in the Brooks and Corey equation to examine the fit to raw data using the estimated parameters.

I.2.3 Resistivity Curve Fitting Procedures

Microsoft® Excel was used to fit Archie's law (Equation 4 in chapter 2) to the electrical resistivity versus moisture content data. The power law curve was fit to data collected during both a wetting and draining sequence (MWC and MDC) since limited data was available and the data did not appear to be hysteretic.

Appendix J

Parameter Correlation Methods and Results

J.1 Introduction

An unknown physical property can be predicted from observations of a second property if the two properties are physically related (or correlated). Linear correlations between properties can be determined using scatterplots, in which observed properties of one variable are plotted against observed properties of another. Linear regression of the observed data provides an equation which describes the linear relationship between X and Y (two physical properties) in the form of $Y= \beta_o + \beta_1 X + \varepsilon$, where β_1 represents the slope of the linear relationship, β_o represents the Y axis intercept of the line passing through the observed data points, and ε represents the random error in the relationship (deviation from the linear relationship). The least squares approach is used to determine the values of the coefficients β_o and β_1 (Schaeffer and McClave, 1995). This approach chooses an estimated equation which minimizes the sum of the squared errors (eqn. 1) by setting the derivatives of SSE with respect to both β_o and β_1 equal to zero and solving for the unknown coefficients.

$$SSE = \sum_{i=1}^{n} \left(y_i - \beta_o - \beta_1 x_i \right)^2 \qquad \text{(J-1)}$$

where SSE is the sum of squared errors, x and y are the observed data, and n is the number of data points.

Multiple regression models, which include higher order terms in the estimation equation or contain more than one independent variable, are derived from the same least

squares approach , however the number of coefficients is increased as the order or number of independent variables increases (Schaeffer and McClave, 1995). For example, if *k* represents the order/number of independent variables in the relationship, then the estimated model now resembles the form of $Y = \beta_o + \beta_1 X_1 + ...\beta_k X_k$, in which there are *k*+1 unknown coefficients. To determine the value of the coefficients, *k*+1 linear equations are needed. The multiple coefficient of determination, R^2, (eqn. 2) is used to measure how well a multiple regression model fits a set of data, where R^2 =1 implies perfect correlation.

$$R^2 = 1 - \frac{SSE}{\sum_{i=1}^{n}\left(y_i - \hat{y}_i\right)^2} \qquad \text{(J-2)}$$

where R^2 is the coefficient of determination, SSE is the sum of squared errors, y is the measured data point, $\hat{y}$ is the predicted data point, and n is the number of data points.

J.2 Methods

We use Microsoft Excel® plotting procedures for graphing parameters and adding trendlines to determine the coefficient of determination and the equation describing a relationship between parameters. Data points which appear to significantly deviate from estimated curves are ignored in some of the relationships to attain higher correlations between parameters.

We plot the van Genuchten curve fitting parameters $1/\alpha$ and n for the MWC, MDC, and PDC against each other to identify hysteretic relationships between wetting and draining curves. We plot electrical resistivity curve fitting parameters (log(*k*) and *m*) versus moisture retention parameters and particle-size distribution parameters to determine the impact of particle-size and pore size distributions on electrical resistivity

measurements. We examine the relationship between saturated hydraulic conductivity and moisture retention characteristics, porosity, grain texture, and sorting to examine the impact on the measured results. We examine the relationship between pore-size distribution, particle-size distribution, and packing (bulk density) to evaluate relevance for predicting hydraulic properties from physical properties of the deposits which are easily attainable. We plot satiation (MDC) versus saturation (PDC) to predict measurements which include entrapped air at saturation from PDC measurements.

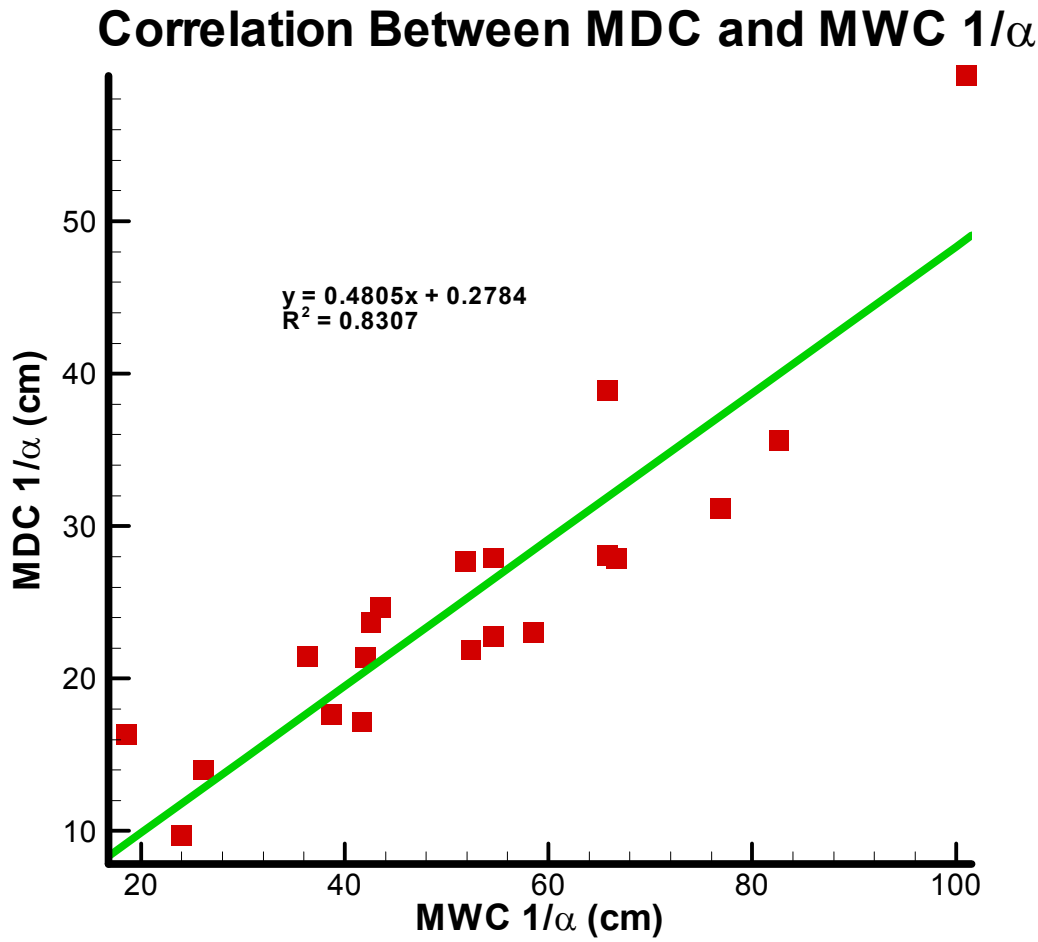

Figure J.1 – Relationship between the van Genuchten parameter α for the MWC and the MDC.

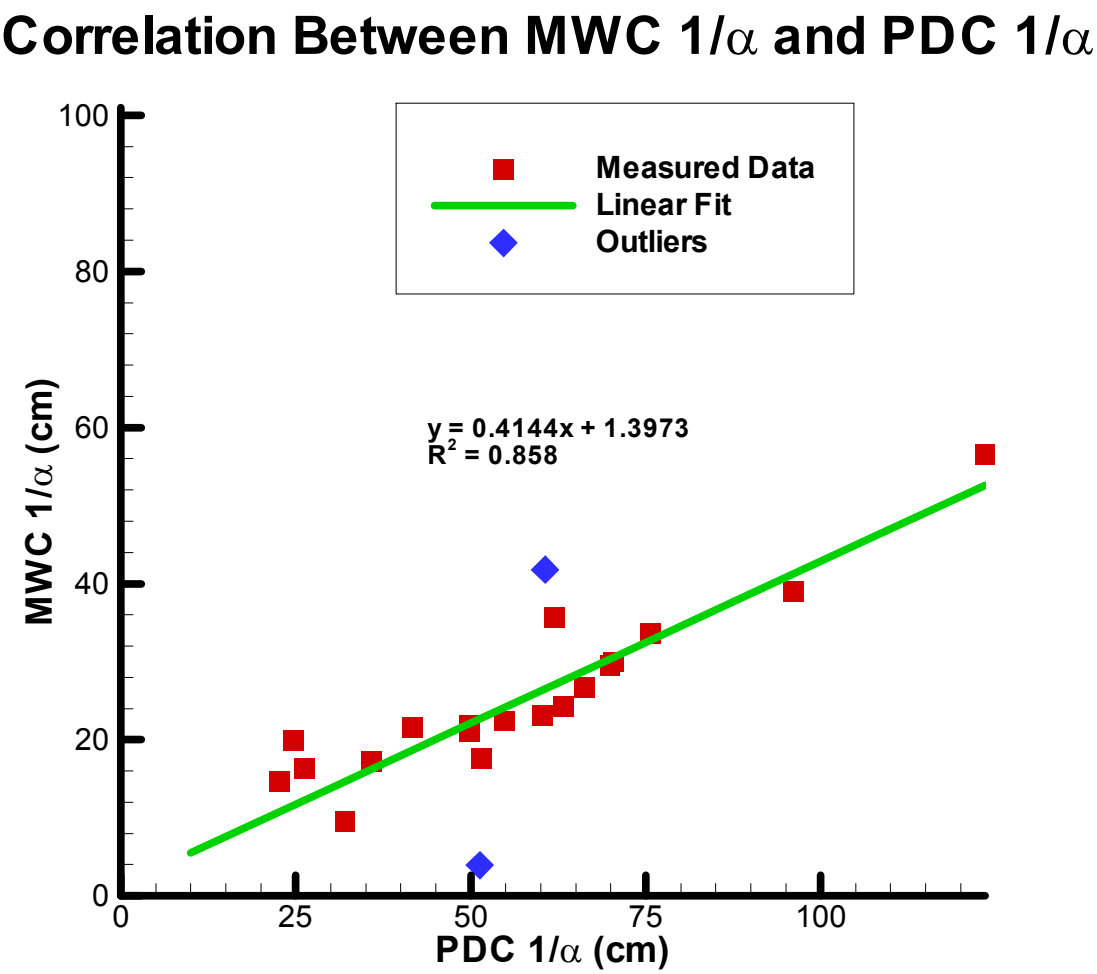

Figure J.2 – Relationship between the van Genuchten parameter α for the MWC and the PDC.

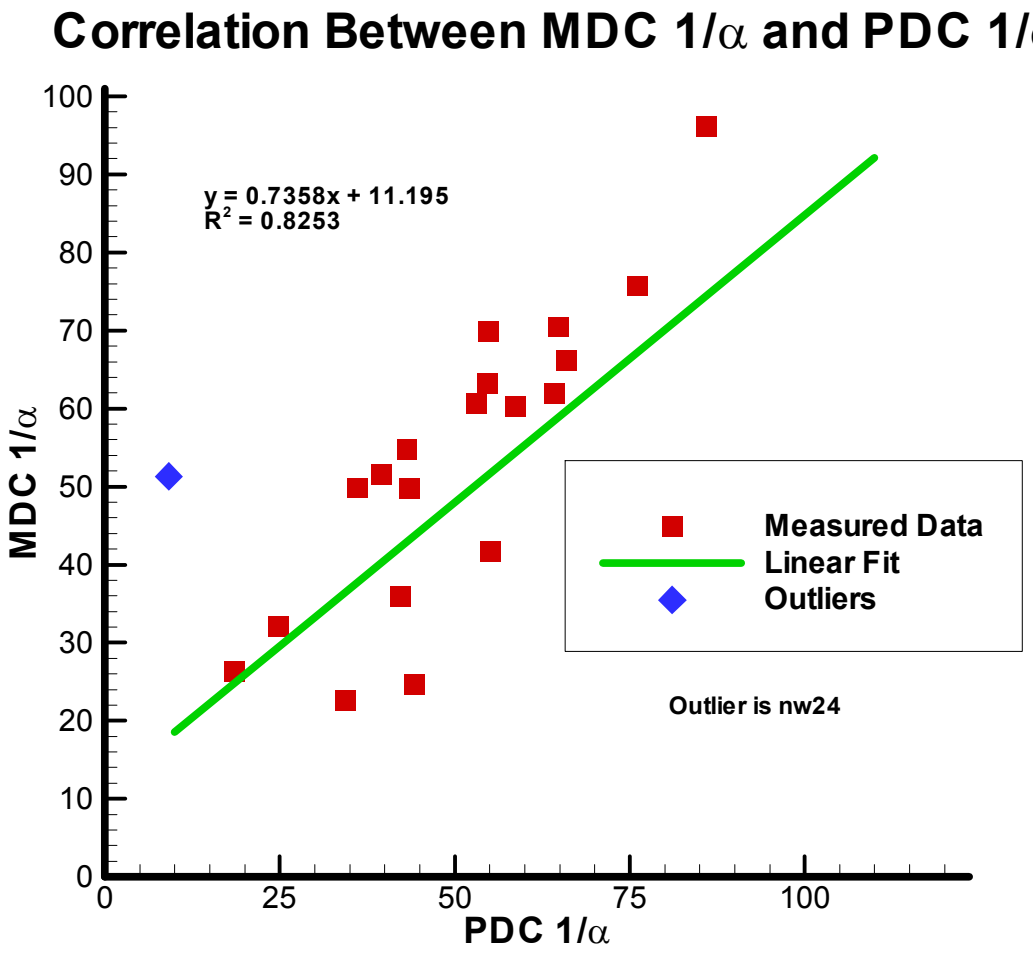

Figure J.3 – Relationship between the van Genuchten parameter α for the MDC and the PDC.

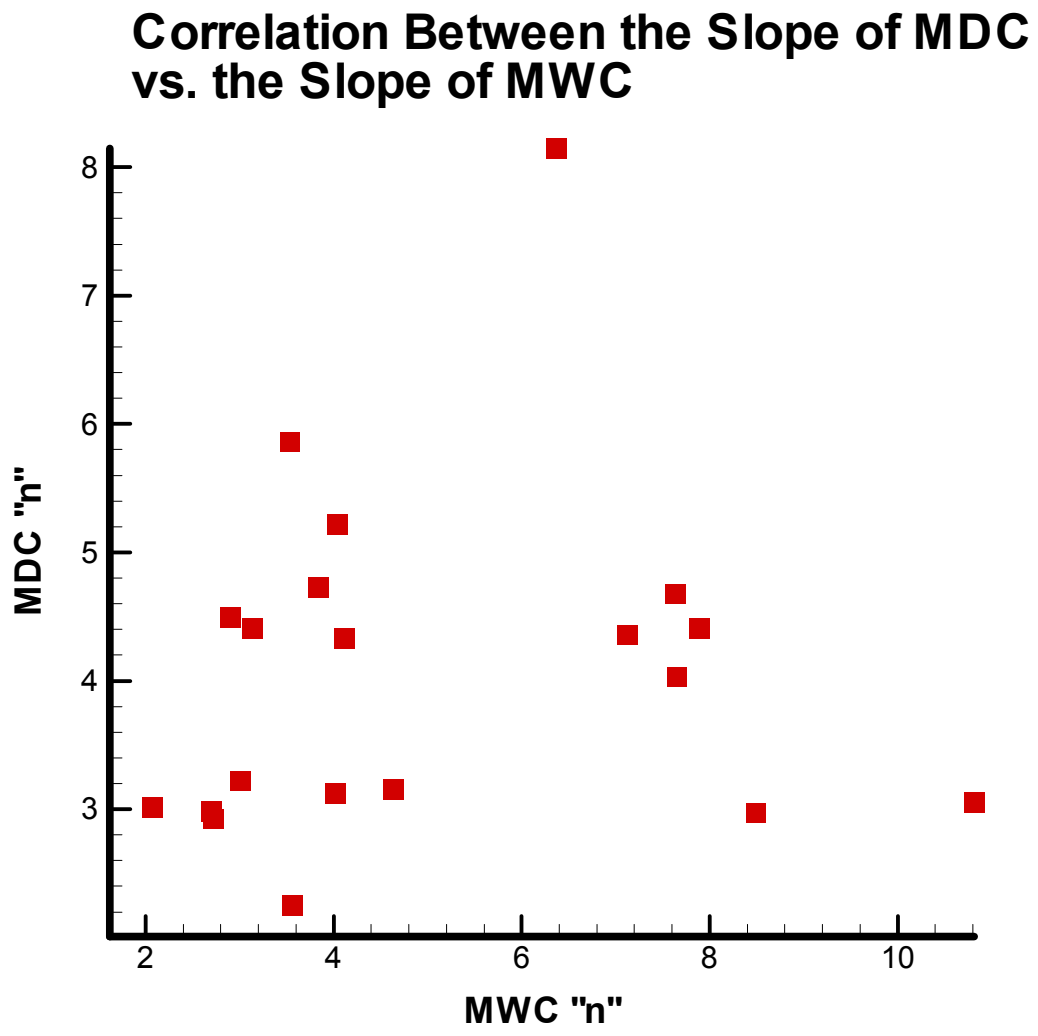

Figure J.4 – Relationship between the van Genuchten parameter *n* for the MDC and the MWC.

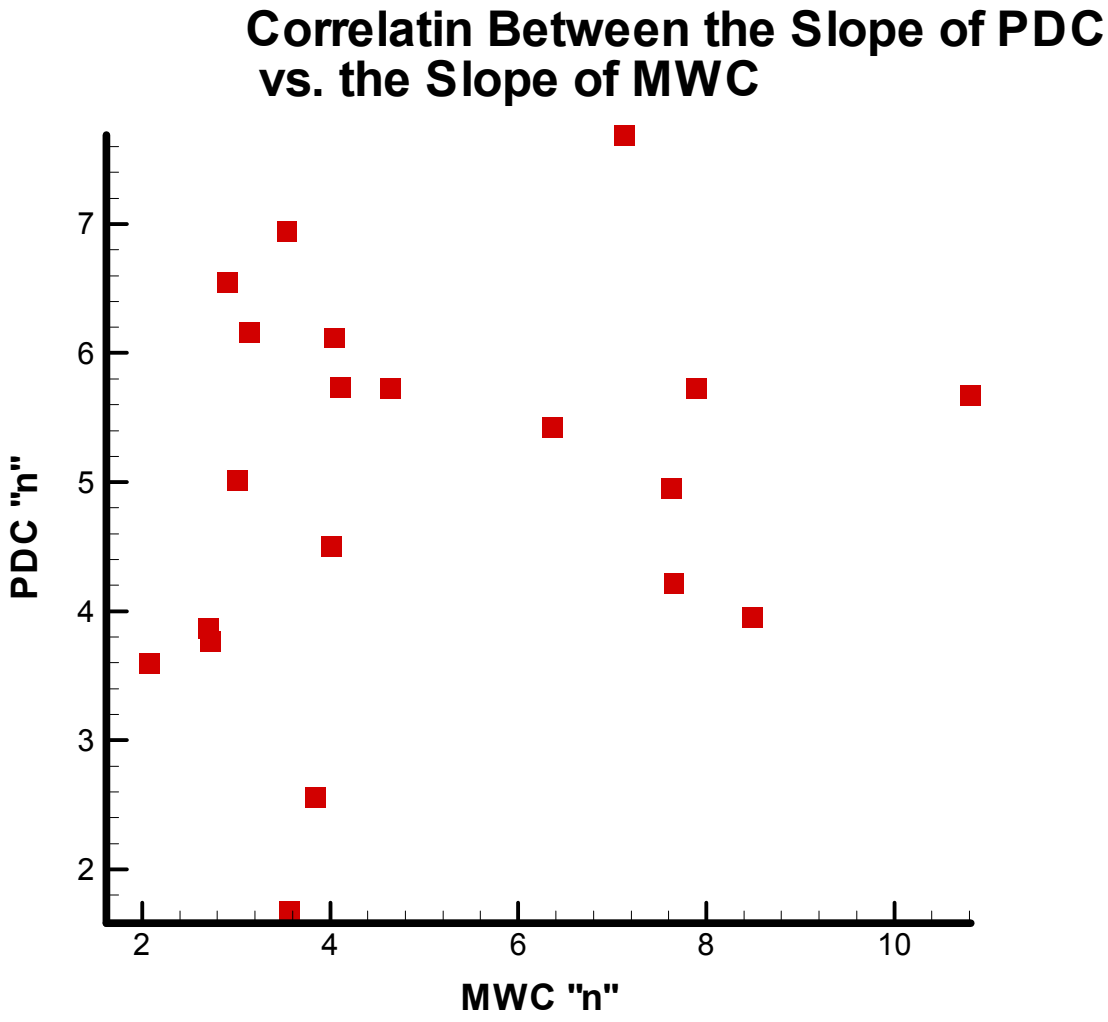

Figure J.5 – Relationship between the van Genuchten parameter *n* for the PDC and the MWC.

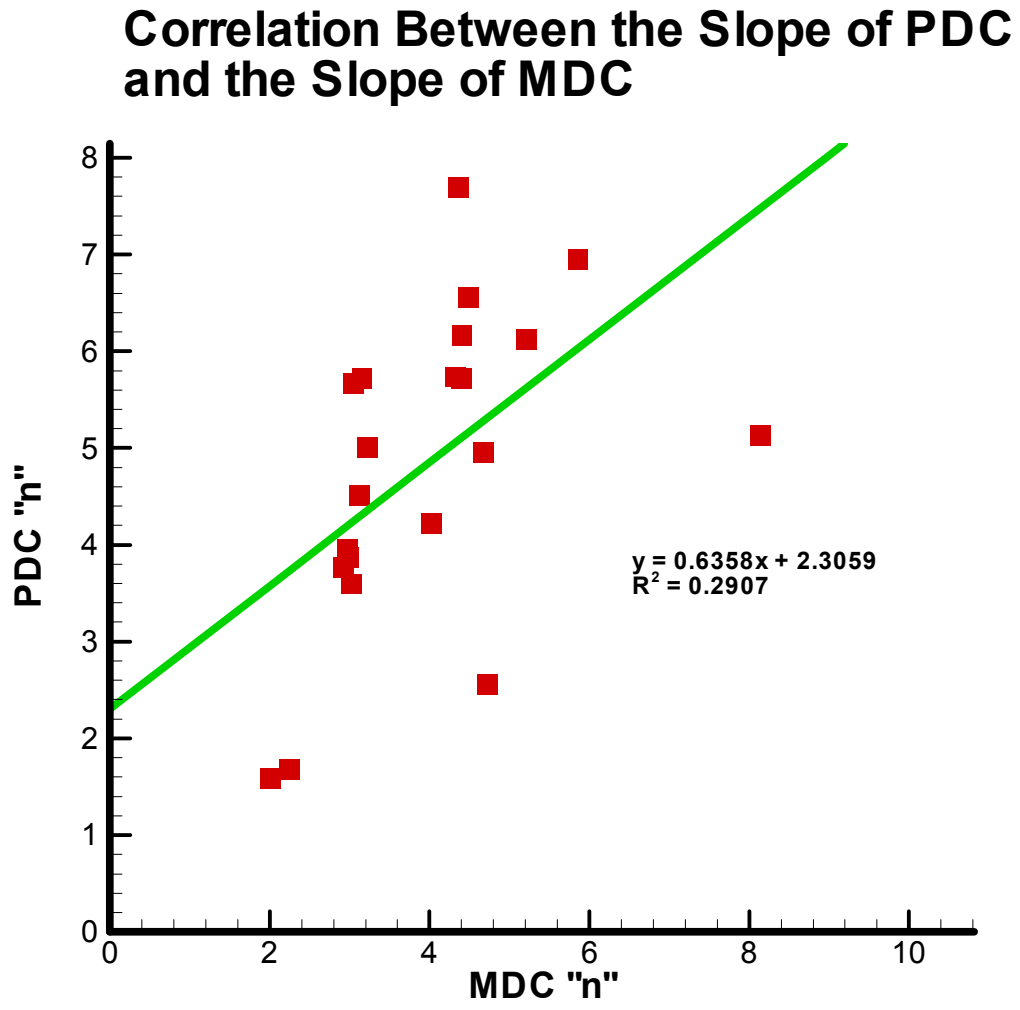

Figure J.6 – Relationship between the van Genuchten parameter *n* for the PDC and the MDC.

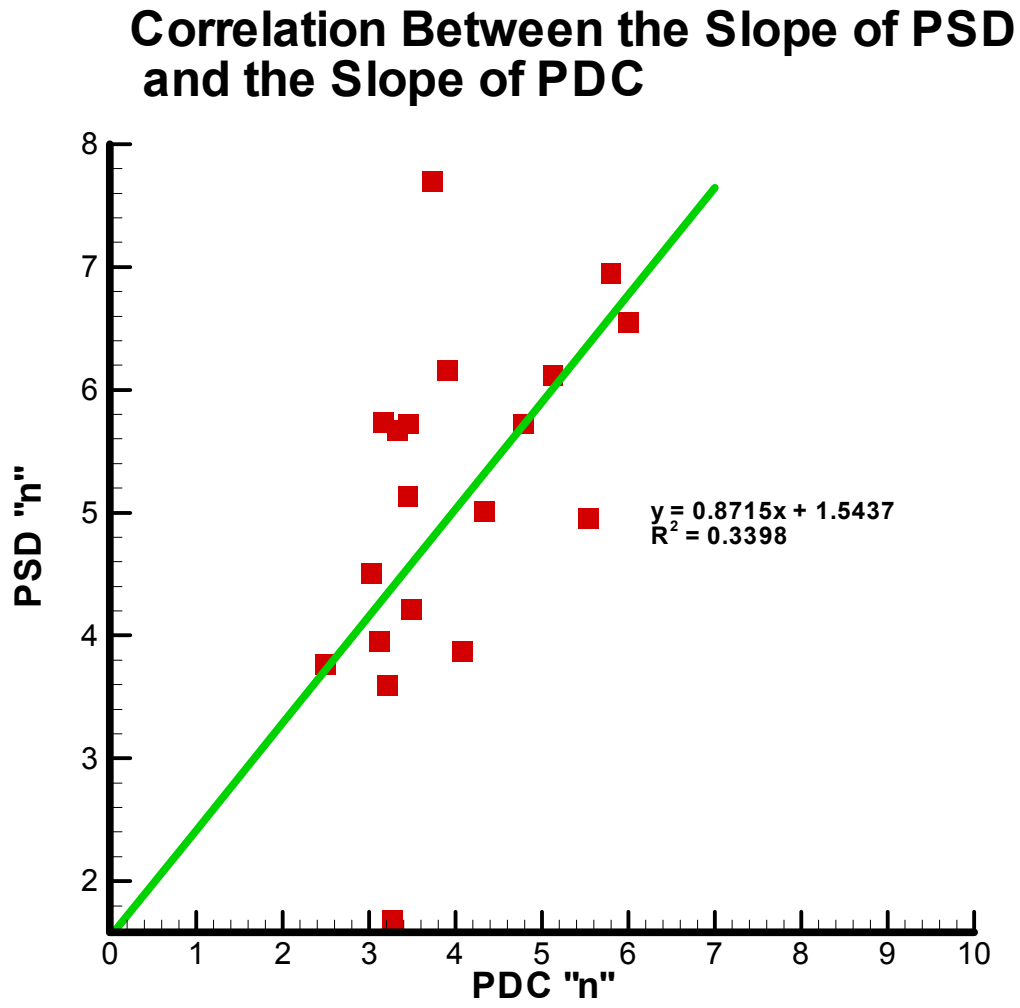

Figure J.7 – Relationship between the slope of the PDC and slope of the PSD.

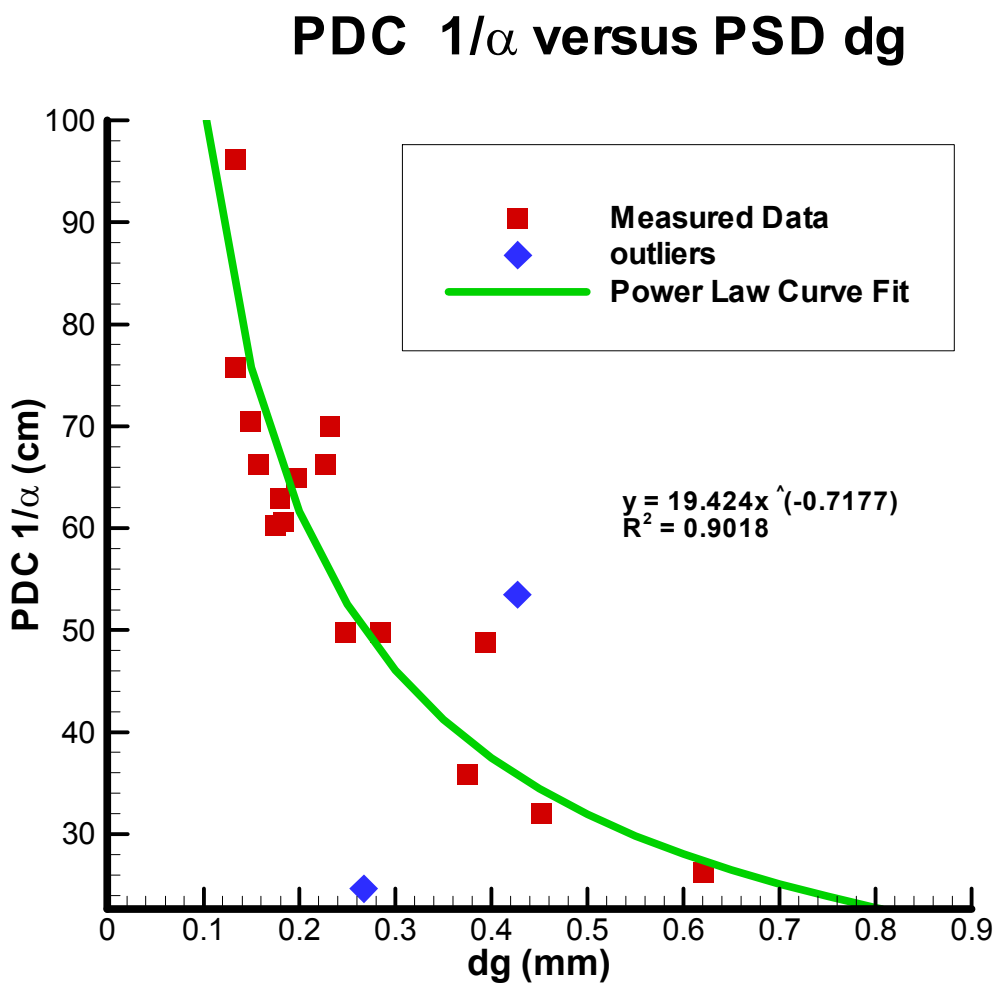

Figure J.8 – Relationship between the van Genuchten parameter α for the PDC and average grain diameter.

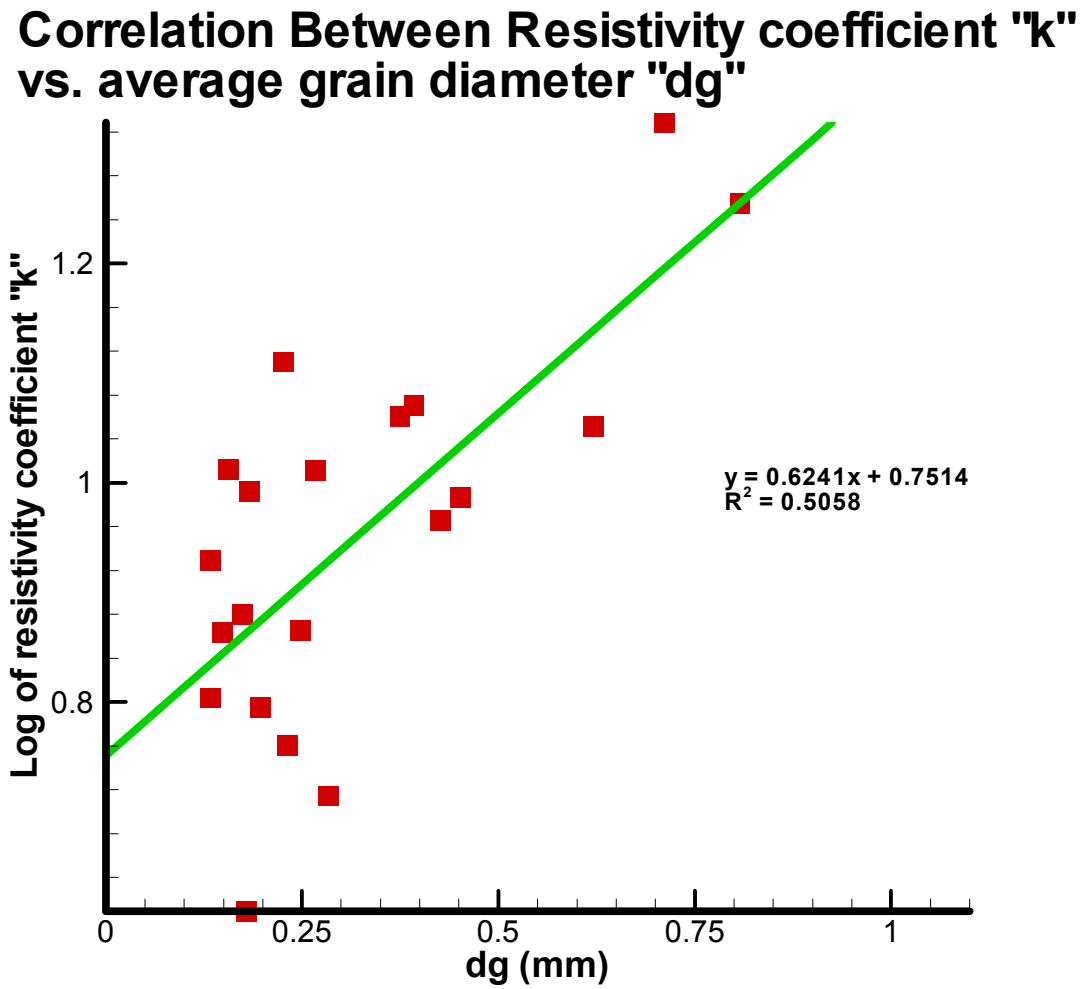

Figure J.9 – Relationship between the resistivity coefficient "k" and slope of the average grain diameter.

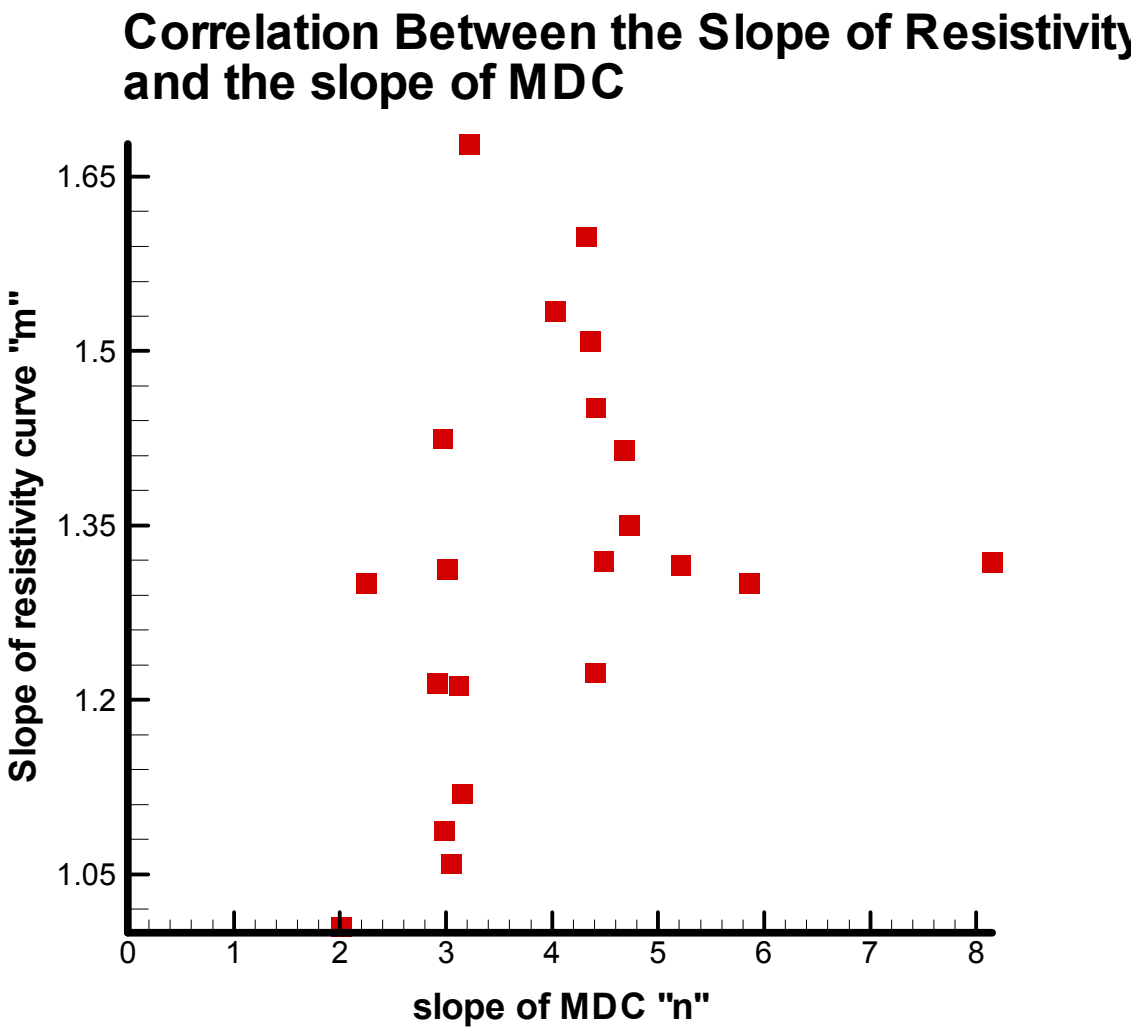

Figure J.10 – Relationship between the slope of the resistivity curve and slope of the MDC.

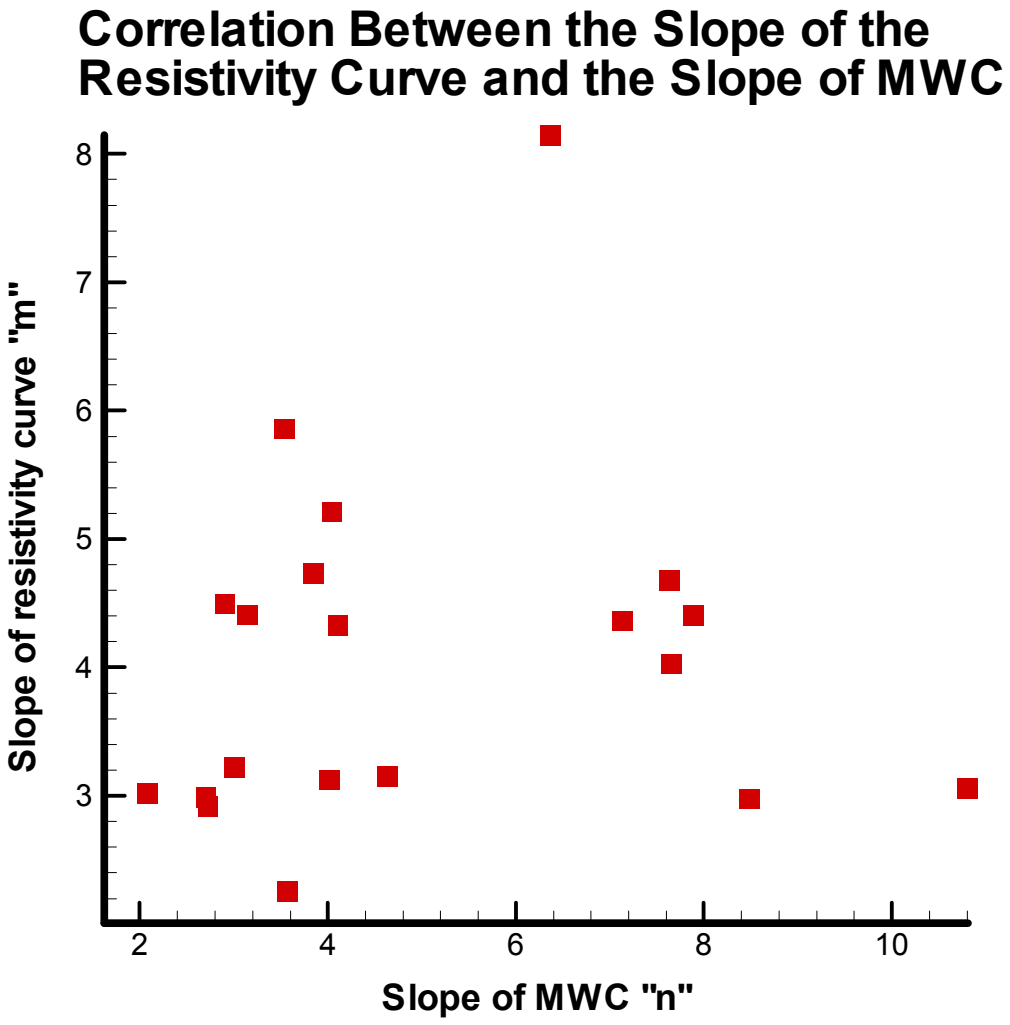

Figure J.11 – Relationship between the slope of the resistivity curve and slope of the MWC.

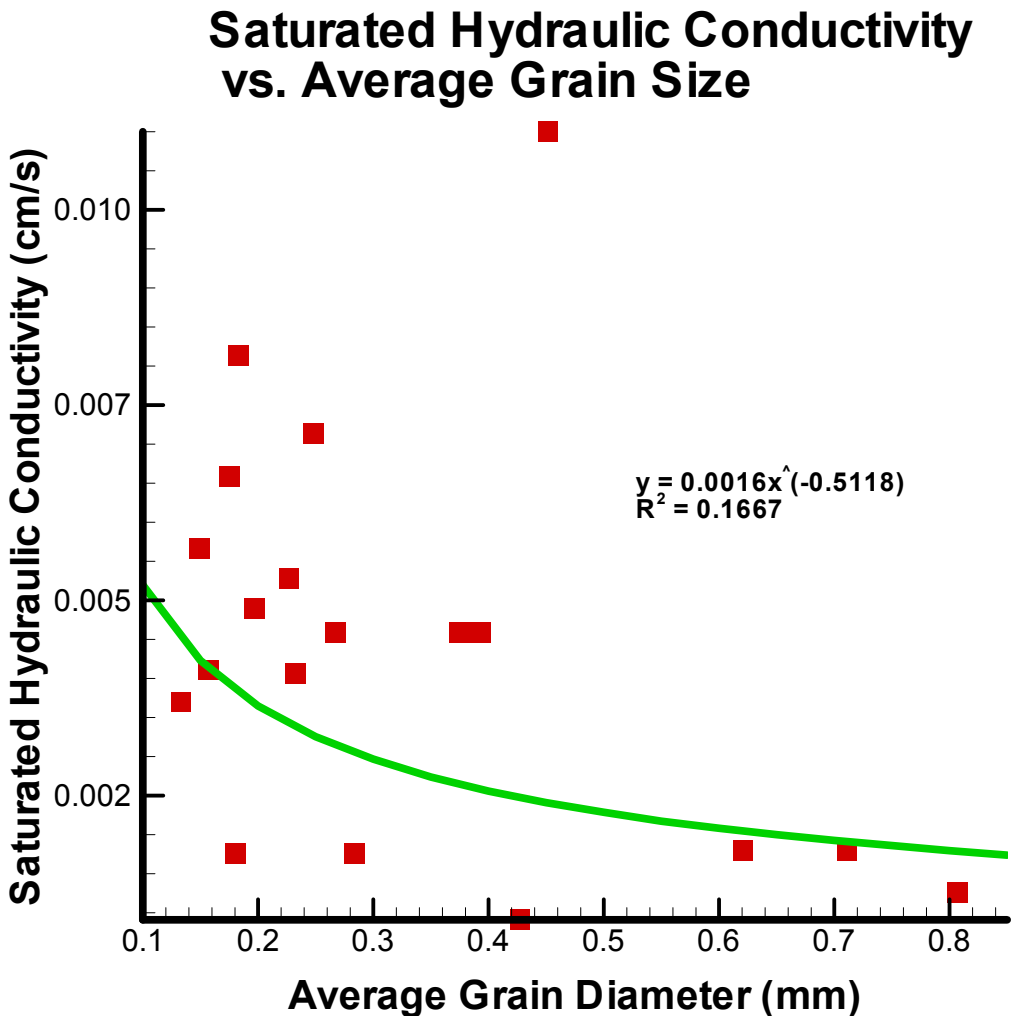

Figure J.12 – Relationship between saturated hydraulic conductivity and the average grain diameter.

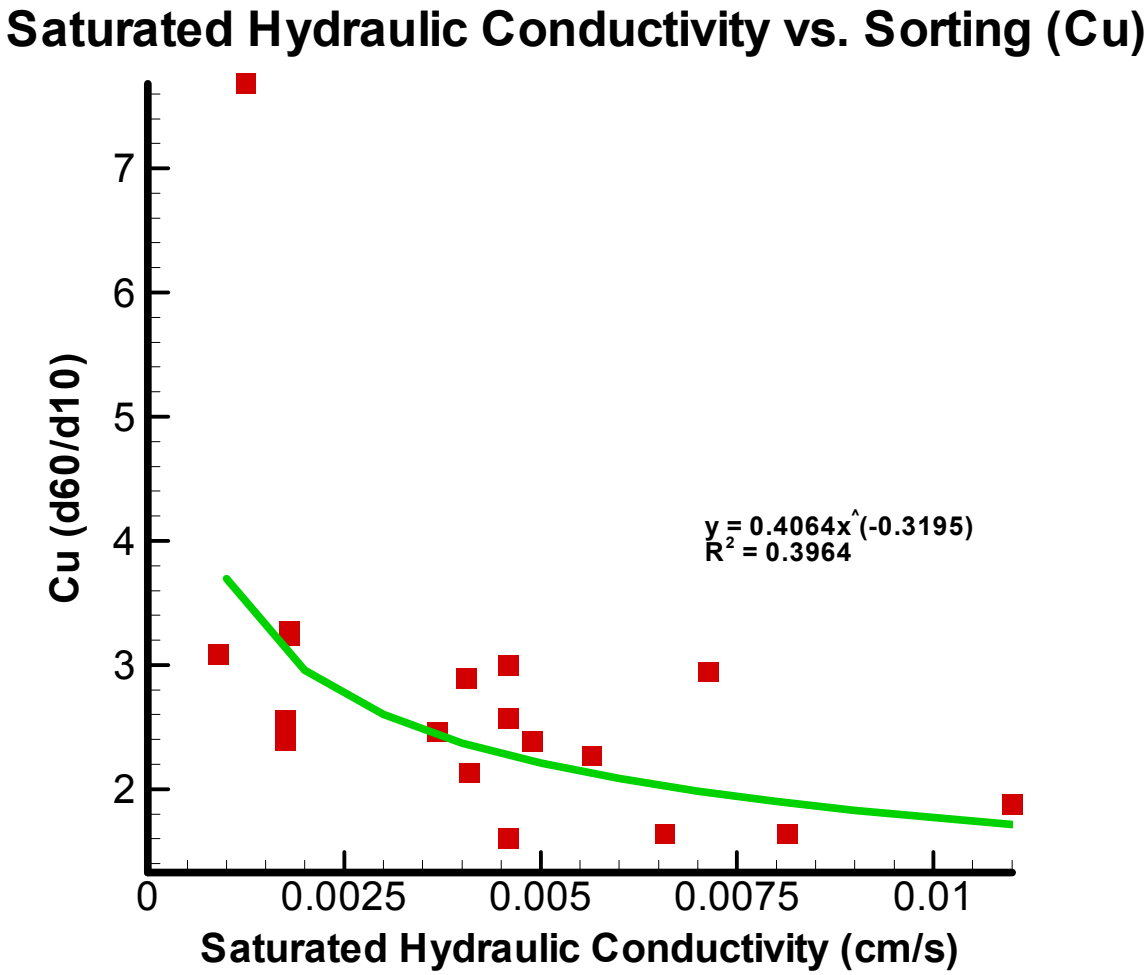

Figure J.13 – Relationship between particle sorting (Cu) and the saturated hydraulic conductivity.

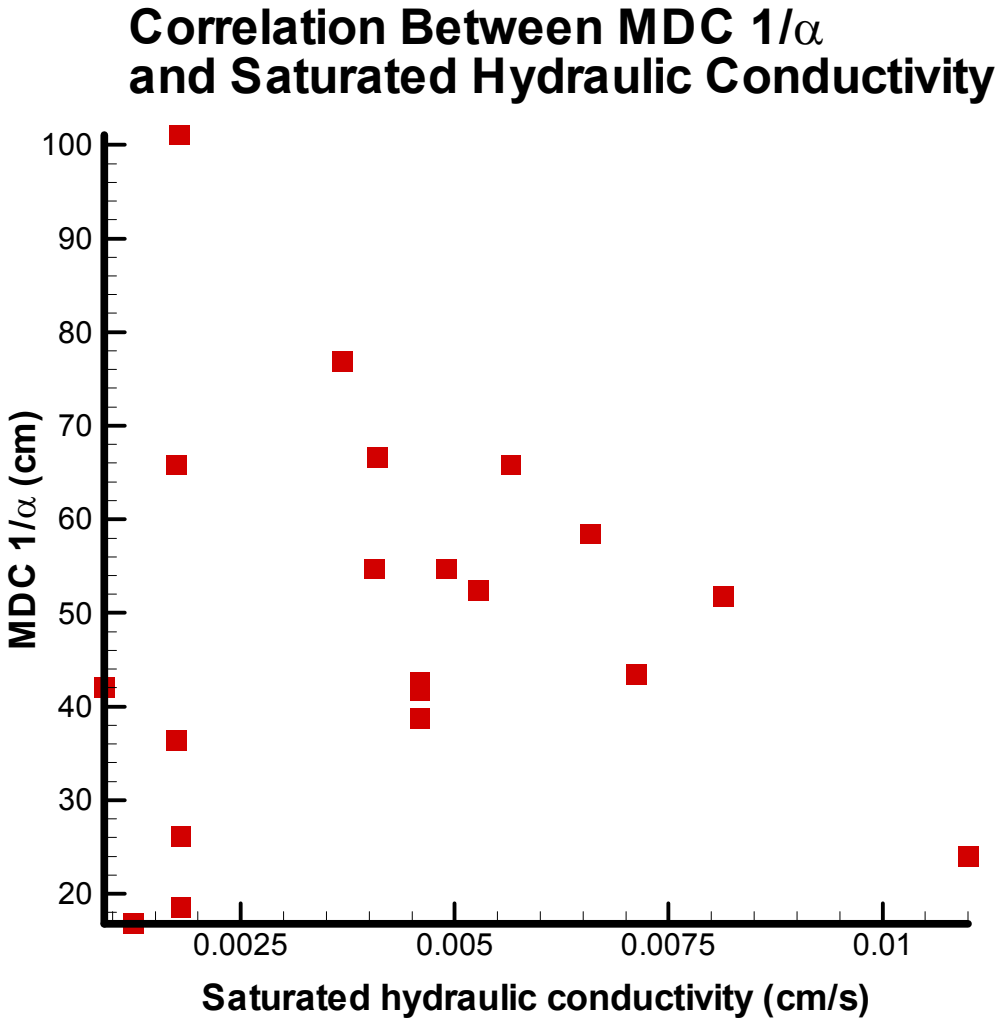

Figure J.14 – Relationship between the van Genuchten parameter α for the MDC and the saturated hydraulic conductivity.

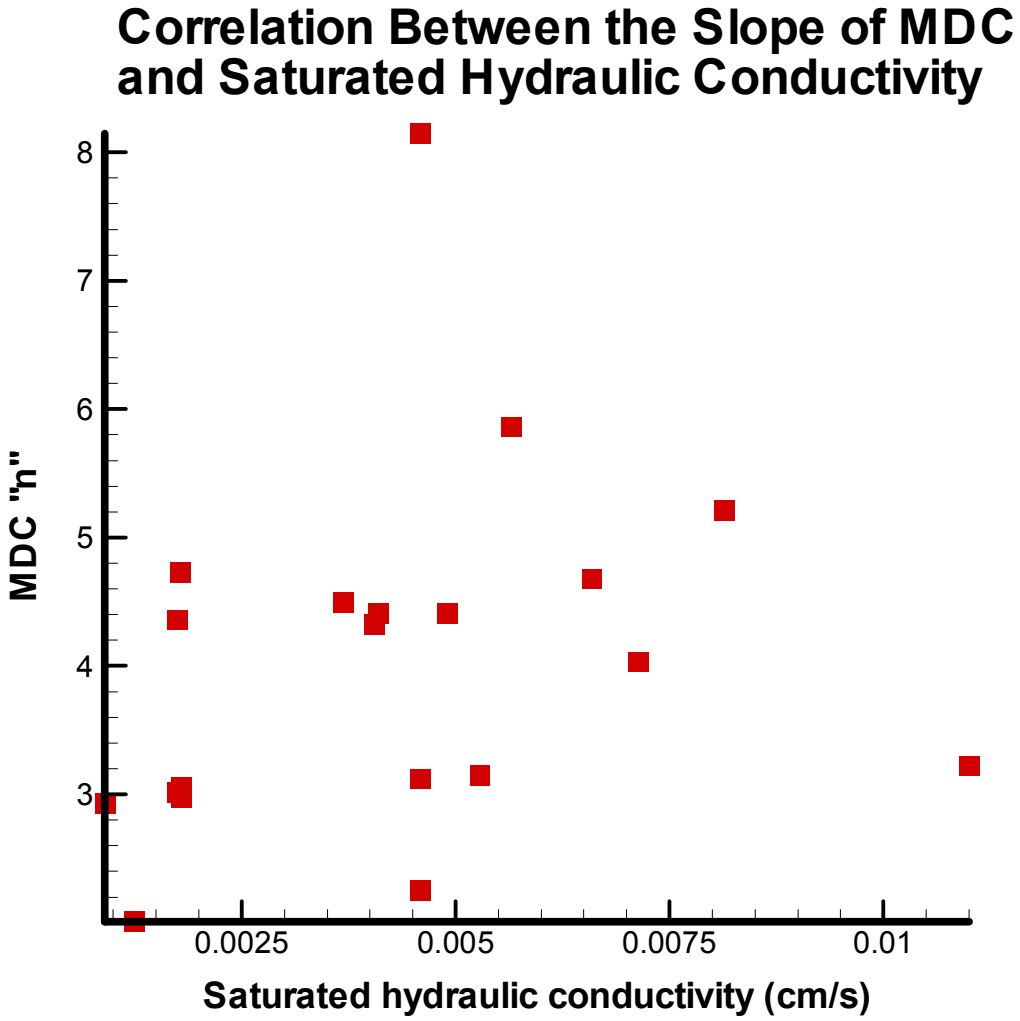

Figure J.15 – Relationship between the van Genuchten parameter *n* for the MDC and the saturated hydraulic conductivity.

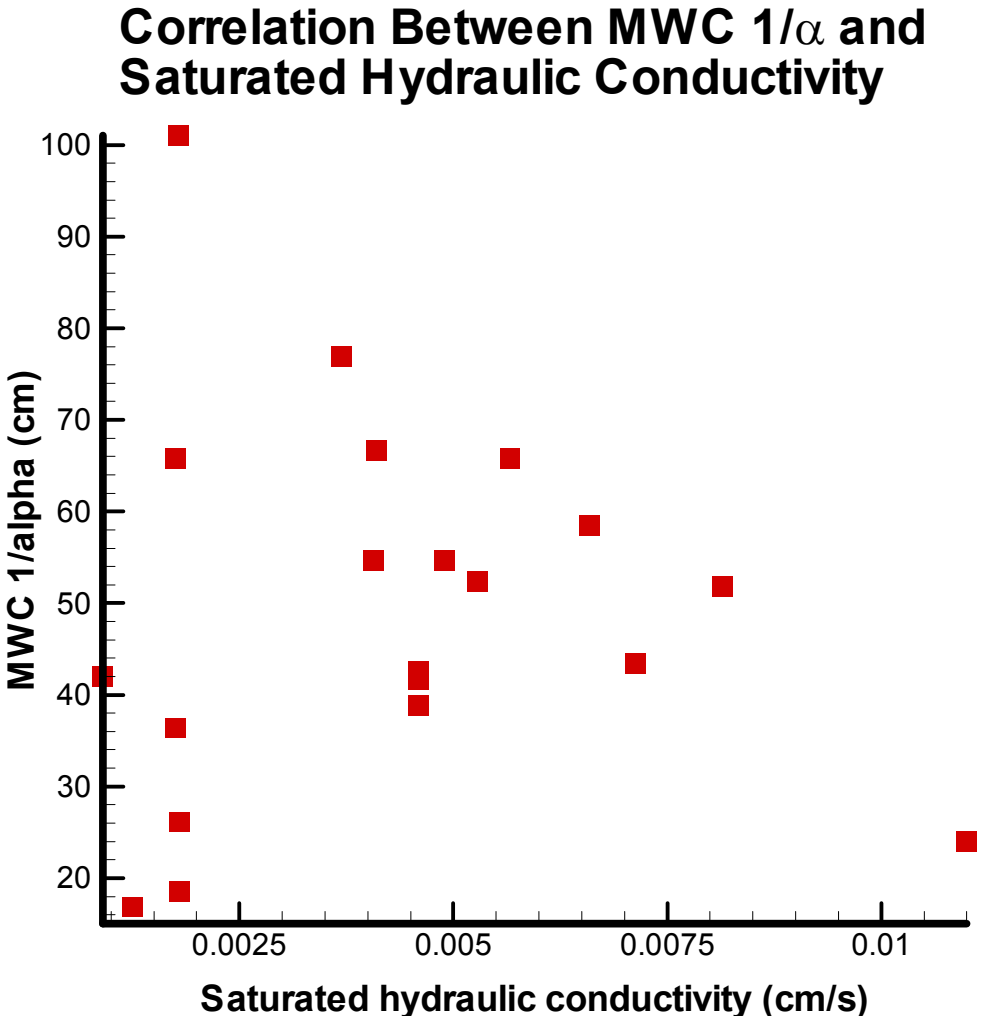

Figure J.16 – Relationship between the van Genuchten parameter α for the MWC and the saturated hydraulic conductivity.

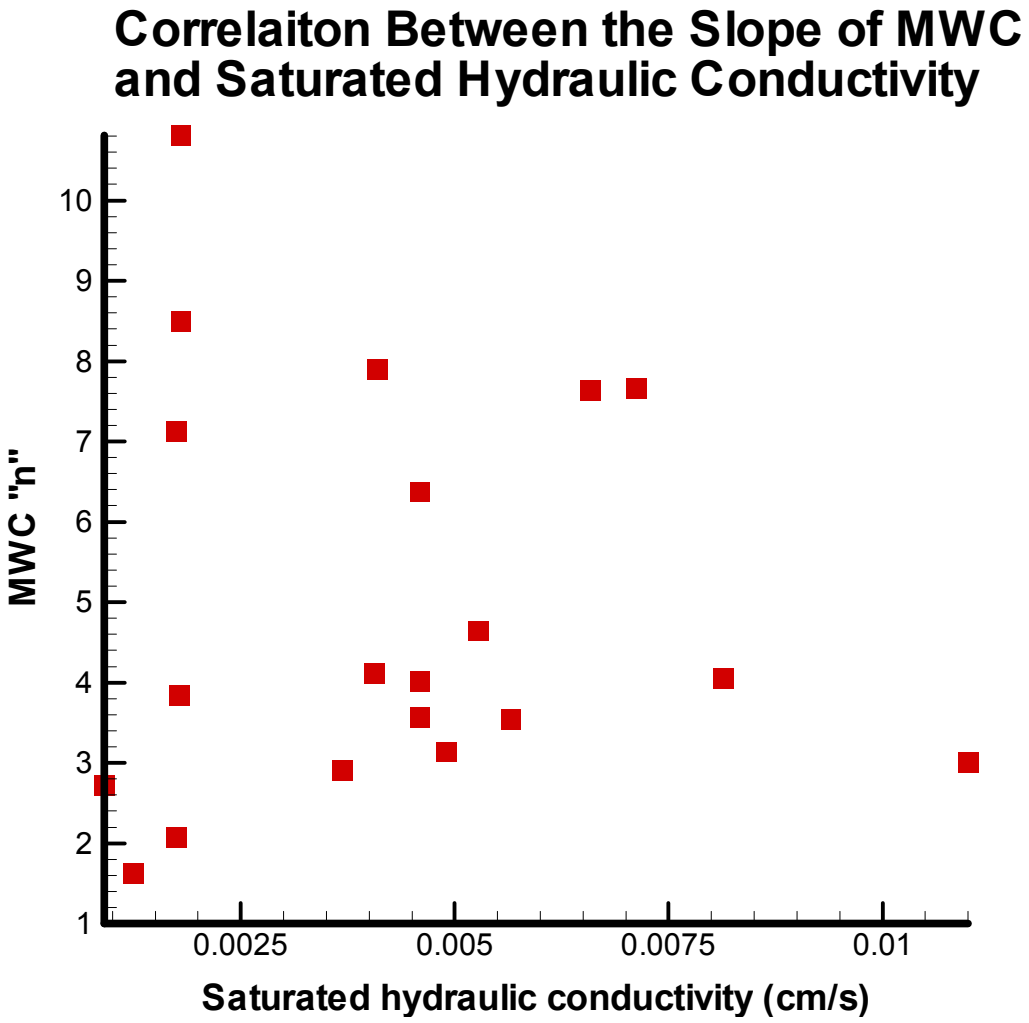

Figure J.17 – Relationship between the van Genuchten parameter *n* for the MWC and the saturated hydraulic conductivity.

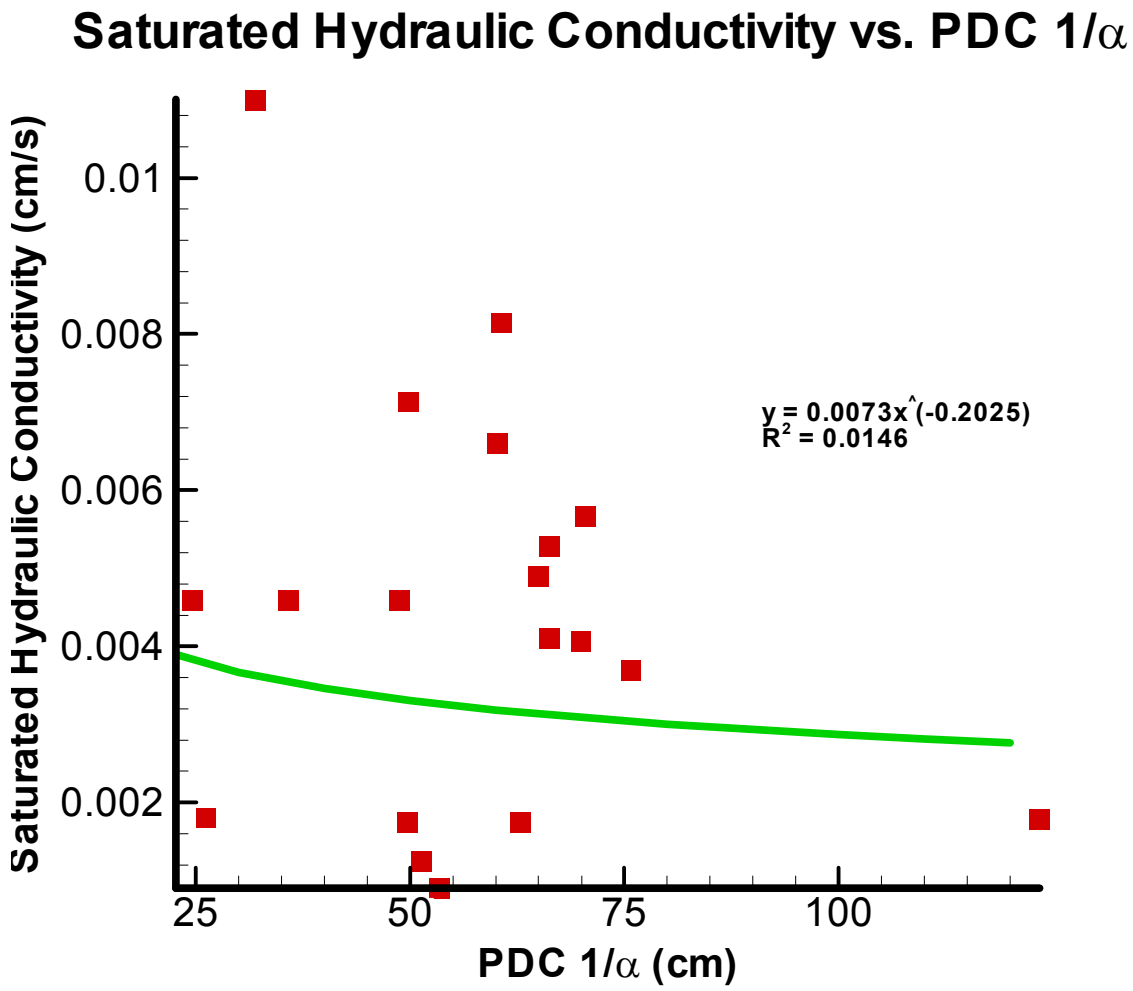

Figure J.18 – Relationship between the van Genuchten parameter α for the PDC and the saturated hydraulic conductivity.

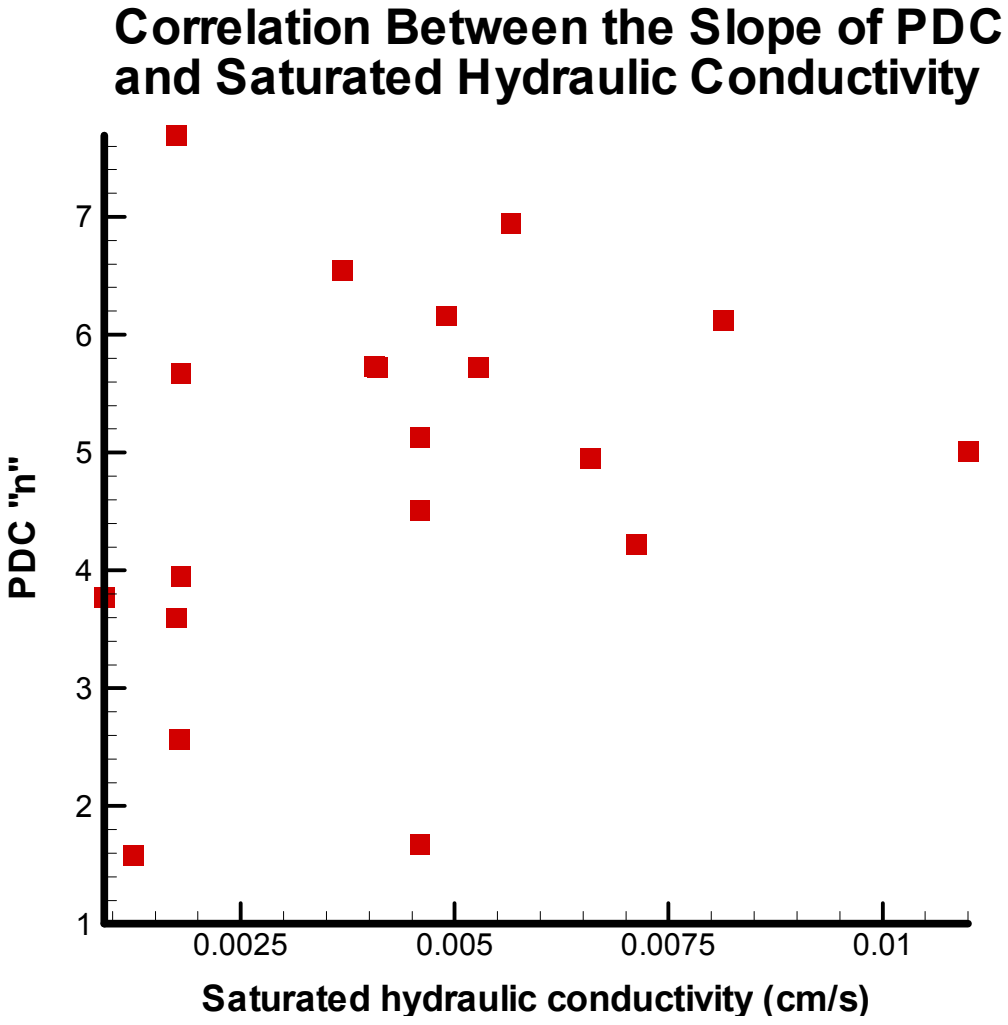

Figure J.19 – Relationship between the van Genuchten parameter *n* for the PDC and the saturated hydraulic conductivity.

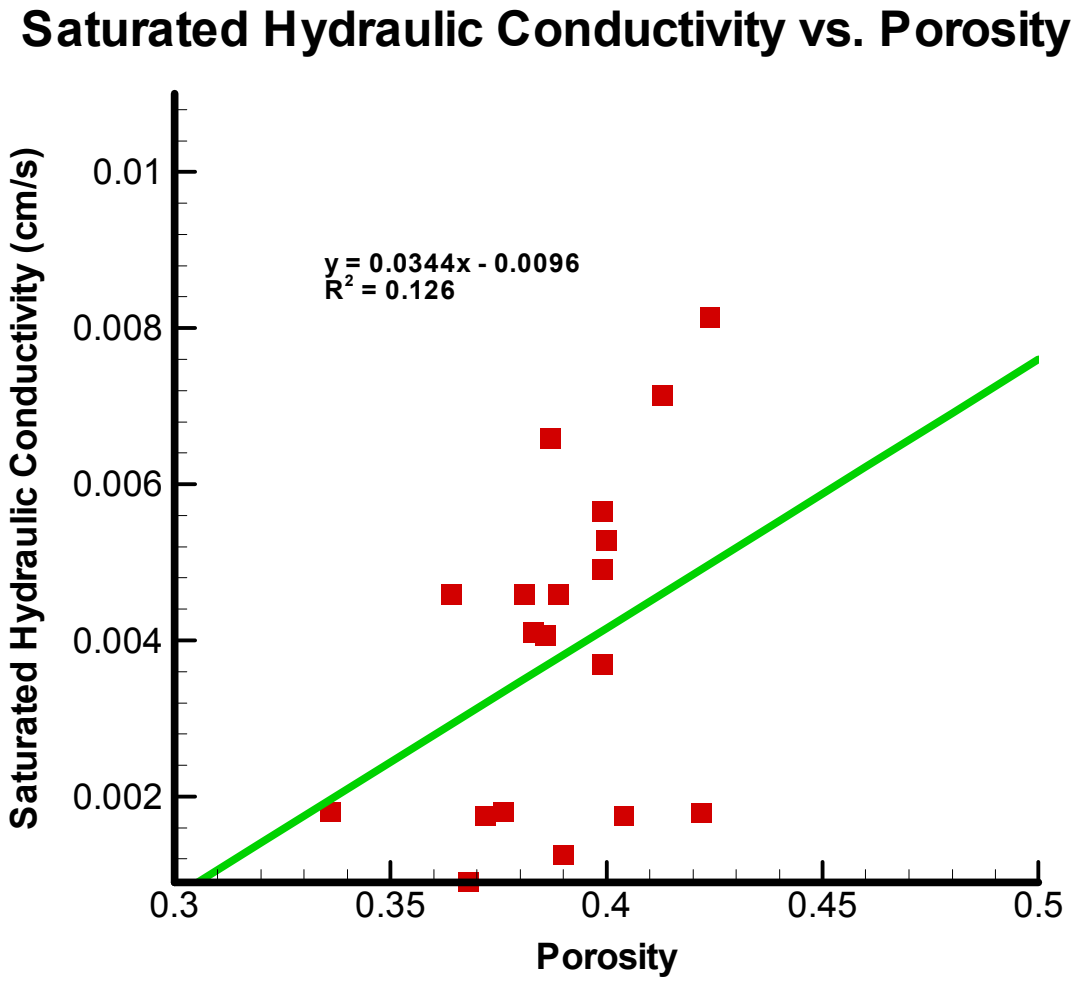

Figure J.20 – Relationship between porosity and the saturated hydraulic conductivity.

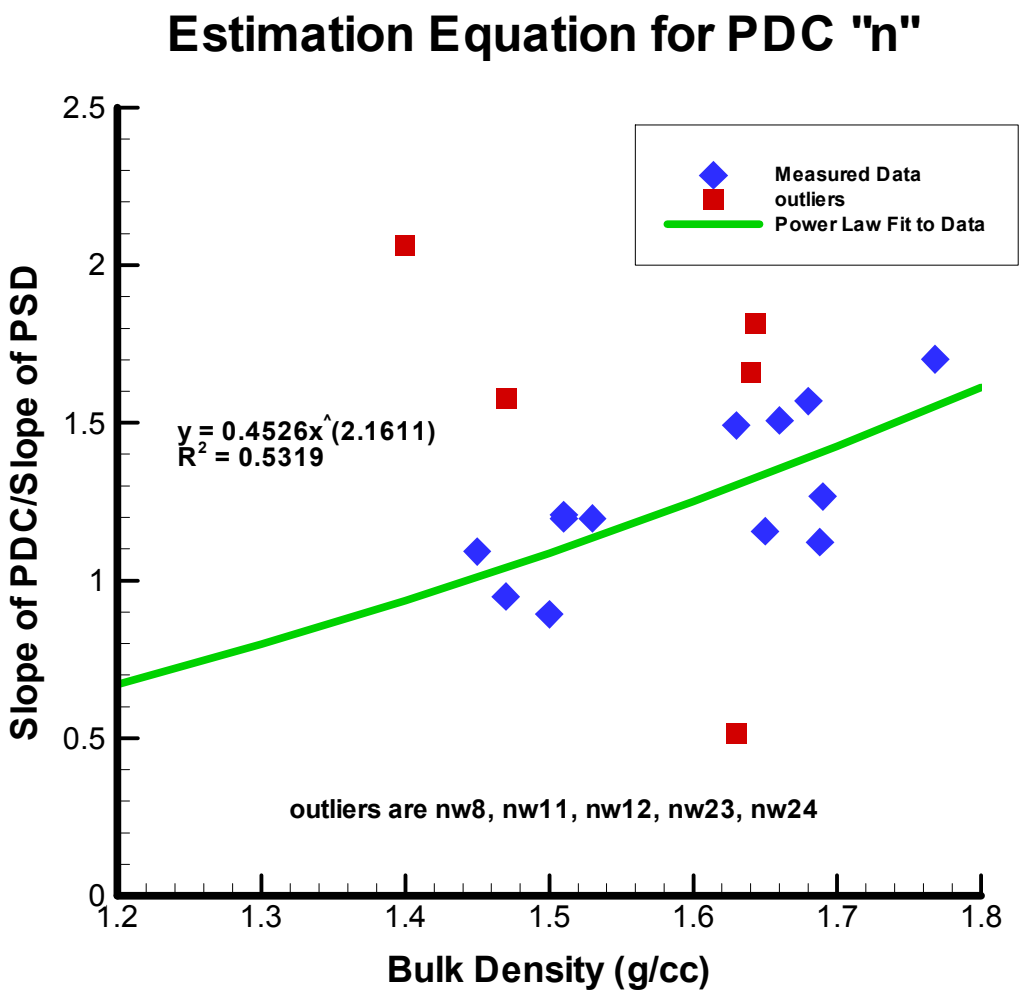

Figure J.21 – Relationship between the slope of the PDC, slope of the PSD, and the bulk density.

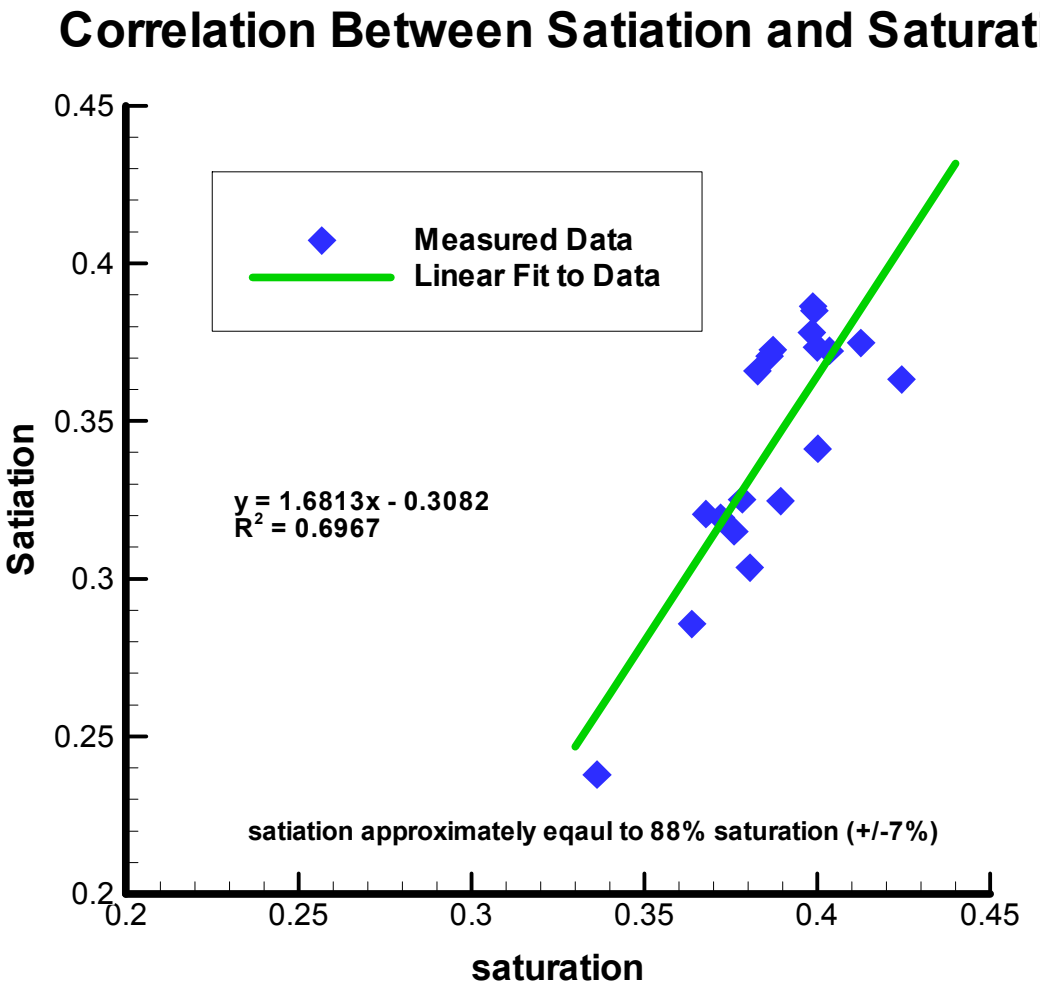

Figure J.22 – Relationship between saturation and satiation.

Appendix K

Measurement Error

K.1 Introduction

Direct measurements of hydraulic properties consist of both the "true" value and measurement error contributed by factors which cannot be completely avoided, such as imprecision and bias in the measuring device and/or researcher errors, such as misread values and transcription errors. In order to determine the relevance of laboratory data, the degree of measurement error should be identified and included in the data, typically in the form of the standard deviation from the mean value (Mandel, 1964).

The two major components of measurement error are precision and accuracy (Scheaffer and McClave, 1995). Precision refers to the reproducibility of measurements and accuracy refers to the ability to produce unbiased measurements. Measurement bias is the result of a constant deviation in the results. For example, measurements which are continually skewed in a particular direction from the "true" value due to improper instrument calibration are considered to be biased. Model estimates are considered biased if the estimated value does not equal the mean value (Isaaks and Srivastava, 1989).

Measurement accuracy is typically determined by comparing results to a known value. Unfortunately, this is difficult to do when measuring hydraulic properties since actual hydraulic properties are rarely known. Measurement precision can be determined by repeating a measurement several times using the same procedure and noting the

deviation in the results. The data would be considered precise within +/- the standard deviation in the repeatability measurements.

K.2 Methods

We examine measurement error by conducting sample repeatability tests for equipment used in the laboratory to measure hydraulic properties of the STVZ site samples. Description of the repeatability tests are included in this appendix along with statistics for the measurements (mean, standard deviation, and coefficient of variation) and measurement data.

K.2.1 Repeatability Tests for Porosity, Moisture Content, and Electrical Resistivity Measurements

Deposits of med-coarse grained sands collected from the infiltration test site were split and repacked into three 100 cc rings to determine the reproducibility of porosity, moisture content, and electrical resistivity measurements made in the laboratory for site characterization. The samples were saturated under a vacuum in the saturation chamber (see Appendix D) then placed in the impedance analyzer (see Appendix F-1) to measure electrical resistivity at saturation. The samples were placed in the pressure chamber to drain the samples to equilibrium moisture content at 1 bar pressure, then weighed to determine volumetric moisture content. Measurements were not made at additional pressures in the pressure chamber due to time constraints. We attempted to measure electrical resistivity after removing the samples from the pressure chambers, however, the samples were very dry after draining under 1 bar pressure, preventing electrical conductance across the samples. The samples were oven dried and the K.3 include the mean, standard deviation, and coefficient of variation (standard deviation divided by the

Table K.1 – Error analysis of porosity measurements made using the saturation chamber.

Sample ID	Sample Mean	Sample Stdev	Coefficient of Variation
36	0.332	0.009	0.027
37	0.321	0.019	0.060
46	0.336	0.014	0.043
average	**0.330**	**0.014**	**0.043**

Table K.2 – Error analysis of moisture content measurements made at 1 bar pressure using the pressure chambers.

Sample ID	Sample Mean	Sample Stdev	Coefficient of Variation
36	0.032	0.008	0.250
37	0.035	0.006	0.171
46	0.037	0.006	0.162
average	**0.035**	**0.007**	**0.200**

Table K.3 – Error analysis of electrical resistivity measurements made at saturation using the impedance analyzer.

Sample ID	Sample Mean	Sample Stdev	Coefficient of Variation
36	47.776	8.561	0.179
37	48.926	8.246	0.169
46	48.828	8.097	0.166
average	**48.510**	**8.301**	**0.171**

mean value) for each sample along with the average statistics of the 3 samples (population statistics).

To determine the reproducibility of moisture content measurements made during a drainage cycle in the hanging column apparatus, we repacked 5 samples with split replicates of fine grained sands collected from the infiltration test site to a bulk density of 1.68 g cm^{-1}, saturated the samples under a vacuum and made measurements at six

separate equilibrium tension heads. We chose this procedure, as opposed repeating measurements, because the drainage process over a range of tension heads alters the grain structure to some degree, making it difficult to reproduce the results. The test results are listed in Table K-5 along with the mean, standard deviation, and coefficient of variation between measurements for the 5 replicate samples.

Table K.5 – Error analysis of moisture content measurements made using the hanging column apparatus.

Tension Head (cm)	Sample Mean	Sample Stdev	Coefficient of Variation
200	0.048	0.003	0.059
100	0.077	0.003	0.036
50	0.319	0.006	0.020
40	0.381	0.013	0.033
30	0.399	0.004	0.009
20	0.402	0.005	0.011
10	0.407	0.005	0.011
0	0.434	0.003	0.007
	average	**0.0052**	**0.023**

K.2.2 Repeatability Test for Tension Head in the Hanging Column

We conducted a repeatability test to determine error in the hanging column tension head measurements and to determine the time required for the samples to reach equilibrium at two different tension heads (50 cm and 100 cm tension). A mini-tensiometer was constructed of ½" ID PVC tubing, ½ bar ceramic porous cup, a rubber septum, and a 15 psi pressure transducer. The tensiometer was placed inside a 100 cc sample ring surrounded by sandy deposits, one of which consisted of uniform medium sized grains (Wedron 510) and the second sample consisted of uniform fine grained sand collected from the infiltration test site. The samples were saturated and allowed to reach equilibrium at the two tensions while a Campbell Scientific 21X data-logger attached to the pressure transducer automatically recorded the pressures every

15 minutes. We noticed a sinusoidal fluctuation in the pressures over time while collecting data for the Wedron 510 sample (this sample was tested first). To reduce background noise, we took an average of 10 readings every 15 minutes during measurements for the fine sand. The results suggest that the precision error in the hanging column pressure measurements is approximately +/- 0.30 cm at 50 cm tension and approximately +/- 0.60 cm at 100 cm tension. These values include the pressure transducer precision, bias in the observed measurement (compared to the pressure transducer reading), and the fluctuations in readings over time (see Appendix B).

K.2.3 Repeatability Test for determination of saturated hydraulic conductivity

Four samples of fine-medium grained sands collected from the sand quarry near the infiltration test site in Socorro were repacked into 100 cc rings, saturated under a vacuum (flushing with CO_2), and placed in the constant head permeameter apparatus (see Figure 2.8). Once steady state flow was established, the volumetric flow rate (Q) and the head difference (ΔH) were measured over a 20 second period. Saturated hydraulic conductivity was calculated from the measured values using Darcys law. This process was repeated ten times for each sample. Table K.6 lists the population and sample variance and standard deviation. Since the samples were not replicates,

Table K.6 – Measurement statistics for K_{sat} values measured for the STVZ sandy alluvial deposits using constant head permeameters.

Sample Statistics:				
Sample ID:	A	B	C	D
mean	1.10E-03	1.05E-03	1.14E-03	8.77E-04
stdev	8.62E-05	1.37E-11	8.70E-05	1.37E-11

Population Statistics:	mean	stdev	Coefficient of variation
	1.04e-03	5.00e-05	4.80E-02

although very similar in texture (collected from the same location), the population statistics provide an estimate of the reproducibility of K_{sat} measurements between similar samples.

K.2.4 Repeatability Test for Particle Size Analysis

We conducted a repeatability test to determine measurement reproducibility for particle size distribution measurements using the sieve method (see Appendix H) by splitting a sample of fine grained sands collected from the infiltration test site to produce 2 replicate samples. We poured each sample in a stack of pre-weighed sieves (stacked in descending order of sieve openings), placed the stack on a shaker table for 10 minutes, and weighed the sieves to determine the mass of grains in each sieve. We repeated this process 5 times each sample. The test results are listed in Table K.7.

Table K.7 – Error analysis of particle size measurements made using the sieve method.

	Sieve No.	Grain Size	Mean fraction by weight	Std Dev	Coefficient of Variation
sample 1	5	pebbles	0.037	0.0007	0.0194
	10	granules	0.031	0.0003	0.0123
	18	VC sand	0.075	0.0016	0.0215
	35	C sand	0.275	0.0037	0.0135
	60	M sand	0.338	0.0023	0.0068
	140	F sand	0.195	0.0049	0.0253
	270	VF sand	0.032	0.0022	0.0686
	Bottom	Silt & clay	0.0135	0.0011	0.0881
			Average all sieves	**0.0021**	**0.0319**
sample 2					
	5	pebbles	0.028	0.0028	0.0984
	10	granules	0.032	0.0002	0.0065
	18	VC sand	0.076	0.0009	0.0125
	35	C sand	0.275	0.0006	0.0024
	60	M sand	0.340	0.0014	0.0042
	140	F sand	0.198	0.0030	0.0154
	270	VF sand	0.034	0.0012	0.0364
	Bottom	Silt & clay	0.014	0.0008	0.0561
			Average all sieves	**0.0014**	**0.0290**

Table K.8 – Repeatability test data for measurements of porosity, moisture content at 1 bar pressures, and electrical resistivity.

Test #	Sample ID	dry samp wt w/ring (g)	wet samp wt w/ring (g)	porosity	Bulk density (g/cc)	ring wt w/cloth (g)	Conduct of wetfluid µS/cm	Impedance at saturation (ohms)	resistivity	equilib wt 1 bar pressure	vol mois content	cond of extracted fluid((µS/cm)
1	36	210.5	243.08	0.319	1.742	32.72	815	670.9	40.254	213.11	0.026	1120
2	36	210.5	245.53	0.343	1.742	32.72	786	620	37.2	213.86	0.033	1060
3	36	210.66	245.08	0.337	1.743	32.72	778	924.4	55.464	213.09	0.024	1241
4	36	209.71	243.51	0.331	1.734	32.72	794	922.9	55.374	213.85	0.041	916
5	36	209.54	243.36	0.331	1.732	32.72	830	843.1	50.586	213.56	0.039	1141
1	37	215.42	248.32	0.322	1.795	32.17	815	709	42.54	219.08	0.036	1120
2	37	215.42	244.93	0.289	1.795	32.17	786	629	37.74	218.65	0.032	1060
3	37	215.09	249.73	0.339	1.792	32.17	778	905.1	54.306	217.71	0.026	1241
4	37	214.46	247.45	0.323	1.786	32.17	794	897.3	53.838	218.38	0.038	916
5	37	214.37	248.15	0.331	1.785	32.17	830	936.8	56.208	218.57	0.041	1141
1	46	213.31	246.68	0.327	1.773	32.3	815	712.5	42.75	217.26	0.039	1120
2	46	213.31	250.09	0.360	1.773	32.3	786	666.6	39.996	217.23	0.038	1060
3	46	213.12	247.43	0.336	1.772	32.3	778	841.8	50.508	215.81	0.026	1241
4	46	211.91	245.96	0.334	1.760	32.3	794	835.1	50.106	215.88	0.039	916
5	46	211.58	244.66	0.324	1.756	32.3	830	1013	60.78	215.99	0.043	1141

Table K.9 – Repeatability data for tension head and moisture content in hanging column experiments.

tension head (cm)	volumetric moisture content (ml/ml)	volumetric moisture content (ml/ml)	volumetric moisture content (ml/ml)	volumetric moisture content (ml/ml)	volumetric moisture content (ml/ml)
	sample 2	sample 4	sample 6	sample 8	sample 1
0	0.429	0.436	0.436	0.435	0.437
10	0.407	0.411	0.399	0.410	0.410
20	0.403	0.406	0.395	0.404	0.406
30	0.400	0.403	0.394	0.400	0.402
40	0.368	0.402	0.374	0.381	0.381
50	0.325	0.323	0.319	0.324	0.309
100	0.081	0.075	0.075	0.079	0.076
200	0.048	0.047	n/a	0.047	0.053

Table K.10 – Repeatability data for hydraulic conductivity measurements in constant head permeameter device.

run		samp A	samp B	samp C	samp D	population mean	population stdev	population Coeff of Variation
1	dH	54.6	54.5	54.5	54.5			
	time (sec)	20	20	20	20			
	vol (cm^3)	7	6	7	5			
	Ksat(cm/s)	1.23E-03	1.05E-03	1.26E-03	8.77E-04	1.10E-03	1.77E-04	1.60E-01
2	dH	54.8	54.5	54.5	54.5			
	time (sec)	20	20	20	20			
	vol (cm^3)	7	6	7	5			
	Ksat(cm/s)	1.22E-03	1.05E-03	1.26E-03	8.77E-04	1.10E-03	1.76E-04	1.59E-01
3	dH	54.9	54.5	54.5	54.5			
	time (sec)	20	20	20	20			
	vol (cm^3)	6	6	7	5			
	Ksat(cm/s)	1.04E-03	1.05E-03	1.26E-03	8.77E-04	1.06E-03	1.57E-04	1.49E-01
4	dH	54.9	54.5	54.5	54.5			
	time (sec)	20	20	20	20			
	vol (cm^3)	7	6	6	5			
	Ksat(cm/s)	1.22E-03	1.05E-03	1.08E-03	8.77E-04	1.06E-03	1.40E-04	1.33E-01
5	dH	54.9	54.5	54.5	54.5			
	time (sec)	20	20	20	20			
	vol (cm^3)	6	6	6	5			
	Ksat(cm/s)	1.04E-03	1.05E-03	1.08E-03	8.77E-04	1.01E-03	9.26E-05	9.13E-02
6	dH	55	54.5	54.5	54.5			
	time (sec)	20	20	20	20			
	vol (cm^3)	6	6	6	5			
	Ksat(cm/s)	1.04E-03	1.05E-03	1.08E-03	8.77E-04	1.01E-03	9.24E-05	9.12E-02
7	dH	55	54.5	54.5	54.5			
	time (sec)	20	20	20	20			
	vol (cm^3)	6	6	6	5			
	Ksat(cm/s)	1.04E-03	1.05E-03	1.08E-03	8.77E-04	1.01E-03	9.24E-05	9.12E-02
8	dH	55	54.5	54.5	54.5			
	time (sec)	20	20	20	20			
	vol (cm^3)	6	6	6	5			
	Ksat(cm/s)	1.04E-03	1.05E-03	1.08E-03	8.77E-04	1.01E-03	9.24E-05	9.12E-02
9	dH	55	54.5	54.5	54.5			
	time (sec)	20	20	20	20			
	vol (cm^3)	6	6	6	5			
	Ksat(cm/s)	1.04E-03	1.05E-03	1.08E-03	8.77E-04	1.01E-03	9.24E-05	9.12E-02
10	dH	55	54.5	54.5	54.5			
	time (sec)	20	20	20	20			
	vol (cm^3)	6	6	6	5			
	Ksat(cm/s)	1.04E-03	1.05E-03	1.08E-03	8.77E-04	1.01E-03	9.24E-05	9.12E-02

Table K.11 – Repeatability data for particle size analysis measurements using dry sieve method.

.	Sieve No.	Grain Size	Wt Sieve + sample	Sieve Wt (g) .	Sample Wt. (g)	% grain size by weight
sample1						
run 1	5	pebbles	529	496.8	32.2	0.0383
	10	granules	499	472.2	26.8	0.0319
	18	VC sand	528.3	462.9	65.4	0.0778
	35	C sand	686.5	449.7	236.8	0.2819
	60	M sand	680.7	392.8	287.9	0.3427
	140	F sand	529.4	372.15	157.25	0.1872
	270	VF sand	388.4	364.2	24.2	0.0288
	Bottom	Silt & clay	398.6	389	9.6	0.0114
				total	840.15	1.0000
run 2	5	pebbles	528.4	496.8	31.6	0.0376
	10	granules	498.3	472.2	26.1	0.0311
	18	VC sand	526.7	462.9	63.8	0.0759
	35	C sand	680.1	449.7	230.4	0.2743
	60	M sand	677.8	392.8	285	0.3393
	140	F sand	536.7	372.15	164.55	0.1959
	270	VF sand	391.4	364.2	27.2	0.0324
	Bottom	Silt & clay	400.4	389	11.4	0.0136
					Total %	1.00
run 3	5	pebbles	528.3	496.8	31.5	0.0375
	10	granules	498.2	472.2	26	0.0309
	18	VC sand	525.9	462.9	63	0.0750
	35	C sand	679.1	449.7	229.4	0.2730
	60	M sand	676.8	392.8	284	0.3380
	140	F sand	538.4	372.15	166.25	0.1979
	270	VF sand	392.4	364.2	28.2	0.0336
	Bottom	Silt & clay	400.87	389	11.87	0.0141
					Total %	1.00
run 4	5	pebbles	527.6	496.8	30.8	0.0367
	10	granules	498.7	472.2	26.5	0.0316
	18	VC sand	525.3	462.9	62.4	0.0744
	35	C sand	679	449.7	229.3	0.2733
	60	M sand	675.9	392.8	283.1	0.3374
	140	F sand	538.6	372.15	166.45	0.1984
	270	VF sand	392.7	364.2	28.5	0.0340
	Bottom	Silt & clay	400.9	389	11.9	0.0142
					Total %	1.00
run 5	5	pebbles	527.4	496.8	30.6	0.0365
	10	granules	498.5	472.2	26.3	0.0314
	18	VC sand	524.6	462.9	61.7	0.0737
	35	C sand	679	449.7	229.3	0.2737
	60	M sand	674.9	392.8	282.1	0.3368
	140	F sand	539.2	372.15	167.05	0.1994
	270	VF sand	392.9	364.2	28.7	0.0343
	Bottom	Silt & clay	400.9	389	11.9	0.0142
					Total %	1.00

Table K.11 – (continued).

.	Sieve No.	Grain Size	Wt Sieve + sample	Sieve Wt (g) .	Sample Wt. (g)	% grain size by weight
sample 2	5	pebbles	524.4	496.8	27.6	0.0335
run 6	10	granules	499	472.2	26.8	0.0325
	18	VC sand	526.9	462.9	64	0.0777
	35	C sand	676.9	449.7	227.2	0.2757
	60	M sand	674.6	392.8	281.8	0.3419
	140	F sand	531.6	372.15	159.45	0.1935
	270	VF sand	390.5	364.2	26.3	0.0319
	Bottom	Silt & clay	400	389	11	0.0133
					Total %	1.00
run 7	5	pebbles	519.5	496.8	22.7	0.0277
	10	granules	498.4	472.2	26.2	0.0320
	18	VC sand	525.7	462.9	62.8	0.0767
	35	C sand	674.3	449.7	224.6	0.2742
	60	M sand	672.95	392.8	280.15	0.3420
	140	F sand	535	372.15	162.85	0.1988
	270	VF sand	392	364.2	27.8	0.0339
	Bottom	Silt & clay	401	389	12	0.0147
					Total %	1.00
run 8	5	pebbles	519.3	496.8	22.5	0.0275
	10	granules	498.5	472.2	26.3	0.0321
	18	VC sand	525	462.9	62.1	0.0759
	35	C sand	674.2	449.7	224.5	0.2744
	60	M sand	671.5	392.8	278.7	0.3406
	140	F sand	535.5	372.15	163.35	0.1997
	270	VF sand	392.5	364.2	28.3	0.0346
	Bottom	Silt & clay	401.4	389	12.4	0.0152
					Total %	1.00
run 9	5	pebbles	518.9	496.8	22.1	0.0270
	10	granules	498.7	472.2	26.5	0.0324
	18	VC sand	524.8	462.9	61.9	0.0757
	35	C sand	674.5	449.7	224.8	0.2750
	60	M sand	669.8	392.8	277	0.3388
	140	F sand	536.6	372.15	164.45	0.2011
	270	VF sand	392.5	364.2	28.3	0.0346
	Bottom	Silt & clay	401.5	389	12.5	0.0153
					Total %	1.00
run 10	5	pebbles	518.7	496.8	21.9	0.0268
	10	granules	498.5	472.2	26.3	0.0322
	18	VC sand	524.3	462.9	61.4	0.0752
	35	C sand	674.7	449.7	225	0.2755
	60	M sand	669.9	392.8	277.1	0.3394
	140	F sand	535.9	372.15	163.75	0.2005
	270	VF sand	392.8	364.2	28.6	0.0350
	Bottom	Silt & clay	401.5	389	12.5	0.0153
					Total %	1.00

Appendix L

Haverkamp and Parlange Estimation Model Calibration to the STVZ Alluvial Sand Deposits

L.1 Introduction

MATHCAD was used to calibrate the Haverkamp and Parlange estimation model to the STVZ site deposits through regression analysis of parameters. Moisture retention and particle size distribution fitting parameters of samples used in calibration were obtained by plotting functional forms to measured data. Appendix J describes the curve fitting procedures.

The estimation equation for the particle index (λ) was determined by plotting the ratio of the pore-size distribution slope to the particle-size distribution slope versus sample dry bulk density. Samples excluded from calibration were extreme outliers in the regression analysis. The anomalous relationship between parameters for these samples may have been due to a high degree of measurement error and/or model error associated with the original Brooks and Corey equation and van Genuchten equation fits to data. Microsoft Excel® was used to fit a power law curve to the data. The equation coefficients were denoted *ex1* and *ex2* representing values for a1 and a2 respectively in the original model. The packing parameter (γ) was also determined from regression analysis of the plot of calculated γ versus the estimated Brooks and Corey fitting parameter λ (estimated from 3-13) . Microsoft Excel® was used to fit a second order polynomial to the data. The fit was verified using a fit command in MATHCAD. Air entry pressure was calculated using the estimated values for the packing parameter and the curve fit determination of d_g (from Equation 3-19). Air entry pressure was also

calculated from the original model estimation equation (Equation 3-14) to determine the appropriate equation for estimating air entry pressure.

Curves were estimated for all the STVZ sandy alluvial using the Brooks and Corey equation for draining sequences (Equations 3-11 and 3-12 assuming saturation is equal to porosity for the PDC). The curves were plotted using the calibrated equations (calibrated fit) and the original model equations (H&P estimate). We include the plot of the original Brooks and Corey fit to data for comparison to the estimated curves.

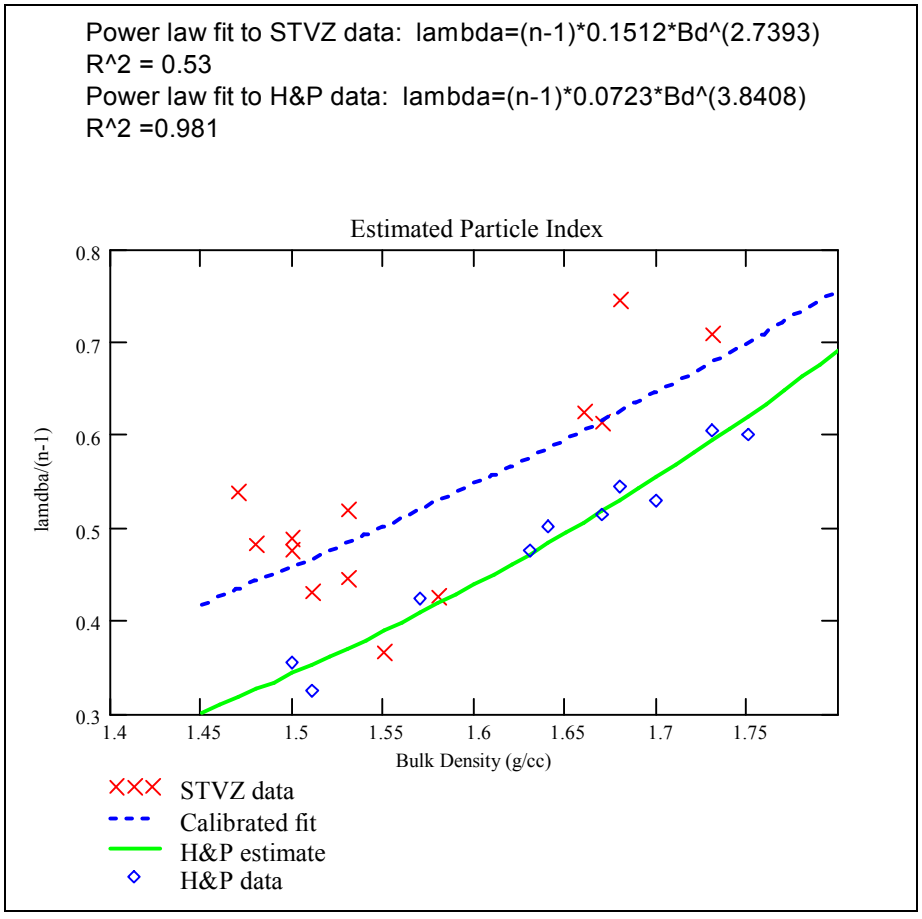

Figure L.1 – Regression analysis for determination of model parameter λ.

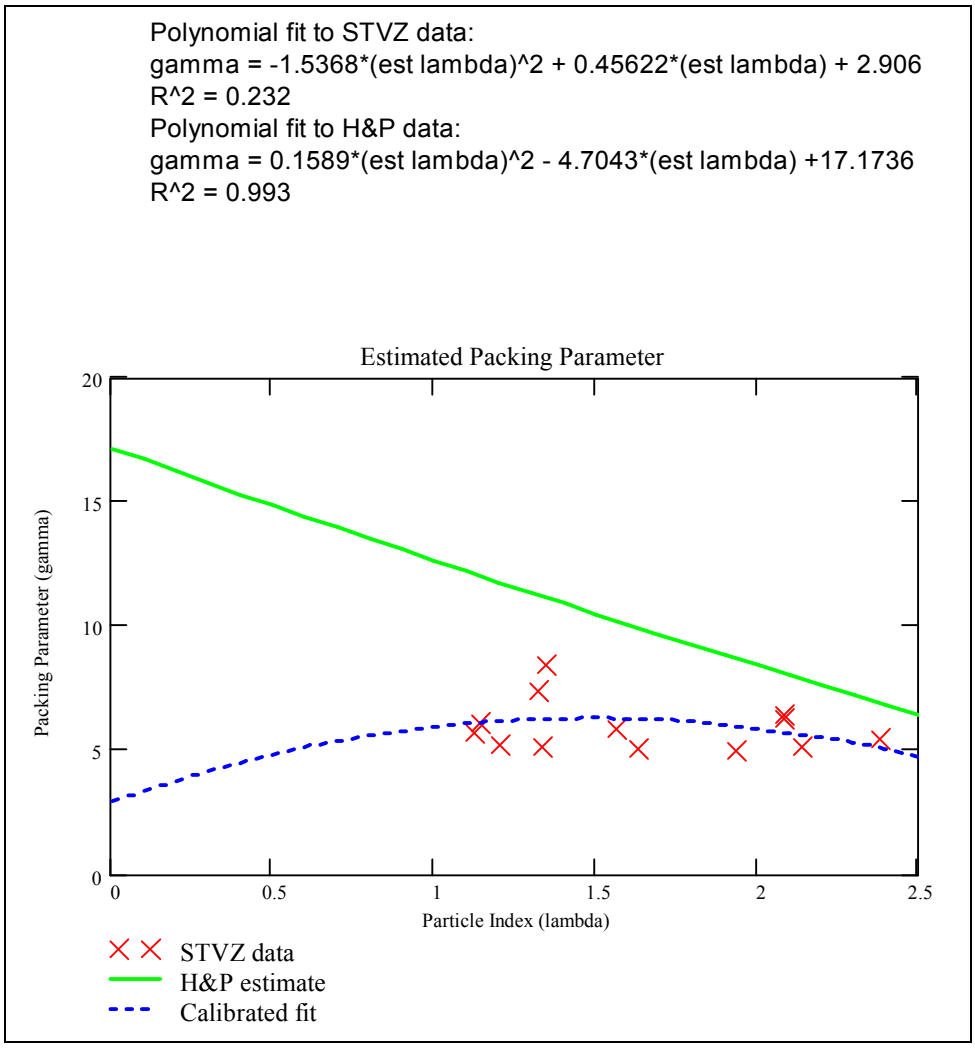

Figure L.2 – Regression analysis to determine the model parameter γ.

Read data from all samples measured in lab:

$alldata := READPRN("input.txt")$

$R := rows(alldata)$ $\quad R = 39$

$r := 1..R$

$hae2_r := alldata_{r,1}$ $\quad n2_r := alldata_{r,3}$ $\quad sat2_r := alldata_{r,5}$ $\quad dg2_r := alldata_{r,7}$

$\mu 2_r := n2_r - 1$

$lam2_r := alldata_{r,2}$ $\quad Bd2_r := alldata_{r,4}$

Estimated parameters for all samples:

$est\lambda_r := (\mu 2_r) \cdot ex1 (Bd2_r)^{ex2}$ $\quad HP\lambda_r := (\mu 2_r) \cdot a1 (Bd2_r)^{a2}$

$est\gamma_r := e1 + e2 \cdot est\lambda_r + e3 \cdot (est\lambda_r)^2$ $\quad HPg_r := b1 + b2 \cdot HP\lambda_r + b3 \cdot (HP\lambda_r)^2$

$m2_r := 1 - \left(\frac{1}{n2_r}\right)$

$\Psi ae1_r := \frac{est\gamma_r \cdot 0.149}{dg2_r \cdot 0.10}$ **Estimated air entry pressure using Laplace Young equation**

Estimated Air Entry Pressure using H&P estimation Equation 32

$\theta ae1_r := \frac{sat2_r}{(1 + HP\lambda_r)}$ $\quad ratio2_r := (1 + HP\lambda_r)^{\left(\frac{-1}{HP\lambda_r}\right)}$

$T3est_r := \left(\frac{\theta ae1_r}{sat2_r}\right)^{-\left(\frac{1}{m2_r}\right)}$ $\quad T2_r := \frac{0.149}{dg2_r \cdot 0.10}$

$\Psi ae2_r := HPg_r \cdot (T2_r) \cdot \left[(T3est_r - 1)^{-\left(\frac{1}{n2_r}\right)} \right] \cdot ratio2_r$

Figure L.3 – Model application to the STVZ samples to estimate moisture retention curves.

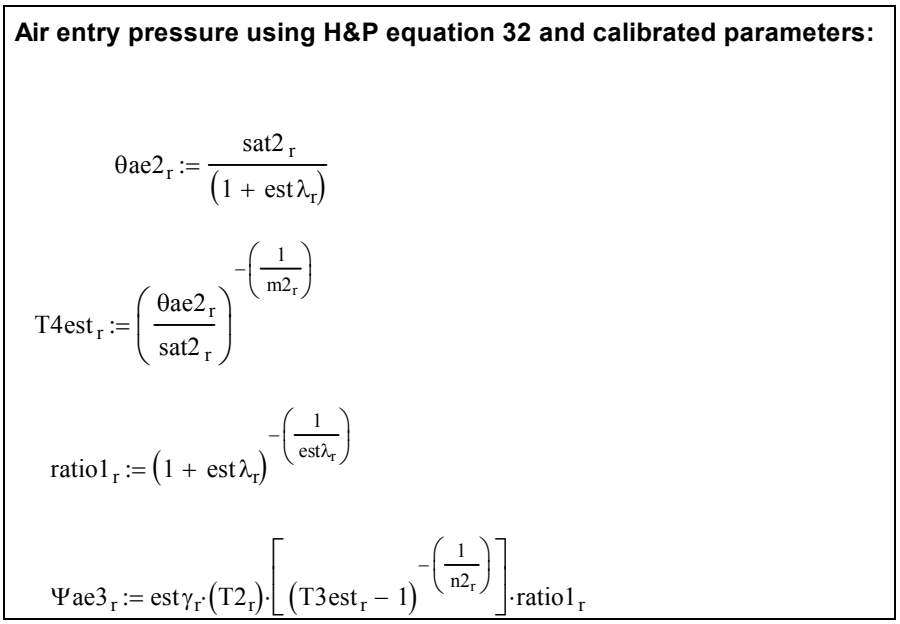

Figure L.4 – Model application to the STVZ samples to estimate moisture retention curves.

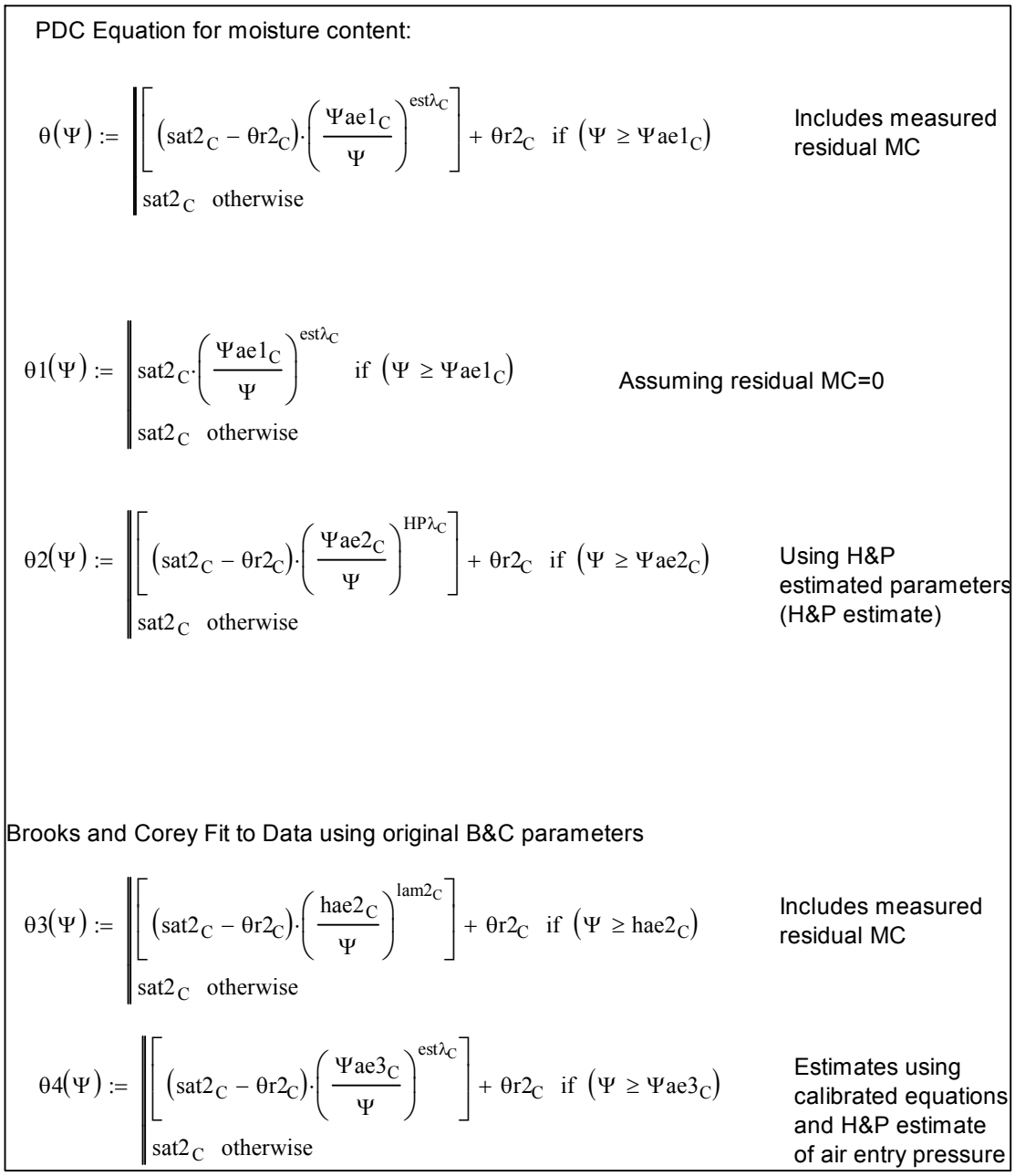

Figure L.5 – Model estimation equations for moisture content using modified version of Brooks and Corey equation.

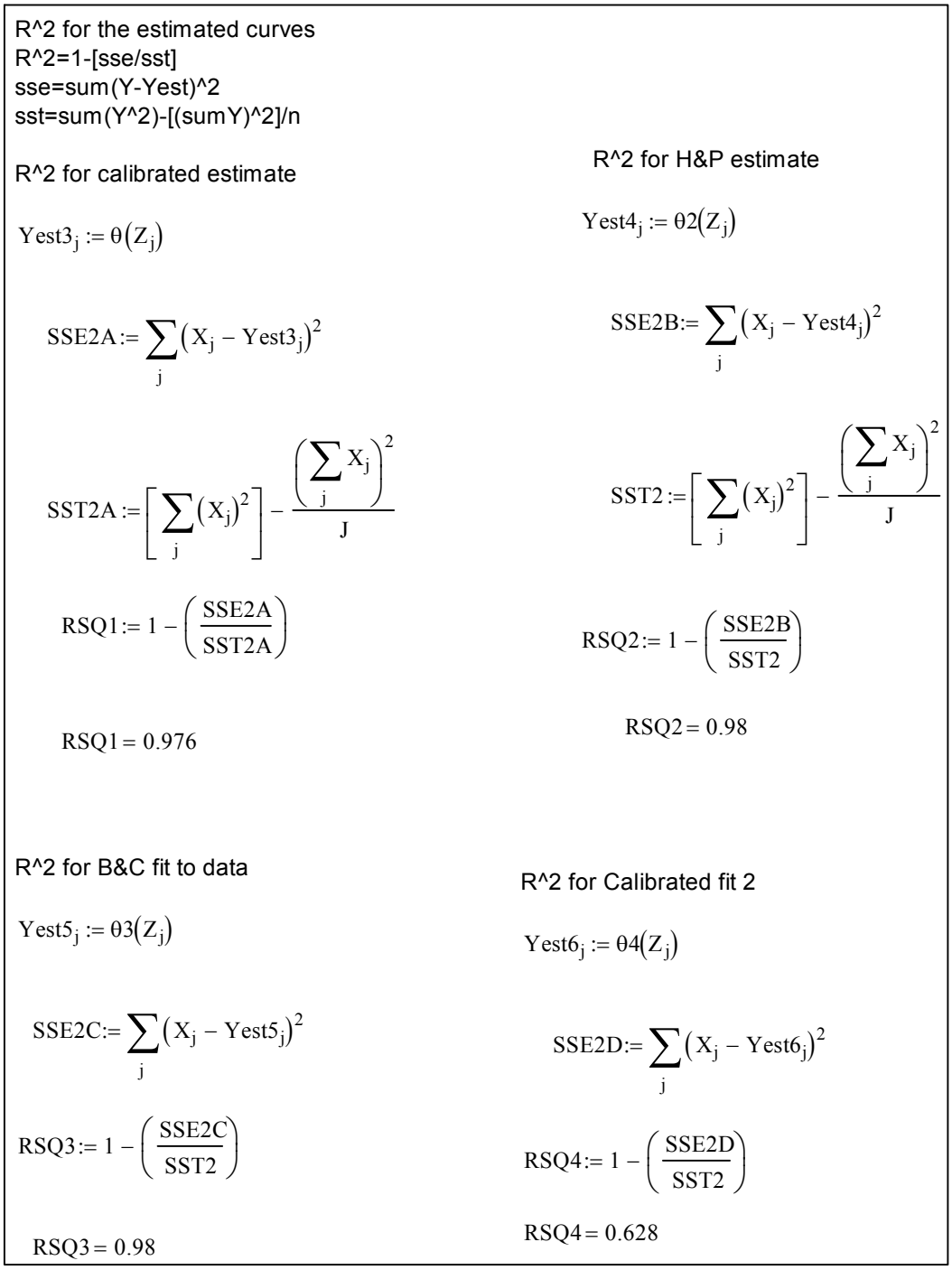

Figure L.6 – Calculation of the coefficient of determination for model estimates of moisture content..

L.2 Original Brooks and Corey fits to STVZ measured data.

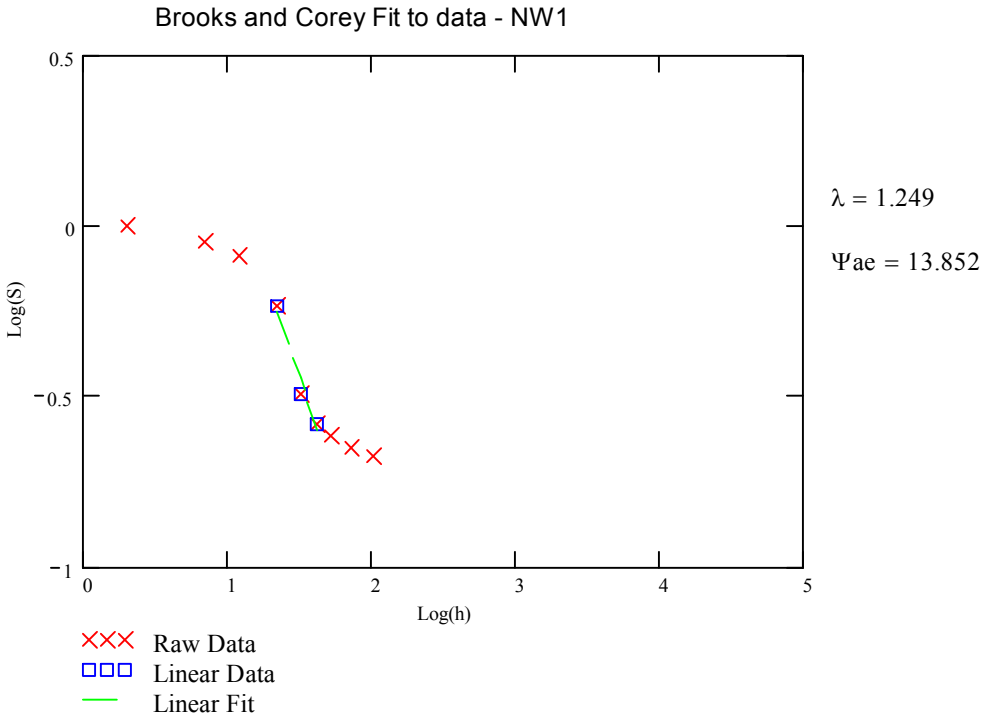

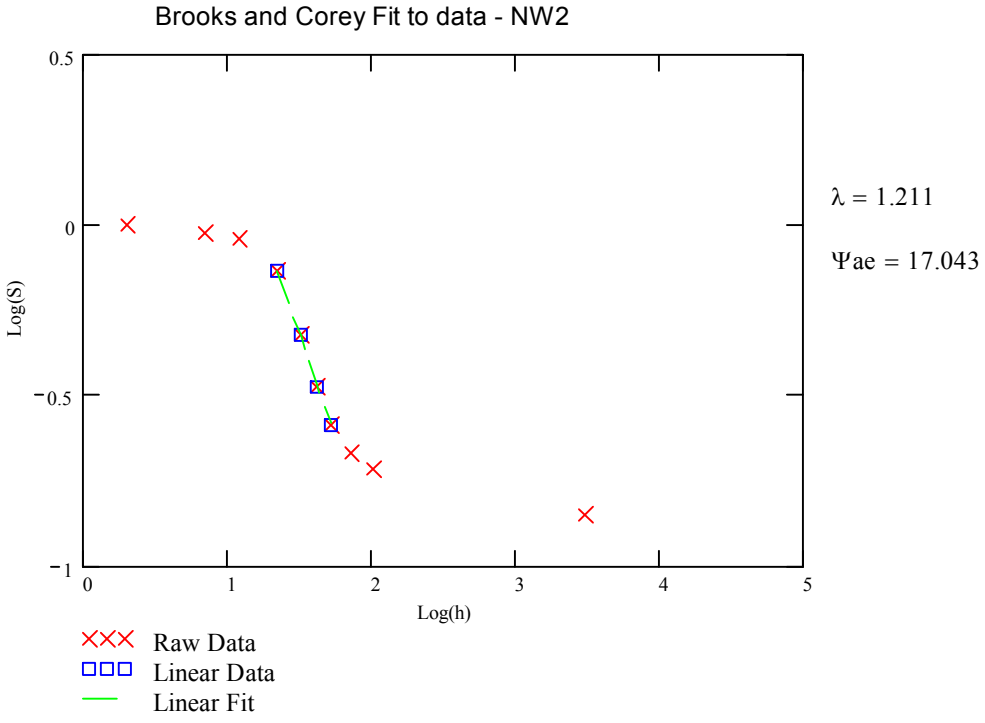

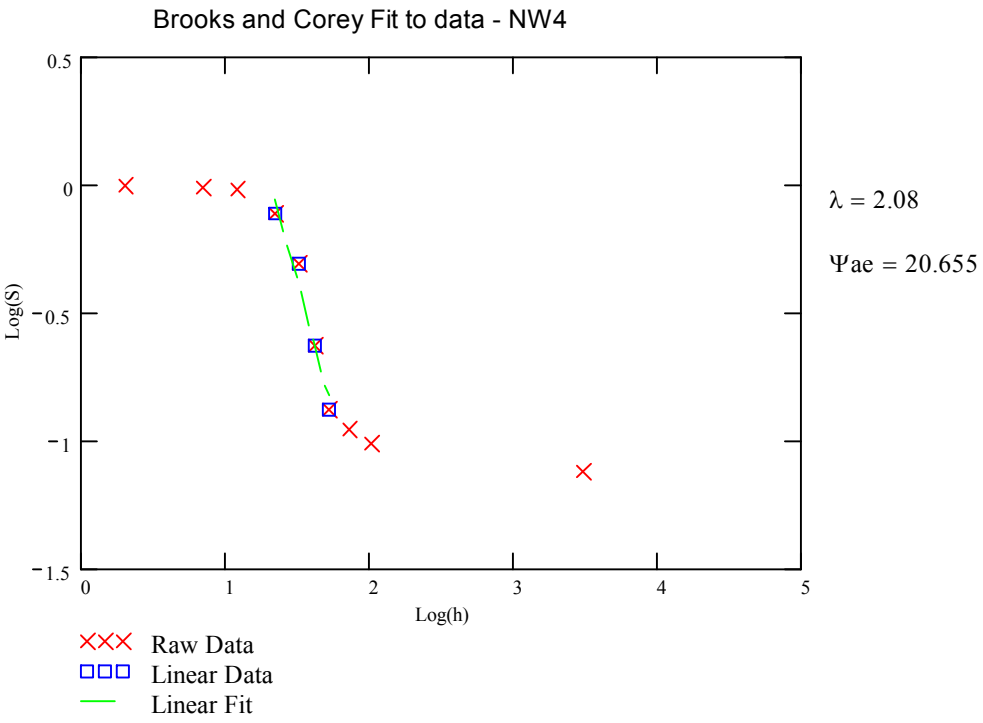
Brooks and Corey Fit to data - NW4
0.5
0
-0.5
-1
-1.5
Log(S)
0
1
2
3
4
5
Log(h)
Raw Data
Linear Data
Linear Fit
λ = 2.08
Ψae = 20.655

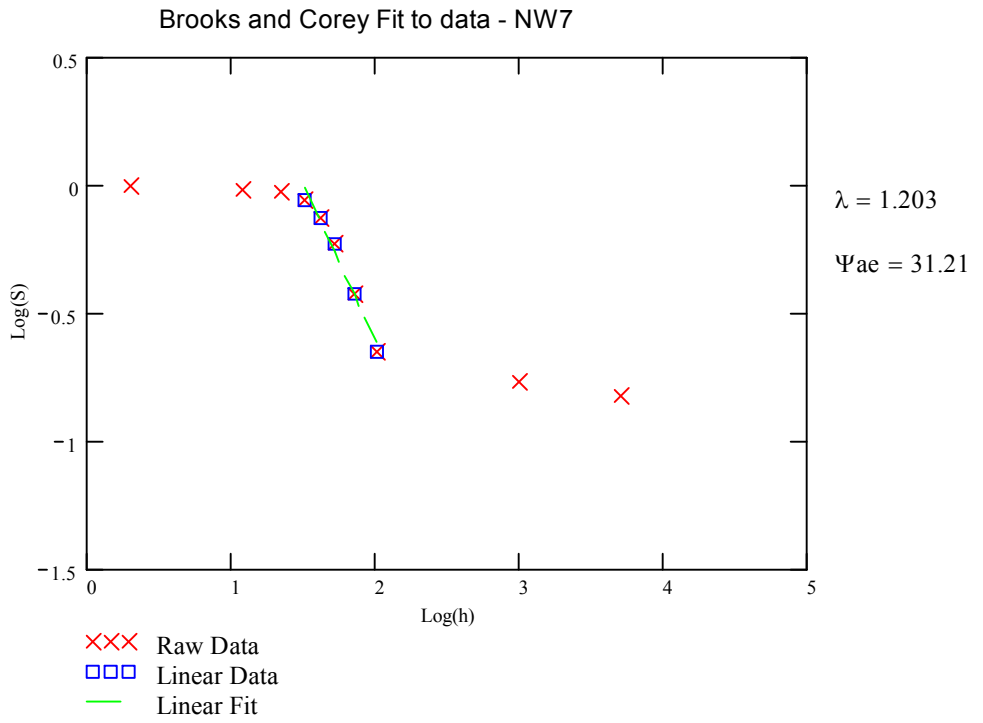
Brooks and Corey Fit to data - NW7
0.5
0
-0.5
-1
-1.5
Log(S)
0
1
2
3
4
5
Log(h)
Raw Data
Linear Data
Linear Fit
λ = 1.203
Ψae = 31.21

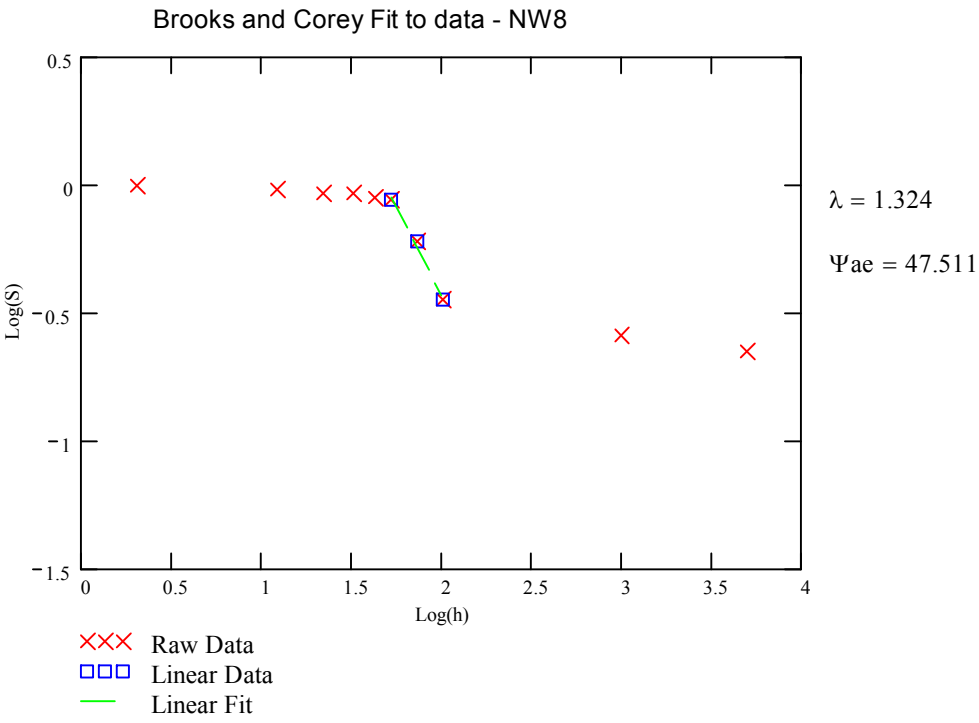
Brooks and Corey Fit to data - NW8
0.5
0
−0.5
−1
−1.5
Log(S)
0
0.5
1
1.5
2
2.5
3
3.5
4
Log(h)
λ = 1.324
Ψae = 47.511
Raw Data
Linear Data
Linear Fit

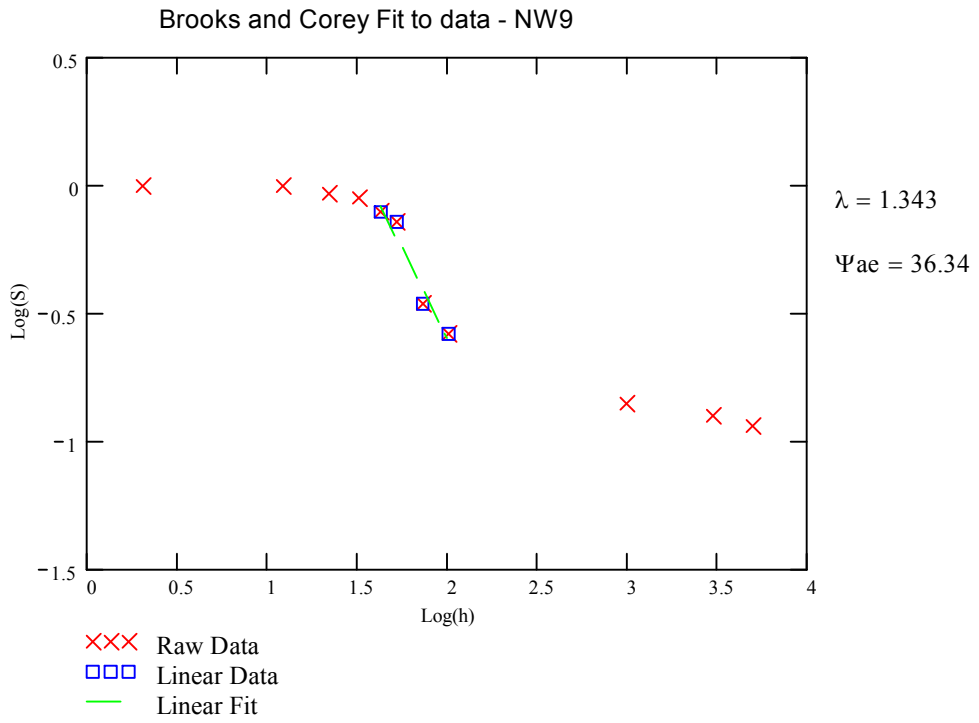
Brooks and Corey Fit to data - NW9
0.5
0
−0.5
−1
−1.5
Log(S)
0
0.5
1
1.5
2
2.5
3
3.5
4
Log(h)
λ = 1.343
Ψae = 36.34
Raw Data
Linear Data
Linear Fit

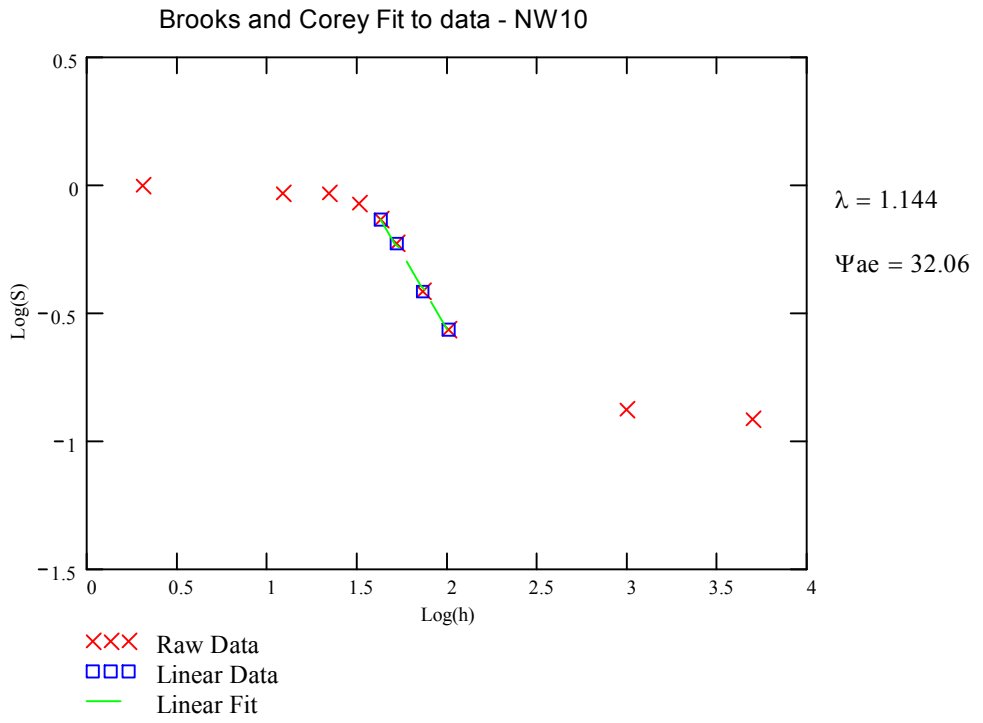
Brooks and Corey Fit to data - NW10
0.5
0
−0.5
−1
−1.5
Log(S)
0
0.5
1
1.5
2
2.5
3
3.5
4
Log(h)
λ = 1.144
Ψae = 32.06
Raw Data
Linear Data
Linear Fit

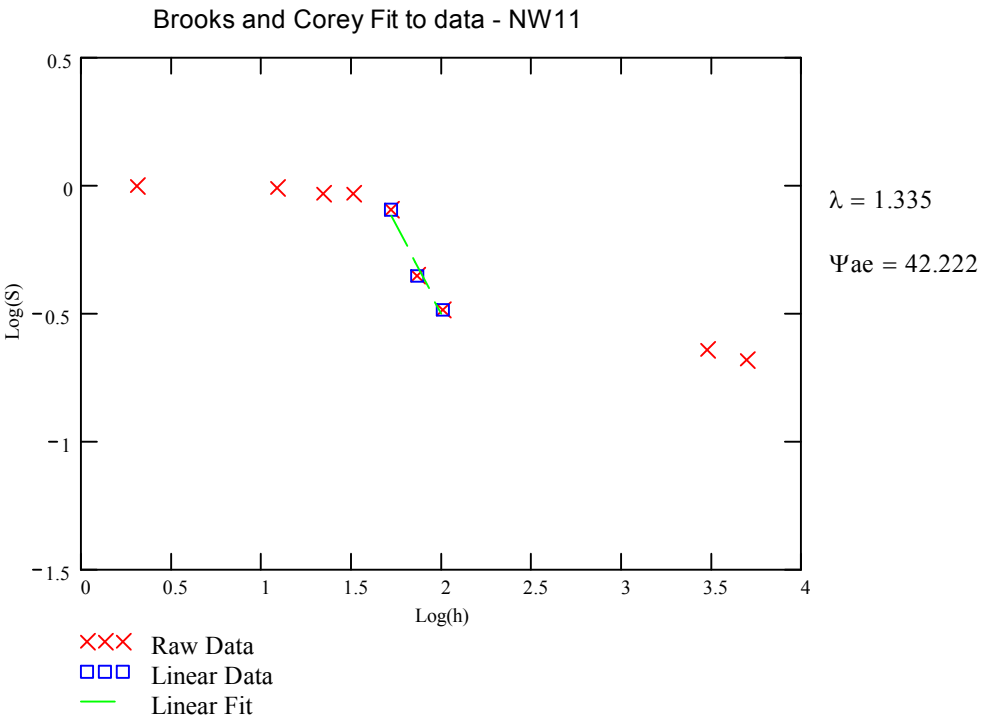
Brooks and Corey Fit to data - NW11
0.5
0
−0.5
−1
−1.5
Log(S)
0
0.5
1
1.5
2
2.5
3
3.5
4
Log(h)
λ = 1.335
Ψae = 42.222
Raw Data
Linear Data
Linear Fit

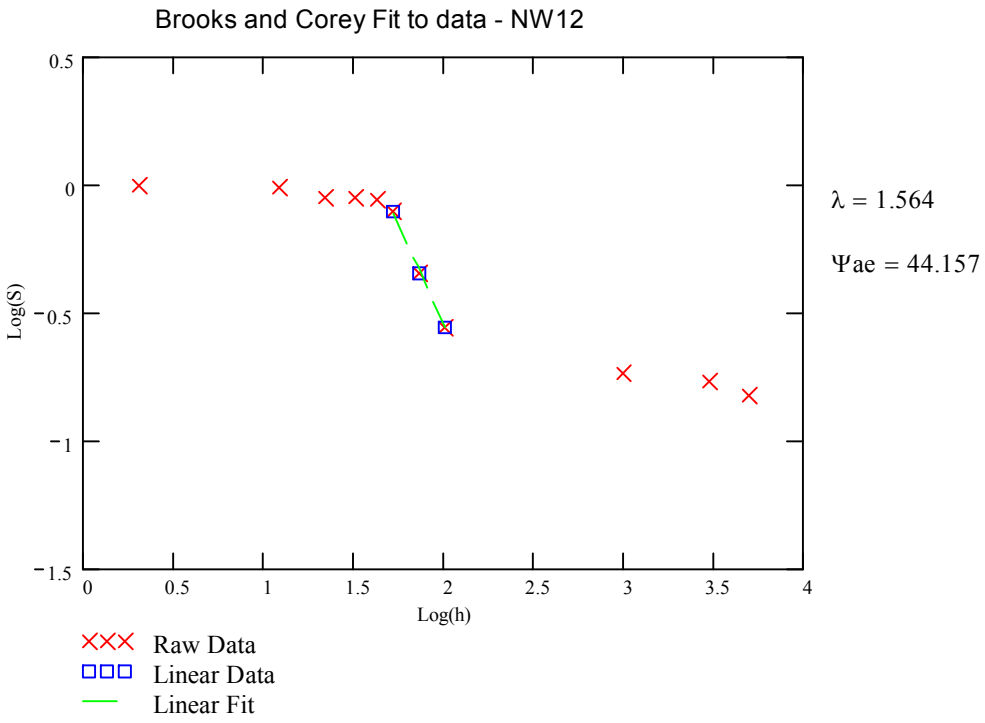
Brooks and Corey Fit to data - NW12
0.5
0
-0.5
-1
-1.5
Log(S)
0
0.5
1
1.5
2
2.5
3
3.5
4
Log(h)
Raw Data
Linear Data
Linear Fit
λ = 1.564
Ψae = 44.157

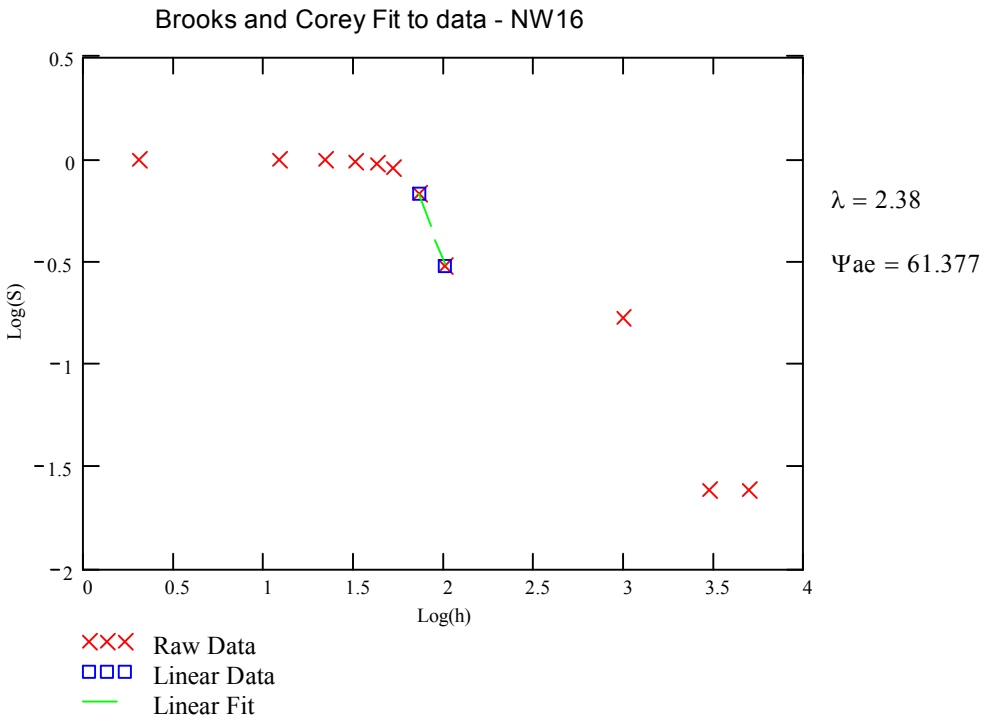
Brooks and Corey Fit to data - NW16
0.5
0
-0.5
-1
-1.5
-2
Log(S)
0
0.5
1
1.5
2
2.5
3
3.5
4
Log(h)
Raw Data
Linear Data
Linear Fit
λ = 2.38
Ψae = 61.377

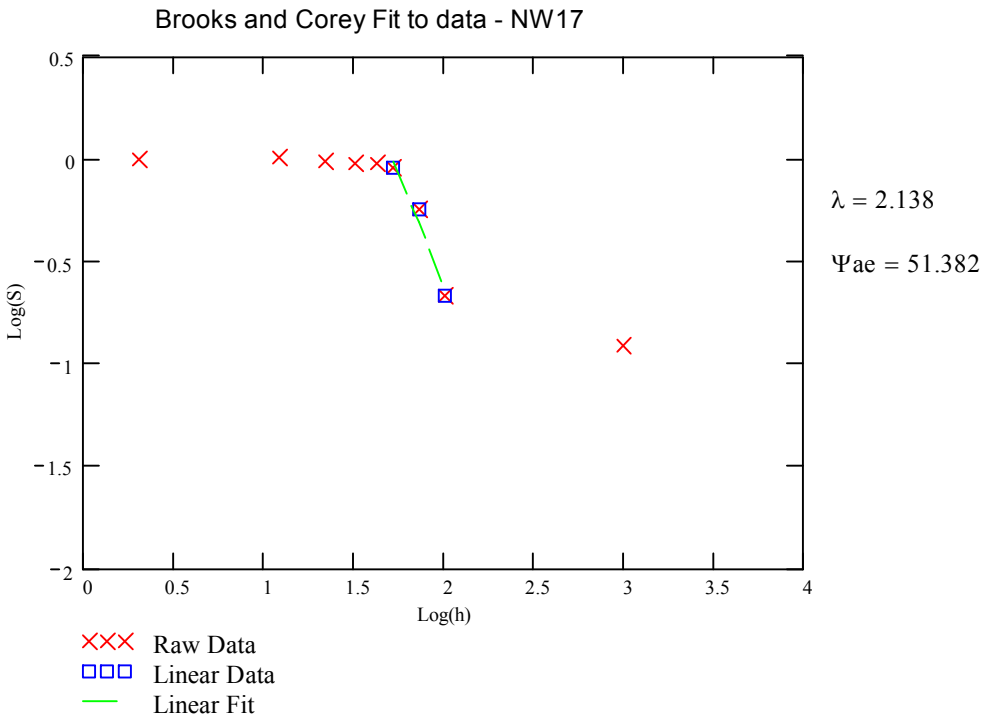
Brooks and Corey Fit to data - NW17
0.5
0
-0.5
-1
-1.5
-2
Log(S)
0
0.5
1
1.5
2
2.5
3
3.5
4
Log(h)
Raw Data
Linear Data
Linear Fit
λ = 2.138
Ψae = 51.382

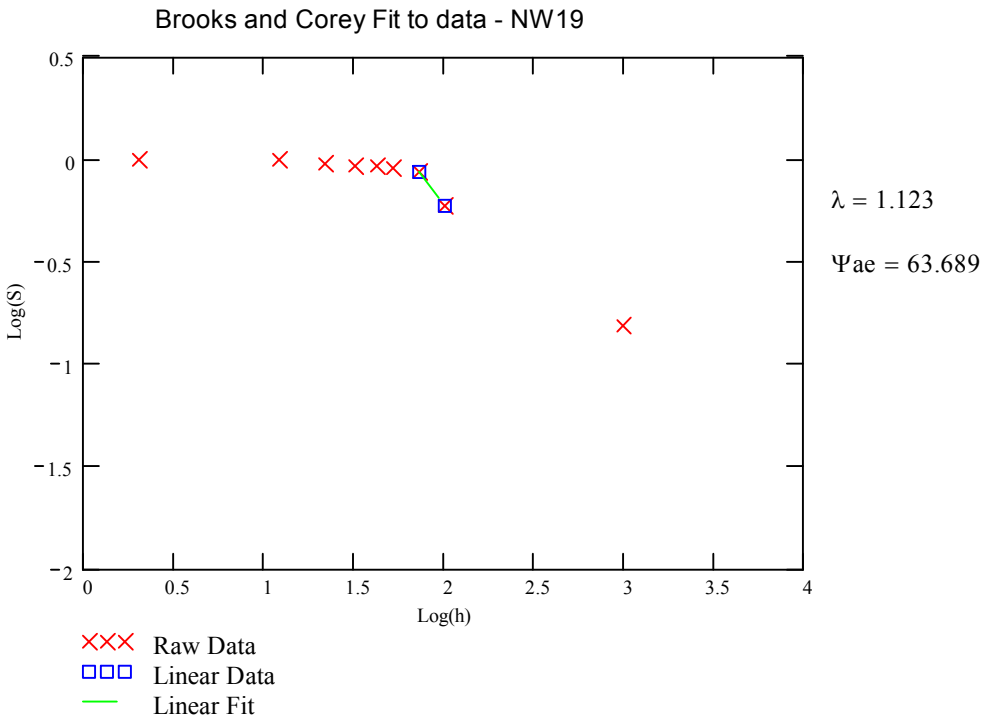
Brooks and Corey Fit to data - NW19
0.5
0
-0.5
-1
-1.5
-2
Log(S)
0
0.5
1
1.5
2
2.5
3
3.5
4
Log(h)
Raw Data
Linear Data
Linear Fit
λ = 1.123
Ψae = 63.689

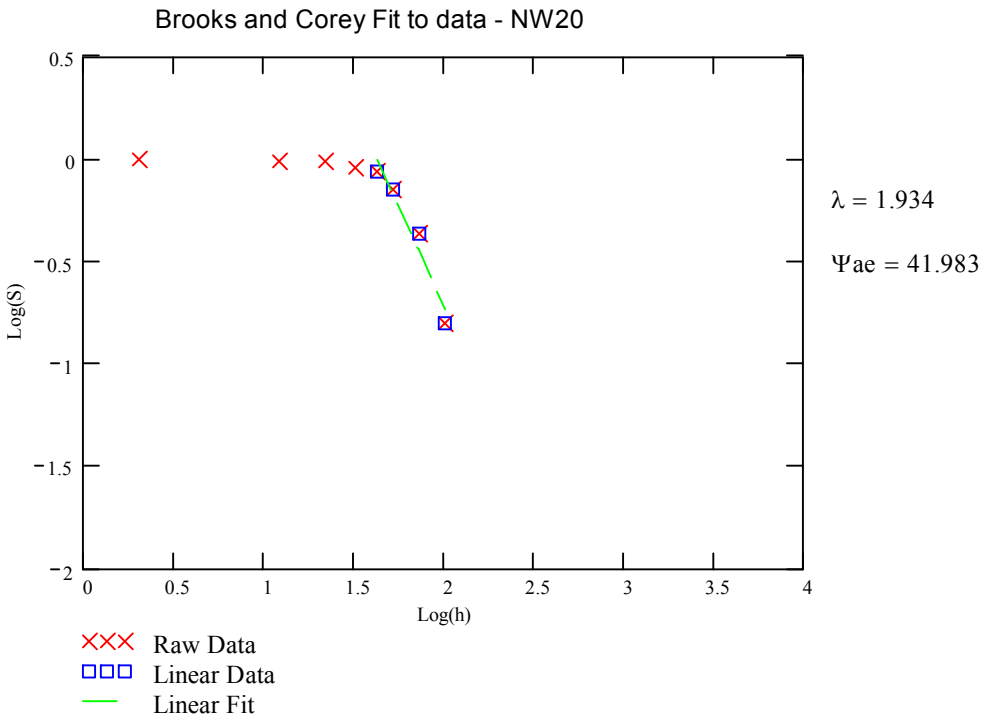
Brooks and Corey Fit to data - NW20
0.5
0
−0.5
−1
−1.5
−2
Log(S)
0
0.5
1
1.5
2
2.5
3
3.5
4
Log(h)
Raw Data
Linear Data
Linear Fit
λ = 1.934
Ψae = 41.983

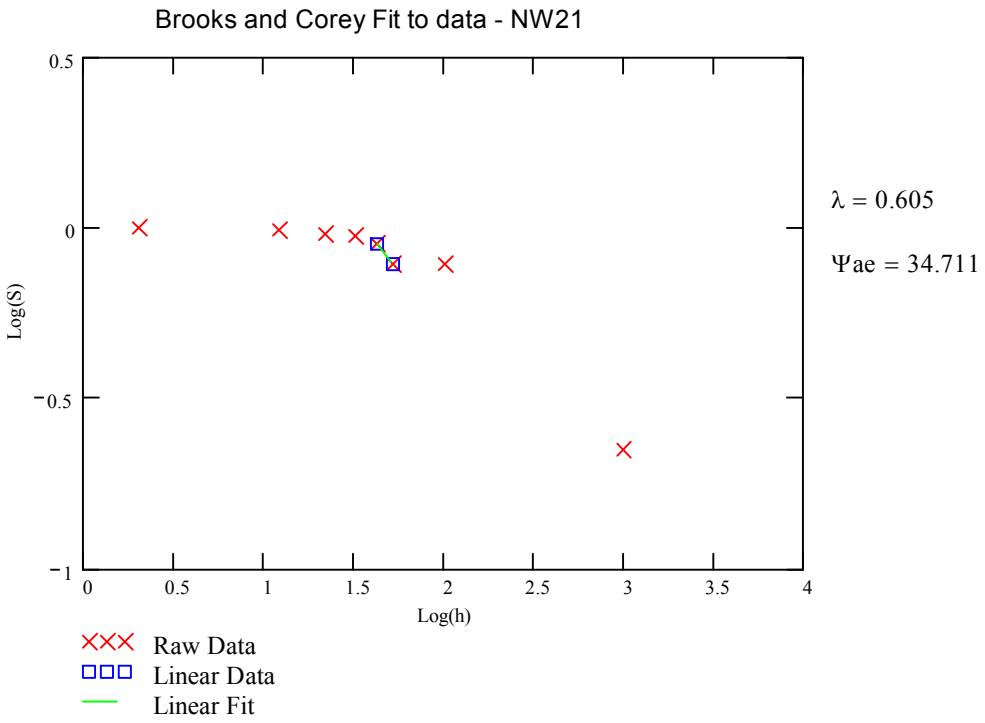
Brooks and Corey Fit to data - NW21
0.5
0
−0.5
−1
Log(S)
0
0.5
1
1.5
2
2.5
3
3.5
4
Log(h)
Raw Data
Linear Data
Linear Fit
λ = 0.605
Ψae = 34.711

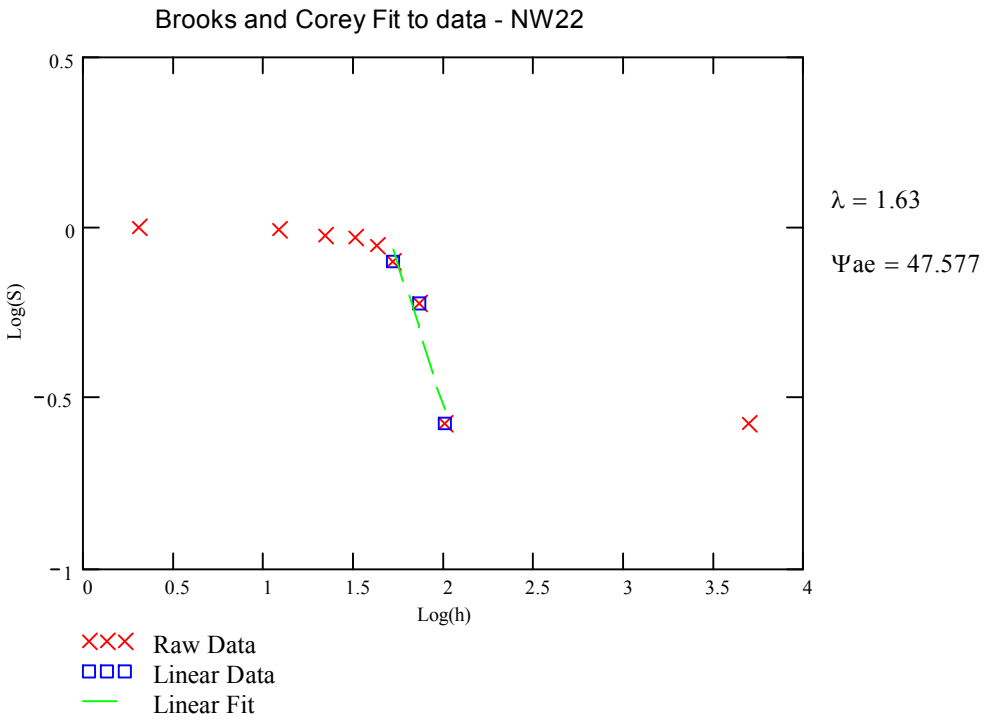
Brooks and Corey Fit to data - NW22
0.5
0
−0.5
−1
Log(S)
0
0.5
1
1.5
2
2.5
3
3.5
4
Log(h)
Raw Data
Linear Data
Linear Fit
λ = 1.63
Ψae = 47.577

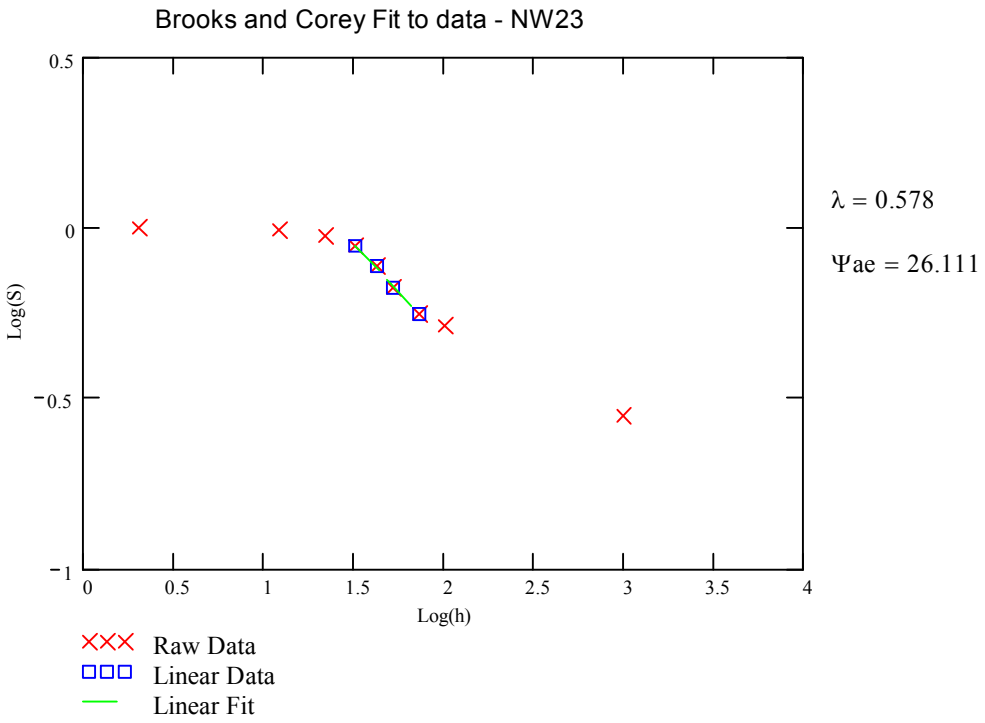
Brooks and Corey Fit to data - NW23
0.5
0
−0.5
−1
Log(S)
0
0.5
1
1.5
2
2.5
3
3.5
4
Log(h)
Raw Data
Linear Data
Linear Fit
λ = 0.578
Ψae = 26.111

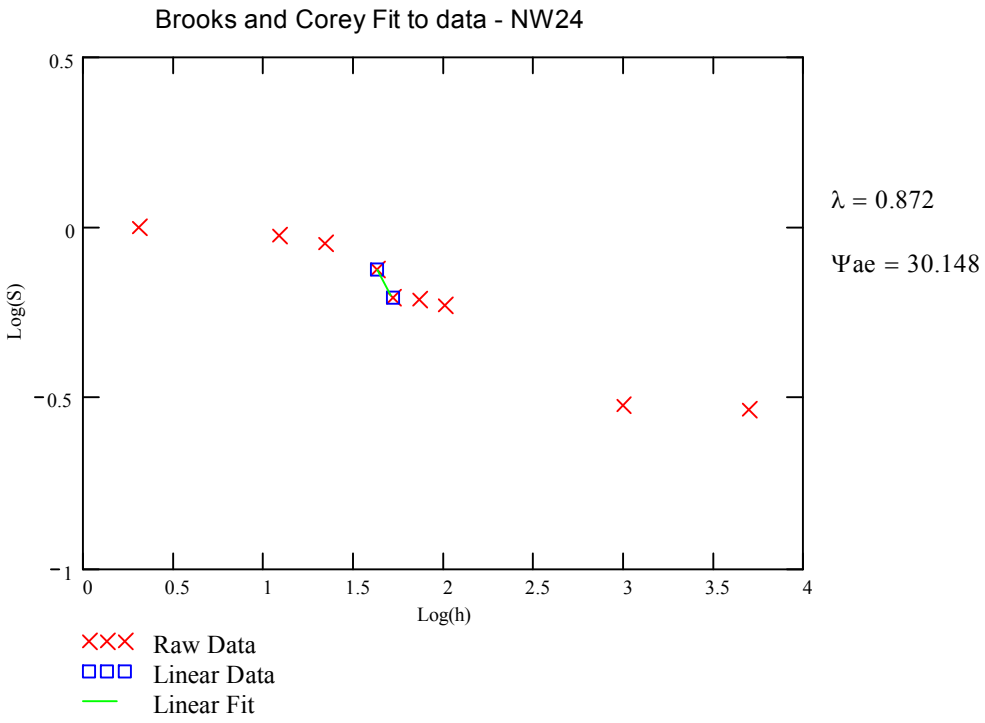
Brooks and Corey Fit to data - NW24
0.5
0
−0.5
−1
Log(S)
0
0.5
1
1.5
2
2.5
3
3.5
4
Log(h)
λ = 0.872
Ψae = 30.148
Raw Data
Linear Data
Linear Fit

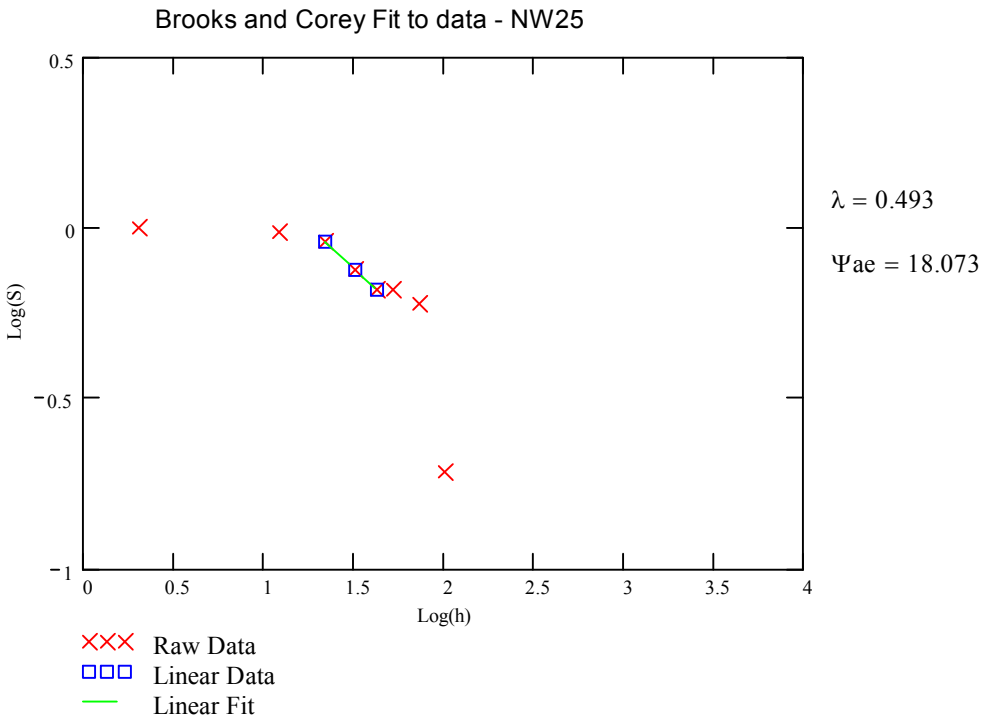
Brooks and Corey Fit to data - NW25
0.5
0
−0.5
−1
Log(S)
0
0.5
1
1.5
2
2.5
3
3.5
4
Log(h)
λ = 0.493
Ψae = 18.073
Raw Data
Linear Data
Linear Fit

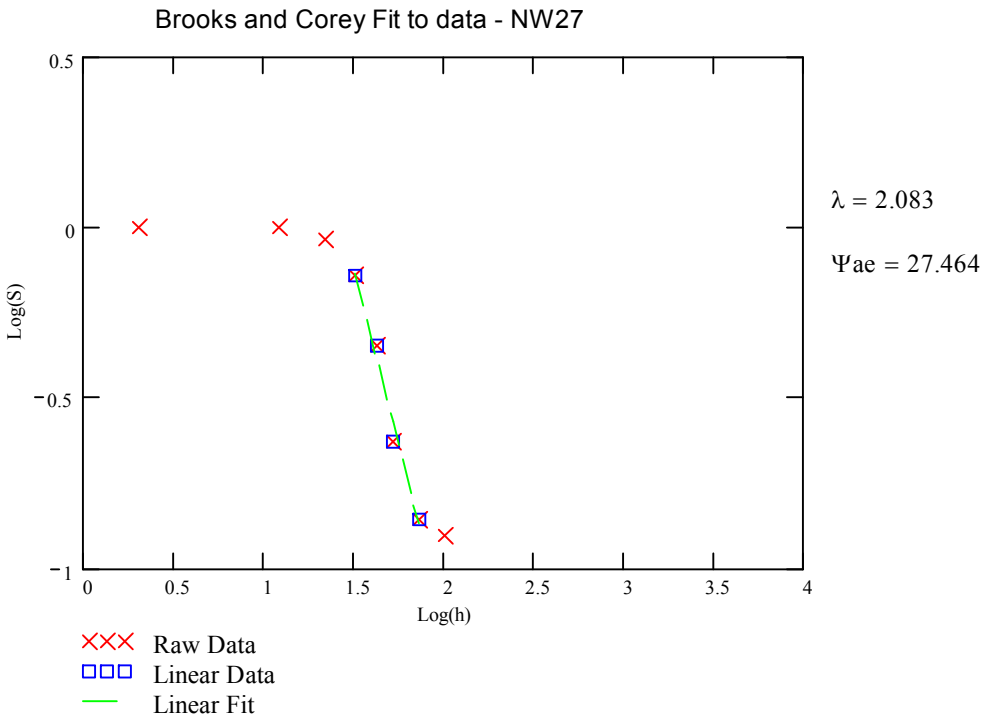
Brooks and Corey Fit to data - NW27
0.5
0
−0.5
−1
Log(S)
0
0.5
1
1.5
2
2.5
3
3.5
4
Log(h)
λ = 2.083
Ψae = 27.464
Raw Data
Linear Data
Linear Fit

Appendix M

Haverkamp and Parlange Estimation Model Results

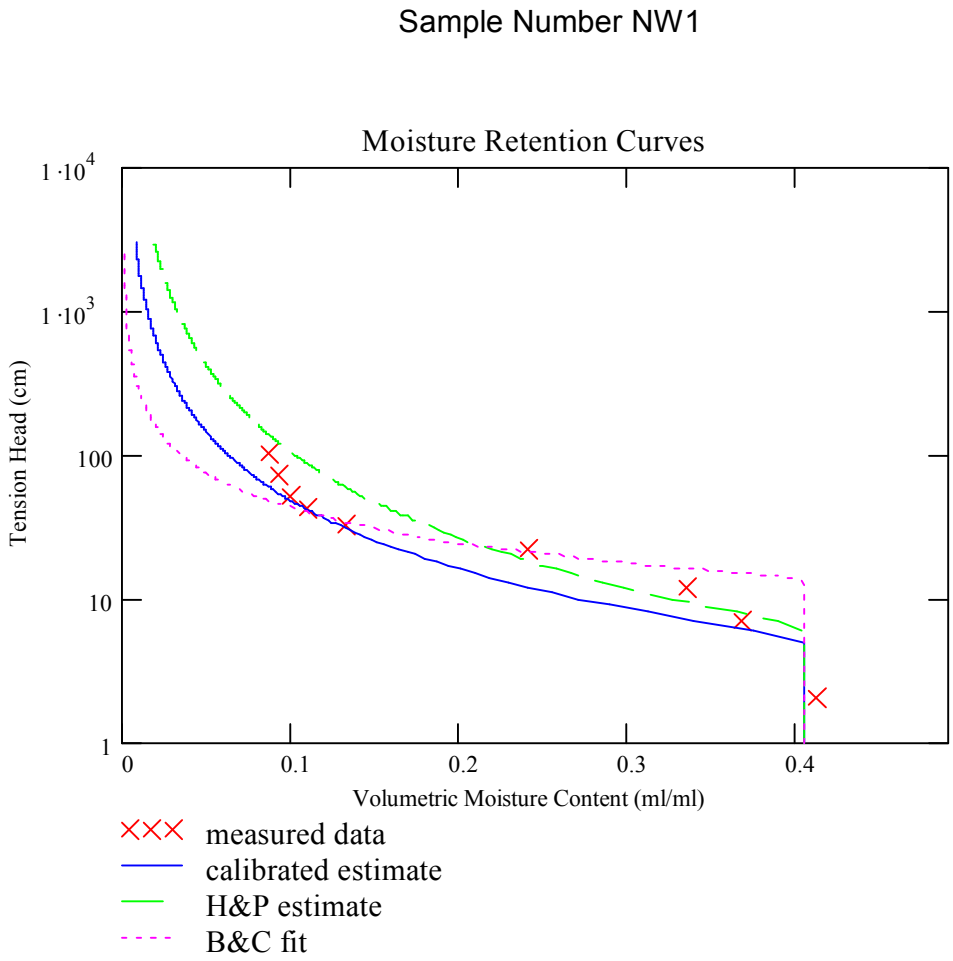

RSQ1 = 0.533
RSQ2 = 0.452
RSQ3 = 0.937

RSQ1= R^2 for calibrated estimate
RSQ2=R^2 for H&P estimate
RSQ3 = R^2 for B&C fit to data

Figure M.1 – Predicted curves versus B&C fit to data – sample NW1. R^2 represents fit to data points not in the very dry or very wet range due to over-saturation in the wet range and lack of hydraulic contact in the dry range.

Sample Number NW2

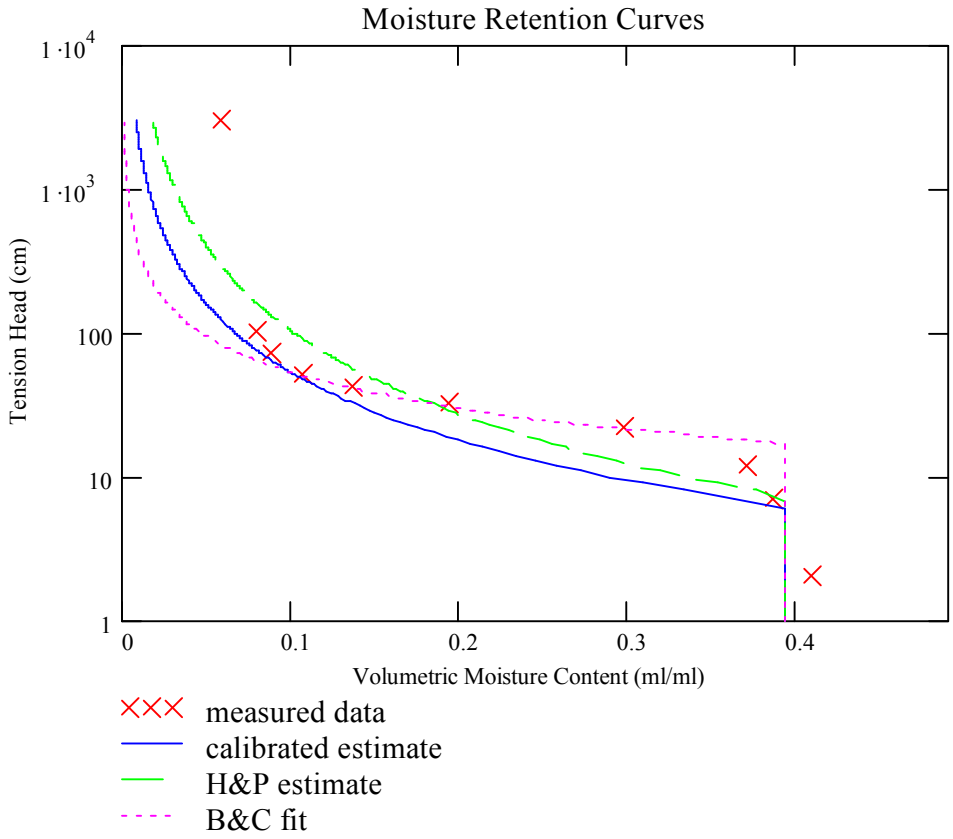

RSQ1 = 0.345
RSQ2 = 0.694
RSQ3 = 0.979

RSQ1= R^2 for calibrated estimate
RSQ2=R^2 for H&P estimate
RSQ3 = R^2 for B&C fit to data

Figure M.2 – Predicted curves versus B&C fit to data – sample NW2. R^2 represents fit to data points not in the very dry or very wet range due to over-saturation in the wet range and lack of hydraulic contact in the dry range.

Sample Number NW4

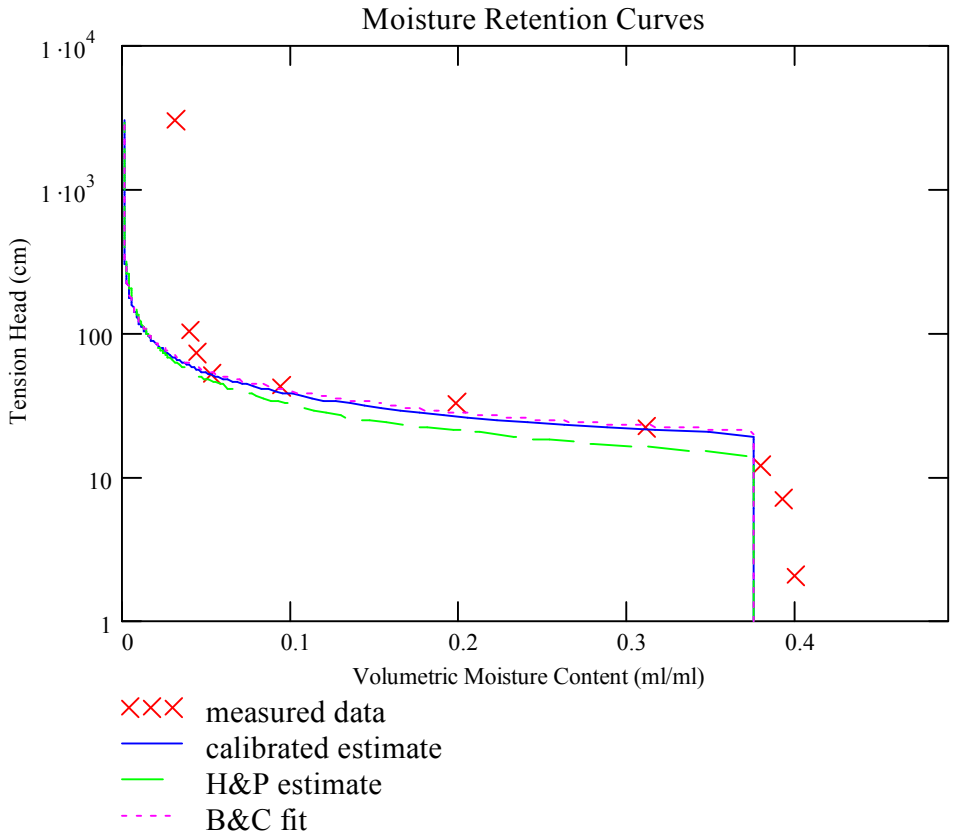

RSQ1 = 0.883
RSQ2 = 0.284
RSQ3 = 0.936

RSQ1= R^2 for calibrated estimate
RSQ2=R^2 for H&P estimate
RSQ3 = R^2 for B&C fit to data

Figure M.3 – Predicted curves versus B&C fit to data – sample NW4. R^2 represents fit to data points not in the very dry or very wet range due to over-saturation in the wet range and lack of hydraulic contact in the dry range.

Sample Number NW7

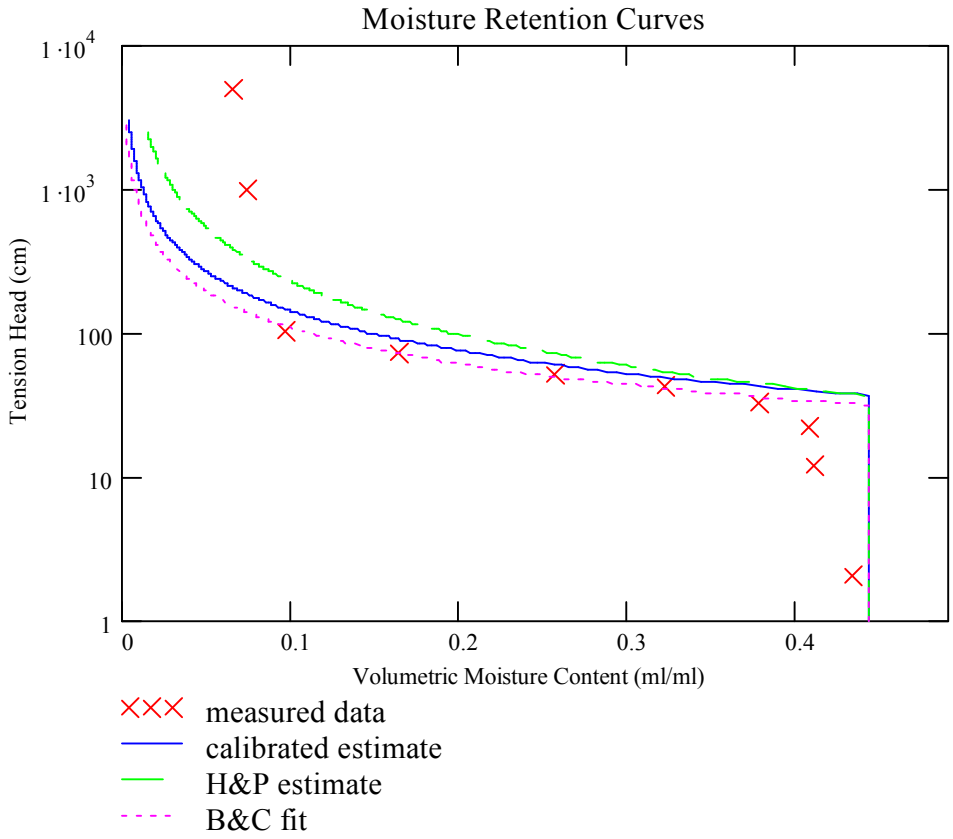

RSQ1 = 0.742
RSQ2 = 0.406
RSQ3 = 0.938

RSQ1= R^2 for calibrated estimate
RSQ2=R^2 for H&P estimate
RSQ3 = R^2 for B&C fit to data

Figure M.4 – Predicted curves versus B&C fit to data – sample NW7. R^2 represents fit to data points not in the very dry or very wet range due to over-saturation in the wet range and lack of hydraulic contact in the dry range.

Sample Number NW8

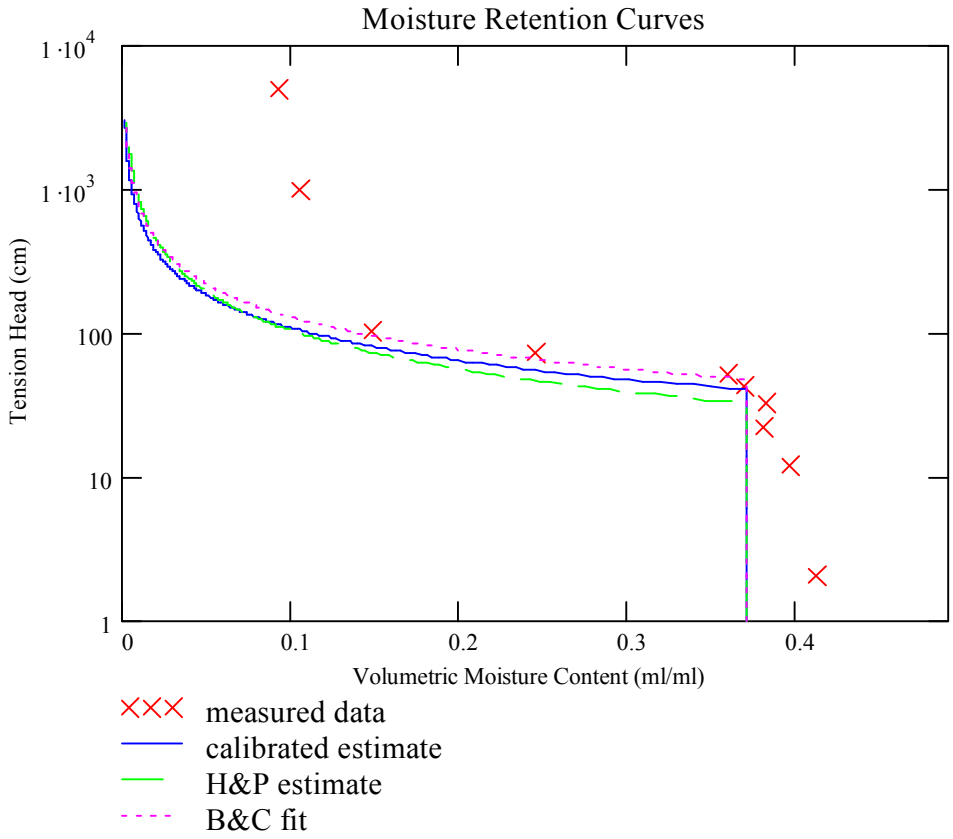

RSQ1 = 0.494
RSQ2 = –0.255
RSQ3 = 0.939

RSQ1= R^2 for calibrated estimate
RSQ2=R^2 for H&P estimate
RSQ3 = R^2 for B&C fit to data

Figure M.5 – Predicted curves versus B&C fit to data – sample NW8. R^2 represents fit to data points not in the very dry or very wet range due to over-saturation in the wet range and lack of hydraulic contact in the dry range.

Sample Number NW9

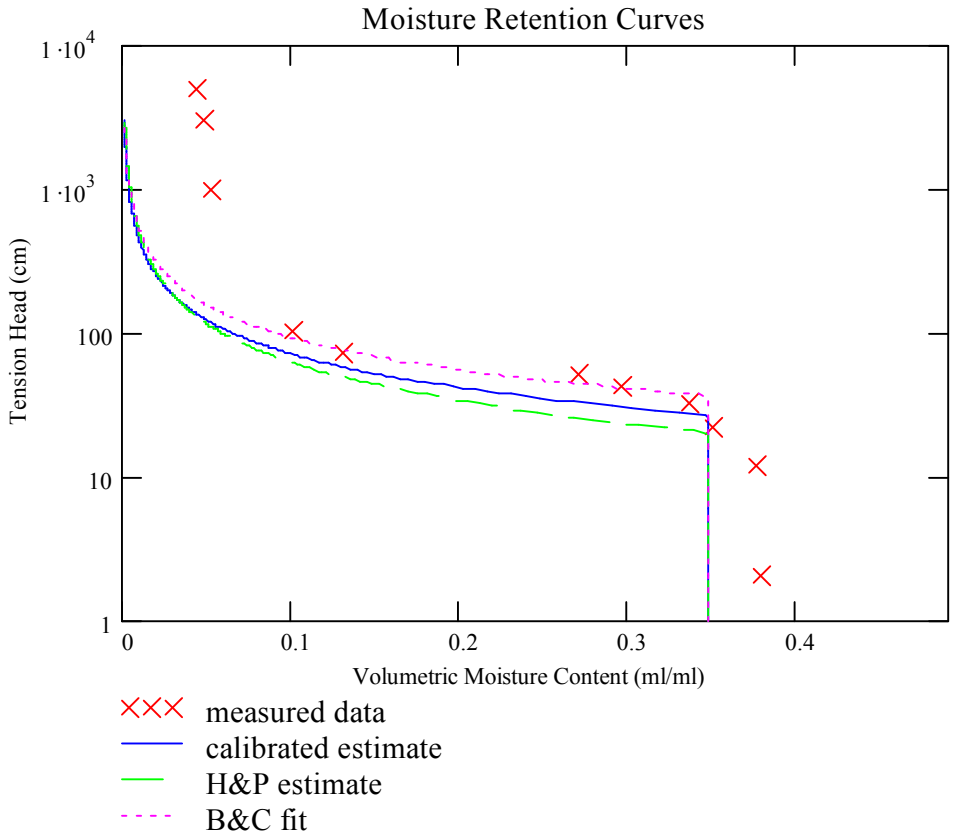

RSQ1 = 0.064
RSQ2 = –0.587
RSQ3 = 0.883

RSQ1= R^2 for calibrated estimate
RSQ2=R^2 for H&P estimate
RSQ3 = R^2 for B&C fit to data

Figure M.6 – Predicted curves versus B&C fit to data – sample NW9. R^2 represents fit to data points not in the very dry or very wet range due to over-saturation in the wet range and lack of hydraulic contact in the dry range.

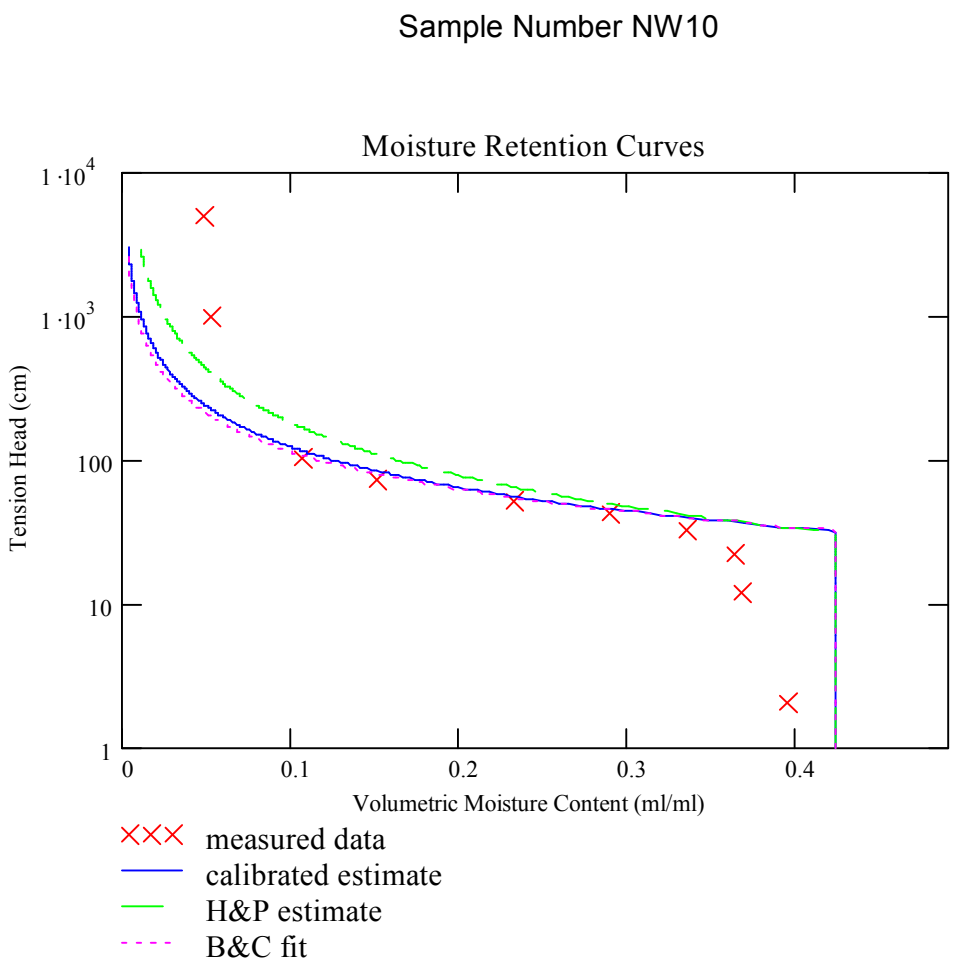

RSQ1 = 0.918
RSQ2 = 0.518
RSQ3 = 0.954

RSQ1= R^2 for calibrated estimate
RSQ2=R^2 for H&P estimate
RSQ3 = R^2 for B&C fit to data

Figure M.7 – Predicted curves versus B&C fit to data – sample NW10. R^2 represents fit to data points not in the very dry or very wet range due to over-saturation in the wet range and lack of hydraulic contact in the dry range.

Sample Number NW11

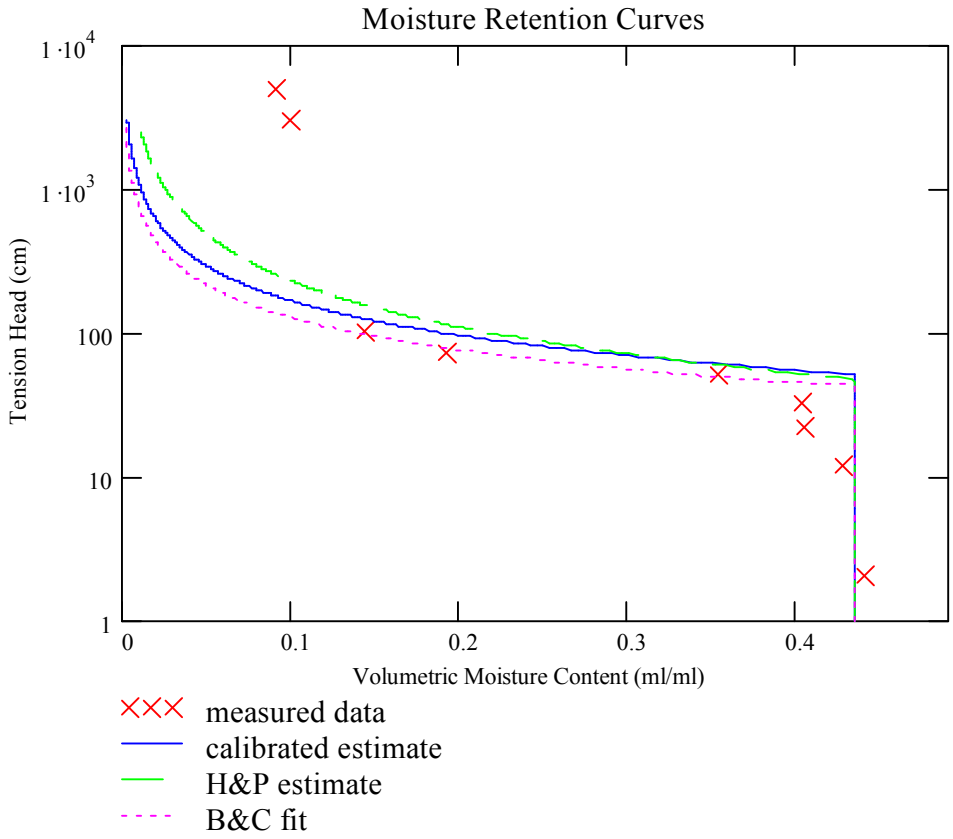

RSQ1 = 0.338
RSQ2 = 0.271
RSQ3 = 0.956

RSQ1= R^2 for calibrated estimate
RSQ2=R^2 for H&P estimate
RSQ3 = R^2 for B&C fit to data

Figure M.8 – Predicted curves versus B&C fit to data – sample NW11. R^2 represents fit to data points not in the very dry or very wet range due to over-saturation in the wet range and lack of hydraulic contact in the dry range.

Sample Number NW12

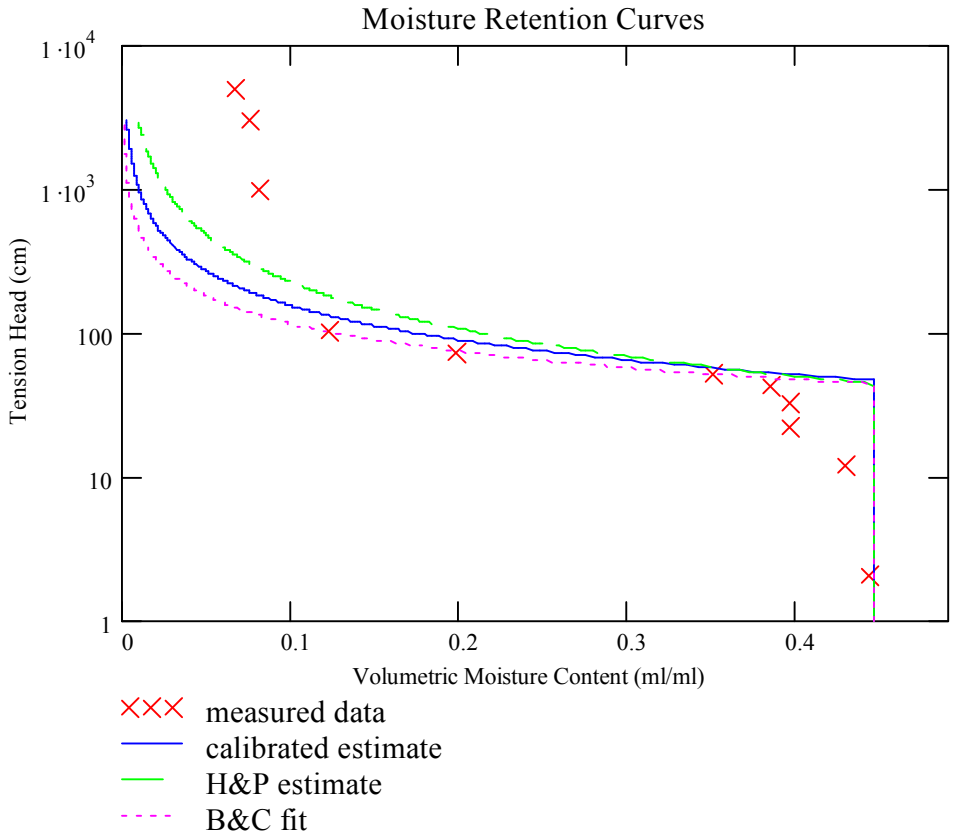

RSQ1 = 0.697
RSQ2 = 0.556
RSQ3 = 0.857

RSQ1= R^2 for calibrated estimate
RSQ2=R^2 for H&P estimate
RSQ3 = R^2 for B&C fit to data

Figure M.9 – Predicted curves versus B&C fit to data – sample NW12. R^2 represents fit to data points not in the very dry or very wet range due to over-saturation in the wet range and lack of hydraulic contact in the dry range.

Sample Number NW16

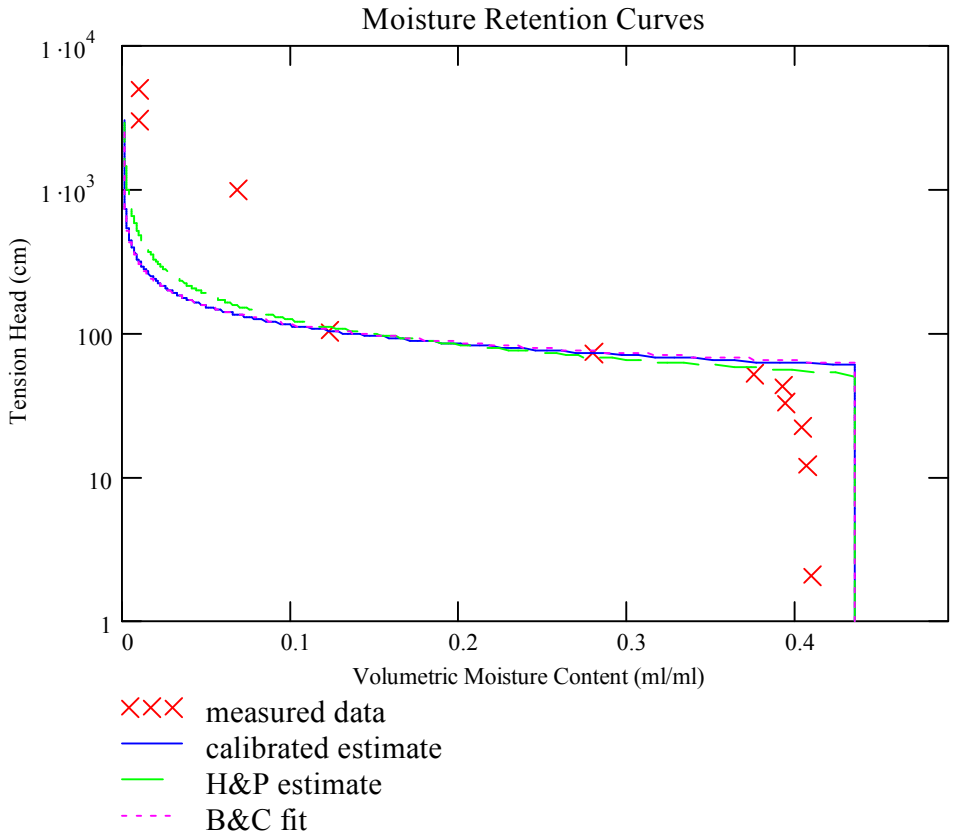

RSQ1 = 0.88
RSQ2 = 0.855
RSQ3 = 0.872

RSQ1= R^2 for calibrated estimate
RSQ2=R^2 for H&P estimate
RSQ3 = R^2 for B&C fit to data

Figure M.10 – Predicted curves versus B&C fit to data – sample NW16. R^2 represents fit to data points not in the very dry or very wet range due to over-saturation in the wet range and lack of hydraulic contact in the dry range.

Sample Number NW17

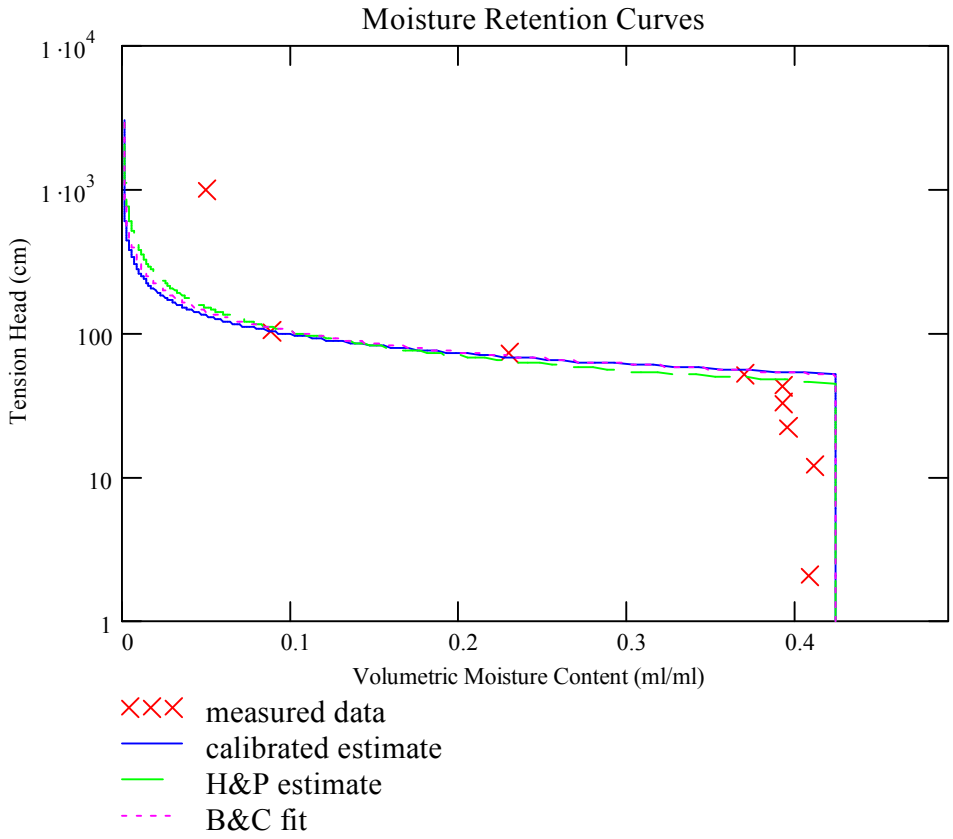

RSQ1 = 0.917
RSQ2 = 0.915
RSQ3 = 0.939

RSQ1= R^2 for calibrated estimate
RSQ2=R^2 for H&P estimate
RSQ3 = R^2 for B&C fit to data

Figure M.11 – Predicted curves versus B&C fit to data – sample NW17. R^2 represents fit to data points not in the very dry or very wet range due to over-saturation in the wet range and lack of hydraulic contact in the dry range.

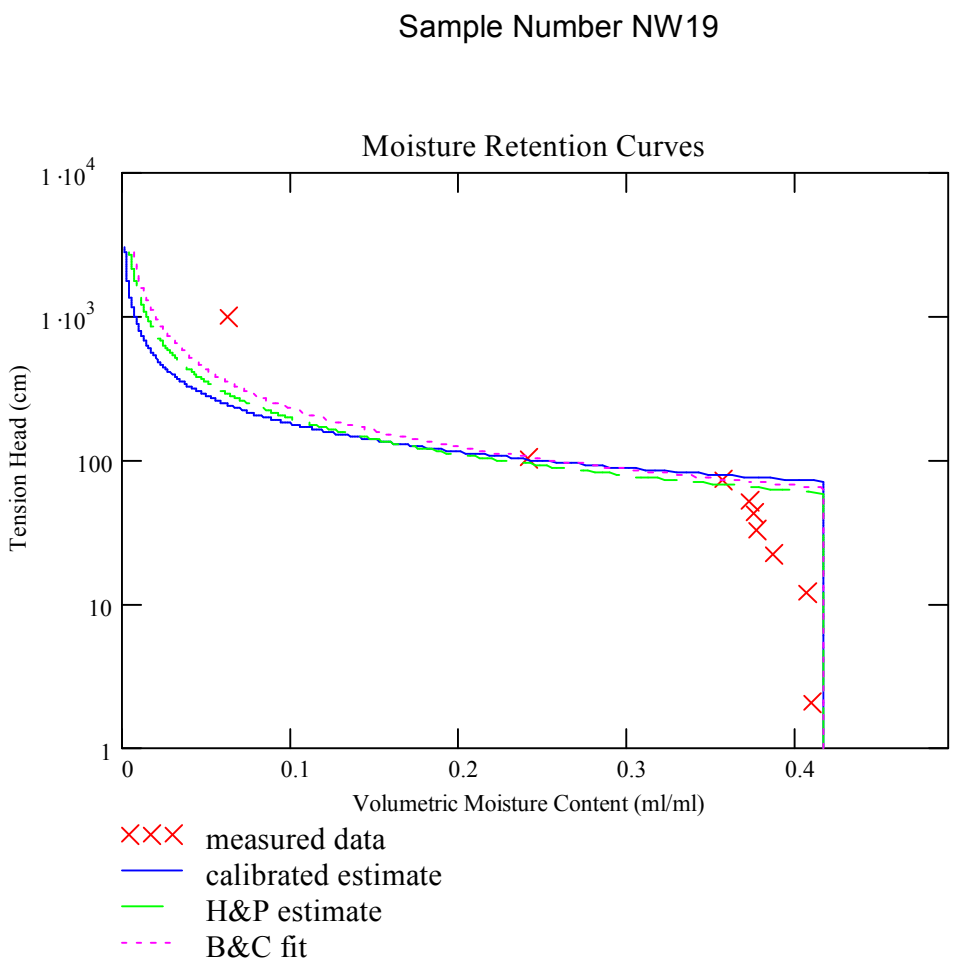

RSQ1 = 0.675
RSQ2 = 0.77
RSQ3 = 0.991

RSQ1= R^2 for calibrated estimate
RSQ2=R^2 for H&P estimate
RSQ3 = R^2 for B&C fit to data

Figure M.12 – Predicted curves versus B&C fit to data – sample NW19. R^2 represents fit to data points not in the very dry or very wet range due to over-saturation in the wet range and lack of hydraulic contact in the dry range.

Sample Number NW20

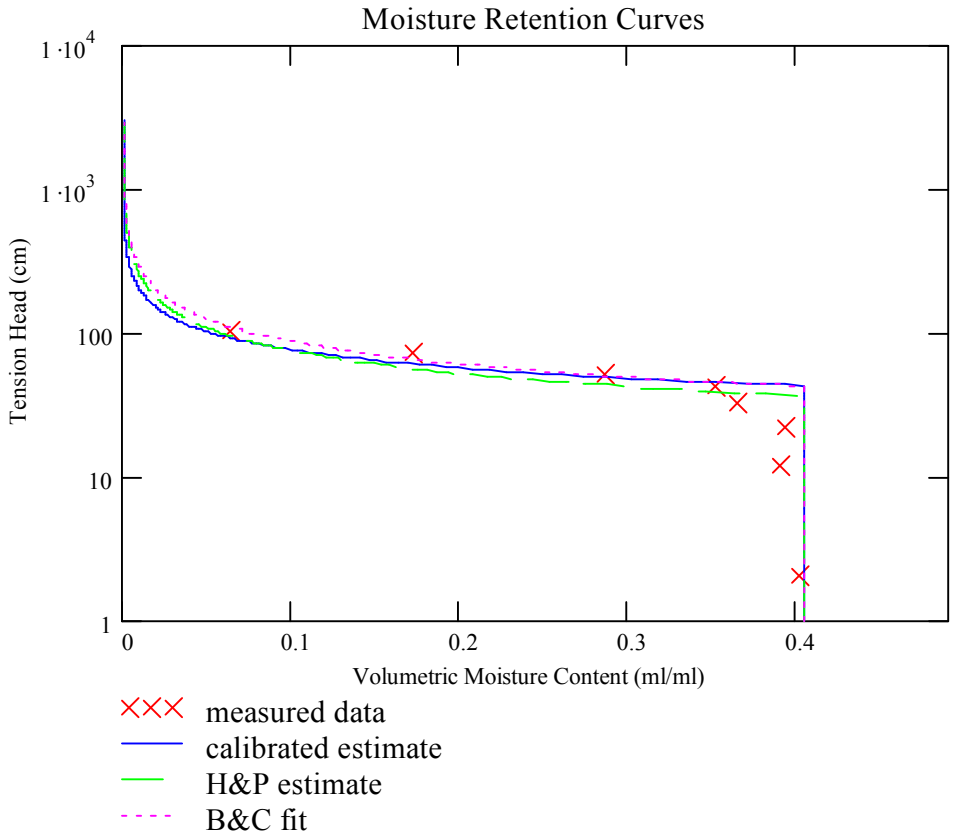

RSQ1 = 0.84
RSQ2 = 0.702
RSQ3 = 0.915

RSQ1= R^2 for calibrated estimate
RSQ2=R^2 for H&P estimate
RSQ3 = R^2 for B&C fit to data

Figure M.13 – Predicted curves versus B&C fit to data – sample NW20. R^2 represents fit to data points not in the very dry or very wet range due to over-saturation in the wet range and lack of hydraulic contact in the dry range.

Sample Number NW21

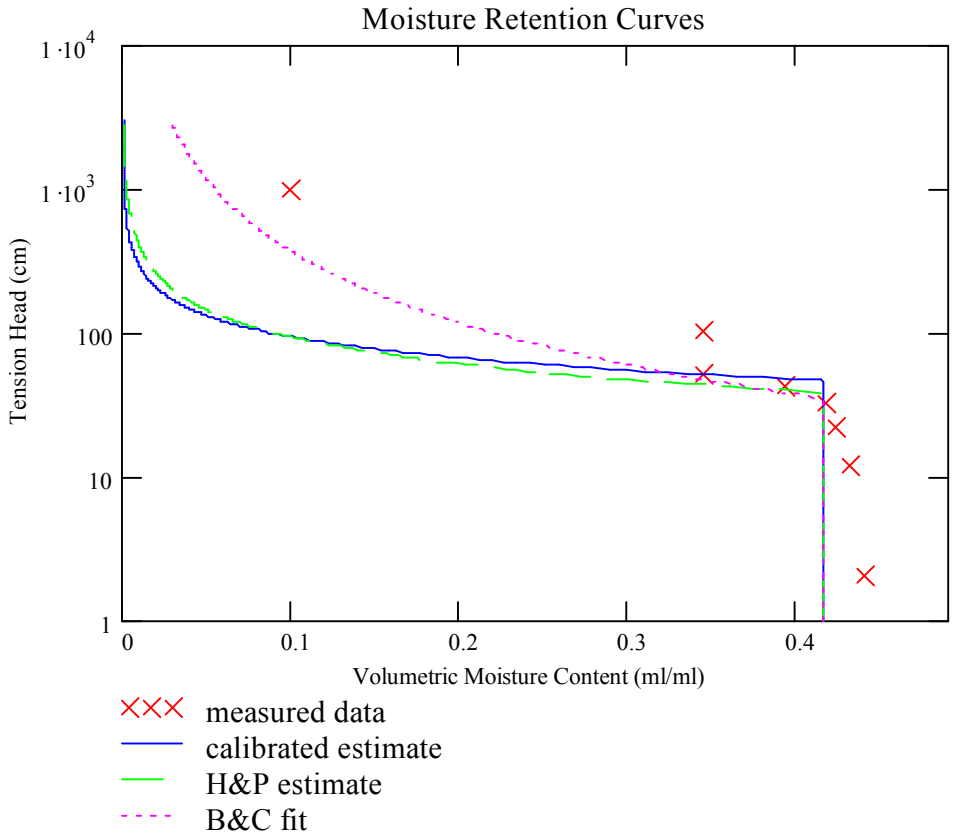

RSQ1 = 0.771
RSQ2 = –2.482
RSQ3 = 0.677

RSQ1= R^2 for calibrated estimate
RSQ2=R^2 for H&P estimate
RSQ3 = R^2 for B&C fit to data

Figure M.14 – Predicted curves versus B&C fit to data – sample NW21. R^2 represents fit to data points not in the very dry or very wet range due to over-saturation in the wet range and lack of hydraulic contact in the dry range.

Sample Number NW22

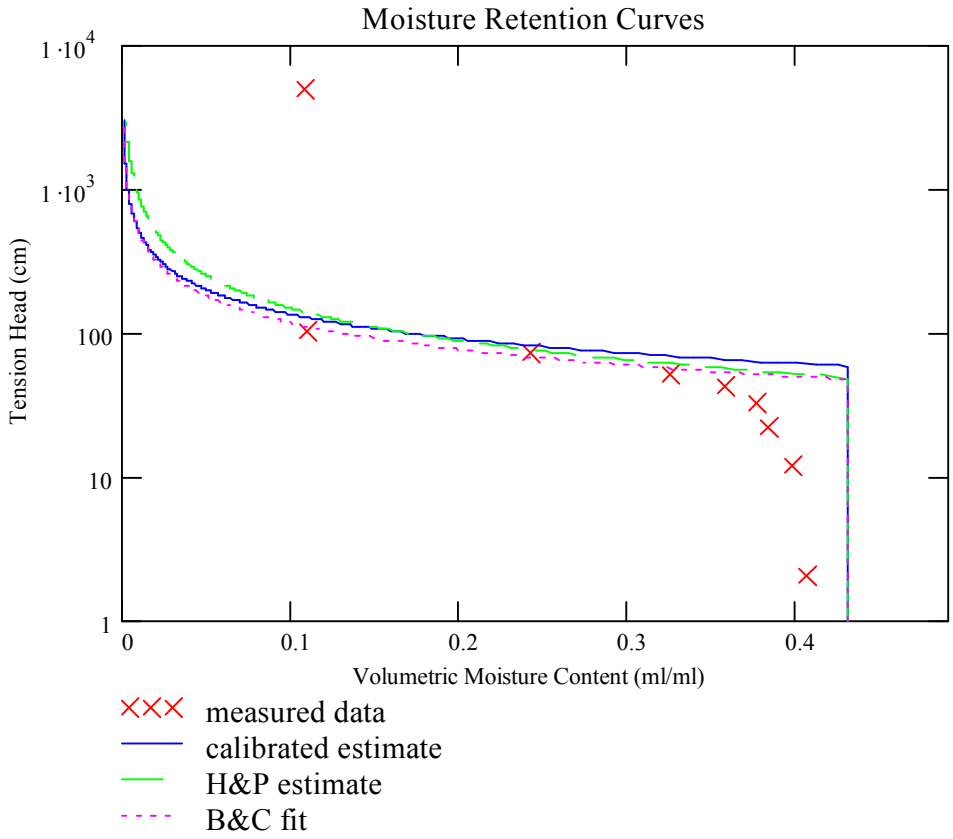

RSQ1 = 0.389
RSQ2 = 0.62
RSQ3 = 0.773

RSQ1= R^2 for calibrated estimate
RSQ2=R^2 for H&P estimate
RSQ3 = R^2 for B&C fit to data

Figure M.15 – Predicted curves versus B&C fit to data – sample NW22. R^2 represents fit to data points not in the very dry or very wet range due to over-saturation in the wet range and lack of hydraulic contact in the dry range.

Sample Number NW23

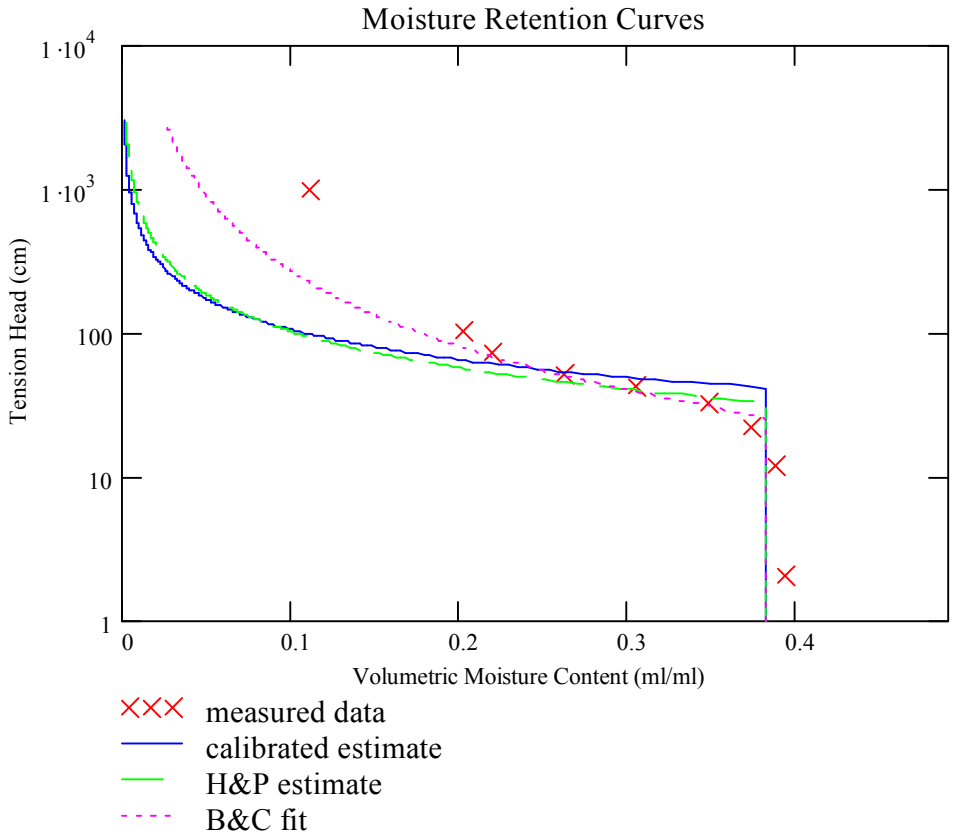

RSQ1 = 0.1
RSQ2 = 0.128
RSQ3 = 0.963

RSQ1= R^2 for calibrated estimate
RSQ2=R^2 for H&P estimate
RSQ3 = R^2 for B&C fit to data

Figure M.16 – Predicted curves versus B&C fit to data – sample NW23. R^2 represents fit to data points not in the very dry or very wet range due to over-saturation in the wet range and lack of hydraulic contact in the dry range.

Sample Number NW24

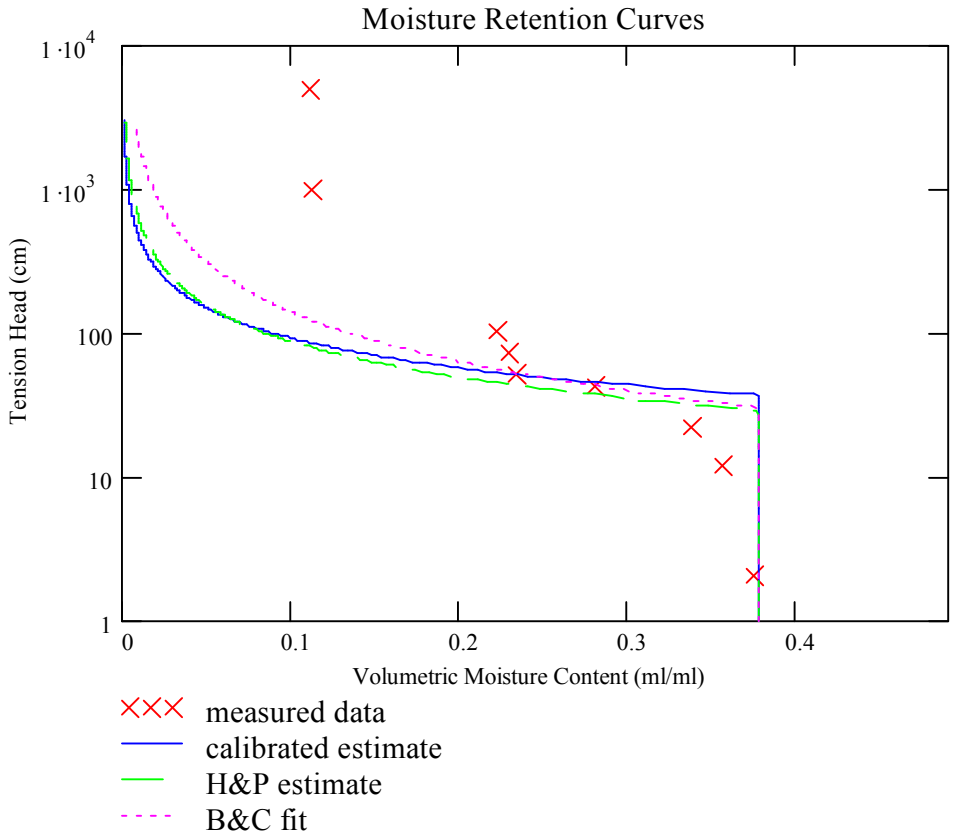

RSQ1 = 0.187
RSQ2 = –2.575
RSQ3 = 0.995

RSQ1= R^2 for calibrated estimate
RSQ2=R^2 for H&P estimate
RSQ3 = R^2 for B&C fit to data

Figure M.17 – Predicted curves versus B&C fit to data – sample NW24. R^2 represents fit to data points not in the very dry or very wet range due to over-saturation in the wet range and lack of hydraulic contact in the dry range.

Sample Number NW25

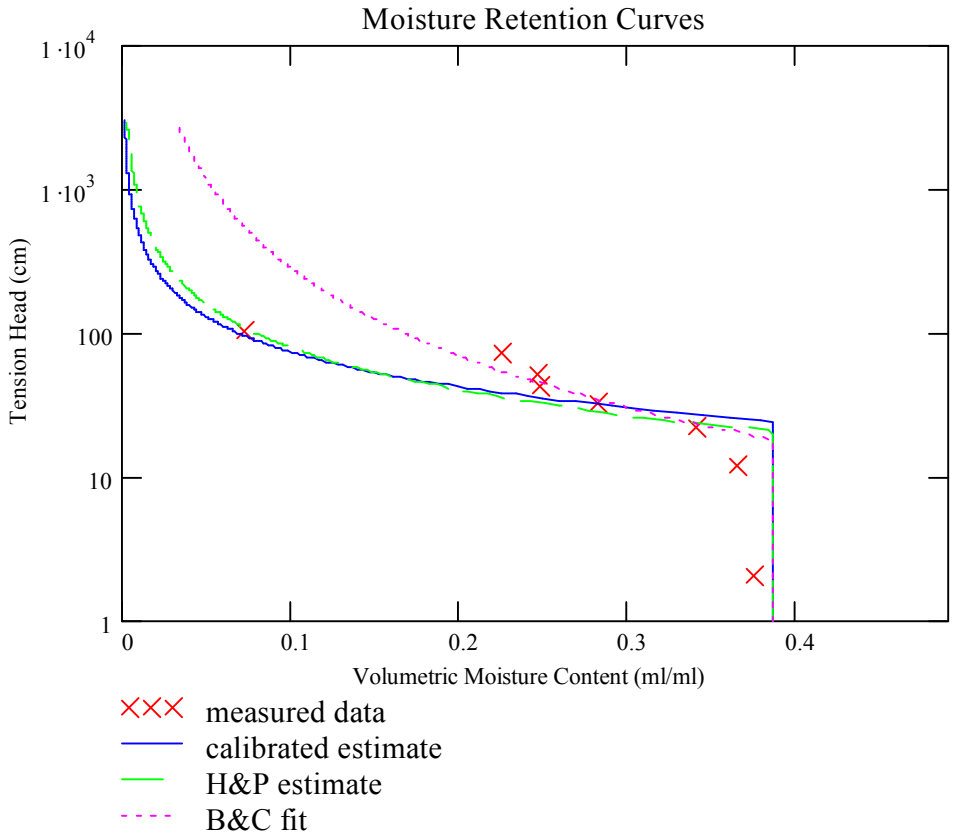

RSQ1 = 0.888
RSQ2 = 0.87
RSQ3 = 0.784

RSQ1= R^2 for calibrated estimate
RSQ2=R^2 for H&P estimate
RSQ3 = R^2 for B&C fit to data

Figure M.18 – Predicted curves versus B&C fit to data – sample NW25. R^2 represents fit to data points not in the very dry or very wet range due to over-saturation in the wet range and lack of hydraulic contact in the dry range.

Sample Number NW27

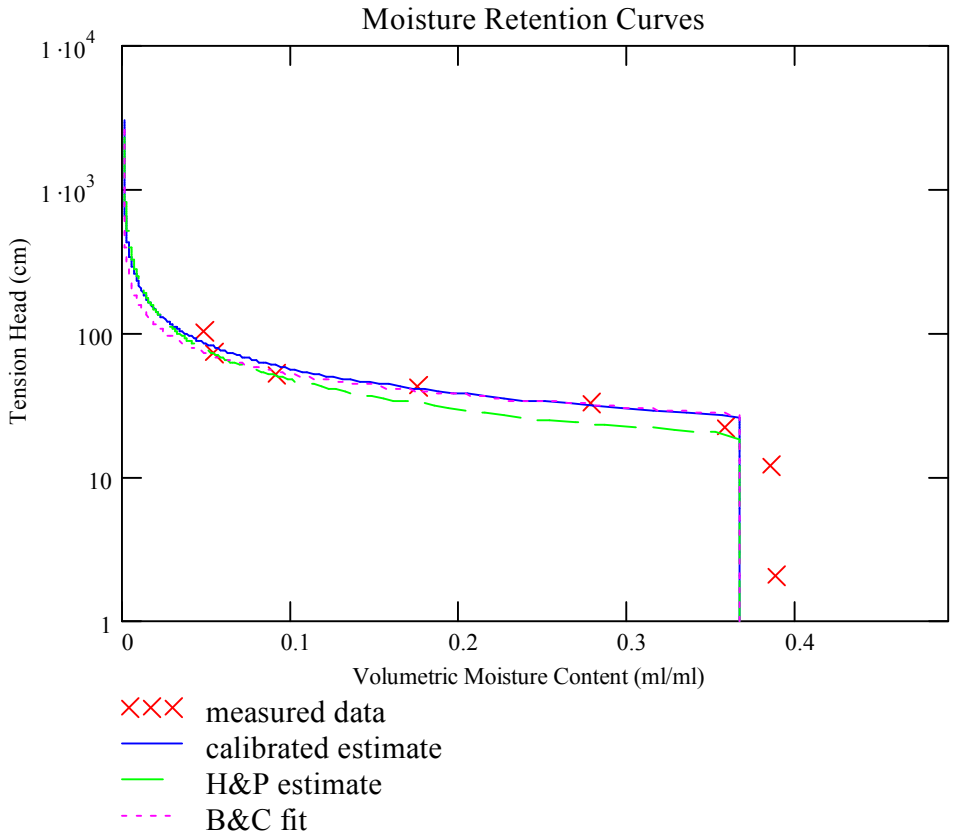

RSQ1 = 0.971
RSQ2 = 0.525
RSQ3 = 0.976

RSQ1= R^2 for calibrated estimate
RSQ2=R^2 for H&P estimate
RSQ3 = R^2 for B&C fit to data

Figure M.19 – Predicted curves versus B&C fit to data – sample NW27. R^2 represents fit to data points not in the very dry or very wet range due to over-saturation in the wet range and lack of hydraulic contact in the dry range.

Appendix N

Fabricated Sample PSD and Brooks and Corey Fit to PDC Data

N.1 Initial Model Application To Fabricated Samples

The empirical model estimation equations determined from model calibration to the STVZ samples were initially used to estimate moisture retention curves for the fabricated samples, however the estimates were extremely poor, therefore we attempted to re-calibrate the model to the fabricated samples to try to improve the estimates. We first tried calibrated the model to all the fabricated samples, but the estimates did not improve significantly, except for the well sorted samples. We then attempted to calibrate the model to several different combination of sample groups to see if we could improve the results. None of the calibrations resulted in improved estimates, however. Figures N.1 to N.12 show the various calibration attempts.

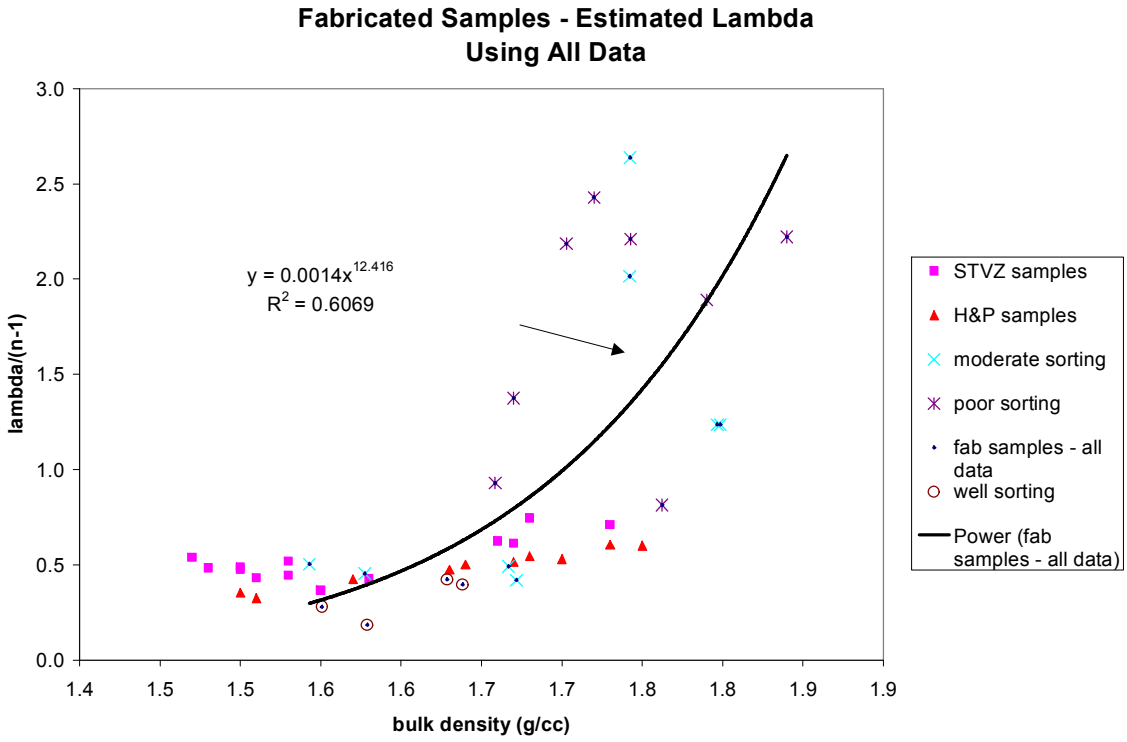

Figure N.1 – Estimated particle index parameter for Haverkamp and Parlange (1986) pedotransfer model using all the fabricated samples.

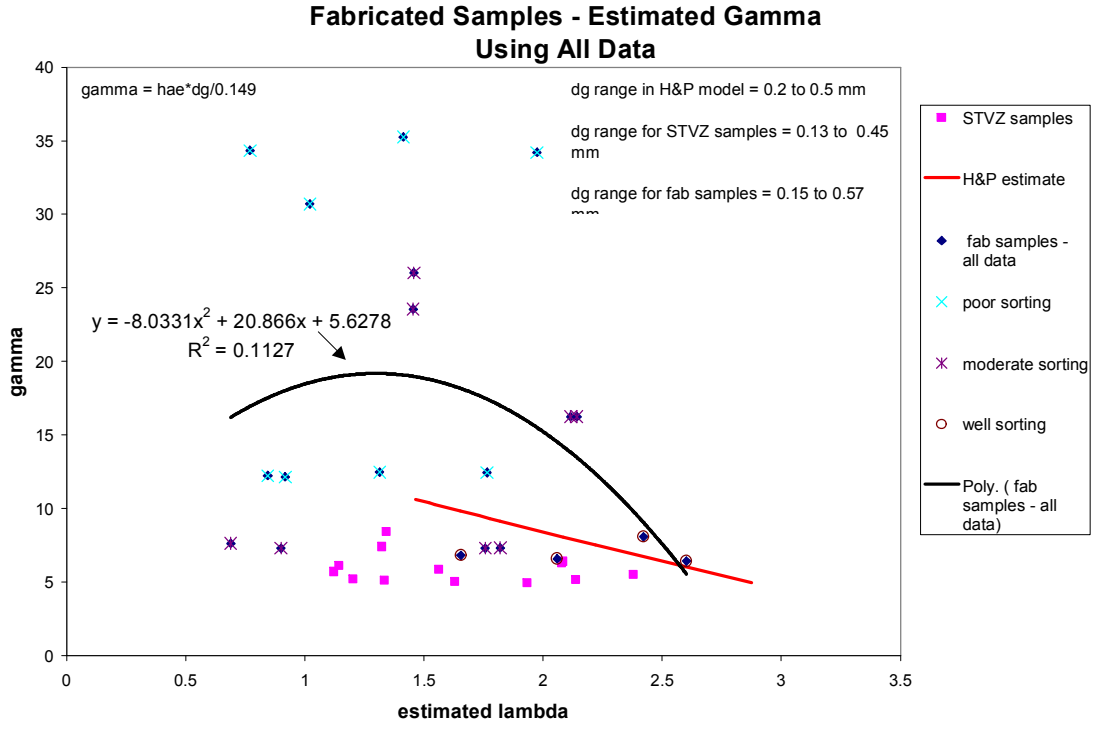

Figure N.2 – Estimated packing parameter for Haverkamp and Parlange (1986) pedotransfer model using all the fabricated samples.

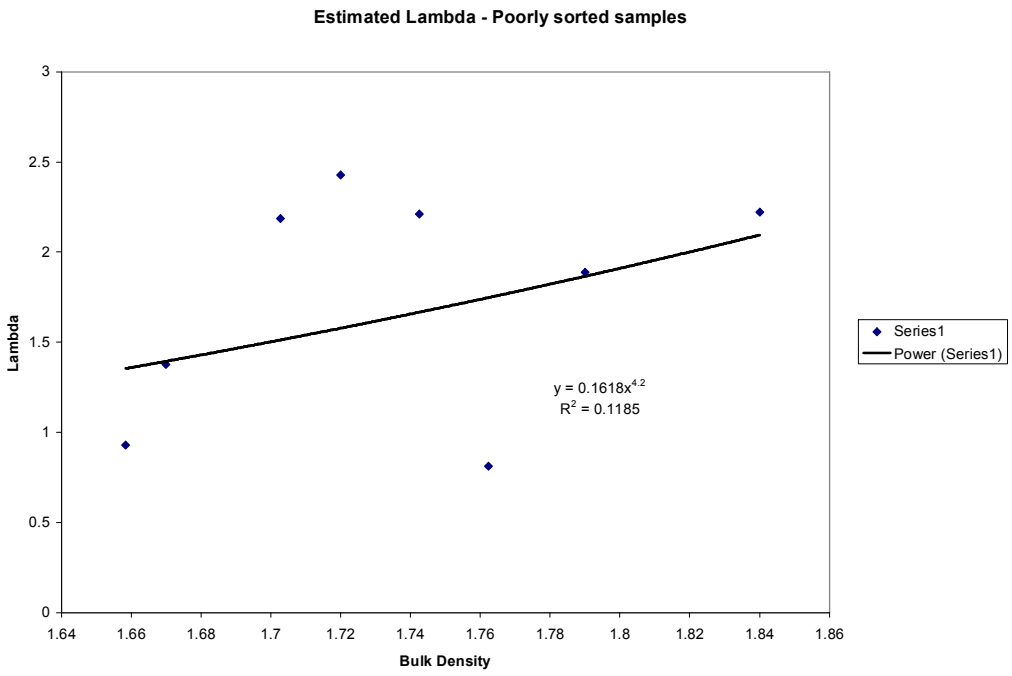

Figure N.3 – Estimated particle index parameter for Haverkamp and Parlange (1986) pedotransfer model using the poorly sorted fabricated samples.

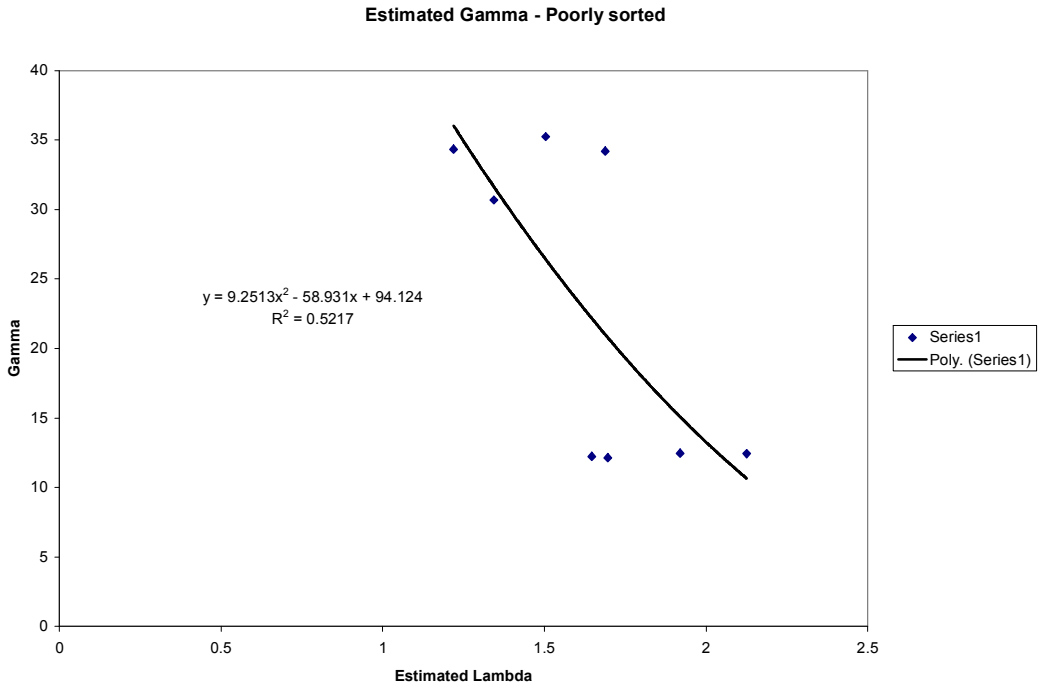

Figure N.4 – Estimated packing parameter for Haverkamp and Parlange (1986) pedotransfer model using the poorly sorted fabricated samples.

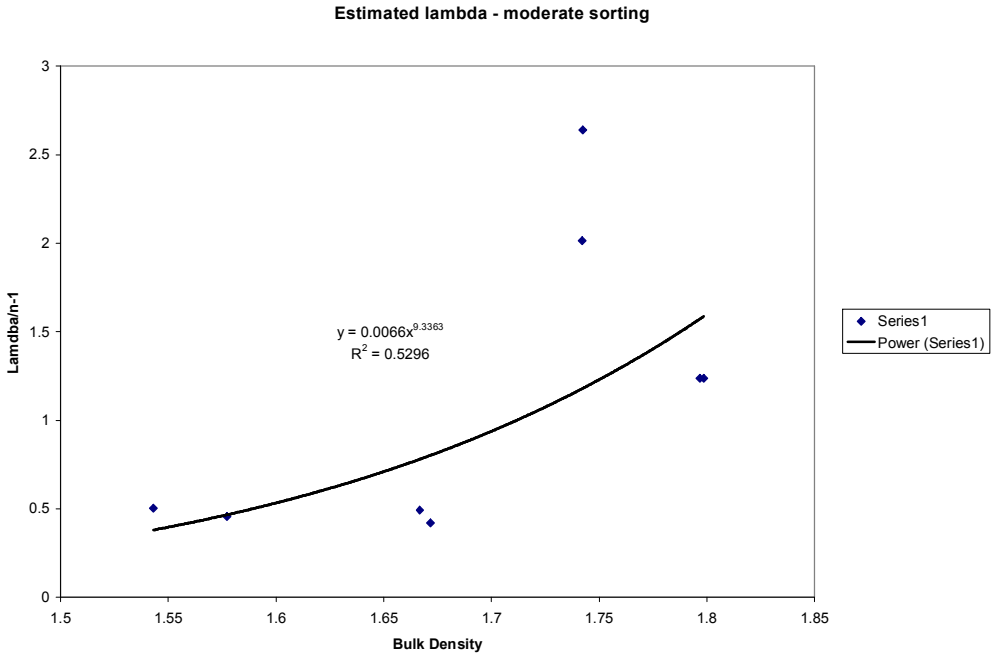

Figure N.5 – Estimated particle index parameter for Haverkamp and Parlange (1986) pedotransfer model using the moderately sorted fabricated samples.

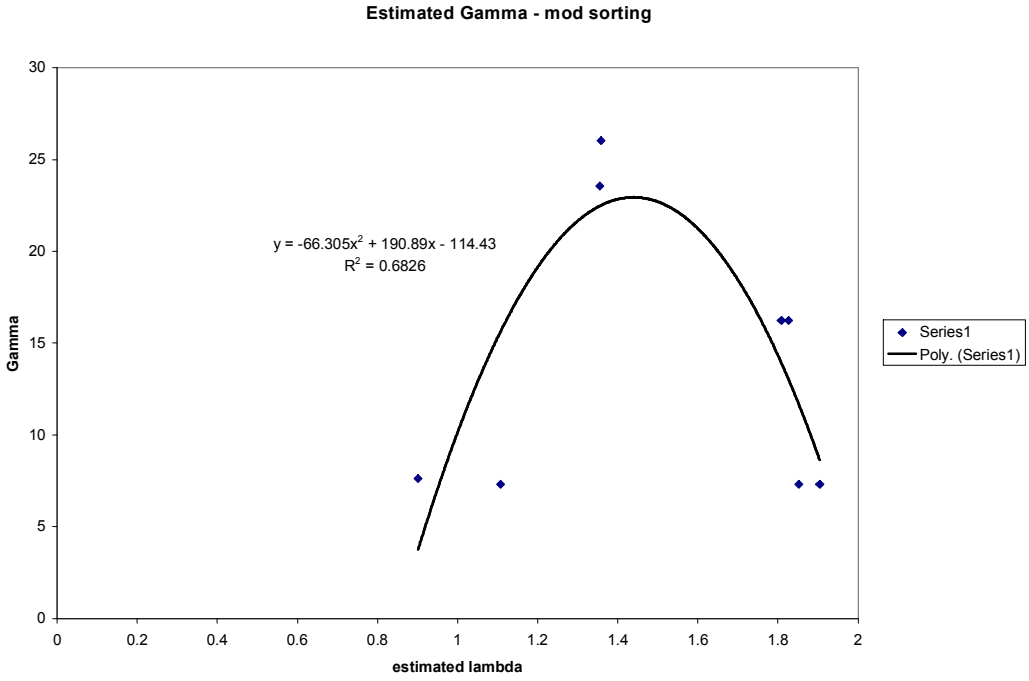

Figure N.6 – Estimated packing parameter for Haverkamp and Parlange (1986) pedotransfer model using the moderately sorted fabricated samples.

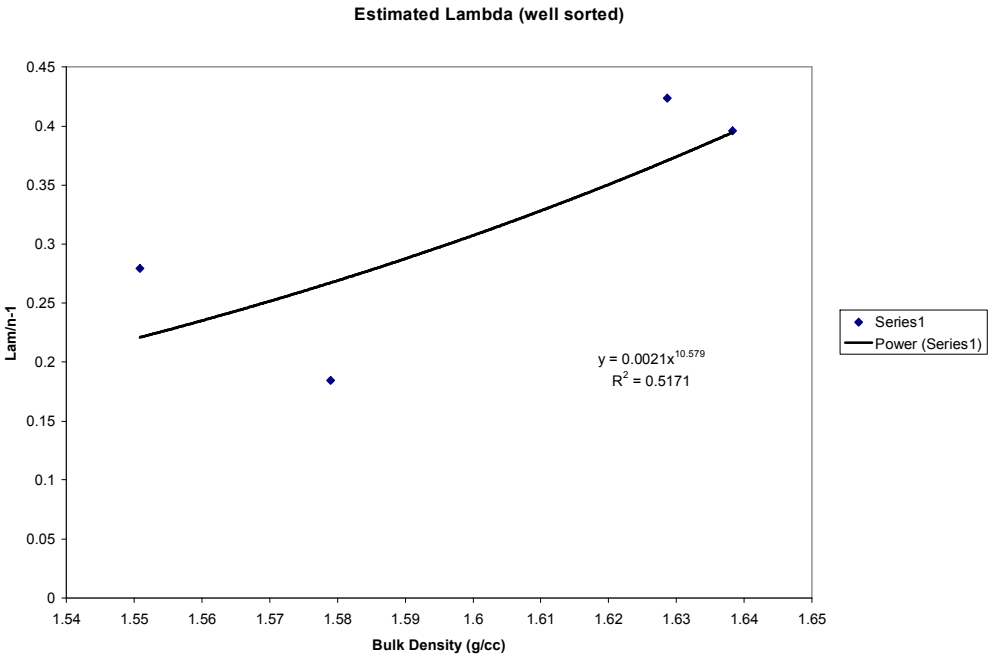

Figure N.7 – Estimated particle index parameter for Haverkamp and Parlange (1986) pedotransfer model using the well sorted fabricated samples.

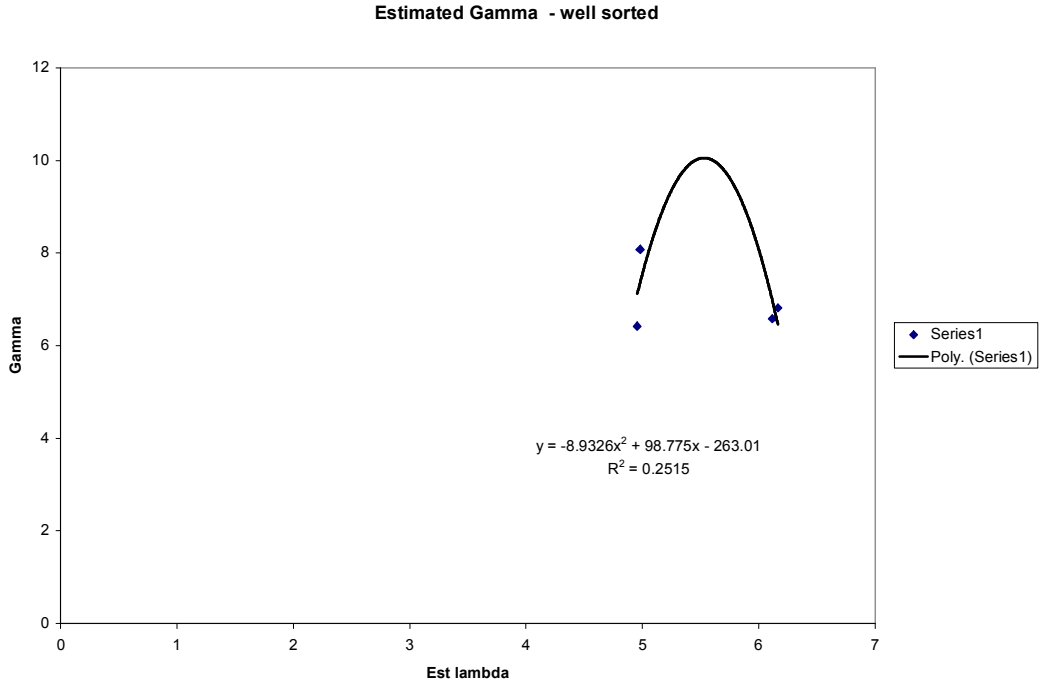

Figure N.8 – Estimated packing parameter for Haverkamp and Parlange (1986) pedotransfer model using the well sorted fabricated samples.

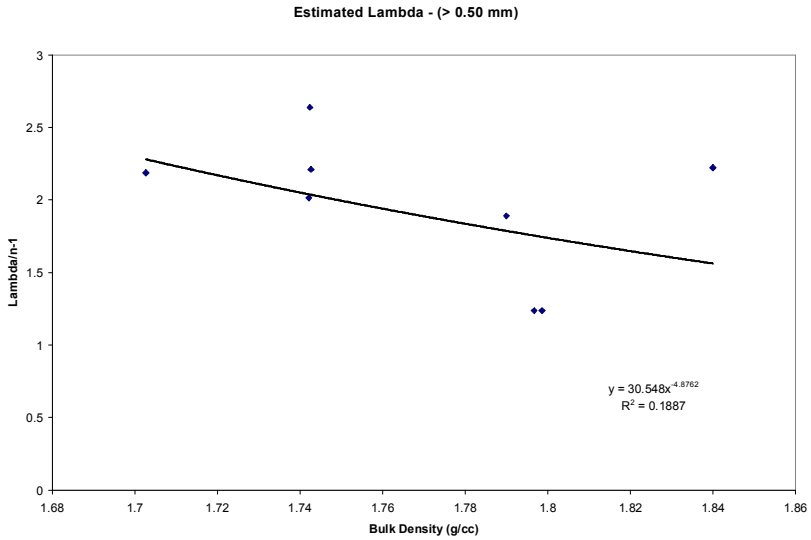

Figure N.9 – Estimated particle index parameter for Haverkamp and Parlange (1986) pedotransfer model using fabricated samples with median particles diameters greater than 0.50 mm.

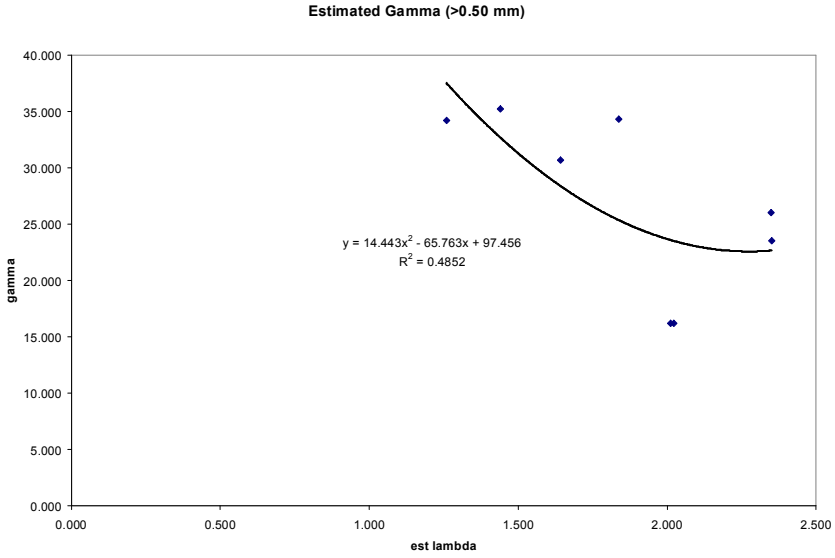

Figure N.10 – Estimated packing parameter for Haverkamp and Parlange (1986) pedotransfer model using fabricated samples with median particles diameters greater than 0.50 mm.

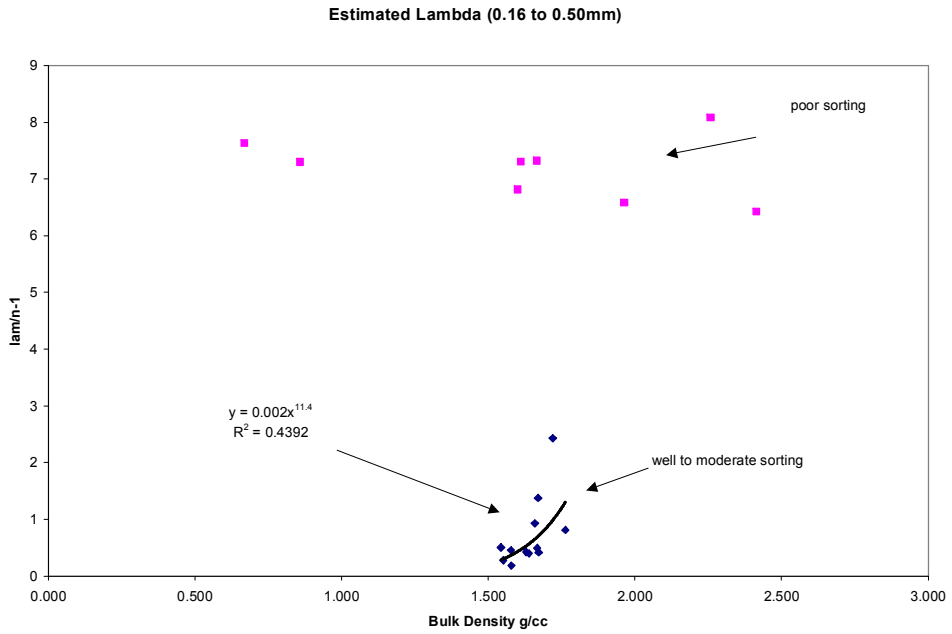

Figure N.11 – Estimated particle index parameter for Haverkamp and Parlange (1986) pedotransfer model using fabricated samples with median particles diameters between 0.16 and 0.50 mm.

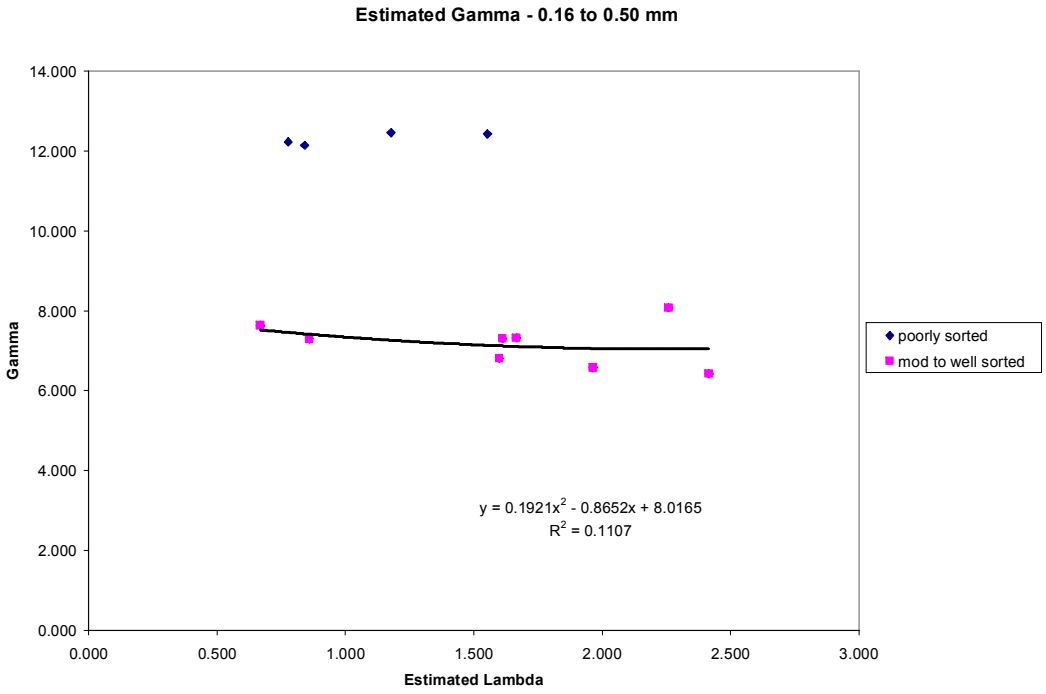

Figure N.12 – Estimated packing parameter for Haverkamp and Parlange (1986) pedotransfer model using fabricated samples with median particles diameters between 0.16 and 0.50 mm.

N.2 Particle Size Distributions for the Fabricated Samples

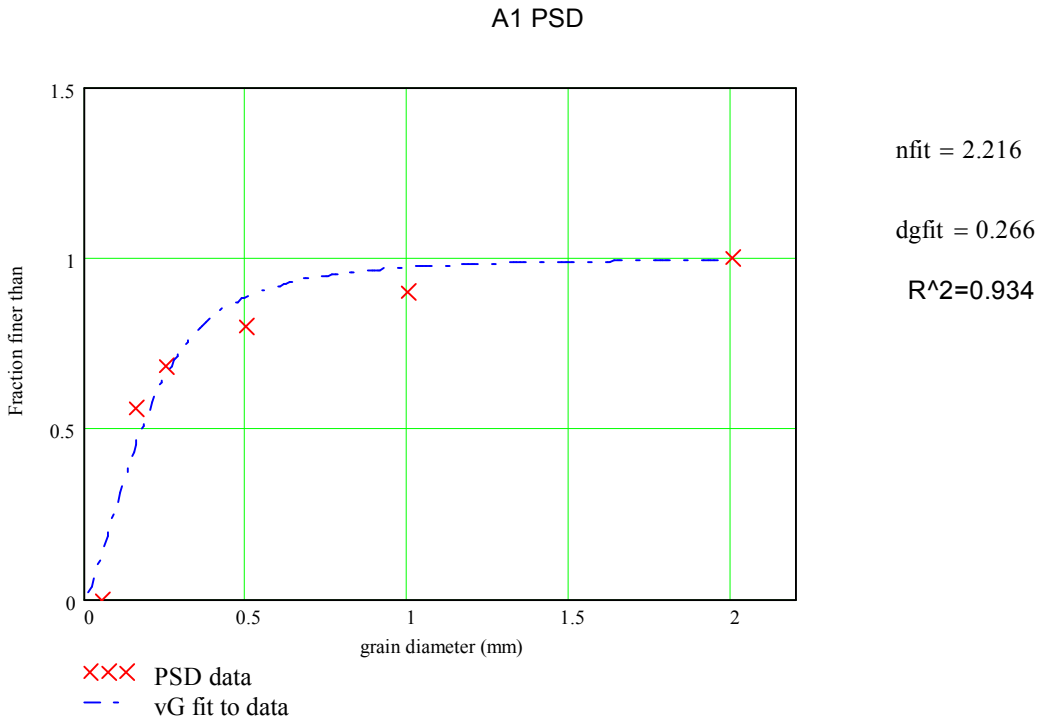

Figure N.13 – Poorly sorted – 0.16mm median grain size.

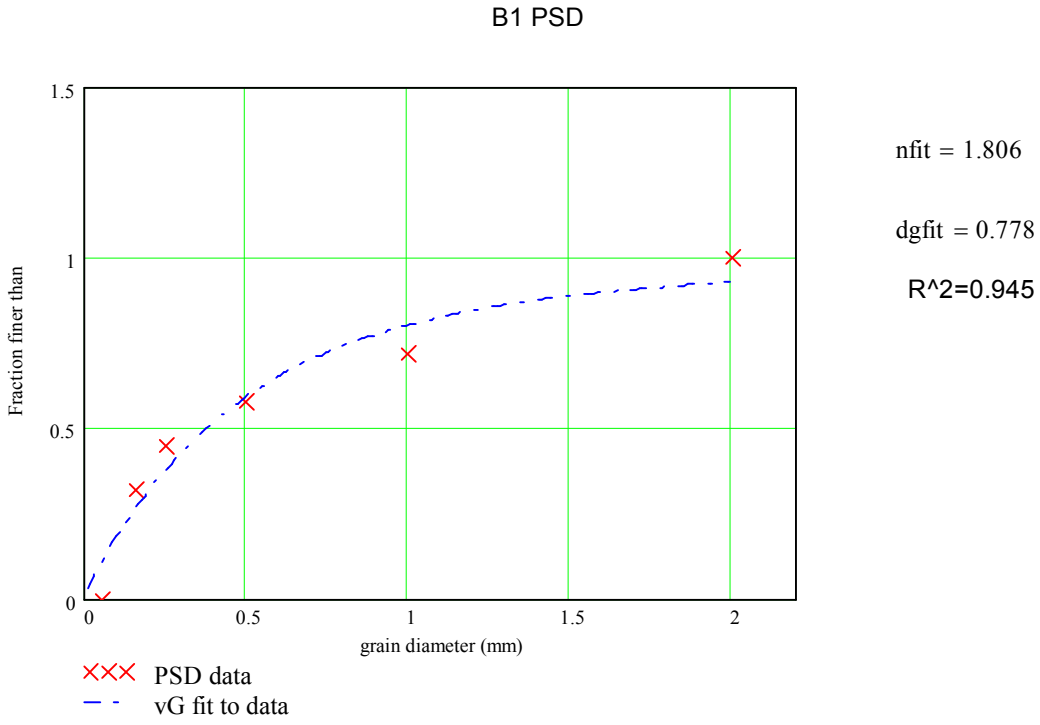

Figure N.14 – Poorly sorted – 0.5mm median grain size.

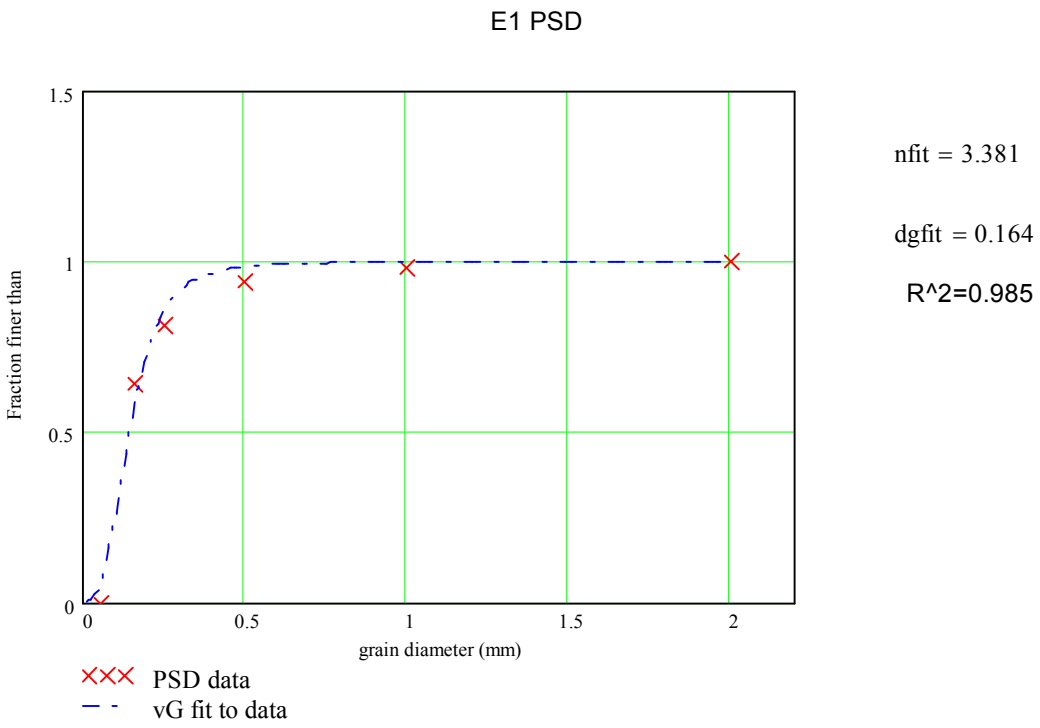

Figure N.15 – Moderately sorted – 0.16mm median grain size.

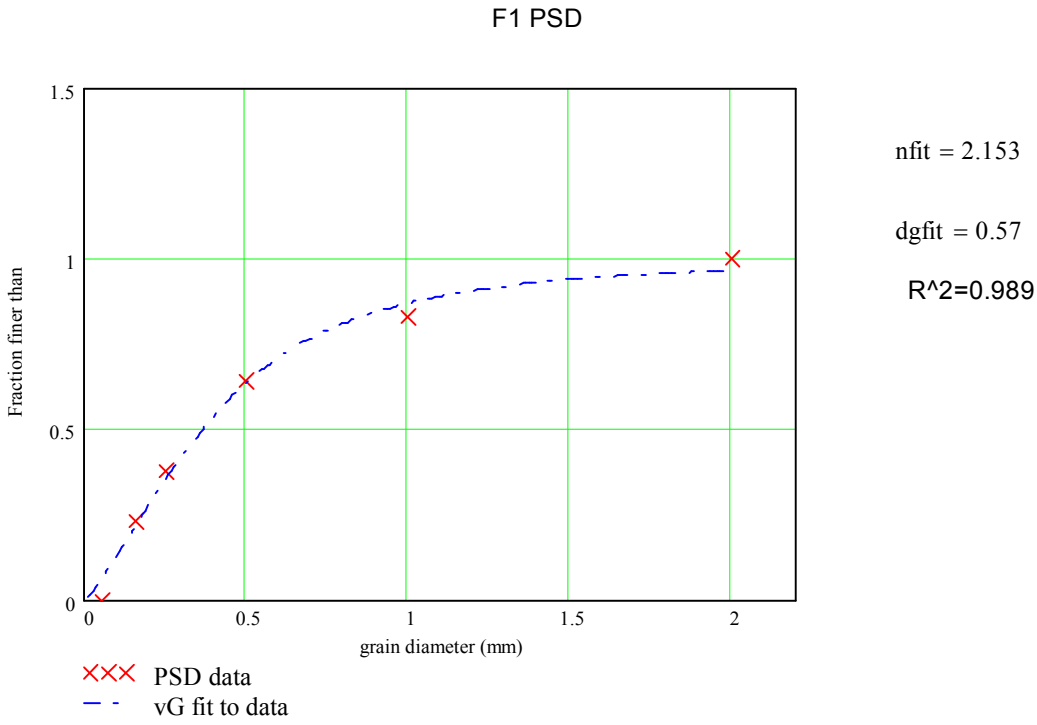

Figure N.16 – Moderately sorted – 0.5mm median grain size.

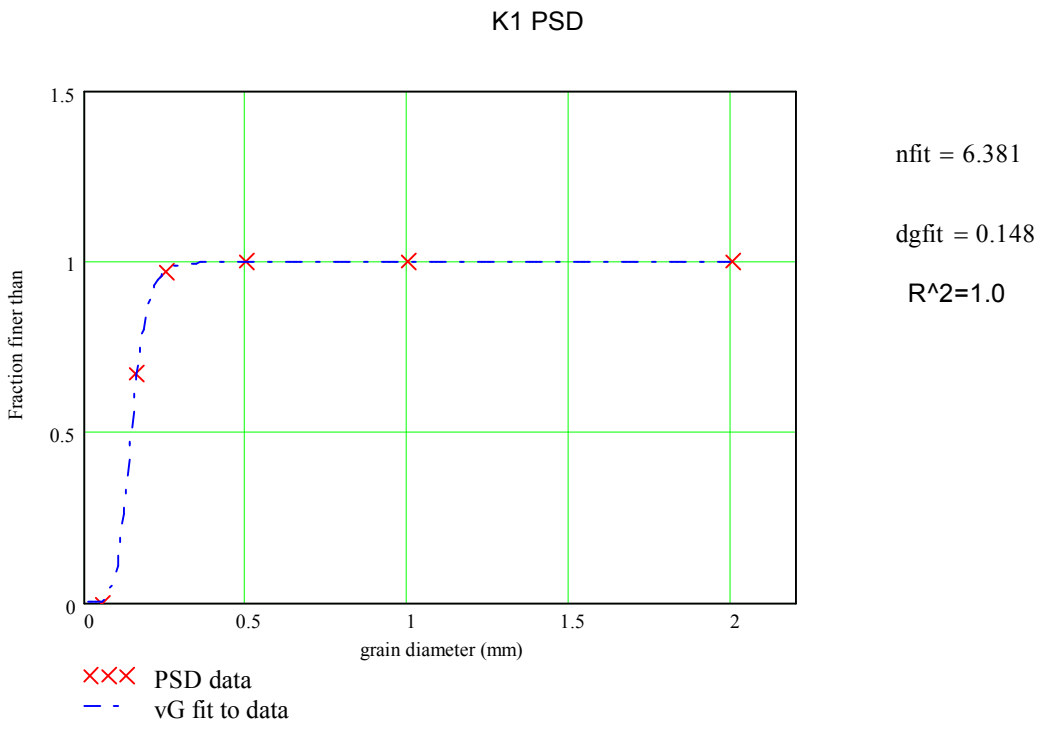

Figure N.17 – Well sorted – 0.16mm median grain size.

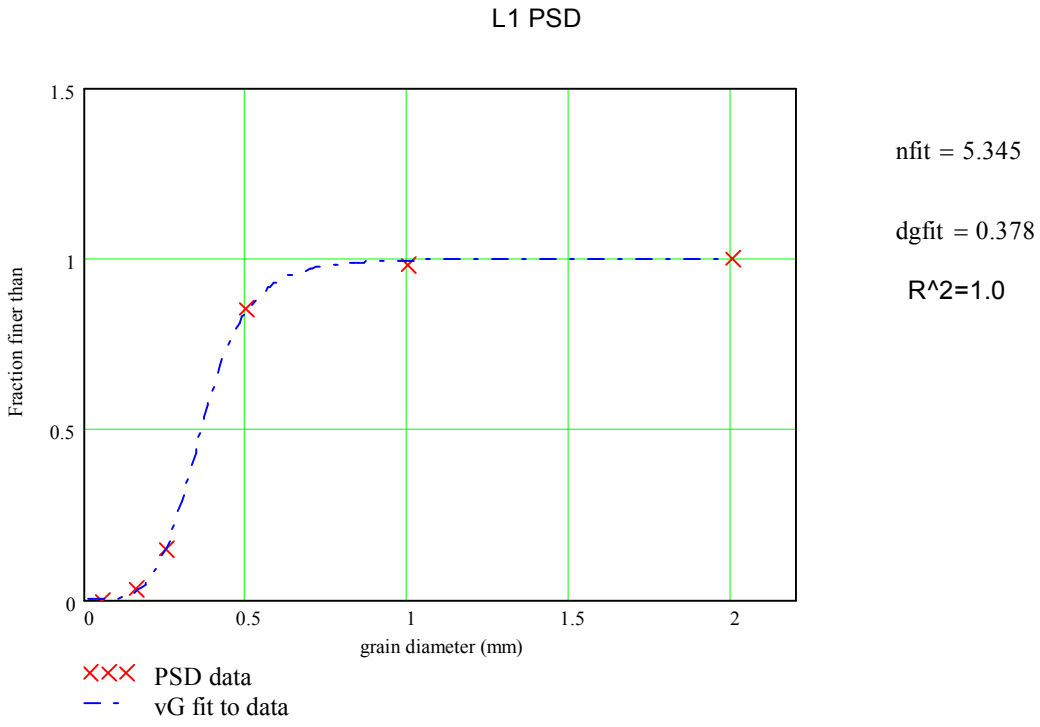

Figure N.18 – Well sorted – 0.5mm median grain size.

N.3 Brooks and Corey equation Fit to PDC data – Fabricated Samples

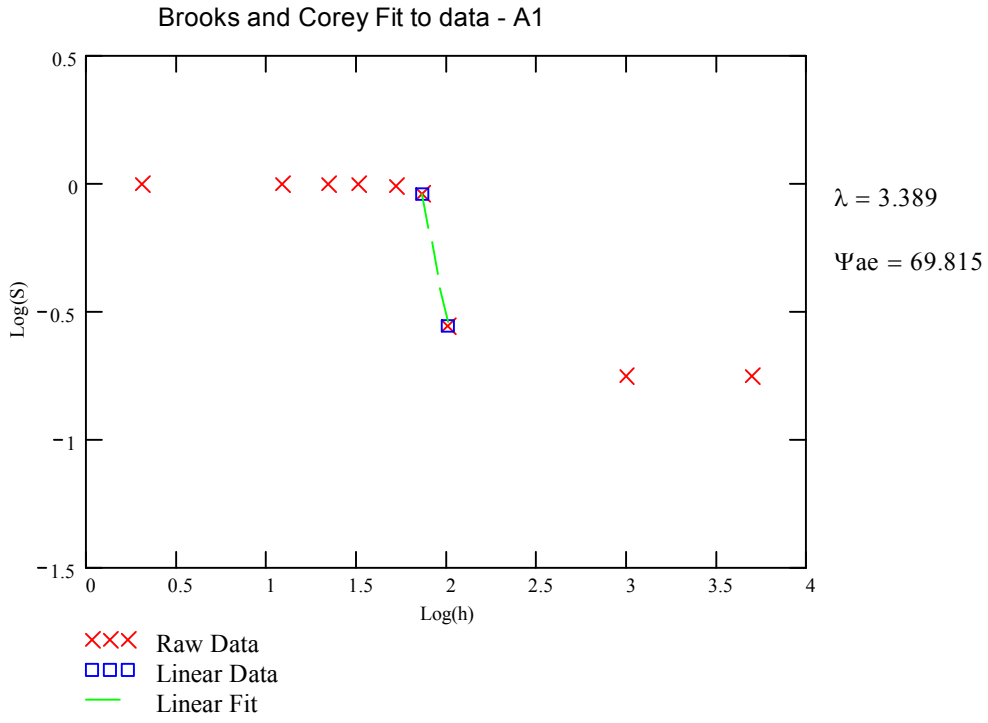

Figure N.19 – Linear Brooks and Corey fit to sample A1.

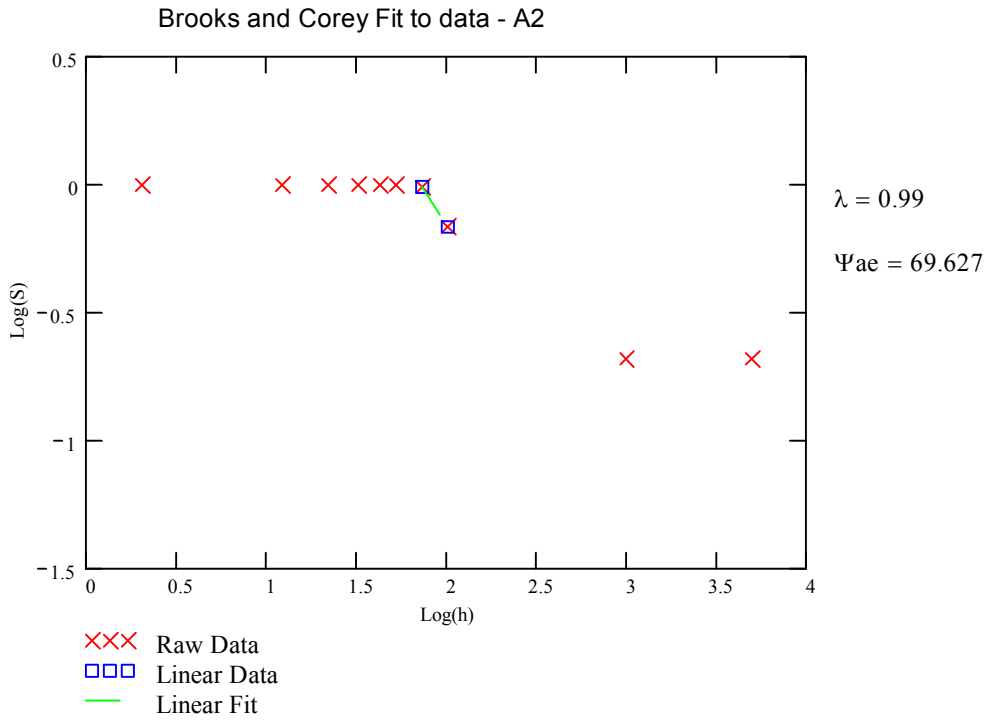

Figure N.20 – Linear Brooks and Corey fit to sample A2.

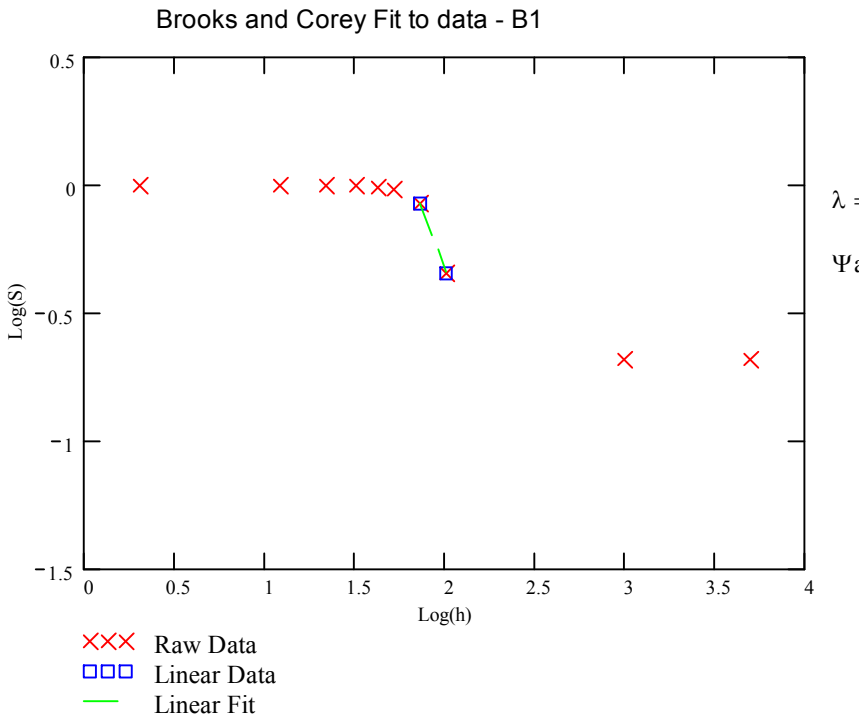

Figure N.21 – Linear Brooks and Corey fit to sample B1.

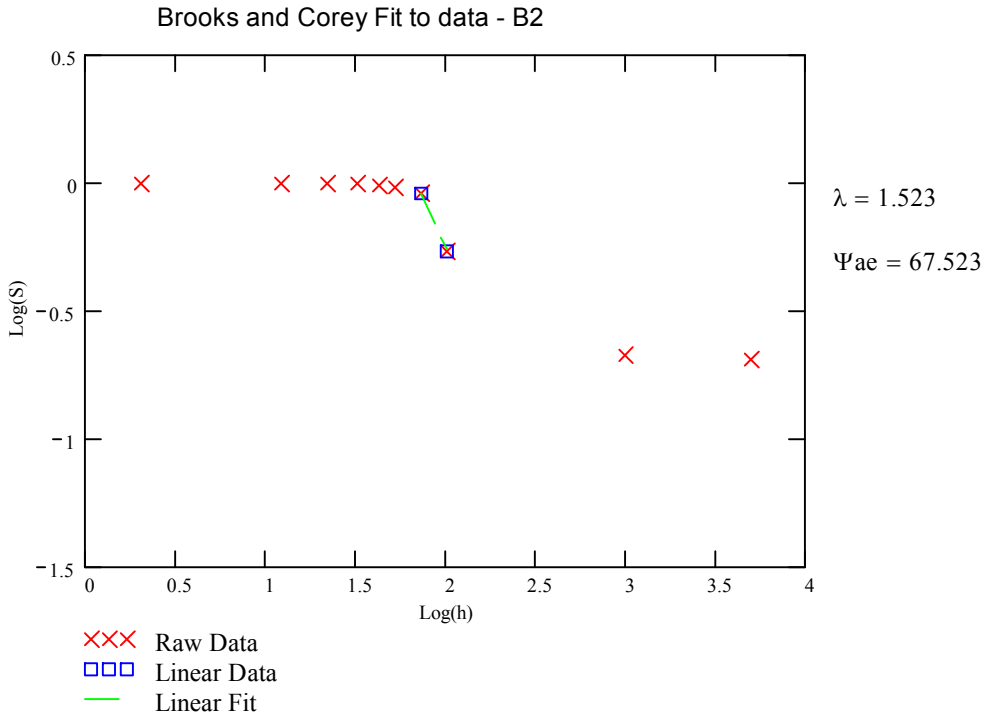

Figure N.22 – Linear Brooks and Corey fit to sample B2.

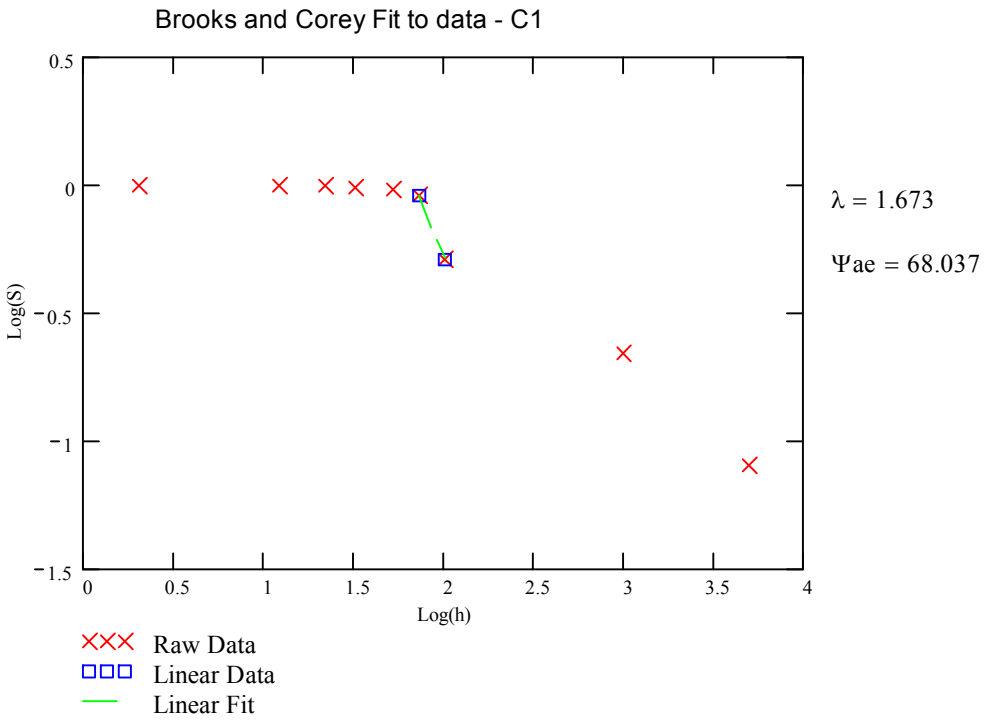

Figure N.23 – Linear Brooks and Corey fit to sample C1.

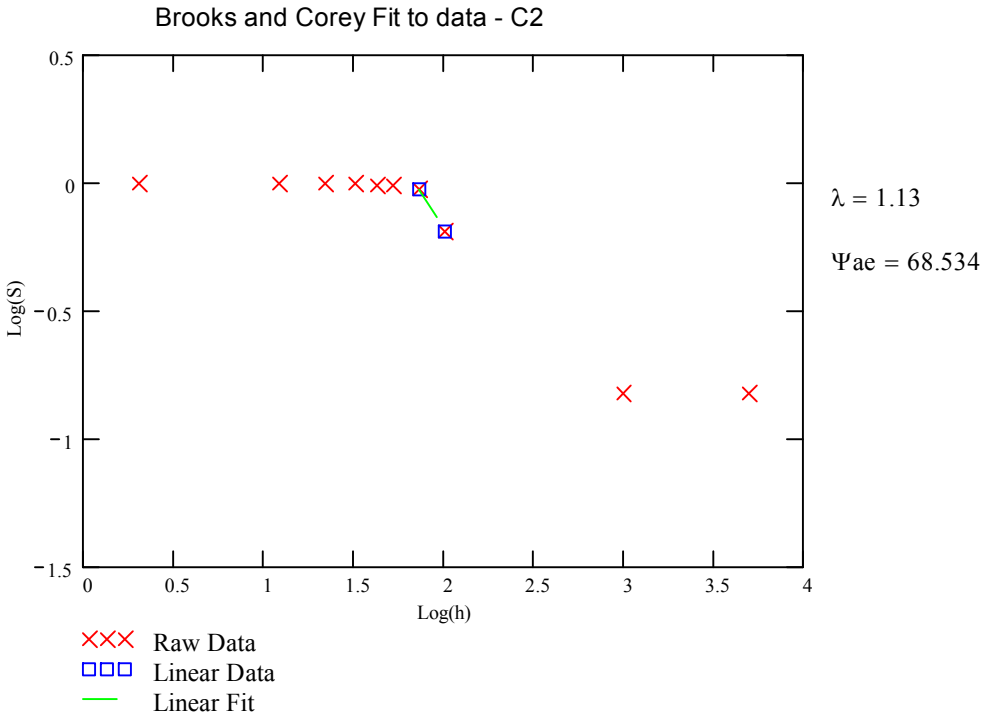

Figure N.24 – Linear Brooks and Corey fit to sample C2.

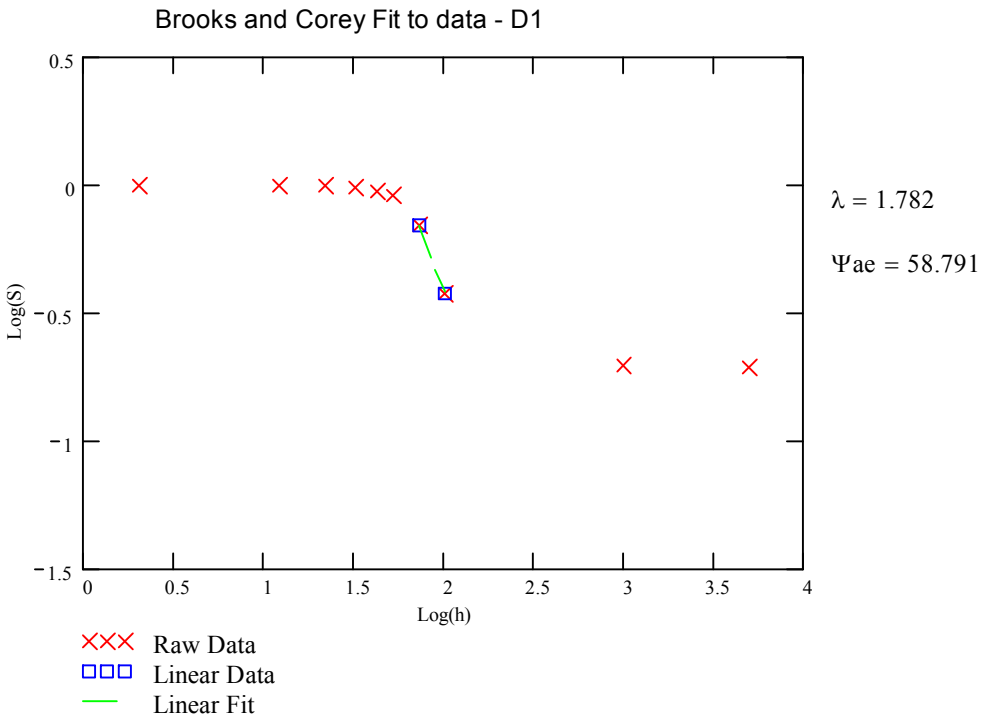

Figure N.25 – Linear Brooks and Corey fit to sample D1.

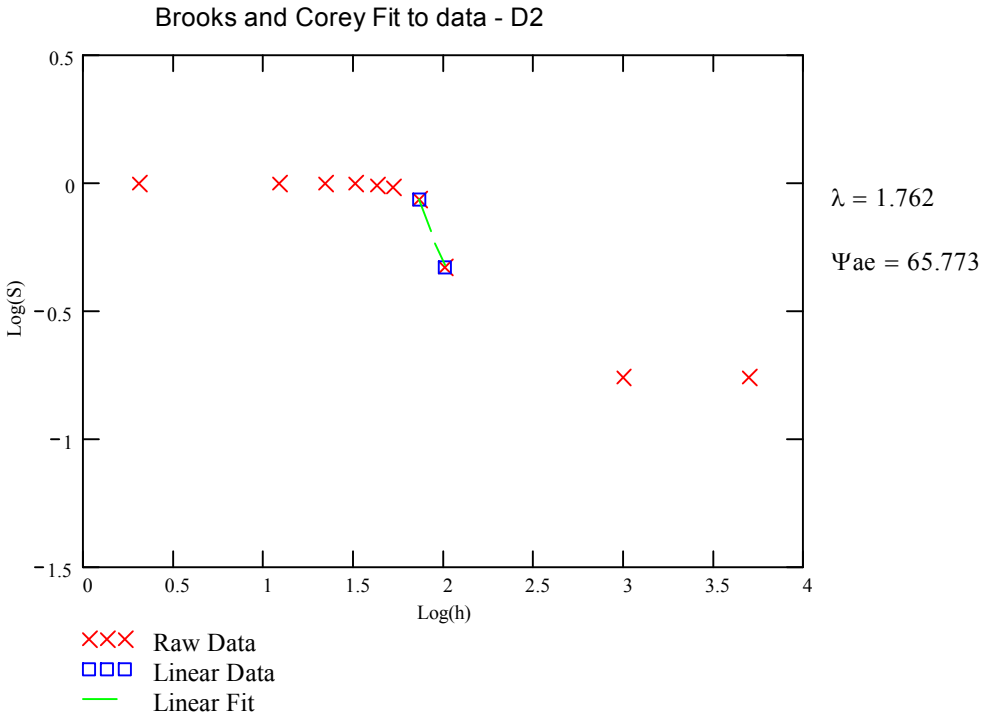

Figure N.26 – Linear Brooks and Corey fit to sample D2.

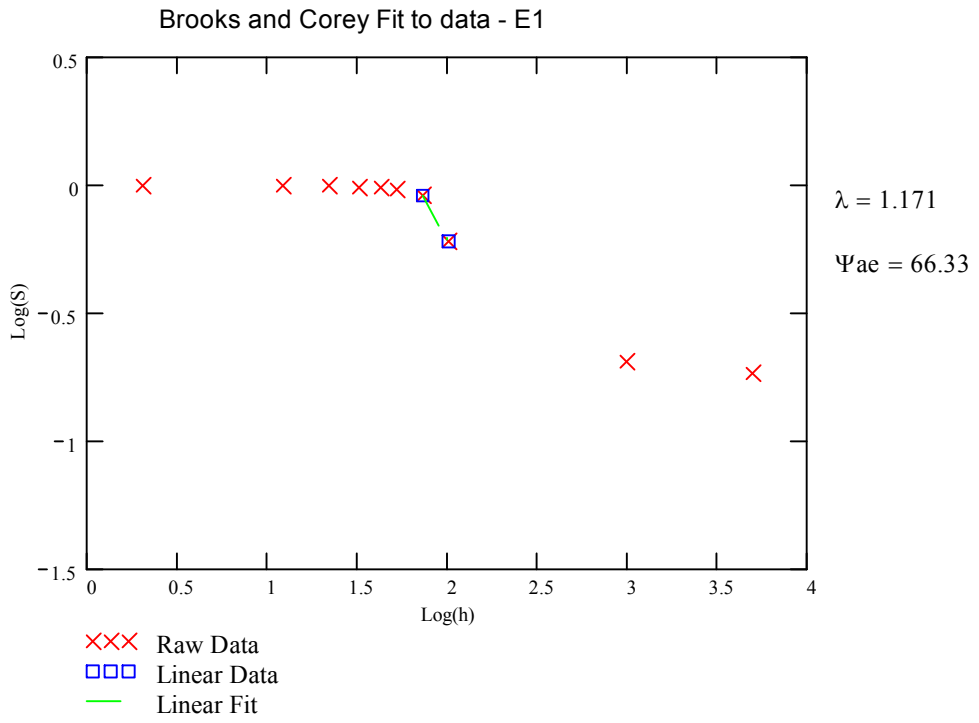

Figure N.27 – Linear Brooks and Corey fit to sample E1.

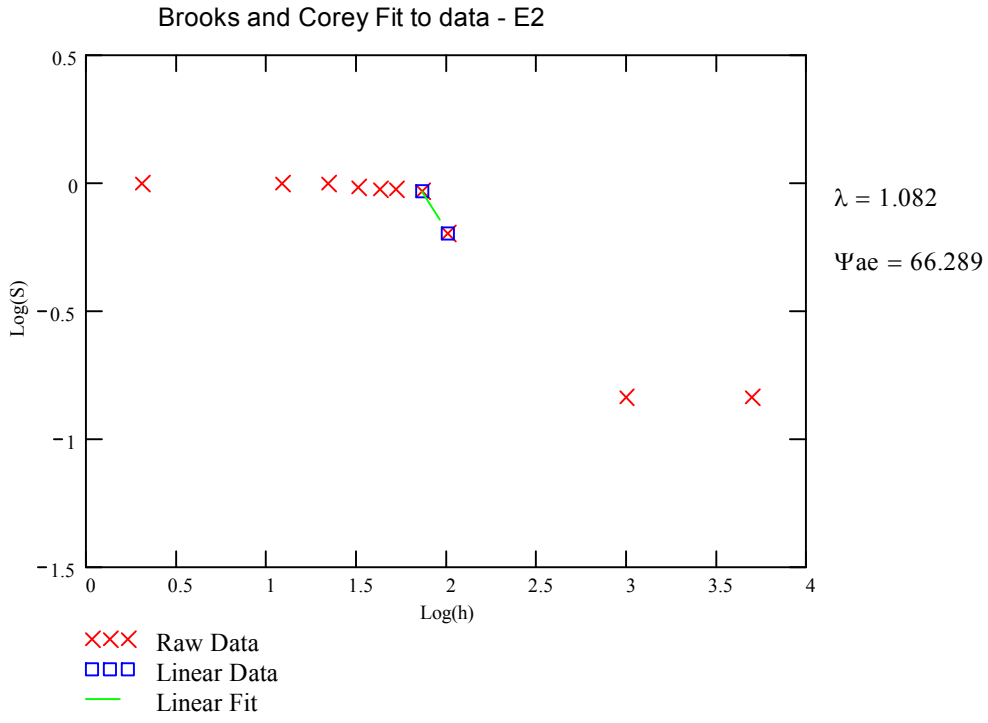

Figure N.28 – Linear Brooks and Corey fit to sample E2.

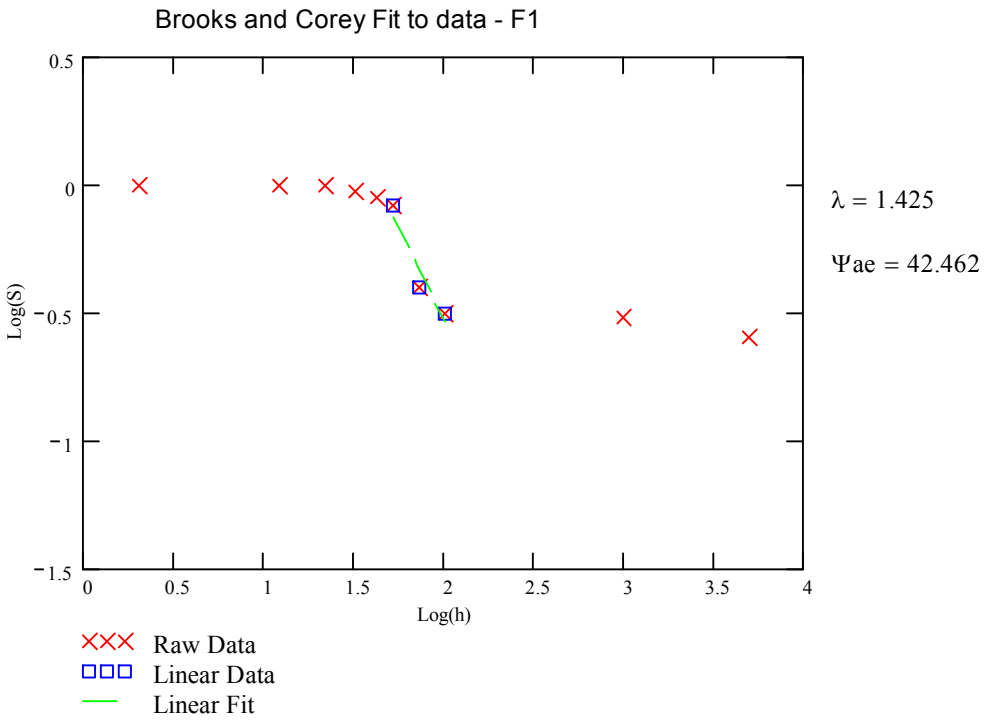

Figure N.29 – Linear Brooks and Corey fit to sample F1.

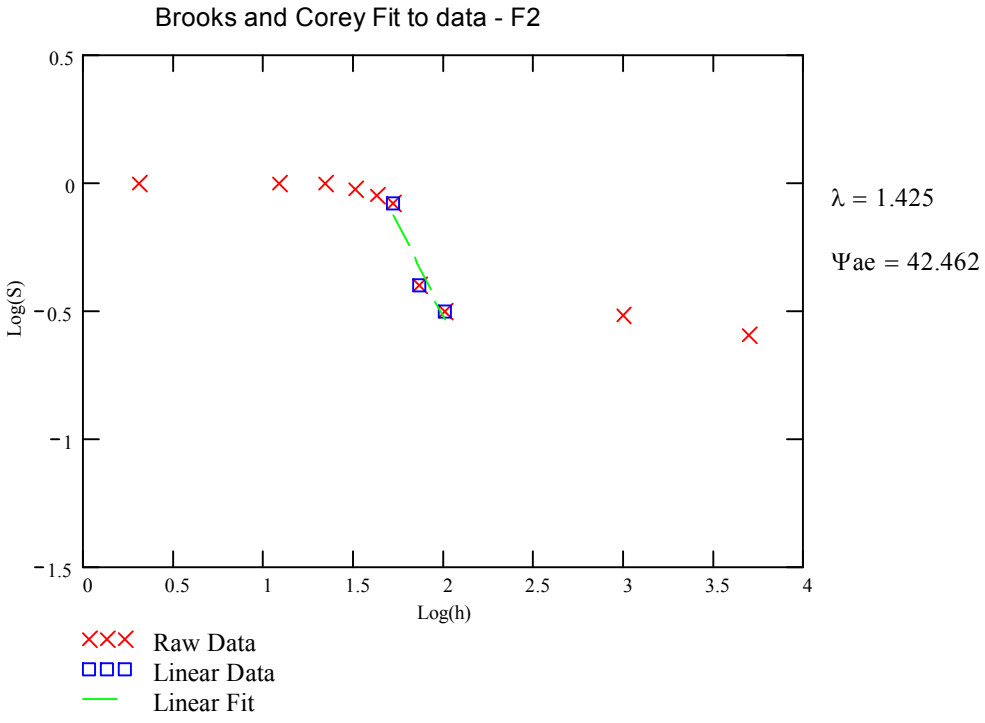

Figure N.30 – Linear Brooks and Corey fit to sample F2.

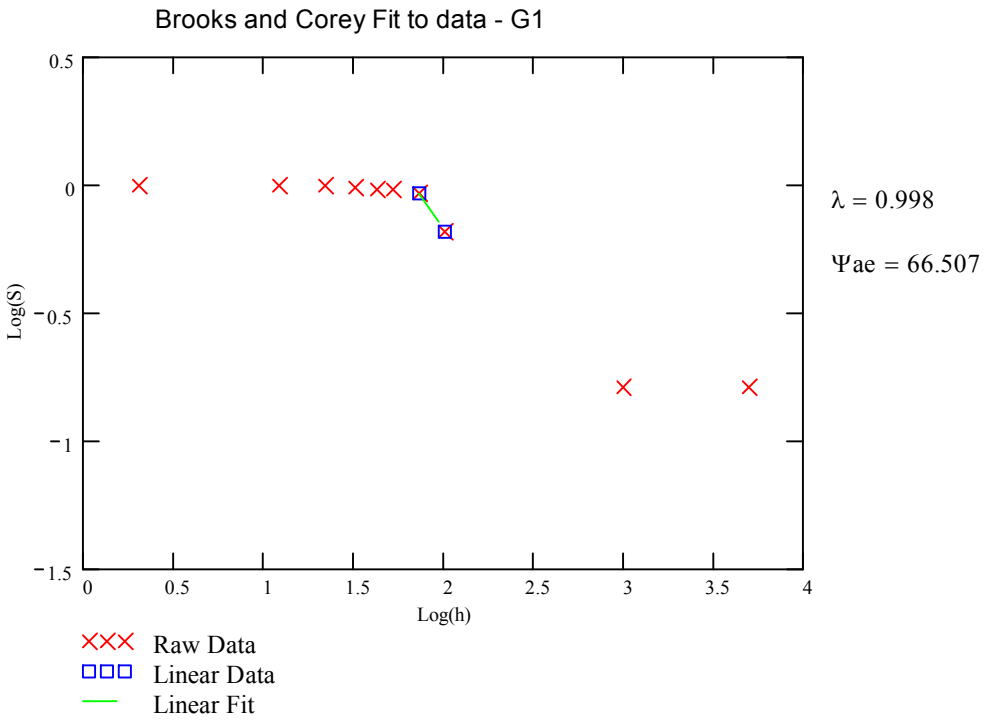

Figure N.31 – Linear Brooks and Corey fit to sample G1.

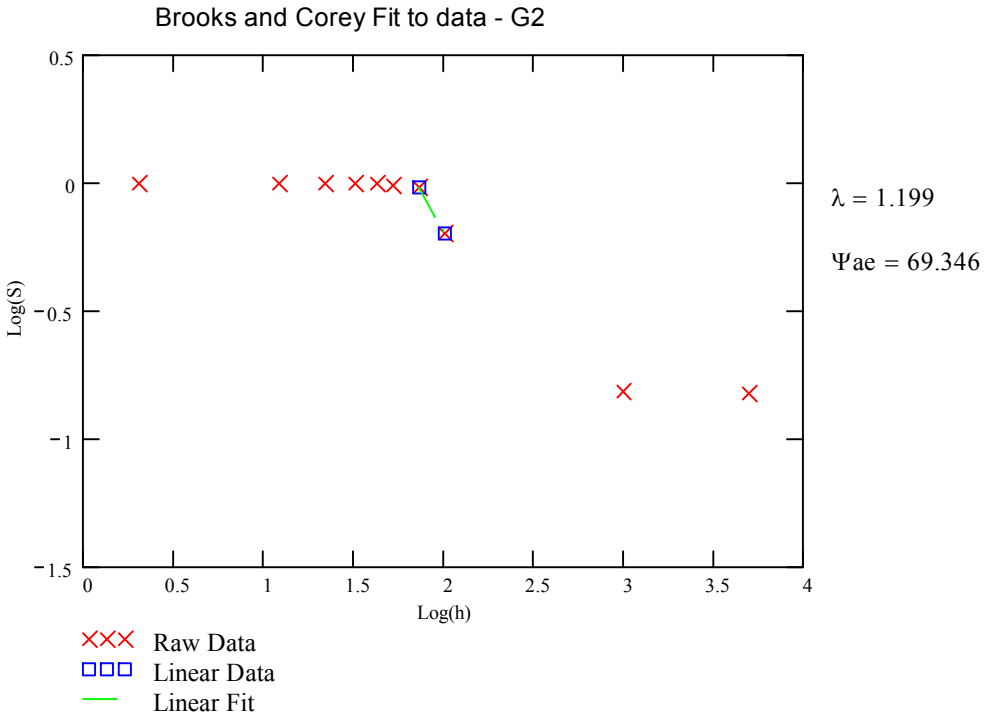

Figure N.32 – Linear Brooks and Corey fit to sample G2.

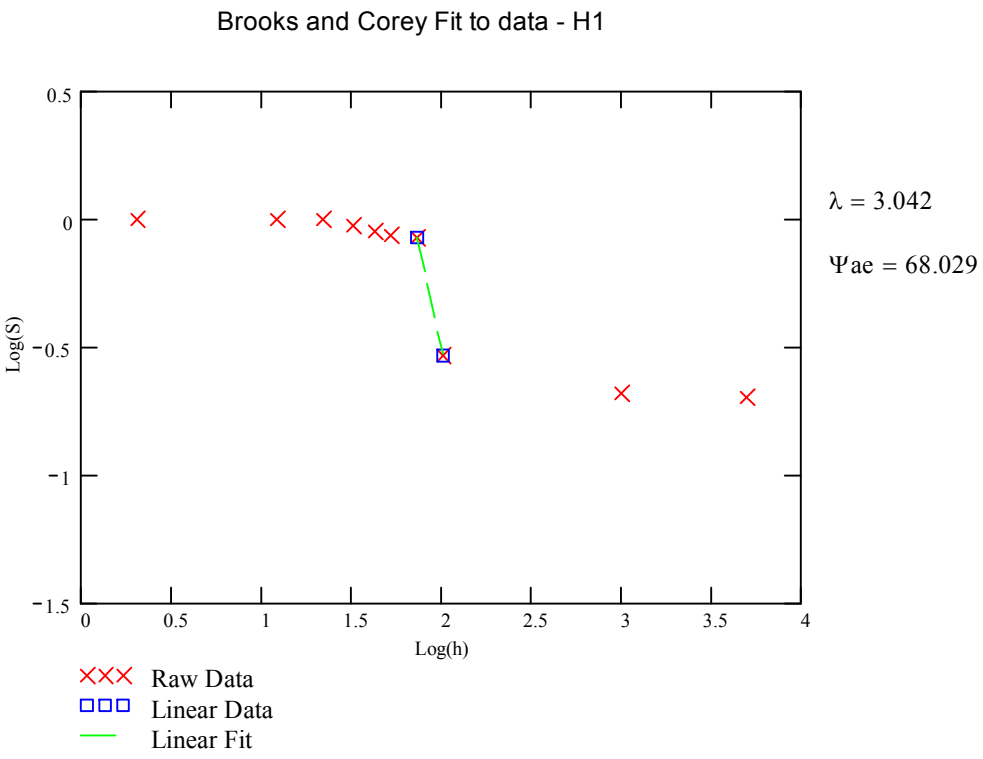

Figure N.33 – Linear Brooks and Corey fit to sample H1.

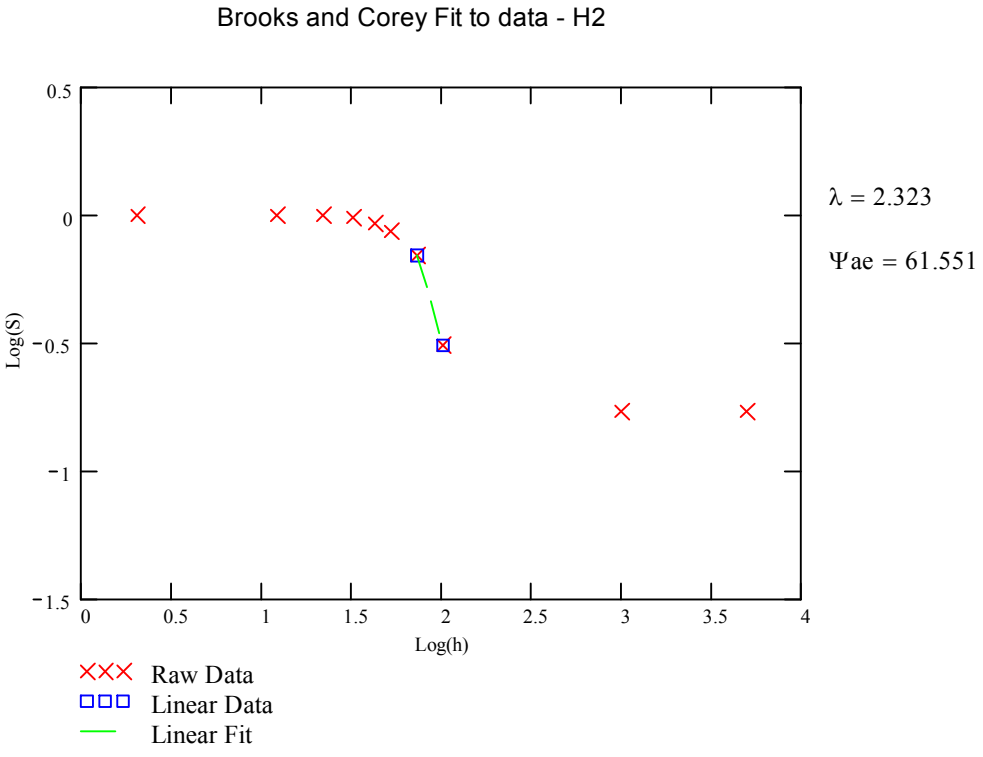

Figure N.34 – Linear Brooks and Corey fit to sample H2.

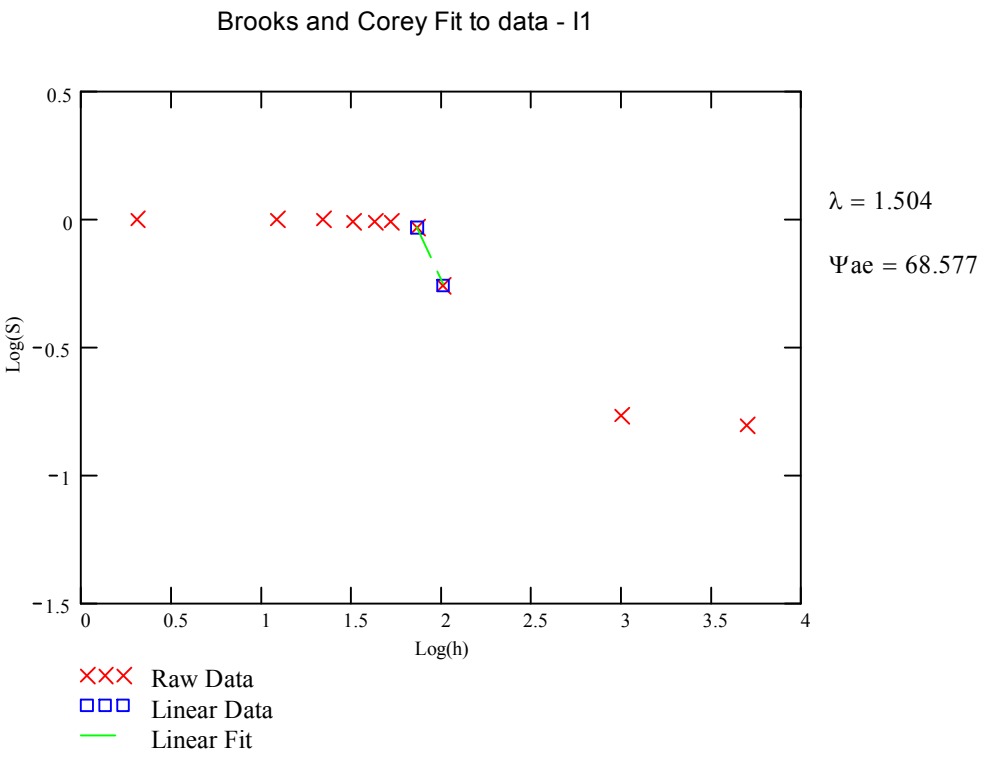

Figure N.35 – Linear Brooks and Corey fit to sample I1.

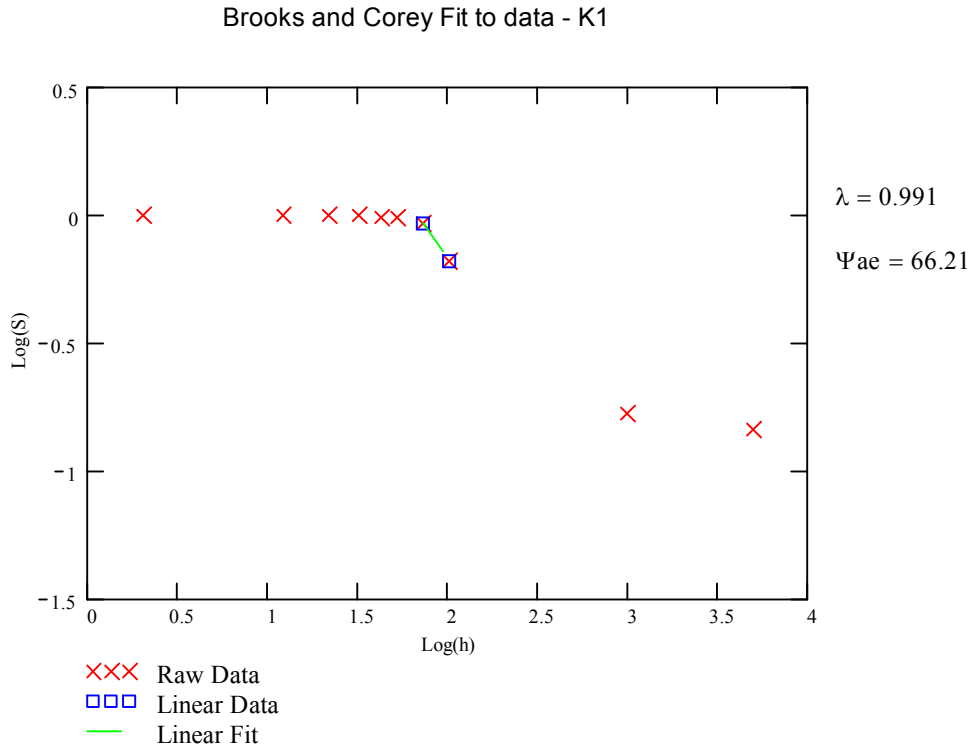

Figure N.36 – Linear Brooks and Corey fit to sample K1.

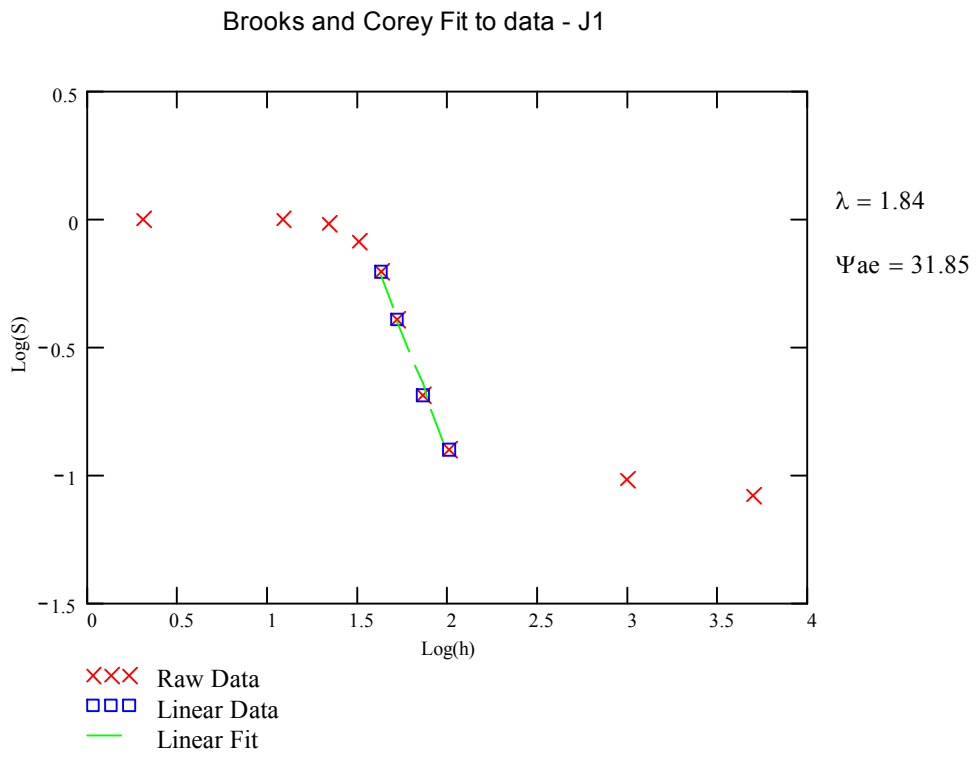

Figure N.37 – Linear Brooks and Corey fit to sample J1.

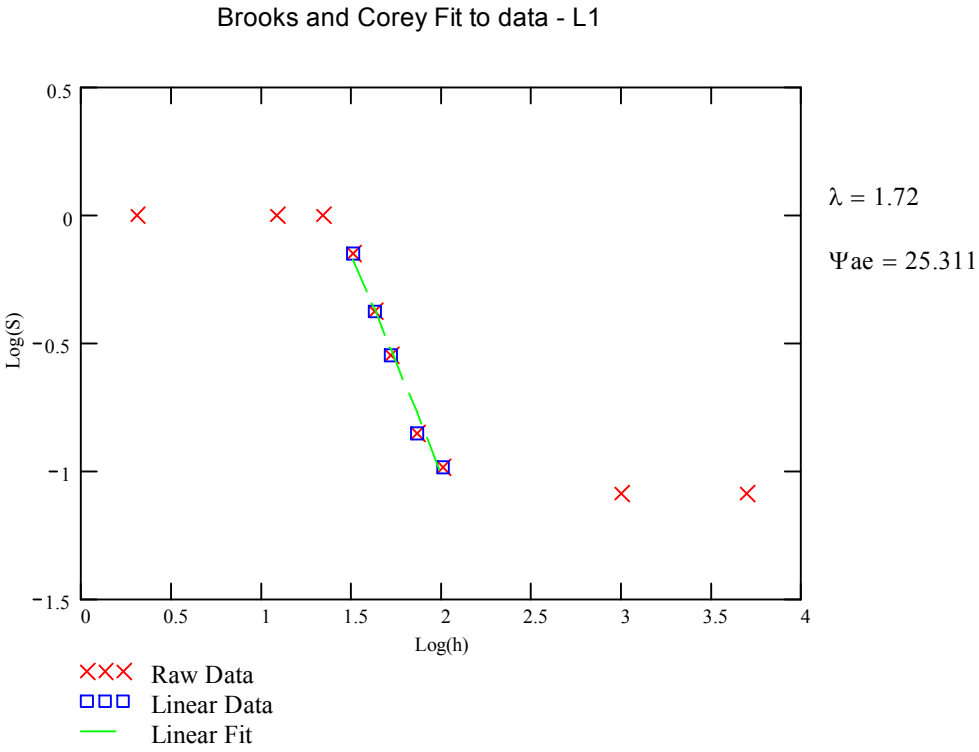

Figure N.38 – Linear Brooks and Corey fit to sample L1.

Appendix O

Modified Parameter Estimation Model Procedures

O.1 Introduction

The van Genuchten equation (Equation 2.1) is used by many researchers to estimate moisture retention and unsaturated hydraulic conductivity properties. For this reason, we examine correlations between pore-size and particle-size distribution parameters (both are described by the van Genuchten equation – see chapter 2) to estimate moisture retention curves from measurements of bulk density and particle-size distributions for sandy alluvial deposits.

We use methods described by Haverkamp and Parlange (1986) to estimate the slope of the PDC moisture retention curve (n). The slope of the moisture retention curve is very sensitive to related parameters used in the curve fitting procedure, i.e. the residual moisture content and saturation. Both these parameters were chosen as free parameters in the RETC program for fitting the van Genuchten equation to measured data (primarily due to uncertainties in the measured values). Weighting of data points can also impact the slope of the curves. Since the curve fitting process is quite subjective, a large degree of uncertainty exists in the slope of the moisture retention curves resulting in poor correlations between parameters. Because we did not observe strong correlations between the slope of the hysteretic curves, we assume n is constant for the MDC, MWC, and the PDC.

We determined that the correlation between the particle size distribution parameter d_g provides a better estimate of α than the Laplace-Young equation (3-4),

therefore we use this relationship to estimate α in the model for the PDC. We use correlations between the PDC and the MWC and MDC to estimate α for these curves. The estimation model was written in MATHCAD by Kristine Baker. Examples of the program functions are included in this appendix. Results are written to output files for analysis.

O.2 MATHCAD program for estimating van Genuchten fitting parameters for MWC, MDC, and PDC moisture retention curves.

Estimation Model for Predicting van Genuchten Parameteric Model Fitting Parameters and Moisture Retention Curves. Written and Developed by Kristine Baker, February 2001.

Read in vG parameters for NW core samples:

$data := READPRN("input.txt")$

$I := rows(data)$ $I = 19$

$i := 1..I$

$Bd_i := data_{i,1}$

$psdn_i := data_{i,2}$ $ratio_i := data_{i,6}$ $mdcn_i := data_{i,10}$

$pdc\alpha_i := data_{i,3}$ $\phi_i := data_{i,7}$ $mwc\alpha_i := data_{i,11}$

$dg_i := data_{i,4}$ $\theta s_i := data_{i,8}$ $mdc\alpha_i := data_{i,12}$

$pdcn_i := data_{i,5}$ $mwcn_i := data_{i,9}$ $\theta r_i := data_{i,13}$

$$m_i := 1 - \left(\frac{1}{pdcn_i}\right)$$

estimated vG "n": y = 0.4526x^2.1611

R^2 = 0.5319

NOTE: Did not use nw8,nw11,nw12,nw23,nw24 in model estimation calibration for "n". Used all samples to calculate gamma.

$$vGn_i := 0.4526\left[\left(Bd_i\right)^{2.1611}\right] \cdot psdn_i$$

estimated gamma: y = 1.0184x^2 - 10.365x + 33.123

R^2 = 0.5357

$$\gamma_i := 1.0184\left(pdcn_i\right)^2 - 10.365 pdcn_i + 33.123$$

estimated satiation: y = 1.6813x - 0.3082

R^2 = 0.6967

$$est\,\theta s_i := 1.6813\phi_i - 0.3082$$

Estimates of 1/alpha:

Using the Laplace Young Equation

est 1/α (cm) =(0.149*gamma)/(dg*0.10)

$$\text{est}\alpha 1_i := \frac{1}{0.149}\cdot dg_i \cdot \frac{.10}{\gamma_i} \qquad \text{alphainv}_i := \frac{1}{\text{est}\alpha 1_i}$$

Using parameter correlation between dg and 1/alpha:
y = 19.424x^(-0.7177)

R^2 = 0.9017

$$\text{est}\alpha 2_i := 19.424\left(dg_i\right)^{-0.7177}$$

Comparison of estimates (1/alpha):

$$\text{diff1}_i := \frac{\text{alphainv}_i}{\text{pdc}\alpha_i} \qquad \text{diff2}_i := \frac{\text{est}\alpha 2_i}{\text{pdc}\alpha_i}$$

$$\text{meandiff1} := \left(\frac{1}{I}\right)\cdot \sum_{i=1}^{I} \text{diff1}_i \qquad \text{meandiff2} := \left(\frac{1}{I}\right)\cdot \sum_{i=1}^{I} \text{diff2}_i$$

$\text{meandiff1} = 1.195$

$\text{stdev}(\text{diff1}) = 0.825$

$\text{meandiff2} = 1.069$

$\text{stdev}(\text{diff2}) = 0.275$

MWCα est: y = 0.4144x + 1.3973

R^2 = 0.858

MDCα est: y = 0.7358x + 11.195

R^2 = 0.8253

$$\text{mwc}\alpha 1_i := 0.4144\text{est}\alpha 2_i + 1.3973 \qquad \text{mdc}\alpha 1_i := 0.7358\text{est}\alpha 2_i + 11.195$$

Read in moisture retention data for NW core samples:

pdc := READPRN("nw21pdc.dat")

R := rows(pdc) R = 8

r := 1.. R

$Z1_r := pdc_{r,1}$ $X1_r := pdc_{r,2}$

mwc := READPRN("nw21mwc.dat")

W := rows(mwc) W = 9

w := 1.. W

$Z2_w := mwc_{w,1}$ $X2_w := mwc_{w,2}$

mdc := READPRN("nw21mdc.dat")

D := rows(mdc)

d := 1.. D D = 10

$Z3_d := mdc_{d,1}$ $X3_d := mdc_{d,2}$

---

k := 2.. 3000 C=Curve Number

$\Psi_k := k$

C := 14

k := 1.. 5000

$\Psi_k := k$

C1=NW1
C2=NW2
C3=NW4
C4=NW7
C5=NW8
C6=NW9
C7=NW10
C8=NW11
C9=NW12
C10=NW16
C11=NW17
C12=NW19
C13=NW20
C14=NW21
C15=NW22
C16=NW23
C17=NW24
C18=NW25
C19=NW27

vG PDC Equation for moisture content:

$$\theta(\Psi) := (\phi_C - \theta r_C)\cdot\left[1 + \left(\frac{\Psi}{est\alpha 2_C}\right)^{vGn_C}\right]^{-m_C} + \theta r_C$$

Includes fitted residual MC

vG MWC Equation for moisture content:

$$\theta 1(\Psi) := (est\theta s_C - \theta r_C)\cdot\left[1 + \left(\frac{\Psi}{mwc\alpha 1_C}\right)^{vGn_C}\right]^{-m_C} + \theta r_C$$

Assuming vG n is the same as PDC

vG MDC Equation for moisture content:

$$\theta 2(\Psi) := (est\theta s_C - \theta r_C)\cdot\left[1 + \left(\frac{\Psi}{mdc\alpha 1_C}\right)^{vGn_C}\right]^{-m_C} + \theta r_C$$

Assuming vG n is the same as PDC

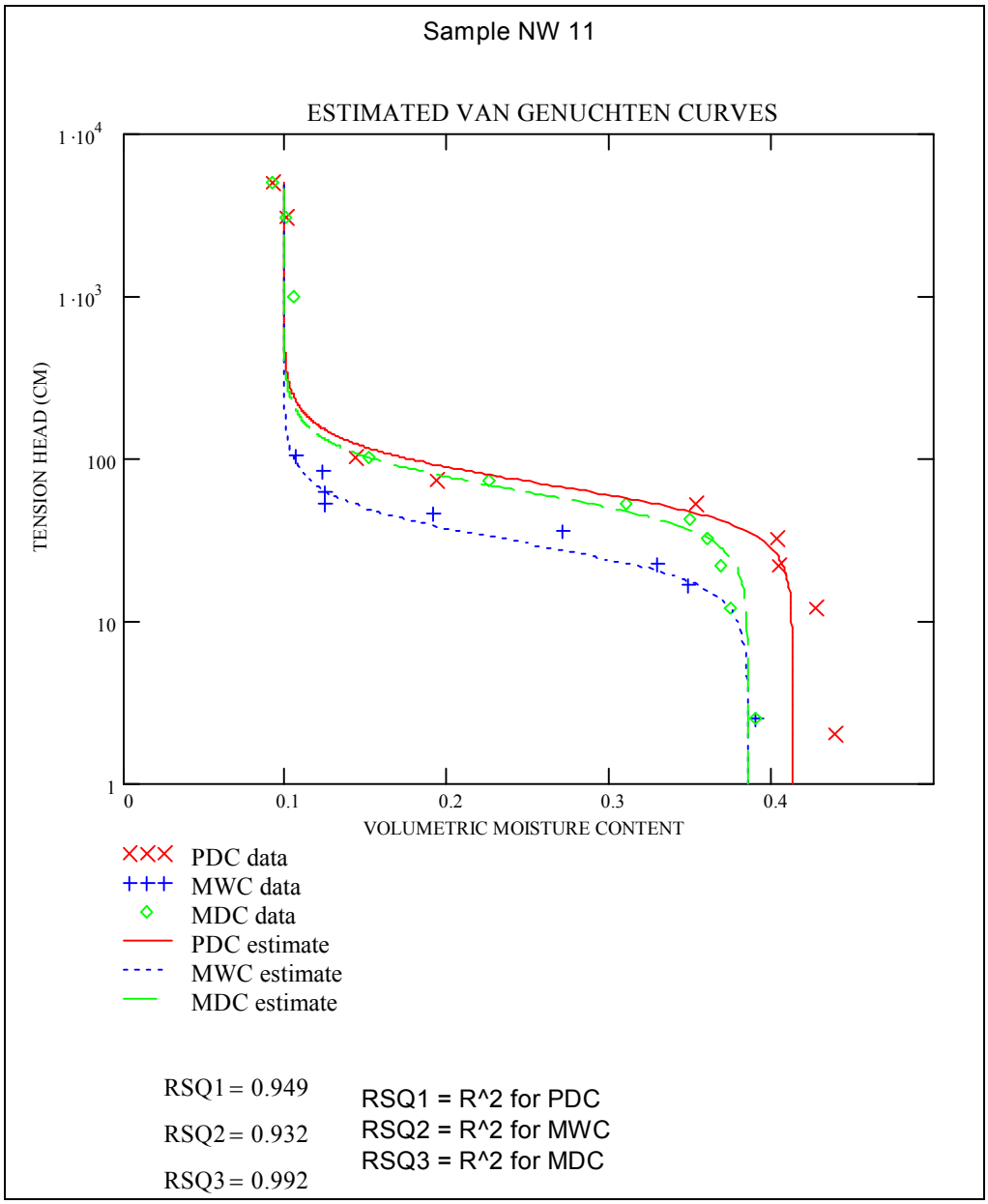
Sample NW 11
ESTIMATED VAN GENUCHTEN CURVES
TENSION HEAD (CM)
1·10^4
1·10^3
100
10
1
0
0.1
0.2
0.3
0.4
VOLUMETRIC MOISTURE CONTENT
PDC data
MWC data
MDC data
PDC estimate
MWC estimate
MDC estimate
RSQ1 = 0.949
RSQ2 = 0.932
RSQ3 = 0.992
RSQ1 = R^2 for PDC
RSQ2 = R^2 for MWC
RSQ3 = R^2 for MDC

R^2 for estimated curves:
R^2=1-[sse/sst]
sse=sum(Y-Yest)^2
sst=sum(Y^2)-[(sumY)^2]/n
Y1=calibrated fit
Y2=H&P est
Y3=B&C fit to data
Y4=calibrated fit using eqn 32

$$Y1_r := \left(\phi_C - \theta r_C\right)\cdot\left[1 + \left(\frac{Z1_r}{est\alpha 2_C}\right)^{vGn_C}\right]^{-m_C} + \theta r_C$$

R^2 for the PDC

$$SSE2 := \sum_r \left(X1_r - Y1_r\right)^2$$

$$SST2 := \left[\sum_r \left(X1_r\right)^2\right] - \frac{\left(\sum_r X1_r\right)^2}{R}$$

$$RSQ1 := 1 - \left(\frac{SSE2}{SST2}\right)$$

$$RSQ1 = 0.378$$

$$Y2_w := \left(est\theta s_C - \theta r_C\right)\cdot\left[1 + \left(\frac{Z2_w}{mwc\alpha 1_C}\right)^{vGn_C}\right]^{-m_C} + \theta r_C$$

R^2 for the MWC

$$Y2_l = 0.076$$

$$SSE2 := \sum_w \left(X2_w - Y2_w\right)^2$$

$$SST2 := \left[\sum_w \left(X2_w\right)^2\right] - \frac{\left(\sum_w X2_w\right)^2}{W}$$

$$RSQ2 := 1 - \left(\frac{SSE2}{SST2}\right)$$

$$RSQ2 = 0.047$$

$$Y3_d := \left(est\theta s_C - \theta r_C\right)\cdot\left[1 + \left(\frac{Z3_d}{mdc\alpha 1_C}\right)^{vGn_C}\right]^{-m_C} + \theta r_C$$

R^2 for the MDC

$$Y2_l = 0.076$$

$$SSE2 := \sum_d \left(X3_d - Y3_d\right)^2$$

$$SST2 := \left[\sum_d \left(X3_d\right)^2\right] - \frac{\left(\sum_d X3_d\right)^2}{D}$$

$$RSQ3 := 1 - \left(\frac{SSE2}{SST2}\right)$$

$$RSQ3 = 0.883$$

$$RS1 := augment(RSQ1, RSQ2)$$

$$RS2 := augment(RS1, RSQ3)$$

$$WRITEPRN("RSQ21.dat") := RS2$$

Appendix P

Modified Parameter Estimation Model Results

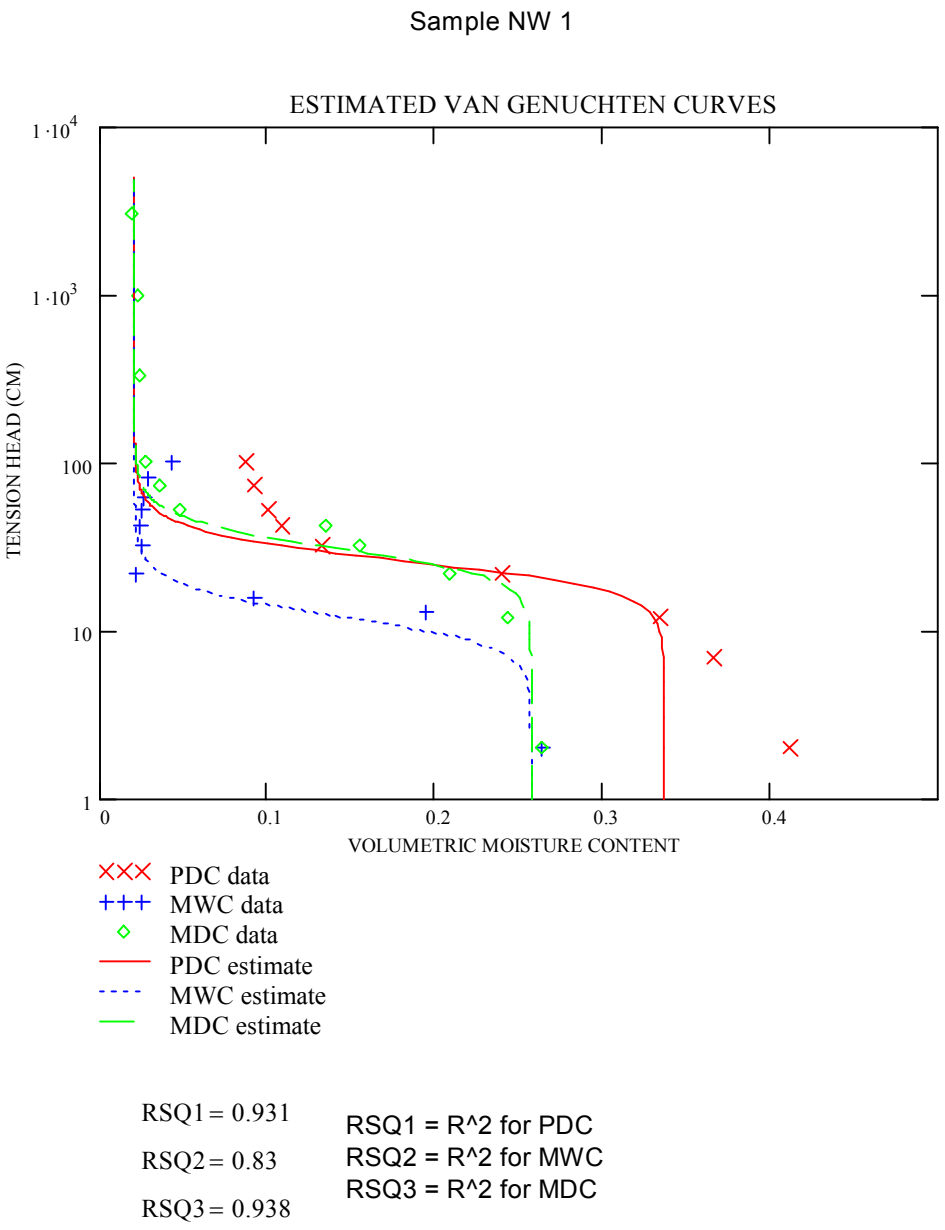

Figure P.1 – Estimated curves for sample NW1 using van Genuchten fitting parameters.

Sample NW 2

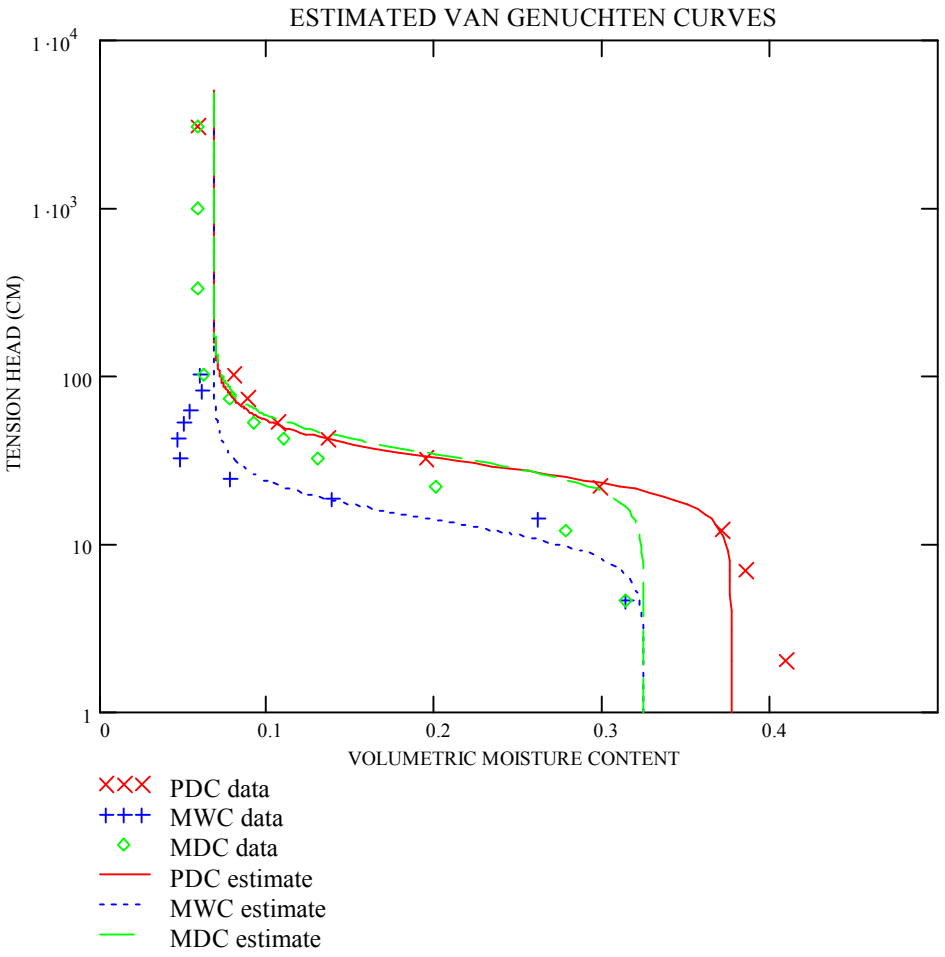

RSQ1 = 0.997

RSQ2 = 0.912

RSQ3 = 0.765

RSQ1 = R^2 for PDC
RSQ2 = R^2 for MWC
RSQ3 = R^2 for MDC

Figure P.2 – Estimated curves for sample NW2 using van Genuchten fitting parameters.

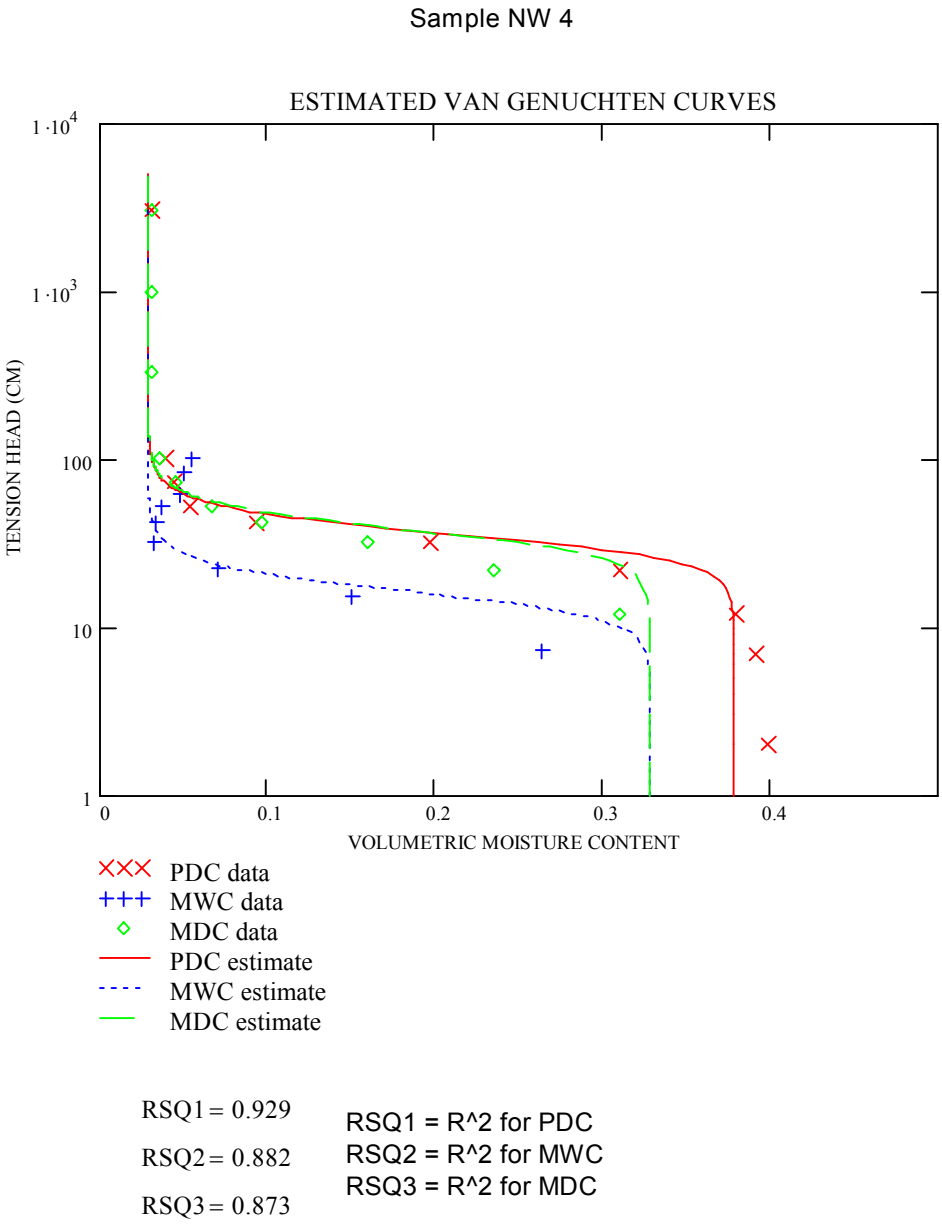

Figure P.3 – Estimated curves for sample NW4 using van Genuchten fitting parameters.

Sample NW 7

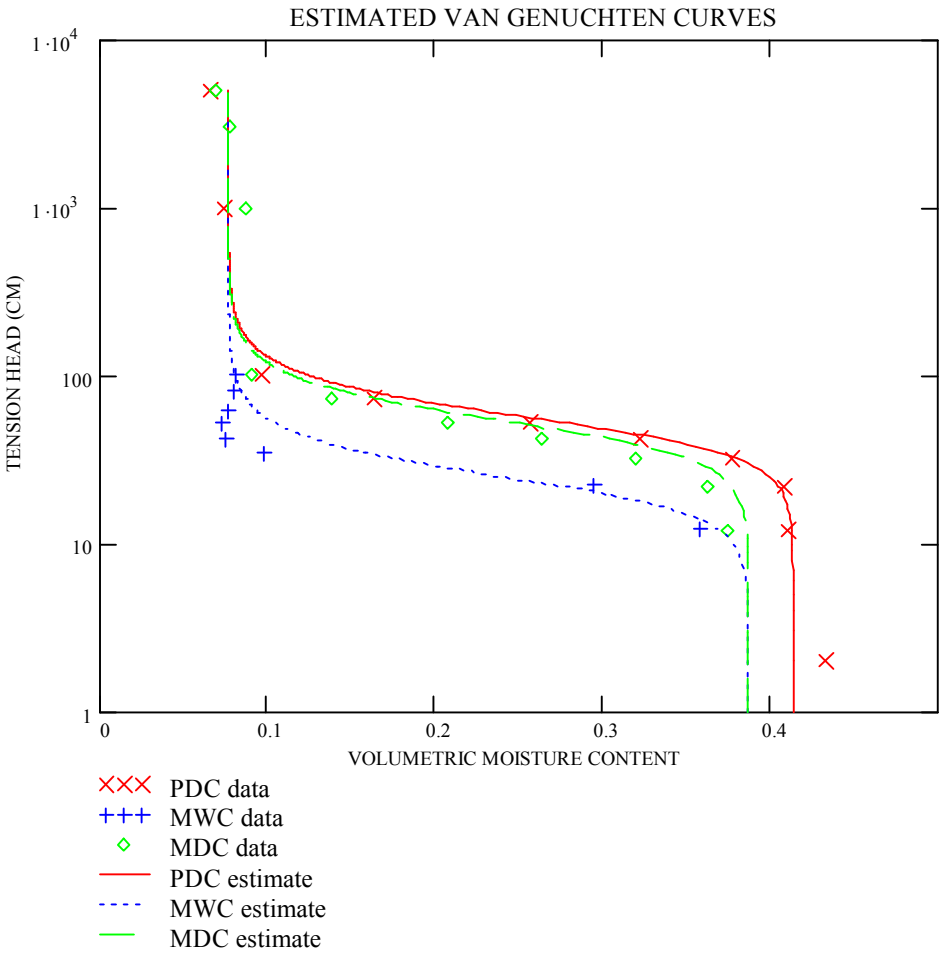

RSQ1 = 0.988

RSQ2 = 0.957

RSQ3 = 0.964

RSQ1 = R^2 for PDC
RSQ2 = R^2 for MWC
RSQ3 = R^2 for MDC

Figure P.4 – Estimated curves for sample NW7 using van Genuchten fitting parameters.

Sample NW 8

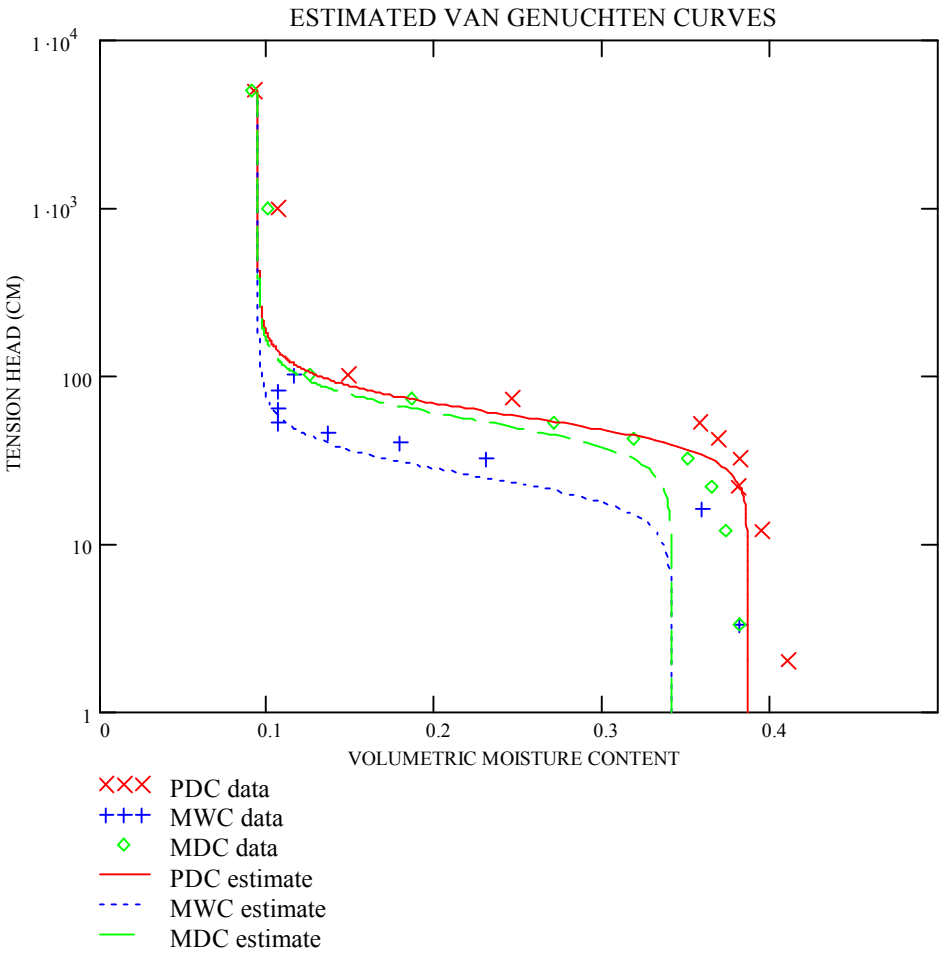

RSQ1 = 0.906

RSQ2 = 0.881

RSQ3 = 0.935

RSQ1 = R^2 for PDC
RSQ2 = R^2 for MWC
RSQ3 = R^2 for MDC

Figure P.5 – Estimated curves for sample NW8 using van Genuchten fitting parameters.

Sample NW 9

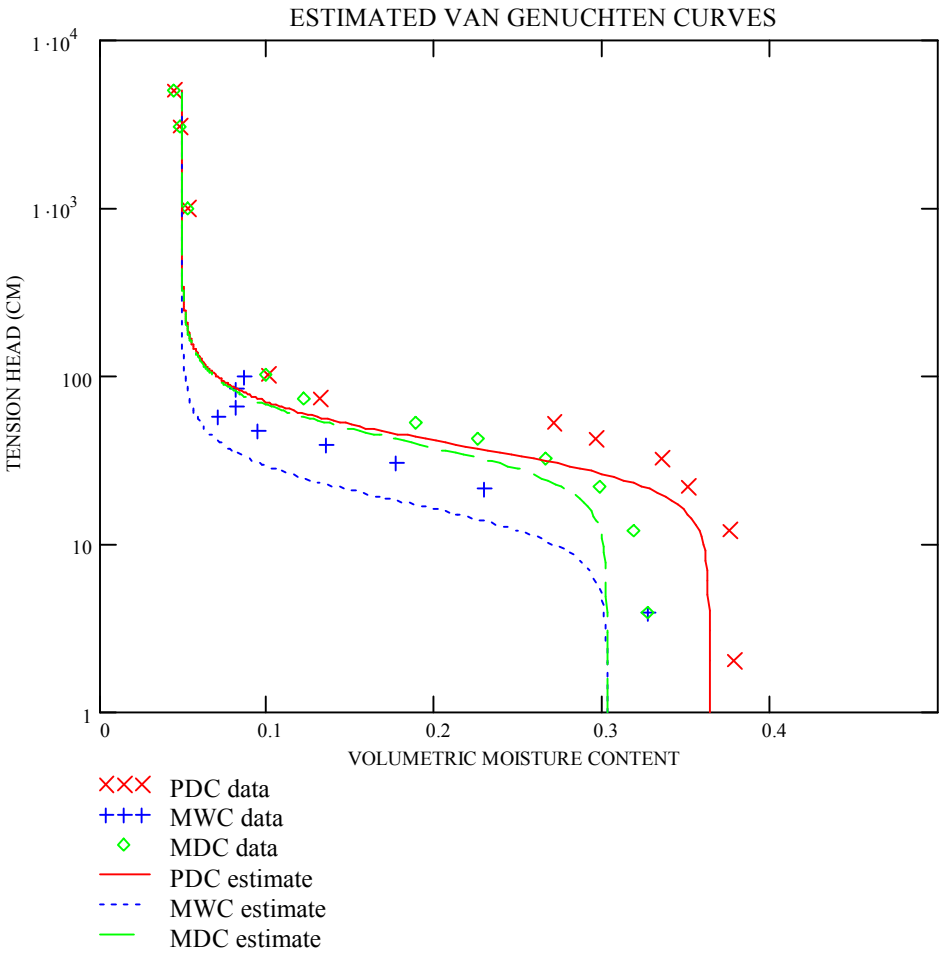

RSQ1 = 0.824

RSQ2 = 0.577

RSQ3 = 0.917

RSQ1 = R^2 for PDC
RSQ2 = R^2 for MWC
RSQ3 = R^2 for MDC

Figure P.6 – Estimated curves for sample NW9 using van Genuchten fitting parameters.

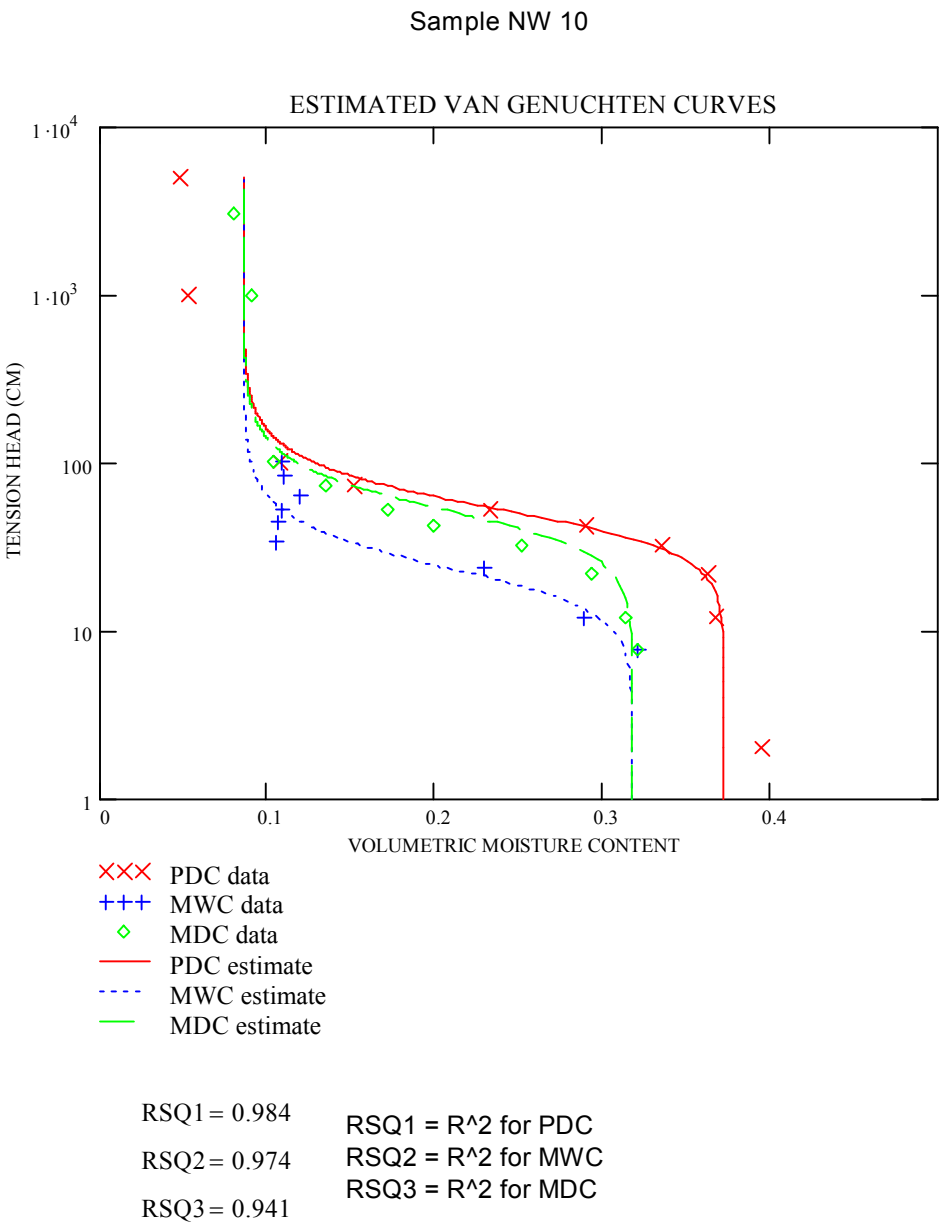

Figure P.7 – Estimated curves for sample NW10 using van Genuchten fitting parameters.

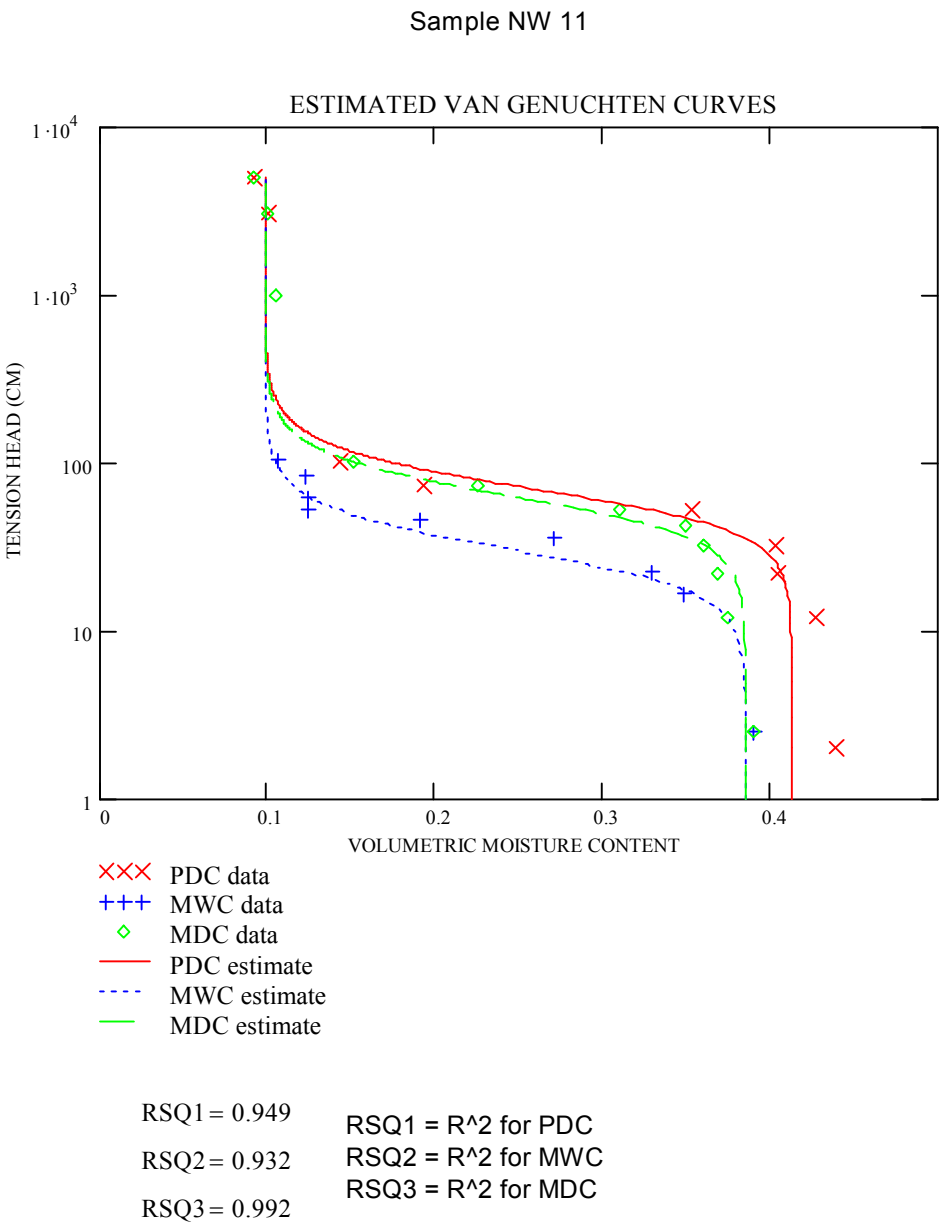

Figure P.8 – Estimated curves for sample NW11 using van Genuchten fitting parameters.

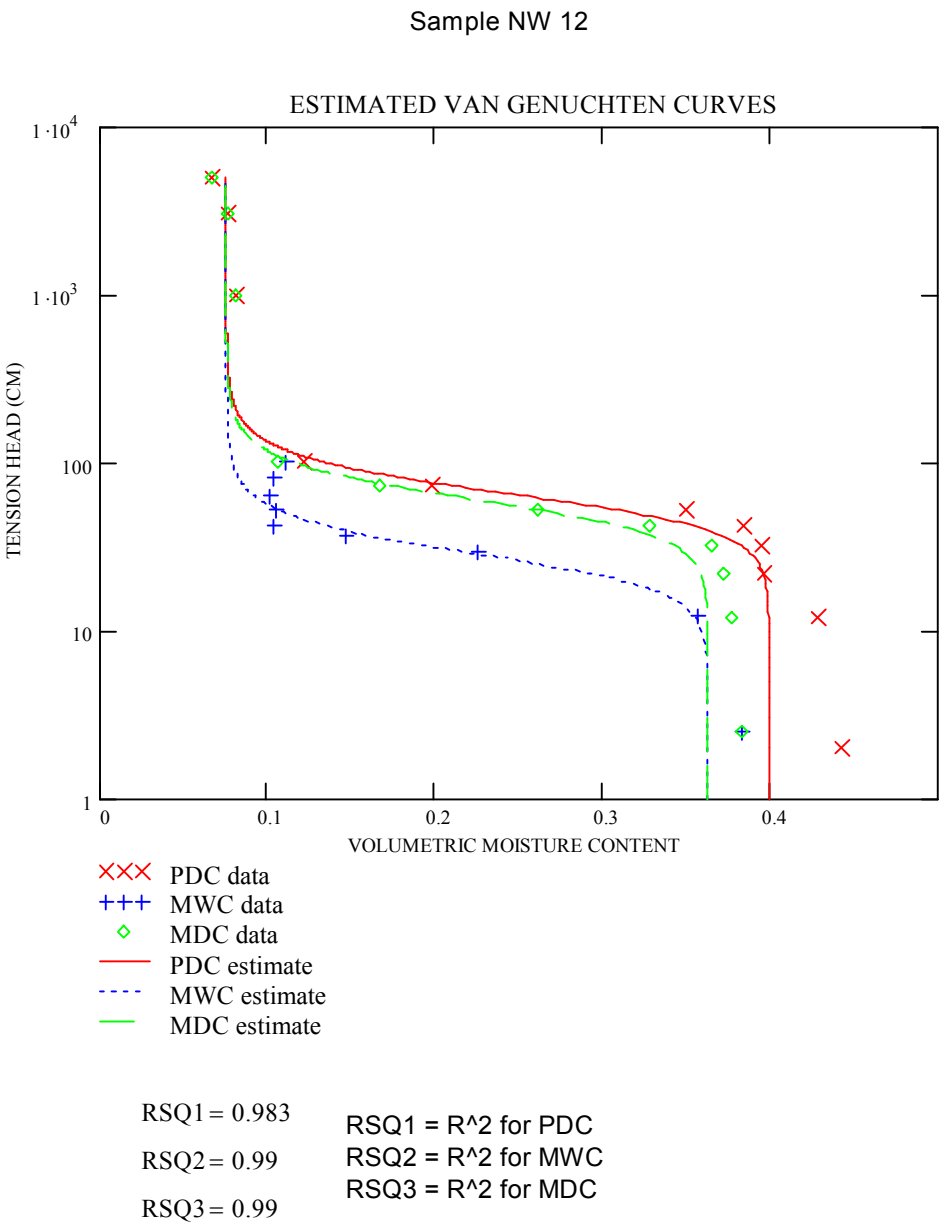

Figure P.9 – Estimated curves for sample NW12 using van Genuchten fitting parameters.

Sample NW 16

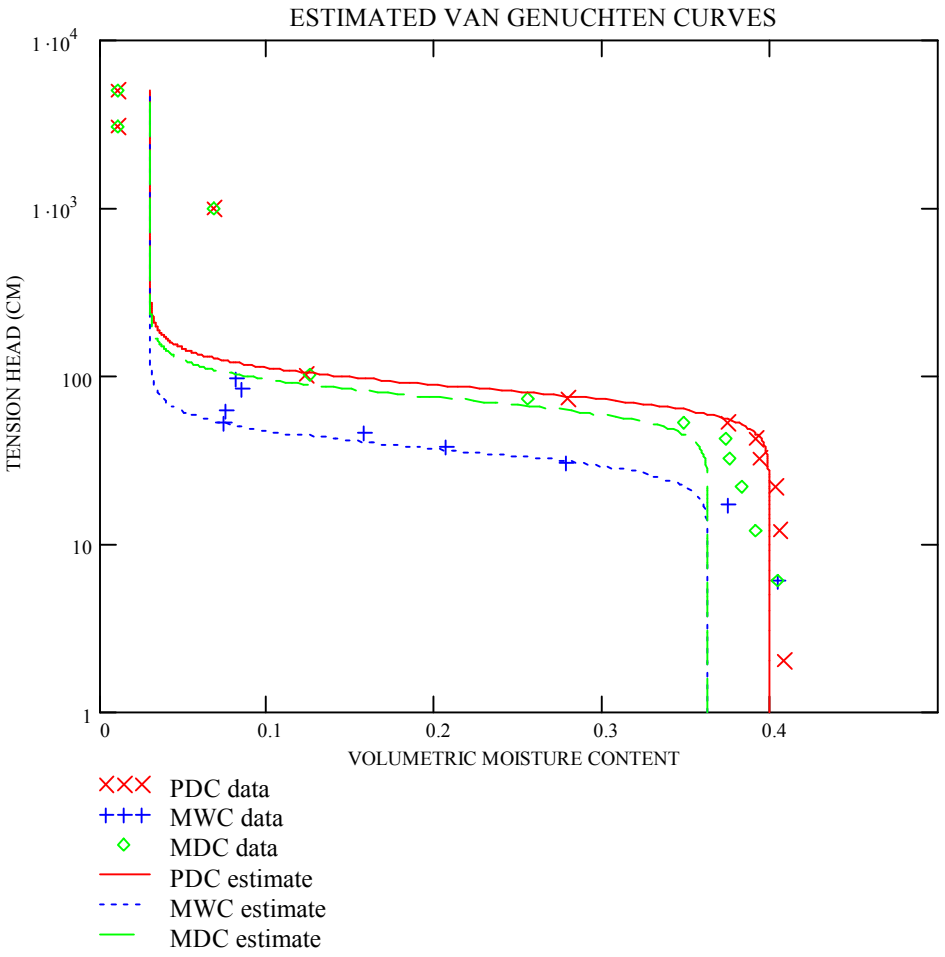

RSQ1 = 0.99

RSQ2 = 0.94

RSQ3 = 0.963

RSQ1 = R^2 for PDC
RSQ2 = R^2 for MWC
RSQ3 = R^2 for MDC

Figure P.10 – Estimated curves for sample NW16 using van Genuchten fitting parameters.

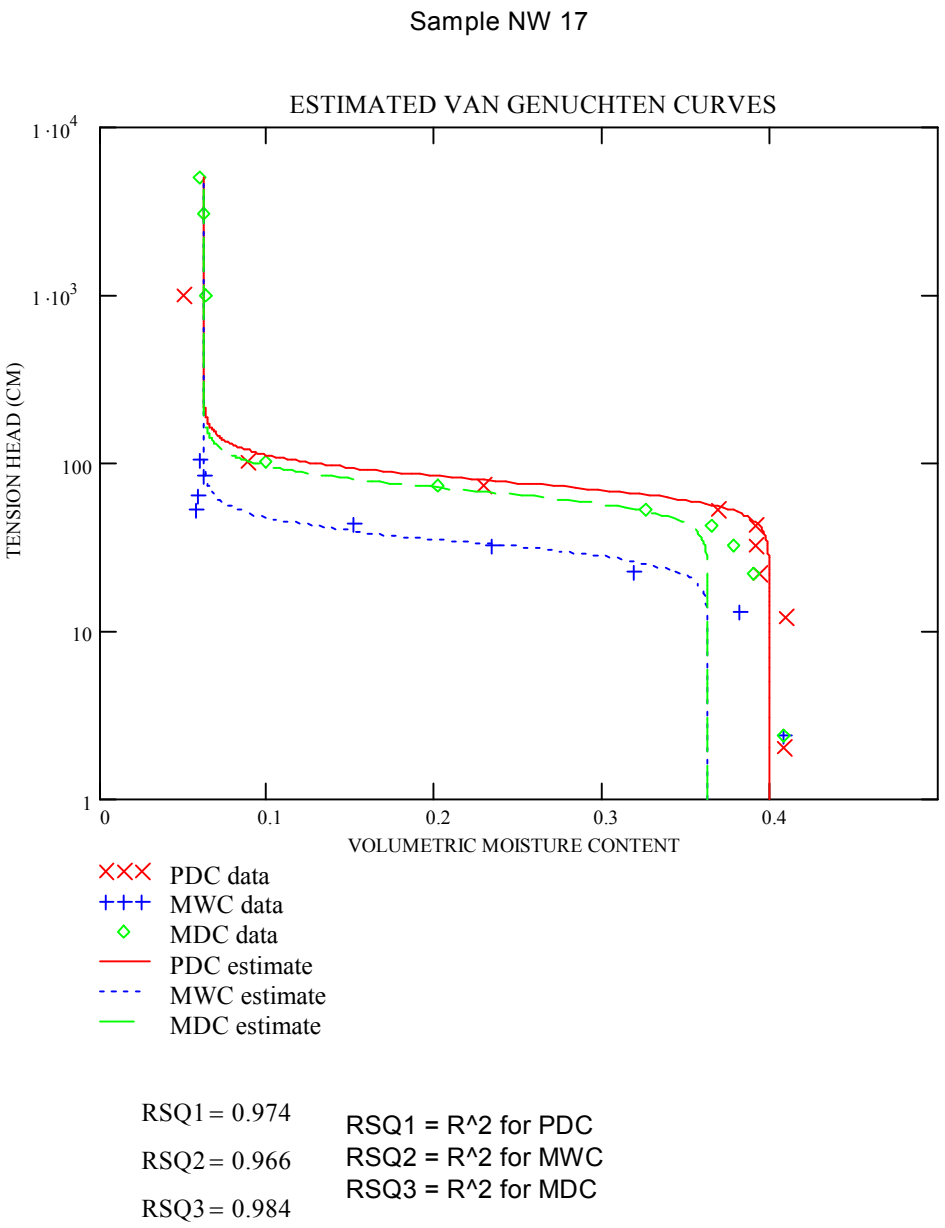

Figure P.11 – Estimated curves for sample NW17 using van Genuchten fitting parameters.

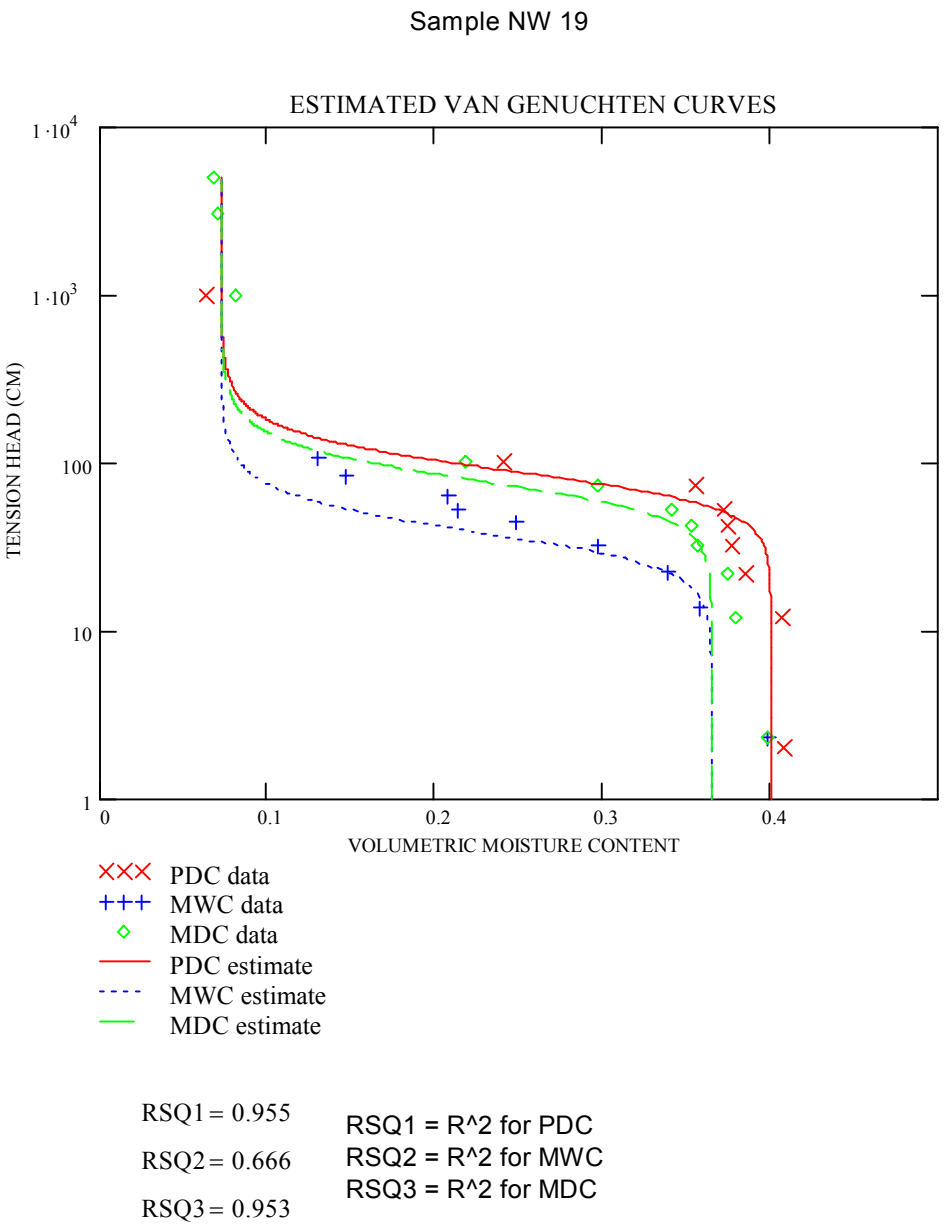

Figure P.12 – Estimated curves for sample NW19 using van Genuchten fitting parameters.

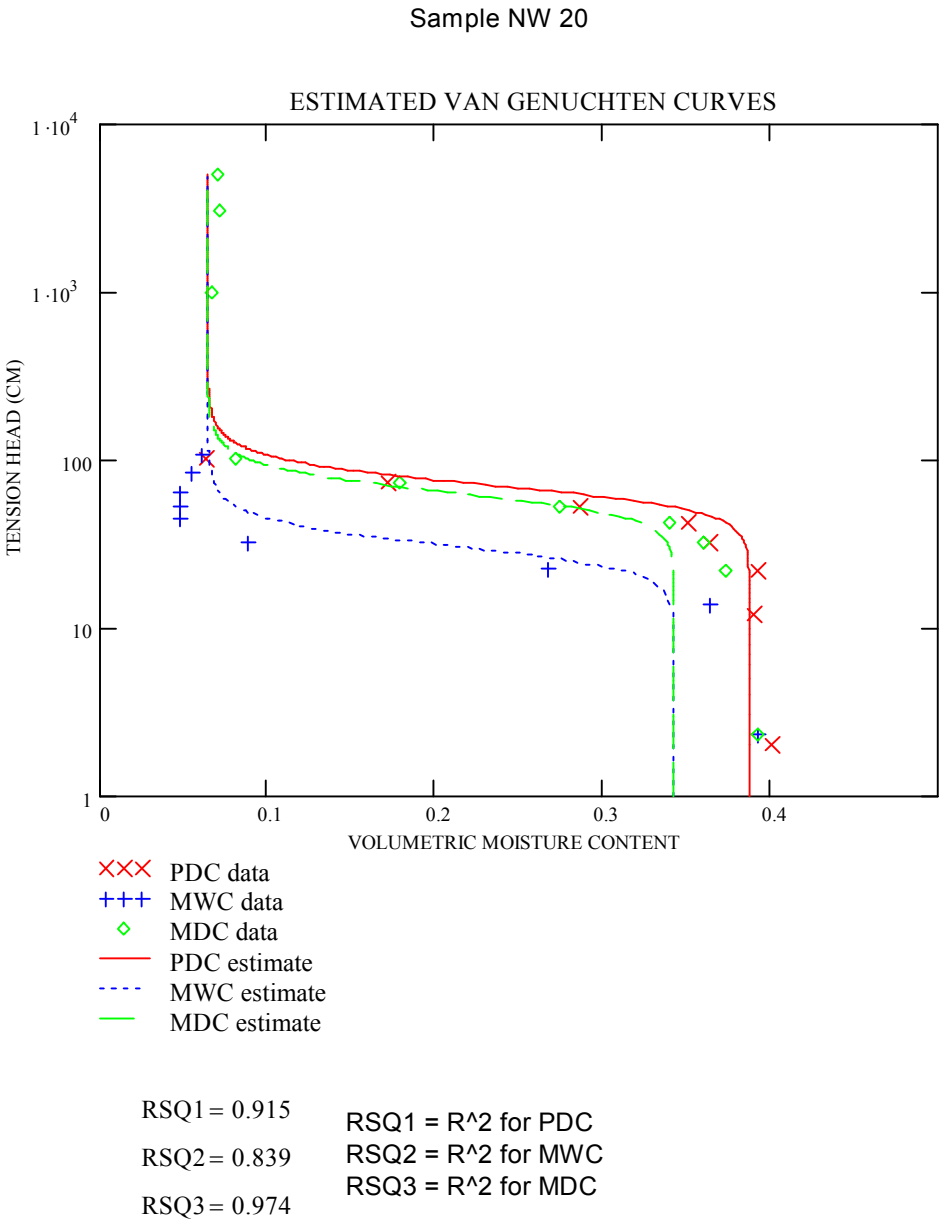

Figure P.13 – Estimated curves for sample NW20 using van Genuchten fitting parameters.

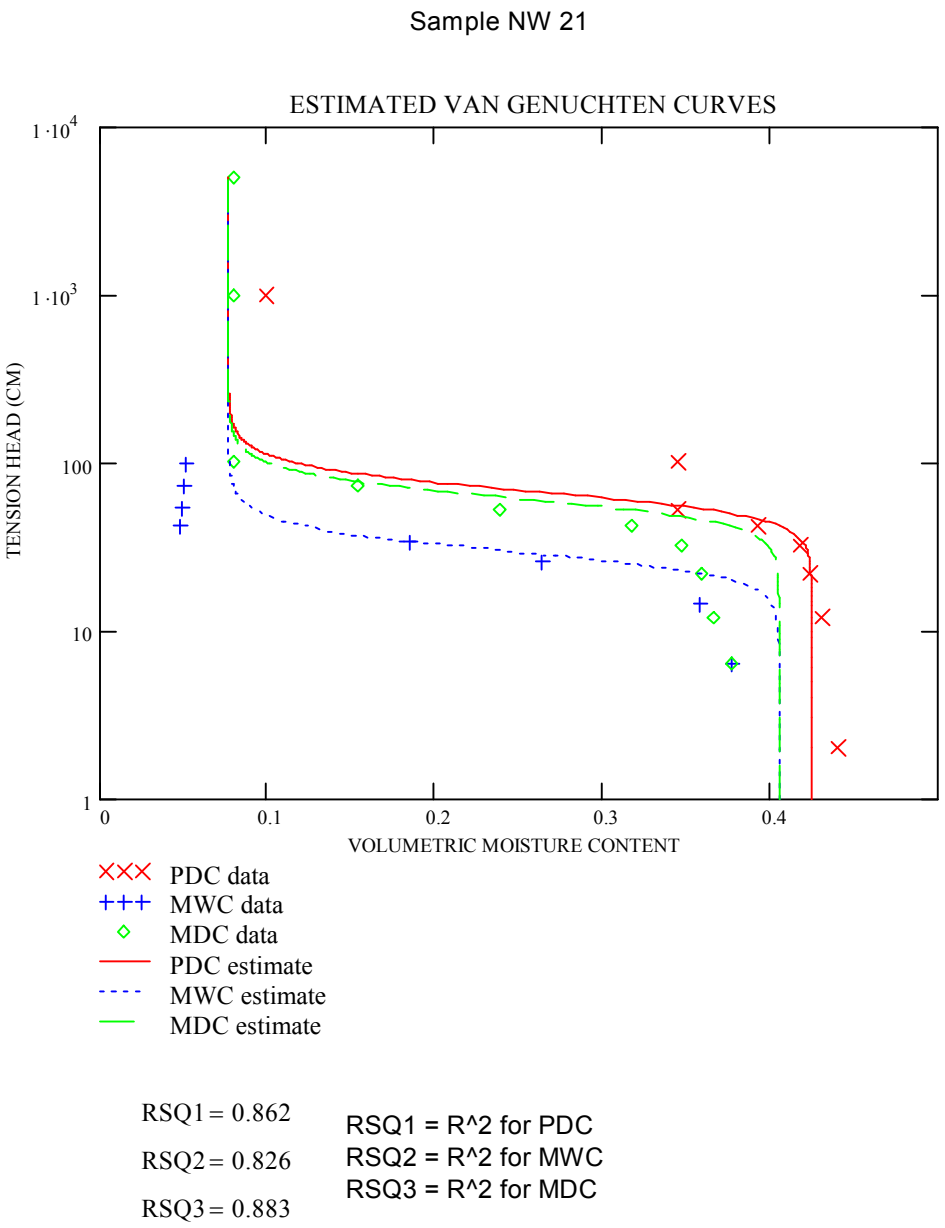

Figure P.14 – Estimated curves for sample NW21 using van Genuchten fitting parameters.

Sample NW 22

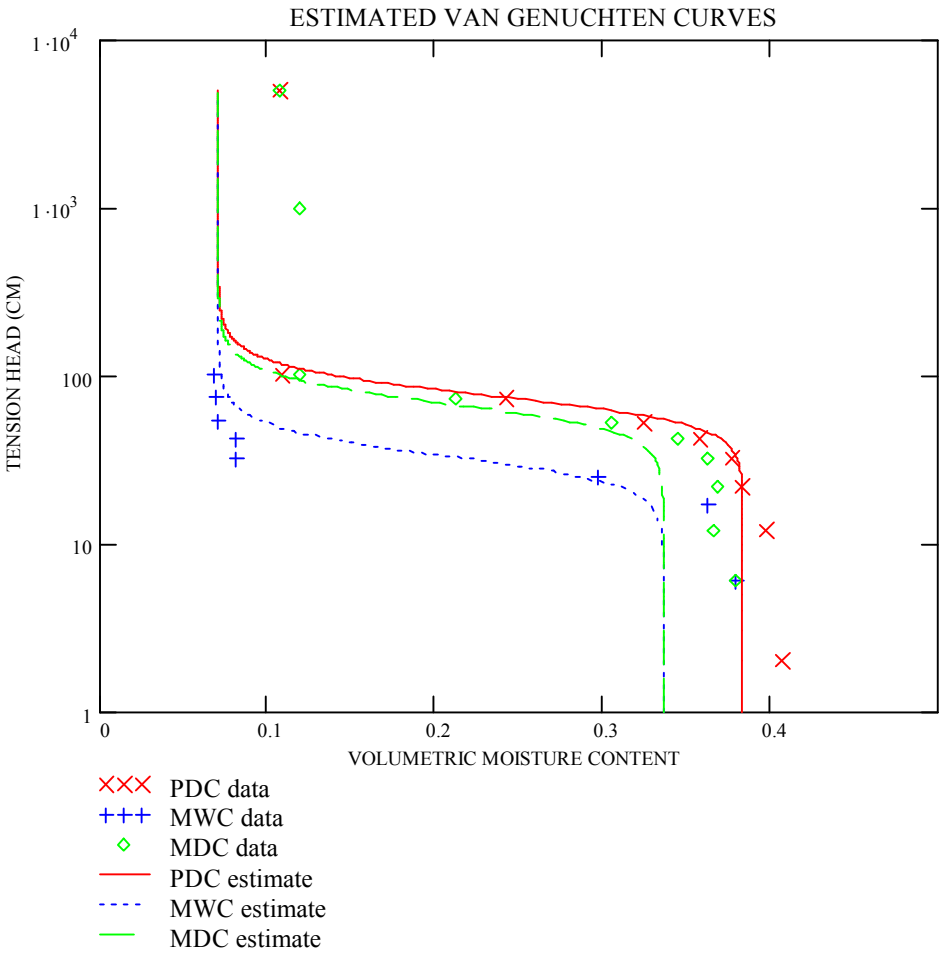

RSQ1 = 0.967

RSQ2 = 0.967

RSQ3 = 0.912

RSQ1 = R^2 for PDC
RSQ2 = R^2 for MWC
RSQ3 = R^2 for MDC

Figure P.15 – Estimated curves for sample NW22 using van Genuchten fitting parameters.

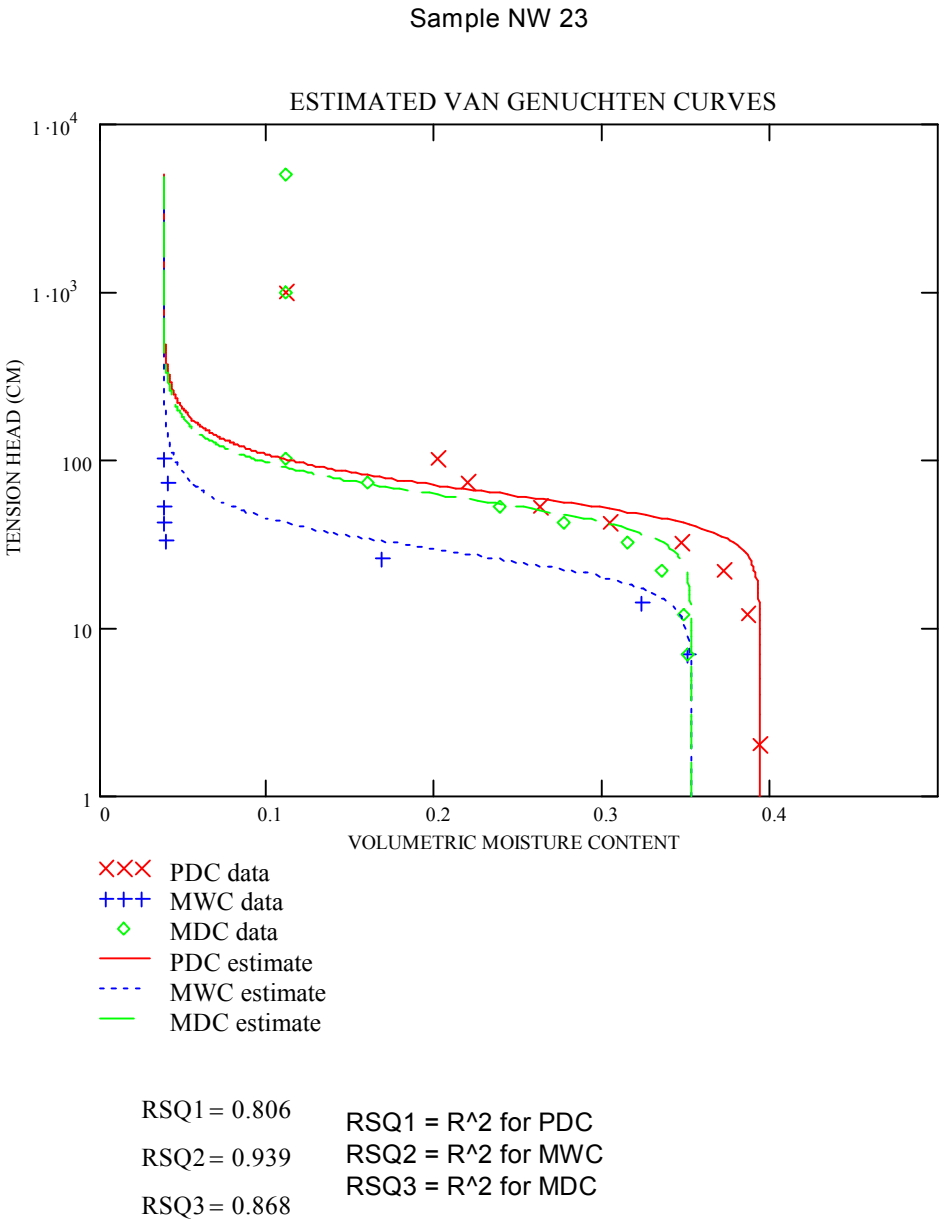

Figure P.16 – Estimated curves for sample NW23 using van Genuchten fitting parameters.

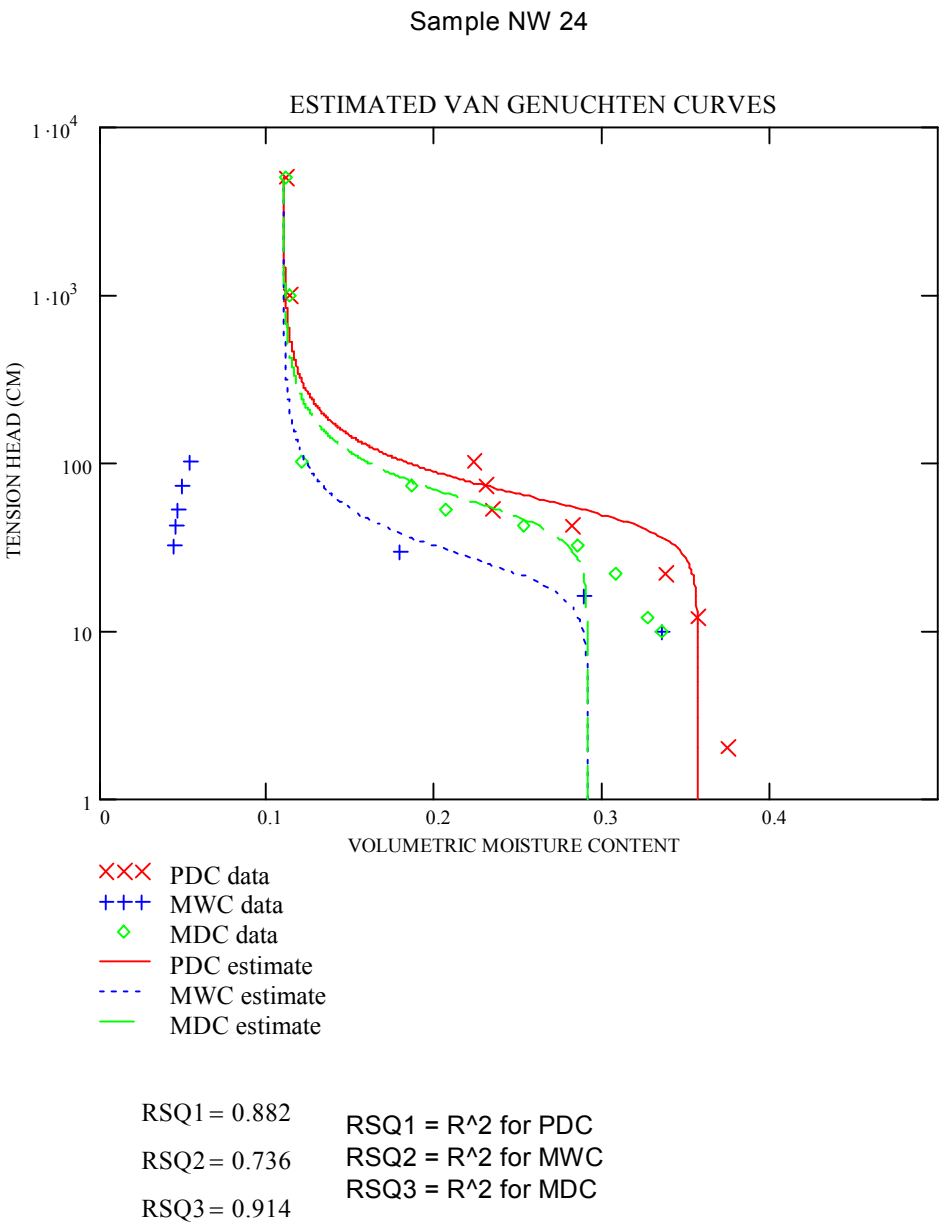

Figure P.17 – Estimated curves for sample NW24 using van Genuchten fitting parameters.

Sample NW 25

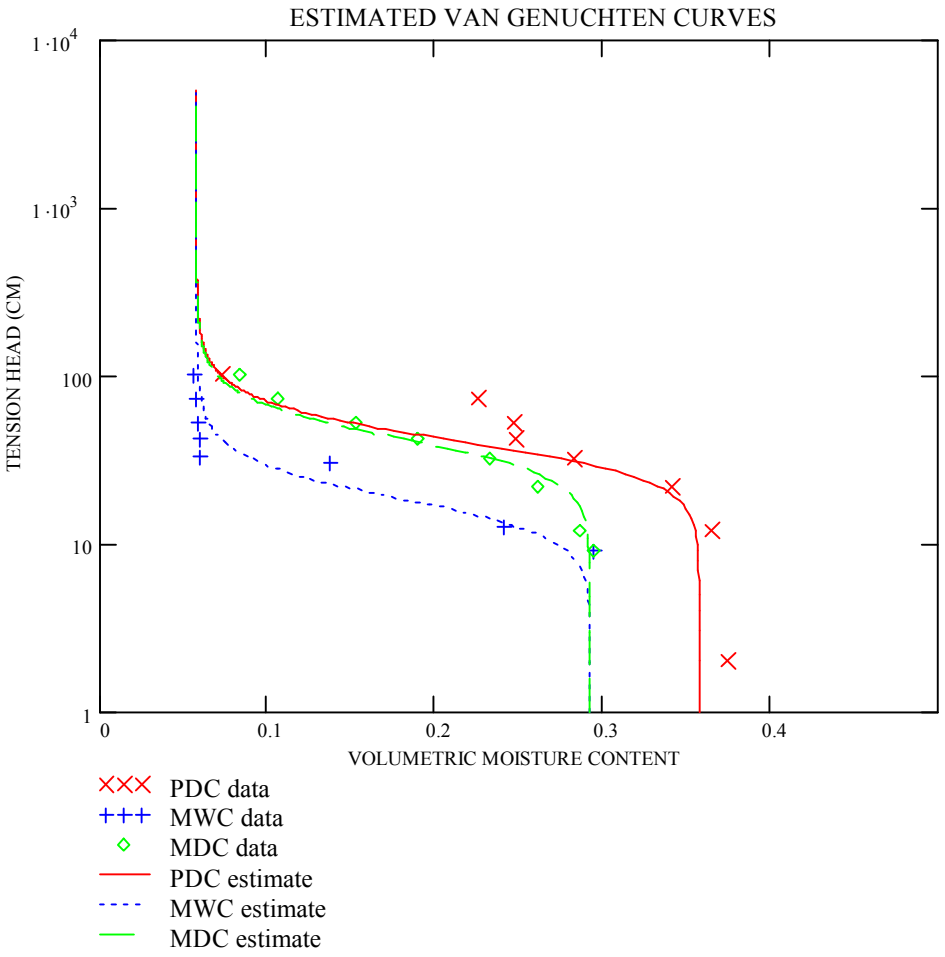

RSQ1 = 0.962

RSQ2 = 0.954

RSQ3 = 0.979

RSQ1 = R^2 for PDC
RSQ2 = R^2 for MWC
RSQ3 = R^2 for MDC

Figure P.18 – Estimated curves for sample NW25 using van Genuchten fitting parameters.

Sample NW 27

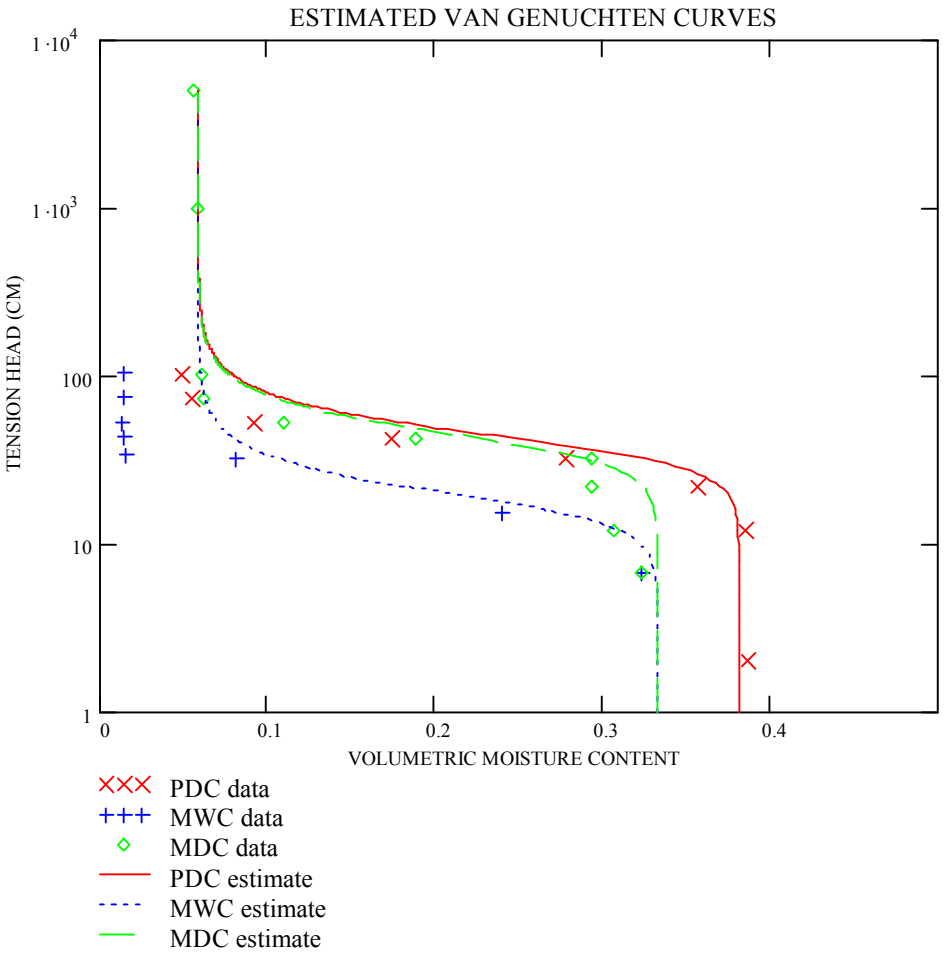

RSQ1 = 0.864

RSQ2 = 0.947

RSQ3 = 0.929

RSQ1 = R^2 for PDC
RSQ2 = R^2 for MWC
RSQ3 = R^2 for MDC

Figure P.19 – Estimated curves for sample NW27 using van Genuchten fitting parameters.

Appendix Q

Model Sensitivity Analysis Procedures

Q.1 Background

Based on the model application results discussed in the previous section, we hypothesize that both the Haverkamp and Parlange (1986) pedotransfer model and the van Genuchten Parameter Estimation Model provide the best predictions for deposits of very similar textures and that the impact of measurement error, sample size, and the number of measured data points along the moisture characteristic curves strongly impacts the model results. To test this hypothesis, we use Monte Carlo simulations (described in Holt, 2000) to examine the optimum conditions for model application.

We use the Haverkamp and Parlange (1986) model with original model coefficient values for a1, a2, b1, b2, and b3 to represent reality. We simulate measurements of moisture characteristic and particle-size distribution data in the presence of error. In order to identify the optimum number of data points for the moisture characteristic curves, we fit the Brooks and Corey (1964) equation to the simulated measurements with an increasing number of data points. We define the optimum number of samples required for model calibration by randomly selecting samples from a total population of artificially generated samples of increasing sample set sizes. We examine the statistics of the results for each model scenario and compare estimated to true moisture characteristic curves. To examine the impact of particle diameters on the model results, we repeat the process using a narrower range of mean particle diameters.

Q.2 Methods

We consider the parameters ϕ, d_g, and n_d to be random variables. Using a uniform distribution, we sample between 0.35 and 0.45 for ϕ, 0.07 mm and 1.0 mm for d_g, and from 2.0 to 6.0 for n_d. We repeat this procedure 1000 times yielding 1000 sets of ϕ, d_g, and n_d. Each set is used to define the true particle-size distribution (3-1) and the bulk density (3-9) of a sample. Using equations (3-13), (3-15), and (3-19) we calculate the sample values of λ, γ, and h_{ae}.

Using our true values of λ, and h_{ae} we estimate the moisture characteristic curve with simple observation errors of weight, length, volume, and pressure. MCC data are then fit with the Brooks and Corey model (3-7). yielding estimates of λ and h_{ae} for the samples. We use our true values of d_g and n_d to estimate the particle-size distribution curve with simple observation errors of weight. PSD data are fit with the van Genuchten equation (3-1) yielding estimates of d_g and n_d for the samples.

To test our hypothesis that the number of data points along the moisture characteristic curve impact the model results, we calculate moisture content in the presence of error at the pressure head data points examined in the laboratory analysis (12 data points) and fit the Brooks and Corey (1964) equation to the simulated log-log moisture retention measurements to determine the fitting parameters λ and h_{ae}. We then calculate moisture content using 20 evenly distributed data points ranging from 0 to 500 cm head and repeat the process for 40, 80, 100 and 250 evenly distributed data points along the curves and then examine the statistics for the ratios of fitted λ and h_{ae} to the true parameters to determine the optimum number of data points required to best define the parameters.

To test the hypothesis that the sample size selected for model calibration impacts the model results, we randomly select 20 samples 1000 times, then randomly select 40 samples 1000 times and repeat the selection using 80,100, and 200 sets of samples all randomly selected 1000 times. For each sample set, we use regression analysis to fit a power law curve to λ, n and ρ_d data to determine the coefficients a1 and a2 for (3-13) and a polynomial curve to the λ and γ data to determine the coefficients b1, b2, and b3 for (3-15). We then examine the mean, variance, median and the 95% confidence intervals for the ratios of the model estimates to the true coefficients for each sample size. We estimate the moisture characteristic curves for the 1000 artificial samples using the mean coefficients of a1,a2, b1, b2 , and b3 obtained using the optimum number of samples. We then plot the model results and the simulated data to examine the model efficiency.

To test our hypothesis that the range of particle diameters for each sample impacts the model results, we repeat the Monte Carlo simulations using a narrower range of mean particle diameters (d_g ranging from 0.10 mm to 0.5 mm) and compare the results to the simulations using the broader range of particle diameters (d_g ranging from 0.07 mm to 1.0 mm).

Q.3 Monte Carlo Simulation Procedures

Objective: There are 3 main objectives:

1) Determine the number of raw data points required along a moisture retention curve for optimum model calibration when observational error is included in the data.

2) Determine the number of samples required for optimum model calibration (particle index and the packing parameter model estimation equations).

3) Examine impact of measurement error on predicted (H&P model) and observed (curves fit to data w/error) MCC and PSD curves.

Methods (copies of Fortran codes are attached at the end of this appendix):

PROCEDURE	SOURCE CODE	INPUT	OUTPUT
1) Generate 1000 random fields for porosity, n, and dg. Calculate other model parameters from H&P model estimation equations.	*genparam2.for*	N/A	*tmoist.dat, tpsd.dat, tgamm.dat,* Output includes 2D arrays (MAX,4) for the model parameters. tmoist includes tsat, thae, tbd, tlam, and tm; tpsd includes tdg and tn; tgamm includes tgam data.
Include randomly generated measurement error to MCC and PSD data. Randomly generated error is uniformly distributed around mean zero and represents 3 standard deviations.	kbmcest.for (Holt, 2000) *psdest.for*	*tmoist.dat* *tpsd*	*HP002mc.prn* *HP002bd.prn* *psd01.out* MCC, Bd, and PSD data w/ error written to output files above.
2) Determine optimum number of data points along moisture retention curves.	*Numpts.for*	*HP002mc.prn*	*Stats1.out* *Stats2.out* *ratios.out* Stats1 is the output file for mean, var, med, 5%, and 95% of the estimates for lambda. Stats2 is the output file for the same stats for estimates of hae. Ratios.out contains ratios of est to true values for lambda and hae for each set of data points examined.
Fit the Brooks and Corey eqn to the MCC data w/error (using optimum # of data pts) to determine lambda and hae values.	*Bcfit.for*	*HP002mc.prn*	Mcfits.dat Output includes fitted values for lambda and h_{ae} for each sample.

PROCEDURE	SOURCE CODE	INPUT	OUTPUT
3) Randomly select X number of samples 1000 times each.	*Select.for*	*Mcfits.dat* HP002bd.prn *Psd01.out*	Param1.prn *Param2.prn* *Param3.prn* *Param4.prn* *Param5.prn* Param files include 1000 (each) randomly selected sample sets of varying number of samples (5 sets).
4) Calibrate estimation model using sample sets selected to determine coefficients for estimation equations (a1, a2, b1, b2, b3).	*Hpeqns.for*	Param1.prn *Param2.prn* *Param3.prn* *Param4.prn* *Param5.prn*	*Coeffs.prn* *Ratios.prn* Stats(1-5).prn Coeffs.prn contains estimated coefficients. Raitos.prn contains ratios of est to true values for the coeffs. Stats(1-5).prn contains mean, var, med, 5%, and 95% for the coefficients..
5 Estimate MCC using estimated coefficients (determined from optimum # of samples used in calibration).	*MATHCAD PROGRAM mcestfit.mcd*	*Coeffs.prn* *Param5.txt* (set of the largest number of samples used in calibration)	Param1.out *Param2.out* *Param3.out* *Param4.out* *Param5.out* An output file is generated for each subset of "X" sample sizes which includes the sample #, the psd and the moisture parameter data: r,Bd,n,dg,sat,hae,lamb

Definition of variables for FORTRAN codes

Variable Name	Definitions
MAX	maximum number of generated curves
COMBO	number of combinations
NPTS	max number of data points along a curve
SETS	number of sets (samples and points)
TOT	MAX*SETS
P(SETS)	size of data points per set
S(SETS)	size of samples per set
sat	porosity
hae	air entry pressure
Bd	dry bulk density
lamb	Brooks and Corey fitting parameter (lambda)
gamm	H&P model parameter (gamma)
r	Randomly selected curve number
n	vG fitting parameter for PSD
dg	vG fitting parameter for PSD
ave	Mean of an array of data
var	Variance of an array of data
med	Median of an array of data
five	5 percentile of an array of data
ninfiv	95 percentile of an array of data
tn,dtg,tsat,tBd,tlamb, tgamm,thae	"true" sample parameters (moisture and particle size)
fn,fdg,fsat,fBd,flamb, fgamm,fhae	"fitted" sample parameters to **observed data** (moisture and particle size)

Q.4 Fortran Codes

```
**********************************************************************
      Program genparam2
**********************************************************************
c     This program will generate MAX random values of porosity, n, and dg.
c     This is the first source code in a series of six sources codes written for
c     evaluation of hydraulic property model predictions.

c     Written by Kristine Baker, March 2000.
**********************************************************************
      Program genparam2

      use DFLIB

      Integer MAX
      Parameter (MAX=1000)

      Integer i,j,nseed

     Real tsat(MAX),thae(MAX),tlam(MAX),tBd(MAX),tn(MAX),tdg(MAX),
     +  tm(MAX),tgam(MAX)
      Real rand,SATdelt,ndelt,dgdelt
      REAL SATmin,nmin,dgmin
      real a1,a2,b1,b2,b3
```

```
c       open output file
        open(1,file='tmoist.dat',status='UNKNOWN')
        open(2,file='tpsd.dat',status='UNKNOWN')
        open(3,file='tgamm.dat',status='UNKNOWN')
        open(4,file='tBd.dat',status='unknown')

c       H&P Model Coefficients
        a1=0.0723
        a2=3.8408
        b1=17.1736
        b2=-4.7043
        b3=0.1589

c       Define parameter boundaries
        SATdelt=0.10
        SATmin=0.35
        ndelt=4.0
        nmin=2.0
        dgdelt=0.93
        dgmin=0.07

c       initialize arrays
        do i=1,MAX
                tsat(i)=0.0
```

```
            tlam(i)=0.0
            thae(i)=0.0
            tBd(i)=0.0
            tn(i)=0.0
            tdg(i)=0.0
            tm(i)=0.0
            tgam(i)=0.0
        end do

c       call random number generator

        nseed = 4853

        CALL SEED(nseed)

        do i=1,MAX
            CALL Random(rand)
            tsat(i)=(rand*SATdelt)+SATmin
            tBd(i)=(1-tsat(i))*2.65
        end do

        do i=1,MAX
            CALL Random(rand)
            tn(i)=(rand*ndelt)+nmin
```

```
            tm(i)=1-(1/tn(i))
            tlam(i)=a1*(tBd(i)**a2)*(tn(i)-1)
            tgam(i)=b1+(b2*tlam(i))+(b3*(tlam(i)**2))
        end do

        do i=1,MAX
            CALL RANDOM(rand)
            tdg(i)=(rand*dgdelt)+dgmin
            thae(i)=(0.149*tgam(i))/tdg(i)
        end do

c       write parameters to output file
        do i=1,MAX
            write(1,99) tsat(i),thae(i),tbd(i),tlam(i),tm(i)
            write(2,999) tdg(i),tn(i)
            write(3,*) i,tgam(i)
            write(4,*) tbd(i)
        end do
99          format(6(f8.4,2x))
999         format(2(f6.4,2x))
        close(1)
        close(2)
        close(3)
        close(4)
```

```
      stop
      end

c     ****************************************************************
      program kbmcest
c     ****************************************************************
c     This program estimates moisture retention data in the presence
c     of measurement error.  The code was originally written by
c     Robert Holt, 1999 to estimate van Genucthen fitting parameters.
c     It has been modified by Kristine Baker, 2000 for estimates of
c     Brooks and Corey fitting parameters.  The code is the 2nd source
c     code in a series of 6 codes used to evaluate pedotransfer model
c     predictions.  This source code must be linked to the following
c     subroutines:  input.for, errors.for, bulkdest.for, and mccurve.for.
c     ****************************************************************

      Include'dimen.inc'
      double precision vV,vL,vW,vP,vvT,vvB
      double precision vphi(MAXSZ2),vtaph(MAXSZ2),vtn(MAXSZ2)
     double precision psii(MAXPSI)
     double precision Lhr,Ldr,Wr
      double precision Lhc,Ldc,Wc
      integer Npts,Npsi,i,j,nV,nL,nW,nP
      character*5 str
```

```
      logical verrcor
      common/nseeds/nV,nL,nW,nP
      common/errparms/vV,vL,vW,vP,vvT,vvB
      common/tparams/vphi,vtaph,vtn
      common/press/psii
     common/ring/Lhr,Ldr,Wr
      common/contain/Lhc,Ldc,Wc
      common/intgrs/Npts,Npsi
      common/chars/str
      common/logi/verrcor
      common/typ/iptype

      double precision EVs(MAXSZ2),ELdc(MAXSZ2),ELhc(MAXSZ2),
     &  EWc(MAXSZ2),EWsc(MAXSZ2)
      double precision ELht(MAXSZ2),ELdt(MAXSZ2),EWbt1(MAXSZ2),
     &  EWsat(MAXSZ2),EWbt2(MAXSZ2,MAXPSI),ELpsi1(MAXSZ2,MAXPSI),
     &  ELpsi2(MAXSZ2,MAXPSI)
      common/bderrors/EVs,ELhc,ELdc,EWc,EWsc
      common/mcerrors/ELht,ELdt,EWbt1,EWsat,EWbt2,ELpsi1,ELpsi2

      double precision tbd(MAXSZ2),ebd(MAXSZ2)
      common/bulkd/tbd,ebd

      double precision EstMC(MAXSZ2,MAXPSI),tMC(MAXSZ2,MAXPSI)
```

```
      common/mcdata/EstMC,tMC

c     Read in random fields
      call input
      write(*,*) 'input complete'

c     Calculate error values
      call errors
      write(*,*) 'errors calculated'

c     Calculate bulk densities
      call bulkdest
      write(*,*) 'bulk densities complete'

c     Calculate Moisture Characteristic Curves
      call mccurve(iptype)

      write(*,*) 'Moisture-Characteristic curves complete'

c     Output results
    open(60,file=str // 'mc.prn',status='unknown')
    open(61,file=str // 'bd.prn',status='unknown')
      do i=1,Npts
        do j=1,Npsi
```

```
            write(60,10) i,j,-psii(j),tMC(i,j),EstMC(i,j)
          end do
          write(61,20) i,tbd(i),ebd(i)
        end do

 10   format(i6,1x,i6,1x,3(1pe10.3,1x))
 20   format(i6,1x,2(1pe10.3,1x))

        close(unit=60)
        close(unit=61)

        end

c       ****************************************************************
Program Psdest
c       ****************************************************************
c       This is the main source code for the PSD estimated van Genuchten
c       curve fitting parameters.  Written by Kristine Baker, April 2000.
c       This code is the 3rd source code in a series of 6 codes written
c       for evaluation of pedotransfer model predictions.  This source code
c       must be linked to the following subroutines:  input.for, fdcurve.for
c       and output.for.
c       Written by Kristine Baker, March 2000.
c       ****************************************************************
```

```
      include 'dimen1.inc'
      external input
      external fdcurve
      external output
      integer i,j
c     initialize arrays
      do i=1,MAX
            tn(i)=0.0
            tdg(i)=0.0
            estn(i)=0.0
            estdg(i)=0.0
            tBd(i)=0.0
            eVol(i)=0.0
            tTotW(i)=0.0
            er1(i)=0.0
            er2(i)=0.0
      end do
      do i=1,NPTS
            avgd(i)=0.0
            tsvW(i)=0.0
            tM(i)=0.0
            er3(i)=0.0
            er4(i)=0.0
            er5(i)=0.0
```

```
      end do
      do i=1,MAX
            do j=1,NPTS
            tfd(i,j)=0.0
            Obsfd(i,j)=0.0
            esoilW(i,j)=0.0
            end do
      end do
      do i=1,RNG
            td(i)=0.0
      end do
c     read random field data and input deck
      call input
      write(*,*) 'input complete'
c     calculate F(d)
      call fdcurve
      write(*,*) 'PSD curves complete'
c     Output results
      call output
      write(*,*) 'Output complete'
      stop
      end
```

```
**********************************************************************
      Program numpts
**********************************************************************
c     This program fits the Brooks and Corey equation to moisture characteristic
c     curves in order to determine the number of points required to obtain the
c     best estimates of lambda and air entry pressures.  This source code is the
c     4th code in a series of 6 codes written to evaluate pedotransfer model
c     predictions.  The code must be linked to the following subroutines:
c     sort.for, Bcfit.for, avevar.for, and calcMC.for.
c     Written by Kristine Baker, March 2000.
**********************************************************************
      include 'param2.inc'
      external sort
      external Bcfit
      external avevar
c     external calcMC

      integer i,j,int,cnt1,cnt2,a1,a2,b1,b2,c1,c2,len1,len2
      real row(MAX),tlamb(MAX),thae(MAX),tsat(MAX),tBd(MAX),X(2),
     +  obsBd(MAX),dat(P),head(P),tmc(MAX,P),
     +  obsmc(MAX,P),psii(MAX),tm(MAX)
      real med1,med2,five1,five2,ave1,var1,ave2,var2,
     +  ninfiv1,ninfiv2,f1,f2
      Real(4) ratio1(MAX),ratio2(MAX),rat1(MAX),rat2(MAX),pt(P)
```

```
      common /samples/i,obsmc,psii,pt
      common /paramdat/X
      character*5 str
      data pt/0.,10.,20.,30.,40.,60.,80.,100.,200.,
     +  330.,1000.,3000./
      str='HP002'
c     open input files
      open(1,file='tmoist.dat',status='OLD')
      open(30,file=str // 'mc.prn',status='old')

C     open debug files
      open(2,file='ratio1.dat',status='unknown')
      open(3,file='ratio2.dat',status='unknown')
      open(4,file='mcfits.dat',status='unknown')

C     open output files
      open(10,file='stats1.out',status='unknown')
      open(20,file='stats2.out',status='unknown')
      open(40,file='ratios.out',status='unknown')

c     read input files
      do i=1,MAX
            read(1,*) tsat(i),thae(i),tBd(i),tlamb(i),tm(i)
      end do
```

```
      do i=1,MAX
            do j=1,P
            read(30,*) row(i),dat(j),head(j),tmc(i,j),obsmc(i,j)
            end do
      end do

c     determine observed porosity for each curve
      do i=1,MAX
            psii(i)=obsmc(i,1)
      end do

c     initialize variables
      med1=0.0
      five1=0.0
      ninfiv1=0.0
      med2=0.0
      five2=0.0
      ninfiv2=0.0
      cnt1=0
      cnt2=0
      a1=0
      a2=0
      b1=0
      b2=0
```

```
      c1=0
      c2=0

      do i=1,MAX
            ratio1(i)=0.0
            ratio2(i)=0.0
            rat1(i)=0.0
            rat2(i)=0.0
      end do
c     SELECT P1-P5 NUMBER OF DATA POINTS ALONG EACH CURVE
c     and calculate log(effS) and log(h)
      do 10 i=1,MAX
            f1=0.0
            f2=0.0
c     call subroutine to calculate moisture content at selected data pts.
c           call calcMC
c     call fitting subroutine - passing "true" values as initial guess,
c     the length of the data, and the X and Y data points.
            call Bcfit
            f1=X(1)                 !air entry
            f2=X(2)                 !lambda
            write(4,99) i,f1,f2,psii(i)
99    format(i4,2x,2(f9.4),2x,f6.4)
c     calculate ratio of estimated lambda vs. true lambda and
```

```
c       estimated hae vs. true hae for every curve/set of datapts selected.
                ratio1(i)=f1/thae(i)
                ratio2(i)=f2/tlamb(i)

c       eliminate zeros from ratios array
                if(ratio1(i).ne.0.0) then
                        cnt1=cnt1+1
                        rat1(i)=ratio1(i)
                end if

                if(ratio2(i).ne.0.0) then
                        cnt2=cnt2+1
                        rat2(i)=ratio2(i)
                end if

10              continue                        !end MAX do loop (i)

C       write arrays to ouput file for observation
c       do i=1,cnt1
c               write(2,*) i,ratio1(i)
c       end do
c       do i=1,cnt2
c               write(3,*) i,ratio2(i)
c       end do
```

```
c       determine mean and variance of arrays
        call avevar(rat1,cnt1,ave1,var1)
        call avevar(rat2,cnt2,ave2,var2)

c       Sort arrays
        call sort(rat1,rat2)

c       determine  median, 5%, and 95% for each ratio array
        len1=MAX-cnt1
        len2=MAX-cnt2
        a1=len1+(cnt1/2)
        a2=len2+(cnt2/2)
        if(cnt1*0.05.gt.1.0) then
                b1=len1+(cnt1*0.05)
        else
                b1=len1+1
        end if
        if(cnt2*0.05.gt.1.0) then
                c1=len2+(cnt2*0.05)
        else
                c1=len2+1
        end if
        if(cnt1*0.95.lt.cnt1) then
```

```
        b2=len1+(cnt1*0.95)
else
        b2=len1+cnt1
end if
if(cnt2*0.95.lt.cnt2) then
        c2=len2+(cnt2*0.95)
else
        c1=len2+cnt2
end if
med1=rat1(a1)
five1=rat1(b1)
ninfiv1=rat2(b2)
med2=rat2(a2)
five2=rat2(c1)
ninfiv2=rat2(c2)

write(10,*) ave1,var1,med1,five1,ninfiv1
write(20,*) ave2,var2,med2,five2,ninfiv2
do i=1,MAX
        write(40,*) ratio1(i), ratio2(i)
end do

write(*,*) 'looped through all sets'
close(1)
```

```
      close(2)
      close(3)
      close(4)
      close(10)
      CLOSE(20)
      close(30)
      close(40)

      stop
      end

c     ************************************************************
      Program select
c     ************************************************************
c     This program  randomly selects X number of samples COMBO
c     number of times where COMBO=number of combinations of X.
c     This source code is the 5th code in a series of 6 codes
c     written for evaluation of pedotransfer predictions.
c     Written by Kristine Baker, March 2000.
c     ************************************************************

      use DFLIB          !when using compaq visual fortran
c     use MSIMSL         !when using fortran powerstation
      include 'arrays.inc'
```

```
      integer nseed1,nseed2
      parameter (nseed1=4250,nseed2=8790)

      integer i,x,y,z,r
      real rand

c     open input files of raw data which includes measurement error
      open(11,file='mcfits.dat',status='OLD')
      open(12,file='HP002bd.prn',status='OLD')
      open(13,file='Psd01out.prn',status='OLD')

      do i=1,MAX
            read(11,*) row(i),hae(i),lamb(i),sat(i)
            read(12,*) row(i),tBd(i),Bd(i)
            read(13,*) tn(i),tdg(i), dg(i),n(i)
      end do

c     Select number of samples selected (X)
      numsamp(1)=S1
      numsamp(2)=S2
      numsamp(3)=S3
      numsamp(4)=S4
      numsamp(5)=S5
c     Select X number of samples at random from set of true curves
```

```
C       and and write psi(theta) data for each curve to output file
        CALL SEED(nseed2)

        do 10 i=1,SETS                  !5 sets of X number of samples
              do 20 y=1,COMBO           !number of combinations of X
samples
                    do 30 x=1,numsamp(i)

                    CALL Random(rand)
                    r=(rand*MAX)+1      !curve array element for theta value

                    if(i.eq.1) then

                    Bd1(y,x)=Bd(r)      !y=combination#, x=curve#
                    n1(y,x)=n(r)
                    m1(y,x)=1-(1/n1(y,x))
                    dg1(y,x)=dg(r)
                    sat1(y,x)=sat(r)
                    aep1(y,x)=hae(r)
                    lamb1(y,x)=lamb(r)
                    gamm1(y,x)=aep1(y,x)*dg1(y,x)/0.149
                    r1(y,x)=r

                    else if(i.eq.2) then
```

```
Bd2(y,x)=Bd(r)                !y=combination#, x=curve#
n2(y,x)=n(r)
m2(y,x)=1-(1/n2(y,x))
dg2(y,x)=dg(r)
sat2(y,x)=sat(r)
aep2(y,x)=hae(r)
lamb2(y,x)=lamb(r)
gamm2(y,x)=aep2(y,x)*dg2(y,x)/0.149
r2(y,x)=r

else if (i.eq.3) then

Bd3(y,x)=Bd(r)                !y=combination#, x=curve#
n3(y,x)=n(r)
m3(y,x)=1-(1/n3(y,x))
dg3(y,x)=dg(r)
sat3(y,x)=sat(r)
aep3(y,x)=hae(r)
lamb3(y,x)=lamb(r)
mcae3(y,x)=sat3(y,x)/(1+lamb3(y,x))
gamm3(y,x)=aep3(y,x)*dg3(y,x)/0.149
r3(y,x)=r
else if (i.eq.4) then
```

```
Bd4(y,x)=Bd(r)                !y=combination#, x=curve#
n4(y,x)=n(r)
m4(y,x)=1-(1/n4(y,x))
dg4(y,x)=dg(r)
sat4(y,x)=sat(r)
aep4(y,x)=hae(r)
lamb4(y,x)=lamb(r)
gamm4(y,x)=aep4(y,x)*dg4(y,x)/0.149
r4(y,x)=r

else if (i.eq.5) then

Bd5(y,x)=Bd(r)                !y=combination#, x=curve#
n5(y,x)=n(r)
m5(y,x)=1-(1/n5(y,x))
dg5(y,x)=dg(r)
sat5(y,x)=sat(r)
aep5(y,x)=hae(r)
lamb5(y,x)=lamb(r)
gamm5(y,x)=aep5(y,x)*dg5(y,x)/0.149
r5(y,x)=r

end if
```

```
30                      continue
20                  continue
10          continue

c           open output files
            open(10,file='param1.prn',status='unknown')
            open(20,file='param2.prn',status='unknown')
            open(30,file='param3.prn',status='unknown')
            open(40,file='param4.prn',status='unknown')
            open(50,file='param5.prn',status='unknown')

            do y=1,COMBO
                  do x=1,numsamp(1)
                   write(10,99) x,r1(y,x),Bd1(y,x),n1(y,x),dg1(y,x),
     +     sat1(y,x),aep1(y,x),lamb1(y,x),gamm1(y,x),m1(y,x)
                  end do
            end do

c           do y=1,COMBO
c                 do x=1,numsamp(2)
c                  write(20,99) x,r2(y,x),Bd2(y,x),n2(y,x),dg2(y,x),
c     +    sat2(y,x),aep2(y,x),lamb2(y,x),gamm2(y,x),m2(y,x)
c      end do
```

```
c       end do

c       do y=1,COMBO
c               do x=1,numsamp(3)
c                write(30,99) x,r3(y,x),Bd3(y,x),n3(y,x),dg3(y,x),
c    +   sat3(y,x),aep3(y,x),lamb3(y,x),gamm3(y,x),m3(y,x)
c     end do
c       end do

c       do y=1,COMBO
c               do x=1,numsamp(4)
c                write(40,99) x,r4(y,x),Bd4(y,x),n4(y,x),dg4(y,x),
c    +   sat4(y,x),aep4(y,x),lamb4(y,x),gamm4(y,x),m4(y,x)
c     end do
c       end do

c       do y=1,COMBO
c               do x=1,numsamp(5)
c                write(50,99) x,r5(y,x),Bd5(y,x),n5(y,x),dg5(y,x),
c    +   sat5(y,x),aep5(y,x),lamb5(y,x),gamm5(y,x),m5(y,x)
c     end do
c       end do
99      format(i3,2x,i4,2x,9(f8.4,2x))
        CLOSE(10)
```

```
      CLOSE(20)
      CLOSE(30)
      CLOSE(40)
      CLOSE(50)
      CLOSE(11)
      CLOSE(12)
      CLOSE(13)
      close(14)

      stop
      end

c     ************************************************************
      Program HPeqns
c     ************************************************************
C     This program reads in MCC data w/error and does a non-linear
c     fit to obtain pedotransfer model estimation equations for
c     model parameters lambda and gamma used to estimate moisture
c     retention curves.  This source code is the 6th code in a series
c     of 6 codes written to evaluate pedotransfer model predictions.
c     Written by Kristine Baker, March, 2000.
c     ************************************************************

c     use MSIMSL   !when using MSfortran powerstation
```

```
      use DFLIB  !when using compaq visual fortran
      include 'param2.inc'

c     This program must be linked to the following external files
      external linefit
      EXTERNAL polyfit
      external avevar
      external sort
      integer LEN,f,i,j,x,y,z,k,indx
      real LX(2),GX(3)
      character*6 str
      common/modparams/gamm,ratio,lamb,Bd
      common/combnum/indx

c     open intput files
      write(*,*) 'Enter param# and return'
      read(*,'(a6)') str
    open(1,file=str // '.prn',status='old')

c     initialize variables
      med1=0.0
      five1=0.0
      ninfiv1=0.0
      med2=0.0
```

five2=0.0

ninfiv2=0.0

med3=0.0

five3=0.0

ninfiv3=0.0

med4=0.0

five4=0.0

ninfiv4=0.0

med5=0.0

five5=0.0

ninfiv5=0.0

ave1=0.0

ave2=0.0

ave3=0.0

ave4=0.0

var1=0.0

var2=0.0

var3=0.0

var4=0.0

var5=0.0

c1=0

c2=0

c3=0

c4=0

```
do i=1,S
        ratio1(i)=0.0
        ratio2(i)=0.0
        ratio3(i)=0.0
        ratio4(i)=0.0
        ratio5(i)=0.0
end do

do i=1,COMBO
        do j=1,S
        samp(j)=0.
        r(j)=0
        Bd(i,j)=0.
        n(i,j)=0.
        dg(i,j)=0.
        sat(i,j)=0.
        hae(i,j)=0.
        lamb(i,j)=0.
        gamm(i,j)=0.
        m(i,j)=0.
        ratio(i,j)=0.0
        end do
end do
```

```
c       READ OBSERVED DATA
        do y=1,COMBO
              do z=1,S
                    read(1,*) samp(z),r(z),Bd(y,z),n(y,z),dg(y,z),
     +        sat(y,z),hae(y,z),lamb(y,z),gamm(y,z),m(y,z)
                    ratio(y,z)=lamb(y,z)/(n(y,z)-1)
              end do
        end do

c       Regression analysis fitting subroutine to determine a1 and a2
        do 10 y=1,COMBO
              indx=y
              call linefit(LX)
              fa1(y)=LX(1)
              fa2(y)=LX(2)

C       Compare estimated values to "true" values (using all samples)
              if(fa1(y).eq.0.0) fa1(y)=0.00001
              ratio1(y)=fa1(y)/a1
              if(fa2(y).eq.0.0) fa2=0.00001
              ratio2(y)=fa2(y)/a2
10      end do
c       Regression analysis fitting subroutine to determine b1,b2,and b3
```

```
      do 20 y=1,COMBO
            indx=y
            call polyfit(GX)
            fb1(y)=GX(1)
            fb2(y)=GX(2)
            fb3(y)=GX(3)
            if(fb1(y).eq.0.0) fb1=0.00001
            ratio3(y)=fb1(y)/b1
            if(fb2(y).eq.0.0) fb2=0.00001
            ratio4(y)=fb2(y)/b2
            if(fb3(y).eq.0.0) fb3=0.00001
            ratio5(y)=fb3(y)/b3
20    end do

      write(*,*) 'looped through all sets'

c     determine mean and variance of arrays
      call avevar(ratio1,S,ave1,var1)
      call avevar(ratio2,S,ave2,var2)
      call avevar(ratio3,S,ave3,var3)
      call avevar(ratio4,S,ave4,var4)
      call avevar(ratio5,S,ave5,var5)
      write(*,*) 'called avevar'
c     Sort arrays
```

```
      call sort(ratio1,COMBO)
      call sort(ratio2,COMBO)
      call sort(ratio3,COMBO)
      call sort(ratio4,COMBO)
      call sort(ratio5,COMBO)
      write(*,*)'sorted ratios'

c     determine  median, 5%, and 95% for each ratio array
      c1=S*0.05
      if(c1.le.0) c1=1
      c2=S*0.95
      c3=S*0.50
      med1=ratio1(c3)
      five1=ratio1(c1)
      ninfiv1=ratio2(c2)
      med2=ratio2(c3)
      five2=ratio2(c1)
      ninfiv2=ratio2(c2)
      med3=ratio3(c3)
      five3=ratio3(c1)
      ninfiv3=ratio3(c2)
      med4=ratio4(c3)
      five4=ratio4(c1)
      ninfiv4=ratio4(c2)
```

```
      med5=ratio5(c3)
      five5=ratio5(c1)
      ninfiv5=ratio5(c2)
      write(*,*) 'calculated stats'

c     open output files
      open(10,file='coeffs.prn',status='unknown')
      open(100,file='ratios.prn',status='unknown')
      open(200,file='stats1.prn',status='unknown')
      open(300,file='stats2.prn',status='unknown')
      open(400,file='stats3.prn',status='unknown')
      open(500,file='stats4.prn',status='unknown')
      open(600,file='stats5.prn',status='unknown')

      do k=1,COMBO
            write(10,99) fa1(k),fa2(k),
     +  fb1(k),fb2(k),fb3(k)
            write(100,99) ratio1(k),ratio2(k),
     +  ratio3(k),ratio4(k),ratio5(k)
      end do
      write(200,99) ave1,var1,med1,five1,ninfiv1
      write(300,99) ave2,var2,med2,five2,ninfiv2
      write(400,99) ave3,var3,med3,five3,ninfiv3
      write(500,99) ave4,var4,med4,five4,ninfiv4
```

```
      write(600,99) ave5,var5,med5,five5,ninfiv5

99    format(5(f9.4,2x))

      close(1)
      close(10)
      close(100)
      close(200)
      close(300)
      close(400)
      close(500)
      close(600)
      stop
      end
```

Appendix R

Model Sensitivity Analysis Results

R.1 Results

Comparison of the Brooks and Corey fitting parameters (λ and h_{ae}) obtained using varying numbers of data points showed very little differences between the true and fitted parameters for all scenarios. The results improved somewhat with increasing number of measurements, but the worst case scenario provided adequate results, indicating that the 12 data points used in the laboratory analysis should have been adequate to define the parameters (see Table M.1).

Increasing the number of samples used in model calibration improved somewhat, however inclusion of conservative measurement error resulted in large standard deviations in model estimation equation coefficients (a1, a2, b1, b2, and b3). Although estimates were still less than ideal, model calibration results improved quite significantly when the range of particle diameters were decreased (d_g ranging from 0.10 mm to 0.50 mm - see Tables M.2 and M.3). This supports our hypothesis that the Haverkamp and Parlange (1986) model provides better results when the model is calibrated to individual geologic units composed of very similar textures.

Table R.1 – Ratio of estimated fitting parameters to true fitting parameters using various number of data points along h(θ) curves.

λ	mean	variance	median	lower limit	upper limit
12 pts	0.993	4.39E-03	1.000	0.929	1.044
20 pts	0.989	7.50E-03	1.000	0.914	1.018
50 pts	0.992	4.14E-03	1.000	0.948	1.013
100 pts	0.995	2.18E-03	1.000	0.951	1.020
250 pts	0.993	2.68E-03	1.000	0.950	1.012
h_{ae}	mean	variance	median	lower limit	upper limit
12 pts	0.996	3.18E-03	1.000	0.924	1.044
20 pts	0.989	7.50E-03	1.000	0.914	1.018
50 pts	0.992	4.14E-03	1.000	0.948	1.013
100 pts	0.995	2.18E-03	1.000	0.951	1.020
250 pts	0.993	2.68E-03	1.000	0.950	1.012

Table R.2 – Statistics for the ratio of estimated to true values for model coefficients for the narrow range of particle diameters (for 1000 combinations of X number of samples).

stats for new dg range (dg=0.10-0.50 mm):						
20 pts		mean	variance	median	5%	95%
	a1	3.2122	0.5745	3.1318	2.1602	4.557
	a2	0.333	0.0172	0.3331	0.1115	0.5428
	b1	1.2213	0.0355	1.2101	0.9327	1.5408
	b2	2.4784	1.8522	2.3727	0.3794	4.7546
	b3	16.8833	292.2631	15.7537	-9.9435	44.8215
40 pts		mean	variance	median	5%	95%
	a1	3.1524	0.2267	3.1124	2.4417	3.9829
	a2	0.3359	0.0078	0.3388	0.1829	0.4726
	b1	1.2085	0.0106	1.1996	1.0531	1.3867
	b2	2.4118	0.5397	2.3464	1.3497	3.7047
	b3	16.4116	75.1001	15.1829	4.0002	31.5743
80 pts		mean	variance	median	5%	95%
	a1	3.174	0.1166	3.1409	2.6561	3.7737
	a2	0.3298	0.004	0.3312	0.2225	0.4327
	b1	1.2026	0.0045	1.1948	1.1049	1.3238
	b2	2.3588	0.2132	2.29	1.724	3.1891
	b3	15.7207	26.9978	14.6341	8.8525	25.1297
100 pts		mean	variance	median	5%	95%
	a1	3.1583	0.0847	3.147	2.6977	3.6474
	a2	0.3319	0.0028	0.3312	0.2472	0.4184
	b1	1.1985	0.0035	1.191	1.1116	1.3022
	b2	2.3227	0.1646	2.2536	1.7503	3.0868
	b3	15.2733	20.6985	14.3427	9.2619	24.1748
200 pts		mean	variance	median	5%	95%
	a1	3.1432	0.0433	3.1288	2.8072	3.4982
	a2	0.3329	0.0015	0.3346	0.2675	0.3953
	b1	1.1917	0.0015	1.1872	1.1331	1.2666
	b2	2.2896	0.0723	2.2499	1.9159	2.8222
	b3	14.9523	8.9742	14.3568	11.1418	20.9208
all data		ratio est/true coeff				
	a1	3.1481				
	a2	0.3308				
	b1	1.183				
	b2	2.2306				
	b3	14.258				

Table R.3 – Statistics for the ratio of estimated to true values for model coefficients for the initial range of particle diameters (for 1000 combinations of X number of samples).

stats for initial d_g range (d_g = 0.07-1.0 mm)						
20 pts		mean	variance	median	5%	95%
	a1	3.5755	1.6723	3.3293	2.0072	6.1419
	a2	0.2792	0.0386	0.2927	-0.0807	0.5724
	b1	1.3105	0.1521	1.3328	0.6054	1.895
	b2	3.2998	6.1389	3.2863	-0.8957	7.3651
	b3	28.7846	885.726	26.9305	-17.2549	79.3955
40 pts		mean	variance	median	5%	95%
	a1	3.4897	0.6295	3.373	2.4284	5.0377
	a2	0.2777	0.0174	0.2855	0.0399	0.4732
	b1	1.2763	0.0634	1.296	0.8263	1.6692
	b2	3.0746	2.5278	3.073	0.3824	5.5845
	b3	26.4089	346.8885	25.406	-2.1047	57.426
80 pts		mean	variance	median	5%	95%
	a1	3.4693	0.3141	3.4141	2.6592	4.3999
	a2	0.2749	0.009	0.2785	0.124	0.4253
	b1	1.2629	0.0346	1.2747	0.9363	1.5375
	b2	2.9636	1.33	2.96	1.0437	4.7531
	b3	24.9526	170.6669	24.3307	5.1222	46.4231
100 pts		mean	variance	median	5%	95%
	a1	3.4517	0.2434	3.41	2.7277	4.3198
	a2	0.2768	0.0069	0.2783	0.1357	0.4079
	b1	1.2578	0.0268	1.2648	0.9832	1.5124
	b2	2.9137	1.0316	2.863	1.3282	4.6235
	b3	24.2682	134.2178	22.6244	7.0945	44.3577
200 pts		mean	variance	median	5%	95%
	a1	3.4263	0.1219	3.3959	2.9155	4.0269
	a2	0.2774	0.0037	0.2795	0.1775	0.3714
	b1	1.2369	0.0141	1.2314	1.0468	1.4406
	b2	2.8048	0.5212	2.73	1.6929	4.0889
	b3	23.2401	65.2925	21.996	11.9246	38.3216
all data		ratio est/true coeff				
	a1	3.4006				
	a2	0.2799				
	b1	1.2017				
	b2	2.4857				
	b3	19.123				

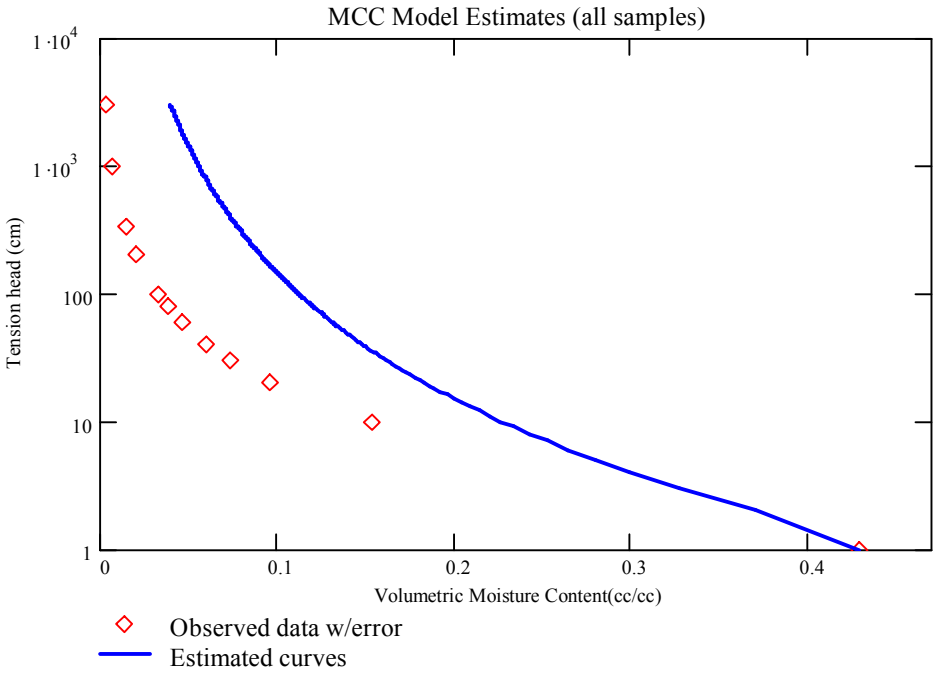

RSQ = 0.599

θ1(0) = 0.429

dg range is from 0.07mm to 1.0mm

Figure R.1 – Example of worst model results for initial range of particle diameters (0.07 to 1.0 mm).

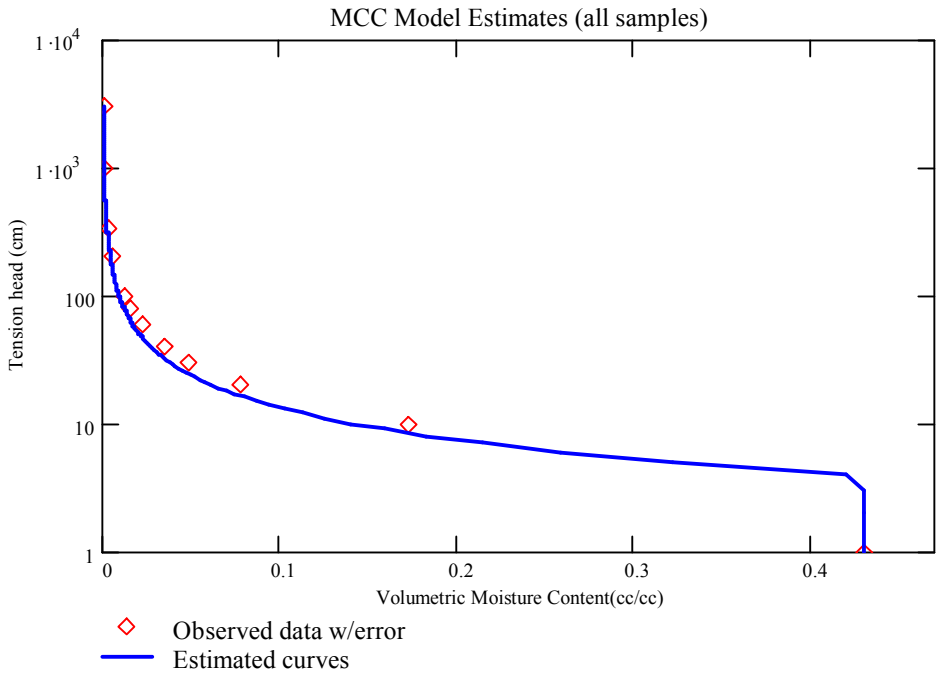

RSQ = 0.991

θ1(0) = 0.43

dg range is from 0.07mm to 1.0mm

Figure R.2 – Example of best model results for initial range of particle diameters (0.07 to 1.0 mm).

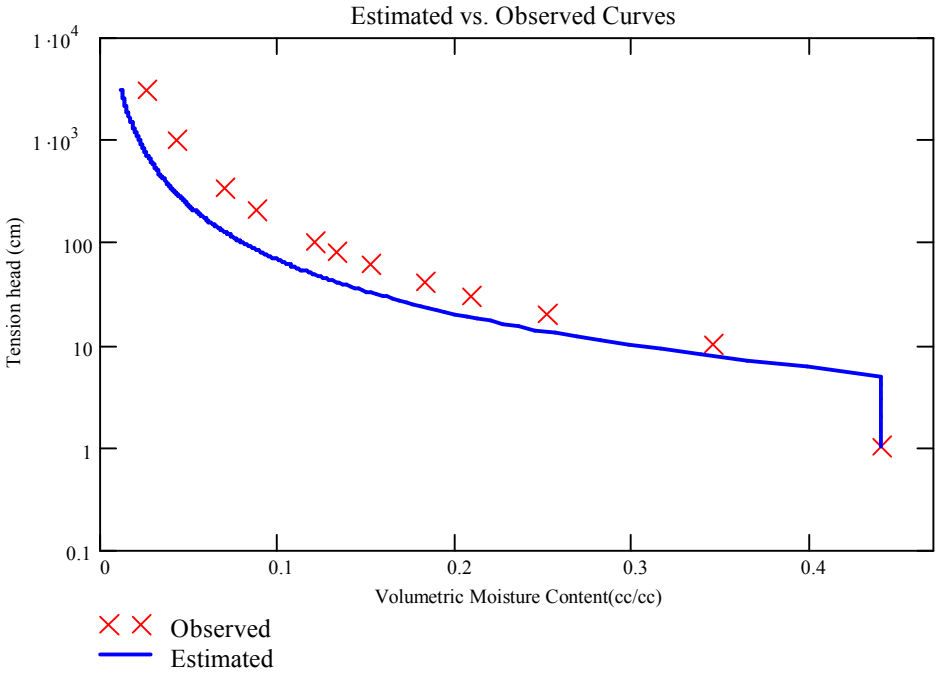

dg range is from 0.10 mm to 0.50 mm

RSQ = 0.894

dg_C = 0.407

θ1(0) = 0.441

Figure R.3 – Example of worst model results for narrow range of particle diameters (0.1 to 0.5 mm).

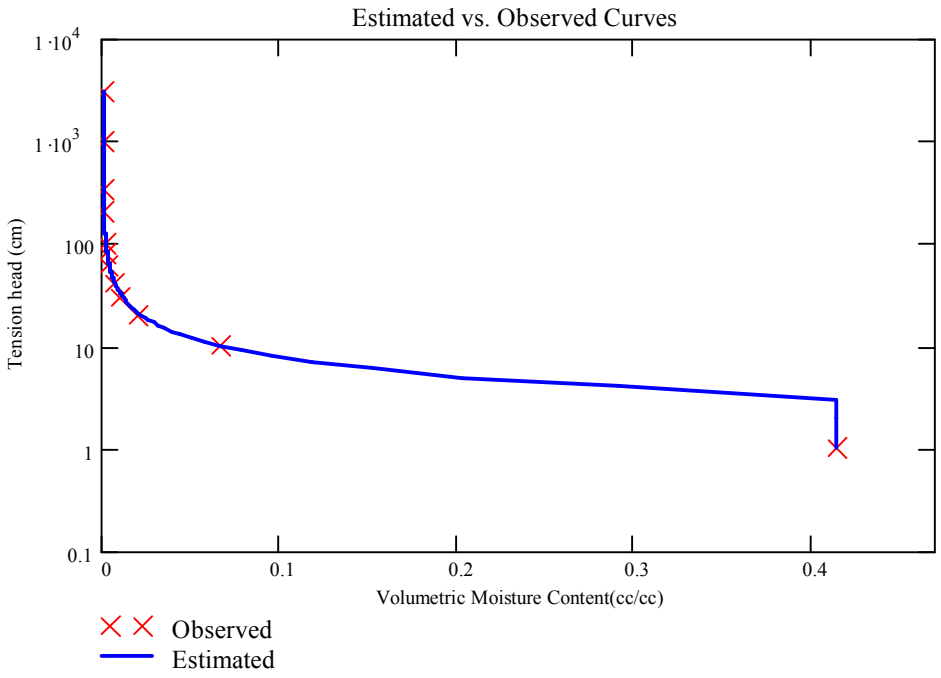

dg range is from 0.10 mm to 0.50 mm

$RSQ = 1$

$dg_C = 0.408$

$\theta 1(0) = 0.414$

Figure R.4 – Example of best model results for narrow range of particle diameters (0.1 to 0.5 mm).

REFERENCES

Alumbaugh, D. L., R. J. Glass, and J. T. McCord, 1996. A Hybrid Hydrologic – Geophysical Inverse Technique for the characterization, monitoring, and risk assessment of leachate in the vadose zone. U. S. Department of Energy, Environmental Management Science Program ER-EM-EMSP-96.

Anderholm, Scott K., 1983. Hydrogeology of the Socorro and La Jencia Basins, Socorro County, New Mexico. New Mexico Geological Society Guidebook, 34th Field Conference, Socorro Region II, pp. 344.

Anderson, S. H. and D. K. Cassel, 1986. Statistical and autoregressive analysis of soil physical-properties of Portsmouth sandy loam. Soil Science Society of America Journal, 50(5): 1096-1104, SEP-OCT 1986.

Arya, L. M., J. L. Feike, P. J. Shouse, and M. T. van Genuchten, 1999. Relationship between the hydraulic conductivity function and the particle-size distribution. Soil Science Society of America Journal, 63:1063-1070.

Arya, L. M., and J. F. Paris, 1981. A physioempirical model to predict soil moisture characteristic from particle-size distribution and bulk density data. Soil Science Society of America Journal, 45: 1023-1030.

ASTM, 1963. Test method for particle-size analysis of soils. Annual book of ASTM standards, ASTM D422-63, American Society for Testing and Materials, Philadelphia, Pennsylvania.

ASTM, 1994a. Standard practice for thin-walled tube geotechnical sampling of soils. Annual book of ASTM standards, ASTM D1587-94, American Society for Testing and Materials, Philadelphia, Pennsylvania.

ASTM, 1994b. Standard test method for capillary-moisture relationships for fine-textured soils by pressure-membrane apparatus. Annual book of ASTM standards, ASTM D3152-72 (reapproved 1994), American Society for Testing and Materials, Philadelphia, Pennsylvania.

ASTM, 1994c. Standard test method for capillary-moisture relationships for coarse and medium textured soils by porous-plate apparatus. Annual book of ASTM standards, ASTM D2325-68 (reapproved 1994), American Society for Testing and Materials, Philadelphia, Pennsylvania.

ASTM, 1994d. Standard test method for permeability of granular soils (constand head). Annual book of ASTM standards, ASTM D2434-68 (reapproved 1994), American Society for Testing and Materials, Philadelphia, Pennsylvania.

ASTM, 1995. Standard practices for preserving and transporting soil samples. Annual book of ASTM standards, ASTM D4220-95, American Society for Testing and Materials, Philadelphia, Pennsylvania.

ASTM, 1999. Standard method for penetration test and split-barrel sampling of soils. Annual book of ASTM standards, ASTM D1586-99, American Society for Testing and Materials, Philadelphia, Pennsylvania.

Brainard, J. R., R. J. Glass, D. L. Alumbaugh, L. Paprocki, D. J. Labrecque, X. Yang, T.-C. J. Yeh, K. E. Baker, and C. A. Rautman, 2000, The Sandia-Tech Vadose Zone Facility: Experimental Design and Data Report of a Constant Flux Infiltration Experiment, Sandia National Laboratories, Publication in Progress.

Brooks, R. H., and A. T. Corey, 1964. Hydraulic properties of porous media. Hydrology Paper No. 3, Colorado State Univ., Fort Collins, Colorado.

Carsel, R. F. and R. S. Parrish, 1988. Developing joint probability distributions of soil water retention characteristics. Water Resources Research, 24(5): 755-769, MAY 1988.

De Backer, L. and A. Klute, 1967. Comparison of pressure and suction methods for soil-water content pressure-head determinations. Soil Science, 104(1): 46-55.

Econony, K. and R. S. Bowman, 1993. Fiberglass encasement method for undisturbed soil cores. Soil Science Society of America Journal, 57:39-41.

Fayer, M. J. and C. S. Simmons, 1995. Modified soil water retention functions for all matric suctions. Water Resources Research, 31(5): 1233-1238.

Fetter, C. W., 1994. Applied Hydrogeology, 3rd edition, Macmillan College Publishing Company, Inc., Oshkosh, WI, pp. 691.

Flint, L. E., 1996. Matrix Properties of Hydrogeologic Units at Yucca Mountain, NV. U.S. Geological Survey, Water Resources Investigations Report 96-XX, 1996.

Gillham, R. W., A. Klute, and D. F. Heermann, 1979. Measurement and numerical simulation of hysteretic flow in a heterogeneous porous medium. Soil Science Society of America Journal, 43(6): 1061-1067.

Gupta, S. C. and W. E. Larson, 1979. A model for predicting packing density of soils using particle-size distribution. Soil Sci. Am. J. 43:758-764.

Haverkamp, R. and J. Y. Parlange, 1986. Predicting the water-retention curve from particle-size distribution: 1. Sandy soils without organic matter. Soil Science, 142(6): 325-339.

Hawley, H. W, 1983, Geomorphic Evolution of Socorro Area of Rio Grande Valley. New Mexico Geological Society Guidebook, 34th Field Conference, Socorro Region II, pp. 334.

Healy, R. W. and P. C. Mills, 1991. Variability of an unsaturated sand unit underlying a radioactive-waste trench. Soil Science Society of America Journal, 55: 899-907, JULY-AUGUST, 1991.

Hillel, D., 1980. Fundamentals of Soil Physics. Academic Press, New York, pp. 413.

Holt, R. M., 2000. Spatial bias in unsaturated hydraulic property estimates: Origin, impact, and relevance. PhD. Dissertation, New Mexico Institute of Mining and Technology, Socorro, NM, August, 2000.

Isaaks, E. H. and R. M. Srivastava, 1989. Applied Geostatistics. Oxford University Press, New York, NY, pp. 561.

Jury, W. A., W. R. Gardner, and W. H. Gardner, 1991. Soil Physics, fifth edition, John Wiley and Sons, Inc., New York, NY, pp. 328.

Istok, J. D., D. O. Blout, L. Barker, K. R. Johnejack, and D. P. Hammermeister, 1994. Spatial variability in alluvium properties at a low-level nuclear waste site. Soil Sci. Soc. Am. J., 58: 1040-1051.

Kaluarachichi J. J. and J. C. Parker, 1987. Effects of hysteresis with air entrapment on water flow in the saturated zone. Water Resources Research, 23(10): 1967-1976.

Klute, A. (ed.), 1986. Methods of Soil Analysis. Part 1. 2nd ed., Number 9 in the series AGRONOMY. ASG, Inc. and SSSA, Inc., Madison, WI, pp. 1188.

Knight, R., 1991. Hysteresis in the electrical resistivity of partially saturated sandstones. Geophysics, 56(12): 2139-2147.

Leij, F. J., W. J. Alves, M. T. van Genuchten, 1996. The UNSODA Unsaturated Soil Hydraulic Database. U.S. Environmental Protection Agency, Office of Research and Development, Washington, DC. EPA/600/R-96/095, August 1996.

Love, D. W., R. F. Reimers, J. W. Hawley, G. D. Johnpeer, and D. J. Bobrow, 1987. Summary of geotechnical investigations near Espanola, New Mexico, in C. Menges, editor, Quaternary tectonics, landform evolution, soil chronologies and glacial deposits--northern Rio Grande rift of New Mexico: Friends of the Pleistocene Field Trip Guidebook, Geology Department, University of New Mexico, Albuquerque, pp. 133-157.

Mallants, D., B. P. Mohanty, D. Jacques, and J. Feyen, 1995. Spatial variability of hydraulic properties in a multi-level soil profile. Soil Science, 161(3): 167-181.

Mandell, J. 1964. The Statistical Analysis of Experimental Data. National Bureau of Standards, Washington, D.C., Dover Publications, Inc., New York, pp. 410.

Mualem, Y., 1976. A new model for predicting the hydraulic conductivity of unsaturated porous media. Water Resources Research, 12: 513-522.

Mualem, Y. and G. Dagan, 1977. Hydraulic conductivity of soils: unified approach to the statistical models. Science Society of America Journal, 42:392-395.

Nimmo, J. R., J. Rubin, and D. P. Hammermeister, 1987. Unsaturated flow in a centrifugal field: Measurement of hydraulic conductivity and testing of Darcy's Law. Water Resources Research, 23(1): 124-134.

Paprocki, L. T., 2000. Characterization of vadose zone in-situ moisture content and an advancing wetting front using cross-borehole ground penetrating radar. M. S. Thesis, New Mexico Institute of Mining and Technology, Socorro, NM, February, 2000.

Prothero, D. R. and F. Schwab, 1996. An Introduction to Sedimentary Rocks and Stratigraphy: Sedimentary Geology. W.H. Freeman and Company, New York, pp. 575.

Rawls, W. J., D. L. Brakensiek, and K. E. Saxton, 1982, Estimating Soil Water Properties Transactions, ASAE, 25(5):1316-1320 and 1328.

Russo, D. W., and G. L. Butters, 1989. Numerical analysis of solute transport during transient irrigation, 1, The effect of hysteresis and profile heterogeneity. Water Resources Research, 25(10): 2109-2118.

Salter, P. J., G. Berry, and J. B. Williams, 1966. The influence of texture on the moisture characteristics of soils: 3. Quantitative relationships between particle size, composition and available water capacity. J. Soil Sci., 17: 93-98.

Scheaffer, R. L. and J. T. McClave, 1995. Probability and Statistics for Engineers. Duxbury Press, Belmont, CA, pp. 745.

Simunek, J. R. Kodesova, M. M. Gribb, and M. T. van Genuchten, 1999. Estimating hysteresis in the soil water retention function from cone penetrometer experiments. Water Resources Research, 35(5): 1329-1345.

Scott, P. S., G. J. Farguhar, and N. Kouwen, 1983. Hysteretic effects on net infiltration. Proceedings of the National Conference on Advances in Infiltration, Dec 12-13, 1983. ASAE Publications; 11-83, Am. Soc. Agric. Eng., pg. 163-170.

Stephens, D. B. and K. R Rehfeldt, 1985. Evaluation of closed-form analytical models to calculate conductivity in a fine sand. Science Society of America Journal, 49(1): 12-19.

Stephens, D. B. and R. Knowlton, 1986. Soil water movement and recharge through sand at a semiarid site in New Mexico. Water Resources Research, 22(6): 881-889, JUN 1986.

Stephens, D. B., 1995. Vadose Zone Hydrology. Lewis Publishers, Boca Raton, LA. pp. 347.

van Genuchten, M. T., 1980. A closed-form equation for predicting the hydraulic conductivity of unsaturated soils. Science Society of America Journal, 44: 892-898.

van Genuchten, M. T., F. J. Leij, and S. R. Yates, 1991. The RETC Code for Quantifying the Hydraulic Functions of Unsaturated soils. U.S. Environmental Protection Agency, Office of Research and Development, Washington, DC. EPA/600/2-91/065, December 1991.

van Genuchten, M. T., M. G. Schaap, B. P. Mohanty, J. Simunek, and F. J. Leij., 1999. Modeling transport processes at the local scale. In: J. Feyen and K. Wiyo (eds.), Modelling of Transport Process in Soils at Various Scales in Time and Space, Wageningen Pers, Wageningen, The Netherlands, pp. 23-45

Vennard, J. K., and R. L. Street, 1982. Elementary Fluid Mechanics. John Wiley and Sons, New York, NY, pp.689.

Yeh, T. C. J. and D. J. Harvey, 1990. Effective unsaturated hydraulic conductivity of layered sands. Water Resources Research, 26(6): 1271-1279, JUN 1990.